The Dissertation Committee for Himanshu Sharma Certifies that this is the approved version of the following dissertation:

Study of Geochemical Interactions during Chemical EOR Processes

Committee:

Kishore K. Mohanty, Supervisor

Gary A. Pope

Upali Weerasooriya

Mojdeh Delshad

Marc A. Hesse

Study of Geochemical Interactions during Chemical EOR Processes

by

Himanshu Sharma, B.E.; M.Tech.

Dissertation

Presented to the Faculty of the Graduate School of

The University of Texas at Austin

in Partial Fulfillment

of the Requirements

for the Degree of

Doctor of Philosophy

The University of Texas at Austin

December 2016

Dedication

Dedicated to my family for their endless love and support.

Acknowledgements

First of all, I would like to thank my PhD supervisor, Dr. Kishore K. Mohanty, for his timely guidance, patience and support. I am thankful to him for being available whenever I needed directions, related to research and otherwise, giving me freedom to pursue research, and guiding me whenever I went astray. I truly value having done research with him; his emphasis on the fundamentals and vast knowledge has helped me immensely. I enjoyed having discussions with him and his amiable personality kept me at ease during these discussions.

I would like to thank Dr. Gary A. Pope for being a valuable mentor and for serving on my PhD committee. I am very grateful to him for being available for discussions. I always enjoyed speaking with him and discussing problems related to geochemistry and surfactant flooding. I enjoyed doing research work with him; his inquisitiveness and systematic approach towards research made working with him a great learning experience.

I would like to thank Dr. Upali Weerasooriya for also being a valuable mentor and for serving on my PhD committee. I am thankful to him for explaining intricate chemistry concepts in simple terms and ensuring that I had a good understanding of the chemistry related to my research. Seeing his enthusiasm towards solving problems using novel concepts has been a valuable experience. In addition, his positive and easy-going disposition made working with him enjoyable.

I would like to thank Dr. Mohdeh Delshad for serving on my PhD committee and answering queries related to UTCHEM.

I am thankful to Dr. Marc Hesse for serving on my PhD committee and for teaching a course on reactive flow in porous media, which helped me immensely in my research.

I am thankful to Dr. Kami Sepehrnoori for his valuable advice during the course of my graduate studies. I am also thankful to him for helping me with UTCHEM-IPHREEQC simulations.

I am thankful to Dr. Robert McNeil for his valuable inputs related to geochemistry.

I would like to thank the administrative staff members for their support: Ms. Barbara Messmore, Ms. Frankie Hart, Ms. Amy Douglas Stewart, Ms. Esther Barrientes and Ms. Diane Landeros. I am also thankful to Gary Miscoe and Glen Baum for ensuring that labs were safe for conducting research.

I would like to thank all my friends and lab members including Luiz, Rubia, Shashvat, Rahul, Gaurav, Ashish, Karthik, Brian, Ayaz, Robin, Kaustabh, Pinaki, Ruth, Ashwin, Gurpreet, Mrinal, Khusboo, Aboulghasem, Jith, Mathieu, Leo, Mohsen, Jun, Nabi, Sophie, Gayani, Nadika, Krishna, Eric, Chammi for their friendship, research related discussions, lunches, and coffee breaks. They truly made research more enjoyable. I am thankful to my department colleagues and other faculty members. I am also thankful to my friends in India for their friendship.

I am thankful to my undergraduate research advisors, Dr. Sirshendu De and Dr. Sunando DasGupta, for giving me the opportunity to conduct research work with them. I value having done research work with them.

I am thankful to this wonderful city, Austin live music, and my own six strings which I enjoyed playing every now and then to take break from research.

Last but not the least; I am thankful to my loving family, especially my parents and sisters, for their endless love, support and encouragement throughout my education.

Study of Geochemical Interactions during Chemical EOR Processes

Himanshu Sharma, Ph.D.

The University of Texas at Austin, 2016

Supervisor: Kishore K. Mohanty

Geochemical interactions of injected fluids with reservoir fluids and minerals determine the fate of the injected species in the porous media. In addition, these interactions could result in affecting the properties of the porous media such as permeability, porosity, and wettability. With a growing energy demand and continuous depletion of easy oil, chemical enhanced oil recovery (CEOR) techniques are being investigated to satisfy future energy needs. An understanding of geochemical interactions that occur during CEOR techniques is essential to make these processes robust and economical, and make reliable field predictions. In this study, geochemical interactions during alkali surfactant polymer (ASP) floods and low salinity wettability alteration in carbonates were investigated.

Experiments were performed to understand interactions of various alkalis in sandstone and carbonate cores containing gypsum. The experiments included single-phase static and transport experiments, surfactant phase behavior experiments and oil recovery corefloods. The ionic compositions of aqueous solutions were carefully monitored to understand the geochemical interactions of these alkalis. The effect of injection rate was investigated to understand if reactions reached equilibrium at the injection rates typically used in lab corefloods. The study showed sodium metaborate to be most suitable, in comparison to sodium carbonate, sodium hydroxide and sodium silicate, for sandstone and carbonate cores containing gypsum. The reaction of

sodium metaborate with gypsum was found to be rate dependent and did not reach equilibrium in the lab corefloods.

Ammonia was investigated as an alternative alkali for ASP floods. Single-phase static and transport experiments were performed to study its interactions with gypsum. Single-phase static and transport experiments were performed to investigate the effect of adding ammonia on surfactant adsorption. Zeta potential measurements were performed using ammonia and sodium carbonate. Ultralow IFT surfactant formulations were developed, using ammonia as the alkali, for cores containing gypsum or otherwise. Polymer stability experiments were performed to identify polymers suitable for ASP corefloods in cores containing gypsum using ammonia as the alkali. The results showed ammonia to maintained a high pH in presence of gypsum without causing any calcium precipitation. The dissolved calcium ions, however, affected surfactant phase behavior and polymer stability. Single-phase static and transport surfactant adsorption experiments showed reduction in surfactant adsorption on sandstones by adding ammonia. The surfactant adsorption results were, however, not obvious for carbonates when ammonia was used as the alkali. Good oil recoveries and low surfactant retentions were observed during ASP corefloods in sandstone and carbonate cores using ammonia.

Interaction of various alkalis with acidic crude oils was also investigated to develop low-cost alkali cosolvent polymer (ACP) floods for such oils. Alkali scans were performed with various alkalis (with and without adding a cosolvent) and low IFT regions were identified. The effect of cosolvent type and divalent cations on the phase behavior results was investigated. ACP corefloods were performed in sandstone cores. The phase behavior experiments showed low IFT regions to vary for different alkalis. ACP corefloods showed good oil recoveries in sandstone cores.

Single-phase static and transport experiments were performed to understand geochemical interactions during low salinity waterfloods in carbonate cores at high

temperatures. Various low-salinity brines were injected in a limestone core and the ionic composition of the effluent samples were monitored. The effect of injection rate on the composition of the effluent ions was investigated. The experiments showed calcite dissolution, dolomitization and sulfate adsorption to occur on injecting low-salinity brines in limestone cores at high temperatures. The reactions reached equilibrium within 2 PV at 1 ft/d when seawater was injected in a limestone core, initially saturated with the formation brine. However, the reactions did not reach equilibrium when the SW was subsequently displaced with SW/50, even after injecting more than 3 PV.

Modeling and simulation work was performed with PHREEQC, UTCHEM and UTCHEM-IPHREEQC to model lab experiments. Single-phase alkali floods and oil recovery corefloods performed using sodium metaborate and ammonia were simulated. A good agreement was obtained between experimental and simulation results. The effect of ion exchange reactions on surfactant floods was investigated. In addition, a mechanistic model was developed for low-salinity wettability alteration in carbonates by incorporating key geochemical interactions observed during the experiments. The model results showed good agreement with effluent ions of static and dynamic experiments, assuming local equilibrium. A good agreement of modeling results was observed with the low salinity oil recovery corefloods reported in the literature.

Table of Contents

List of Tables

List of Figures

CHAPTER 1. INTRODUCTION

1.1 Motivation

A substantial portion of our energy needs is satisfied by fossil fuels. The near-term future predictions, shown in Figure 1.1, indicate that crude oil is going to provide a significant portion of our energy needs. Even though the energy output from renewable and nuclear energy is going to increase in the future, about 78% of our energy demand is likely to be satisfied by fossil fuels in 2040. Enhanced oil recovery (EOR) techniques will be required so that the future energy demand can be satisfied. By making these processes more robust and economical, the energy demand can be satisfied likewise.

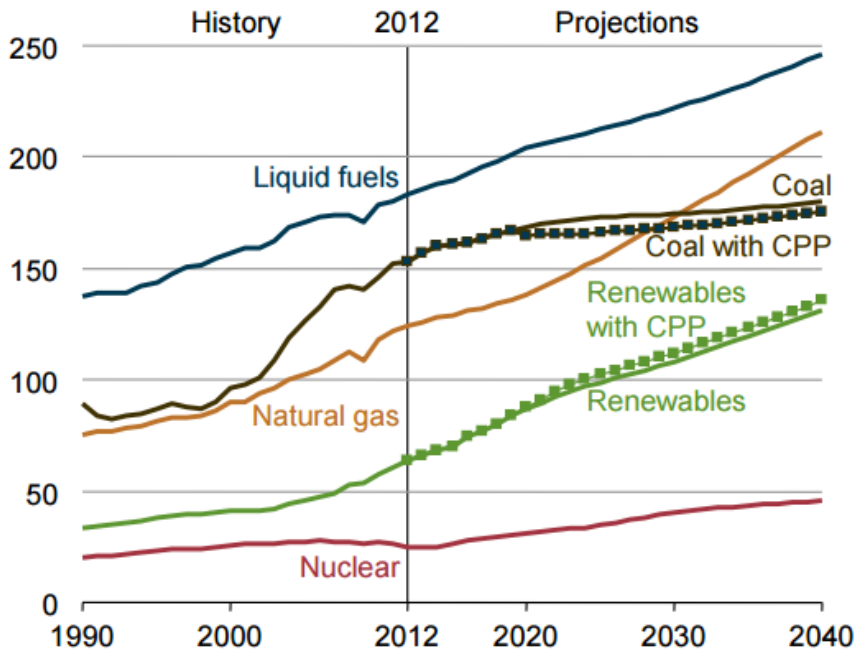

Figure 1.1: World future energy demand in quadrillion Btu by energy source (IEA, 2016)

A schematic of various phases and species that are typically present or injected in an oil reservoir during an EOR process is shown in Figure 1.2. The geochemical interactions between these species, in the process of achieving equilibrium, could result in changing the properties of the injected fluids, in-situ fluids, produced fluids and the reservoir.

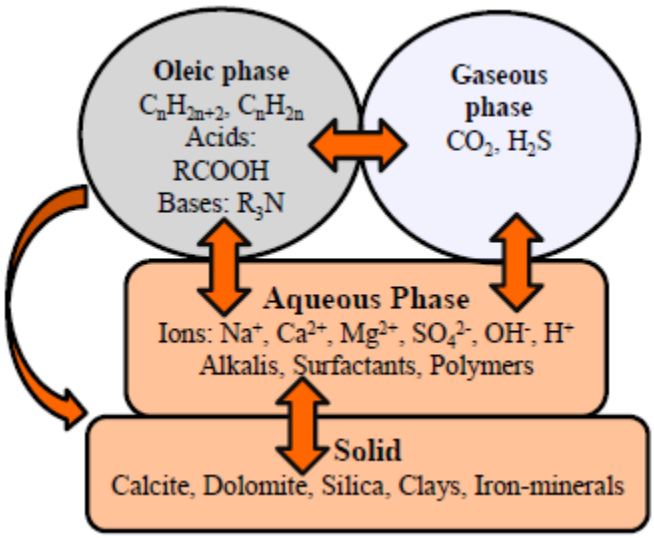

Figure 1.2: A schematic of various species and phases present in an oil reservoir

For instance, severe plugging near the production well was reported by He et al. (2007) during an ASP pilot test in Daqing field due to the dissolution of minerals in the reservoir and their subsequent precipitation due to cooling and depressurization near the production well. Austad (2009) reported an increase in oil recovery from carbonates on injecting brines with carefully designed compositions. They postulated the interactions of ions in these brines with the carbonate matrix to be responsible for improving the oil

recovery. Similarly, Venkataraman (2014) reported change in the phase behavior envelope during CO_2 injection due to precipitation and dissolution reactions. An understanding of geochemical interactions is therefore critical in designing robust and economical recovery of hydrocarbons.

1.2 Research Objective

The objective of this study is to investigate geochemical interactions during alkali surfactant polymer (ASP) floods, alkali cosolvent polymer (ACP) floods, and low salinity waterfloods in carbonates. Both experimental and modeling work was performed to obtain a better understanding of these interactions. In addition, attention was given to understand if reactions reached equilibrium in lab experiments. The specific objectives of this research work are listed below.

1. Understand the interactions of various alkalis in the presence of gypsum and identify alkalis that can be used to perform ASP floods in reservoirs containing gypsum. Develop ASP formulations and investigate the role of geochemical interactions on ASP floods designed using these alkalis. Model lab results in UTCHEM and PHREEQC.

2. Identify an alternate alkali to perform ASP floods, economically. Develop surfactant formulations using this alkali and perform ASP corefloods to tests the effectiveness of the alkali in lowering surfactant adsorption on sandstones and carbonates. Lastly, understand the role of geochemical interactions on surfactant formulations developed using this alkali. Model lab results in UTCHEM and PHREEQC.

3. Understand the interactions of various alkalis with acidic crude oils and develop ACP formulations for such oils. Understand the effect of geochemical interactions and cosolvent type on ACP floods. Perform ACP corefloods to tests these formulations.

4. Understand geochemical interactions during low salinity waterfloods in carbonates by performing single-phase static and transport experiments. Develop a mechanistic model for the process in PHREEQC and UTCHEM-IPHREEQC, and simulate single-phase lab results and oil recovery corefloods.

1.3 Description of the chapters

The dissertation is organized into seven chapters. In Chapter 2, review of the literature on alkali floods, surfactant floods, polymer floods, and low salinity waterfloods in carbonates in given. Chapter 3 focusses on the materials and methods adopted in this study. The chapter discusses experimental procedures and measurement techniques in detail. Chapter 4 discusses the results of ASP and ACP corefloods performed using various alkalis. This chapter is divided into three sections: the results obtained using sodium metaborate and ammonia are discussed in the first two sections. The last section discusses the results of ACP floods using various alkalis. In particular, the interactions of these alkalis in the presence of gypsum is discussed. The results of single-phase and multiphase simulations using PHREEQC and UTCHEM, respectively, are discussed in Chapter 5. The focus of these simulations is on modeling lab results and further investigating the geochemical interactions during ASP and ACP floods. The results of single-phase static and dynamic experiments to investigate geochemical interactions

during low salinity waterfloods in carbonates is discussed in Chapter 6. A mechanistic model developed for the wettability alteration process is also discussed. The results are summarized in Chapter 7 and the main conclusions are listed. In addition, recommendations for future work are given in Chapter 7.

CHAPTER 2. LITERATURE SURVEY

Oil production from a reservoir is often broadly categorized into three stages: primary recovery, secondary recovery, and tertiary recovery. The primary oil recovery is due to the natural drive in the oil reservoir: reservoir pressure, aquifer drive or gas cap. Oil recovery during this stage is typically about 10-15% OOIP. During the secondary recovery, a fluid is injected (typically water) to maintain or increase the reservoir pressure and displace the oil towards the production wells. The cumulative oil recovery after this stage is around 30-35% OOIP, thus leaving a large quantity of oil unrecovered. The factors responsible for a low oil recovery after primary and secondary floods can be broadly classified into two categories. The low oil recovery is due to either a low macroscopic sweep efficiency or a low microscopic sweep efficiency (or both). Note, however, that in the case of heavy oils or shales, the low oil recovery is the result of poor transport of oil in the porous media; due to the high viscosity of heavy oils and due to an ultra-low permeability of shale reservoir, respectively. The macroscopic sweep efficiency is an indicator of the total volume of the reservoir that comes into contact with the injected fluids. The microscopic sweep efficiency dictates the amount of oil that is recovered from the areas that are contacted by the injected fluid. The combination of both these parameters determines the overall recovery from an oil reservoir. Enhanced oil recovery techniques are needed to improve these sweep efficiencies, and ultimately, the oil recovery from an oil reservoir. In this chapter, a review of EOR techniques is made. However, the focus of this chapter remains on chemical EOR techniques, especially on

alkali/surfactant/polymer floods and low salinity wettability alteration. A review of geochemical interactions during these EOR processes is also given. Note that additional techniques to improve the oil recovery such as hydraulic fracturing, treatment of formation damage, conformance control with gels, and so on, are not discussed here.

2.1 EOR techniques

The objective of any EOR technique is to recover the residual oil left after primary and secondary recovery. It was briefly discussed earlier that this oil is left behind due to a low macroscopic sweep efficiency or a low microscopic sweep efficiency or both. Low macroscopic sweep efficiency is the consequence of an insufficient contact of the injected fluid with the reservoir. Reservoir heterogeneity, viscous fingering and gravity override are mainly responsible for a low macroscopic sweep efficiency. Reservoir heterogeneity could be due to the presence of layers, vugs or fractures in the reservoirs. In such a case, the injected fluids choose the path of least resistance and bypass through high permeability channels, resulting in insufficiently contacting the reservoir fluids and leaving a large amount of oil behind. Viscous fingering occurs when the mobility of the displacing phase is more than that of the phase being displaced. Viscous fingering is common in waterflooding of viscous and heavy oils, and during gas floods. Due to a relatively higher mobility of the displacing phase, it fingers through the phase being displaced and creates a path of least resistance. As a result, a large part of the reservoir is not contacted. Gravity override also results in lowering the macroscopic sweep efficiency due to a density difference between the displacing and the displaced

phase. This is especially detrimental during gas floods where the gas passes through the upper section of the reservoir owing to buoyancy. One of the objectives of an EOR process, therefore, is to improve the macroscopic sweep efficiency. During the secondary recovery stage, a large amount of oil is left unrecovered even in areas which are swept by the injected fluid due to a low microscopic efficiency. A low microscopic efficiency is the result of high capillary forces between oil and the injected fluids, and an unfavorable wettability of the rock. Therefore, another objective of an EOR process is to improve the microscopic efficiency.

By one classification, EOR techniques can be divided into thermal and non-thermal methods as shown in Figure 2.1. However, others have classified them into three categories: thermal recovery, chemical injection and gas injection. Note that this classification is not very strict and hybrid methods have been developed. In addition, wettability alteration techniques using surfactants and low salinity brines which can be classified under chemical EOR techniques are not given in Figure 2.1.

Thermal methods are usually applied to viscous or heavy oils, and the main purpose is to lower the viscosity of the oil (Figure 2.2). Due to a lowered viscosity, the fluidity of the oil in the porous media is enhanced, and it can be displaced more effectively by the injected fluids. Thermal methods include steam drive, steam assisted gravity drainage (SAGD), hot water injection, in-situ combustion, electrical heating, cyclic steam stimulations (CSS), vapor extraction (VAPEX) and so on (Thomas, 2008). Thermal methods are attractive for heavy oils, especially after improvements in

horizontal drilling techniques. However, these methods have various disadvantages such as the heat loss in formations with thick laminations. They rely heavily on the vertical permeability of the reservoir. In addition to the cost involved in heating a reservoir, thermals methods also have high carbon footprints.

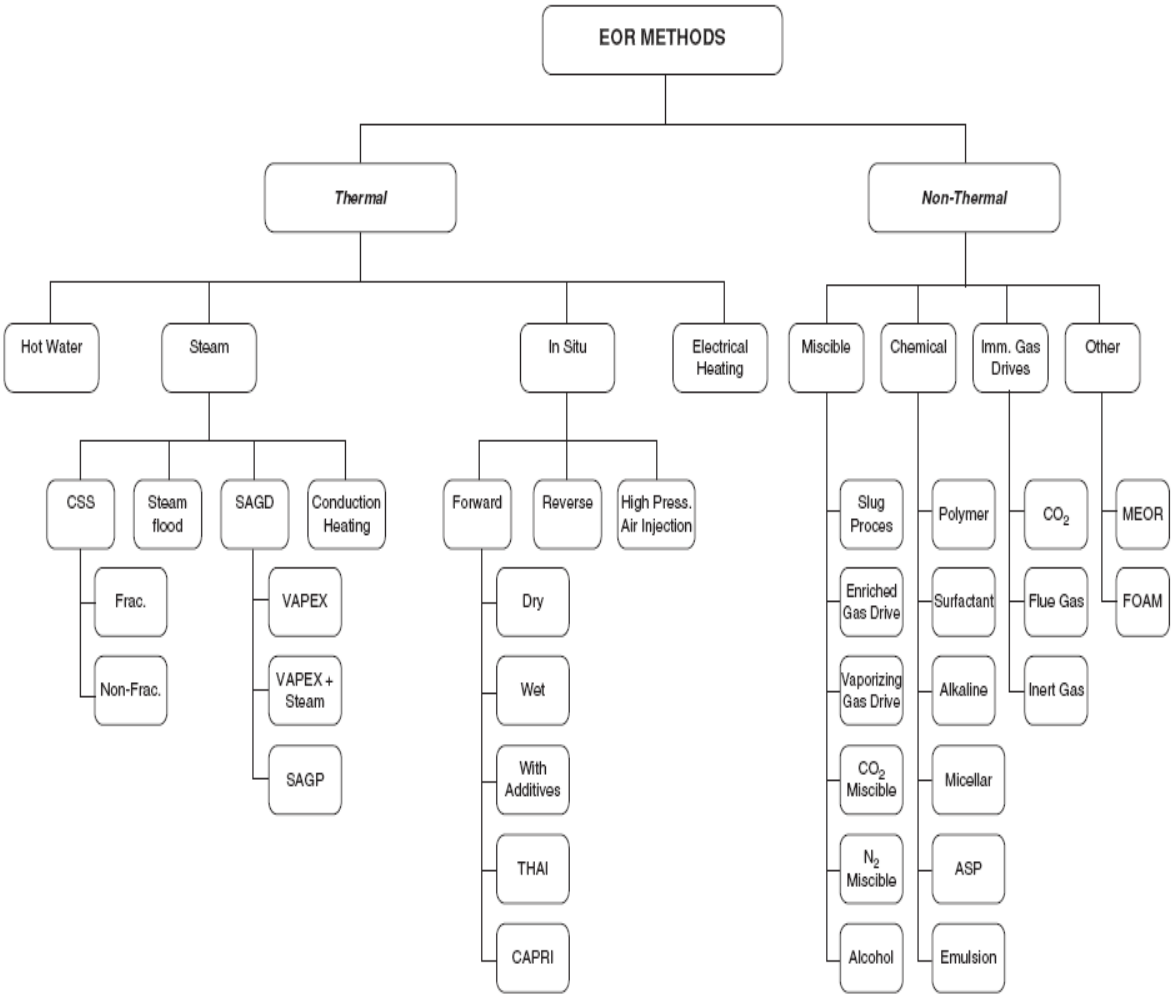

Figure 2.1: A list of EOR techniques (Thomas, 2008)

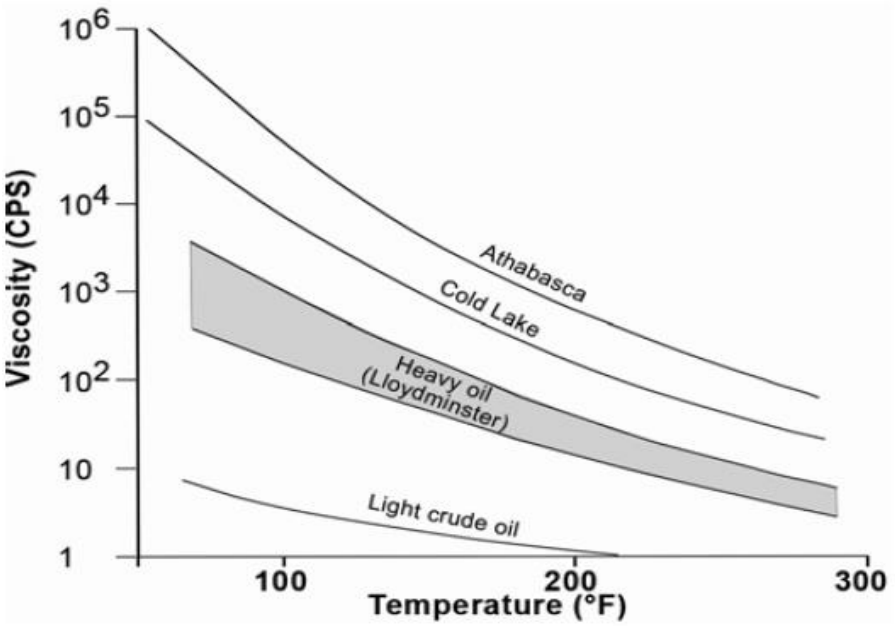

Figure 2.2: Reduction in oil viscosity with an increase in temperature of Canadian heavy oils (Raicar and Proctor, 1984)

Non-thermals methods mainly consist of chemical or gas injection. Microbial EOR techniques are also being investigated. Depending on the experimental conditions, chemical or gas injection can displace the oil in a miscible or an immiscible manner. Gas injection is usually performed with hydrocarbon gas. However, CO_2 and N_2 are also used depending on their availability and reservoir conditions. Recently, increased use of CO_2 for improving oil recovery is being considered to reduce global warming (IEA, 2015).

Injection of gas in an oil reservoir results in swelling of oil and reduction in oil viscosity. In addition, it develops miscibility with oil above a certain temperature and pressure. Gas injection is a mature EOR technique and has been applied in many fields (Alverado & Manrique, 2010). However, the technique suffers from severe limitations

due to low density and low viscosity of gas; the gas tends to sweep the top portion of a reservoir due to its low density and results in viscous fingering due to its low viscosity. In addition, reservoir heterogeneity further lowers the oil recovery. Foams are being studied, using surfactants and nanoparticles, to address these challenges (Singh & Mohanty, 2015; Singh & Mohanty, 2016).

Chemical EOR is another technique to improve oil recovery, which involves the injection of chemicals that can increase macroscopic sweep efficiency, microscopic sweep efficiency or both. A list of chemicals typically injected during this technique includes surfactants, polymers, alkalis, solvents, and their combinations. Low salinity brines have shown to improve the oil recovery from oil wet sandstone and carbonate rocks. A detailed discussion of alkali surfactant polymer (ASP) floods and low salinity wettability alteration is presented next.

2.2 Polymer floods

A polymer is added to the aqueous phase to increase its viscosity and lower its mobility. A lowered mobility of the aqueous phase promotes oil displacement in a stable manner, and reduces the effects of layering and reservoir heterogeneity on oil recovery; thus improving the macroscopic sweep efficiency. Recent studies have also found an improvement in microscopic sweep efficiency with viscoelastic polymers (Huh & Pope, 2008; Koh et al., 2016). A brief review of polymer floods is presented here.

2.2.1 Mechanisms of oil recovery

During a waterflood, a large quantity of oil is left unrecovered if there is an unfavorable mobility ratio and reservoir heterogeneity. Similar to waterfloods, miscible floods (using surfactants for example) are also affected viscous fingering and reservoir heterogeneity. The mechanisms by which a polymer can address these issues are discussed below.

An immiscible displacement in the porous media can be classified into three regions depending on the capillary number and viscosity ratio as shown in Figure 2.3 (Lenormand et al., 1988); regions showing stable displacement, capillary fingering and viscous fingering, respectively. During the waterflood of light oil, the viscosity ratio is often less than 1 and the capillary numbers is around 10^{-7}. As a result, the displacement is capillary dominant and viscous fingering is not observed. However, a substantial number of oil reservoirs are known to contain viscous and heavy oils, and waterflooding these reservoirs results in bypassing a substantial amount of oil due to viscous fingering.

Doorwar & Mohanty (2015) in their waterflood experiments observed an increase in oil recovery of viscous oils (at a given viscosity ratio) by slowing down the injection velocity in water-wet cores. Worawutthichanyakul (2016) studied the effect of rock wettability on the displacement of viscous oils during the waterflood, and observed lowering of oil recovery with a decrease in the injection velocity in oil-wet rocks. Chuoke et al. (1959), Peters & Flock (1981), and Doorwar & Mohanty (2016) developed dimensionless numbers to estimate the onset on viscous fingering and predict oil recovery

in the viscous-fingering regime. Viscous fingering is also observed during miscible displacement due to unfavorable viscosity ratio between the displacing and the displaced phase. Koval (1963) developed an analytical solution based on the fractional flow theory to account for viscous fingering and heterogeneity during a miscible displacement. Lake (2010) discusses conditions for stable displacement during a miscible flood. Polymers may be added in such cases to lower the mobility ratio and improve the oil recovery.

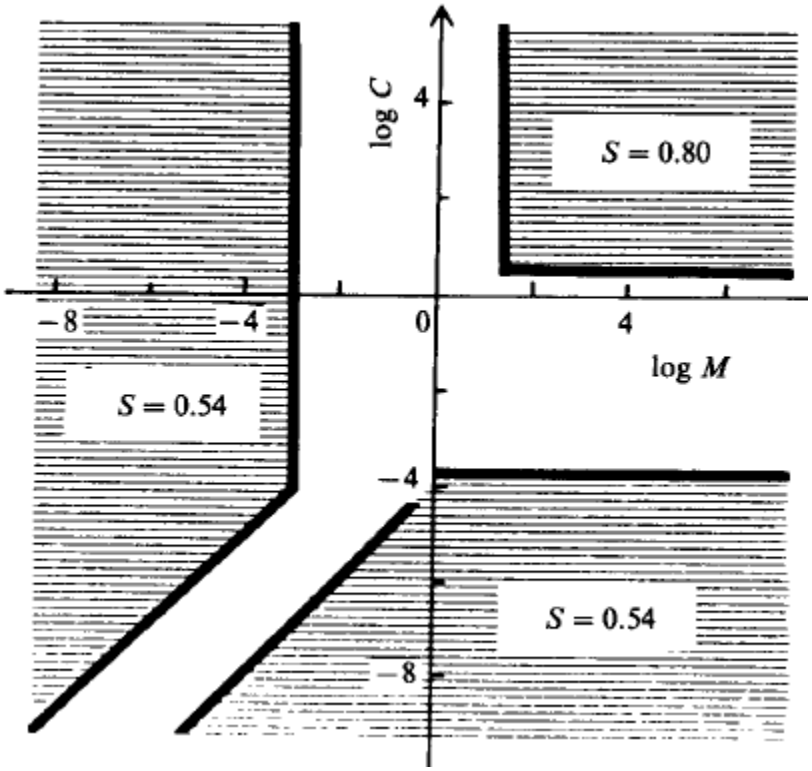

Figure 2.3: Lenormand phase-diagram for immiscible displacement (Lenormand et al., 1988)

In addition to viscous fingering, reservoir heterogeneity could also result in by pass of the injected fluids through high permeability channels. One such situation is when layers of different permeabilities exist in a reservoir. Waterflooding of such a reservoir

results in bypassing of the injected fluid through the high permeability layer. The addition of a polymer to the waterflood brine could improve the oil recovery in this situation (Sorbie, 1991). The polymer could divert the flow by promoting cross-flow between various layers. A schematic of flow through two layers of different permeability and the corresponding pressure profile, with and without cross-flow, is shown in Figure 2.4 (a). When a polymer solution is injected in such a reservoir, the injected polymer flows easily through the high permeability channel. This could result in a lateral buildup of a pressure gradient between these layers, and consequently, the crossflow of fluids between these layers and an additional oil recovery. Note that, the cross-flow is affected by parameters such as the permeability contrast between layers, the vertical permeability, and so on. The analysis is also applicable to surfactant floods, where polymer is typically added to the surfactant slug.

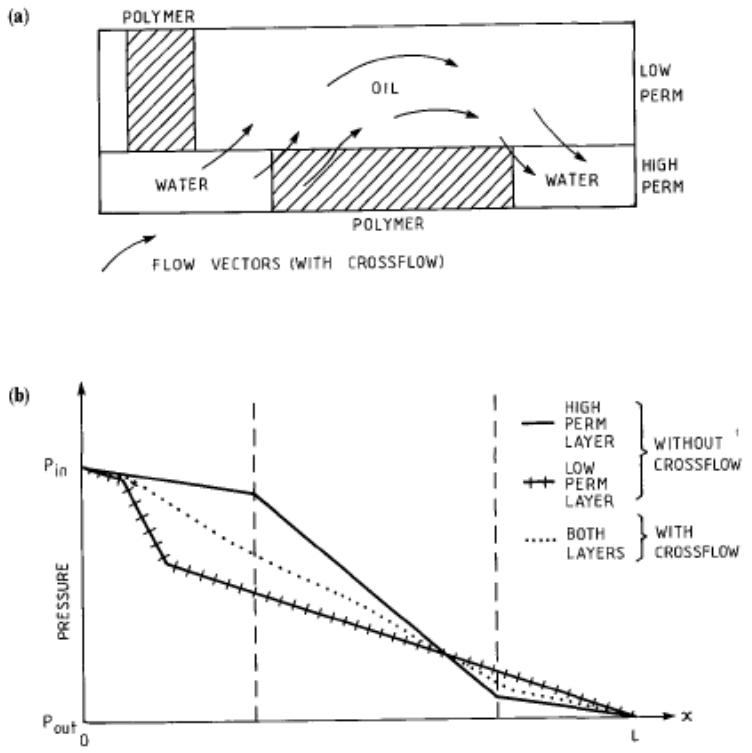

Figure 2.4 (a): Simple representation of crossflow in two layered reservoir (a) Schematic (b) Pressure profile with and without cross-flow (Sorbie et al., 1991)

Polymer addition helps in improving the oil recovery even in homogenous reservoirs due to the fractional flow effect. The fractional flow curves for waterflood and polymer flood, respectively, with a given oil are shown in Figure 2.4 (b). The figure shows that the addition of polymer results in shifting the fractional flow curve to the right. Addition of polymer delays the water breakthrough as well as lowers the water-cut after water breakthrough. As a result, oil can be recovered much faster on adding polymer. A detailed discussion of fractional flow theory is presented by Pope (1980).

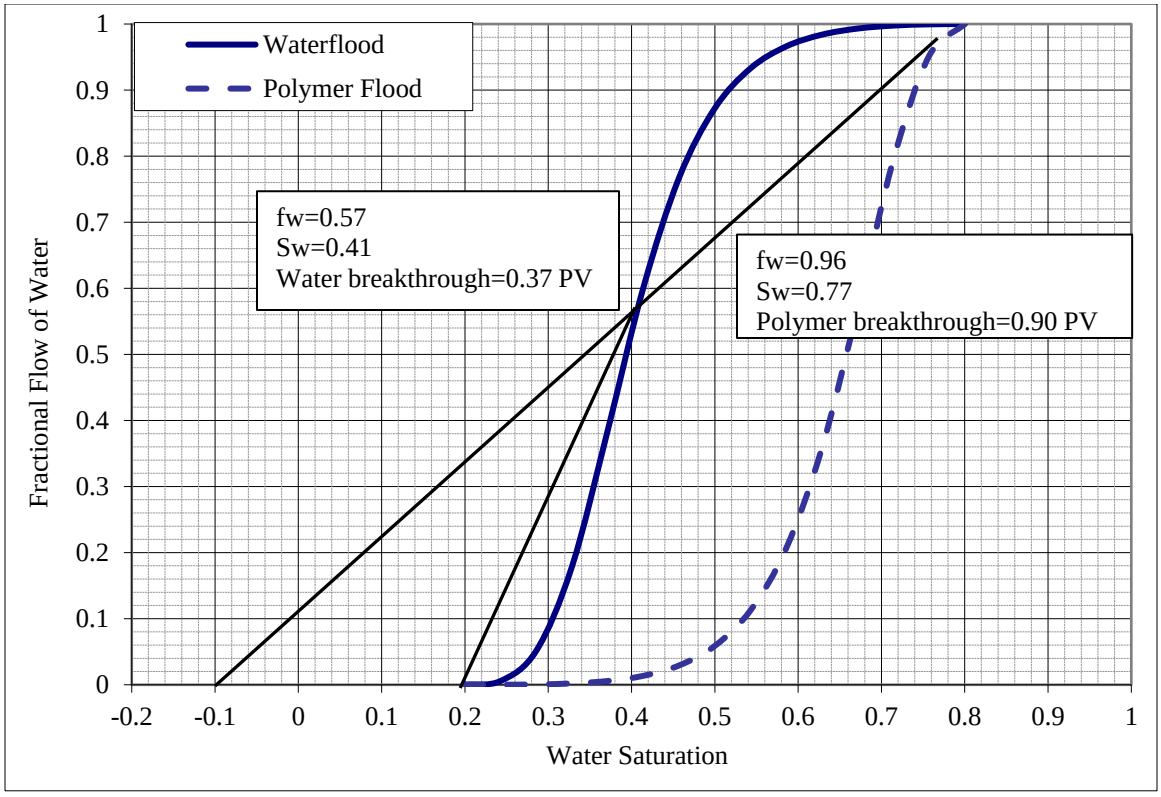

Figure 2.4 (b): Fractional flow curves for waterflood and polymer flood for a given oil

2.2.2 Polymer types

Polymers commonly used for EOR can be classified into two categories: Polyacrylamides and Polysaccharides (biopolymers). Polyacrylamide polymers (PAM) are partially hydrolyzed, about 20-30%, such that they are water soluble as well as not very sensitive to salinity and hardness (Shupe, 1981). During the hydrolysis of PAM, the amide group ($-CONH_2$) transforms into a carboxylic group ($-COO^-$) and the polymer develops negative charges which extend the polymer due to electrical repulsion (Figure 2.5). Other polymers derived from HPAM polymers includes 2-acrylamide-2-

methylpropane sulfonic acid (AMPS) or N-vinyl pyrrolidones (NVP) polymers. The typical molecular weight of HPAM polymers range from 2-20 million Daltons. Due to the negative charges on these polymers, these polymers show sensitivity towards hardness and salinity. In the presence of high salinity or hardness brines, the negative charges are shielded by cations and the polymer chain is shrunk, resulting in a loss of viscosity.

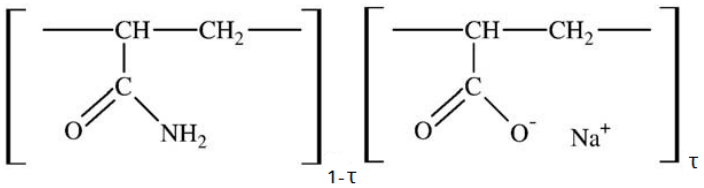

Figure 2.5: Chemical structure of partially hydrolyzed polyacrylamide

Polysaccharide polymers are formed by bacterial fermentation. The structure of Xanthan, a well-studied EOR polymer, is shown in Figure 2.6. Other biopolymers incudes scleroglucan and schizophyllan, and similar to Xanthan, these polymers also have polysaccharides as the building blocks. Biopolymers are known to for insensitivity towards high hardness and salinity, tolerance to shear degradation and good thermal stability around the neutral pH (Seright & Henrici, 1990). These polymers, however, show thermal degradation at high pH. In addition, biopolymers have poor filtration due to the presence of cell debris and are susceptible to bacterial attack in the porous media. The molecular weight of these polymers range between 2-6 million Daltons (Veibke, 2005; Leonharth et al., 2014; Rivenq et al., 1992)

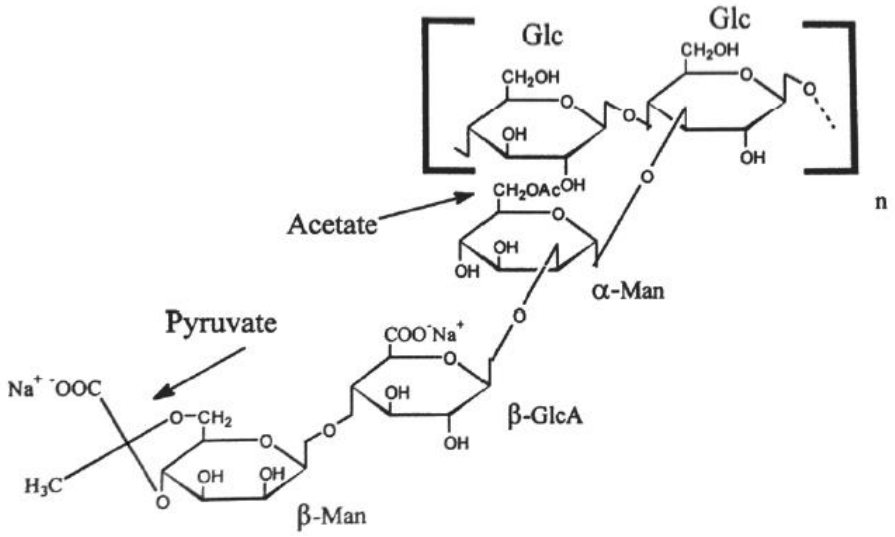

Figure 2.6: The repeating unit of Xanthan polymer (Veibke, 2005)

2.2.3 Polymer stability

In this section, the stability of only polyacrylamide polymers is discussed since these polymers were mainly used in this study. Polymer stability study is important to ensure that the polymer does not degrade in the porous media. HPAM polymers are susceptible to chemical degradation in the presence of divalent cations. In addition, these polymers can undergo thermal degradation at high temperature. These polymers have shown to undergo precipitation with divalent cations depending on the degree of hydrolysis (τ) of the polymer. HPAM polymers stability studies show that these polymers are susceptible to precipitation in the presence of calcium ions when $\tau > 0.35$. However, their chemical stability is also a function of calcium concentration, temperature and salinity (Zaitoun et.al, 1983; Levitt and Pope, 2008). Further, HPAM hydrolysis is faster under acidic or alkaline conditions, compared to the neutral pH. Levitt et al. (2011)

studied HPAM hydrolysis in detail and observed significant hydrolysis within 1-2 months in the presence of Na_2CO_3 at room temperature. Levitt and Pope (2008) performed experiments with extensively hydrolyzed PAM and recommended using HPAM with calcium ions below the concentration of 400 ppm at high salinity at 23 ºC. However, this calcium concentration is also a function of temperature. Replacing some acrylate moieties with monomer units such as 2-acrylamide-2-methylpropane sulfonic acid (AMPS) or N-vinyl pyrrolidone (NVP) have shown to increase the calcium tolerance of these polymers. Levitt and Pope (2008) observed a four-fold increase in calcium tolerance with AMPS substituted PAM. The ter-polymers of NVP, AMPS and AM moieties are found to be even more tolerant to divalent cations and showed good transport behavior in porous media (Vermolen et al., 2011; Kulawardana et al., 2012). In addition to chemical degradation, polyacrylamide polymers can also undergo thermal degradation at high temperature in the presence of iron, oxygen and free-radical generating impurities (Muller, 1981a; Muller, 1981b; Ramsden et al., 1986). Levitt (2009) found HPAM polymers prepared at a high pH to be stable even in the presence of iron after removing oxygen. Seright et al. (2015) found HPAM polymers to be stable from 23 °C to 90 °C after one week, when oxygen level was below 200 ppb and iron concentration ranged from 5 ppm to 30 ppm.

2.2.4 Polymer transport in porous media

Polymer transport in the porous media is governed by its rheology and interactions in the porous media. In this section, techniques to incorporate polymer

rheology and its interactions with porous media is discussed. Polymers commonly used in chemical EOR are shear thinning at small to moderate shear rates. The polymer rheology in this shear rate can be represented by the power law model shown below (Equation 2.1). For a complete representation, Carreau model may be used (Equation 2.2).

$$\mu_{app} = K\dot{\gamma}^{(n-1)} \tag{2.1}$$

$$\frac{\mu-\mu_\infty}{\mu_o-\mu_\infty} = \left(1 + \left(\frac{K}{\mu_o}\right)^{\frac{2}{n-1}}\dot{\gamma}^2\right)^{\frac{n-1}{2}} \tag{2.2}$$

where $\mu_{app}$and $\dot{\gamma}$ are the apparent viscosity and shear rate in the porous media. K and n are constants. μ_o and μ_∞ are viscosities at low and high shear rates.

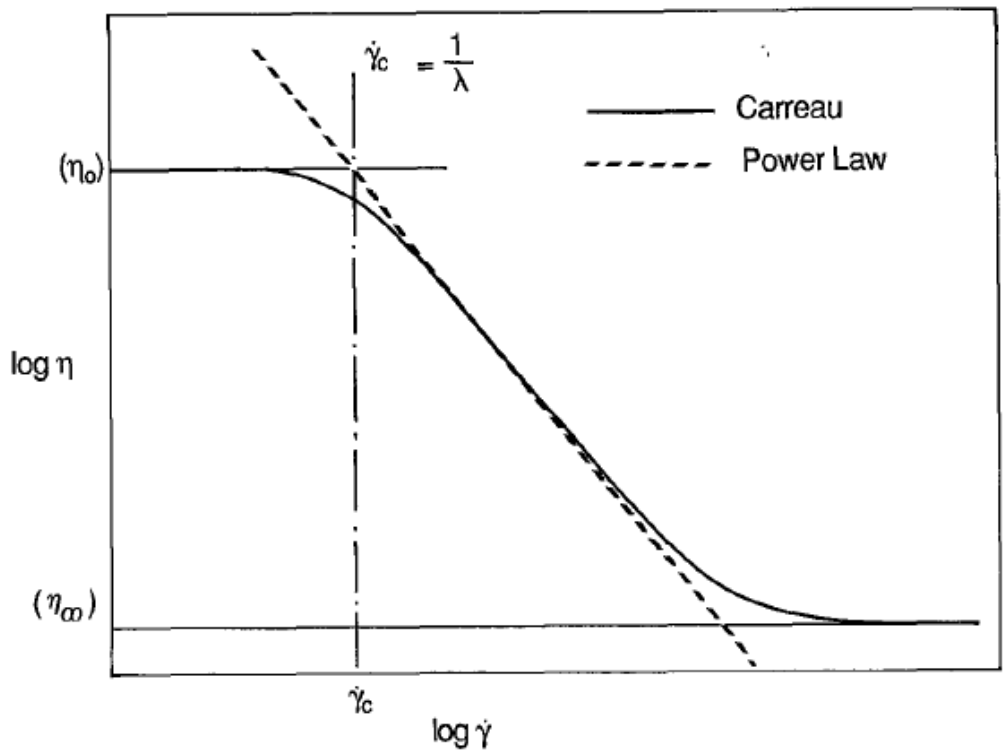

Figure 2.7: Comparison of the Carreau and power law model (Sorbie, 1991)

When a polymer solution is injected in the porous media, the mobility of the aqueous phase is reduced in comparison to that without the polymer. This mobility reduction on the addition of polymer is represented by the term known as the resistance factor (R_F).

$$R_F = \frac{\lambda_w}{\lambda_p} = \frac{K_w/\mu_w}{K_p/\mu_p} \tag{2.3}$$

where λ_w and λ_p are the mobility of the brine and the polymer, respectively, in the porous media.

After a polymer flood, the brine mobility in the porous media is often reduced. The measure of the reduction in brine permeability due to polymer injection is called as the residual resistance factor.

$$R_{RF} = \frac{\lambda_w}{\lambda_{wp}} = \frac{K_w/\mu_w}{K_{wp}/\mu_{wp}} \tag{2.4}$$

where λ_w and λ_{wp} are the mobility of the brine before and after polymer injection, respectively, in the porous media.

Other parameters that govern the transport of polymers in the porous media includes the inaccessible pore volume and polymer retention. Due to a varied pore structure, the injected polymer is not able to access the pores below a certain radius. The portion of the total pore volume which is not accessible to the polymer is known as the inaccessible pore volume. Inaccessible pore volume can range from 1-2% to 25-30%

depending on the polymer and the porous media (Green and Willhite, 1998). Polymer retention includes polymer adsorbed on the rock surface due to the negative charge on HPAM polymers as well as the polymer that is trapped mechanically. The retention in the porous media depends on parameters such as polymer type, molecular weight, rock properties, brine composition and temperature. Typical field retention values of polymers range from 7 $\mu g/cm^3$ bulk volume to 150 $\mu g/cm^3$ bulk volume (Lake, 2010). Inaccessible pore volume tends to accelerate polymer transport, while polymer retention tends to retard it.

2.2.5 Field studies

Injection of polymer solution to improve the oil recovery is a mature technique and has been implemented in the field at several occasions. Sandiford (1964) discussed the results of successful polymer injection in a heavy oil sandstone reservoir. Hydrolyzed polyacrylamide was used as the polymer. Gao (2011) reviewed the field application of polymer floods for improving the recovery of heavy oils. Polymer injection resulted in additional oil recovery and reduction in water-cut in Bohai Bay, offshore China (Liu et al., 2010). Other field case studies include East bodo reservoir, Alberta (Wassmuth et al., 2009); Tambaredjo field, Suriname (Manichand et al., 2010); Bati Raman, Turkey (Topgudar, 2010); Marmul field, Oman (Koning et al., 1988). Delamaide et al. (2013) reported the results of a successful polymer flood in Pelican Lake field in Alberta, a heavy oil reservoir. The primary recovery from the reservoir was poor due to little solution gas and high viscosity. Horizontal wells were drilled to maximize the benefits of

polymer injection. During the field injection, a 25% OOIP incremental oil was produced with a water-cut of less than 60%. Other examples of polymer field trials include Daqing field in China (Wang et al., 2008) and Mangala in India (Prasad et al., 2014). The oil viscosities in these fields ranged from 9-22 cP. Manrique et al. (2006) give a summary of the field implementation of chemical floods in carbonate reservoirs in the US.

2.3 Alkali floods

2.3.1 Mechanisms of oil recovery

The use of alkali for improving oil recovery is not a new practice, in fact, one of the earliest patents on the use of alkalis for increasing oil recovery was filed by Atkinson (1927). However, most of the studies related to the role of alkali in improving oil recovery were performed from mid-seventies to mid-eighties. Jennings et al. (1974) attributed the increase in oil recovery to the generation of in-situ soap, due to the reaction of alkali with surface-active organic acids present in oil, which resulted in decreasing the IFT. Johnson (1976) summarized the following mechanisms for an increase in oil recovery on adding an alkali (a) Emulsification and entrainment (b) Wettability reversal (water-wet to oil-wet or oil-wet to water-wet) (c) Emulsification and entrapment. In the emulsification and entrainment process, Subkow (1942) proposed that addition of an alkali results in reaction with acidic components of bitumen, lowering of IFT and emulsification. This results in subsequent entrainment in the flowing aqueous phase. In wettability reversal process, Wagner et al. (1959) observed alteration of rock wettability towards a water-wet state on increasing the pH, and thus an increase in the oil relative

permeability and the oil recovery. Cooke et al. (1974), however, observed the rock wetting state to change towards an oil-wet state on adding alkali; this resulted in making the oil film continuous that could flow. In the emulsification and entrapment process, Jennings et al. (1974) proposed that addition of an alkali resulted in lowering the IFT and emulsification; these emulsions could block the smaller pore throats resulting in improving the areal and the vertical sweep efficiently.

2.3.2 Alkali types

Strong alkalis such as sodium hydroxide (NaOH), sodium silicate (Na_2SiO_3) and potassium hydroxide(KOH) were initially used for alkali floods (Cambell, 1977; McAuley, 1977). However, due to their high reactivity towards the reservoir rocks, milder alkalis were preferred. Sodium carbonate was found to be less reactive compared to stronger alkalis and has since become the standard alkali for chemical floods (Burk, 1987). Sodium metaborate was also investigated as an alternative alkali (Flaaten et al., 2008). Unlike other alkalis, little information is available on the use of ammonia (NH_3) in alkaline flooding (Cooke et al., 1974; Jennings, 1975; Mayer et al., 1983; Martin et al., 1985). Nelson et al. (1984) found ammonia to be equally effective in their oil displacement experiments. They also recommended using ammonia to reduce co-surfactant requirements. Pursley et al. (1973) used the combination of sodium carbonate and (less expensive) ammonia to reduce divalent ions in the formation brine and satisfy rock consumption during their surfactant flooding pilot test at Loudon, Illinois.

2.3.3 Reactions of alkalis

Most petroleum reservoir rocks are either silica or carbonate based. Silica-based sands and sandstones are composed of quartz, layered aluminosilicates (montmorillonite, kaolinite, illite, chlorite and mixed layer minerals), and non-layered aluminosilicates (feldspar, zeolites). Carbonate reservoirs consist mainly of dolomite and calcite, but are often accompanied with trace amounts of other minerals such as gypsum (or anhydrite), pyrite, siderite **,** etc. Reservoir mineralogy is one of the key factors governing the alkali consumption and its transport in the porous media. Several studies have been performed to understand the interactions of various alkalis with sandstones and carbonates.

Jennings et al. (1974) emphasized on the importance of estimating alkali consumption for a successful field operation. De Zabala et al. (1982) introduced a model to take into account the in-situ soap generation and sodium/hydrogen exchange in the porous media as shown below.

Step 1: Distribution of the molecular acid between the oleic and aqueous phase:

$$HA_o \longleftrightarrow HA_w \tag{2.5a}$$

$$K_D = \frac{[HA_w]}{[HA_o]} \tag{2.5b}$$

Step 2: Aqueous phase hydrolysis:

$$HA_w + OH^- \longleftrightarrow A_w^- + H_2O \tag{2.6a}$$

$$K_A = \frac{[H^+][A_w^-]}{[HA_w]} \tag{2.6b}$$

They concluded that alkaline flooding should be performed at high pH to overpower the chromatographic ion-exchange retardation of the hydroxide ions. Bunge et al. (1982) developed a mass action equilibrium model to study the effects of pH, salinity and temperature on hydroxide uptake during sodium-hydrogen exchange and sodium-calcium exchange and proposed three mechanisms of hydroxide consumption as shown below.

(1) Reversible rock adsorption or ion exchange

The reaction shown below is the sodium-hydrogen exchange reaction. This reaction is responsible for alkali consumption in sandstones. Ion exchange reactions are fast reaction and laboratory results can be scaled to the field with a high degree of confidence.

$$MH + NaOH \longleftrightarrow MOH + H_2O \tag{2.7}$$

(2) Congruent and incongruent dissolution

The reactions shown below is an example of congruent dissolution. The dissolution of a mineral results in introducing species in the aqueous phase depending on its equilibrium constant. The dissolution on silica in an alkaline medium is shown below.

$$SiO_2(s) + OH^- + H_2O \longleftrightarrow H_3SiO_4^- \tag{2.8}$$

However, depending on the pH of the aqueous solution, the actual species in the aqueous can vary as shown by the equations below and Figure 2.8.

$$H_3SiO_4^- + OH^- \longleftrightarrow Si(OH)_2O_2^{2-} + H_2O \tag{2.9a}$$

$$Si(OH)_2O_2^{2-} + OH^- \longleftrightarrow Si(OH)O_3^{3-} + H_2O \quad (2.9b)$$

$$Si(OH)O_3^{3-} + OH^- \longleftrightarrow SiO_4^{4-} + H_2O \quad (2.9c)$$

$$SiO_2(quartz) + 2H_2O \longleftrightarrow Si(OH)_4 \quad (2.9d)$$

$$SiO_2(amorphous) + 2H_2O \longleftrightarrow Si(OH)_4 \quad (2.9e)$$

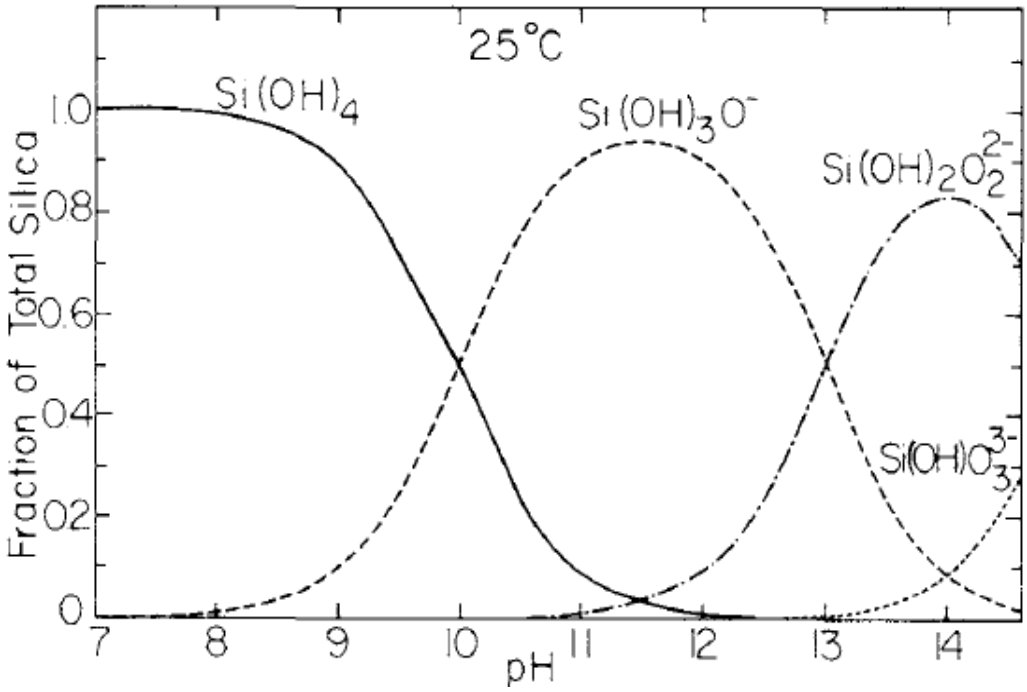

Figure 2.8: Soluble silica speciation calculated based on the equations given above (Bunge et al., 1982)

Incongruent dissolution occurs when the dissolution of one mineral is also accompanied by the precipitation of another. For example, precipitation of calcium hydroxide due to the reaction of sodium hydroxide with gypsum is an example of incongruent dissolution.

$$CaSO_4(s) + NaOH \longleftrightarrow Ca(OH)_2(s) + Na_2SO_4 \quad (2.10)$$

(3) Precipitation of insoluble hydroxides occurs due to the precipitation of hardness ions present in the pore fluid and exchanged from the surface. For example, the precipitation of calcium ions at high pH after sodium-calcium exchange is shown below

$$2Na^{+} + M_2Ca \longleftrightarrow 2MNa + Ca^{2+} \tag{2.11}$$

where, M is the exchange site.

Bunge et al. (1985) presented the chromatographic theory of simultaneous ion-exchange with precipitation of divalent cations for studying the effectiveness of alkaline preflush (instead of soft brine) to remove divalent cations. They showed that re-dissolution of the precipitated cations on injecting a low pH solution, following the alkaline slug, may increase the concentration of divalent cations behind the preflush. Novosad et al. (1984) performed experiments to calculate cation exchange capacity (CEC) and hydrogen exchange capacity (HEC) of Berea sandstone by monitoring the sodium concentration in the effluent. Their experiments also showed that mineral dissolution is a slow process while ion-exchange is fast. Southwick (1985) performed batch mixing experiments to study quartz dissolution in sodium hydroxide and sodium silicate and its effect on the alkalinity. They proposed an alternative method to estimate alkali loss due to the reaction with silica based on the useful alkalinity, instead of the change in the pH. They observed significant differences in alkalinity loss estimates based on their method. Mohnot et al. (1987) performed batch experiments of sodium hydroxide with commonly occurring reservoir rock minerals and observed that, at high alkali concentration and temperature, kaolinite consumes more hydroxide than montmorillonite. Contrary results were observed under mild conditions. Huang et al. (1986) studied the

consumption of sodium hydroxide and sodium orthosilicate in the presence of clays and found montmorillonite to show highest consumption.

ASP floods were mainly investigated for sandstone reservoirs in the past. Recently, very few studies have been performed on carbonate reservoirs. Mohnot et al. (1989) performed alkali consumption studies of sodium hydroxide with carbonates and observed that useful alkalinity loss was greatest for gypsum, high for dolomite and insignificant for calcite. Precipitation/dissolution mechanisms were responsible for alkalinity consumption in the case of dolomite and gypsum. Further, they observed that the loss of useful alkalinity was lower for dolomite (also it is a slow reaction) because of buffering action of carbonate ions that are produced due to the dissolution of dolomite. The addition of sulfate ions decreased alkalinity loss in the case of gypsum. Further, they observed that useful alkalinity was released in the case of gypsum due to calcium hydroxide dissolution on lowering the pH. Lopez-salinas et al. (2011) performed simulations that showed that when 1 % Na_2CO_3 is used as alkali, even 0.1 % anhydrite could retard the alkali breakthrough by 0.7 pore volumes. Many alternative alkalis have been investigated for as a result for reservoirs containing gypsum and divalent cations. Burger et al. (2006) suggested using an organic alkali in ASP formulations that is able to tolerate high salinity and hardness. Kazempour et al. (2011) performed single-phase alkali injection experiments with NaOH, Na_2CO_3 and $NaBO_2$ in Berea and Minnelusa cores (containing gypsum) and observed little pH change and permeability damage by $NaBO_2$ injection in Minnelusa core. Levitt et al. (2011) discussed various challenges encountered in carbonate reservoirs for ASP flooding, in particular, the uncertainty about

presence of anhydrite or gypsum which limits the use of conventional alkalis. They further ruled out the possibility of using chelating agents like EDTA in the presence of anhydrite.

2.3.4 Field studies

Nutting (1925) reported the first field trial of an alkali flood using Na_2CO_3. Johnson (1976) reviewed field studied of alkali floods performed in the 1960s and 70s. Leach et al. (1962) reported the results of sodium hydroxide injection in Harrisburg field, Nebraska where additional oil recovery was observed, however, much lower compared to the injected alkali volume. Emery et al. (1970) performed sodium hydroxide injection in Singleton field in Nebraska and recovered additional oil. Cooke et al. (1974) performed sodium carbonate injection in a southeast Texas field and observed addition oil recovery. However, a delay in alkali breakthrough was observed. Graue and Johnson (1974) reported results of alkali injection in a large-scale field and observed an increase in oil recovery. Sheng (2016) summarized the results of eight field scale alkali-polymer (AP) injection; four in Canada, two in the US and two in China. These fields include Cessford (Canada), Black creek (Canada), Horsefly Lake (Canada), Wrentham (Canada), Xing Long Tai (China), Yang Sang Mu (China), Isenhour unit (USA) and Moorcroft West (USA). These floods were mainly performed in sandstone reservoirs using sodium carbonate as the alkali and polyacrylamide as the polymer.

2.4 Surfactant floods

2.4.1 Mechanisms of oil recovery

It was realized very early that a large amount of oil is left unrecovered in the waterflood regions due to high capillary forces due to a high IFT between water and oil. Subsequent studies showed that oil recovery from a reservoir could be improved by increasing the capillary number; defined as the ratio of viscous forces to capillary forces (Stegemeier, 1974; Chatzis & Morrow, 1984; Delshad et al., 1986; Mohanty et al., 1987; Kamath et al., 2001). The plot between residual oil saturation and capillary number is termed as the capillary desaturation curve (CDC) curve (Figure 2.9). Note that CDC curve depends on many parameters such as rock pore structure, rock wettability, among others. Due to an upper limit on the pressure drop that can be achieved in the field, reduction of IFT between oil and water is a more practical approach to improve the recovery of trapped oil. A reduction of interfacial tension and improvement in oil recovery was observed on adding an alkali to acidic crude oils (discussed previously). However, it was soon realized that the low IFT region was at a very low alkali concentration, and the propagation of this low alkali concentration in the field seemed unlikely due to geochemical interactions of the alkali with reservoir fluids and minerals. Nelson et al. (1984) proposed the addition of a co-surfactant with the alkali to shift the low IFT region to a higher salinity. This process was termed as the co-surfactant enhanced alkaline flooding and is now commonly known as the ASP flooding. The type of surfactants that can be used for conducting SP or ASP floods is discussed next.

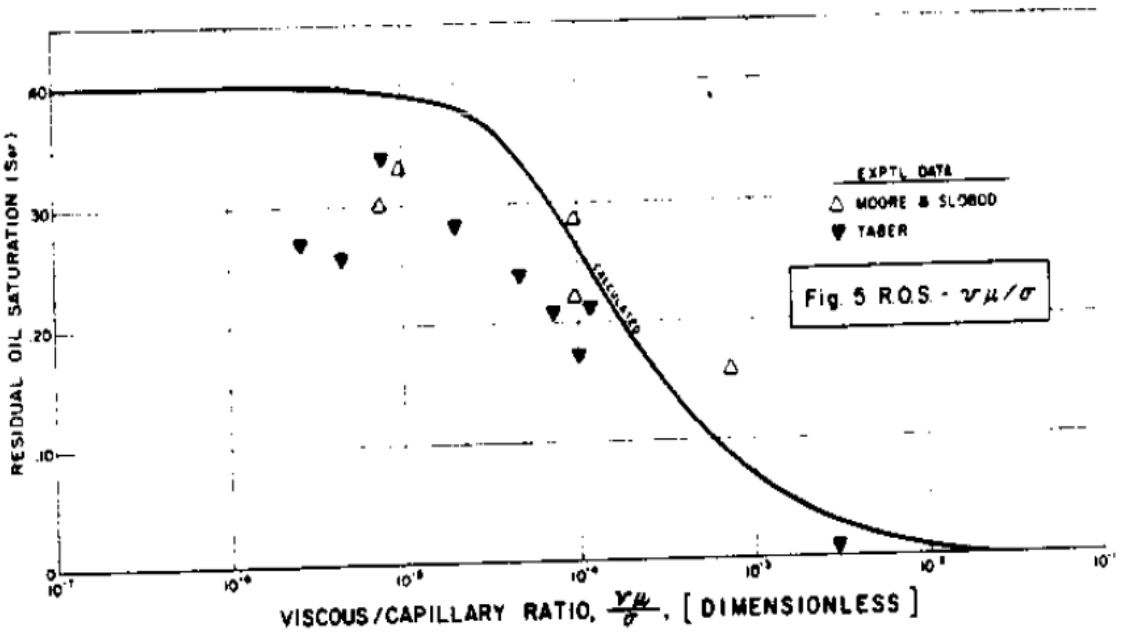

Figure 2.9 Capillary desaturation curve showing lowering on residual oil saturation with increasing capillary number (Stegemeier, 1974)

2.4.2 Surfactant types

Surfactants can be broadly classified into the following categories based on the charge on the surfactant molecule: anionic surfactants, cationic surfactants, non-ionic surfactants and zwitterionic (or amphoteric) surfactants. Anionic surfactants are commonly used in ASP or SP floods because these surfactants are able to give ultralow IFT with crude oils. Non-ionic and cationic surfactants have mainly been studied for wettability alteration (discussed later). Zwitterionic surfactants are typically used in foam floods. A brief description of these surfactants is given below. However, the focus in this section will be on anionic surfactants.

(a) Anionic surfactants

Anionic surfactants that are commonly used in chemical EOR include alkyl benzene sulfonates (ABS), alpha olefin sulfonates (AOS), internal olefin sulfonates (IOS), alcohol sulfates, alcohol ether sulfates and alcohol ether carboxylates. These surfactants have negatively charged polar head groups which provide them their hydrophilic nature.

Alkyl benzene sulfonates are extensively used in the detergent industry and have shown to give ultralow IFT with crude oils (Doe et al., 1976). These surfactants have alkyl chain attached to a sulfonated aromatic ring (Figure 2.10). These surfactants have poor tolerance towards divalent cations and therefore water softening (or chelation of divalent cations) is required to use these surfactants.

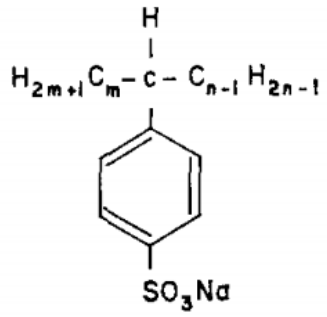

Figure 2.10: Representative alkyl benzene sulfonate structure (Doe et al., 1976)

Alpha olefin sulfonates are produced by the sulfonation of linear alpha olefins (Figure 2.11). These surfactants are known to show good detergency, foaming and

wetting properties (Farazadeh et al., 2008). Due to the presence of hydroxyl bond, these surfactants have good tolerance to divalent cations.

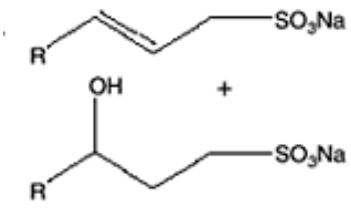

Figure 2.11: Representation of alpha olefin sulfonates

In the case of internal olefin sulfates, sulfonation reaction takes place at any location along the chain since the double bond is randomly distributed. Two main sulfonated species are formed at the end of sulfonation, neutralization and hydrolysis besides other surface active species; hydroxyl alkane sulfonate and alkene sulfonate as shown in Figure 2.12 (Barnes et al., 2010). Due to the branching and distribution of sulfonated species, formation of ordered structures (such as liquid crystals, viscous gels, macro-emulsions) is minimized in an oil-brine-surfactant system. This improves the transport of phases in the porous media. IOS surfactants come with a variety of hydrophobes; most commonly C_{15-18}IOS, C_{19-23}IOS, C_{24-28}IOS. These surfactants have shown good performance in oil recovery experiments in sandstone and carbonate cores (Levitt et al., 2006; Zhao et al., 2008).

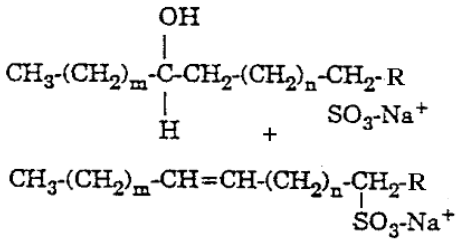

Figure 2.12: Representation of internal olefin sulfonates

Alcohol ether sulfate surfactants are an important class of anionic surfactant commonly used in chemical EOR. These surfactants are prepared by the ethoxylation or propoxylation of an alcohol followed by the sulfation. The chemical formulae of alcohol alkoxy sulfate surfactants is shown in Figure 2.13. Some commonly used alcohol ether sulfate surfactants include C_{12-13}-7PO-sulfate and C_{12-13}-13PO-sulfate. Ether sulfates with large hydrophobes (C_{20} to C_{32}) have also been developed for crude oils with high EACN numbers (Adkins et al., 2012). Addition of ethylene oxide (EO) groups increases their hydrophilicity and improve their aqueous stability. On the other hand, addition of proplylene oxide (PO) groups increases their hydrophobicity. The ratio of EO and PO groups can be adjusted such that the surfactant is surface active and has enough aqueous stability. Addition of EO and PO groups also improves the calcium tolerance of these surfactants because EO and PO groups result in internal complexation of calcium ions. These surfactants are also good foaming agents.

Figure 2.13: Chemical representation of alcohol alkoxy sulfate surfactants (Barnes et al., 2010)

Earlier studies have shown these surfactants to be unstable at temperatures exceeding 65 °C (Talley, 1988). The hydrolysis reaction of ether sulfates is shown below (reaction 2.12a). In acidic conditions, hydrolysis of the sulfate group takes place resulting in the release of bisulfate (HSO_4^-) ions. Bisulfate ions further lower the pH of the solution and expedite the hydrolysis process. Addition of an alkali has found to stabilize ether sulfate surfactants at high temperatures (Adkins et al., 2010).

$$R - O - CH_2 - CH_2 - O - SO_3^- + H^+ = R - O - CH_2 - CH_2 - OH + HSO_4^- \quad (2.12a)$$

$$R - O - CH_2 - CH_2 - O - SO_3^- + OH^- = R - O - CH_2 - CH_2 - OH + SO_4^{2-} \quad (2.12b)$$

Ether sulfate hydrolysis can also occur at extremely high pH values as shown by the reaction 2.12b. Therefore, the stability of ether sulfates at high temperatures is enhanced when the solution pH is adjusted within a certain range.

Alcohol ether carboxylate have been developed as an alternative to ether sulfates. Carboxylate surfactants are not new *per se*; the oldest known carboxylate surfactant was formed by neutralization of fatty acids. However, ether carboxylate surfactants have been

developed recently. These surfactants have been found to be stable under alkaline and non-alkaline conditions up to 120 °C (Lu et al., 2014). Similar to alcohol ether sulfates, these surfactants also have good tolerance for divalent cations due to the presence of EO and PO groups. The chemical representation of this class of surfactants is shown in Figure 2.14.

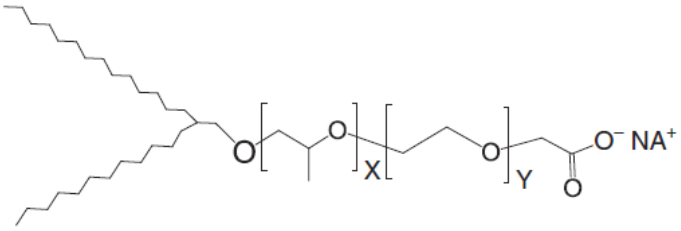

Figure 2.14: Chemical representation of alcohol ether carboxylate surfactants (Lu et al., 2014)

(b) Non-ionic surfactants

Non-ionic surfactants consist of hydrophobic and hydrophilic parts; the hydrophobic part, however, does not dissociate in aqueous solutions. Examples of non-ionic surfactants include alcohol ethoxylates, alkyl phenolethoxylates, amides, alkyl polyglucosides and fatty glucamides. These surfactants are commonly used as a co-surfactant in low IFT formulations and wettability altering formulations (Sharma et al., 2011). These surfactants are not aqueous stable at high temperatures due to the cloud point effects of EO and PO groups; however, they have good tolerance to divalent cations. A chemical representation of alcohol ethoxylates is shown in Figure 2.15.

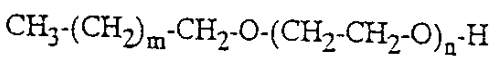

Figure 2.15: Chemical representation of alcohol ethoxylates

(c) Cationic surfactants

Cationic surfactants are quaternary ammonium compounds that have positively charged polar head group. These surfactants usually do not give ultralow IFT and are mainly used in foam floods and wettability alteration (Sharma et al., 2011). Recently, cationic gemini surfactants have shown to alter the wettability of oil-wet carbonate cores (Ghosh et al., 2016). Switchable surfactants have been developed that acquire positive charge under acidic conditions for foam floods using CO_2 (Cui et al., 2014). Due to the positive charge, these surfactants are being studied mainly for carbonate reservoirs since these rocks are positively charged at neutral pH; due to similar charges, cationic surfactants may have lower adsorption on the rock surface (Hahn, 2015). The chemical representation of a cationic surfactant is shown in Figure 2.16.

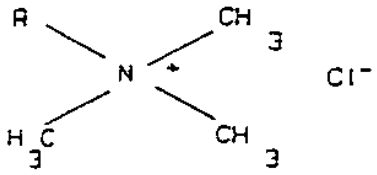

Figure 2.16: Chemical representation of a cationic surfactant

(d) Zwitterionic surfactants

Zwitterionic surfactants contain both positive and negative charges as shown in Figure 2.17. These surfactants are mainly used as foam boosters and viscoelastic surfactants. These surfactants are stable in high temperature and high salinity environment.

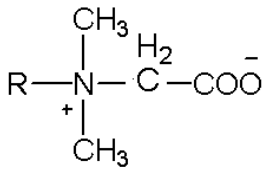

Figure 2.17: Chemical representation of a zwitterionic surfactant

2.4.3 Surfactant transport in porous media

When an aqueous solution containing the surfactant is injected into the porous media, the surfactant interacts with oil and brine (and other ions from the rock) present in the porous media and forms various phases depending on the in-situ conditions. Winsor classified these microemulsion phases into three categories; going from Winsor type I (or type II-) to Winsor type III to Winsor type II with increasing effective salinity. The term effective salinity is used to also include the effect of additional variable such as the concentration of divalent cations, cosolvent type and amount, water-oil ratio, and so on. Additional discussion on these micro-emulsion phases is made in chapter 3. In addition to these microemulsion phases, emulsions (or macro-emulsions) may also form. Unlike micro-emulsions, emulsions (or macro-emulsions) are thermodynamically unstable and have droplet sizes larger than 0.1 μm (Bourrel & Schechter, 1988).

(a) Surfactant phase behavior and oil recovery

The multiphase flow phenomena during surfactant floods has been investigated in great detail and conditions have been identified to maximize the oil recovery and minimize the surfactant retention (Healy et al., 1976; Glover et al., 1979; Nelson & Pope, 1978; Hirasaki et al., 1983). A negative salinity gradient has been proposed to obtain high

oil recovery and minimize surfactant retention. A negative salinity design ensures encountering Winsor type III window, corresponding to an ultralow IFT, in the porous media. It was observed that the polymer drive salinity controlled the amount of surfactant retention. The trapped surfactants may be remobilized by sufficiently lowering the drive salinity. The effect of divalent ions and surfactant dilution on surfactant phase behavior was investigated (Glover, 1979; Nelson, 1982). Modeling and simulation work was performed to model surfactant floods (Pope, 1980; Pope et al., 1978; Hirasaki, 1981). Delshad et al. (1996) developed a three-dimensional, multicomponent, multiphase compositional simulator to model chemical floods.

(b) Effect of geochemical reactions

The effect of cation exchange reactions on surfactant floods has been investigated in the past because these reactions are critical in a sandstone reservoir; surfactant floods were mainly considered for sandstone reservoirs (Pope et al., 1978; Lake & Helfferich, 1978; Hill et al., 1977; Pope, 1980; Hirasaki, 1982). These studies identified the effect of various parameters such as dispersion, pre-flush, and cation exchange with clays and surfactants on surfactant floods. In addition, the effect of mineral dissolution was investigated. Bhuyan et al. (1991) later developed a comprehensive geochemical module in UTCHEM, called EQBATCH, to include a larger set of geochemical reactions in alkaline/surfactant polymer flooding simulations. The program was later further improved by Luo et al. (2016). UTCHEM-IPHREEQC was developed by Kazemi et al. (2014) by coupling UTCHEM with IPHREEQC (the USGS geochemical modeling tool)

which enabled users to incorporate the comprehensive geochemistry framework of IPHREEQC in UTCHEM simulations.

(c) Surfactant retention

Surfactant retention in the porous media consists of adsorption on the rock matrix and trapping in the residual oil phase. A vast literature is available on the adsorption of anionic surfactants on sandstone and carbonate rocks. A number of forces are responsible for surfactant adsorption on a solid surface such as electrostatic forces, covalent bonding, hydrogen bonding, non-polar interactions, among others. Zhang & Somasundaran (2006) reviewed surfactant adsorption of single and mixture of surfactants. Adsorption of an ionic surfactant on an opposite charged surface can be divided into four regions. At a low surfactant concentration (region I in Figure 2.18), surfactant adsorption is the result of the electrostatic interaction between individually charged monomers with the charged surface. In region II, surfactant molecules begin to form surface aggregates due to interactions between the hydrocarbon chains. In region III, adsorption continues due to lateral attraction. In region IV, when the surfactant concentration is above the critical micelles concentration (CMC), no additional adsorption takes place.

Adsorption of anionic surfactants on the rock can be lowered by lowering the surface charge of the rock. Studies have found that this can be achieved by adding an alkali to the surfactant formulation. The isoelectric points of various minerals present in an oil reservoir are found to be at pH values ranging from 2 to about 9. Therefore, increasing the pH makes these rocks negatively charged and lowers the adsorption of

anionic surfactants (typically used in chemical EOR). Studies have found lowering of surfactant adsorption on increasing the pH in sandstones (Somasundaran & Hanna, 1979; Krumrine et al., 1982; Somasundaran et al., 1983). However, the results are not obvious in case of carbonates (Hirasaki et al., 2008).

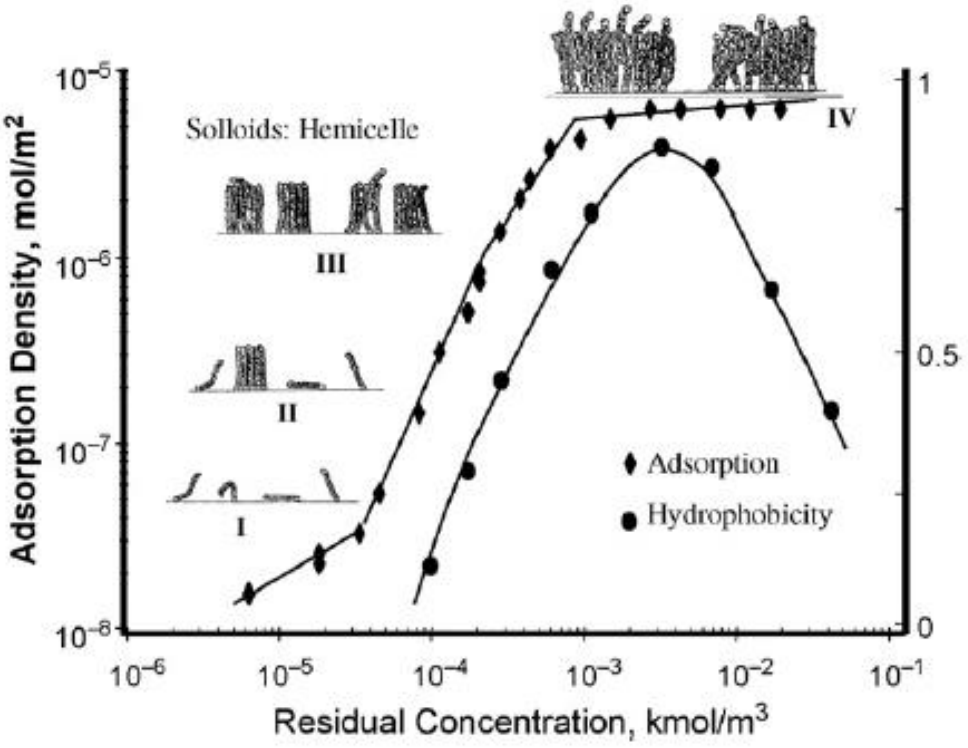

Figure 2.18: Surfactant adsorption isotherm and hydrophobicity of sodium dodecyl sulfate on alumina at pH 6.5 (Zhang & Somasundaran, 2006)

Surfactant is also retained in the porous media by trapping in the residual oil phase and as viscous emulsions. Studies have found that this surfactant retention can be lowered by sufficiently lowering the salinity of the polymer drive and preventing the formation of viscous emulsion by using a mixture of surfactants (preferably branched) and cosolvents (Healy et al., 1976; Glover et al., 1978; Nelson & Pope, 1978; Sahni,

2009). More recently, addition of a given amount and type of cosolvent has shown to lower surfactant retention in coreflood experiments (Jung et al., 2016). Also, lower surfactant retention has been observed in a reduced environment (Wang, 1993).

(d) Effect of alkali

It was previously discussed that addition of an alkali to acidic crude oils results in generation of in-situ surfactants. These in-situ surfactants, in combination with synthetic surfactants, are very effective in giving an ultralow IFT formulation that requires less synthetic surfactant and is effective in improving the oil recovery (Yang et al., 2010; Aitkulov & Mohanty, 2016). Additionally, in-situ surfactants have been observed to improve the surfactant phase behavior by showing the low IFT over a wider salinity window (Liu et al., 2010). Salager et al. (1979) developed a mixing rule to incorporate the effect of mixture of surfactants on optimum salinity and the corresponding solubilization ratio. The similar mixing rule has been used to model the effect of soap on surfactant phase behavior in ASP simulations (Mohammadi et al., 2009)

(e) Effect of cosolvent and microemulsion viscosity

Cosolvents are low molecular weight alcohols and ethers (typically C3 to C5) that are used for improving the surfactant phase behavior. Commonly used cosolvents include isobutyl alcohol (IBA), isopropyl alcohol (IPA), triethylene glycol monobutyl ether (TEGBE). Recently developed cosolvents include IBA-$(EO)_n$, Phenol-$(EO)_n$, Diisopropylamine (DIPA), DIPA-$(EO)_n$. Addition of a cosolvent has shown to increase the aqueous stability and lower the equilibration time of a surfactant formulation, and

minimize the formation of viscous gels (Sanz and Pope, 1995; Levitt et al., 2006; Flaaten et al., 2008). Addition of cosolvents has also shown to lower the microemulsion viscosity; surfactant formulations with lower microemulsion viscosities have shown lower retentions in oil recovery corefloods (Walker et al., 2012). However, addition of cosolvents also results in increasing the IFT. Short-hydrophobe surfactants have been developed as alternatives of traditional cosolvents. These surfactants have shown to improve the surfactant phase behavior, similar to traditional cosolvents, without increasing the IFT (Upamali et al., 2016).

As mentioned previously, addition of a cosolvent is found to affect microemulsion viscosity and surfactant retention in the porous media. Microemulsion viscosity is also found to be critical in gravity stable corefloods (Lu & Pope, 2015). Studies have been being performed to investigate rheology of micro-emulsions in the porous media (Humphry et al., 2013). A new model has recently been developed for microemulsion rheology (Tagavifar et al., 2016).

2.4.4 ACP floods

Recently, Fortenberry et al. (2015) developed alkali cosolvent polymer (ACP) floods for sufficiently active crude oils. This process is similar to the alkaline flooding; no synthetic surfactant is added and reduction in IFT is due to the reaction of an alkali with naphthenic acids present in the crude oil. However, ACP floods address the challenges that have traditionally been encountered in alkaline flooding such as obtaining low IFT region at low alkali concentration and formation of viscous emulsions. In ACP

floods, a cosolvent is added with the alkali that helps in overcoming these challenges. Addition of a cosolvent lowers the emulsion viscosity, lowers equilibration time and shifts the low IFT region to a higher alkali concentration. The new ethoxylated cosolvents (IBA-$(EO)_n$, Phenol-$(EO)_n$), due to their hydrophilic nature, are very effective in shifting the low IFT regions to a desired alkali concentration. Also, typically a positive slope is observed on the activity map when salinity scans are performed using only an alkali. However, addition of a hydrophilic cosolvent has shown to lower this slope. A less steep slope is helpful in designing a robust salinity gradient design. Note that, unlike ASP floods, ACP floods do not require addition of synthetic surfactants and therefore these processes are much more economical (given that the oil is sufficiently acidic).

2.4.5 Field studies

A large number of ASP field studies are reported in the literature. French et al. (1973) reported the results of ASP flood in Benton field in Illinois. A pre-flood low-salinity brine was injected to displace the high salinity brine. The ASP slug consisted of sodium tripolyphosphate, sodium sulfonate and Dow Pusher 520. Permeability damage was observed in the flood possibly due to the precipitation of calcium phosphate. Incremental oil recovery was observed in the pilot test. Gilliland et al. (1976) reported the results of a surfactant flood in the Big Muddy field in Wyoming. The surfactant slug contained 2.5% sodium sulfonate, 3% alcohol and 0.2% NaOH. A biopolymer was used for increasing the viscosity of the slug to 6 cP; biocides were added to avoid bacterial growth. An increase in oil production was observed in the pilot test. Bragg & Gale (1983)

reported the results of Louden field surfactant flood. Bacterial degradation of Xanthan polymer was observed in the flood. In addition, due to the presence of 12 ppm ferrous iron was present in the formation brine, 75 ppm sodium hydrosulfite was added to prevent oxidation of iron and subsequent cross linking on the polymer. Acetic acid was added to prevent iron precipitation. A cumulative oil recovery of about 60% and a surfactant retention of 0.35 mg/g rock was observed during the surfactant flood. Falls et al. (1994) observed an additional oil recovery of 38% of the waterflood residual oil in a sandstone reservoir in offshore Gulf of Mexico. Wang et al. (1997) reported the ASP pilot test results in Daqing oil field. The oil viscosity at the reservoir temperature (45 °C) was 11.5 cP. The reservoir porosity and permeability was 26% and about 500 md. An incremental oil recovery of about 20% OOIP over waterflood and 10% OOIP over polymer flood was observed. Zhijian et al. (1998) reported the results of a successful ASP pilot test in Gudong oil field in China. The oil viscosity was 41.3 cP at the reservoir temperature of 68 °C. An incremental oil recovery of 13.4% OOIP or 30% ROIP was observed. Qi et al. (2000) reported the results of the ASP pilot test in Karamay oil field. About 25% OOIP incremental oil recovery was achieved. In this test, sodium carbonate was used as the alkali, petroleum sulfonates as the surfactant and hydrolyzed polyacrylamide as the polymer. The oil contained acidic components which generated in-situ surfactants on reacting with the alkali. A pre-flush of sodium chloride was injected to pre-condition the reservoir for the ASP flood. Vargo et al. (2000) reported the ASP pilot results of the Cambridge Minnelusa field. The field had the porosity and permeability of 18% and 845 md, respectively; the oil viscosity of 31 cP at the reservoir temperature of

55 °C. Injection of ASP slug in this field resulted in an incremental oil recovery of 28.1% OOIP. Pandey et al. (2016) reported results of a successful ASP pilot in Mangala field, India. The reservoir contained a 15 cP oil at the temperature of 65 °C. Sodium carbonate was used as the alkali, alcohol ether sulfate and IOS as the surfactants and hydrolyzed polyacrylamide as the polymer. A polymer pilot test was previously conducted in the same area. ASP flood resulted in increasing additional 20% of the pilot STOIIP oil after the polymer flood. Additional ASP field studies are reported by Alvarado & Manrique (2010) and Manrique et al. (2006).

2.5 Wettability alteration

Wettability is defined as the tendency of one fluid to spread on or adhere to a solid surface in the presence of other immiscible fluids. For a crude oil-brine-rock system, various situations may arise depending on the preference of the solid towards oil and water. Figure 2.19 shows four situations in which water can spread on a solid surface in presence of oil. In Figure 2.19 shows that water has more preference to adhere on the surface in case (d) compared to case (a). The other two cases show the intermediates preference. The wettability of a reservoir rock is critical in governing the distribution and flow of fluids in it. Figure 2.20 shows the distribution of fluids in rocks with different wetting states. The left-most image in Figure 2.20 shows water films covering the grain particles indicating that the rock is water-wet. The right-most image shows oil film covering the grains indicating that the rock is oil wet state. The middle image shows that the rock is mixed-wet.

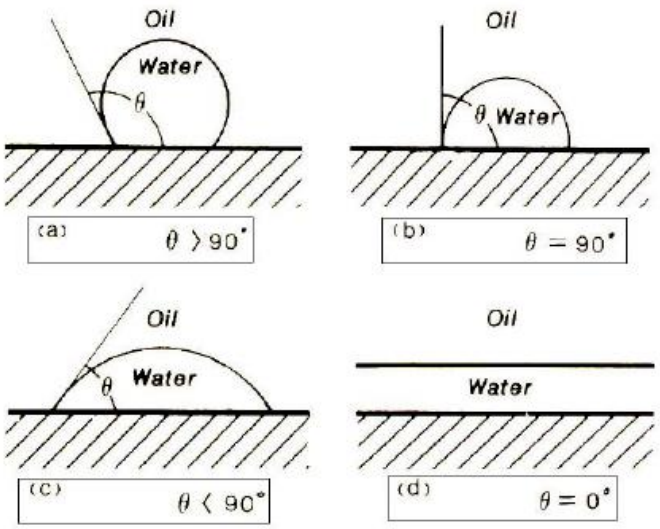

Figure 2.19: Equilibrium contact angles for different wetting states (Peters, 2012)

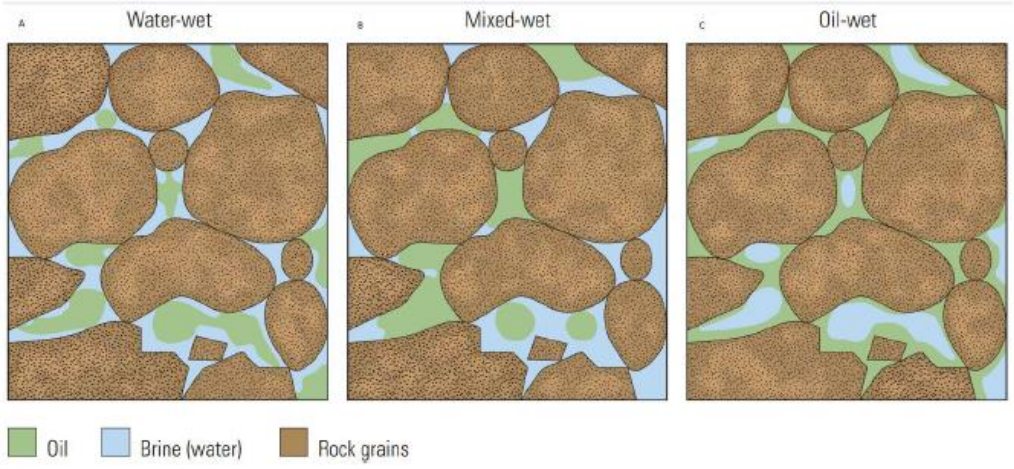

Figure 2.20: Distribution of fluids in rocks of different wettability (Abdallah, 2007)

It is believed that the rock surfaces were water-wet before oil invaded them. The wettability alteration of the surface on oil invasion was due to the surface active agents present in the oil. The surface active agents were polar compounds containing nitrogen,

oxygen and sulfur functional groups such as phenols and carboxylic acids. Buckley et al. (1997) presented various mechanisms responsible for making a surface oil-wet. The waterflood performance of a reservoir is dependent on its wetting state. The relative permeability, capillary pressure, electrical properties, dispersion and waterflood behavior is found to depend on the rock wettability (Anderson, 1986). In a water-wet rock, the relative permeability of water is low compared to that of the oil and thus oil can flow more easily. In addition, water imbibition, due to high capillary forces, results in improving the oil recovery (Morrow, 1990). In an oil-wet reservoir, on the other hand, an early water breakthrough is observed due to its higher relative permeability compared to that of the oil. A significant amount of connected oil is left behind, in this case, compared to discontinuous oil blobs in the case of a water-wet rock. Salathiel (1973) proposed the concept of mixed-wettability where water occupied the small pores and oil occupied the big pores. In such a situation, it is possible to obtain low saturation of oil since both oil and water remain continuous up to very low saturations.

2.5.1 Mechanisms of oil recovery

A substantial amount of oil is known to exist in carbonate reservoirs. However, due to the oil-wet nature of these reservoirs, not much oil is recovered from them during primary and secondary floods. The presence of fractures in these reservoirs further lowers the oil recovery due to bypassing of injected fluids through fractures. Oil recovery from these reservoirs can be improved by wettability alteration. Wettability alteration involves changing the wetting state of an oil-wet rock towards a water-wet state, which results in

increasing the oil relative permeability. In addition, the oil recovery from oil-wet fractured reservoirs can be improved by spontaneous imbibition; the wetting fluid imbibes from fracture to matrix, thus displacing the oil. At the molecular scale, the wetting state of a surface is dependent on the forces acting at the oil/brine and brine/oil interfaces. The oil/brine interface is typically negatively charged at neutral pH due to dissociation of carboxylic acids present in crude oil in the aqueous phase. The brine/rock interface for a carbonate surface is positively charged in the presence of formation brine due to a high concentration of divalent cations in the brine. Due to dissimilar charges at the two interfaces, the brine film between them collapses and brings the oil in contact with the rock surface. The carboxylic acids present in the oil change the wettability towards an oil-wet state, the degree of which is dependent on the amount of acid present in the oil, brine composition, temperature and so on.

2.5.2 Lab measurement techniques

Various techniques exist to characterize the wettability of a surface in the laboratory. Somasundaran & Zhang (2006) summarized various techniques to measure the wettability such as contact angle measurement, bubble pick up, micro-floatation, film floatation and so on. Various techniques exist to characterize the wetting state of the porous media such as the Amott wettability index, USBM, Amott-USBM and so on. Two such techniques widely used are discussed.

(a) Contact angle measurement

Contact angle measurement is performed using a smooth surface. An immiscible phase is placed on the surface in presence of another immiscible phase and the system is allowed to equilibrate. The equilibrium contact angle is measured to estimate the surface wettability. Figure 2.21 shows an example of contact angle measurement where an oil film is in contact with the surface in presence of water. At equilibrium, force balance gives the Young's equation:

$$\sigma_{os} = \sigma_{ws} + \sigma_{ow} cos\theta \tag{2.13}$$

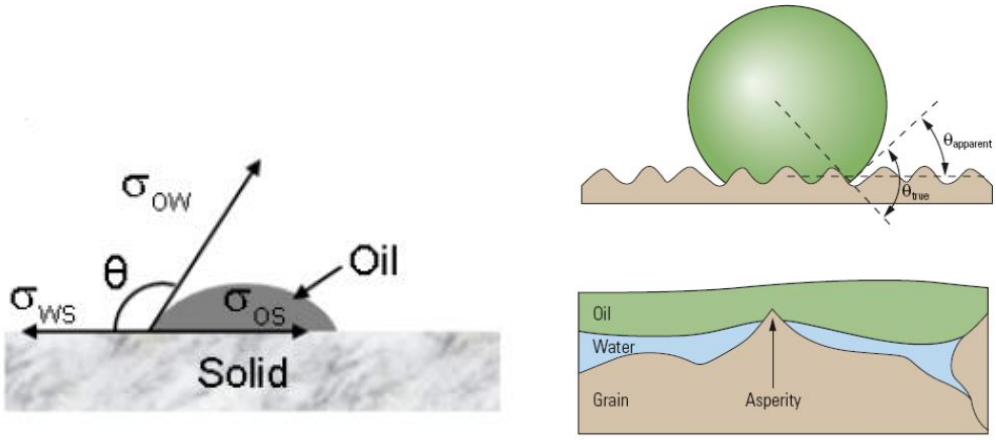

(a) **(b)**

Figure 2.21: Equilibrium contact angle of an oil film in presence of water

Note, that in reality a surface is not perfectly smooth and asperities on the surface may affect the results as shown in Figure 2.21 (b) as discussed by Abdallah et al. (2007). Due to the asperities, the true contact angle may be different than the apparent contact angle.

(b) Amott-Harvey index

Amott-Harvey index is a technique to measure the wettability of a core. In this technique, a core saturated with a given fluid (say oil) is immersed in an immiscible fluid (say water) and spontaneous imbibition of the second fluid is measured. Forced imbibition of the second fluid is then performed. The process is repeated with the core now initially saturated with the second fluid. The ratio of the saturation change of a fluid due to spontaneous imbibition to total saturation change (due to spontaneous and forced imbibition) is calculated for both the fluids. The difference between these indices, (I_1-I_2), gives the wetting preference of fluid phase 1 over phase 2. Figure 2.22 shows the measurements performed for obtaining the Amott-Harvey index.

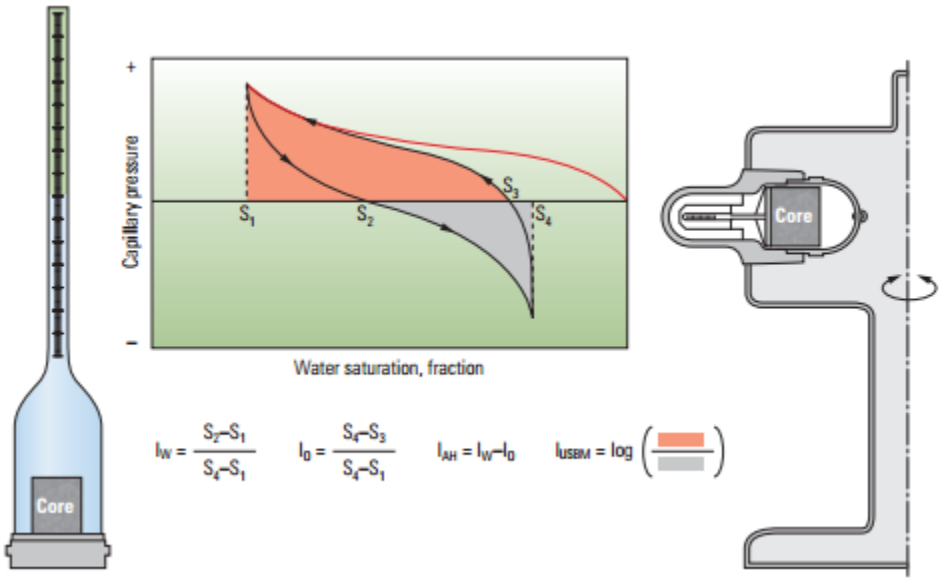

Figure 2.22: Capillary pressure curves obtained for measuring Amott-Harvey index (Abdallah et al., 2007)

2.5.3 Wettability alteration in carbonates

There are two main approaches to alter the wettability in carbonates. In the first approach, wettability alteration is achieved with the use of surfactants. Cationic surfactants, such as Dodecyl trimethyl ammonium bromide (DTAB), have shown to alter the wettability of oil-wet chalk cores and improve the oil recovery (Standnes & Austad, 2000; Standnes & Austad, 2003). Anionic surfactants have also shown to improve the oil recovery from oil-wet carbonates (Seethepalli et al., 2004; Adibhatla & Mohanty, 2008). Sharma & Mohanty (2013) observed wettability alteration and additional oil recovery at high temperature and salinity by using a dual surfactant system consisting of cationic and non-ionic surfactants.

Recent studies have found low salinity brines or modified brines to alter the wettability and improve oil recovery from carbonates at high temperatures. However, unlike sandstones, the mechanisms responsible for the additional oil recovery in carbonate reservoirs are not very well understood. In carbonates, the ionic composition of a brine is found to be more important than the total dissolved solids and wettability altering effects have been observed with high salinity brines such as seawater (Yousef et al., 2010). It is believed that potential determining ions, such as calcium, magnesium and sulfate, play a key role in altering the wettability of carbonates at high temperature (Strand et al., 2005). Sulfate ions, in presence of divalent cations, can alter the wettability of carbonates at high temperatures by adsorbing on the surface, thus making the rock surface negatively charged and triggering the release of attached acids. Divalent cations,

such as calcium and magnesium ions, promote the release of acid by complexing with it. The hypothesis was confirmed by further studies conducted by Strand et al. (2006), Tweheyo et al. (2006), Zhang (2007), Austad (2008), Fathi et al. (2012), Chandrasekhar & Mohanty (2013). Other mechanisms have also been proposed recently to explain the process (Hiorth et al., 2010). Many studies have observed wettability alteration and an increase in oil recovery with modified brines including seawater, diluted seawater and brines with high sulfate concentrations (Yousef et al., 2010; Fathi et al., 2011; Chandrasekhar & Mohanty, 2013). In addition, anions such as phosphate and borate have also shown to alter the wettability in carbonates (Vo et al., 2012). An increase in oil recovery on injecting diluted seawater in carbonate cores containing anhydrite has been reported (Austad et al., 2015). Additional oil recovery has also been observed by selectively removing Na^+ and Cl^- ions, possibly due to a better interaction of potential determining ions with carbonate surface. Selectively increasing the sulfate ions in these brines have shown to further improve the oil recovery. Removing 90% NaCl in seawater or increasing the sulfate concentration has shown low salinity effects (Puntervold et al., 2015).

The studies discussed above agree that wettability alteration in carbonates with low salinity or modified brines is the result of a complex interplay of geochemical interactions at the oil/brine and brine/rock surfaces. Due to the complexity of these interactions, it is difficult to understand the effect of various parameters (such as mineralogy, temperature, salinity and so on) and make reliable field predictions. A mechanistic model that can tackle the geochemistry of the system and relate it to surface

wettability in a reliable manner is therefore required. Many attempts have been made to model this process. Hiorth et al. (2010) first reported a single-phase model that included interactions at the oil/brine and solid/brine interface such as surface complexation reactions and dissolution/precipitation reactions, and the effect of such interactions on disjoining pressure. They proposed calcite dissolution to be the main mechanism responsible for wettability alteration. However, recent studies dismissed the role calcite dissolution alone in altering the wettability (Austad, 2009; Mahani et al., 2015). Qiao et al. (2015) recently developed a multiphase model to include the interactions at oil/brine and brine/rock interfaces and obtained good agreements with the static imbibition data.

2.5.4 Field studies

Field studies using low salinity brine in carbonate reservoirs is scarce in the literature. Yousef et al. (2012) reported the results of the first single-well pilot test where they observed a reduction in oil saturation on injecting seawater. Many field studies have been performed on sandstones where additional oil recovery was observed on injecting low salinity brines (Webb et al., 2004; McGuire et al., 2005; Lager et al., 2008; Vledder et al., 2010).

CHAPTER 3. MATERIALS AND METHODS

The objective of this study was to understand the role of geochemical interactions during chemical EOR processes. A comprehensive approach was followed to understand these interactions, and their significance, with the help of carefully designed experiments and simulations. The type of experiments performed in this study can broadly be classified into three categories: (a) Single-phase static experiments which involved understanding interactions of crushed cores with aqueous solutions. The aqueous solutions consisted of salts, alkalis, surfactants and their combinations. The list of static experiments includes alkali-rock interactions, brine-rock interactions, surfactant adsorption experiments and zeta potential measurements. (b) Single-phase transport experiments were performed to understand the interactions of various aqueous species with the porous media. One of the reasons to perform these experiments was to understand if the geochemical interactions reach equilibrium at flow rates which are typically used in laboratory experiments. Further, useful insights were obtained from these experiments. The list of single-phase transport experiments includes alkali transport experiments in sandstone and carbonate cores, single-phase surfactant corefloods, and low salinity brine corefloods in limestone cores at high temperatures. (c) Multiphase experiments, including oil recovery corefloods, were performed to further investigate the role of geochemical interactions. In this chapter, materials and methods used in this study are discussed. This chapter is divided into two main sections. In the first section, the materials used in this study are discussed which includes chemicals, equipment, and

analytical instruments. In the second section, the methodology followed to perform experiments and analyze samples is discussed.

3.1 Materials

3.1.1 Brines and Alkalis

The brines consisted of aqueous solutions prepared by adding laboratory grade salts such as sodium chloride, calcium chloride, magnesium chloride, sodium sulfate obtained from Fisher Scientific. The alkali solutions were prepared by adding salts such as sodium carbonate, sodium metaborate, sodium hydroxide, sodium phosphate, sodium silicate which were also obtained from Fisher Scientific. Ammonia solutions were prepared by adding ACS grade ammonium hydroxide solution consisting of 30% (v/v) ammonia.

3.1.2 Polymers

Polymers used in the study were commercially available polyacrylamide polymers, sulfonate substituted and vinyl substituted polyacrylamide polymers obtained from SNF Floerger (Cedex, France) in powdered form. The average molecular weights of these polymers were about 2 to 20 million Da. These polymers include FP 3630S, FP 3330S, AN-125 and SAV 550.

3.1.3 Surfactants

Surfactants used in the study were commercially available alkoxy sulfate and internal olefin sulfonate surfactants obtained from Shell chemicals and Stepan chemicals. Alkoxy carboxylate surfactants were obtained from Harcros chemicals.

3.1.4 Solvents and cosolvents

The organic solvents and chemicals such as Toluene, chloroform, cyclohexane, acetone and methanol were obtained from Fisher Scientific. The cosolvents such as isobutanol (IBA), triethylene glycol monobutyl ether (TEGBE), phenols were obtained from Huntsman chemicals.

3.1.5 Crude oils

The oils used in this study consisted of active and inactive crude oils having viscosities between 2 cP to 350 cP at their respective reservoir temperatures (Table 3.1). The temperature of these reservoirs ranged from 30 °C to 120 °C.

Table 3.1: Properties of the crude oil used in this study

Crude oil	Viscosity	Acid number (mg KOH/g oil)
1	3 cP at 55 °C	Inactive oil
2	105 cP at 38 °C	1.25
3	5 cP at 25 °C	Inactive oil
4	8 cP at 59 °C	Inactive oil
5	113 cP at 59 °C	5.0
6	14 cP at 59 °C	2.0
7	350 cP at 30 °C	3.5

3.1.6 Cores

Reservoir (and outcrop) sandstone and carbonate cores were used in the study. The outcrop sandstone cores include Berea sandstone cores, Bentheimer sandstone cores, and Bandera brown sandstone cores. The clay content in Berea sandstone cores and Bandera brown sandstone cores was about 5-11% and 18%, respectively. The outcrop carbonate cores include Texas cream limestone cores, Indiana limestone cores, Silurian dolomite cores and Estaillades limestone cores. The outcrop cores were purchased from Kocurek Industries. Gypsum was present in some of the reservoir sandstone and carbonate cores.

3.1.7 Borosilicate tubes

Surfactant phase behavior experiments were performed in 5 mL graduated borosilicate tubes obtained from Fisher Scientific. The tapered ends of the tubes were sealed by using a propane torch. For microemulsion viscosity measurements, the samples were prepared in 50 mL borosilicate tubes. Surfactant aqueous stability experiments were performed in 20 mL plastic screwcap borosilicate vials. Alkali samples were prepared in plastic vials, instead of glass vials since glass consumption was observed in the presence of an alkali. These tubes were used for experiments up to a temperature of about 70 °C. For high temperature experiments, borosilicate tubes were obtained from the glass workshop of the chemistry department at the University of Texas at Austin. These tubes were sealed using a propane torch to avoid evaporation of

samples at high temperatures. No leak was detected in these tubes even at 120 °C when properly sealed.

3.1.8 Gases

Nitrogen and argon were used for filtering brines, polymer and surfactants, and for displacing oxygen from aqueous solutions. Propane was used for sealing glass tubes. These gases were obtained from Praxair.

3.1.9 Equipment

3.2 Preparation of stock solutions

The aqueous solutions were prepared in 18.2 MΩ (ASTM D1193 standard) deionized water (DI) obtained from ThermoFisher Scientific. Brine stock solutions, having concentrations three to four times the actual brine concentrations, were prepared. Similarly, surfactant and polymer stock solutions were prepared. Actual aqueous solutions were prepared by diluting stock solutions using DI water. This method was adopted to maintain consistency between different samples. In cases where a brine salinity or hardness was too high to prepare a concentrated stock solution, the brine was prepared in 4 L plastic jars. The following equipment were mainly used for preparing the stock solutions.

Weighing Balance

The electronic weighing balance used for measuring samples was purchased from Radwag USA. The least count of the weighing balance was 0.01 g.

Stirrer

The magnetic stirrers used for mixing liquid samples were purchased from VWR International. The stirrers were equipped with heating coils to perform mixing at a desired temperature.

Filtering system

Bell filter press station was used for filtering oil and aqueous solutions. The working pressure of the equipment was 15 psi. Nitrogen or argon was used for maintaining the pressure. Millipore membrane filters of 0.45 to 1.2-micron pore size were used in the bell filters. All the aqueous solutions (brines, alkali solutions, surfactant and polymer slugs) were filtered with at least 0.45 micron filters. Oils were filtered with 1.2 micron filters at reservoir conditions. In-line filters were also used, in some cases, for filtering oil during injection.

3.3 Preparation of samples

Actual samples were prepared from the stock solutions using the equipment given below. These samples include alkali samples, surfactant phase behavior samples, surfactant aqueous stability samples, polymer stability samples, HPLC samples, IC samples and so on. These samples were prepared by carefully adding given amounts of solutions with high precision pipettors. For high temperature experiments (roughly>70 °C), samples were prepared in glass tubes which were then sealed using a propane torch to avoid loss due to evaporation.

Pipettors

High precision pipettors, purchased from Fisher scientific, were used for measuring a given amount of liquid carefully. Different pipettors were used for accurately dispensing samples in the range of 0-20 μL, 20-200 μL, and 200-1000 μL. Pipettors' tips were also obtained from Fisher Scientific. In addition, Eppendorf repeater dispenser was purchased mainly for dispensing polymer solutions and oils.

Glass tube sealing station

Glass tubes were sealed using a propane torch to prevent the evaporation of samples and to create an inert environment. Before sealing the tubes, argon was passed through the samples to remove volatile components as well as oxygen.

3.4 Coreflood setup

Linear corefloods were performed in outcrop and reservoir cores to investigate geochemical interactions and multiphase phenomena. The equipment used for performing corefloods are given below.

Heat shrink tubing

FEP heat shrink tubes, purchased from Geophysical Supply Company, were wrapped around cores to prevent them from getting contaminated. The tubes were also used for making composite cores. The following method was used for putting a heat shrink tube. A tube of given length and diameter was placed on a core, after which heat

was applied with a heat gun. The tube shrank on heating and covered the core uniformly. Attention was given not to introduce air pockets while applying the heat.

Core holder

Stainless steel Hassler-type coreholders designed to accommodate 1.5" diameter and 1' long cores were obtained from Core Laboratories. The image and schematic of the core holder are shown in Figures 3.1 (a) and 3.1 (b), respectively. The coreholder was able to maintain a maximum pressure of 7000 psi.

The coreholder consisted of a hollow steel cylinder (316 stainless steel) with end caps, made up of the same material, attached to it. Ports for applying confining pressure and connecting pressure transducers were available in the cylinder. On the inside, a cylindrical rubber sleeve was placed between the two end caps. The core was placed in the rubber sleeve. The annulus between the sleeve and the coreholder was filled with mineral oil for applying the confining pressure. On the outside, the end caps were attached with end plugs which were in-turn attached with spacers and distributors. Spacers were used so that the distributor was properly in contact with the core. Distributors were used for distributing the injected fluids into the core evenly. O-rings were placed at key locations to make the coreholder leak proof.

Figure 3.1(a): Image of Hassler-type core holder used in experiments

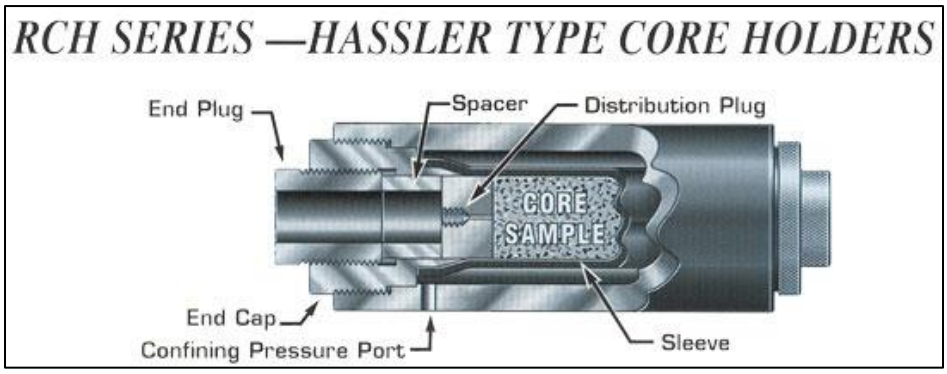

Figure 3.1(b): Schematic of Hassler type core holder

Vacuum pump

A Welch 1400 B-01 type vacuum pump was used to maintain a pressure of -14 psi. The vacuum pump was mainly used for removing air from the core before saturation, degassing aqueous solutions and preparing brine columns.

Pumps

Teledyne ISCO 500 D syringe pumps were used for injecting fluids. The pump can store up to 507 mL of fluid, and maintain minimum and maximum pressures of 10 psi and 3750 psi, respectively. The pump can be operated at constant pressure or constant rate modes. In the constant pressure mode, the pump can maintain the desired pressure by injecting or retrieving the fluid. The pump is run in the constant pressure mode mainly for testing the coreflooding system for leaks, purging the lines and maintaining confining pressure. Oil injection was usually performed at constant pressure. The constant rate mode was used for injecting fluids during a coreflood. The pump was usually filled with mineral oil (or DI water in some occasions). The pump fluids were used for displacing injection fluids, which were kept in glass or steel accumulators. A pressure limit was usually set on the pump to avoid the system pressure from exceeding a given pressure.

Steel accumulators and glass columns

The injection fluids were not filled directly into the pump as some of these fluids could be corrosive. Steel accumulators were instead used, particularly at high temperature and pressure. The volume of accumulators varied from 500 mL to 1000 mL. The accumulator was equipped with a floating piston which separated the injection fluid with the displacing fluid. DI water was typically used as the displacing fluid when steel accumulators were used. These accumulators were also used for injecting oil. Steel accumulators were not used for injecting aqueous solutions, especially polymers, and surfactants, as even a trace amount of iron could be detrimental to them.

Aqueous solutions such as brines, alkalis, surfactants, and polymers were injected using glass columns. The volume of these columns ranged from 75 mL to 300 mL, and they tolerated a maximum pressure of about 30-35 psi. The aqueous solutions were filled in the column with the help of vacuum. The vacuum was used to also degas the aqueous solution. These solutions were displaced from the glass columns by injecting a lighter fluid, such as the mineral oil, from the top. Since the glass columns could tolerate a maximum pressure of 30-35 psi, a pressure limit of 30-35 psi was always set on the pump when these columns were used. Similar to glass columns, polycarbonate columns were manufactured in the machine shop of the petroleum and geosystems engineering department. These columns could work up to a maximum pressure of 50-60 psi.

Convection oven

Blue M 146 series standard mechanical convection oven, having a maximum temperature rating of 350 °C, was used to maintain samples and perform corefloods at desired temperatures.

Pressure gauge and transducers

Pressure gauges were obtained from Omega and were mainly used for measuring air porosity, air permeability, and brine permeability. Pressure transducers, purchased from Rosemount and Cole Palmer, were used for measuring differential pressure across various sections of the core. The pressure transducers converted pressure values to electrical signals and transmitted them to a data acquisition card (DATAQ) which stored

the data on a computer. The raw voltage data was converted to pressure with the help of calibration plots.

Fractional collector

A Retriever 500 fraction collector was used for collecting effluent samples automatically. In this study, the fractional collector was usually programmed to collect 0.1 pore volume samples.

Back pressure regulators

Spring loaded back pressure regulators were purchased from Swagelok to maintain backpressure of up to 100 psi during corefloods at high temperatures.

Valves and tubing

The tubing (plastic and stainless steel) and valves used for making connections were obtained from Swagelok. The internal diameter of these tubes was 1/8". Two-way and three-way valves were used for diverting the flow of fluids in desired lines. Additional valves were obtained from HiP for high-pressure experiments (pressure exceeding 2000 psi). Other related items such as steel ferrule, stainless steel nuts, two-way and three-way connectors were obtained from Swagelok. A tube cutter was purchased from Grainger to cut steel tubings of desired lengths. In addition, Hestalloy tubing was purchased to perform high temperature and high salinity experiments.

3.5 Analytical instruments

3.5.1 Refractometer

Fisher Scientific handheld refractometer was used for measuring the salinity of aqueous solutions. The refractometer gave accurate salinity measurements for sodium chloride brines. However, it must be calibrated for measuring the salinity of other samples.

3.5.2 pH and ORP meters

Portable pH and ORP meters were purchased from Oakton and used for measuring the pH and oxidation-reduction potential of aqueous solutions. pH meter was used mainly for measuring the pH of static experiments' samples and coreflood effluents. ORP meter was mainly used for experiments performed under reduced conditions.

3.5.3 Ion chromatography

Dionex ICS 3000 ion chromatograph (IC) was used for measuring the concentration of cations (Na^+, Ca^{2+}, Mg^{2+}, K^+) and anions (usually Cl^-, $SO4^{2-}$) in aqueous solutions. Before using the IC, the lines were purged with DI water to remove air, and the column was cleaned to remove residue ions from the previous run. The concentration of each ion was kept roughly below 300 ppm in the samples. Note that these samples must be free from oil, polymer or other impurities. 0.2 micron filters were used for filtering samples before diluting them. Separate anion and cation standards stocks were prepared which contained 4000 ppm of each ion. Cations and anions standards, ranging from 1 ppm to 300 ppm, were prepared by diluting their respective stock solutions with DI

water. Standard samples were used for preparing calibration plots for each ion. A characteristic peak was obtained for each ion, the area under which was calculated to obtain the concentration of unknown samples based on the calibration chart.

3.5.4 Inductively coupled plasma-mass spectroscopy (ICP-MS)

In addition to IC, ICP-MS was used for measuring the ionic composition of an aqueous solution. ICP-MS was mainly used to obtain the concentration of total boron in sodium metaborate experiments. The sample preparation procedure for ICP-MS was similar to that of IC. The samples must be free from oil, polymer, and other impurities. The samples must be filtered through 0.2 micron filters. ICP samples were prepared by diluting the filtered samples with 2% nitric acid.

3.5.5 Acoustic zeta probe

Acoustic zeta probe instrument, obtained from Colloidal Dynamics, was used for measuring zeta potential of crushed rock samples (Figure 3.2). The instrument was equipped with a stirrer that kept particles suspended while the measurements were being performed. The instrument was designed based on the electro-kinetic sonic amplitude (ESA) effect; a MHz voltage was applied across the particles which made them vibrate and generate ultrasound waves. Particle vibration was dependent on the particle charge. These waves were picked up by a piezoelectric transducer and converted to dynamic mobility and zeta potential values based on the calibration readings.

Figure 3.2: Colloidal dynamics acoustic zeta probe instrument

3.5.6 High performance liquid chromatography (HPLC)

Surfactant concentrations in chemical flood samples were measured using HPLC obtained from Dionex. In addition to the total surfactant concentration, the instrument provides a distribution of components present in a surfactant. Chemical flood samples were treated to remove polymer, oil, and fine particles. The treated samples were filtered and diluted to the extent such that they could be detected reliably by the instrument. Standard samples were prepared for calibration from the injected surfactant slugs after treating them similarly.

After preparing standard and unknown samples, they were placed in the sampling tray. A given amount of sample was injected into the chromatography column, along with the mobile phase consisting of 0.1M ammonium acetate solution and acetonitrile.

Nitrogen was used as the carrier gas. Depending on the preference of the surfactant components, they partitioned between the mobile phase and the chromatography column (stationary phase) and their elution times differed. The effluent samples from the column were nebulized with nitrogen and detected with an evaporative light scattering detector (ELSD). Surfactant peaks were obtained at given elution times, the area under which were used for quantifying surfactant amounts.

3.5.7 Rheometer

Bulk rheology measurements were performed using the Texas Instruments AR-G2 rheometer. Usually, 2° cone-and-plate geometry was used for measurements which required less than one mL sample. Concentric cylinder geometry was used, in some cases, which required 8-10 mL samples. The rheometer was very accurate at a high shear rate but not at very low shear rates due to a lower limit of 0.2 μNm on the minimum torque. The rheometer came with a Peltier plate to perform measurements at a given temperature.

3.6 Methods

3.6.1 Surfactant phase behavior

Surfactant phase behavior experiments were performed to identify ultralow IFT surfactant formulations. Aqueous solutions were prepared in graduated borosilicate tubes by adding given amounts of surfactant solution. The salinity of the samples was systematically increased by adding electrolyte (alkali or sodium chloride, typically), starting from the base brine. Cosolvent was typically added to reduce the equilibration

time, lower the microemulsion viscosity and improve the aqueous stability. After adding given amounts of aqueous solutions, the aqueous levels in the tubes were recorded. A given amount of oil was then added to the samples. The oil volume fraction was typically changed from 10% to 50%. Argon was then purged into the tubes to remove volatile gases and create an inert environment, after which the tubes were sealed using a propane torch. The tubes were inspected for possible leaks, after which they were mixed and kept in a convection oven set at a given temperature for equilibration. The tubes were mixed from time to time. Additional aqueous samples were prepared similarly, without oil, to obtain the aqueous stability limit of the surfactant formulation at the reservoir temperature. The surfactant formulation, cosolvent type, and their concentrations were systematically varied to identify a surfactant formulation which showed ultralow IFT in the desired salinity window and aqueous stability at least up to the optimum salinity (the concept of optimum salinity is explained below).

Winsor type phase transition, as shown in Figure 3.3, was observed as the salinity of the samples was systematically increased. The transition in phase behavior was the result of a change in surfactants' preference towards oil and the aqueous phase as the salinity was increased. An increase in salinity resulted in increasing surfactants' preference to partition into the oil phase. As a result, more oil was solubilized in the aqueous phase with increasing salinity, thus giving Winsor Type-I (also known as Type II-) phase behavior or oil-in-water microemulsions. This phase behavior showed a clear oil phase and a microemulsion phase. The change in the aqueous level of the respective tubes was used for calculating the amount of oil solubilized. In Winsor type I region, the

volume of the microemulsion phase was more than the original aqueous phase volume, and hence the interface between oil and microemulsion was higher than the aqueous level recorded during sample preparation. The amount of oil solubilized was recorded as the solubilization ratio using the following equation.

$$\sigma_{oil} = \frac{V_o}{V_s} \tag{3.1}$$

where σ_{oil}, V_o, V_s are oil solubilization ratio, volume of oil solubilized and volume of the surfactant. IFT is the interfacial tension between oil and the microemulsion phase in dyne/cm and is estimated to be (Huh, 1979):

$$IFT = \frac{0.3}{{\sigma_{oil}}^2} \tag{3.2}$$

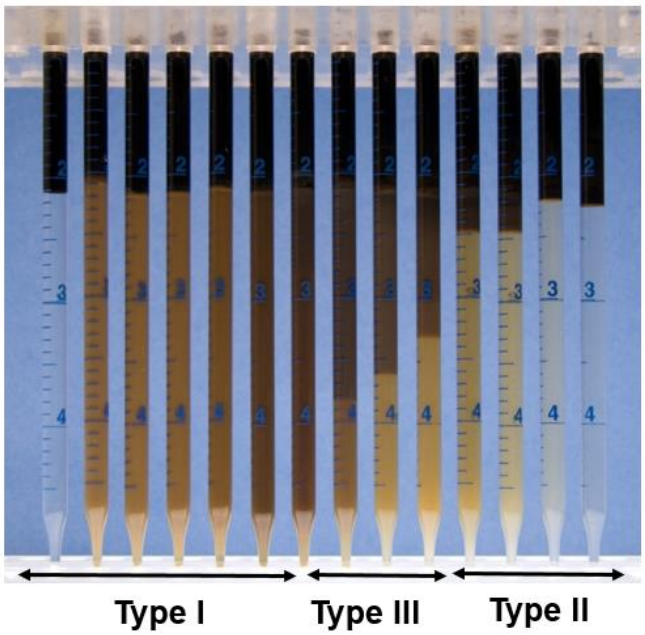

Figure 3.3: Winsor type phase behavior with increasing salinity

As the salinity was further increased, more oil was solubilized resulting in the formation of a separate phase consisting of surfactants, solubilized oil, and solubilized water. At such conditions, three phases exist (Winsor type III region); clear aqueous phases at the bottom, a microemulsion phase in the middle and a clear oil phase at the top. Note that since the microemulsion phase consisted of both solubilized oil and water, the solubilization ratios of both oil and water were calculated. Similarly, Type II (or Type II+) or water-in-oil type microemulsions were observed at higher salinities in which case water was solubilized in the oil phase. These tubes showed a clear aqueous phase and an oil-rich microemulsion phase. The amount of water solubilized was calculated based on the change in original oil-water interface. Water solubilization ratio and IFT between water and the microemulsion phase can be obtained similarly from equations 3.1 and 3.2.

The solubilization ratios were plotted, as a function of salinity, as shown in Figure 3.4. The optimum salinity is the point at which both oil and water solubilization ratios are equal. The interfacial tension at optimum salinity was obtained by using Huh's equation (equation 3.2). A solubilization ratio of more than 10 at the optimum salinity was used as a rule to thumb for identifying an ultralow IFT formulation.

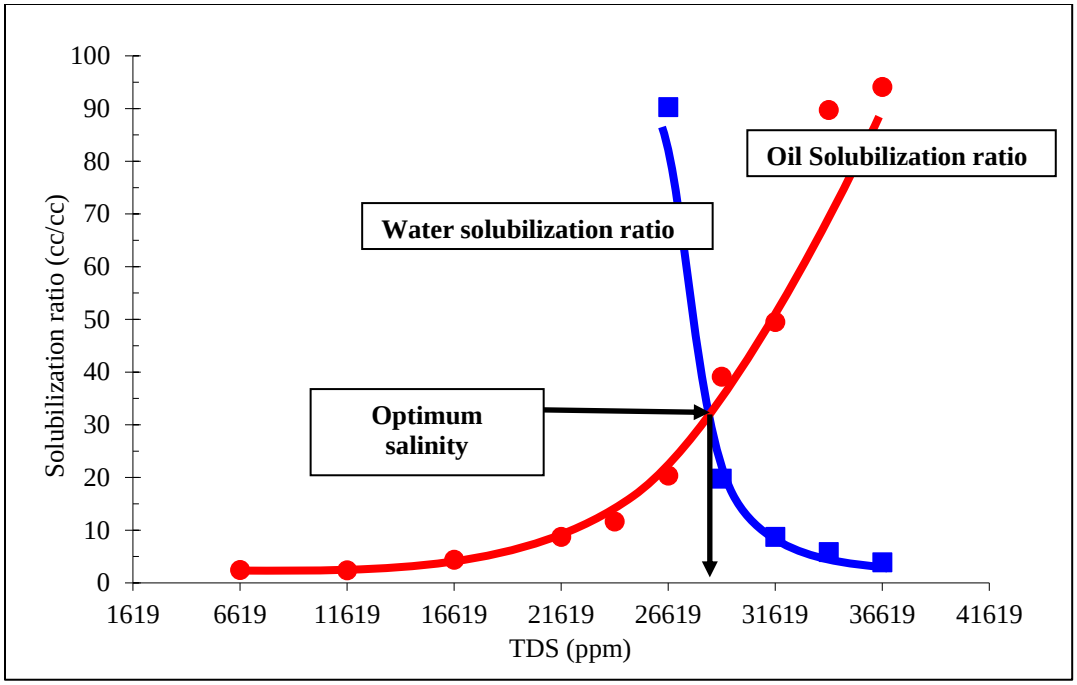

Figure 3.4: Oil and water solubilization ratios as a function of salinity

In the case of acidic crude oils, activity maps (Figure 3.5) were prepared by changing the oil to water ratio. Note that this experiment was performed when an alkali was added to the surfactant formulation. The purpose of this test was to identify the change in optimum salinity as the oil-water ratio was varied. The change was observed due to a change in the amount of soap generated due to different oil-water ratio. The amount of soap generated is directly related to the amount of oil; samples with 50% oil have more soap than that of 10% oil. As a result, the soap to surfactant ratio varied which affected the optimum salinity window. Activity maps were used for designing surfactant floods such that negative salinity gradient is achieved; Type II phase behavior ahead of the surfactant slug, followed by ultralow IFT in Type III region and Type I phase

behavior in the polymer drive. ACP formulations were also developed following the same procedure, however, no synthetic surfactant was added in these experiments.

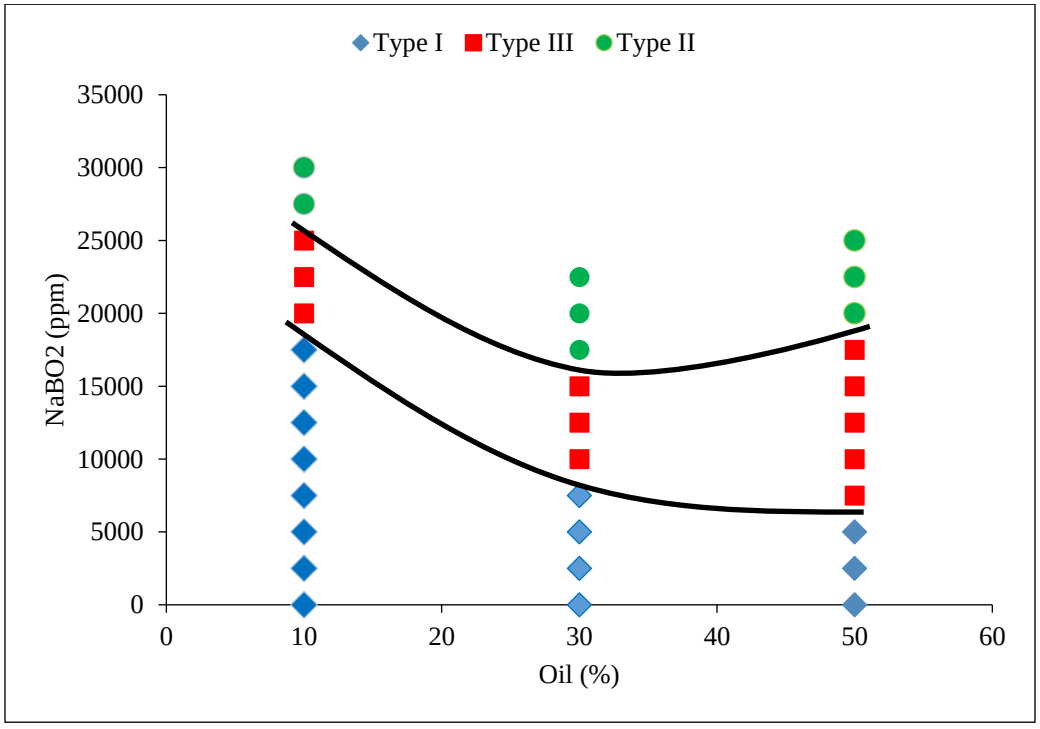

Figure 3.5: Activity map for an acidic crude oil

3.6.2 Polymer preparation

Polymer stock solutions containing 5000 ppm to 10,000 ppm polymer were prepared by carefully weighing a given amount of polymer and adding it to 0.1 NaCl brine. The polymer was added on the shoulder vortex slowly while the solution was being mixed so that the polymer particles do not aggregate. The polymer solution was stirred slowly for 24 hours, after which it was filtered through 1.2 μm membrane filter using the bell press filtration system under a constant pressure of 15 psi. The filtered amount was collected in a graduated cylinder, and the volume of polymer collected was noted at

different times. Filtration ratio was obtained using the equation 3.3, which gave an indication of the time taken to filter a given amount of polymer at the beginning and the end of the filtration. Filtration ratio was used as an indicator of the polymer solution quality; a filtration ratio of 1 indicated that the filter paper was not plugged during filtration and the filtration rate of the polymer under a constant pressure was constant throughout the filtration process. On the other hand, a filtration ratio of more than 1 indicated that the filter paper was getting plugged as the polymer was being filtered. In our study, a filtration ratio of less than 1.2 was used as a standard for selecting good polymer solutions.

$$FR = \frac{\Delta t_{80-100}}{\Delta t_{40-60}} \tag{3.3}$$

Where, Δt_{40-60} and Δt_{80-100} is the time taken to filter 20 mL polymer after filtering 40 mL and 80 mL, respectively.

Note that although filtration ratio is a good indicator of polymer quality, it does not guarantee that plugging would not occur in the cores. This is likely to be governed by the pore throat size distribution of the core.

3.6.3 Polymer stability experiments

Polymer stability experiments were performed to identify polymers that were stable under the experimental conditions. In this study, polymer stability experiments were performed mainly to identify polymers that could be used in surfactant floods in cores containing gypsum when ammonia was used as alkali. Aqueous solutions were

prepared by adding a given amount of polymer, salts, and alkalis in glass ampules. The glass tubes were ordered from the chemistry department at the University of Texas at Austin to avoid leaks at high temperatures. The oxygen from the samples was removed by purging nitrogen or argon for 30-60 mins. The oxygen level in the polymer samples was carefully monitored by using oxygen strips. After the oxygen concentration was below a few ppb, sodium dithionite was added to establish reduced conditions. In addition, a polymer protection package consisting of IPA and thiourea was added to remove free radicals. The tubes were sealed using a propane torch and left to equilibrate at a given temperature. A sample was allowed to equilibrate for a given time, after which the tube was carefully broken, and the oxygen level was immediately measured to make sure that the tubes did not leak in the oven. After making sure that the tube did not leak, the pH and viscosity of the polymer solution were measured using a pH meter and the rheometer, respectively. A detailed procedure to perform the polymer stability experiments is discussed by Lee (2015).

3.6.4 Static brine-rock/alkali-rock experiments

Static experiments were performed to study the interaction of various ions present in a brine or alkali solution with various minerals. The purpose of these tests was to understand the equilibrium composition of such as system. A given amount of mineral was crushed with a ball mill, after which it was sieved to obtain the desired size fraction. These crushed solids were washed with DI water or low salinity NaCl or KCl brine (depending on the case) to remove the impurities. Note that cleaning was particularly

important in the case of sandstones where clays were usually loaded with divalent cations. These samples were first washed with a high salinity NaCl brine (~100,000 ppm) to remove divalent cations from clays and then equilibrated in low salinity NaCl brine (~10,000 ppm). The solids were removed from the DI water or NaCl brine, washed with ethanol and allowed to dry in a convection oven.

A given amount of crushed solid was placed in a glass or plastic vial followed by adding the desired amount of an aqueous solution. Plastic vials were used for preparing alkali-rock samples to avoid errors due to an alkali-glass reaction. Enough solid was added so that it was not completely consumed by the reactions. The glass vials were closed properly using plastic screw caps and then allowed to equilibrate at the desired temperature. In the case of very high temperature experiments (>80 °C), the samples were prepared in glass vials which were then sealed using a propane torch to avoid the evaporation of samples. These samples were mixed from time to time. In addition, they were weighted from time to time to identify leaks. After equilibrating for a desired amount of time, the samples were analyzed for the pH and the ionic composition using a pH meter and the IC (or ICP-MS), respectively.

3.6.5 Static surfactant adsorption experiments

Static surfactant adsorption experiments were performed to study the adsorption of surfactants on crushed solids under a given condition. A core was crushed, sieved and cleaned using the procedure described above. Note that removing the divalent cations attached to clays was essential to obtain reliable results. The specific surface area of the

solid sample was measured by performing the BET measurement. A given amount of solid was added to glass vials followed by adding a surfactant solution. The solid to liquid ratio was kept close to 1 in these experiments. However, the ratio was dependent on various parameters such as the total surfactant concentration in the formulation, specific surface area of the solid and so on. The salinity of the surfactant formulation was kept at the optimum salinity since the surfactant slug injection was usually performed at the optimum during coreflood experiments. The glass vials were sealed using plastic screw caps and allowed to equilibrate at the required temperature. Note that the surfactant samples must be aqueous stable at the experimental conditions.

After equilibrating the samples for a given duration, the supernatant solution was separated, filtered and analyzed using HPLC for surfactant concentration. A calibration plot of surfactant concentration versus area obtained from HPLC was prepared to obtain surfactant concentrations of the unknown samples. Surfactant adsorption was calculated based on the change in the surfactant concentrations using the formula given below:

$$Surfactant\ adsorption\left(\frac{mg}{g\ rock}\right) = \frac{10*(Co(wt\%)-C(wt\%))M_{liq}\ (g)}{M_{rock}\ (g)} \tag{3.4}$$

where C_o = initial surfactant concentration in wt%, C = final surfactant concentration in wt%, M_{surf} = Total mass of the liquid solution in grams, and M_{solid} = mass of solid in grams.

3.6.6 Zeta potential measurements

Zeta potential measurements were performed to study the change in surface composition and surface charge in the presence of different brines and alkalis. These measurements were performed using a Colloidal Dynamics acoustic zeta probe, shown in Figure 3.2. The instrument automatically performed background salinity corrections which is required especially for high salinity measurements. A given amount of rock was crushed, sieved and cleaned as described previously. Samples consisting of 250 g aqueous solutions and about 1 wt% solids were prepared and allowed to equilibrate overnight before the measurements were performed. The samples were then transferred into the measuring cup, with the zeta-probe immersed in it, and allowed to equilibrate for 10 minutes. The zeta potential of each sample was measured five times, and the mean value was reported. The measurements reported in this study were performed at 25 °C.

3.6.7 Single-phase brine or alkali floods

Single-phase brine or alkali floods were performed to understand the geochemical interactions of aqueous solutions with fluids and minerals present in a core. These studies were useful in gaining additional insight into geochemical interactions. In this study, these experiments were performed mainly for two chemical EOR processes; ASP floods in sandstone and carbonate cores and low-salinity-brine transport in carbonate cores. The schematic of the experimental setup is shown in Figure 3.6.

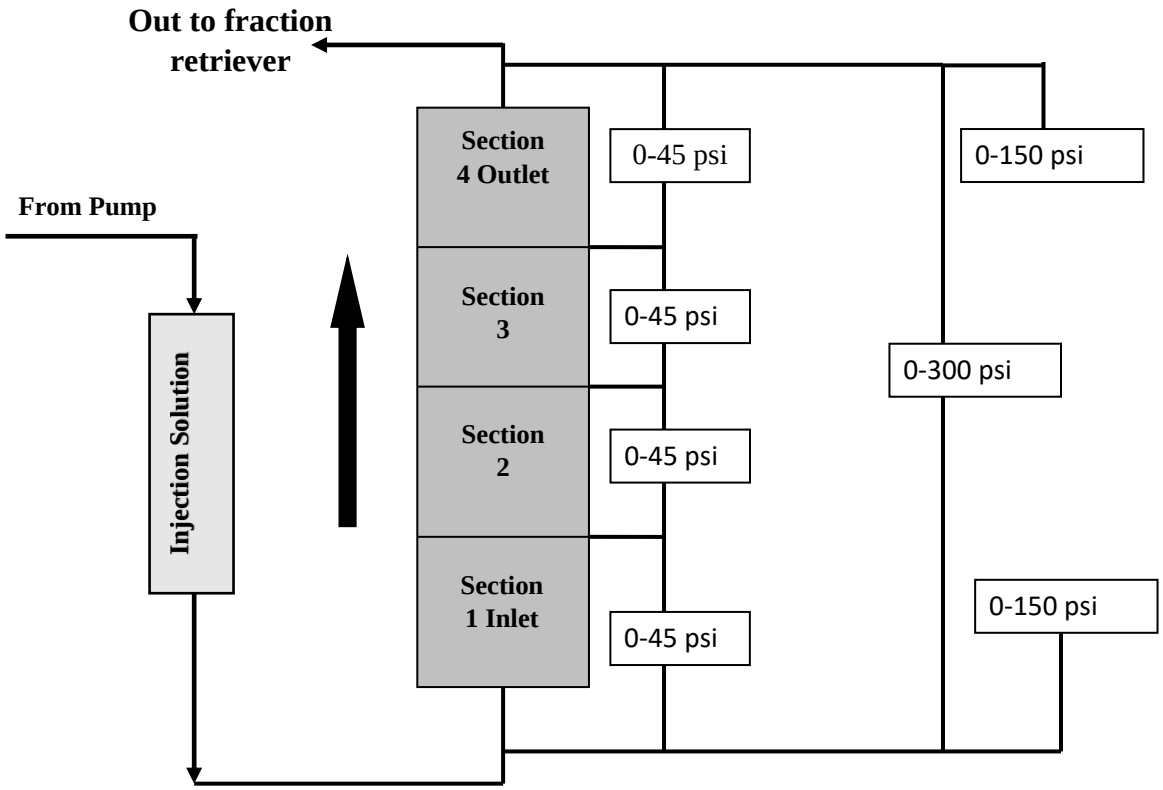

Figure 3.6: Schematic of the experimental setup

During ASP floods, it is critical that the alkali transports with the surfactant, without a significant delay, so that surfactant adsorption on the rock can be minimized. To ensure that alkali does not retard significantly, studying its interactions with reservoir fluids and minerals is essential. Unfavorable interactions may result in alkali propagation delays, permeability damage, and alkali loss. An example of such unfavorable interactions includes precipitation of alkali with reservoir fluids and minerals, ion exchange with the rock, dissolution of clay minerals and so on. In addition, it is crucial that these studies are performed keeping in mind that the residence time of injected fluids

in the reservoir is much larger than in the lab. In this study, slow flow rate experiments were therefore performed to understand the long term effect of such interactions. Single-phase transport of low salinity brines in carbonate cores was similarly studied to understand the interactions of potential determining ions. Single-phase floods in cores of known mineral compositions facilitated in creating controlled environment to perform such studies. The detailed procedure to perform these tests are given below.

Core characterization

The experiment started with a fresh core or a core which had been cleaned to remove oil and other chemicals from a previously coreflood. The core was dried beforehand by keeping it overnight at 80 °C. The length, diameter, and mass of the core were measured, after which a heat shrink tubing was placed over it. In this study, cores of 1.5" diameter and 1' length were used. Dummy cores (usually made up of steel) were used in case of shorter cores to fill the remaining space. The core was placed in a clean coreholder (cleaned to remove brine, oil and other chemicals from the previous flood). The ends of the coreholder were properly tightened ensuring that the distributors were in contact with the core. Before applying a confining pressure with mineral oil or DI water, a confining pressure of 100 psi was applied with air. Air was used initially because one could detect leaks in the overburden without damaging the core. After applying the pressure, the air connection was disconnected, and a pressure gauge was attached to monitor the confining pressure. If no leak was detected, then air pressure was released. A confining pressure of 800-1000 psi was established by injecting mineral oil or DI water

with pump. It was ensured that no air got trapped in the overburden chamber when a liquid was used for overburden. The pump, attached to the overburden, was allowed to run for a few hours at constant pressure and the liquid level in the pump was carefully monitored to identify possible leaks. Once the overburden pressure was stable and no leak was detected, air porosity and permeability measurements were performed.

Air permeability and porosity

Air permeability was measured by injecting air at constant pressure from the core inlet. Air flow rate was obtained by connecting the outlet of the core air flow meter. A differential pressure transducer was connected to the core to measure the pressure drop across it. Air flow rate and pressure drop across the core were recorded once these values stabilize. Such measurements were repeated 4-5 times by changing air pressure. The pressure drop across the core is related to the flow rate by using equation 3.5, which is derived for compressible fluids from mass balance and Darcy's law.

$$Q = \frac{K_{air}A\left(P_{in}^2 - P_{std}^2\right)}{2\mu_{air}LP_{std}} \tag{3.5}$$

where, K_{air} is the air permeability, P_{in} and P_{std} are inlet and outlet pressures, respectively. L, A and μ_{air} are the length of the core, cross sectional area of the core and viscosity of air, respectively.

Note that air permeability is usually higher than the actual permeability due to the slippage on the wall. Klinkenberg correction should be applied by plotting K_{air} vs

inverse of average pressure. The intercept of the curve gives corrected permeability and slope of $K_L b$

$$K_{air} = K_L \left(1 + \frac{b}{P}\right) \tag{3.6}$$

where, K_L is the corrected permeability, P is the average pressure and b is a constant

Air porosity was obtained using the Boyle's law. Air filled inside a pump of volume V_1 (known) and maintained at a pressure of P_1 was connected to the core of volume V_2 (unknown) containing air at a given pressure P_2. The valve connecting the pump and the core was opened, and the system was allowed to achieve a steady state. The final pressure of the system was recorded using a pressure gauge. The porosity of the core is obtained by solving the equation given below.

$$P_1V_1+P_2V_2 = P(V_1+V_2) \tag{3.7}$$

Note that this test was performed at a constant temperature and absolute pressure values were used in the equation given above. The dead volume of the system was subtracted from V_2 to obtain the core pore volume.

Initial brine saturation

The air inside the core was removed next to prepare the core for brine saturation. Vacuum and CO_2 lines were connected to separate lines at the core inlet. A pressure gauge was connected at the core outlet to monitor the vacuum inside the core. The CO_2 line was closed and vacuum was applied until the pressure gauge reading was steady at a value below -13.5 psi. At this point, vacuum line was closed, and CO_2 line maintained at

a pressure of about 10-15 psi was opened. The line was kept open until the system pressure stabilized. The CO_2 line was closed, the vacuum line was opened, and this process was repeated 3-4 times. The vacuum was applied at the end to remove CO_2 from the core, after which the desired brine was injected at a constant pressure. The amount of brine that went into the core was recorded to obtain the pore volume (which was compared with the value obtained from air porosity).

Tracer test

Tracer test experiment was performed next by displacing the brine initially present in the core with another brine of different salinity at the injection rate of 5-10 ft/d. The purpose of the tracer test was to investigate if the core was homogeneous and also confirm the pore volume of the core. The effluents from the core were collected using an automatic fractional collector as samples of 0.1 pore volume. The volumes and the salinities of effluent samples were recorded. The effluent salinity was normalized between the salinities of the initial brine and the injected brine and plotted against cumulative volume injected to obtain the tracer test curve. In an ideal situation without dispersion, the normalized effluent salinity would have changed from 0 (corresponding to initial brine salinity) to 1 (corresponding to injected salinity) in a step-wise manner. However, due to dispersion, an ‘S’ shaped curved is observed in reality. This effluent salinity profile can be modeled using the convection-dispersion equation shown below. For a homogeneous core, one pore volume is the volume corresponding to the normalized salinity of 0.5.

$$\frac{\partial C}{\partial t} + \nabla \cdot (\overline{u}C) - \nabla \cdot \left(\overline{D}\nabla C\right) = 0 \tag{3.8}$$

Where, $\overline{D}$ is the dispersion coefficient tensor.

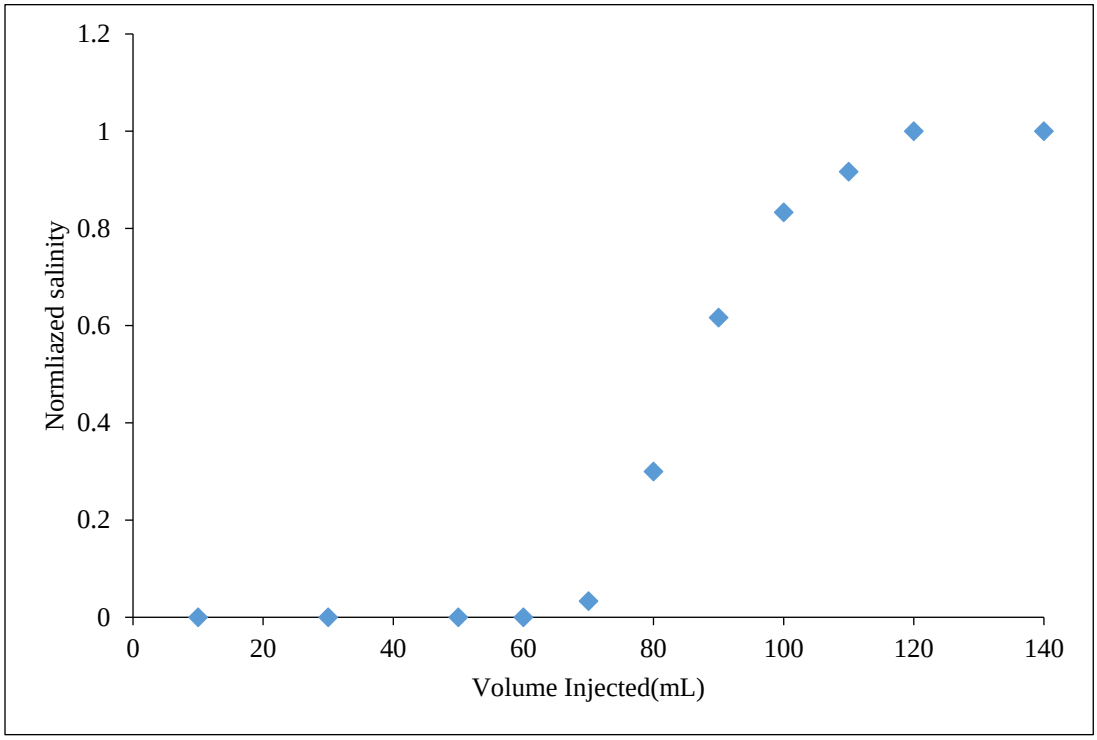

Figure 3.7: Results of a tracer test experiment. Normalized salinity of effluent samples is plotted against volume of tracer test brine injected

After the tracer test, initial conditions were established by injecting many pore volumes of the formation brine at the reservoir temperature and allowing it equilibrate with the core for at least one day.

Brine permeability

After saturating the core with the formation brine, the brine permeability was measured by injecting the brine at different flow rates and recording the differential

pressure drop across the core after a steady state was achieved. During the measurement, the maximum pressure drop across the core was kept below 20-22 psi. Such measurements were repeated 4-5 times at different flow rates. Darcy law was used to obtain core permeability from the following equation.

$$Q = \frac{KA}{\mu}\frac{\Delta P}{L} \tag{3.9}$$

Brine/Alkali flood

A desired brine or alkali solution was prepared and filtered, using the procedure described previously, and inspected for any signs of precipitation. The pH (and the ORP in the case of reduced solutions) was measured, after which it was filled in a glass column or a steel accumulator. The column or accumulator was connected to the experimental setup and allowed to heat to the desired temperature. While heating the brine solution (or alkali solution), the pressure in the column or accumulator was continuously monitored to prevent it from exceeding to undesirably high values. A pump, running at a given constant pressure, was connected to the brine column or accumulator, especially when overnight heating was required. After heating the solution, it was injected into the core at a desired flow rate, and the effluent samples were collected using an automatic fractional collector. The pressure drop across the core was monitored using differential pressure transducers. Note that a maximum pressure limit was set on injection pumps to avoid pressures to reach to unacceptably high values during the corefloods.

Effluent analysis

The volume of effluent samples was recorded after which they were analyzed for the pH, the salinity, and the ionic composition. Before performing the ion analysis, it was ensured that the effluent samples were clear and did not have any precipitates. If precipitates were observed, then they were re-dissolved before the samples were analyzed (usually by acidifying the samples). The precipitation could be the result of cooling or depressurization of the effluent samples; cooling or depressurization (and the escape of dissolved gases) could make the effluent sample supersaturated leading to precipitation.

3.6.8 Single-phase surfactant adsorption

Single-phase surfactant adsorption experiments were performed to understand the effect of adding various alkalis on surfactant adsorption. The experiments were performed in two ways; (a) Continuous surfactant slugs were injected at their respective optimum salinities and delays in the effluent surfactant concentrations were obtained. Based on the delay, the surfactant adsorption was calculated. (b) A given amount of surfactant slug was injected at optimum salinity followed by a polymer drive at a lower salinity. The amount of surfactant collected in the effluent was obtained from HPLC based on which the surfactant adsorption was obtained. Single-phase surfactant adsorption experiments were performed separately because in the presence of oil, surfactants might get retained in the core by other mechanisms such as by trapping in the residual oil phase or as viscous emulsions. Therefore, single-phase surfactant adsorption experiments were performed to create a controlled environment to study the effect of

alkali on surfactant adsorption. Note that the absolute surfactant adsorption values obtained from these experiments may not be applicable in the field because the presence of oil in actual corefloods may have an effect on these values. However, these experiments served the purpose of comparing different corefloods under similar conditions.

3.6.9 Initial oil saturation and core aging

Cores were aged in crude oils to make them oil wet. The degree of oil wetness that can be achieved by core aging depends on many factors such as rock type, oil acid number, oil saturation, formation brine composition, temperature of aging and so on. After saturating a core with formation brine, by following the procedure described in section 3.4.7, oil was injected at reservoir temperature at a constant pressure of about 200-400 psi. The effluents from the core were collected in a graduated cylinder to estimate the initial oil saturation based on the amount of brine collected. The injection was continued until no more water was produced. The core was said to have reached the initial oil saturation. The initial oil saturation of a core depends on a number of parameters such as oil viscosity, core heterogeneity, core permeability and so on. The core was then placed in a glass cylinder and oil was poured into the cylinder to entirely submerge the core. The cylinder was sealed with a screw cap and placed at 80 °C for 3-4 weeks. In case of a low viscosity oil, it may not be possible to achieve high initial oil saturations which is desirable to achieve oil wetness. In such a case, vacuum saturation method was adopted to increase the initial oil saturation. Instead of saturating the core

with formation brine after vacuuming, only a given amount of formation brine was injected. Rest of the core was saturated with the oil.

3.6.10 Oil recovery corefloods

Oil flood

After saturating the core with oil as described in section 3.4.9, oil was injected at a constant flow rate and the differential pressure drop was recorded when a steady state was reached. Such measurements were repeated at least 3-4 times. Oil permeability at initial water saturation (Ko at Swi) was obtained from this data by using the Darcy equation (equation 3.9). Oil relative permeability at the initial water saturation was obtained by dividing the oil permeability by the brine absolute permeability (Kro=Ko/K).

Waterflood

Waterflood was typically performed before the chemical flood to observe the benefits of injecting chemicals for improving the oil recovery from waterflooded reservoirs. During a waterflood, the desired brine was filtered and transferred to a glass column or steel accumulator and allowed to heat up to the experimental temperature. The brine was displaced at a constant velocity, typically 1 ft/d and the effluent samples were collected using an automatic fractional collector. The differential pressure drop was simultaneously recorded. The injection was continued till no additional oil was produced. In the case of oil-wet cores, the core outlet may not reach the residual oil saturation to waterflood because of capillary end effect. Capillary end effects result in increasing the oil saturation at the core outlet. To remove these artifacts, the injection was performed at

a higher velocity (typically 10 ft/d) such that the pressure drops were sufficiently high to remove the end effects. The amount of oil collected was measured visually and the residual oil saturation after waterflood was obtained based on mass balance.

Brine injection was performed at different flow rates and the differential pressure data across the core was recorded. This data was used for calculating the brine permeability at the residual oil saturation from equation 3.9. The brine relative permeability (Krw) at the residual oil saturation (Sorw) was obtained by dividing the brine permeability at Sorw with the absolute permeability. This data is later used in designing the chemical flood.

Surfactant flood design

To design a good surfactant flood, the following three conditions must at least be satisfied: the flood should result in ultralow IFT in the porous media; the flood should have sufficient mobility control at various interfaces (microemulsion-oil bank, surfactant slug-microemulsion, surfactant slug-polymer drive); and last, the surfactant retention should be minimum so that injected surfactant is sufficient to transport through the porous media.

The first condition is achieved by developing an ultralow IFT surfactant formulations and then achieving the desired salinity in the core by designing a correct salinity gradient. Typically, negative salinity design is preferred. However, if the formation brine salinity is lower than the optimum salinity, then either a pre-flush slug is injected to increase the salinity, or the surfactant slug is injected above the optimum

salinity (given that it is aqueous stable). In addition, the transition from the surfactant slug salinity to the polymer drive salinity must not be abrupt, else Winsor type III window may not be achieved in the core. The effect of geochemical interactions must be kept in mind when designing the salinity gradient. For example, the dissolution of gypsum could result in increasing the calcium concentration in the surfactant slug which could drive the surfactant system into Winsor type II. Similarly, ion exchange reactions may result in changing the effective salinity of the surfactant slug (discussed in chapter 5). In addition, salinity design may change based on the activity map (for acidic crude oils).

The mobility requirement is achieved by adding a sufficient amount of polymer to the surfactant slug and polymer drives. The requirements can be estimated based on the mobility of the oil bank and shear rate in the core (discussed next) at the reservoir condition. Note that the effect of geochemical reactions in the porous media on polymer viscosity must be taken into account when deciding the polymer concentration. The polymer must not plug the porous media and be able to propagate through it without degradation.

The third condition of low surfactant retention is achieved by designing a good surfactant system which does not result in forming viscous emulsions or gels and is aqueous stable at the injection salinity. An alkali is typically added to lower the surfactant adsorption on rock matrix. The trapping of surfactant in the residual oil phase is avoided

by designing the salinity gradient such that Winsor type I is achieved in the polymer drive.

Polymer requirement

The type of polymer required for a surfactant flood is dictated by many parameters such as the reservoir temperature, the brine salinity and hardness, the reservoir permeability, the mineralogy and so on. Based on these parameters, a polymer is chosen such that it is stable under reservoir conditions, propagate without plugging the reservoir and is economical. Given that the type of polymer is known, its minimum concentration in the surfactant slug (and polymer drives) is decided such that the surfactant flood is performed in a stable manner. The schematic of displacement during surfactant flood (Figure 3.8) shows that the injection of surfactant slug results in making an oil bank followed by a microemulsion phase. The oil bank consists of both oil and the formation brine in a given ratio (known as the out-cut). For a stable displacement, the mobility of the surfactant slug should be at least equal to that of the microemulsion phase, which should in-turn be lower than the mobility of the oil bank. Similarly, mobility of the polymer drive should be at least equal or lower than that of the surfactant slug.

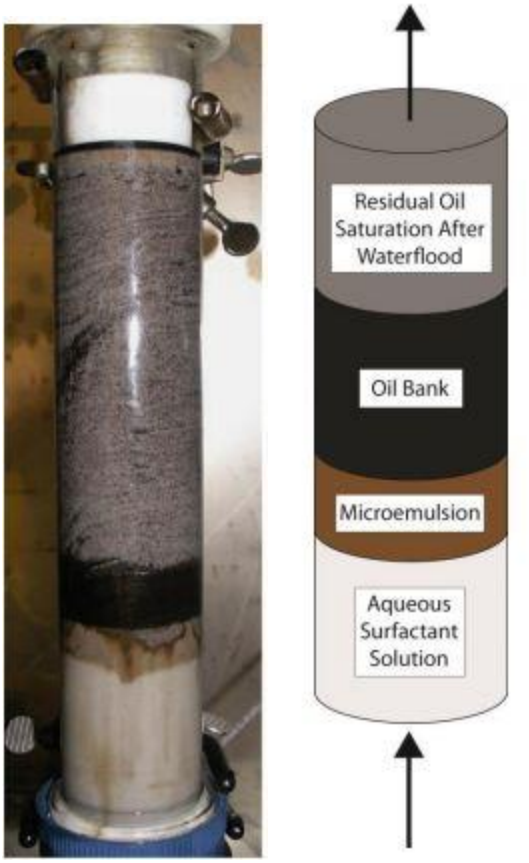

Figure 3.8: Oil displacement during surfactant flood (Lu, 2014)

For simplicity, the relative mobility of the oil bank was used in deciding the polymer concentrations in the surfactant slug and the polymer drives in the study (Gogarty, 1967). The relative mobility of the oil bank at a given oil saturation can be written as the sum of the relative mobility of the oil and the mobility of the water in the oil bank.

$$\lambda_{total} = \lambda_{oil} + \lambda_{water} \tag{3.10}$$

where λ_{total}, λ_{oil}, λ_{water} are the relative mobility of the oil bank, oil phase and water phase, respectively. The total relative mobility can be considered as the inverse effective viscosity of the oil bank; the above equation can be written as,

$$\frac{1}{\mu_{oil\,bank}} = \frac{K_{ro}}{\mu_o} + \frac{K_{rw}}{\mu_w} \tag{3.11}$$

$$\mu_{oil\,bank} = \frac{1}{\frac{K_{ro}}{\mu_o} + \frac{K_{rw}}{\mu_w}} \tag{3.12}$$

The relative permeability of oil and water is written using Corey's equation as shown below,

$$K_{ro} = K_{ro,max}\left(\frac{S_o - S_{or}}{1 - S_{or} - S_{wc}}\right)^{n_o} \tag{3.13}$$

$$K_{rw} = K_{rw,max}\left(\frac{S_w - S_{wc}}{1 - S_{or} - S_{wc}}\right)^{n_w} \tag{3.14}$$

where, $K_{ro,max}$ and $K_{rw,max}$ are the end point relative permeabilities of oil (at initial water saturation) and water (at residual oil saturation after waterflood). A plot is obtained between water saturation and total mobility by varying the water saturation from S_{wi} to $(1\text{-}S_{orw})$. The minima on that curve gives the minimum mobility of the surfactant slug for a stable displacement. The viscosity of the surfactant slug is obtained by taking its reciprocal.

Now that the minimum viscosity of the surfactant slug is known, the shear rate in the core is calculated next using the equation given below. Since polymers used in

chemical floods are shear thinning, the shear rate calculation plays a key role in deciding polymer concentration.

$$\dot{\gamma_{eq}} = C\left(\frac{3n+1}{4n}\right)^{\frac{n}{n-1}} \frac{4u}{\sqrt{8kk_{rw}\varphi S_{rw}}} \tag{3.15}$$

where

- u, the Darcy velocity (q/A)
- k, the absolute permeability
- k_{rw}, the water relative permeability
- S_{rw}, the water saturation
- Φ, the porosity
- C, a correction factor that depends on the rock characteristics
- n, the power law coefficient

Surfactant injection

A surfactant slug was prepared and filled in a glass column by vacuum. The air inside the slug was removed by vacuum and the column was placed in the oven to heat up to the desired temperature. Glass columns containing polymer drives were simultaneously filled in glass columns and kept in the oven. The slug was injected using mineral oil (injected from the top) at a constant velocity, typically at 1 ft/d. The effluent samples were collected using an automatic fractional collector and the differential

pressure drop across the core was recorded. A given amount of surfactant slug was injected after which the flood was continued by injecting polymer drives. Usually about 2 pore volumes were injected in total. The tubes collected were capped immediately to preserve the samples and then analyzed.

Effluent analysis

The effluent samples collected from the coreflood were analyzed for the oil recovery (visually), the pH (by pH meter), the surfactant concentration (by HPLC), the ionic composition (by ion chromatography) and the salinity (by refractometer). For running samples in HPLC and ion chromatography, the oil from them must be removed, and the polymer must be degraded. In addition, all the surfactant in a given sample should be dissolved in the aqueous phase. This was achieved by adding a solution consisting of 1% bleach and 5% TEGBE in a given proportion (usually keeping sample: solution ratio of 1:3). The samples were kept at 60 °C for a few hours for polymer degradation. Same procedure was performed using the injected surfactant slug, which was used for making the calibration standards.

Core cleanup

After chemical flood, the core can be reused after cleaning it so that the oil, the polymer and the surfactants are removed. The procedure to clean the core is the following. Note that the injection rate must be slow during the core cleanup so that the injected solutions get enough time to interact with the core fluids.

1. Injection of several pore volumes (2-3 PV) of 1,000 ppm hypochlorite in brine to degrade and remove polymer. About 0.5% KCl may be added to avoid damage from clays in sandstones
2. Injection of several pore volumes of brine to displace hypochlorite solution. The brine should have at least 0.5% KCl, especially in case of sandstones.
3. Injection of several pore volumes of 100% methanol to desorb and remove surfactants from rock.
4. Injection of many pore volumes of a mixture of 50% toluene and 50% methanol until clear effluent is observed and the oil concentration in the effluent is below the detection limit.
5. Injection of several pore volumes of 100% methanol to remove toluene.
6. Injection of several pore volumes of brine to remove methanol and measure the brine permeability and effluent pH. If the brine permeability and pH are close to the original values before the chemical flood, then the core is considered to be restored and ready to use for another experiment.

CHAPTER 4. CHEMICAL FLOODS WITH ALTERNATIVE ALKALIS

Incorporating an alkali to surfactant formulations is beneficial as alkalis have shown to lower surfactant adsorption, generate soap on interacting with acidic crude oils and improve surfactant phase behavior. Sodium carbonate is typically used as an alkali, however, it has limitations under certain circumstances as was discussed in chapter 2. In this chapter, results of the study performed using alternative alkalis will be discussed. The study involved understanding various aspects of chemical EOR using these alkalis. Single-phase static and transport experiments were performed to understand the geochemical interactions of these alkalis with the porous media, especially in the presence of gypsum. Zeta potential measurements were performed to study the effect of adding alkalis on sandstone and carbonate rocks. Static and dynamic single-phase surfactant adsorption experiments were performed using different alkalis in sandstone and carbonate rocks. Surfactant phase behavior and polymer stability experiments were performed to develop robust formulations. Interactions of different alkalis with acidic crude oils were studied to develop optimum alkali cosolvent polymer (ACP) formulations. Oil recovery corefloods were performed in sandstone and carbonate rocks to compare these alkalis. The chapter is divided into three sections; the first and second section discuss the results obtained with sodium metaborate and ammonia, respectively. The third section discusses the results of alkali cosolvent polymer (ACP) floods performed using different alkalis.

4.1 Sodium metaborate as an alternative alkali for ASP floods

In this section, the results obtained with sodium metaborate will be discussed. The motivation of this study was to develop surfactant formulations using sodium metaborate for sandstone and carbonate reservoirs, thus serving as an alternate to sodium carbonate in situations where sodium carbonate is not suitable or easily available. In addition, a particular focus of this study was to understand geochemical interactions of sodium metaborate in the presence of gypsum or anhydrite. Single-phase static and transport experiments were performed to understand geochemical interactions between sodium metaborate and gypsum. Surfactant formulations were developed which were used in static surfactant adsorption experiments, to compare sodium metaborate with sodium carbonate, and oil recovery corefloods. The list of experiments performed using sodium metaborate is shown in Table 4.1.

Table 4.1: List of experiments performed using sodium metaborate

Experiment	Description of experiment
4.1	Alkali interactions in the presence of gypsum at 53 °C using (a) No alkali (b) Na_2CO_3 (c) $NaBO_2$ (d) Na_2SiO_3+$Na_2B_4O_7$ (e) $NaBO_2$
4.2	Alkali interactions in presence of calcium chloride (a) NaBO2 fixed to 5000 ppm (b) Calcium fixed to 2000 ppm
4.3	Static surfactant adsorption results on Silurian dolomite (a) No alkali (b) Sodium metaborate (c) Sodium carbonate
4.4	Single-phase alkali flood in a carbonate core containing gypsum using (a) CH_3COONa (b) Na_2CO_3 (c) $NaBO_2$
4.5	Single-phase $NaBO_2$ flood in a carbonate core containing gypsum at varying flow rates
4.6	Single-phase $NaBO_2$ flood in a sandstone core containing gypsum

4.7	Surfactant phase behavior results using oil#1 with NaBO2 as alkali (a) IBA-3EO as cosolvent (b) IBA as cosolvent
4.8	Surfactant phase behavior experiments results obtained with crude oil-2
4.9	Oil recovery ASP coreflood CF-1 in a sandstone core containing gypsum using (a) surfactant formulation-4.6(a) at 1 ft/d (b) surfactant formulation-4.6(b) at 0.25 ft/d
4.10	Oil recovery ASP corefloods using formulation 4.8 (a) Tertiary ASP coreflood CF-3 (b) Secondary ASP coreflood CF-4

4.1.1 Static experiments

The use of sodium carbonate is often limited to sandstone reservoirs because carbonate reservoirs often contain gypsum, which dissolves to produce calcium ions which in turn precipitate on interacting with sodium carbonate. The purpose of these experiments was to understand the interaction of alternative alkalis with gypsum. Single-phase static experiments were first performed to screen the potential alkalis. These alkalis were later used for performing single-phase corefloods in sandstone and carbonate cores containing gypsum. Some of the parameters measured in these experiments include solution pH and ionic composition.

Experiment 4.1: Interactions of alkalis in the presence of gypsum

Static experiments were performed to screen potential alkalis for gypsum containing reservoirs. The list of alkalis tested includes sodium carbonate, sodium silicate, sodium metaborate, sodium hydroxide and their combinations as shown in Table 4.2. These alkalis were mixed with 1.25% sodium chloride and an excess amount of gypsum in plastic bottles and allowed to equilibrate at 53 °C for a given duration. After

equilibration, the supernatant solution was measured for pH and ionic composition. The detailed procedure followed to perform these experiments and measurements is described in chapter 3.

Experiment 4.1(a) serves as the base case where no alkali was added to the aqueous solution. The pH of the supernatant solution remained neutral, at 6.8, after 2 days and the calcium and sulfate concentrations were found to be about 1,082 ppm and 2,560 ppm, respectively. Note that the aqueous solutions consisted of only sodium chloride; no calcium or sulfate ions were initially added to the aqueous solution, and the presence of these ions in the supernatant solutions was due to the dissolution of gypsum. Similar experiments were performed with different alkalis, keeping their concentrations similar in molar terms. In the presence of sodium carbonate (case 4.1(b)), the pH decreased from the initial pH of about 11.4 to 8.1 within two days. In addition, the sulfate concentration increased to about 53,000 ppm, indicating the transition of sodium carbonate to calcium carbonate which decreased the pH and increased the sulfate ions concentration. The calcium concentration was about 441 ppm, indicating that sodium carbonate was possibly completely consumed. In the presence of sodium metaborate (case 4.1(c)), the pH remained at 10.9 and the calcium, boron and sulfate concentrations were found to be about 1,490 ppm, 2,490 ppm and 26,500 ppm, respectively, after 2 days of equilibration. The decrease in boron concentration from 6,400 ppm (corresponding to 3.84% sodium metaborate) to 2,490 ppm and the increase in sulfate concentration to 26,500 ppm indicated the precipitation of a calcium-boron compound. The pH stayed to about 10.9 in spite of the precipitation and not all the boron was consumed in the

presence of gypsum, unlike sodium carbonate. The concentrations remained about the same after equilibrating for 25 days. An experiment was similarly repeated using a lower concentration of sodium metaborate (case 4.1(e)) which showed a reduction in boron concentration from 2,100 ppm to 1,600 ppm. The pH, calcium and sulfate ions were found to be about 10.4, 1,600 ppm and 8,000 ppm, respectively, after 2 days. The supernatant solutions remained essentially the same after 25 days as well. A combination of sodium silicate and borax was tested in case 4.1(d) which showed the pH of 11.4 after 2 days. The calcium and sulfate concentrations were found to be about 695 ppm and 64,000 ppm, respectively, indicating excess precipitation of the alkali solution with gypsum. Sodium sulfate was added in case 4.1(f) with sodium metaborate to suppress gypsum dissolution by the common-ion effect. The sulfate ions in the supernatant were about 39,000 ppm (about 10,000 from Na_2SO_4, rest from gypsum dissolution), a value similar to that observed in case 4.1(c), suggesting that sodium sulfate did not help in suppressing gypsum dissolution in this case. The equilibrium was instead controlled by the precipitation of calcium-boron complex. These experiments showed that, among the alkalis that were tested, sodium metaborate was most suitable in the presence of gypsum because it maintained a high pH and did not show as much reactivity towards gypsum, especially at a lower concentration, as sodium silicate or sodium carbonate.

Table 4.2: Static experiments with alkalis in presence of gypsum

	Alkali	Alkali (wt%)	Alkali (M)	Day 2				Day 25		
Experiment				pH	Ca (ppm)	B (ppm)	SO4 (ppm)	pH	Ca (ppm)	SO4 (ppm)
4.1 (a)	No Alkali	-	-	6.8	1,082	-	2,560	6.9	850	2,600
4.1 (b)	Na_2CO_3	6.11	0.58	8.1	441	-	53,302	8.3	-	52,692
4.1 (c)	$NaBO_2$	3.84	0.58	10.9	1,489	2,490	26,551	10.9	1,497	22,105
4.1 (d)	Na_2SiO_3 +$Na_2B_4O_7$	3.52 +5.82	0.28+ 0.15	11.4	695		64,146	-	-	-
4.1 (e)	$NaBO_2$	1.28	0.19	10.4	1,604	1,594	7,974	10.3	1,324	6,934
4.1(f)	$NaBO_2$ + Na_2SO_4	3.0 + 1.5	0.45 + 0.10	10.95	1,600	2,698	39,350	10.9	-	-

Experiment 2: Alkali interactions in presence of calcium chloride

Since gypsum is only sparingly soluble in water, it was not possible to differentiate the precipitate that formed due to the reactions with alkali from the solid, which was initially present in the samples. Therefore, another set of experiments was performed by using calcium chloride, instead of gypsum, since calcium chloride is soluble in water. These experiments were performed mainly with sodium metaborate as it was found to be most effective from the previous results. In experiment 4.2(a), the amount of sodium metaborate was fixed to 5000 ppm and the calcium chloride was increased up at 5,000 ppm using calcium chloride. In experiment 4.2(b), the calcium concentration was kept fixed to 2,000 ppm and the sodium metaborate amount was

increased up to 5,000 ppm. The results of these experiments are shown in Figures 4.1(a) and 4.1(b), respectively. Calcium precipitation was observed on addition of sodium metaborate. A decrease in both calcium and boron concentrations was observed on increasing the calcium concentration (Figure 4.1(a)); more decrease in both calcium and boron concentrations at higher initial calcium concentrations. Similarly, it can be seen from Figure 4.1(b) that calcium loss was higher at a higher boron concentration. The calcium concentration in the presence of 3,330 ppm and 5,000 ppm sodium metaborate was found to be about 490 ppm and 436 ppm, respectively. These results further confirmed that calcium ions precipitate in the presence of sodium metaborate. The calcium ions, however, did not completely precipitate even in the excess sodium metaborate, unlike with sodium carbonate. The pH of these solutions remained at from about 10.5 to 10.7.

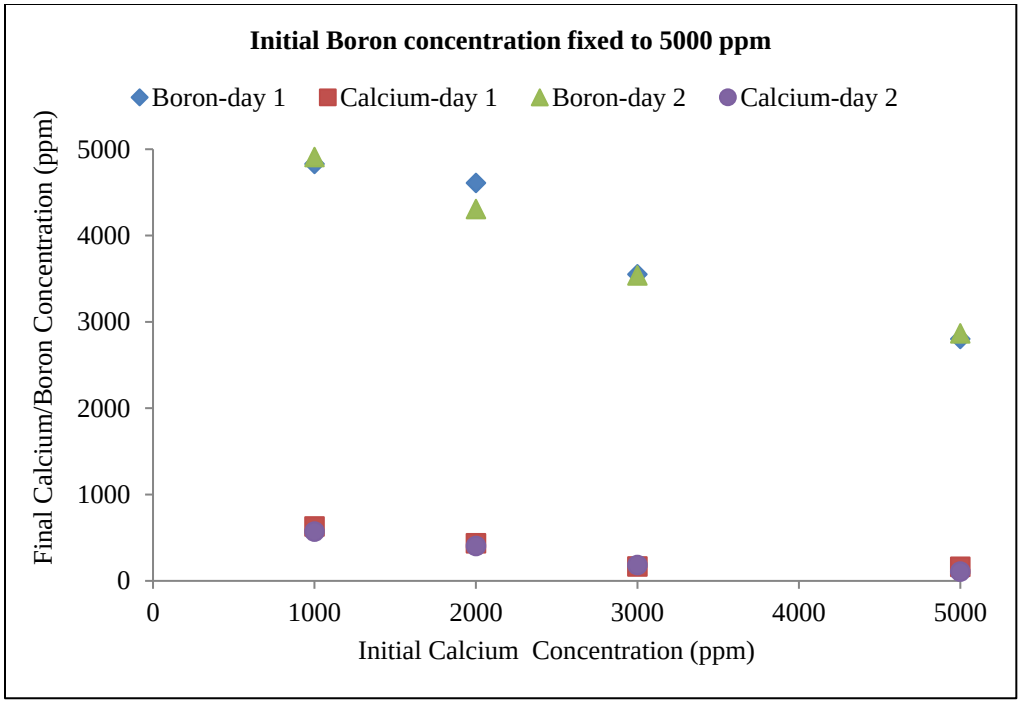

Figure 4.1(a): Effect of increasing initial calcium concentration on calcium and boron concentration in the aqueous solutions

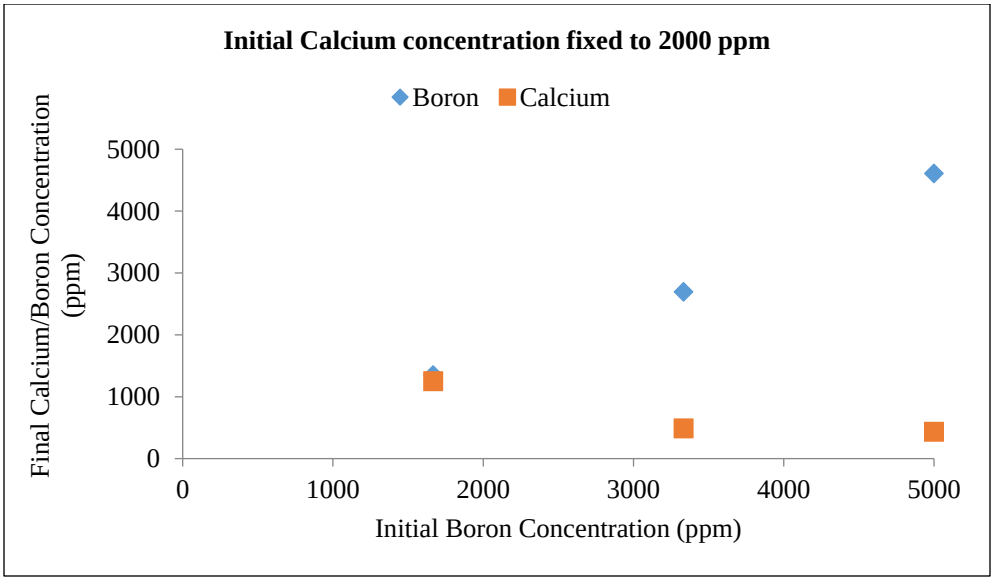

Figure 4.1(b): Effect of increasing initial NaBO2 concentration on calcium and total boron concentration in the aqueous solutions

Experiment 4.3: Static surfactant adsorption results on Silurian dolomite (a) No alkali (b) Sodium metaborate (c) Sodium carbonate

Static surfactant adsorption experiments were performed near the optimum salinity to compare sodium metaborate and sodium carbonate in terms of their effectiveness in reducing surfactant adsorption on Silurian dolomite. Note that this experiment was performed to screen potential alkalis and the adsorption numbers, by themselves, may not apply to oil recovery corefloods. Crushed Silurian dolomite of 140-200 mesh size and 0.4 m^2/g specific surface area was mixed with surfactant solution keeping the solid to liquid ratio of 1 (3 grams each). The surfactant formulation consisted of C_{12-13}-7PO-SO_4 and C_{12-13}-13PO-SO_4 surfactants. The total surfactant concentration was varied from 0.25 wt% to 1 wt%, keeping the alkali (or NaCl) concentration fixed. The results showed that both sodium metaborate and sodium carbonate were equally effective in lowering the surfactant adsorption (see Figure 4.2). The surfactant adsorption in the absence of alkali was about 1.0-1.3 mg/g rock. On adding sodium carbonate, it reduced to about 0.4-0.8 mg/g rock. Similarly, on adding sodium metaborate, the surfactant adsorption reduced to about 0.5-0.6 mg/g rock. These results show that sodium metaborate can be equally effective in lowering the surfactant adsorption on Silurian dolomite surfaces.

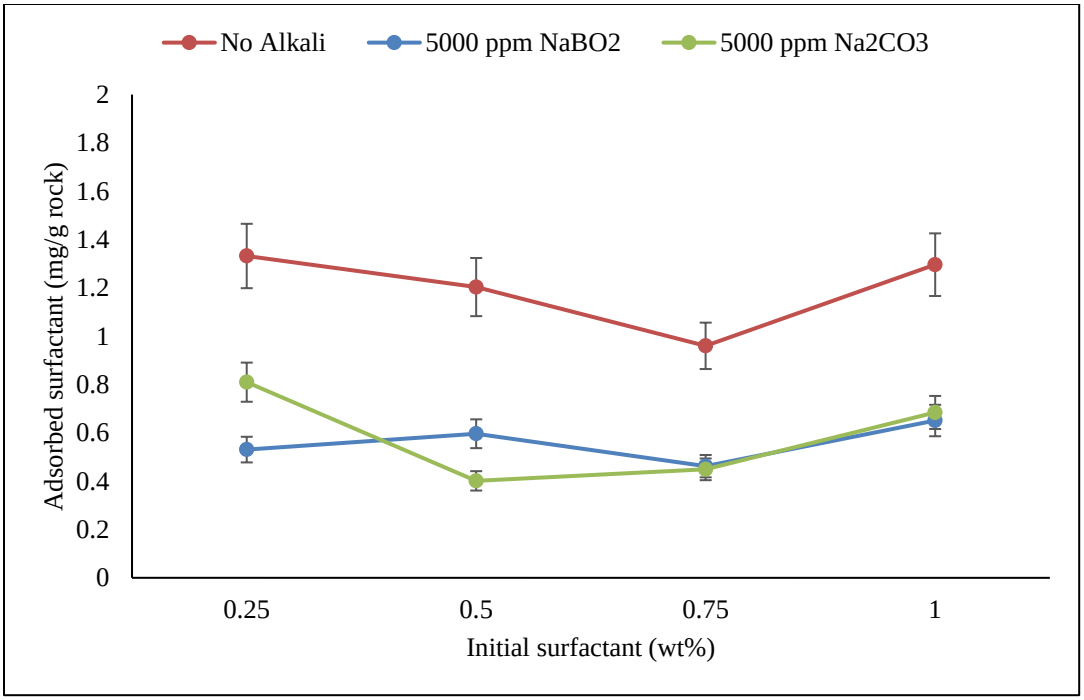

Figure 4.2: Static surfactant adsorption on Silurian dolomite using no alkali, sodium carbonate and sodium metaborate

4.1.2 Single-phase alkali transport experiments

Alkali transport experiments were performed in sandstone and carbonate cores containing gypsum. In these experiments, alkali solutions were continuously injected in the core and effluent pH and ions, and pressure drop across the core was measured. The experimental procedure for conducting these experiments is described in detail in chapter 3. The purpose of these experiments was to study the reactions of these alkalis in a dynamic mode and, equally importantly, to understand if reactions reach equilibrium at the velocity of 1 ft/d which is typically used in laboratory coreflood experiments. Sodium metaborate and sodium carbonate were injected in a carbonate core containing gypsum.

In addition, sodium acetate was used in experiment 4.4 to perform a similar coreflood as sodium acetate had shown to maintain a pH of about 8.5-9 and tolerate divalent ions (Winters, 2012). The change in permeability was carefully monitored in single-phase corefloods.

Experiment 4.4: Single-phase alkali floods in a carbonate core containing gypsum (a) Sodium acetate (b) Sodium carbonate (c) Sodium metaborate

In this experiment, various alkalis were injected through a carbonate core containing gypsum at 0.167 ft/d. The compositions of formation brines and injected alkali solutions, core properties and experimental conditions are given in Table 4.3 and 4.4. At the end of each flood, the core was cleaned by injecting several pore volumes of sodium chloride solution. The effluent pH, sulfate and calcium compositions from this experiment are shown in Figures 4.3-4.5. From Figure 4.3, it can be seen that the effluent pH on injecting sodium acetate was about 8 even after 3 pore volumes, lower than the injected pH of 8.21. Since this pH was not high enough for performing ASP floods, sodium acetate was not pursued further as an alternative to conventional alkalis. A possible reason for not seeing a high pH propagation with sodium acetate is that its pKa is around 4.8, much lower than 8.5. The effluent sulfate and calcium concentrations on injecting sodium acetate were about 100 ppm and 400 ppm, respectively, as shown in Figures 4.4 and 4.5, respectively. The scatter in the calcium ions data in Figure 4.5 is possibly due to dilution error, especially due to low calcium concentrations. Note that no calcium or sulfate ions were included in the sodium acetate solution and the presence of these ions in the effluents indicates the presence of gypsum in the core.

The effluent pH on injecting sodium carbonate was found to be about 10.3 after 3 pore volumes, lower than the injected pH of 10.8. From Figure 4.3, it can be seen that the effluent pH increased gradually due to the interaction of sodium carbonate with gypsum. These interactions were more evident from the effluent sulfate data shown in Figure 4.4, which showed an increase in sulfate concentration from about 440 ppm to 22,000 ppm as the formation brine was displaced with sodium carbonate. A corresponding decrease in calcium ions was observed, indicating the precipitation of calcium carbonate.

The effluent pH on injecting sodium metaborate solution was found to be 9.2 at 1 pore volume and reached a steady state value of about 9.6 at 1.5 pore volume, indicating a good pH propagation. The effluent sulfate and calcium ions were found to be about 800 ppm and 100 ppm, respectively. Note that the effluent sulfate concentration on using sodium metaborate was much lower than that with sodium carbonate showing that sodium metaborate did not interact with gypsum as much as sodium carbonate. In addition, good pH propagation was observed with sodium metaborate. These preliminary results indicated the possibility of using sodium metaborate for ASP floods in the presence of gypsum. Additional experiments were therefore performed in other cores (containing gypsum) using sodium metaborate.

Table 4.3: Composition of formation brine and injected solutions

Salts (ppm)/Brines	Formation brine	Sodium carbonate solution	Sodium metaborate solution	Sodium acetate solution
NaCl	30,000	30,000	30,000	30,000
Na2CO3	-	30,000	-	-
NaBO2	-	-	30,000	-
CH3COONa	-	-	-	30,000
TDS (ppm)	**30,000**	**60,000**	**60,000**	**60,000**

Table 4.4: Properties of the core used in experiment 4.3

Core	Length (inches)	Diameter (inches)	Porosity (%)	Permeability (md)	Temperature (°C)	Gypsum
Carbonate	3.0	1.5	24	101	50	Yes

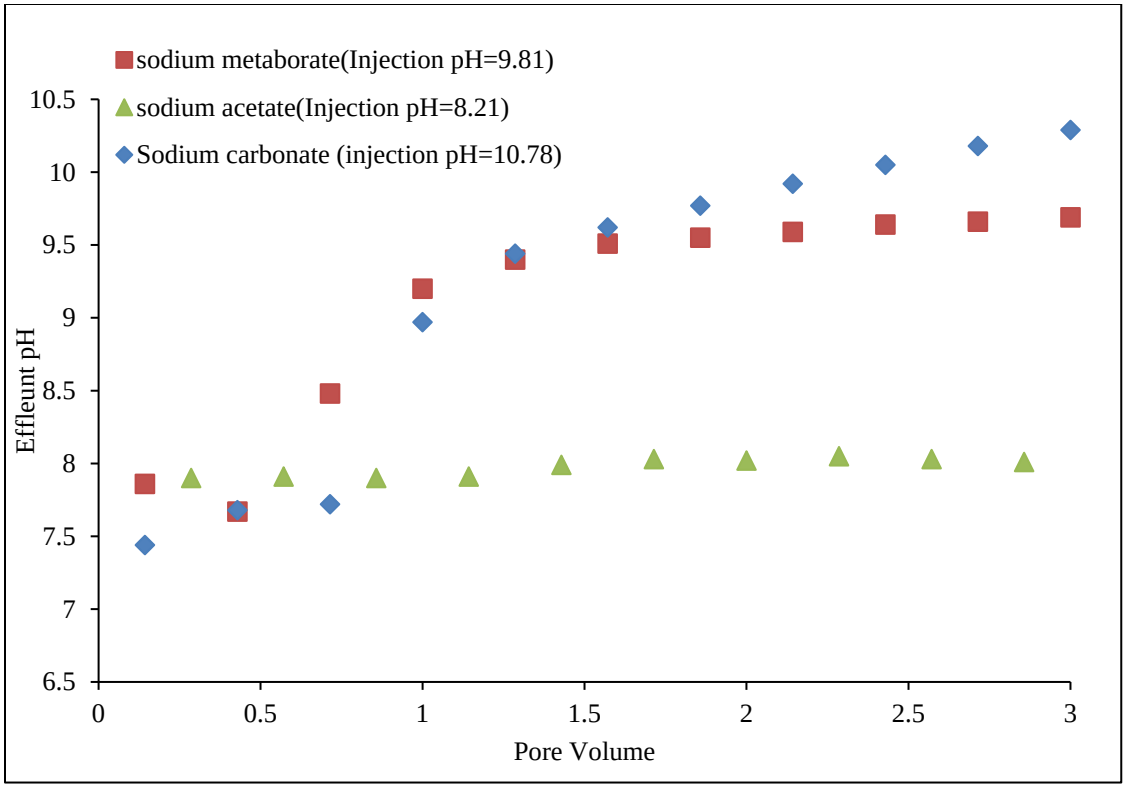

Figure 4.3: Effluent pH on injecting sodium metaborate, sodium carbonate and sodium acetate in a carbonate core containing gypsum at 50 °C

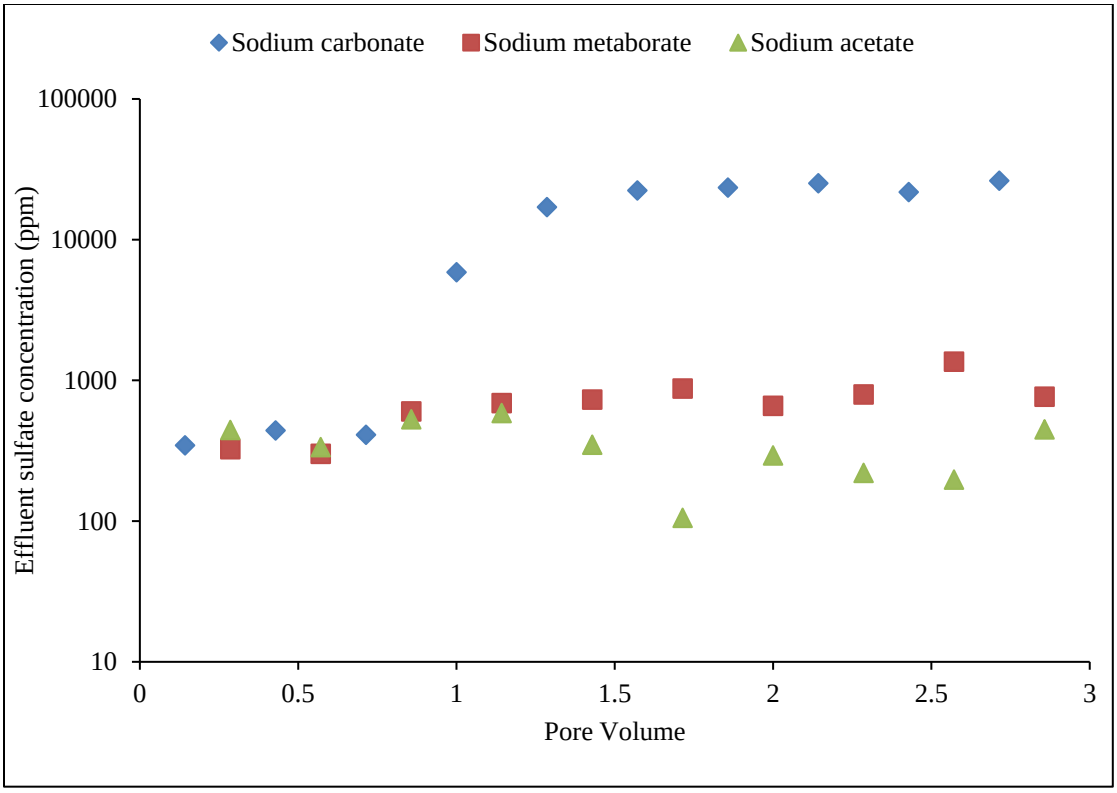

Figure 4.4: Effluent sulfate ions on injecting sodium carbonate, sodium metaborate and sodium acetate in a carbonate core with gypsum at 50 °C

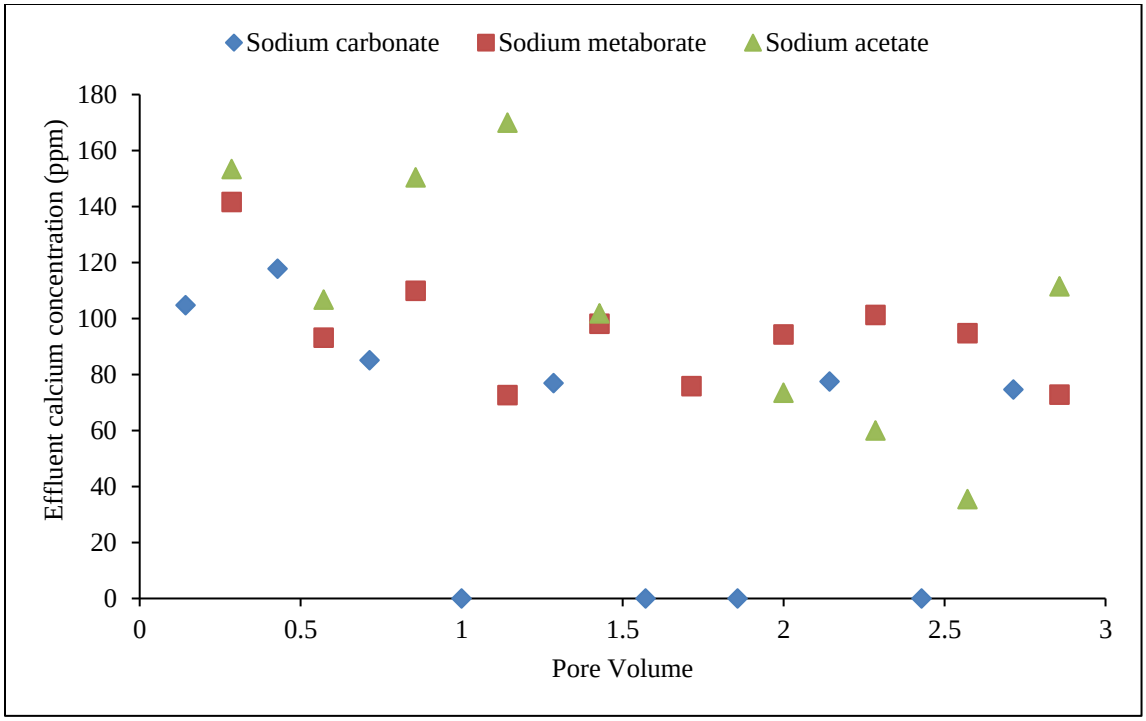

Figure 4.5: Effluent calcium ions on injecting sodium metaborate, sodium carbonate and sodium acetate in a carbonate core containing gypsum at 38 °C

Experiment 4.5: Single-phase sodium metaborate flood in a carbonate core containing gypsum at varying flow rates

Sodium metaborate was injected into another carbonate core to obtain further insights into its interactions in the presence of gypsum. The composition of the formation brine and the injected alkali solution, core properties and experimental conditions are given in Table 4.5 and 4.6. The core was initially saturated with 10,000 ppm NaCl brine and shut-in for one day. The core was then flushed with 10,000 NaCl brine, and effluent samples were analyzed for calcium and sulfate concentrations to confirm the presence of gypsum (Table 4.7). From Table 4.7, it can be seen that equal moles of calcium and

sulfate ions were present in the effluent samples indicating the presence of gypsum. The core was then continuously flooded with the alkali solution at 0.67 ft/day and the effluent pH, calcium, sulfate and total boron concentrations were measured. The effluent pH results, shown in Figure 4.6, showed an increase in pH to 10.3 at 1 pore volumes and 10.8 at 1.5 pore volumes, after which it became steady. The effluent boron concentration, shown in Figure 4.7, showed that it also broke through at about 1 pore volumes and reached the injected concentration at about 1.5 pore volumes indicating no noticeable delays in its transport. The effluent calcium and sulfate ions are shown in Figures 4.8 and 4.9. The calcium concentration decreased from about 800 ppm, in the formation brine, to about 320 ppm when sodium metaborate was injected due to the precipitation of calcium-boron compound. This is clearer from Figure 4.9 which shows the molar concentrations of effluent ions. It can be seen that initially calcium and sulfate amounts were equal (about 22 mM at 0.4 pore volumes) because both the ions resulted from the dissolution of gypsum. On injecting sodium metaborate, the calcium amount decreases from 22 mM to 7.9 mM while sulfate decreases from about 22 mM to 12.5 mM; more decrease in calcium ions compared to sulfate ions indicating calcium precipitating on injecting sodium metaborate. Note that sulfate ions did not interact with other ions or the rock surface in this particular system and therefore they served as a reference to compare the extent of calcium precipitation in these experiments. Any decrease in calcium concentration compared to sulfate, in molar terms, indicated calcium precipitation. The decrease in sulfate concentration itself on injecting sodium metaborate was possibly due to the decrease in salinity when the formation brine was displaced with sodium

metaborate solution; gypsum was found to be more soluble at high salinity. This dissolution behavior of gypsum is discussed in detail in the second part of this chapter.

Table 4.5: Composition of formation brine and injected solutions

Salts (ppm)/Brines	Formation brine	Sodium metaborate solution
NaCl	10,000	10,000
NaBO2	-	30,000
TDS (ppm)	**10,000**	**40,000**

Table 4.6: Properties of the core used in experiment 4.4

Core	Length (inches)	Diameter (inches)	Porosity (%)	Permeability (md)	Temperature (°C)	Gypsum
Carbonate	7.93	1.485	19.3	68	55	Yes

Table 4.7: Effluent calcium and sulfate ions on injecting NaCl brine through the core

Sample #	SO4 (ppm)	Ca (ppm)	SO4 (mM)	Ca (mM)
1	6256.14	2660.24	65.168125	66.506
2	5873.39	2628.15	61.18114583	65.70375
3	5952.83	2381.75	62.00864583	59.54375
4	5870.56	2474.29	61.15166667	61.85725

Table 4.8: Core permeability at the beginning and end of experiment 4.4

Experiment	Core permeability (md)
Initial permeability	68
Permeability after injecting 4 pore volumes of NaBO2 at 1 ft/d	61
Permeability after injecting 6 pore volumes of NaBO2 at slow velocities	57

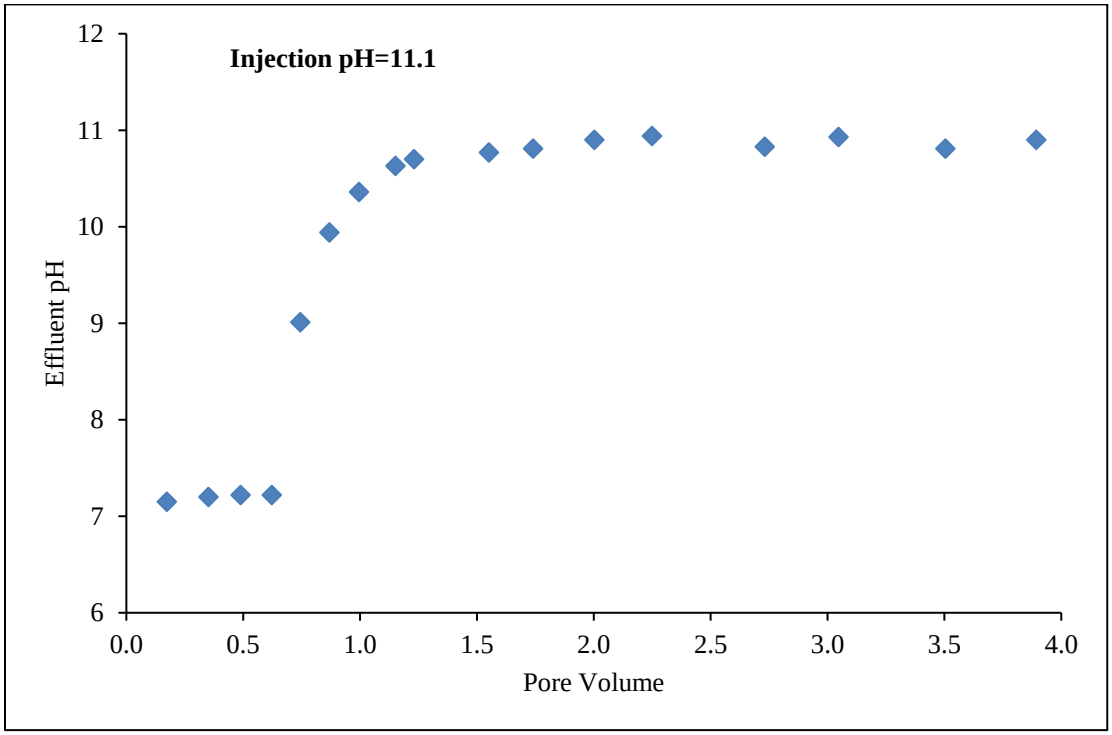

Figure 4.6: Effluent pH on injecting NaBO2 (experiment 4.4) in a carbonate core containing gypsum at 0.67 ft/d

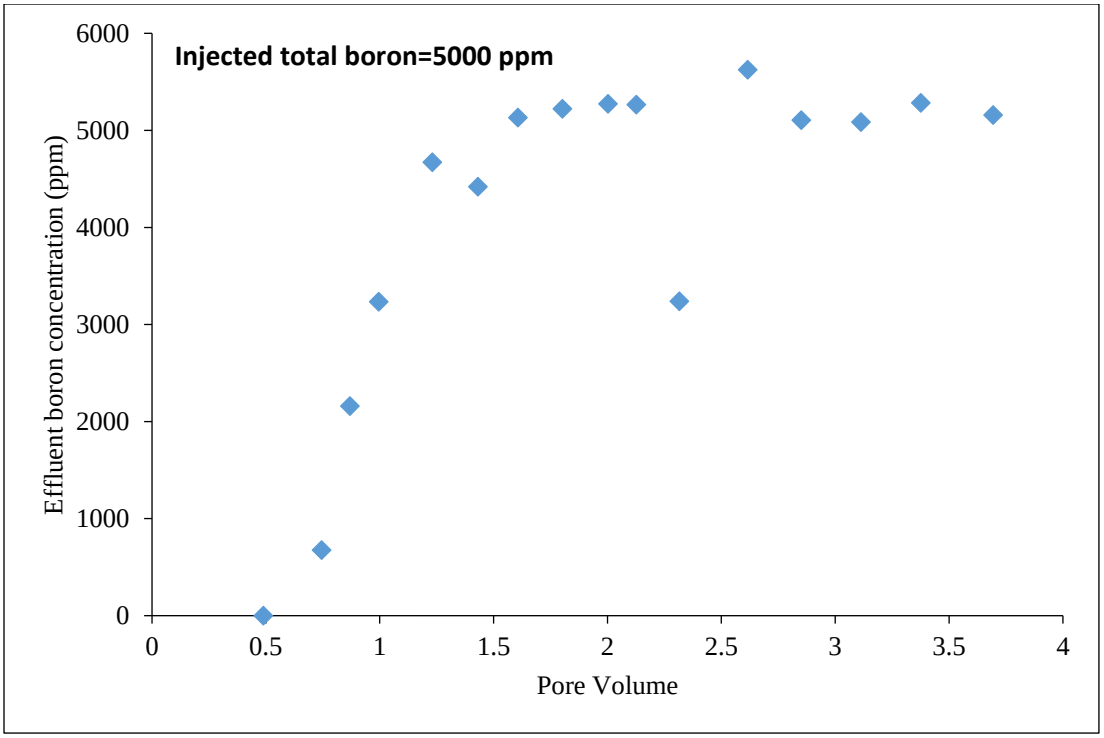

Figure 4.7: Effluent boron concentration on injecting NaBO2 (experiment 4.4) in a carbonate core containing gypsum at 0.67 ft/d

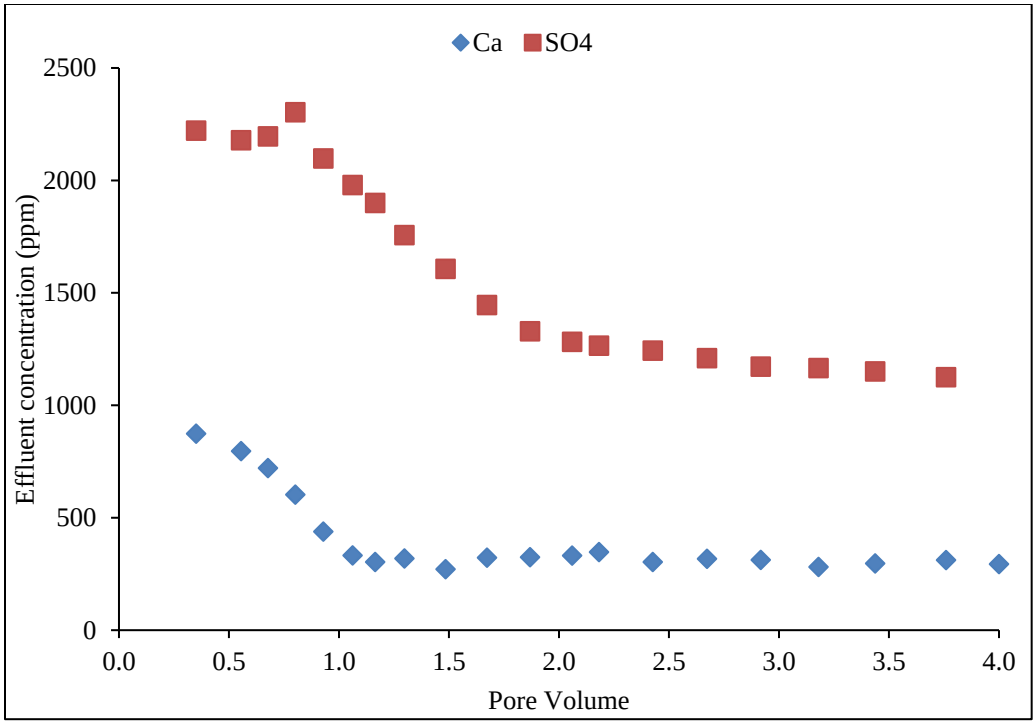

Figure 4.8: Effluent calcium and sulfate concentrations on injecting NaBO2 (experiment 4.4) in a carbonate core containing gypsum at 0.67 ft/d

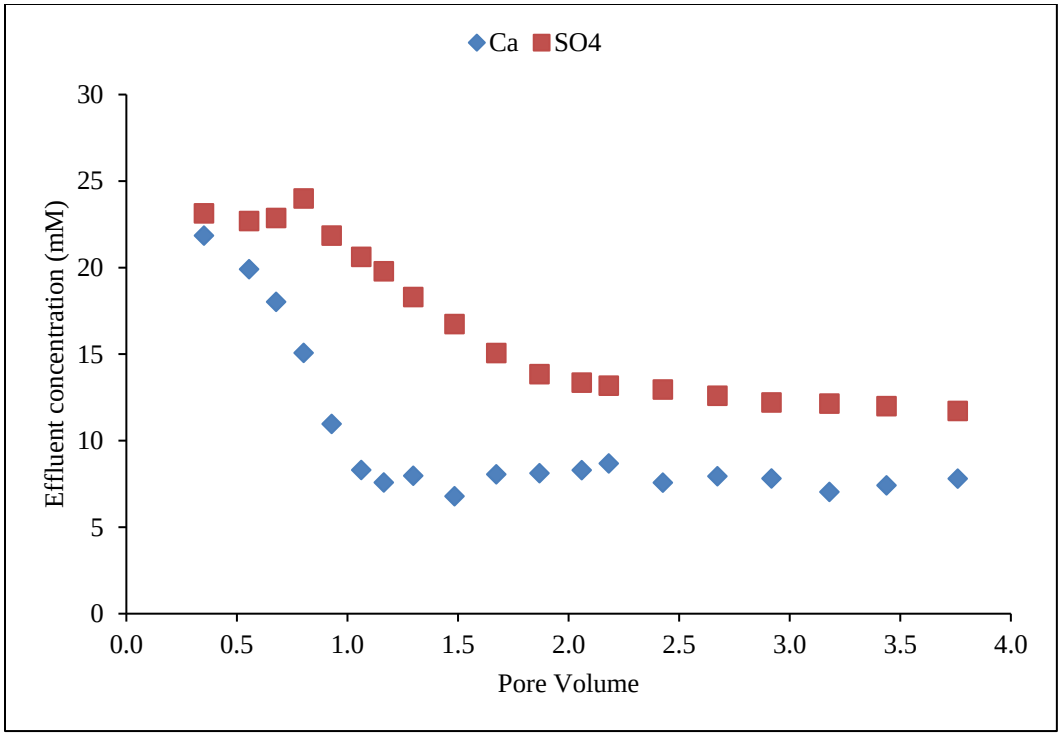

Figure 4.9: Effluent calcium and sulfate concentrations in mM on injecting NaBO2 (experiment 4.4) in a carbonate core containing gypsum at 0.67 ft/d

The core was cleaned by injecting many pore volumes of sodium chloride brine and the effluent pH, salinity, and ions were monitored. A reason to perform this test was to understand if the precipitation of calcium in the presence of sodium metaborate was reversible or irreversible. The effluent salinity and pH data (Figure 4.10) shows that the effluent salinity decreased to the injected amount in about 1.5 pore volumes after starting the cleaning process. The pH, however, stayed to about 9.3 even after injecting 2.3 pore volumes of the 10,000 ppm NaCl brine. The calcium and sulfate concentrations were almost equal after injecting 2 pore volumes of the brine, as expected due to gypsum dissolution and no boron was detected indicating that the core was cleaned (Figures 4.11 and 4.12). It further indicates that at this injection rate, the re-dissolution of precipitated

calcium-boron complex was insignificant; else the boron concentration would have stayed at a non-zero concentration and calcium ions must have been higher than sulfate.

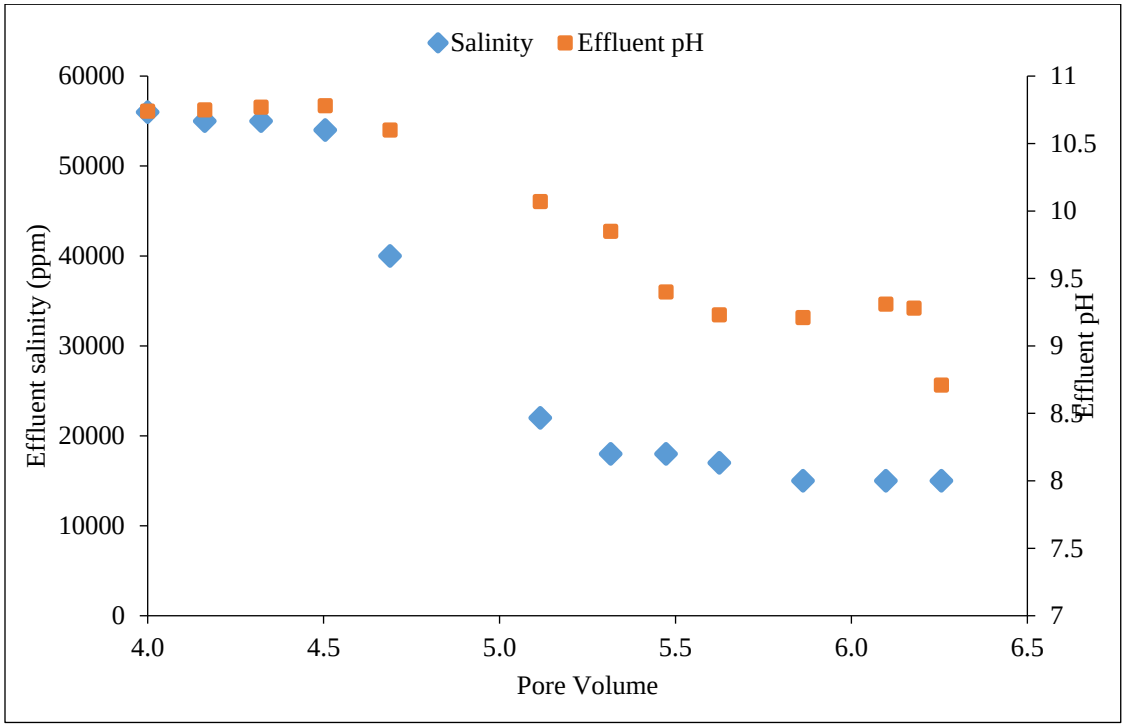

Figure 4.10: Effluent salinity and pH when the core was cleaned after injecting 4 pore volumes of NaBO2 at 0.67 ft/d

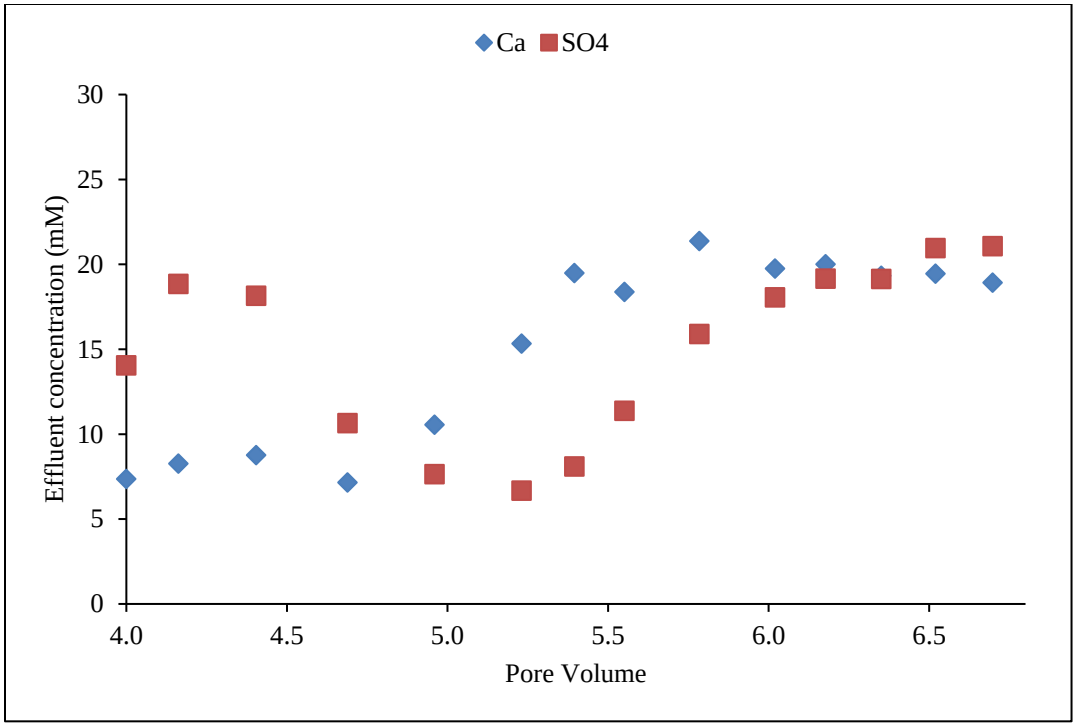

Figure 4.11: Effluent calcium and sulfate concentrations when the core was cleaned after injecting 4 pore volumes of NaBO2 at 0.67 ft/d

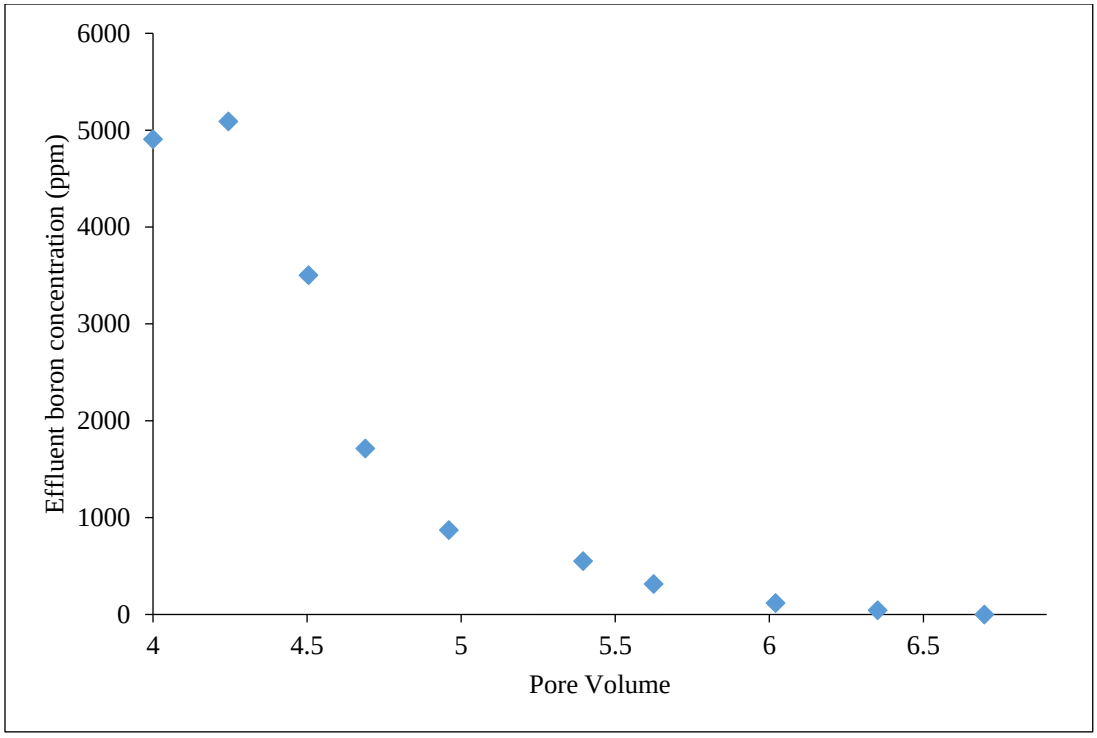

Figure 4.12: Effluent boron concentration when the core was cleaned after injecting 4 pore volumes of NaBO2 at 0.67 ft/d

The experiments so far showed sodium metaborate to perform well in cores containing gypsum, both in terms of pH propagation and permeability change. These experiments were performed keeping the residence time of the alkali solution inside the core to about 1 day. In the field, however, the residence time of the injected fluids is much higher than a day. Therefore, slow flow rate experiments were performed to understand the long-term interactions of sodium metaborate in the presence of gypsum. After cleaning the core, sodium metaborate solution was continuously injected at varying flow rates and the effluent pH, calcium and sulfate ions were measured. At least 2 pore volumes were injected at a given rate. The results are shown in Figures 4.13 and 4.14. Figure 4.13 shows effluent pH data, and calcium and sulfate concentration in molar

terms. It can be seen that at a slower injection rate, the difference between sulfate and calcium concentrations increased; indicating that more calcium precipitated at a slower injection rate. The steady state values of sulfate ions were found to be about 35 mM (3,400 ppm), 22 mM (2,100 ppm) and 15 mM (1,440 ppm) corresponding to the injection rates of 0.1 ft/d, 0.17 ft/d and 0.32 ft/d, respectively. The calcium concentration, on the other hand, reached a steady state value of about 7 mM (280 ppm). These results showed that equilibrium was not achieved in the previous floods which was performed on injecting sodium metaborate at 1 ft/d. The pH in all the different flow rates was steady at around 10.3. The steady state sulfate concentrations were plotted, as an indication of the extent of reaction, with the corresponding injection rates to estimate if an equilibrium was achieved at the slowest velocity of 0.01 ft/d in these experiments. The results (Figure 4.15) show a linear trend between effluent sulfate and injection rate, indicating that equilibrium was not reached even at the slowest flow rate.

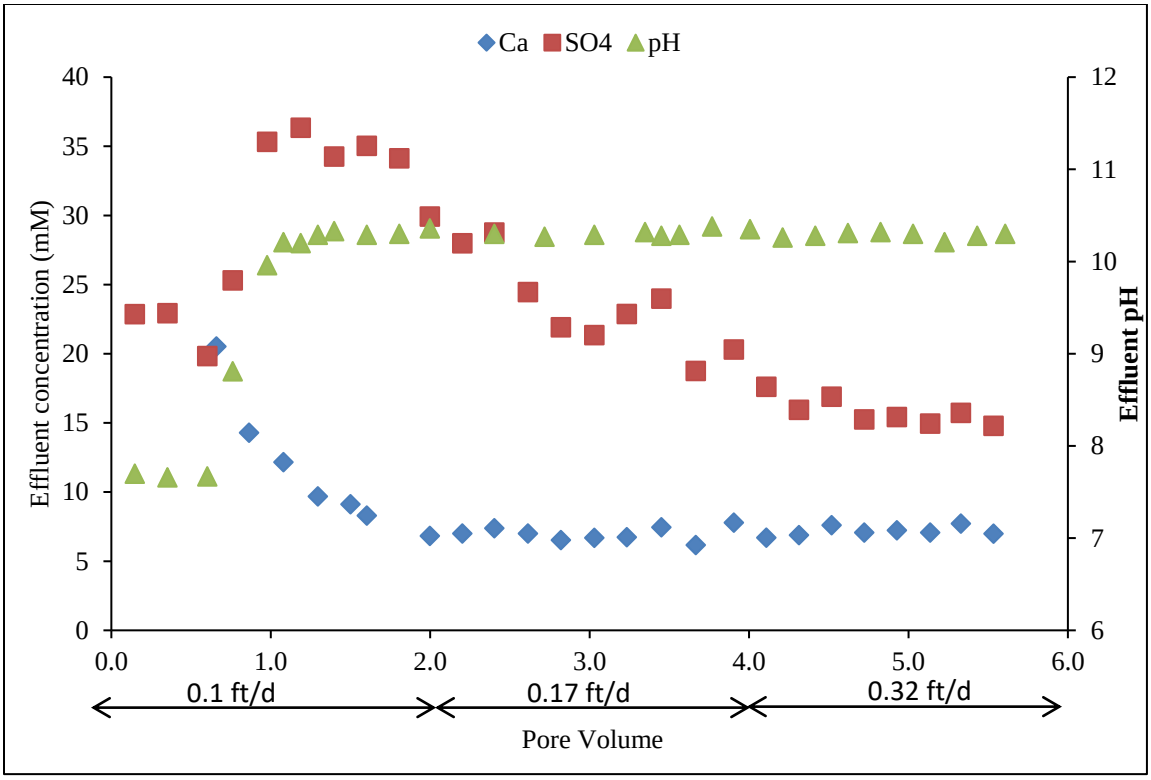

Figure 4.13: Effluent pH, calcium and sulfate ions concentrations on injecting sodium metaborate at different injection rates in a carbonate core containing gypsum

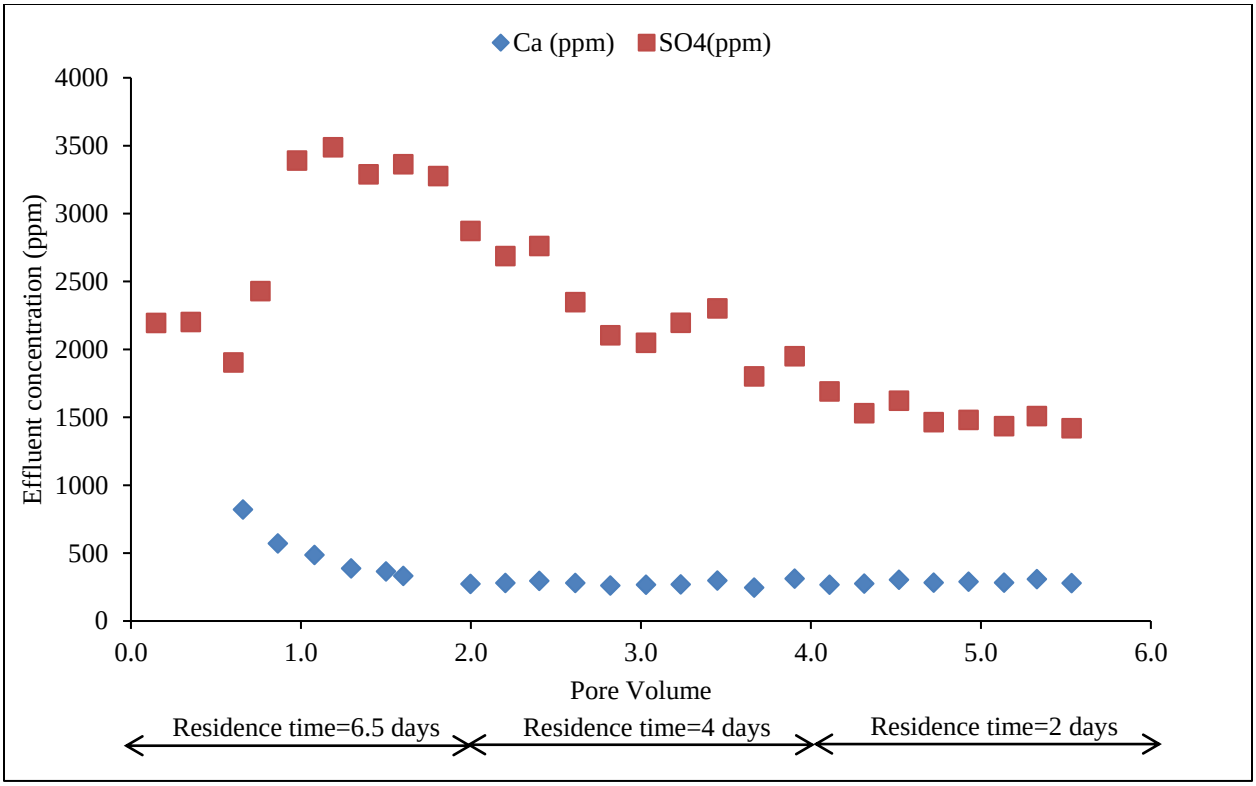

Figure 4.14: Effluent calcium and sulfate ions on injecting sodium metaborate in a core with gypsum at different injection rates

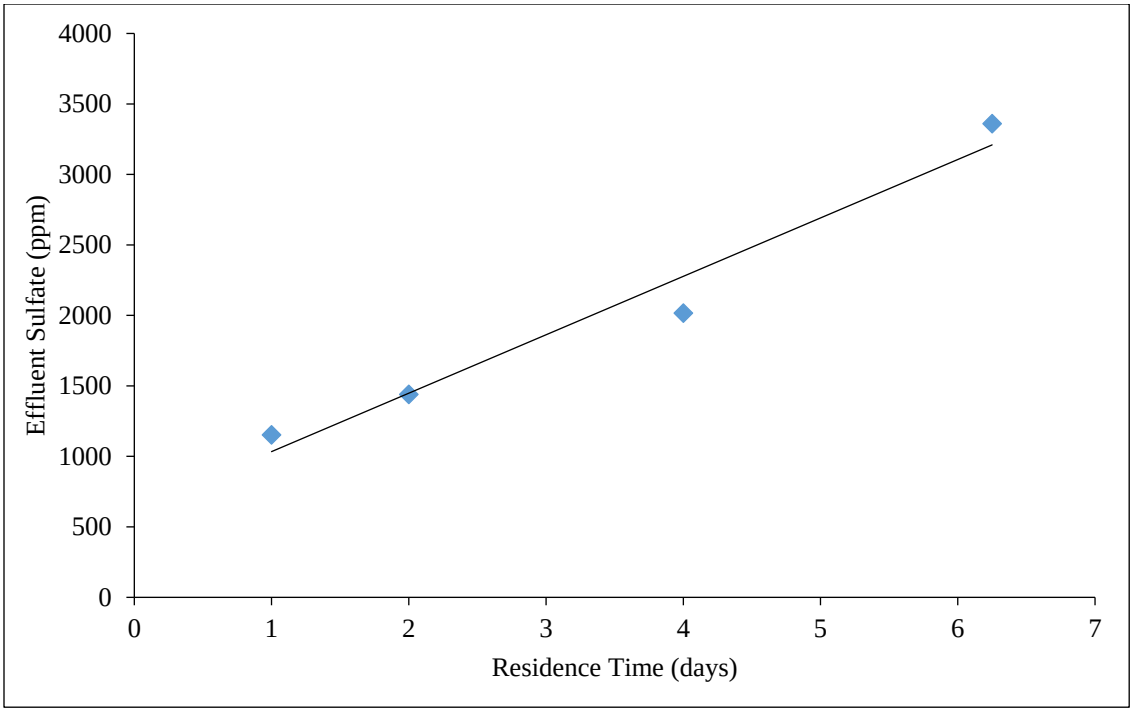

Figure 4.15: Effluent sulfate ions on injecting sodium metaborate in a core with gypsum as a function of residence time

Another experiment was therefore repeated at an even slower injection rate of 0.044 ft/d, corresponding to the residence time of 15 days. The effluent pH and ion data is shown in Figures 4.16 and 4.17, respectively. Figure 4.17 shows that the pH stayed at about 10.0 even at 0.044 ft/d injection velocity. The effluent sulfate ions, however, increased further to about 5,000 ppm, indicating that even more calcium was getting precipitated at this flow rate, compared to the previous experiment. The effluent calcium concentration was about 150 ppm after 2 pore volumes. The steady state sulfate values were again plotted with the corresponding injection rates (Figure 4.18), which showed that the reactions were approaching towards equilibrium at this flow rate. The

approximate equilibrium sulfate concentration was found to be about 5,500 ppm on extrapolating the curve. Very little change in the permeability was observed during this experiment; from 68 md at the beginning of the experiment to 56 md at the end (Table 4.8).

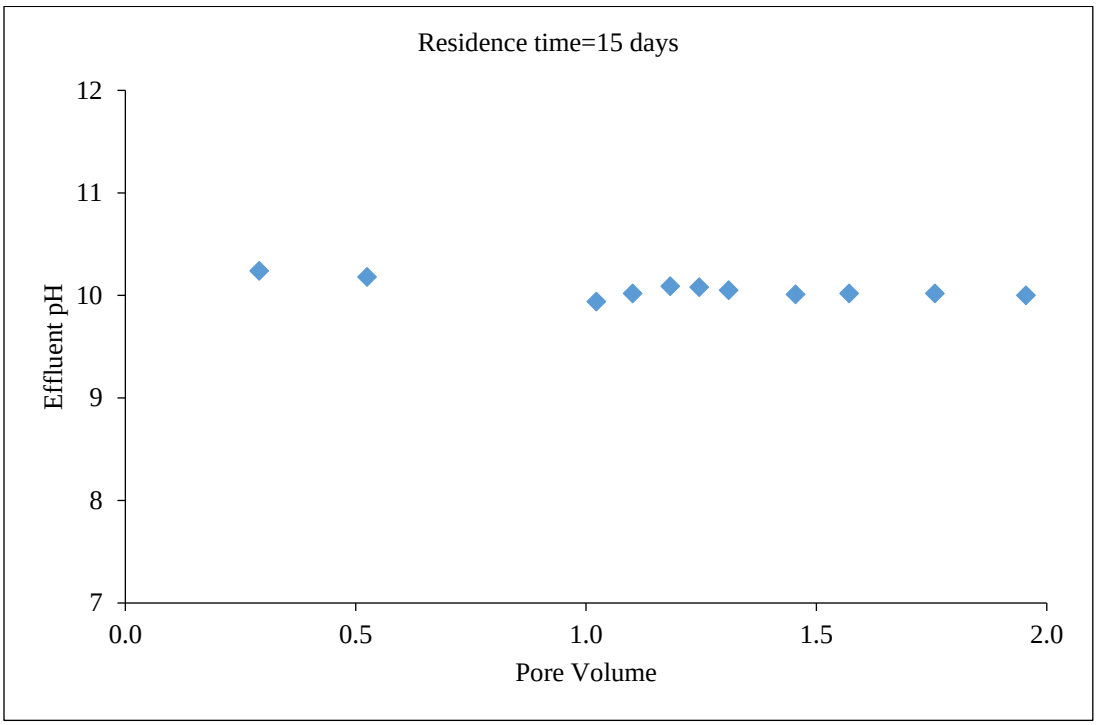

Figure 4.16: Effluent pH on injecting sodium metaborate at 0.044 ft/d in a carbonate core with gypsum

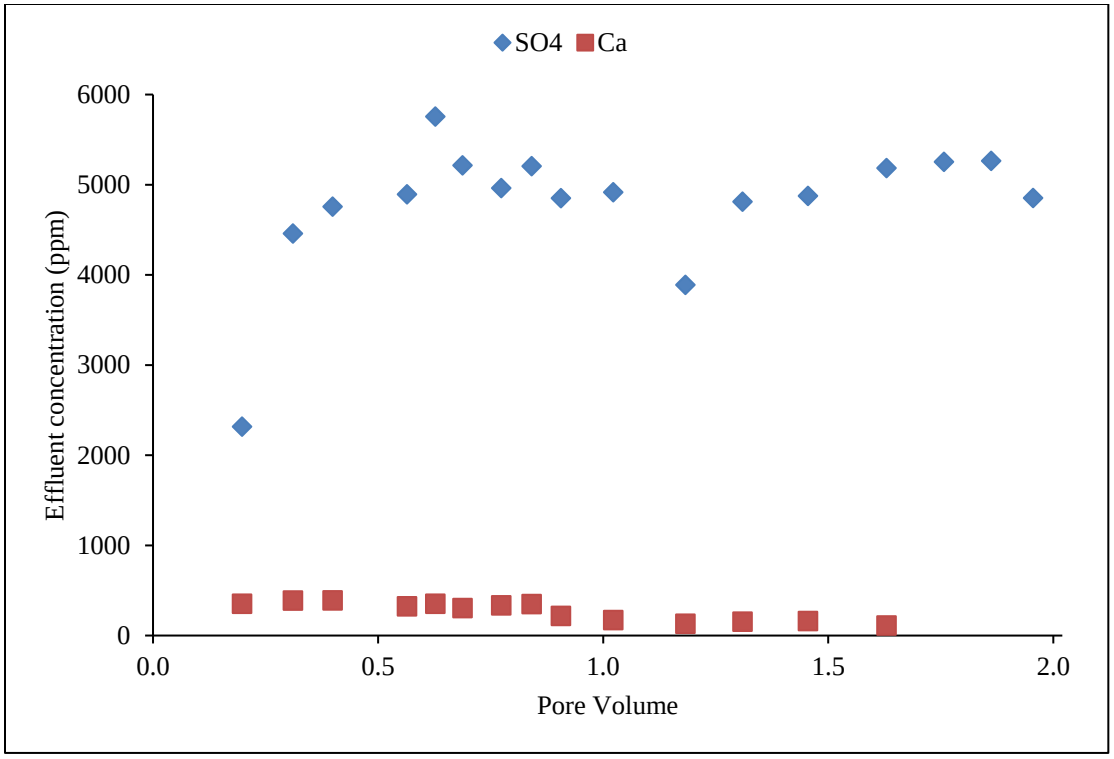

Figure 4.17: Effluents calcium and sulfate ions on injecting sodium metaborate at 0.044 ft/d through a carbonate core with gypsum

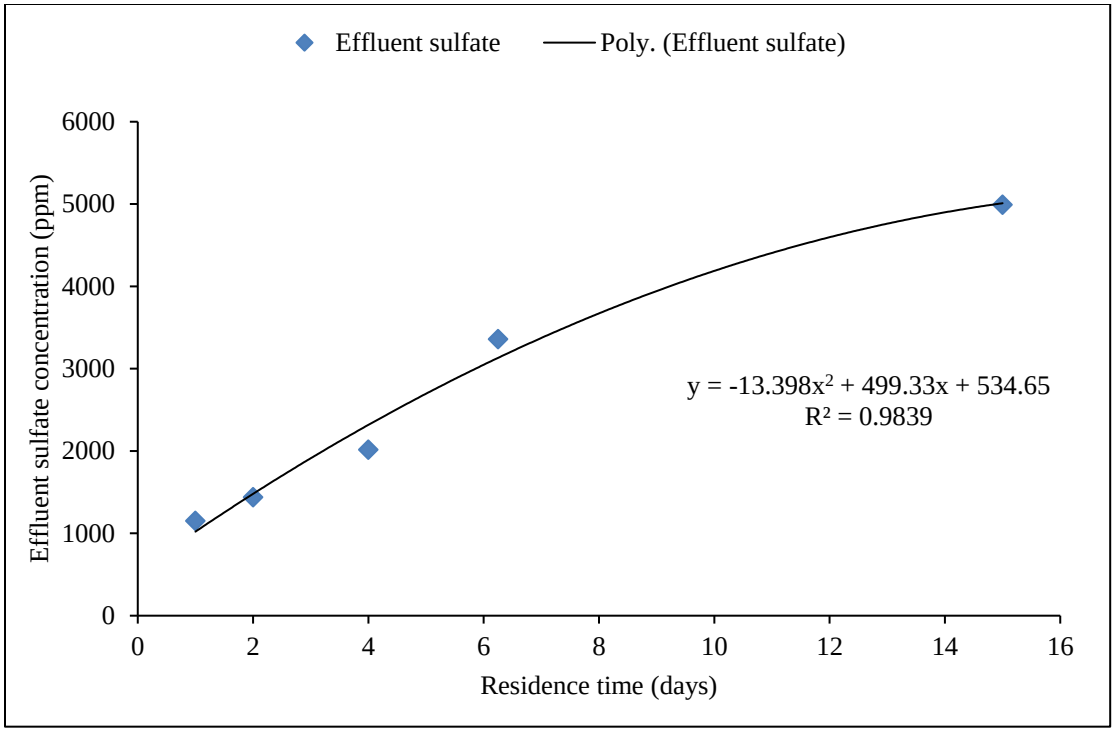

Figure 4.18: Effluent sulfate concentration as a function of residence time on injecting sodium metaborate in a carbonate core with gypsum

Some precipitate was observed in the tubes containing the effluent samples after they cooled down to room temperature. The precipitate was re-dissolved by acidifying the samples before the ions were measured by ion chromatography. Solid particles from a few samples were analyzed using SEM-EDS to estimate their compositions. Figure 4.19(a) shows the SEM image and 4.20 shows the elemental composition of the precipitate. It can be seen from Figure 4.19 that the precipitate appeared amorphous. The exact composition of the precipitate was not obtained from the elemental analysis. However, it mainly contained calcium (Figure 4.19(b)).

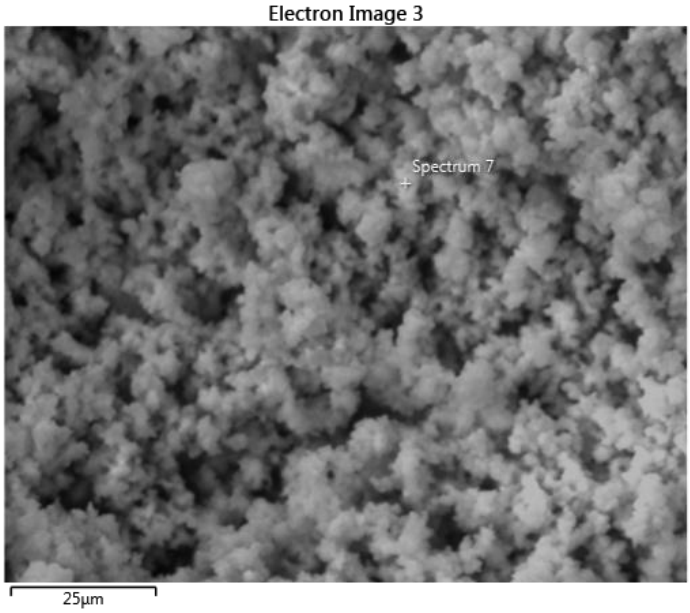

Figure 4.19(a): SEM image of the precipitate observed in effluent samples obtained on injecting sodium metaborate in a carbonate core with gypsum

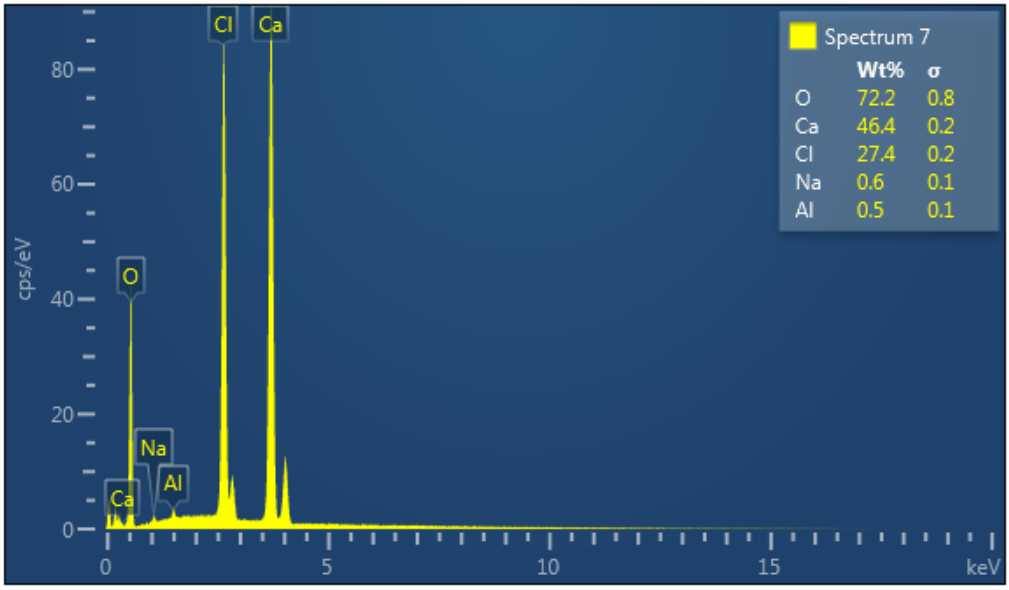

Figure 4.19(b): Elemental composition of the precipitate shown in Figure 4.19(a)

Experiment 4.6: Single-phase sodium metaborate injection in sandstone core with gypsum

Sodium metaborate showed high pH propagation in the static and dynamic experiments and even though calcium precipitation was observed, very little change in permeability was observed as a result of the precipitation; far less than sodium carbonate. As a result, sodium metaborate was used for conducting ASP corefloods in a sandstone core containing gypsum. The properties of the core and the experimental conditions are shown in Table 4.9. Single-phase sodium metaborate flood was first performed at 1 ft/d in the core to confirm that the results in this core were in agreement with the previous results. The compositions of the formation brine and the injected alkali solution are given in Table 4.10. The results of the single-phase alkali transport experiment showed good pH propagation and no plugging in the core as shown in Figure 4.20(a). The pH increased to 9.7 and 10.4 after 1 and 1.5 pore volumes, respectively. The pressure drop remained constant at about 1.5 psi.

The effluent calcium and sulfate concentrations (Figure 4.20(b)) were almost equal before the breakthrough, thus representing initial equilibrium state when the core was saturated with 80,000 ppm NaCl brine. The sulfate concentration was higher than the calcium concentration after 1 pore volumes. This was mainly due to the precipitation of calcium ions, dissolved from gypsum, in the presence of sodium metaborate. Other possible reasons for a substantial increase in sulfate concentration at 1 pore volume is unclear. The sulfate concentration slowly decreased after 1 pore volume while calcium

concentration remained to about 560 ppm (Figure 4.20(c)). Equilibrium was not achieved by injecting about 2 pore volumes of the alkali solution.

Table 4.9: Properties of the sandstone core used in experiment 4.5

Core	Length (inches)	Diameter (inches)	Porosity (%)	Permeability (md)	Temperature (°C)	Gypsum
Sandstone	11.2	1.48	19.2	80	55	Yes

Table 4.10: Formation brine and injected alkali solution composition for experiment 4.5

Salts (ppm)/Brines	Formation brine	Sodium metaborate solution
NaCl	80,000	-
NaBO2	-	30,000
TDS (ppm)	**80,000**	**30,000**

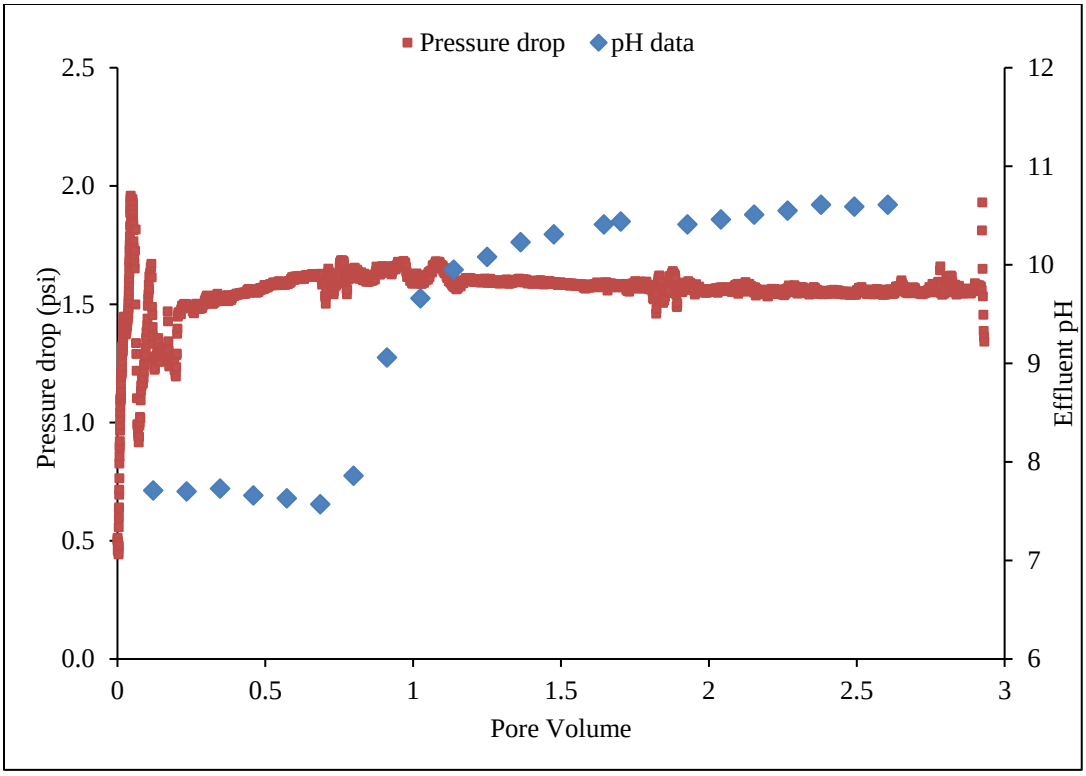

Figure 4.20 (a): Effluent pH and pressure drop across the core on injecting sodium metaborate in a sandstone core with gypsum

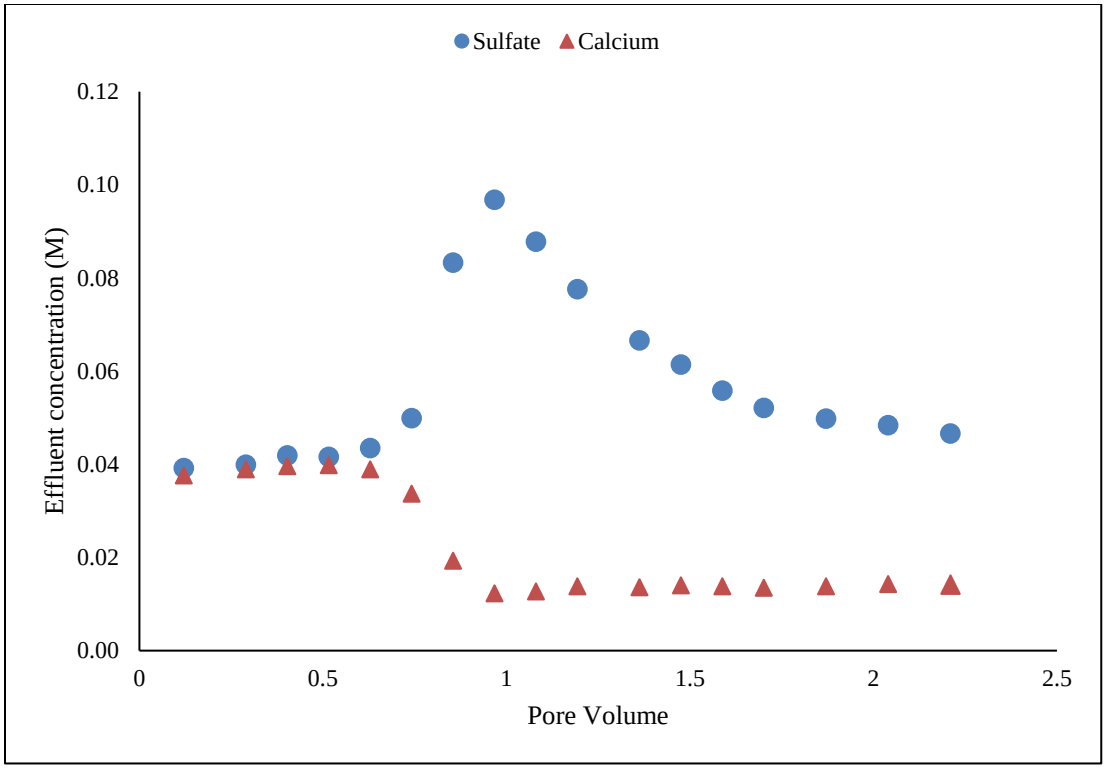

Figure 4.20(b): Effluent calcium and sulfate concentration, in mol/kg, during experiment 4.5

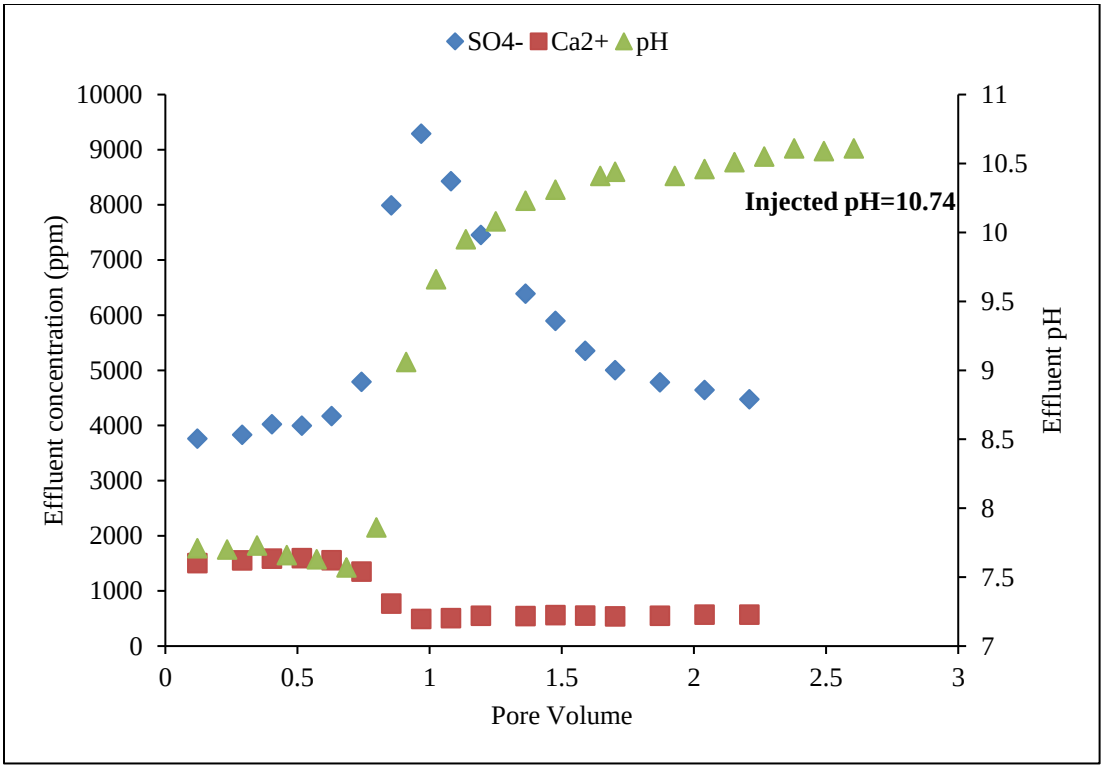

Figure 4.20(c): Effluent pH, calcium and sulfate concentration (in ppm) during experiment 4.5

4.1.3 Surfactant phase behavior experiments

Surfactant phase behavior experiments were performed to obtain ultralow IFT surfactant formulations to be used in oil recovery corefloods. The experiments involved mixing an aqueous solution, consisting of alkali and electrolytes, with crude oil in a given proportion. The electrolyte concentration was increased to obtain Winsor type phase transitions. The solubilization ratio plots, giving the amount of oil or water solubilized in the microemulsion phase, and activity maps, showing a change in ultralow IFT region with oil/water ratio, were prepared. In addition, aqueous stability samples were prepared, without oil, by increasing the electrolyte concentration for a given amount of surfactant

(and cosolvent) concentration. The detailed procedure to perform these experiments is discussed in chapter 3.

Experiment 4.7 (a): Surfactant phase behavior results with oil#1

Surfactant phase behavior experiments were performed with oil#1 using sodium metaborate as the alkali. The detailed procedure to perform surfactant phase behavior and identify the ultralow IFT formulations is described in chapter 3. The viscosity of the oil at the reservoir temperature of 55 °C was about 3 cP. The base brine had the salinity of 1,608 ppm and sodium metaborate was used to increase the salinity. The formulation consisting of 0.5% $C_{12\text{-}13}$-13PO-SO4, 0.5% $C_{19\text{-}18}$ IOS and 1% IBA-3EO showed ultralow IFT with optimum salinity at 39,000 ppm and aqueous stability up to 41,619 ppm, corresponding to the alkali concentration of 3.75 wt%. The solubilization ratio at the optimum salinity was found to be about 17, corresponding to the interfacial tension of 0.001 dynes/cm as per Huh's equation.

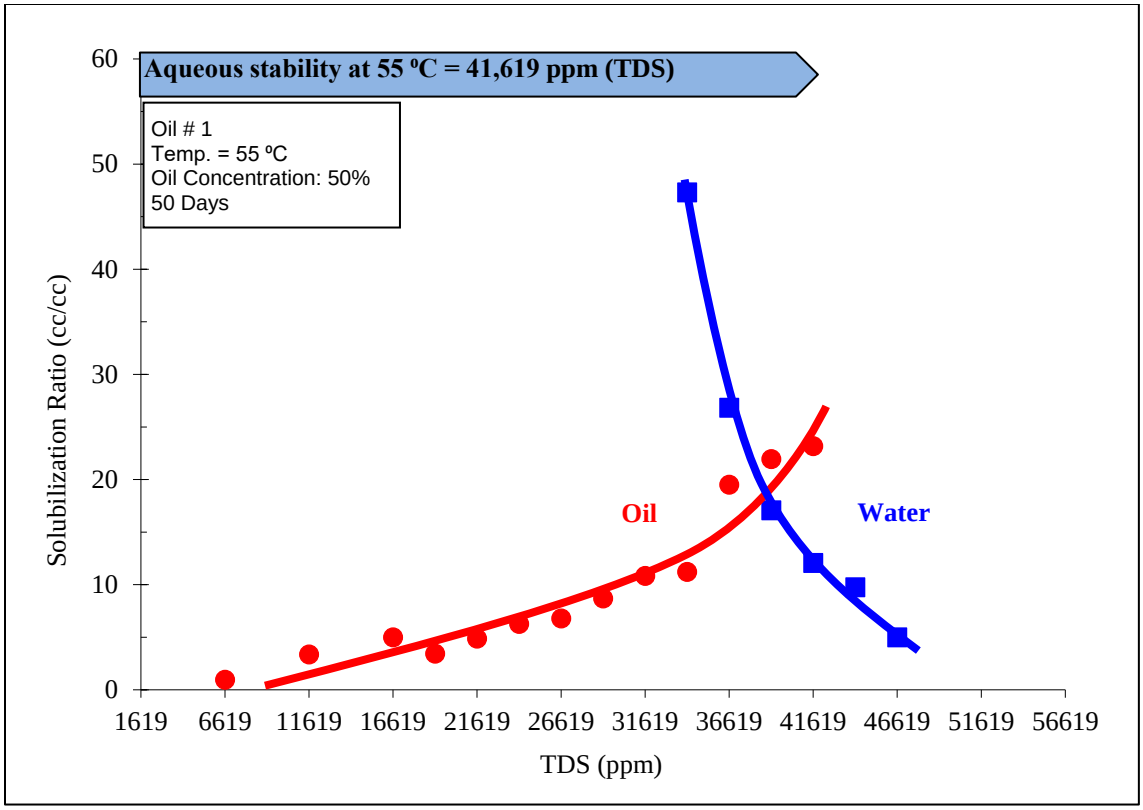

Figure 4.21: Solubilization ratios and aqueous stability results for experiment 4.6(a)

Experiment 4.7 (b): Modified formulation using IBA as cosolvent

The previous surfactant formulation was further optimized by replacing 1% IBA-3EO with 0.5% IBA. The rest of the formulation was kept the same, that is, 0.5% C_{12-13}-13PO-SO4, 0.5% C_{19-18} IOS. The solubilization ratio of about 30 was observed at the optimum salinity, clearly indicating that very low IFT was obtained with this surfactant formulation. The optimum salinity also reduced to 27,500 ppm, lowering the alkali concentration from 3.75%, in the previous formulation, to 2.4%. The formulation was aqueous stable up to 25,500 ppm. Although the aqueous stability limit of the formulation

was little less than the optimum salinity of 27,500 ppm, the formulation resulted in good oil recovery in the coreflood due to a high salinity of the formation brine (discussed later).

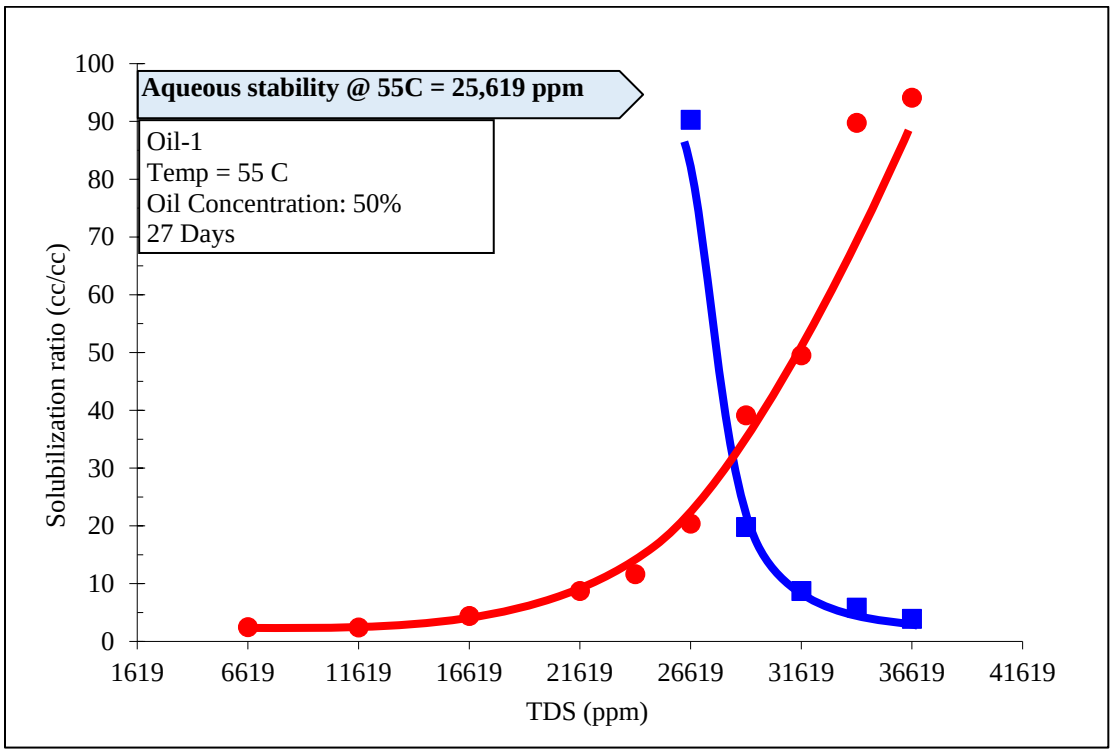

Figure 4.22: Solubilization ratios and aqueous stability results for experiment 4.6(b)

Experiment 4.8: Surfactant phase behavior experiment with crude oil-2

Surfactant phase behavior experiments were performed to identify an ultralow IFT surfactant formulation with a viscous crude oil (oil#2) using the procedure described in chapter 3. The viscosity of the oil at the reservoir temperature of 38 °C was 105 cP. Starting with the base brine of about 35,000 ppm, sodium metaborate was used to increase the salinity. A surfactant formulation consisting of 0.75 wt% $C_{12\text{-}13}$-7PO-SO_4,

0.25% C_{12-13}-13PO-SO_4 and 2% TEBGE showed an ultralow IFT formulation which was aqueous stable up to the optimum salinity. The solubilization plot for 30% oil using this surfactant formulation showed a solubilization ratio of about 8 at 10,000 ppm sodium metaborate (see Figure 4.23), which corresponded to an IFT of 0.0046 from Huh's equation. The surfactant formulation was aqueous stable up to the optimum salinity.

The ratio of oil and aqueous surfactant solution was varied, from 10% oil to 50% oil, to obtain the activity diagram (see Figure 4.24). Activity diagrams are useful in understanding the effect of soap on the optimum salinity in the case of active oils. This knowledge is crucial in designing a coreflood, especially for deciding the slug and polymer salinities (and salinity gradient). From Figure 4.23, it can be seen that the Winsor type III region was between 7,500 ppm-17,500 ppm sodium metaborate for 50% oil, 10,000-15,000 ppm sodium metaborate for 30% oil and 20,000 ppm-25,000 ppm sodium metaborate for 10% oil. Such an activity diagram is typical for an active crude oil and is the result of the change in soap to surfactant ratio (lower for 10% oil compared to 50%). This type of activity map is favorable because of the ease in designing an effective salinity gradient and obtaining Winsor type I phase behavior in the polymer drive.

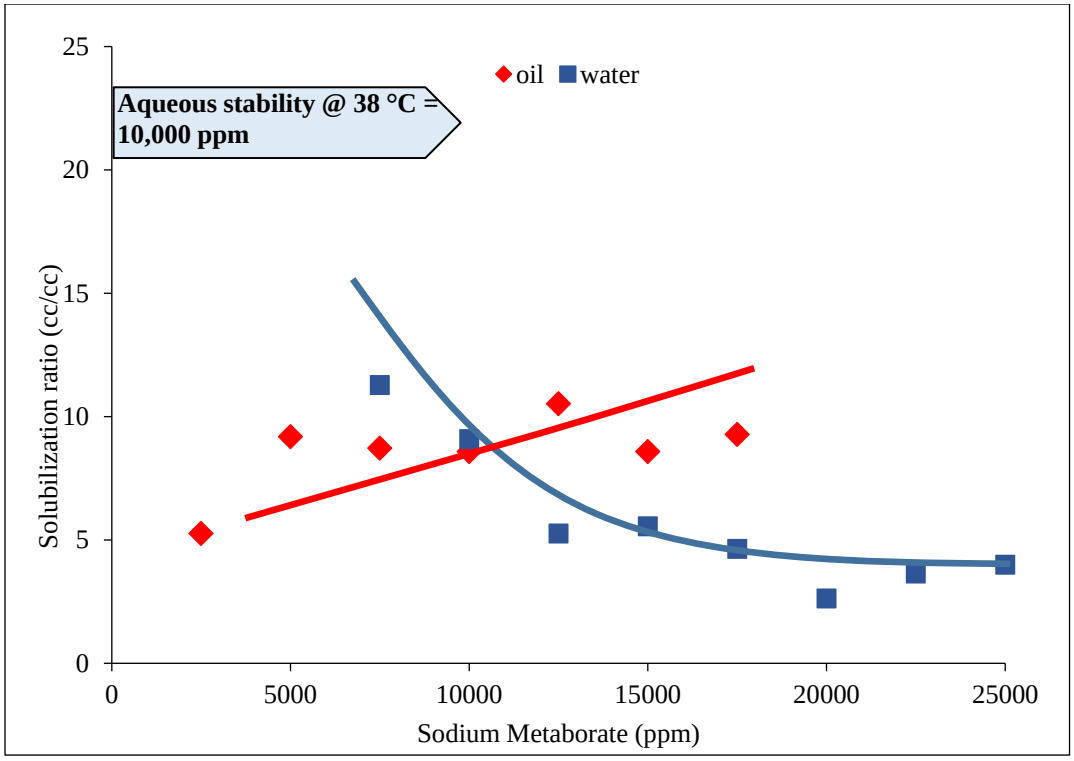

Figure 4.23: Solubilization plot for crude oil-2 using surfactant formulation 4.8

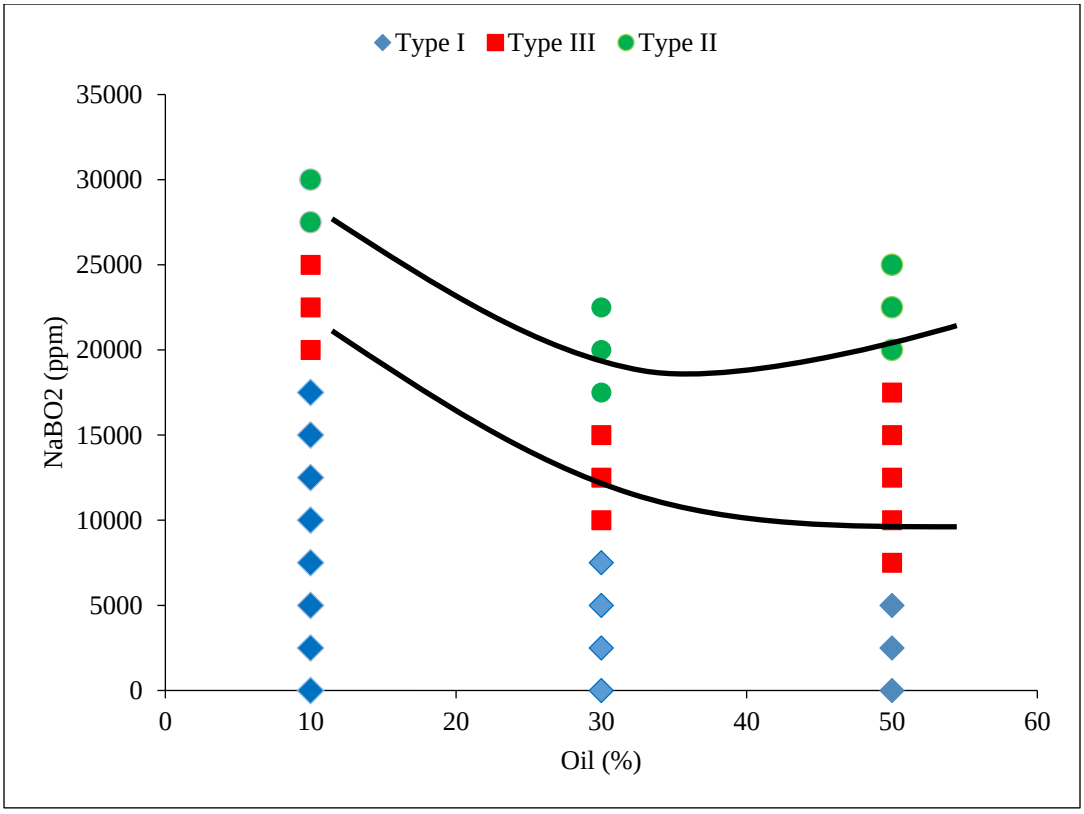

Figure 4.24: Activity map diagram for crude oil 2 and surfactant formulation 4.8

4.1.4 Oil Recovery Corefloods

Experiment 4.9 (a): ASP coreflood CF-1 in sandstone core containing gypsum

Oil recovery corefloods were performed in sandstone cores containing gypsum using sodium metaborate as the alkali. The core properties, oil properties, experimental conditions and ionic compositions of the formation brine, waterflood brine, chemical slugs are given in Tables 4.11 and 4.12. The detailed procedure followed to perform oil recovery corefloods, including the methods used for deciding critical parameters such as the salinity gradient, polymer requirements in the surfactant slug and polymer drives is

discussed in chapter 3. The tracer test result of the core (Figure 4.25) showed that the core was fairly homogeneous.

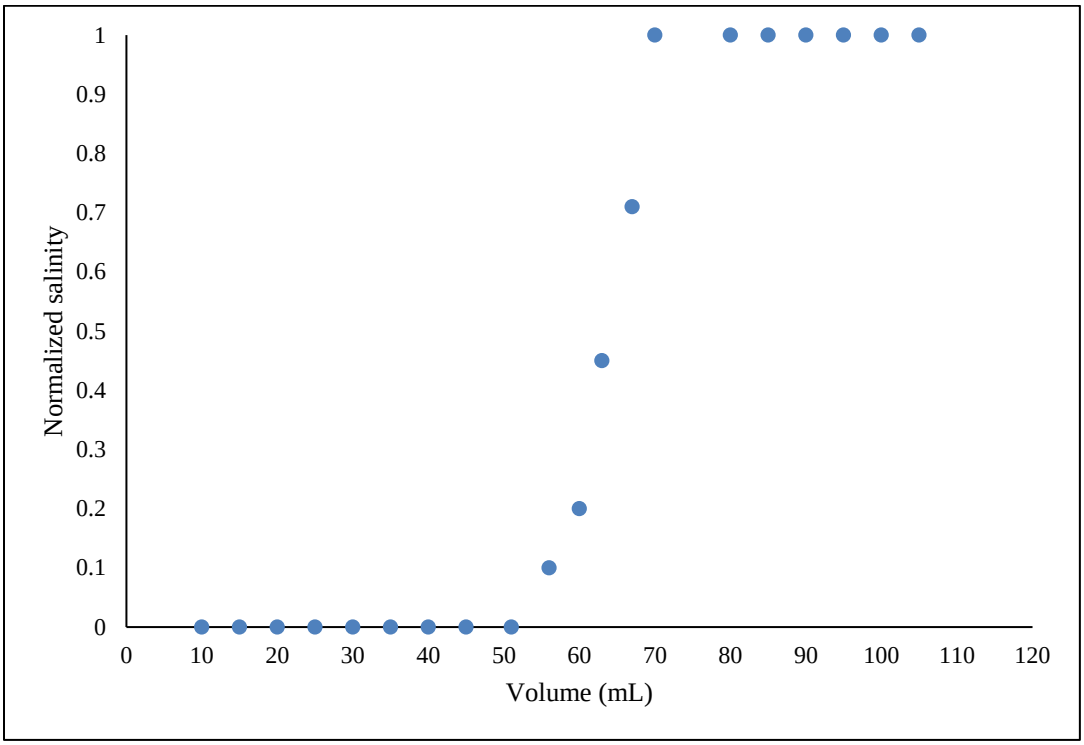

Figure 4.25: Tracer test result of the core used for coreflood experiment 4.7(a)

Table 4.11: Properties of the core used in coreflood CF-1

Core	Length (inches)	Diameter (inches)	Porosity (%)	Permeability (md)	Temperature (°C)	Gypsum
Sandstone	11.2	1.48	19.2	80	55	Yes

Table 4.12: Ionic compositions of the formation brine, waterflood brine and chemical slugs. In addition, $NaBO_2$ was added to the chemical slugs

Ions	Formation/Waterflood brine (ppm)	ASP slug (ppm)	Polymer drive 1 (ppm)	Polymer drive 2 (ppm)
Ca^{2+}	1,500	0	0	0
Mg^{2+}	644	0	0	0
Na^{+}	56,100	539	539	539
HCO_3^{-}	0	740	740	740
Cl^{-}	86,488	177	177	177
SO_4^{2-}	3,875	208	208	208
$NaBO_2$	**-**	**37,500**	**10,000**	**-**
TDS	**147,509**	**39,164**	**11,664**	**1,608**

The presence of gypsum in the core was confirmed by continuously injecting 10,000 ppm NaCl solution at 0.5 ft/d. The effluents from this flood were collected and analyzed for calcium and sulfate ions using ion chromatography (Figure 4.26). It can be seen from this plot that substantial calcium and sulfate ions (about 500 ppm and 2,000 ppm, respectively) were present in the effluent samples clearly indicating the presence of gypsum.

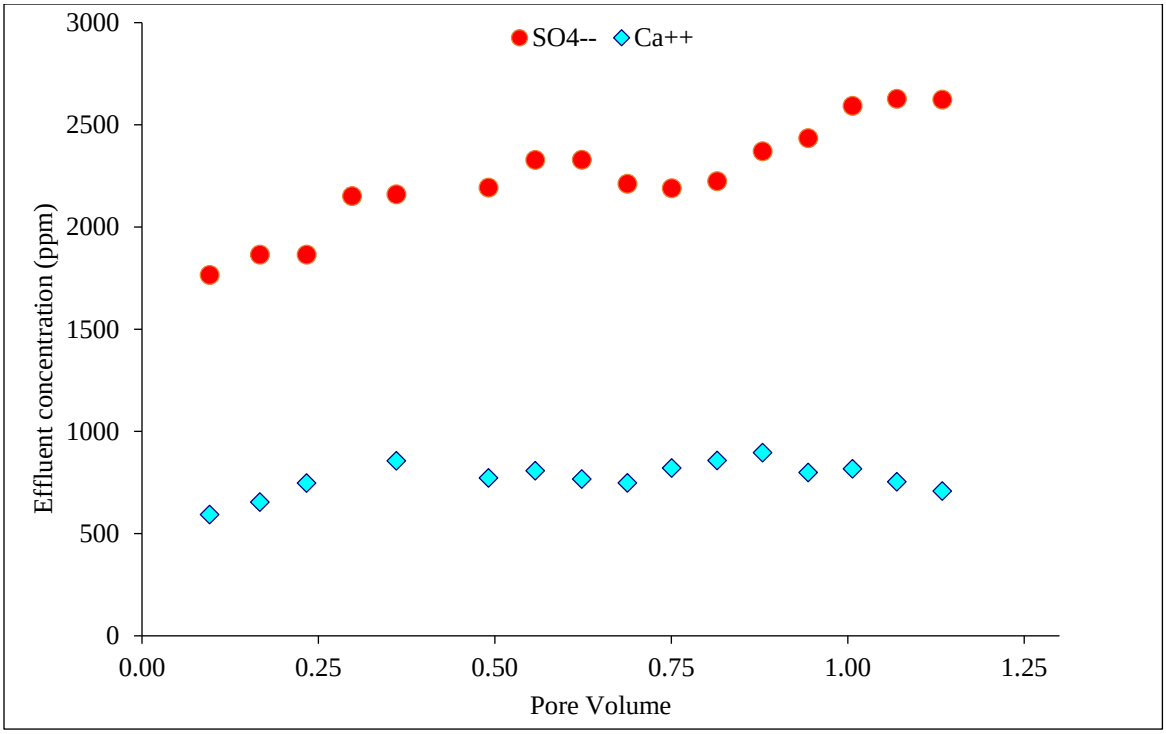

Figure 4.26: Effluent calcium and sulfate concentrations on injecting soft brine in a sandstone core to confirm the presence of gypsum before coreflood CF-1

The core was prepared, oil flooded and then waterflooded at experimental conditions as per the procedure described in chapter 3. The residual oil saturation after waterflood was about 0.18. 0.4 pore volume ASP slug, developed in experiment 4.7(a), was injected at the optimum salinity at 1 ft/d, followed by 0.2 pore volume of polymer drive 1 and 1.4 pore volumes of polymer drive 2 with decreasing salinities. A negative salinity gradient was achieved in the coreflood. Figures 4.27 and 4.28 show that about 99% of the residual oil, left after waterflood, was recovered, thus reducing the residual oil saturation to 0.01. Most of the oil was recovered within 1.3 pore volumes indicating a good surfactant formulation and salinity gradient, favorable mobility ratio and low

surfactant retention. The pH at 1 pore volume was about 10, indicating a good pH propagation. The surfactant retention in the coreflood was found to be 0.197 mg/g rock and 45% of the injected surfactant was recovered. The pressure drop data showed that no permeability damage was observed during the coreflood.

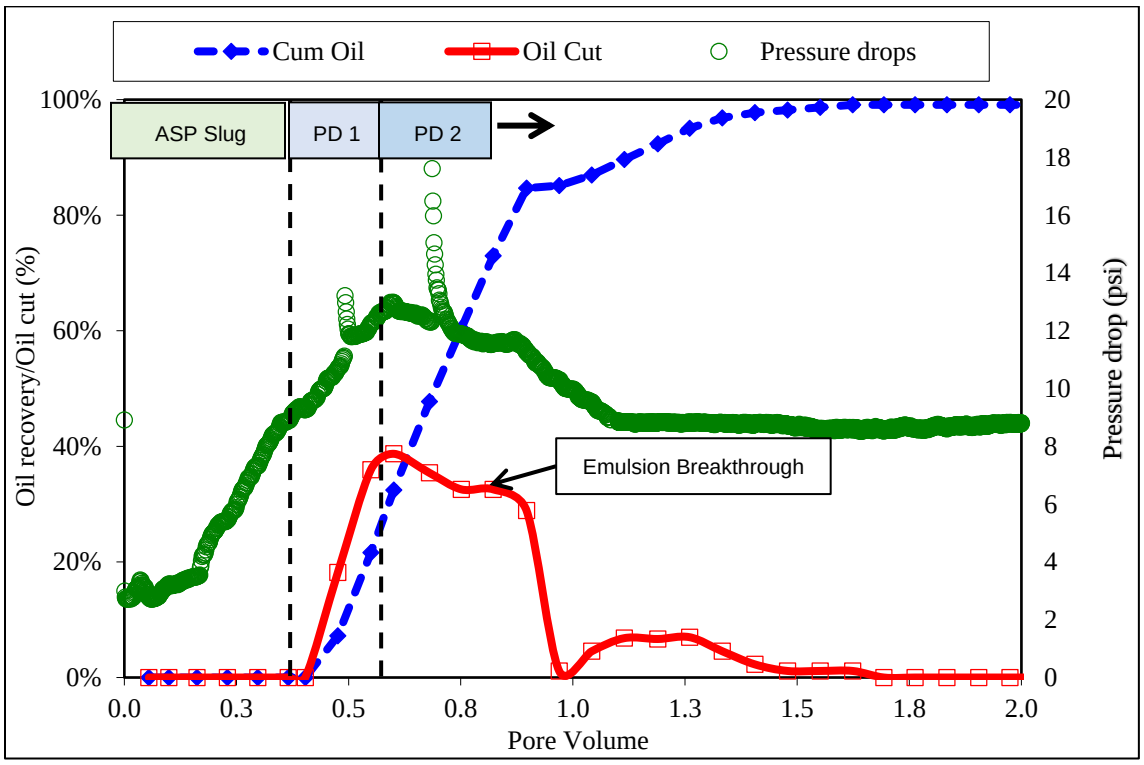

Figure 4.27: Oil recovery, oil cut and pressure drop during the ASP coreflood CF-1

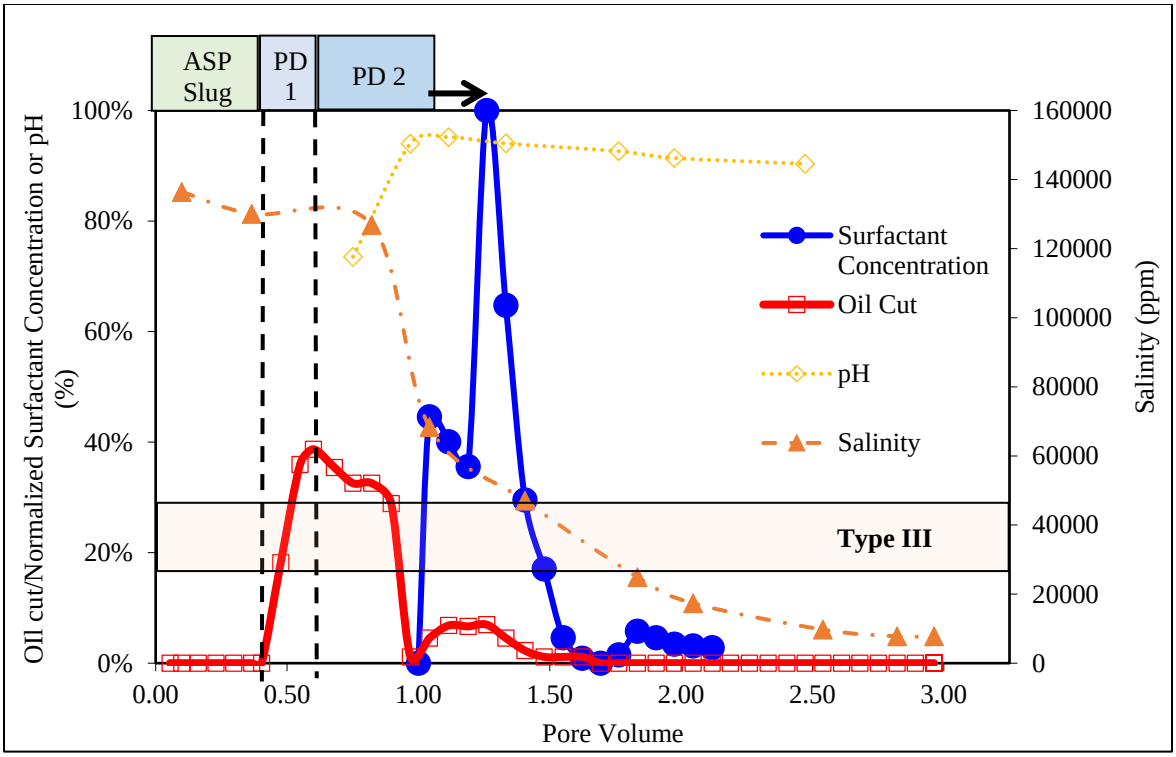

Figure 4.28: Oil cut, effluent surfactant concentration, salinity and pH observed during ASP coreflood CF-1. Note the pH value of x is shown here as 10x% on the primary y axis

Experiment 4.9 (b): ASP coreflood CF-2 in sandstone core containing gypsum

The coreflood was repeated in another similar core using the formulation developed in experiment 4.7(b). The tracer test result of this core is shown in Figure 4.29. The presence of gypsum in the core was tested by injecting 10,000 ppm NaCl brine. The effluent calcium and sulfate concentrations are shown in Figure 4.30, clearly indicating the presence of gypsum in the core. The main purpose of this coreflood was to study the longer term interaction of sodium metaborate with gypsum. Therefore, the residence time in the coreflood was increased from 1 day to 5 days by injecting the slugs for 6 hours at 1

ft/d and then shutting the experiment for 18 hours, and continuing this scheme for the rest of the coreflood. The details of the coreflood, including the composition of the ASP slug and polymer drive, are shown in Table 4.13 and 4.14. 0.25 pore volume ASP slug was injected at a slightly under-optimum salinity followed by 1.8 pore volumes of polymer drive of a lower salinity. The results of the coreflood are shown in Figure 4.31. It can be seen that a negative salinity gradient was achieved during the coreflood. About 94% of the residual oil after waterflood was recovered during the chemical flood, reducing the oil saturation to 0.01. Similar to the previous case, most of the oil was recovered within 1.3 pore volumes indicating good surfactant formulation and salinity gradient, favorable mobility ratio and low surfactant retention. The surfactant retention in the coreflood was found to be about 0.23 mg/g rock and 19% of the injected surfactant was recovered. The pH at 1.5 pore volume was about 9.8, lower than that of the previous case. The effluent ions in the coreflood samples were measured using ion chromatography, shown in Figure 4.32. It can be seen from the figure that the calcium and sulfate concentration remained constant before 1 pore volume, as expected, but the calcium concentration decreased after 1 pore volume because of the interaction of sodium metaborate with calcium ions leading to its precipitation.

Table 4.13: Properties of the core used in the ASP coreflood CF-2

Core	Length (inches)	Diameter (inches)	Porosity (%)	Permeability (md)	Temperature (°C)	Gypsum
Sandstone	11.9	1.48	24.0	86	55	Yes

Table 4.14: Ionic compositions of the formation brine, waterflood brine, and chemical slugs

Ions	Formation/Waterflood brine (ppm)	ASP slug (ppm)	Polymer drive 1 (ppm)
Ca^{2+}	1,500	0	0
Mg^{2+}	644	0	0
Na^{+}	56,100	539	539
HCO_3^{-}	0	740	740
Cl^{-}	86,488	177	177
SO_4^{2-}	3,875	208	208
$NaBO_2$	**-**	**24,000**	**10,000**
TDS	**147,509**	**25,664**	**11,664**

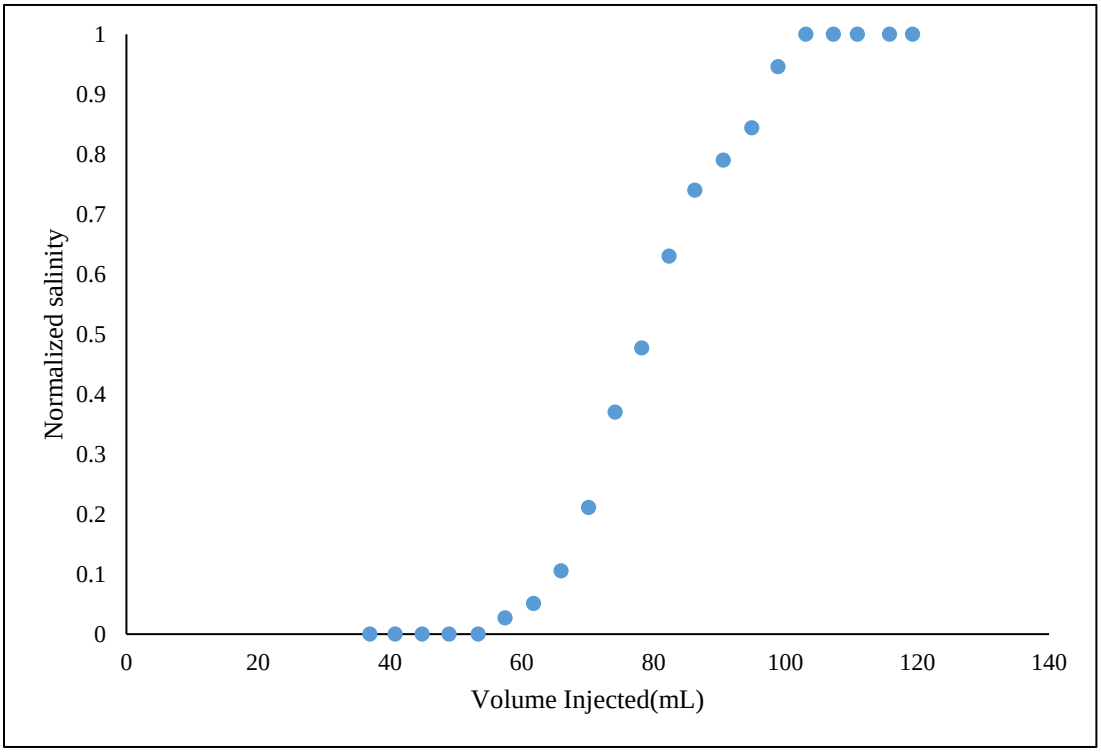

Figure 4.29: Tracer test results of the core used in coreflood CF-2

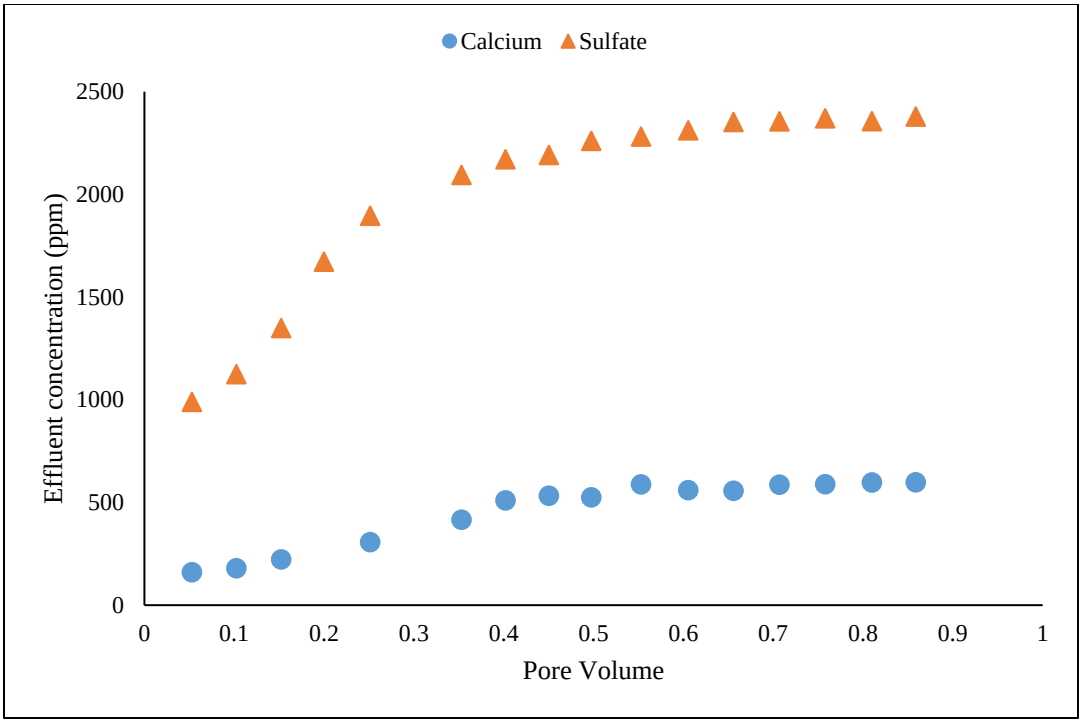

Figure 4.30: Effluent calcium and sulfate concentrations on injecting soft brine in a sandstone core to confirm the presence of gypsum before coreflood CF-2

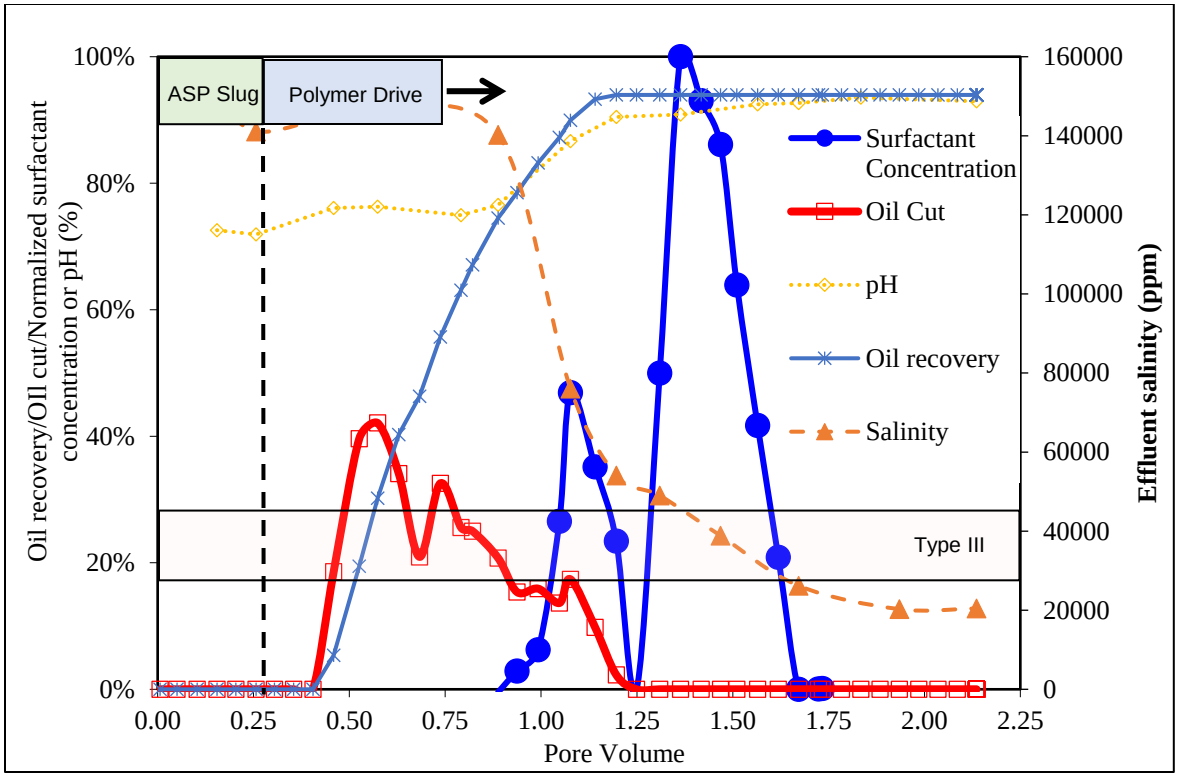

Figure 4.31: Oil recovery, oil cut, effluent surfactant concentration, pH and salinity for the ASP coreflood CF-2. Note that the pH value of x is represented as 10x% on the primary y axis

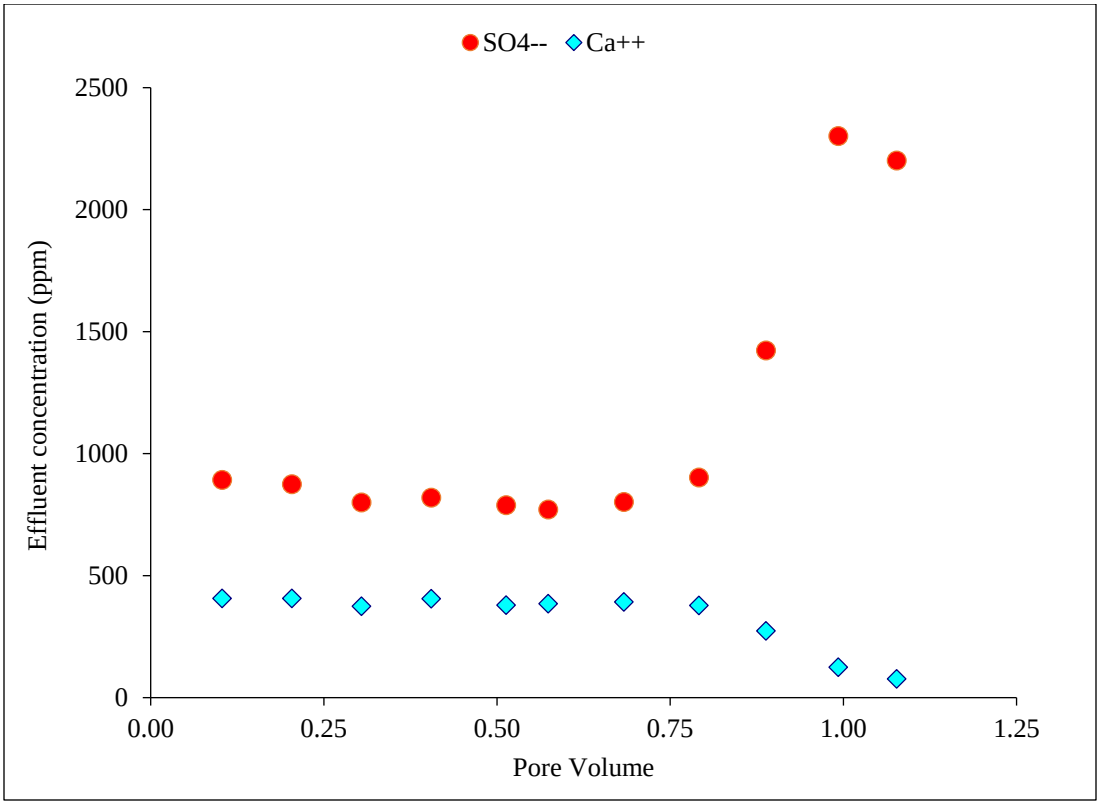

Figure 4.32: Effluent calcium and sulfate ions obtained during the ASP coreflood CF-2

Sodium metaborate was used as the alkali to perform ASP floods in Silurian dolomite core using a viscous crude oil-2 of 105 cP at 38 °C. The core properties and brine compositions are given in Tables 4.15 and 4.16, respectively. Using the surfactant formulation developed in Experiment 4.8, two oil recovery ASP corefloods were performed in Silurian dolomite cores; a tertiary ASP coreflood and a secondary ASP coreflood. Secondary ASP coreflood was also performed to compare with the tertiary ASP coreflood since fingers created during waterflood may affect the oil recovery in the subsequent chemical flood.

Experiment 4.10 (a): Oil recovery coreflood CF-3

The coreflood was setup, oil flooded and then waterflood at experimental conditions as per the procedure described in chapter 3. Coreflood parameters, including compositions of the ASP slug and polymer drives, are given in Table 4.17. The initial oil saturation after oil flood was about 0.84 and reduced to 0.44 after waterflood. A pre-flush of 0.4 pore volume, corresponding to the optimum salinity, was injected after waterflood so that a favorable salinity gradient is achieved. 0.3 pore volume of ASP slug was then injected at 1 ft/d, followed by two polymer drives of 0.5 pore volumes each of decreasing salinities. The waterflood brine was injected at the end. The coreflood results (Figure 4.34) showed that the cumulative oil recovery increased from 47% (after waterflood) to 92% after the chemical flood. The critical oil saturation after the chemical flood was about 6%. Most of the oil was recovered within 1.2 pore volumes, after starting the chemical flood, indicating a favorable mobility ratio, good surfactant formulation and salinity gradient design. The pH stayed at around 10 during the coreflood.

Table 4.15: Properties of the core used in ASP corefloods CF-3 and CF-4

Core	Length (inches)	Diameter (inches)	Porosity (%)	Permeability (md)	Temperature (°C)	Gypsum
Silurian dolomite	11.95	1.47	18.8	80.1	38	No

Table 4.16: Composition of the various brines used in the ASP corefloods CF-3 and CF-4

Salt	Formation/Waterflood brine (ppm)	Preflush	ASP slug (ppm)	Polymer drive 1 (ppm)	Polymer drive 2 (ppm)
NaCl	30,700	30,700	30,700	30,700	30,700
Na_2SO_4	4,800	4,800	4,800	4,800	4,800
$NaBO_2$	-	10,000	10,000	10,000	-
TDS	**35,500**	**45,500**	**45,500**	**45,500**	**35,500**

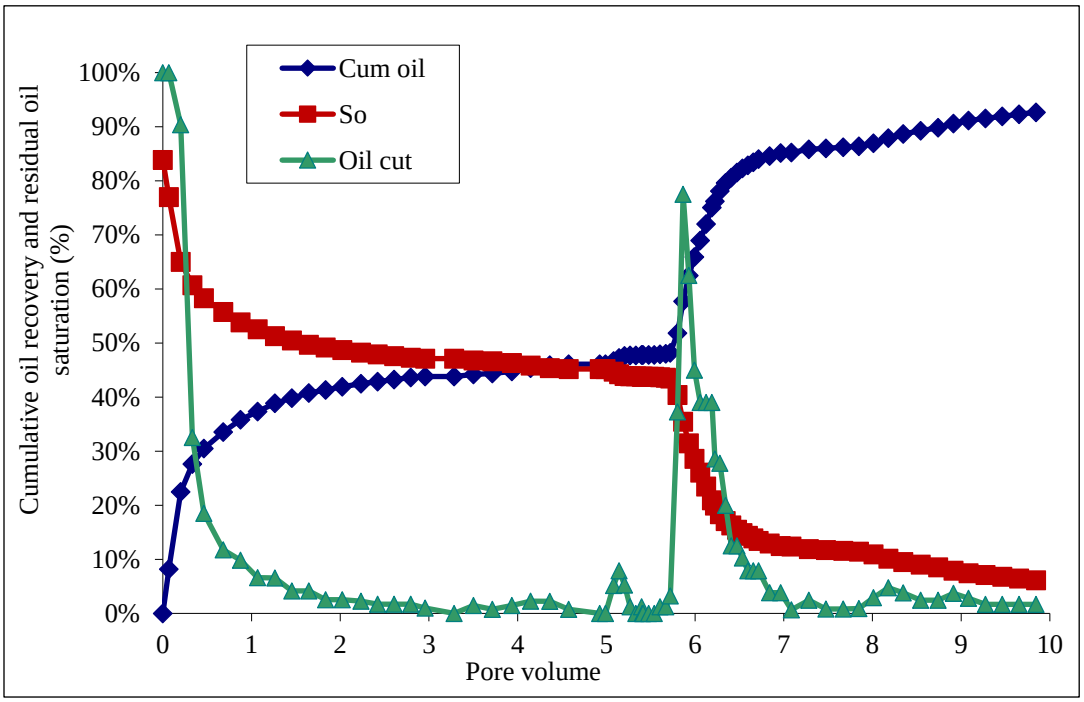

Figure 4.34: Oil recovery, oil cut and residual oil saturation during waterflood and tertiary ASP coreflood 4.10(a)

Experiment 4.10 (b): Oil recovery coreflood CF-4

The previous chemical flood was performed at the secondary stage keeping the slug compositions and amounts same as the previous case. The oil saturated core, containing formation brine at the residual saturation, was flooded with 0.3 pore volumes of ASP slug followed by two polymer drives of 0.5 pore volumes each. Waterflood brine was injected at the end. The results of the coreflood are shown in Figure 4.35. The oil recovery from the coreflood was about 95%, reducing the critical oil saturation from 70% to 3.1%. A stable oil bank was observed and most of the oil was recovered within 1.5 pore volumes. The pH of the effluent sample reached to about 10 and a low surfactant retention of about 0.13 mg/g rock was observed.

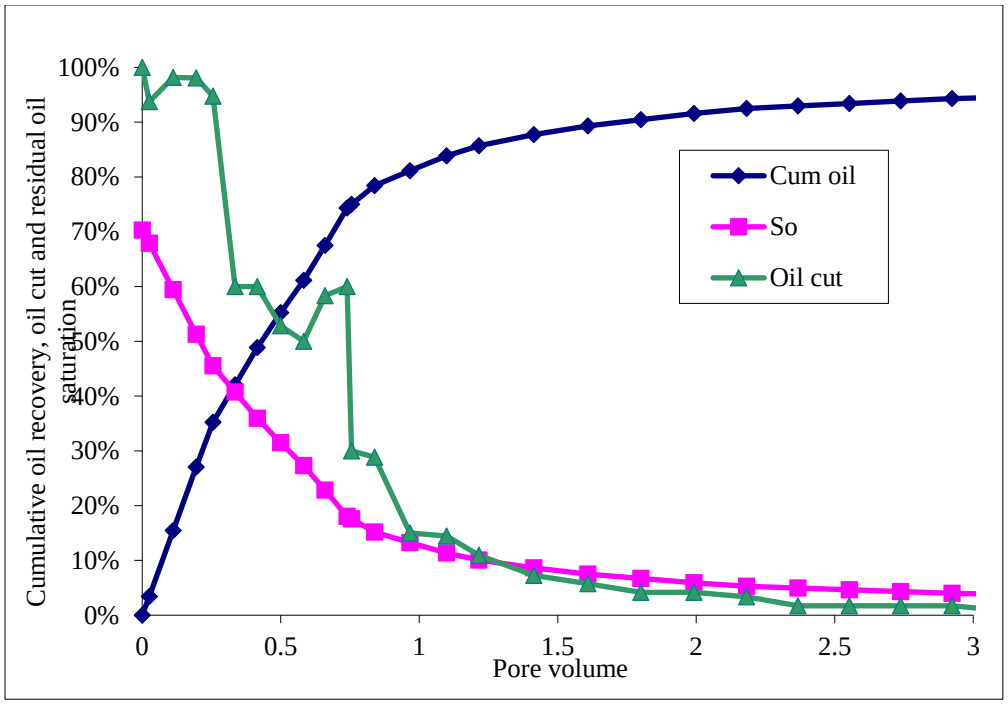

Figure 4.35: Oil recovery, oil cut and residual oil saturation for secondary ASP coreflood 4.10(b)

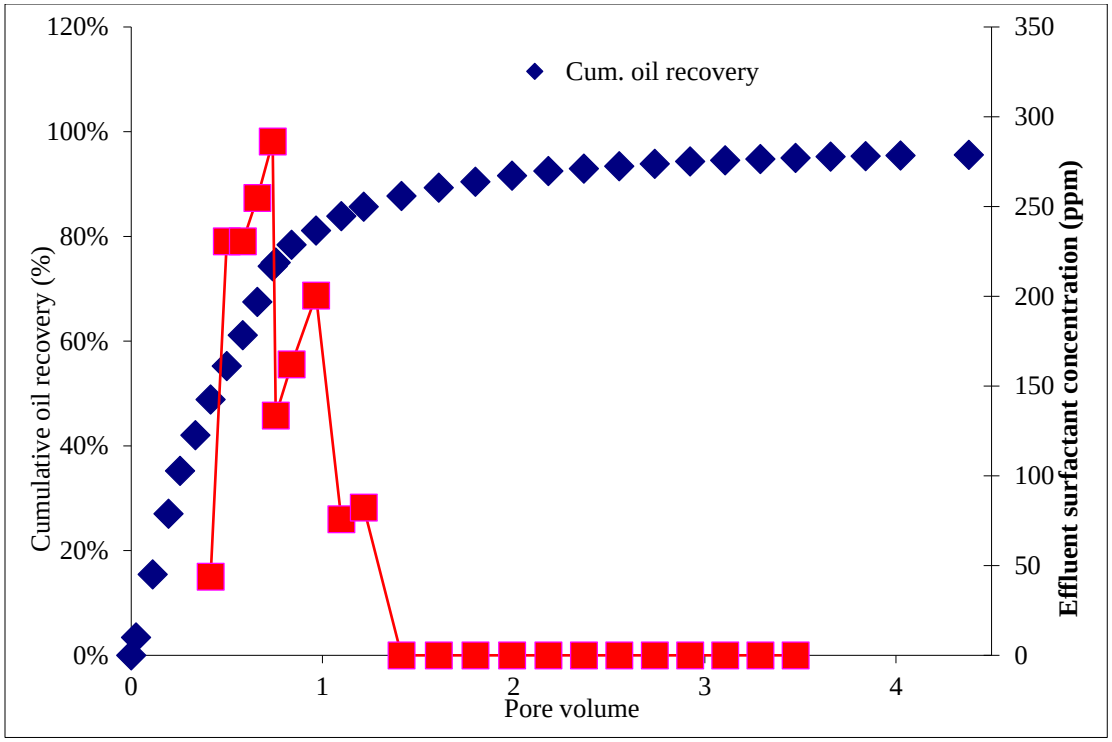

Figure 4.36: Cumulative oil recovery and effluent surfactant concentration during secondary ASP coreflood 4.10(b)

Table 4.17: Comparison of oil recovery ASP corefloods CF-1 to CF-4 using sodium metaborate as alkali

Experiment (Core)		CF-1	CF-2	CF-3	CF-4
Core		Sandstone with gypsum	Sandstone with gypsum	Silurian dolomite	Silurian dolomite
ASP Slug	Surfactants	0.5% C_{12-13}-13PO-SO_4 0.5% C_{19-23} IOS	0.5% C_{12-13}-13PO-SO_4 0.5% C_{19-23} IOS	0.75% C_{12-13}-7PO-SO_4 0.25% C_{12-13}-13PO-SO_4	0.75% C_{12-13}-7PO-SO_4 0.25% C_{12-13}-13PO-SO_4
	Co-solvent	1% IBA-3EO	0.5% IBA	2% TEBGE	2% TEBGE
	Alkali	3.75% $NaBO_2$	2.4% $NaBO_2$	1% $NaBO_2$	1% $NaBO_2$
	TDS (ppm)	39,000	25,664	45,500	45,500
	Polymer	2500 ppm FP 3330S	2750 ppm FP 3630S	4500 ppm FP 3630S	4500 ppm FP 3630S
	Slug size	0.4 PV	0.25 PV	0.3 PV	0.3 PV
Polymer Drive 1	Alkali	1% $NaBO_2$	1% $NaBO_2$	1% $NaBO_2$	1% $NaBO_2$
	TDS (ppm)	11,664	11,664	45,500	45,500
	Polymer	2000 ppm FP 3330S	2500 ppm FP 3330S	4500 ppm FP 3630S	4500 ppm FP 3630S
	Slug size	0.2 PV	1.8 PV	0.5 PV	0.5 PV
Polymer Drive 2	Alkali	-	-	-	-
	TDS (ppm)	1,664	-	35,500	35,500
	Polymer	1000 ppm FP 3330S	-	4500 ppm FP 3630S	4500 ppm FP 3630S
	Slug size	1.4 PV	-	0.5 PV	0.5 PV
Oil Saturation After Chemical Flood (Sorc)		1%	2%	6.1 %	3.1 %
Total Oil Recovery		99%	94%	92.7%	95.6%
Surfactant Retention (mg/g rock)		0.197	0.231	n.a.	0.127

A summary of sodium metaborate experiments is given below:

1. Static surfactant adsorption experiments showed reduction in surfactant adsorption on Silurian dolomite on adding sodium metaborate. The extent of decrease in surfactant adsorption with sodium metaborate was similar to that with sodium carbonate.

2. Surfactant phase behavior experiments with sodium metaborate showed classical Winsor type phase behavior. Soap generation was observed on adding sodium metaborate to acidic crude oils. Good pH propagation and low surfactant adsorption were observed in ASP floods in carbonate rocks using sodium metaborate as the alkali.

3. Sodium metaborate was studied for ASP floods in cores containing gypsum or anhydrite. Single-phase static and transport experiments with sodium metaborate showed that, unlike sodium carbonate, sodium metaborate was able to maintain and propagate a high pH in cores containing anhydrite. Note that precipitation was observed in both the cases. However, the extent of precipitation of sodium metaborate with gypsum was much less than that of sodium carbonate.

4. The alkali transport experiments showed that the interaction of sodium metaborate with gypsum was dependent on the injection rate. More gypsum dissolution was observed when sodium metaborate was injected slowly. The effluent pH stayed at around 10 even at the flow velocity 1/15 ft/d; the equilibrium was however not achieved. The results show the importance of performing experiments not only at 1 ft/d but also at slow flow rates, especially when slow reactions are involved.

5. Static experiments were performed to study the interaction of sodium metaborate with calcium ions (using calcium chloride). The experiments showed precipitation of calcium ions in the presence of sodium metaborate. The extent of precipitation was dependent on the amount of sodium metaborate; more precipitation was observed on using higher sodium metaborate concentration.

4.2 Ammonia as an alternative alkali for ASP floods

The previous results showed that sodium metaborate was as effective as sodium carbonate in lowering the surfactant adsorption and was able to tolerate gypsum much better than sodium carbonate. Some precipitation was however still observed when sodium metaborate was injected in cores containing gypsum. Ammonia was therefore investigated as an alternate alkali in sandstone and carbonate cores, especially in cores containing gypsum. The interaction of ammonia with gypsum was investigated by static experiments. Ammonia was injected in Berea sandstone cores to study the pH propagation. Ammonia was then injected in cores containing gypsum and the effluent ions and pH were analyzed. Zeta potential measurements were performed with ammonia on sandstone and carbonate surfaces. Surfactant phase behavior study was performed with ammonia and ultralow IFT surfactant formulations were developed. Polymer stability experiments were performed. Oil recovery corefloods were performed using these surfactant formulations in sandstone and carbonate cores, some of which contained gypsum. The corefloods showed good oil recovery and high pH propagation even with

0.5 wt% ammonia. In this section, results obtained with ammonia will be discussed. The list of experiments discussed in this section is given in Table 4.18.

Table 4.18: List of experiments performed using ammonia

Experiment	Description of experiment
ASP floods in core containing gypsum	
4.11	Single-phase static experiments using ammonia in the presence of (a) Gypsum (b) Calcium chloride
4.12	Single-phase ammonia transport in Berea sandstone
4.13	Single-phase ammonia transport in a carbonate core containing gypsum
4.14	Surfactant phase behavior results using ammonia as alkali with (a) oil-1 (b) oil-3 (c) oil-4
4.15	Polymer stability experiments results in presence of ammonia and calcium ions
4.16	Oil recovery ASP coreflood using surfactant formulation 4.14 (d) in Berea sandstone (a) CF-5 (b) CF-6 (c) CF-7
4.17	Oil recovery coreflood using surfactant formulation 4.14 in a carbonate core containing gypum (a) ASP coreflood CF-8 (b) SP coreflood CF-9
4.18	Single-phase corefloods in a carbonate core containing gypsum (a) SP coreflood CF-10 (b) ASP coreflood CF-11 (c) SP coreflood CF-12
4.19	Oil recovery ASP coreflood CF-13 in a sandstone core containing gypsum using the surfactant formulation 4.14 (a)
ASP floods in cores without gypsum	
4.20	Zeta potential measurements using ammonia and sodium carbonate on (a) crushed Bandera brown sandstone (b) crushed Silurian dolomite
4.21	Single-phase surfactant adsorption on crushed Bandera brown sandstone
4.22	Single-phase surfactant adsorption on crushed Silurian dolomite
4.23	Single-phase dynamic surfactant adsorption experiments in sandstone
4.24	Single-phase dynamic surfactant adsorption experiments in carbonates

Table 4.18 (continued)

4.25	Surfactant phase behavior experiments with crude oil-3
4.26	Oil recovery corefloods in Berea sandstone cores using surfactant formulation 4.25 (a) ASP coreflood CF-14 (b) SP coreflood CF-15

4.2.1 Static experiments

Experiment 4.11(a): Single-phase static experiments using ammonia in the presence of gypsum

Static experiments were performed to study the interactions of ammonia in the presence of gypsum. An excess amount of gypsum was mixed with aqueous solutions containing ammonia and allowed to equilibrate for about 2 days, after which the pH and ionic compositions of the supernatant solutions were measured. For comparison, the same experiment was repeated without adding an alkali and also with sodium carbonate. The results (see Table 4.19) showed that the pH, calcium and sulfate concentrations of the supernatant solution when no alkali was added were about 6.8, 1,082 ppm and 2,560 ppm, respectively. On adding sodium carbonate, the sulfate concentration increased to about 53,000 ppm indicating excessive precipitation of calcium carbonate and a resultant decrease in pH to 8.1 (from the initial value of about 11.4). A similar experiment with ammonia showed no signs of precipitation; the pH stayed at the initial value of about 11.1 and, the concentrations of calcium and sulfate ions were similar to the experiment that was performed without adding an alkali.

Table 4.19: Static alkali-gypsum experiments samples

	Alkali	wt% Alkali	Day 2		
Experiment			pH	Ca (ppm)	SO4 (ppm)
4.11 (a)	No Alkali	-	6.8	1,082	2,560
4.11 (b)	Na_2CO_3	6.11	8.1	441	53,302
4.11 (c)	NH_3	0.67	11.1	1,312	2,584

Experiment 4.11(b): Single-phase static experiments using ammonia in the presence of calcium chloride

In the previous experiment, ammonia showed no calcium precipitation or pH decrease in the presence of gypsum. Experiments were repeated with calcium chloride salt, which is very soluble in water unlike gypsum. Calcium concentration was varied using calcium chloride, from 2,500 ppm to 10,000 ppm, keeping the ammonia concentration fixed to 0.9 %. The solutions were equilibrated at 59 °C and were analyzed for pH change and signs of precipitation. No precipitation was observed in any of the equilibrated samples, shown in Figure 4.37, and the pH stayed to about 11 confirming the previous observations with gypsum.

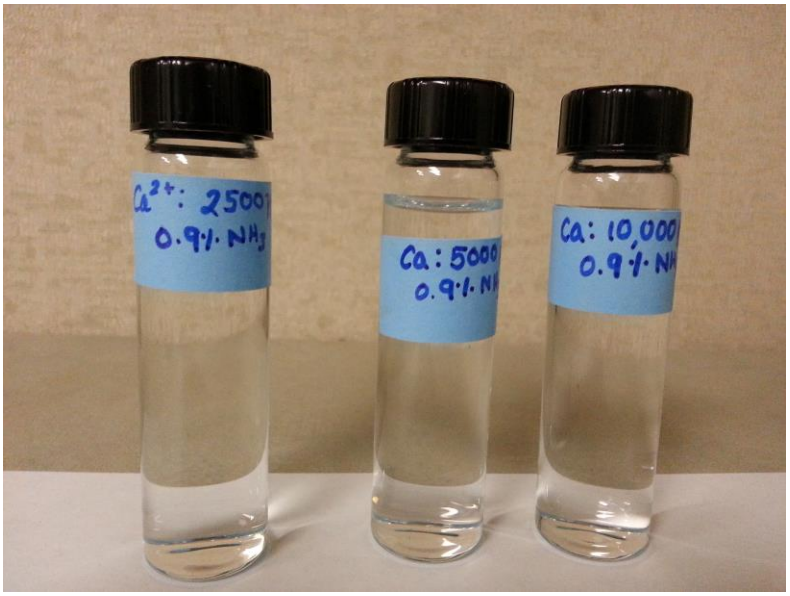

Figure 4.37: Aqueous samples prepared by adding 0.9% NH_3 and up to 10,000 ppm calcium

4.2.2 Single-phase ammonia transport in cores containing gypsum

Experiment 4.12: Single-phase ammonia transport in Berea sandstone

The existing literature on the use of ammonia is very scarce and therefore single-phase transport experiments were first performed in Berea sandstone, a typical sandstone porous media, at room conditions. The core properties are given in Table 4.20. The core was initially saturated with 80,000 ppm NaCl brine. This brine was displaced with 10,000 ppm NaCl brine containing 0.3 wt% ammonia. The effluent ions were collected in a sealed environment and measured for salinity and pH. From the results, shown in Figure 4.38, it can be seen that a pH value of about 10.2 was recorded at 1 pore volume indicating a good pH propagation in the Berea sandstone core only by adding 0.3 wt%

ammonia. Single-phase ammonia transport experiments were performed next in carbonate cores containing gypsum.

Table 4.20: Properties of the Berea core used in experiment 4.12

Core	Length (inches)	Diameter (inches)	Porosity (%)	Permeability (md)	Temperature (°C)	Gypsum
Berea Sandstone	12	1.48	21.2	650	22	No

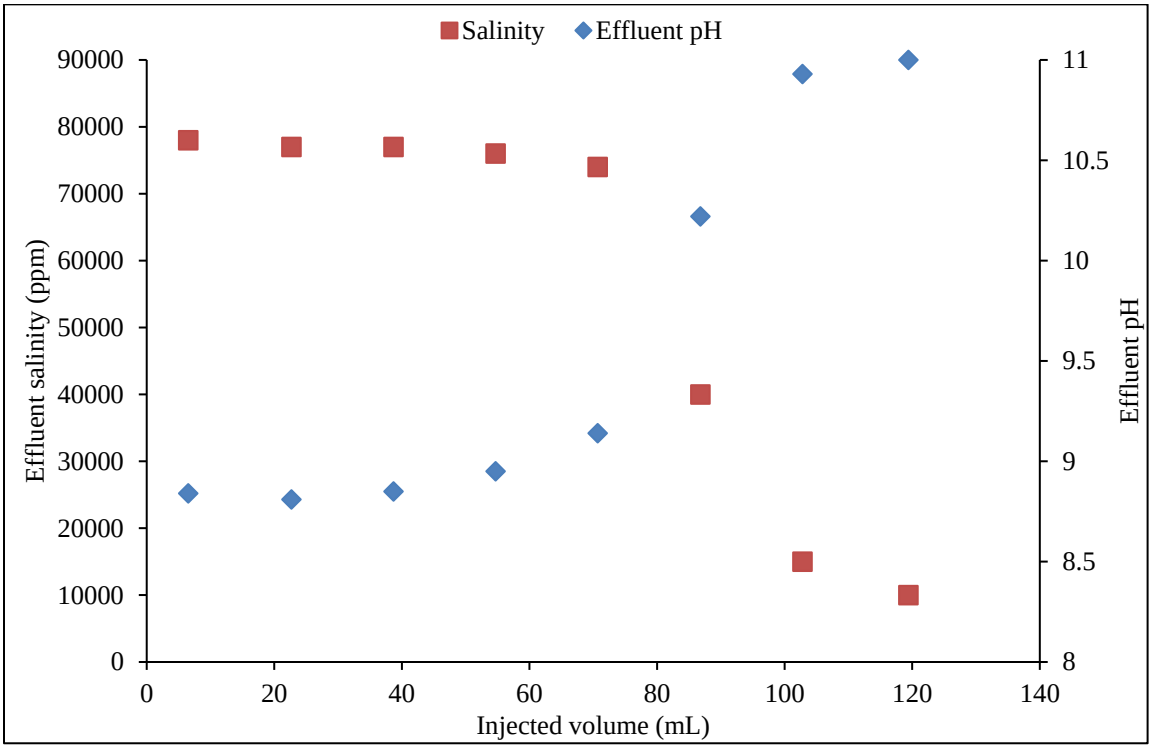

Figure 4.38: Effluent pH and salinity during single-phase alkali coreflood experiment 4.12

Experiment 4.13: Single-phase ammonia transport in carbonate core with gypsum

A carbonate core containing gypsum was used for studying ammonia transport in the presence of gypsum. The core properties are given in Table 4.21. The core was fairly homogeneous as can be seen from tracer test results (Figure 4.39). After accounting for dead volume corrections, the pore volume of the core from the tracer test result was found to be 64 mL. The presence of gypsum in the core was tested using the procedure described in chapter 3. The effluents from the core on injecting NaCl brine were collected and analyzed for calcium and sulfate concentrations using ion chromatography. The presence of calcium and sulfate ions in the effluent indicated the presence of gypsum. It has been observed that the dissolution reaction of gypsum reaches equilibrium within 1-2 days and the effluent calcium and sulfate ions obtained from cores containing gypsum corresponded to the equilibrium values.

Table 4.21: Properties of the core used in single-phase ammonia coreflood

Core	Length (inches)	Diameter (inches)	Porosity (%)	Permeability (md)	Temperature (°C)	Gypsum
Carbonate	12	1.48	19.5	453	22	Yes

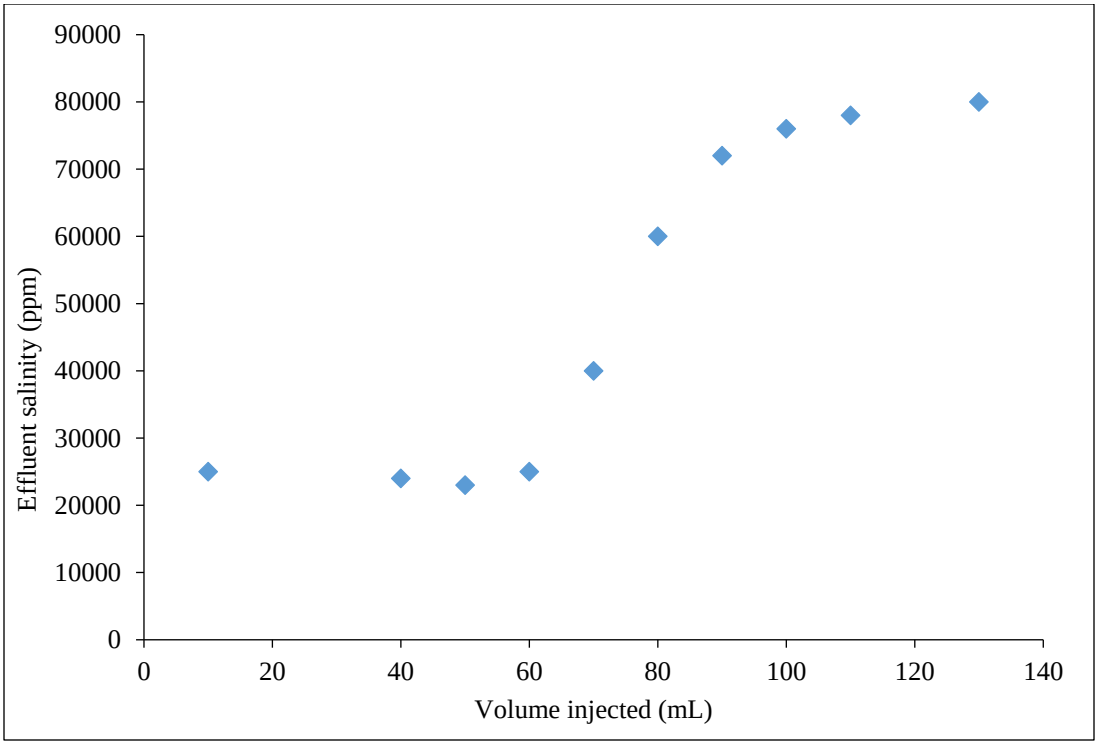

Figure 4.39: Tracer test result of the carbonate core containing gypsum

Single-phase alkali transport experiments were performed in the carbonate core containing gypsum using ammonia at 0.25 ft/d room conditions. The effluent samples were carefully collected in plastic tubes, which were capped soon after the collection and analyzed for pH, salinity, calcium and sulfate concentrations. The effluent concentration of ammonia obtained by acid-base titration. The effluent pH and ammonia concentration were plotted against pore volumes as shown in Figure 4.40 (a). Effluent calcium and sulfate ions were similarly plotted and are shown in Figure 4.40 (b). From Figure 4.40(a), it can be seen that a pH of about 9.8 and ammonia concentration of 0.15 wt%, 50% of the injected amount, was observed at 1 pore volume indicating a good pH and ammonia

transport. The effluent calcium and sulfate ions, shown in Figure 4.40(b), were equal throughout the coreflood indicating that no calcium precipitation occurred during the flood. The concentration decreased from about 55 mM when the core was saturated with 8% NaCl brine to 30 mM when 0.3% ammonia in 1% NaCl was injected. This decrease in the concentration of calcium (or sulfate) ions was due to the dependence of gypsum dissolution on salinity; more dissolution at a higher salinity. The concentration of calcium and sulfate ions are also shown in parts per million in Figure 4.40(c) to give an idea of the equilibrium calcium concentration in the presence of gypsum during this experiment. The calcium concentration ranged from about 1000 ppm to 2000 ppm when the salinity of the aqueous solution was 8% NaCl and 1% NaCl (with 0.3% ammonia), respectively.

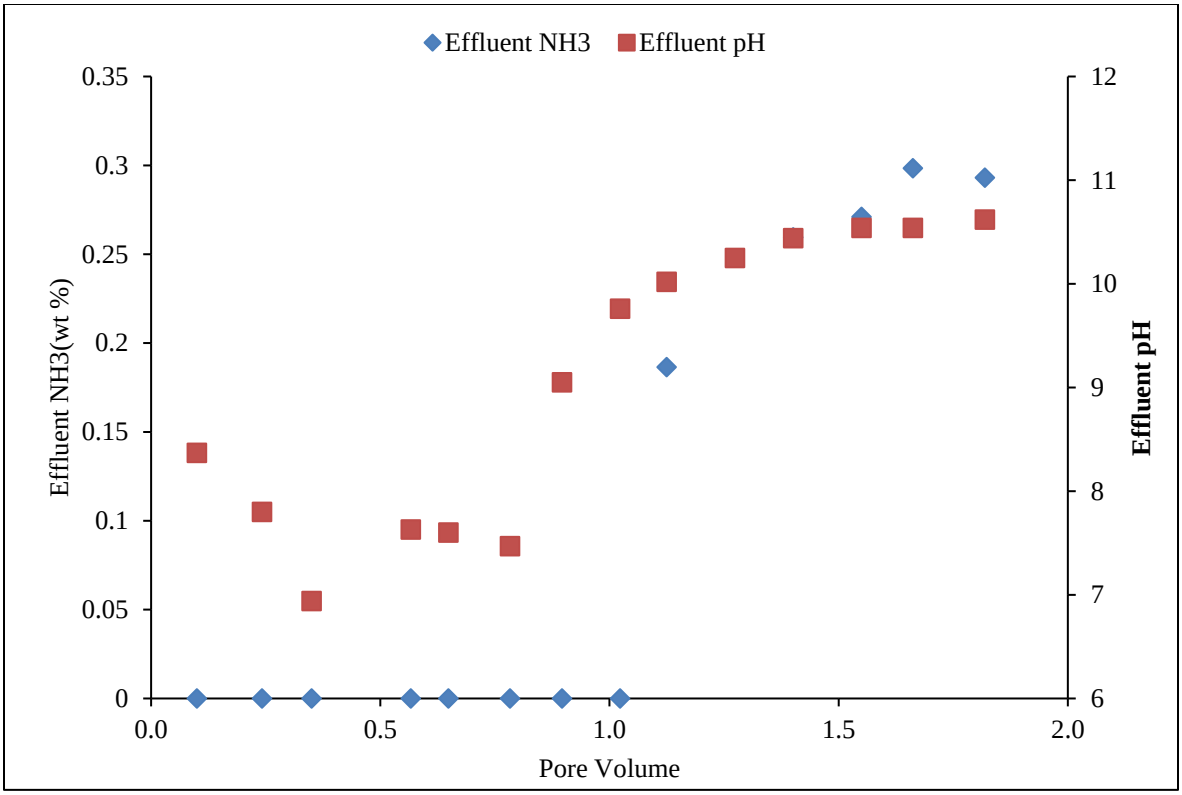

Figure 4.40(a): Effluent pH and ammonia concentration obtained from experiment 4.13

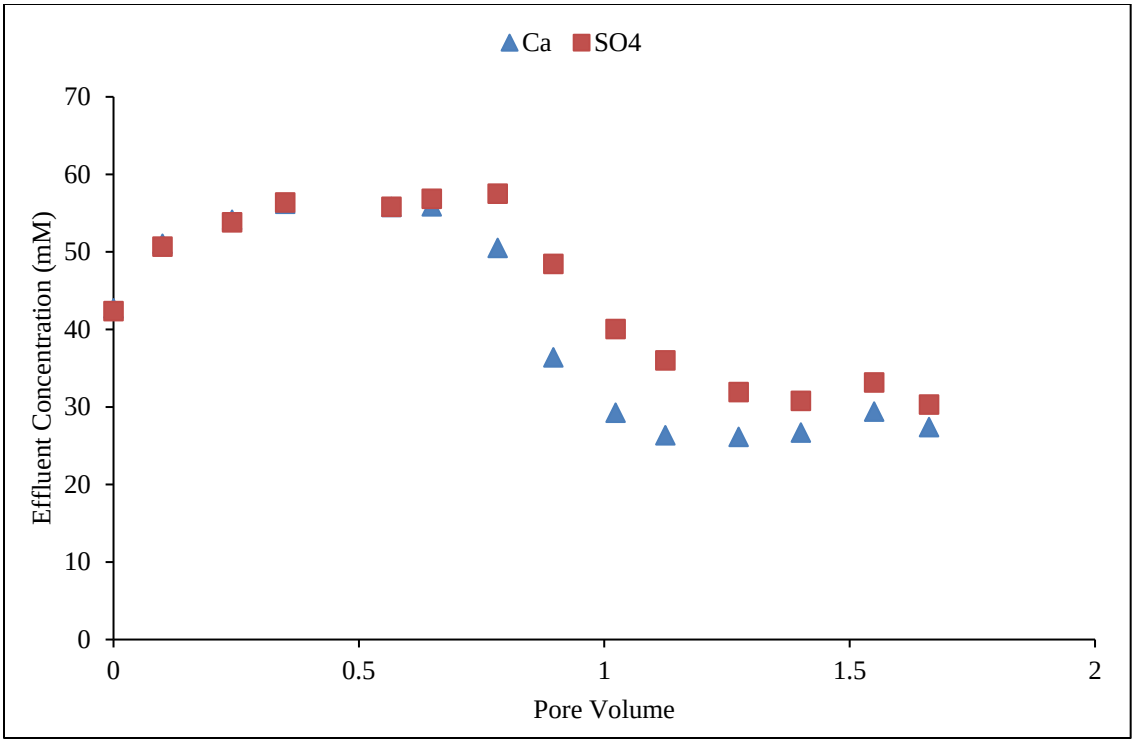

Figure 4.40(b): Effluent calcium and sulfate ions (in mM) obtained during experiment 4.13

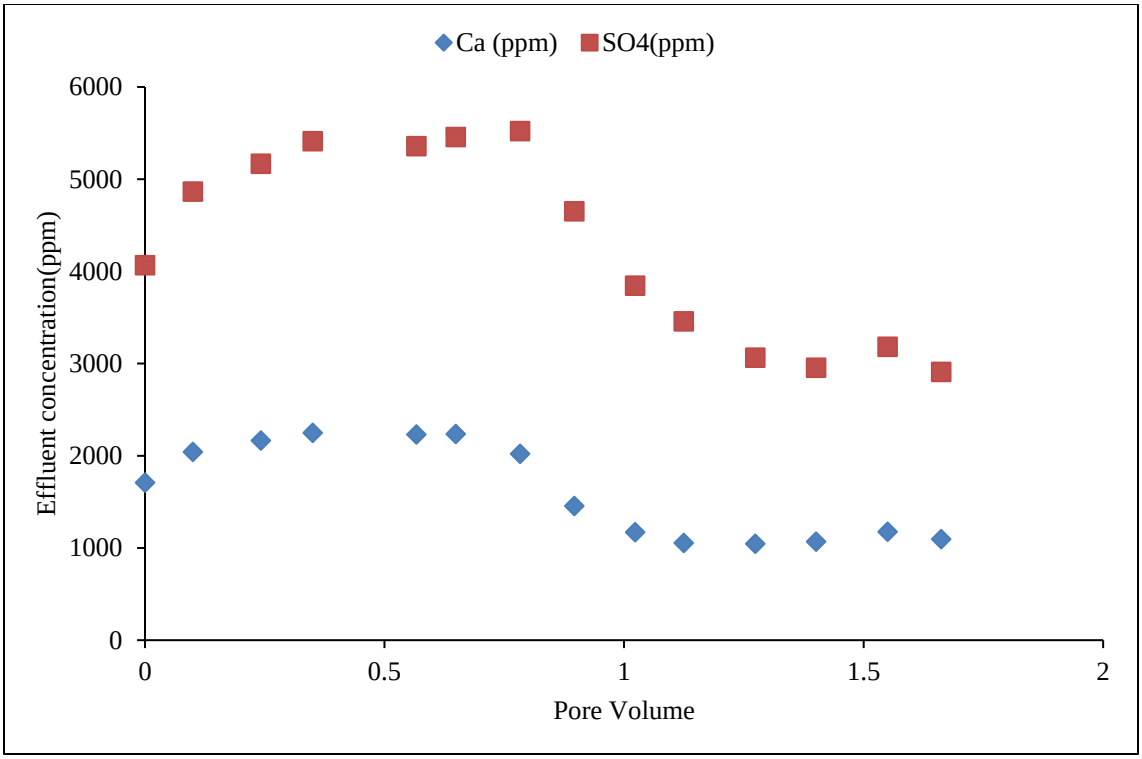

Figure 4.40(c): Effluent calcium and sulfate ions (in ppm) obtained during experiment 4.13

4.2.3 Surfactant phase behavior experiments

Experiment 4.14: Surfactant phase behavior using ammonia

Surfactant phase behavior experiments were performed to obtain ultra-low IFT surfactant formulations using ammonia as the alkali. The detailed procedure to perform surfactant phase behavior is given in chapter 3. In the experiments using ammonia, the concentration of ammonia was fixed and the salinity was increased by adding salts. This procedure was adopted because ammonia does not add much to salinity and increasing only ammonia concentration did not show Winsor type phase behavior transitions. The electrical conductance of aqueous solutions prepared by adding a given amount of

ammonia or NaCl was measured to get an idea of the salinity that a given amount of ammonia provides. The results are shown in Figure 4.41. From this figure, it can be seen that when NaCl concentration was increased from 0 to 5 wt%, the electrical conductance increased from 0 to 80,000 uS. When the ammonium hydroxide (containing 30% ammonia by volume) was increased from 0 to 5 wt%, the electrical conductance increased to only about 1000 uS. This value is equivalent to about 0.2 wt% NaCl.

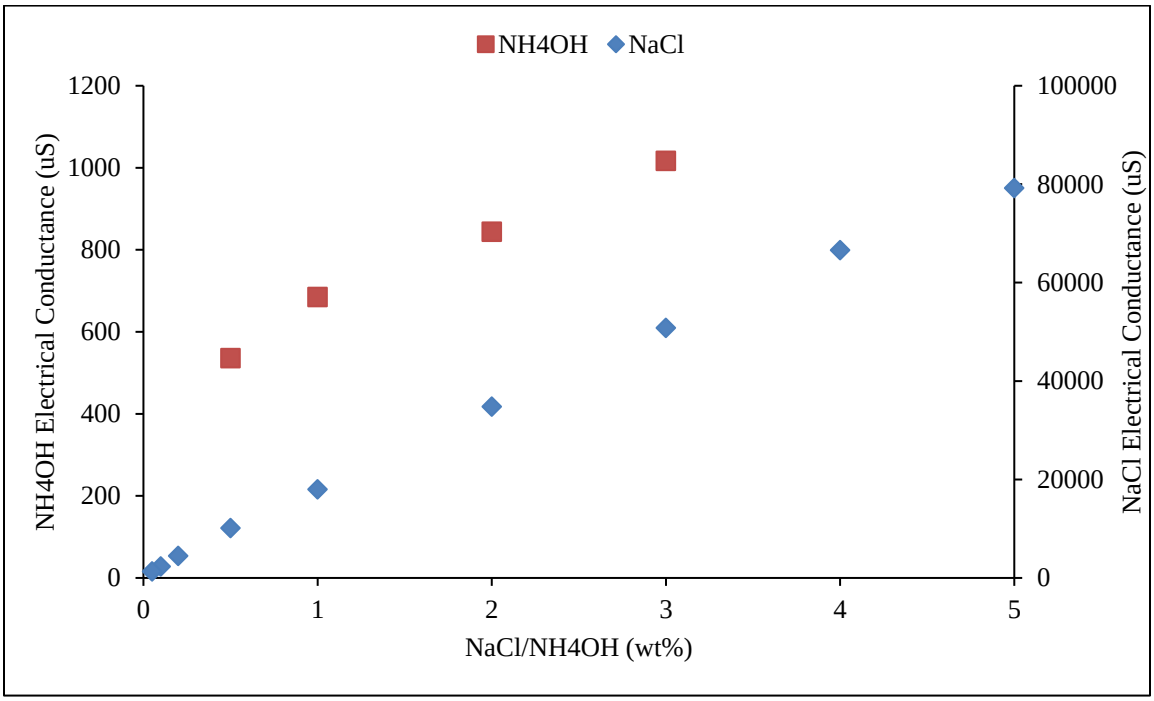

Figure 4.41: Electrical conductance of samples prepared by adding NaCl or NH_4OH in DI water

Experiment 4.14(a): Surfactant phase behavior using oil#1

From the previous experiments, it is clear that calcium ions can be up to 2000 ppm, depending on temperature and brine composition, in cores containing gypsum when

ammonia is used as the alkali. Experiments were therefore also performed to understand the effect of free calcium ions on interfacial tension, optimum salinity and aqueous stability. The surfactant formulation, developed previously with sodium metaborate and oil#1, gave an ultralow IFT surfactant formulation with ammonia. The same formulation was then repeated with 500 ppm and 1000 ppm calcium ions but did not show low IFT. The formulation was therefore modified to 0.5 wt% C_{12-13}-13PO-SO_4, 0.5% C_{15-18} IOS, and 1% IBA-3EO which showed ultralow IFT without calcium and with up to 1,000 ppm calcium ions (Figures 4.42(a) and 4.42(b)) The optimum salinity decreased from about 67,000 ppm to 41,000 ppm as the concentration of calcium ions was increased from 0 ppm to 1,000 ppm. The solubilization ratios were more than 10, corresponding to the IFT of less than 0.003 dynes/cm using Huh's equation both with and without calcium ions. The solution was aqueous stable up to 55,000 ppm but was not aqueous stable in the presence of calcium ions. During the ASP coreflood, the ASP slug was injected at its aqueous stability limit of 55,000 ppm. There was no problem in injecting the slug since the calcium ions were picked up only after the slug interacted with gypsum in the core. These results will be discussed in detail.

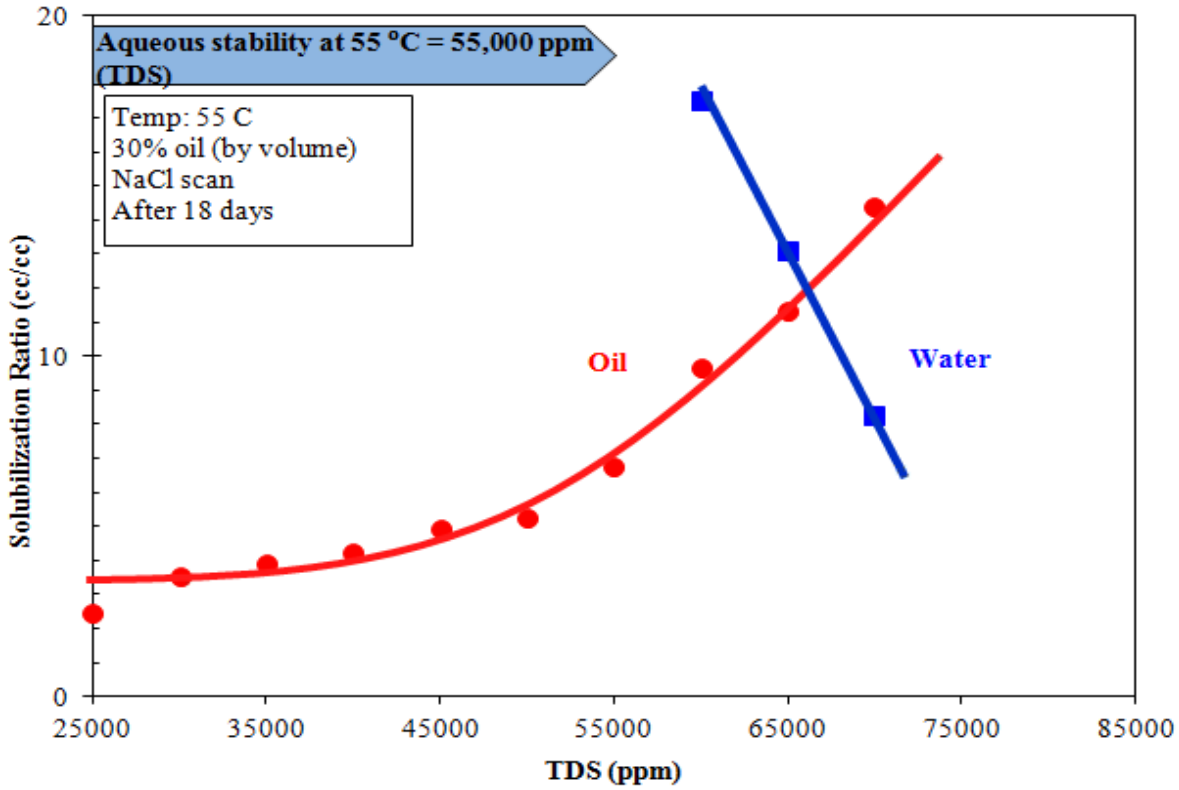

Figure 4.42 (a): Oil and water solubilization ratios of a low IFT surfactant formulation developed for crude oil-1 in the absence of calcium ions

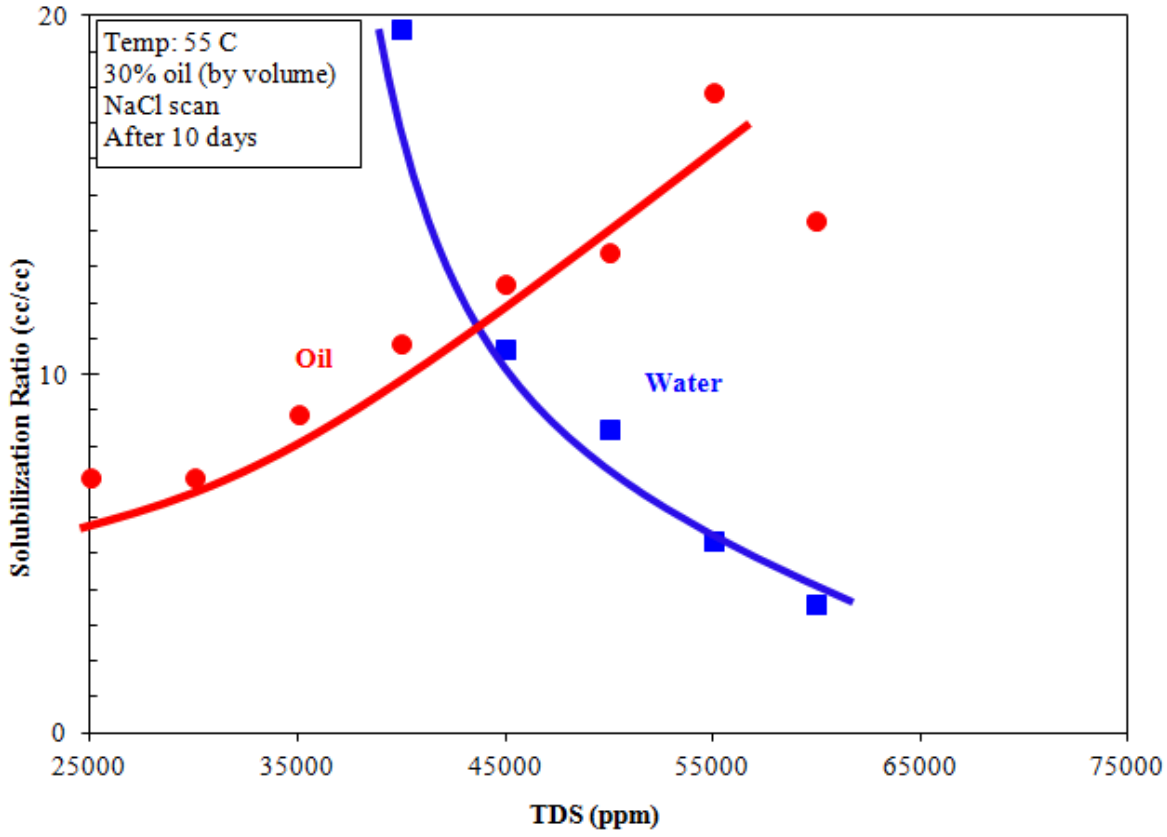

Figure 4.42(b): Oil and water solubilization ratios of a low IFT surfactant formulation developed for crude oil-1 in the presence of 1000 ppm calcium ions

Experiment 4.14(b): Surfactant phase behavior using oil#3

Experiments were performed using oil#3, having a viscosity of 5 cP at 25 °C, to obtain ultralow IFT surfactant formulations in the presence of calcium ions. A surfactant formulation consisting of 0.15% $C_{12\text{-}13}$-7PO-SO_4, 0.15% $C_{19\text{-}23}$ IOS, 0.2% $C_{12\text{-}13}$-30PO-35EO-SO_4 and 1.5% TEGBE gave both ultralow IFT and aqueous stability up to optimum salinity at 25 °C. The solubilization plots with 800 ppm calcium and 1200 ppm calcium are shown in Figures 4.43(a) and 4.43(b), respectively. The solubilization ratios

at their respective optimum salinity were more than 20 in both the cases. A shift in optimum salinity from 52,000 ppm to 48,000 ppm was observed as the calcium concentration was increased from 800 ppm to 1200 ppm.

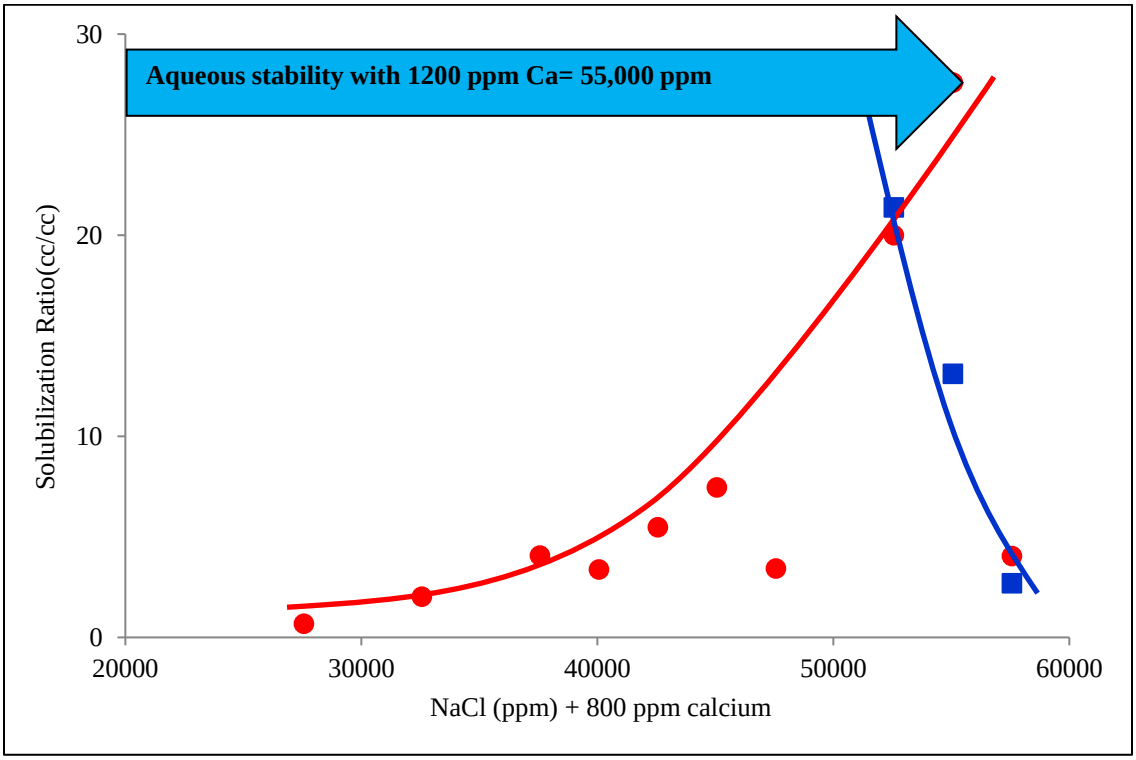

Figure 4.43(a): Oil and water solubilization plots in presence of 800 ppm calcium for an ultralow IFT formulation developed with crude oil-3

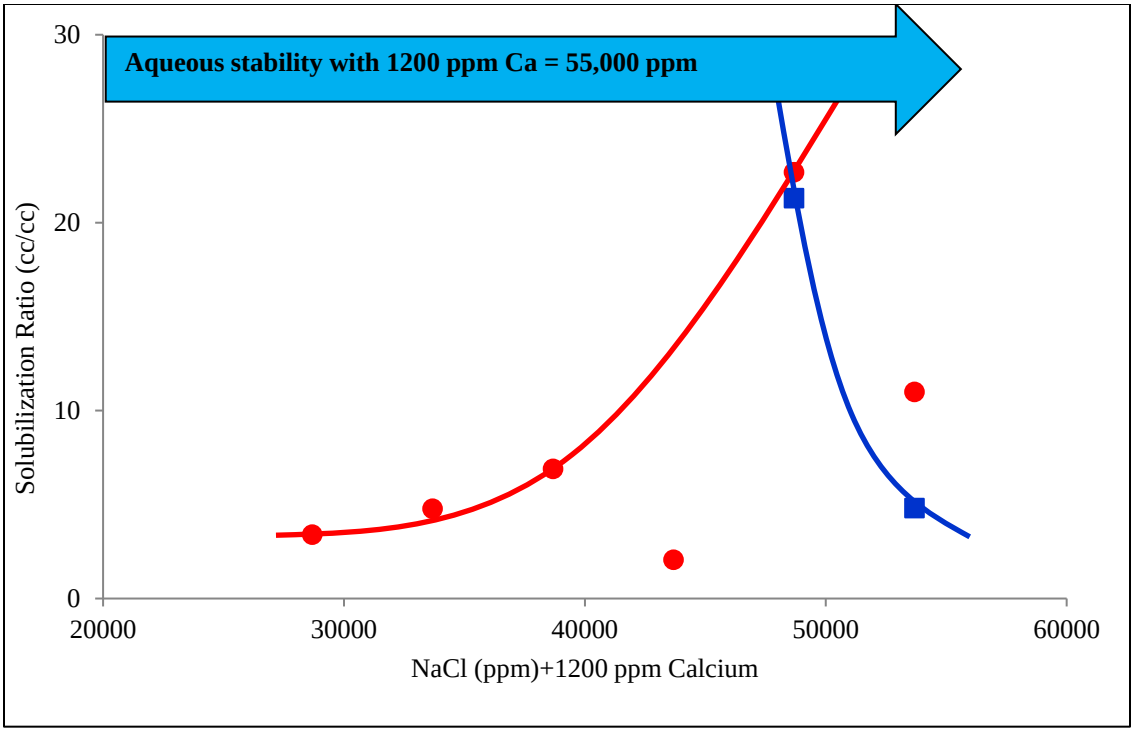

Figure 4.43(b): Oil and water solubilization plots in presence of 1200 ppm calcium for an ultralow IFT formulation developed with crude oil-2

Experiment 4.14(c): Surfactant phase behavior using oil#4

Surfactant phase behavior experiments with performed with oil#4, having a viscosity of 8 cP at 59 °C, using 0.65% C_{28}-25PO-45EO-carboxylate, 0.45% C_{15-18} IOS, 0.25% C_{19-28} IOS, 1% TEGBE and effect of calcium ions were studied. The surfactant formulation showed ultralow IFT with no calcium and 1000 ppm calcium ions, was aqueous stable at optimum salinity in both the cases and showed a decrease in optimum salinity by 10,000 ppm NaCl on increasing calcium ions to 1000 ppm. The solubilization plots with and without calcium ions are shown in Figures 4.44(a) and 4.44(b), respectively.

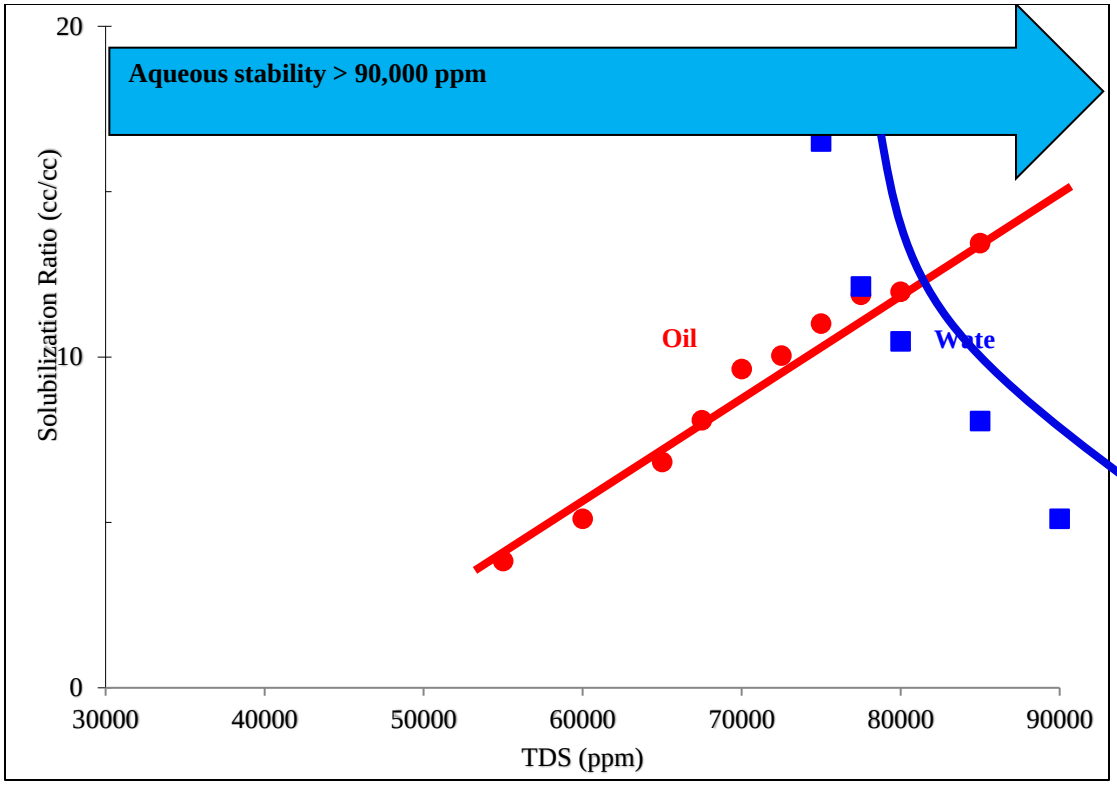

Figure 4.44(a): Oil and water solubilization ratios for an ultralow IFT surfactant formulation and crude oil-4 in the absence of calcium ions

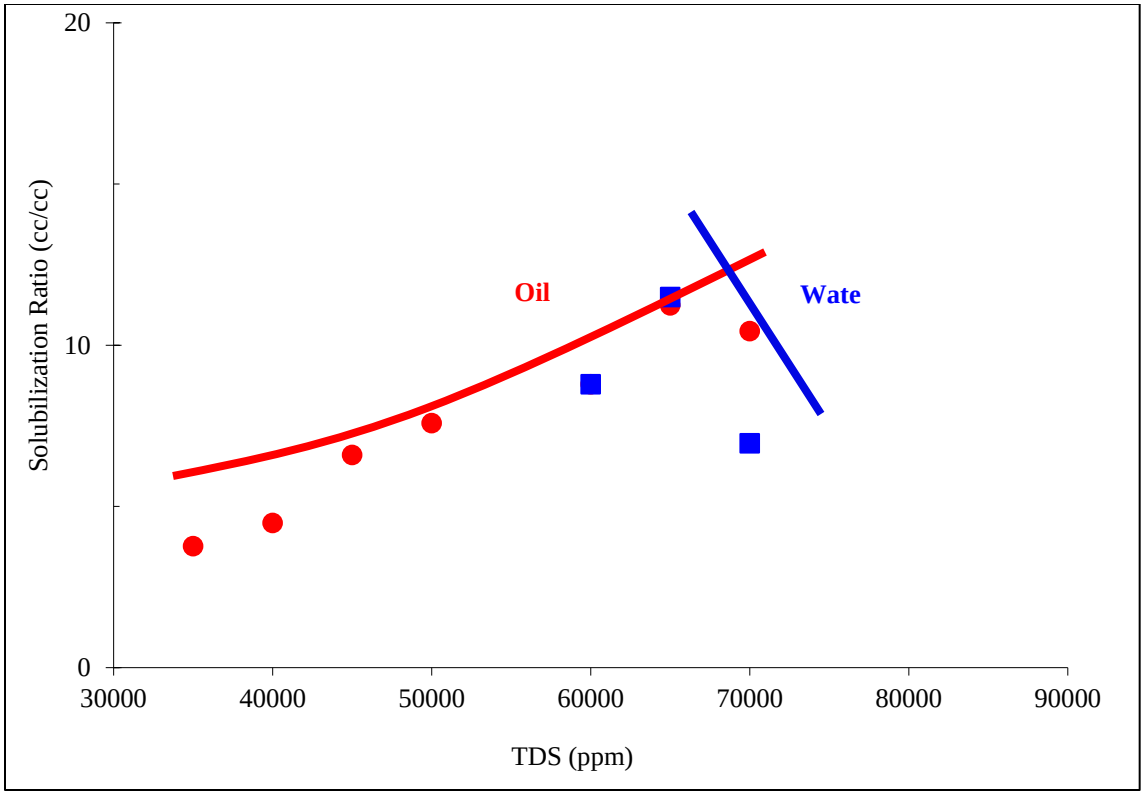

Figure 4.44(b): Oil and water solubilization ratios for an ultralow IFT surfactant formulation and crude oil-4 in the presence of 1000 ppm calcium

4.2.4 Polymer stability experiments

Experiment 4.15: Polymer stability in presence of calcium ions and ammonia

Polymer selection study was performed next to identify polymers that can be used to perform ASP floods, using ammonia as alkali, in cores containing gypsum. It was previously shown that the concentration of calcium ions and pH of the aqueous solution in equilibrium with gypsum, when ammonia was used as the alkali, could be as high as 2000 ppm and 11, respectively. High pH could expedite the hydrolysis of polyacrylamide polymers and precipitate it in the presence of calcium ions. Experiments were performed

HPAM, 2-acrylamide-2-methylpropane sulfonic acid (AMPS) and N-vinyl pyrrolidone (NVP) polymers in the presence of ammonia and up to 1000 ppm Ca at 59 ºC. Initial screening experiments showed precipitation of HPAM polymer samples under these conditions. SAV 550 (NVP polymer) and AN-125 (AMPS polymers) were found to be stable under similar conditions. Aqueous solutions containing fixed NaCl concentration, 0.6% NH_3, up to 3000 ppm polymer and 1000 ppm Ca were prepared in glass ampules and kept at 59 ºC**.** These samples were observed visually for any signs of chemical degradation and viscosity measurements were performed from time to time using the TI ARG2 rheometer. The results obtained using AN-125 polymer are shown in Figure 4.45. The polymer solution remained clear and retained its viscosity even after 20 days at 59 °C. The pH of polymer samples was about 10.2 after 20 days.

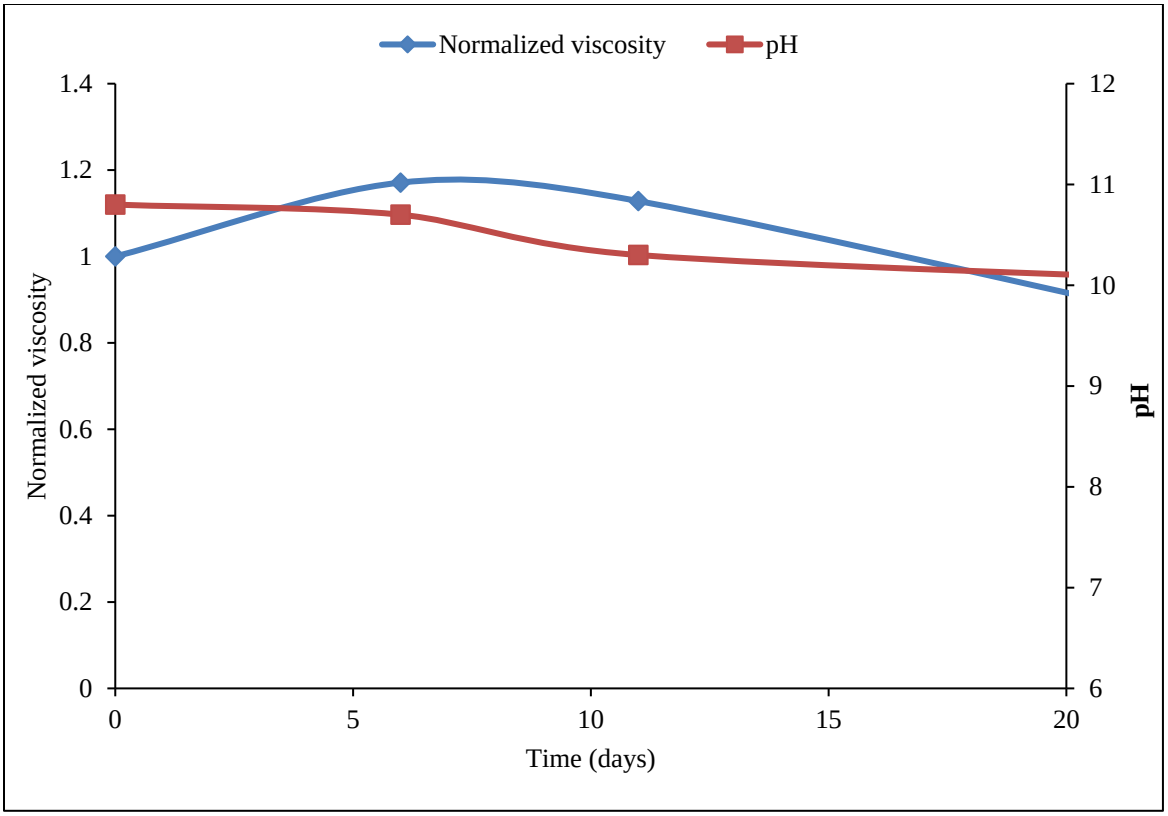

Figure 4.45: pH and viscosity (at 10 sec^{-1} shear rate and 25 ºC) of AN-125 samples in the presence of 1000 ppm Ca^{2+} kept at 59 ºC.

4.2.5 Oil recovery corefloods

Experiment 4.16(a): Oil recovery core CF-5 in Berea sandstone

The surfactant formulation developed with oil#4 was first tested in Berea sandstone core before moving on to the reservoir cores. The viscosity of the oil at 59 °C was about 8 cP. The core properties, experimental conditions and ionic compositions of the formation brine, waterflood brine, ASP slug, and polymer drive(s) are given in Tables 4.22 and 4.23. More details of the coreflood are given in Table 4.33(a). The detailed procedure followed to perform oil recovery corefloods, including the methods used for deciding critical parameters such as the salinity gradient, polymer requirements in the surfactant

slug and polymer drives is discussed in chapter 3. The tracer test result of the core is shown in Figure 4.46, which showed that the core was fairly homogeneous. The pore volume from the tracer test results was found to be about 72 mL (after correcting for dead volumes). The tracer brine was then displaced with formation brine. Oil was injected next at reservoir temperature at a constant pressure of 200 psi to establish initial oil saturation. The initial oil saturation was found to be 0.66. Waterflood was performed next at 1 ft/d, and an oil recovery of about 44% OOIP was observed, reducing oil saturation from 0.66 to 0.37. 0.25 pore volume of ASP slug was injected at 60 °C at 0.05 mL/min, corresponding to 1 ft/day, followed by 0.5 pore volume injection of polymer 1 and 1.4 pore volume injection of polymer 2. The salinity of the formation brine was 75,000 ppm while the optimum salinity of the formulation was 70,000 ppm. 0.25 pore volume of ASP slug was injected at 65,000 ppm (type I) followed by 0.5 pore volume of polymer 1 at 45,000 NaCl and 1.4 pore volume of polymer 2 at 25000 ppm NaCl. The effluent samples were collected using automatic fractional collector and analyzed for oil recovery, polymer viscosity, pH, salinity and surfactant concentration. The results of the ASP coreflood are shown in Figure 4.47.

The effluent pH increased to about 9.8 on injecting about 1 pore volume indicating a good pH propagation. The oil recovery results show that a stable oil bank was not formed during the coreflood and oil recovery was observed even after 3.3 pore volumes. It was suspected that the polymer perhaps degraded in the container which resulted in an unfavorable mobility ratio at the surfactant slug-oil bank and surfactant-polymer interfaces. The effluent polymer viscosities, shown in Figure 4.48, were

compared with the initial viscosities of the ASP slug and polymer slugs. The effluent viscosity was about 37 cP even after injection 1.8 pore volumes, lower than initial viscosities of chemical slugs suggesting possible degradation of the polymer during the experiment. The tertiary oil recovery and residual oil saturation after 3.5 pore volumes were 65% and 0.13, respectively.

Table 4.22: Properties of the core used in the ASP coreflood CF-5

Core	Length (inches)	Diameter (inches)	Porosity (%)	Permeability (md)	Temperature (°C)	Gypsum
Berea Sandstone	12	1.5	19.5	594	59	No

Table 4.23: Ionic composition of the brines used in the ASP coreflood CF-5

Salt	Formation/Waterflood brine (ppm)	ASP slug (ppm)	Polymer drive 1 (ppm)	Polymer drive 2 (ppm)
NaCl	70,000	60,000	35,000	20,000
Na_2SO_4	5,000	5,000	5,000	5,000
NH_3	-	0.9 wt%	0.45 wt%	-
TDS	**75,000**	**65,000**	**40,000**	**25,000**

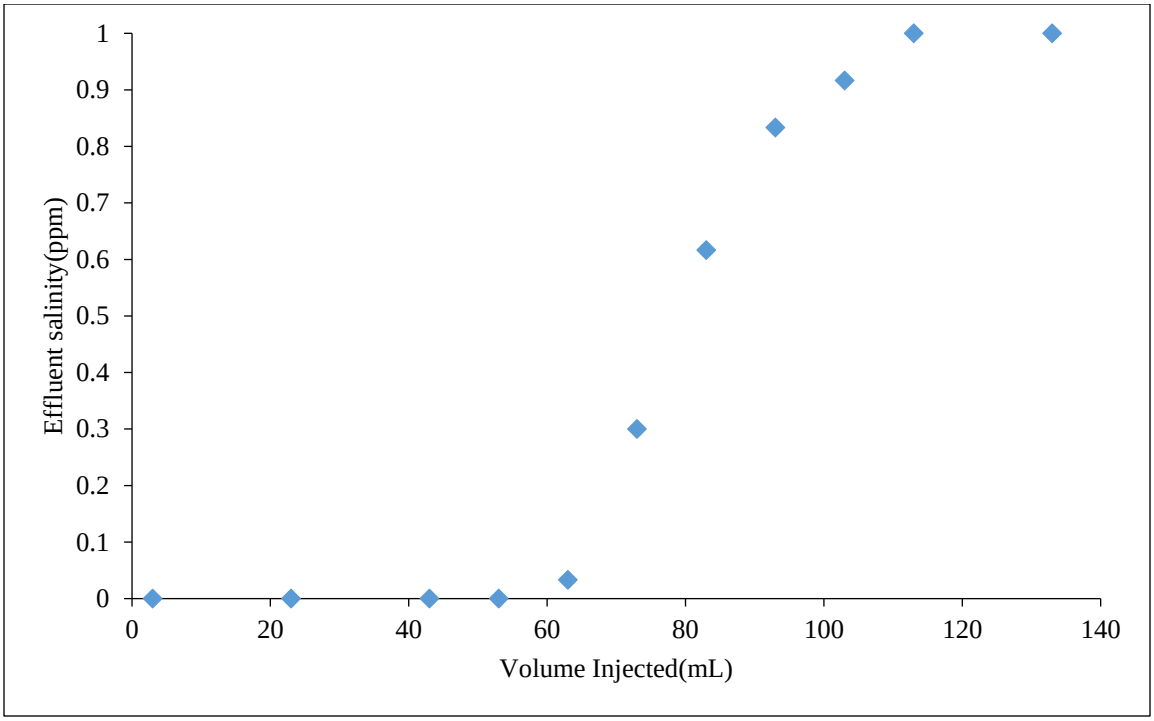

Figure 4.46: Tracer test results of the sandstone core used in ASP coreflood CF-5

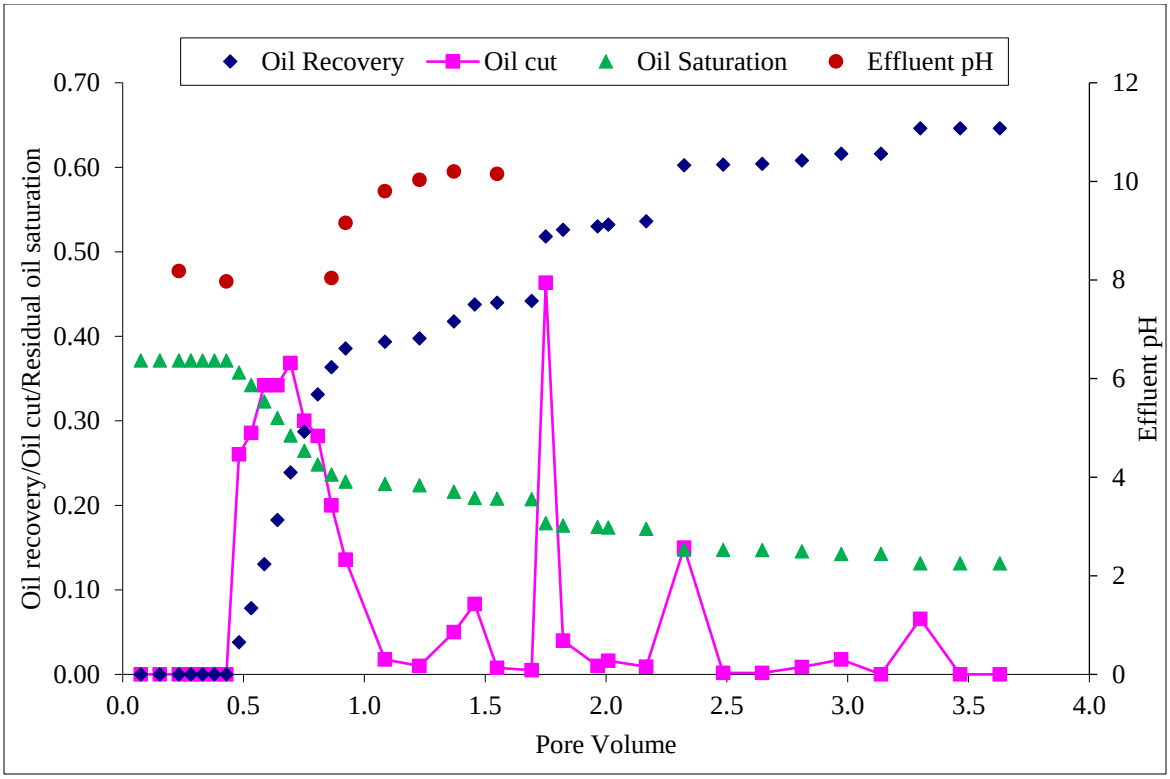

Figure 4.47: Oil recovery, oil cut, residual oil saturation and effluent pH obtained from ASP coreflood CF-5

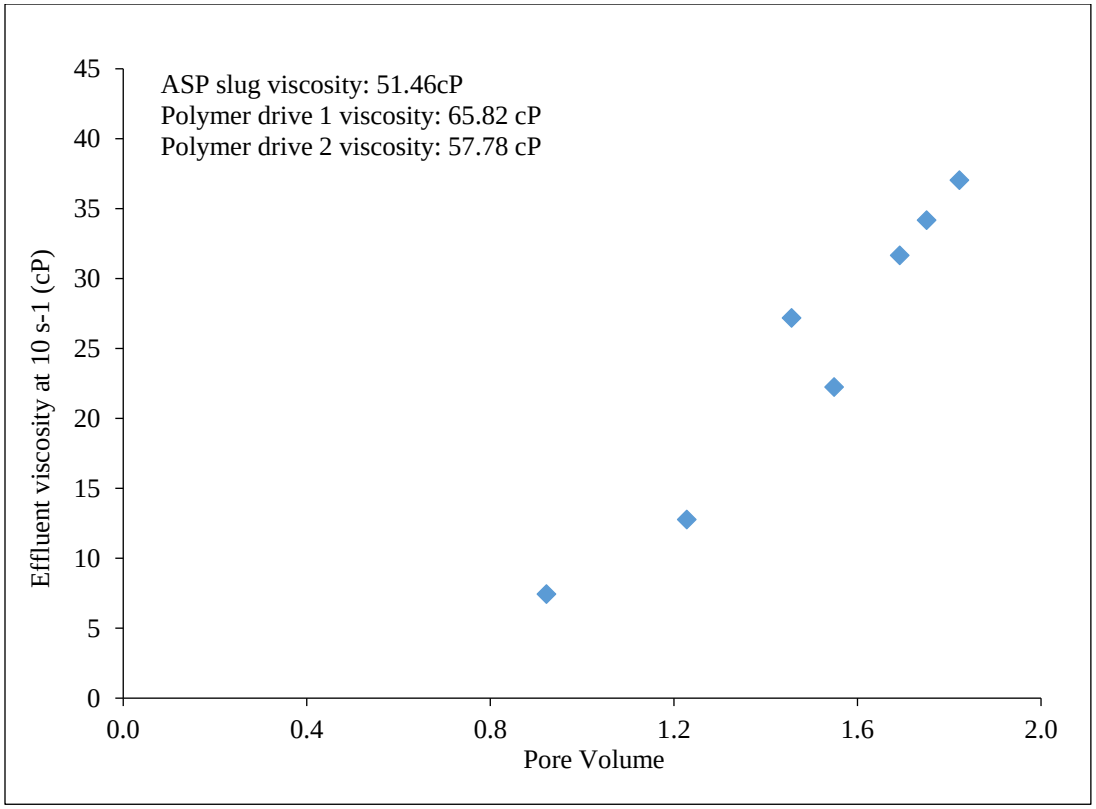

Figure 4.48: Viscosity of the effluent samples collected during ASP coreflood CF-5

Experiment 4.16 (b): Oil recovery coreflood CF-6 in Berea sandstone

The source of polymer degradation in the previous experiment was identified to be the small amount of rust in the steel accumulator that was used to inject the chemical slugs. In the following experiments, glass columns were used instead, and mineral oil was used to displace the chemical slugs. The previous coreflood was repeated in another Berea sandstone core. The core properties and brine salinities are given in Tables 4.24 and 4.25. More details of the coreflood are given in Table 4.33(a). The tracer test results of this core are, given Figure 4.49, shows that the core was fairly homogeneous. The core

was flooded with the formation brine following the tracer test and then with oil#4 at a constant pressure of 200 psi at reservoir temperature to establish the initial oil saturation. The core was then waterflooded at 1 ft/d till no oil was produced. Waterflood resulted in lowering the oil saturation from about 0.65 to 0.38.

0.25 pore volume of ASP slug was then injected followed by the polymer drive at 1 ft/d, and effluents were analyzed for oil recovery, pH, surfactant concentration, polymer viscosity and salinity.

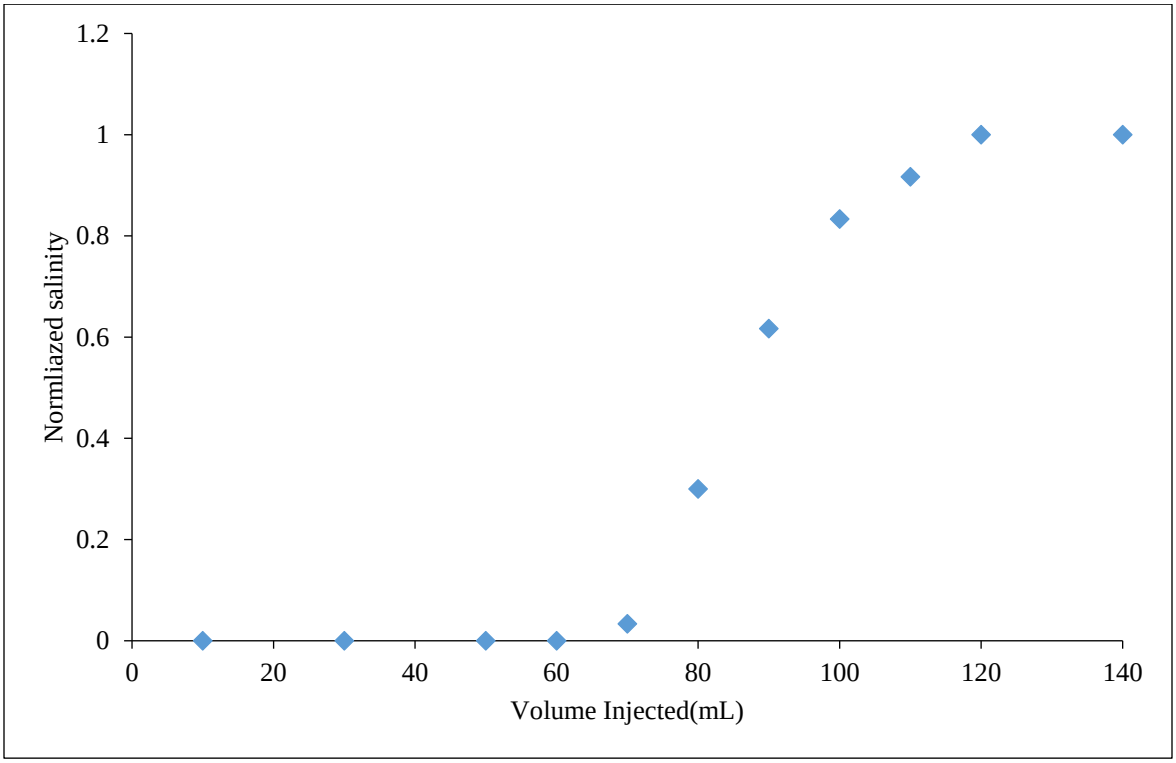

Figure 4.49: Tracer test results of the Berea sandstone core used in the ASP coreflood CF-6

The oil recovery results are shown in Figure 4.50. About 75% of oil left after waterflood was recovered on after a total injection of 2.5 pore volumes. A good oil bank

of about 40-50% oil cut was observed, however, the oil cut was not maintained long enough. The residual oil saturation after the chemical flood was reduced to about 0.097 from 0.38 (left after waterflood). The effluent pH after 1 pore volume was about 9.5. The effluent salinity showed a gradual transition from Winsor type II to Winsor type III to Winsor type I as the formation brine was displaced with surfactant slug and polymer drive. The effluent polymer viscosity data (Figure 4.51) showed no signs of polymer degradation, unlike the previous case. All the injected surfactant was retained resulting in a surfactant retention of 0.33 mg/g rock.

Table 4.24: Properties of the core used in the ASP coreflood CF-6

Core	Length (inches)	Diameter (inches)	Porosity (%)	Permeability (md)	Temperature (°C)	Gypsum
Berea Sandstone	12	1.5	21	620	59	No

Table 4.25: Ionic composition of the brines used in the ASP coreflood CF-6. Note that since ammonia dissociates partially, it is not added to TDS

Salt	Formation/Waterflood brine (ppm)	ASP slug (ppm)	Polymer drive 1 (ppm)
NaCl	85,000	75,000	52,500
Na_2SO_4	-	-	-
NH_3	-	0.9 wt%	0.45 wt%
TDS	**85,000**	**75,000**	**52,500**

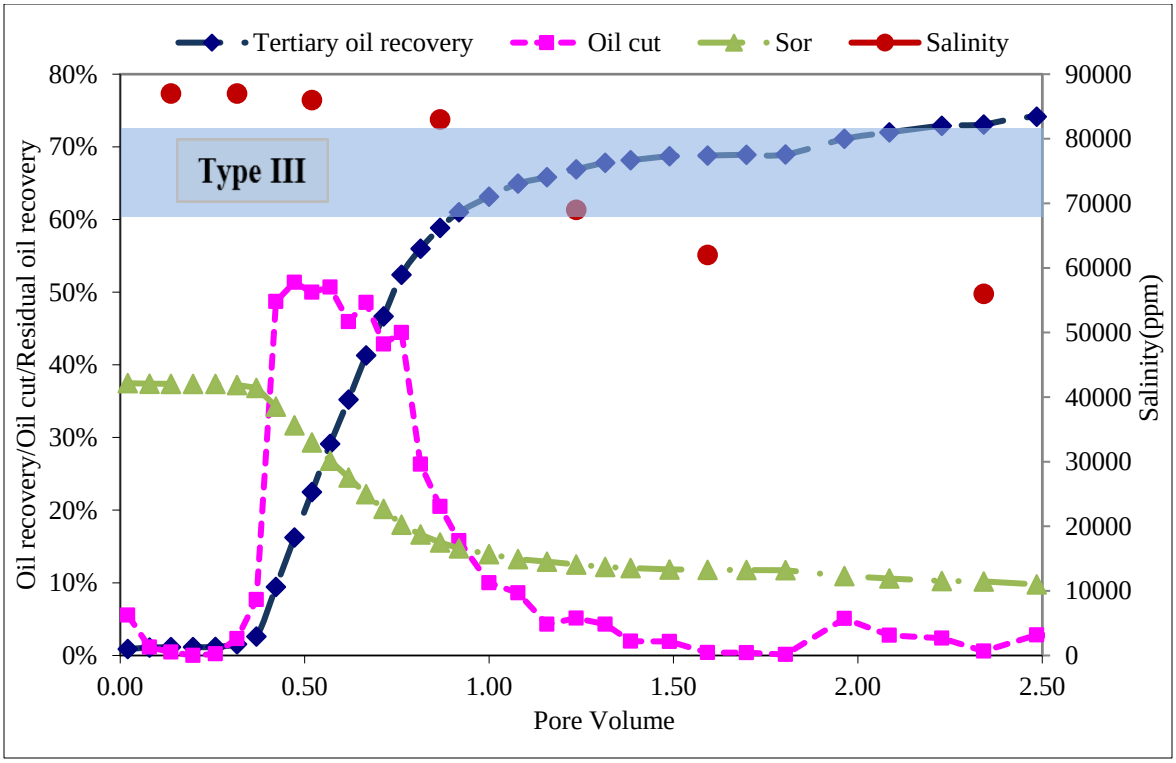

Figure 4.50: Oil recovery, oil cut, residual oil saturation and effluent salinity obtained from the ASP coreflood CF-6

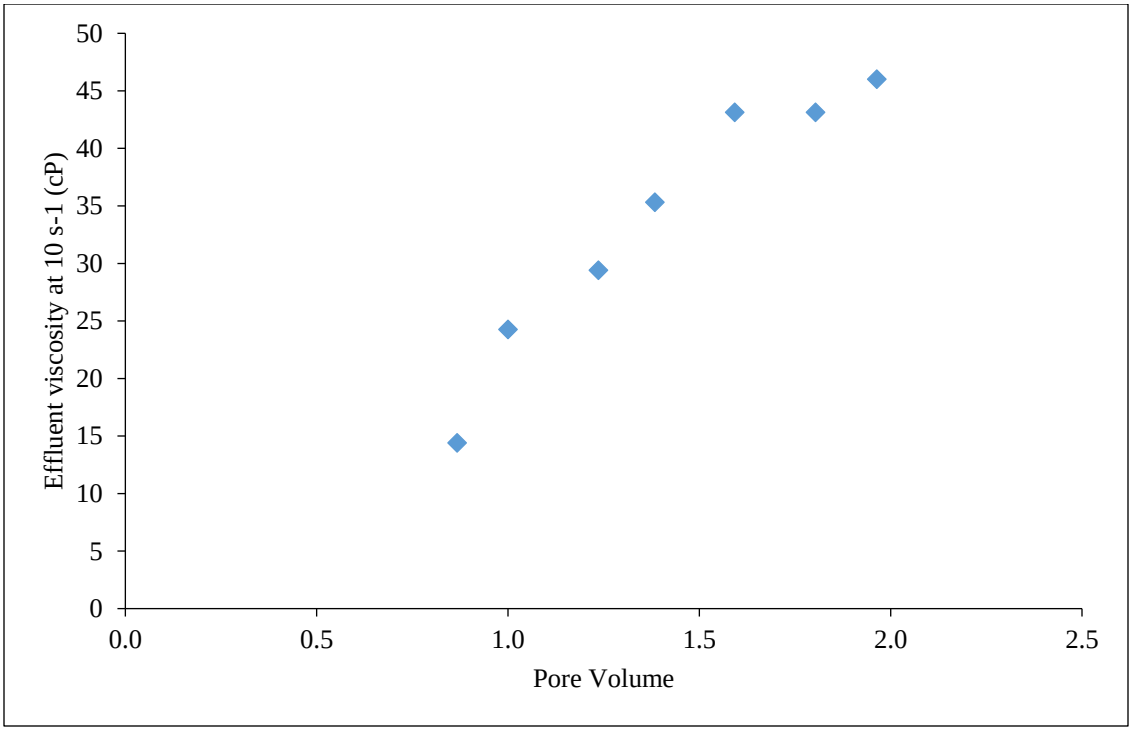

Figure 4.51: Viscosity of the effluent samples collected during the ASP coreflood CF-6

Experiment 4.16 (c): Oil recovery coreflood CF-7 in Berea sandstone

The previous coreflood was repeated in a Berea sandstone core. In this experiment, the ASP slug size was increased to 0.4 pore volumes since all the surfactant was retained in the previous coreflood. The properties of the core and compositions of the brines are given in Table 4.26 and 4.27. The core characterization, initial oil saturation, and waterflooding procedure were the same as described previously. The oil recovery results of the Berea coreflood is summarized in Table 4.33(a) and Figure 4.52. Waterflood was conducted with 90,000 ppm NaCl brine which left a residual oil saturation of about 34%. 0.4 PV ASP slug was then injected followed by the polymer drive. The ASP slug had the salinity of 80,000 ppm NaCl and contained 1.35%

surfactant, 0.9% NH_3 and 3500 ppm FP3630. About 80% of the oil left after waterflood was recovered by 1.5 pore volumes of the chemical flood. The oil-bank broke through at about 0.35 pore volumes and a high oil cut of about 50% was observed; the oil saturation decreased to about 7% from about 34%. A pH of 10.5 was observed after 1 pore volumes. The salinity in the polymer drive was 60,000 ppm. The cumulative oil recovery, including waterflood recovery, was about 88%. The tertiary oil recovery was 78% ROIP. No surfactant was observed in the coreflood effluent. The most likely reason for a high surfactant retention was because the effective salinity of the polymer drive was not low enough to give Winsor type I phase behavior. This coreflood in the Berea core showed that the surfactant formulation was effective in mobilizing oil, but the surfactant retention was high.

Table 4.26: Properties of the core used in the ASP coreflood CF-7

Core	Length (inches)	Diameter (inches)	Porosity (%)	Permeability (md)	Temperature (°C)	Gypsum
Berea Sandstone	11.65	1.48	20.5	409	59	No

Table 4.27: Ionic composition of the brines used in the ASP coreflood CF-7

Salt	Formation/Waterflood brine (ppm)	ASP slug (ppm)	Polymer drive 1 (ppm)
NaCl	90,000	80,000	60,000
NH_3	-	0.9 wt%	0.45 wt%
TDS	**90,000**	**80,000**	**60,000**

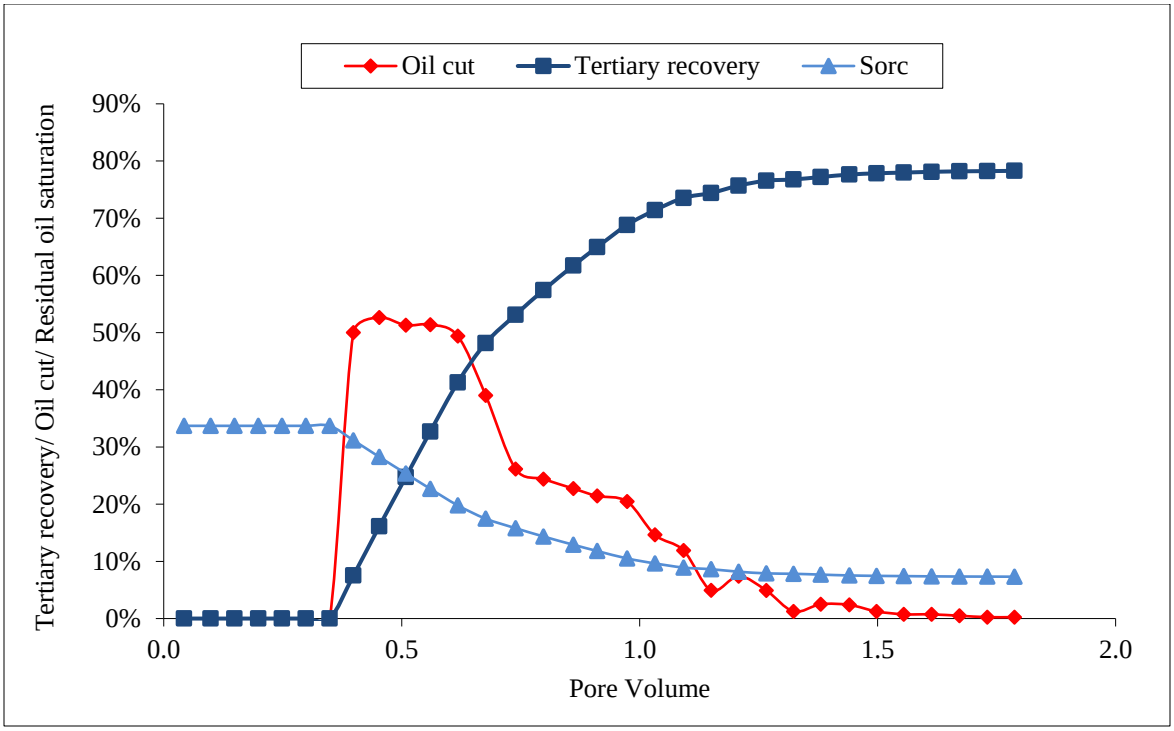

Figure 4.52: Oil recovery, oil cut and residual oil saturation during the ASP coreflood CF-7

Experiment 4.17 (a): Oil recovery coreflood CF-8 in a carbonate core containing gypsum

After testing the formulation (formulation#) in outcrop cores, corefloods CF-5 to CF-7, the formulation was tested in a reservoir core containing gypsum. The polymer stability experiments showed AN-125 to be better suited for such conditions of high pH (with ammonia) and high calcium ions (due to gypsum dissolution). The surfactant formulation was tested with and without calcium and was found to give ultralow IFT and good aqueous stability even in the presence of calcium ions. This test was important to understand the effect of calcium ions, dissolved from gypsum, on surfactant phase

behavior so that the chemical flood can be designed favorably. The use of sodium sulfate to reduce gypsum dissolution (and thus calcium concentration) was studied through simulations with PHREEQC (discussed in chapter 5). The results showed that addition of 10,000 ppm sodium sulfate was likely to reduce the calcium pickup from gypsum by almost 50%, thus enhancing polymer stability, improving surfactant phase behavior and overall making the coreflood design more robust.

The carbonate core, previously used for single-phase ammonia flood, was used for performing oil recovery coreflood. The core was cleaned by injecting many pore volumes of sodium chloride brine. The presence of gypsum in the core was confirmed by measuring the effluent ions obtained by injecting brine consisting of only sodium chloride salt. The core properties, brine composition and experimental conditions are given in Table 4.28 and 4.29. The procedure described previously was followed to prepare the coreflood setup and establish initial oil saturation. Waterflood was then performed at 1 ft/d and oil recovery and pressure drop were recorded. The waterflood brine consisted of only sodium chloride salt and the effluent samples after waterflood were tested for calcium and sulfate ions to again confirm the presence of gypsum. A chemical flood consisting of 0.4 pore volumes of ASP slug, 0.5 pore volumes of polymer drive 1 and 1.2 pore volume of polymer drive 2 was performed. The salinity was gradually reduced from 90,000 ppm, in the formation brine to 35,000 in the polymer drive 2. 10,000 ppm sodium sulfate was added to the surfactant slug and polymer drive to reduce gypsum dissolution. AN-125 and FP 3630 were used as the polymers in the surfactant slug and polymer drives, respectively. The details of the compositions of

surfactant slug and polymer drives are given in Table 4.33(b). The coreflood results are shown in Figures 4.53-4.55. The oil saturation reduced from about 0.29, after waterflood, to 0.05 after the chemical flood. The chemical flood resulted in a tertiary oil recovery of about 81%, increasing cumulative oil recovery from 57% (after waterflood) to 91%. A maximum pressure drop of 4.5 psi/ft was observed at 1 ft/d injection rate, which reduced to about 2 psi/ft at the end of the chemical flood. No sign of plugging was observed during the experiment. The effluent salinity data (Figure 4.54) indicated that type III region was encountered during the flood. A surfactant retention of 0.24 mg/g rock was observed and 43% of the injected surfactant was recovered. A pH value of 10 was obtained at 1 pore volumes indicating good pH propagation during the chemical flood. The effluent calcium ions were reduced substantially, both due to lowering of salinity and addition of sodium sulfate (Figure 4.55). The calcium and sulfate concentrations were about 1,700 ppm and 5,400 ppm, respectively, in the formation brine. Note that no calcium or sulfate was added to the formation brine and these ions were the result of gypsum dissolution.

Table 4.28: Properties of the core used in the ASP coreflood CF-8

Core	Length (inches)	Diameter (inches)	Porosity (%)	Permeability (md)	Temperature (°C)	Gypsum
Carbonate	11.65	1.48	0.20	480	59	Yes

Table 4.29: Ionic composition of the brines used in the ASP coreflood CF-8

Salt	Formation/Waterflood brine (ppm)	ASP slug (ppm)	Polymer drive 1 (ppm)	Polymer drive 2 (ppm)
NaCl	90,000	70,000	40,000	25,000
Na_2SO_4	-	10,000	10,000	10,000
NH_3	-	0.9 wt%	0.45 wt%	-
TDS	**90,000**	**80,000**	**50,000**	**35,000**

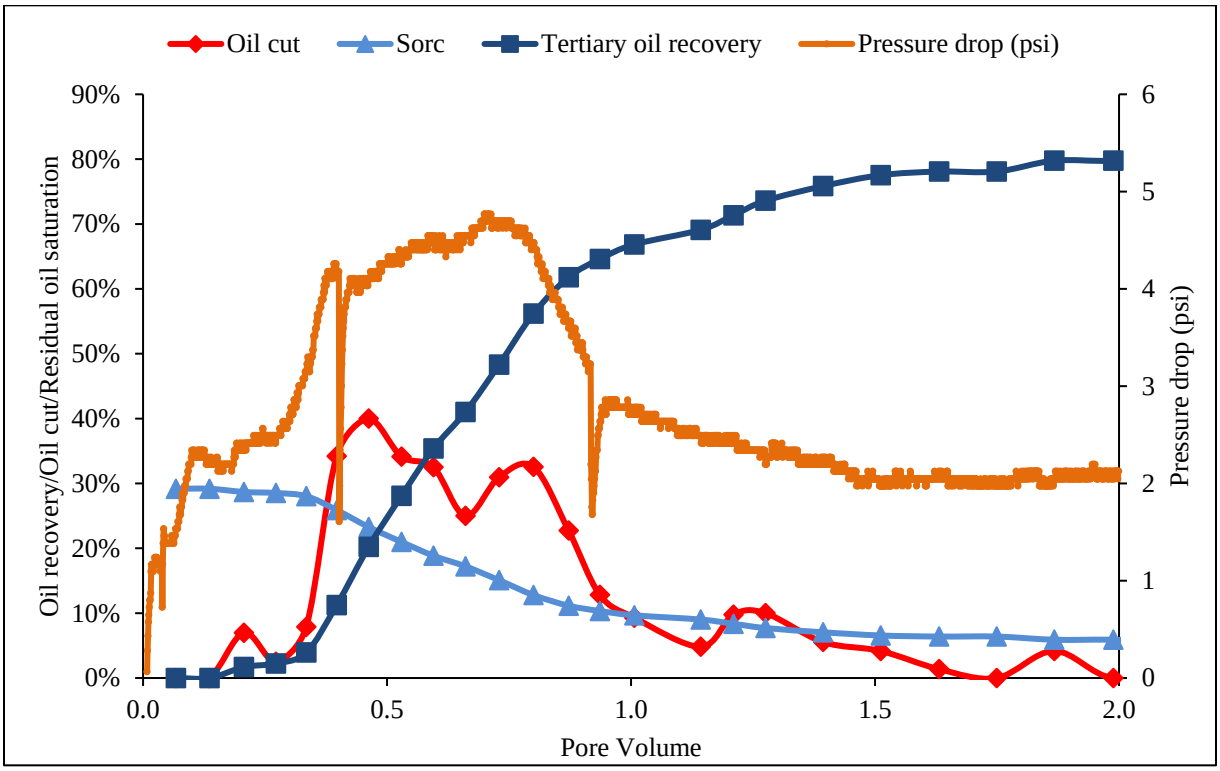

Figure 4.53: Oil recovery, oil bank, residual oil saturation and pressure drop during the ASP coreflood CF-8

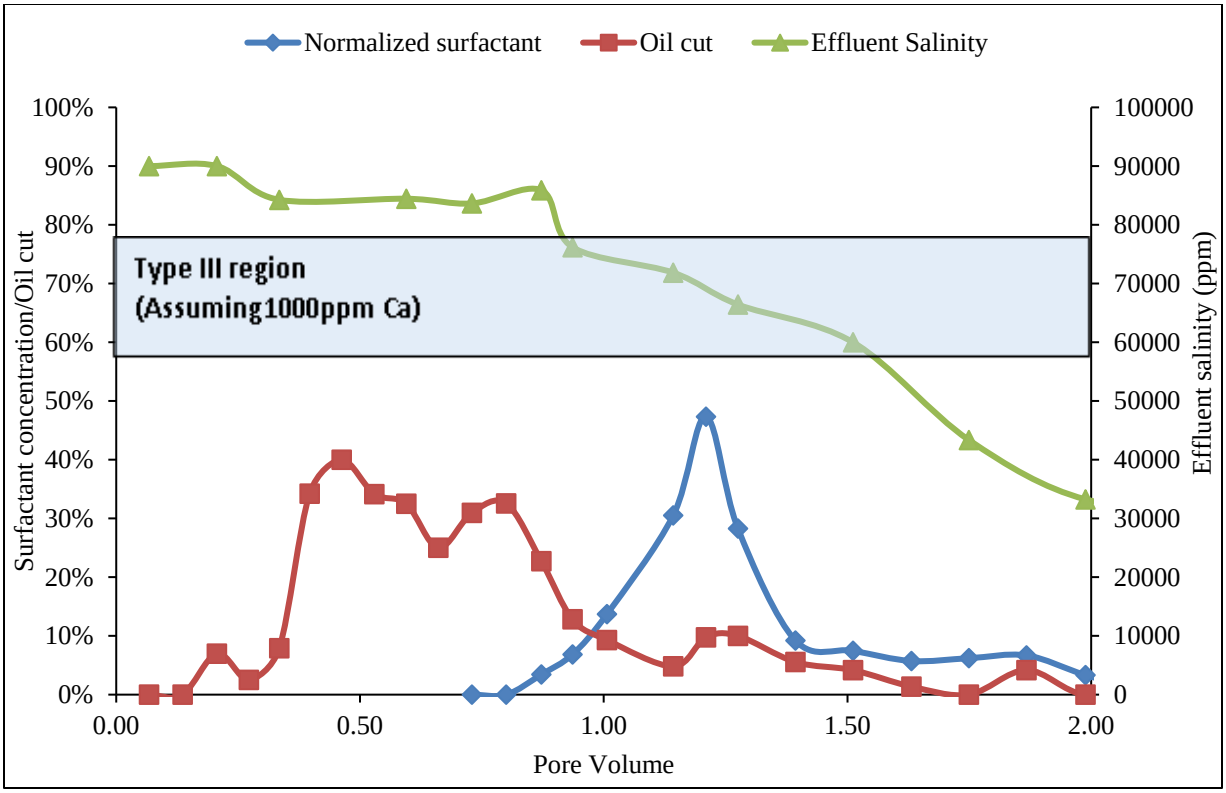

Figure 4.54: Oil bank, effluent surfactant concentration and salinity during the ASP coreflood CF-8

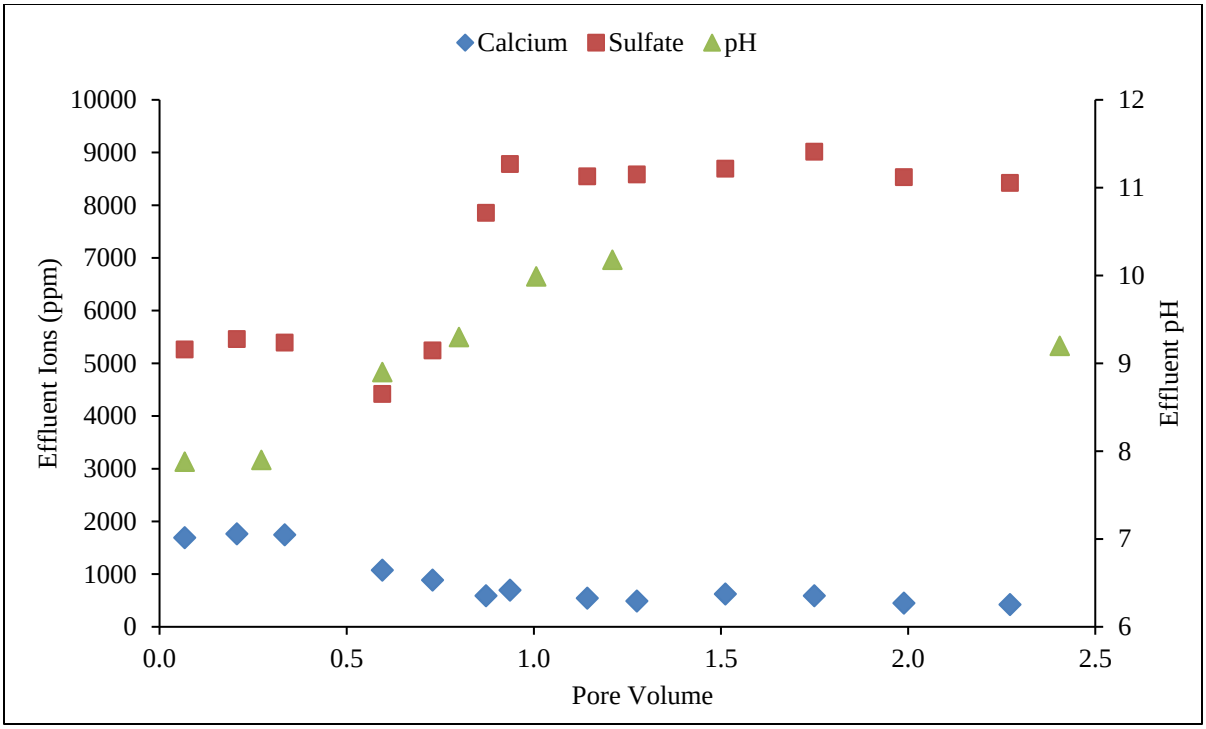

Figure 4.55: Effluent pH and ions during the coreflood CF-8

Experiment 4.17 (b): Oil recovery SP coreflood CF-9 in a carbonate core containing gypsum

After coreflood CF-8, the core was cleaned by injecting many pore volumes of brine, bleach, toluene and methanol as per the procedure described in chapter 3. The presence of gypsum in the core was confirmed by analyzing the core effluent ions obtained by injecting sodium chloride brine as described in chapter 3. SP coreflood was performed using oil-4 after cleaning the core used in coreflood CF-8. The salinity design and composition of the slugs in coreflood CF-9 was similar to that of coreflood CF-8, except no alkali was added to the surfactant slug in coreflood CF-9. The core properties

and brine compositions can be found in Table 4.28 and 4.29. Since no alkali was added to the surfactant slug, FP 3630S was used in the surfactant slug (and polymer drives), instead of AN-125. The details of the slugs are given in Table 4.13(b). This coreflood was performed to understand the benefits of adding ammonia, in terms of surfactant adsorption in particular. The coreflood characterization was performed using our standard method and initial oil saturation was established. The core was waterflooded to establish residual oil saturation to waterflood, after which the chemical flood was performed. The chemical flood design was kept as close to that of coreflood CF-8 as possible. No ammonia was added to the surfactant slug and FP 3630 was used in the surfactant slug and polymer drives. The oil recovery results of the coreflood are shown in Figure 4.56. The oil recovery during the chemical flood was about 85%, reducing the oil saturation to about 4%. A good oil bank and low surfactant retention of 0.2 mg/g rock were observed. The pressure drop data was very similar to that of coreflood CF-8.

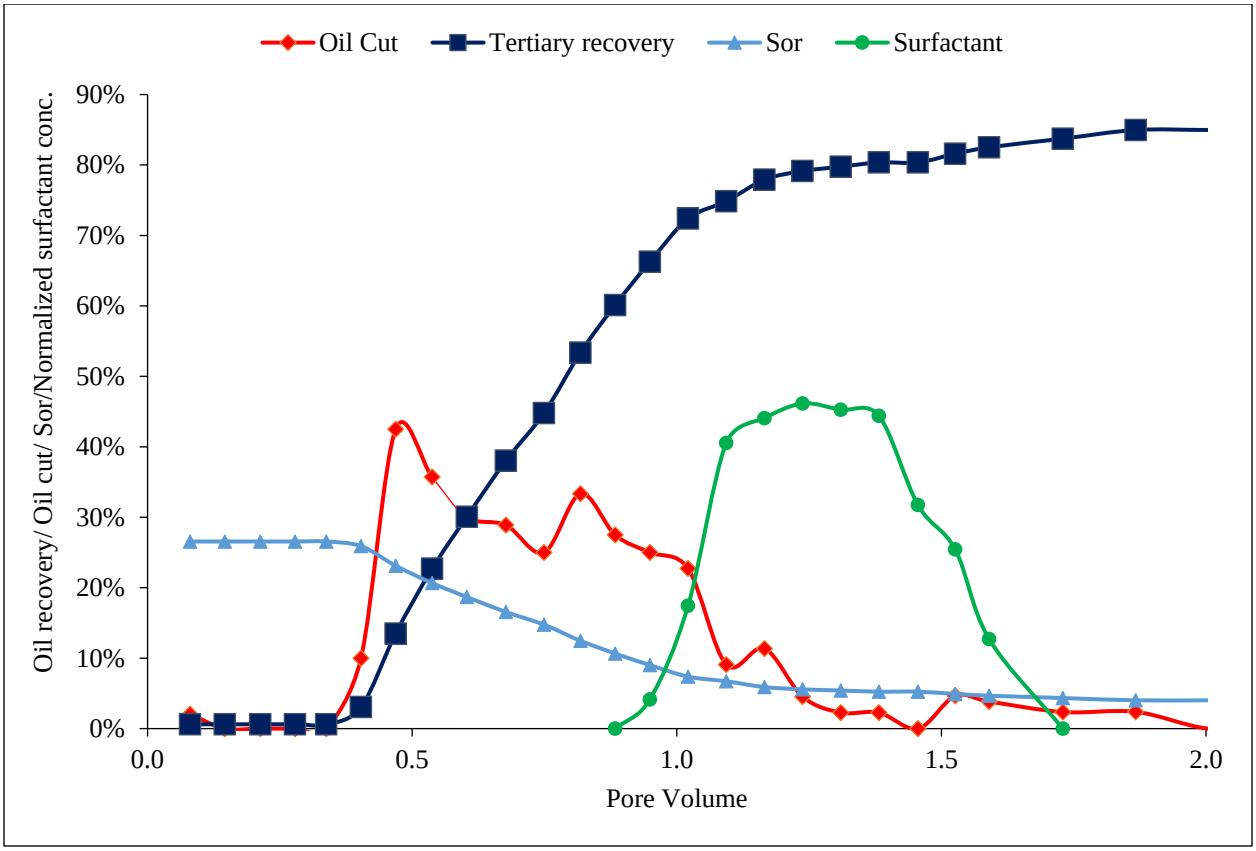

Figure 4.56: Oil recovery, oil cut, residual oil saturation and effluent surfactant concentration obtained from the SP coreflood CF-9

A comparison of coreflood CF-8 and 9 showed no obvious benefit of adding ammonia to surfactant formulations in the case of carbonate cores containing ammonia. Note that this surfactant retention consisted of both surfactant adsorption and phase trapping. However, an alkali usually helps in lowering only the adsorption. Single-phase chemical floods were therefore performed to study the effect of adding ammonia on surfactant adsorption only. The carbonate core was cleaned, after coreflood CF-9, using the core cleaning procedure described in chapter 3 and was used to perform single-phase

chemical floods (CF-10, 11 and 12). Note that no oil was injected into the core in these experiments and the chemical flood was performed after saturating the core with formation brine at reservoir temperature.

Experiment 4.18: Single-phase chemical floods (a) SP coreflood CF-10 (b) ASP coreflood CF-11 (c) SP coreflood CF-12

Three single-phase corefloods, CF-10-12, were performed after cleaning the carbonate core which were used in corefloods CF-8 and CF-9. The same surfactant formulation was used (surfactant formulation#4.14(c)). The injection sequence in these corefloods was the same as the respective oil recovery ASP or SP corefloods. The details of surfactant slug and polymer drives for corefloods CF-10, 11 and 12 are shown in Table 4.33(b). The core properties and brine compositions can be found in Table 4.28 and 4.29. The core was cleaned after each flood as per the cleaning procedure described in chapter 3, after which, the presence of gypsum in the core was confirmed by injecting sodium chloride brine and measuring the effluent ions with ion chromatography. Coreflood CF-10 was a single-phase SP flood where chemical slugs were injected into the core initially saturated with formation brine. The effluent samples were collected and analyzed for surfactant concentration using HPLC to obtain surfactant adsorption. Coreflood CF-11 (single-phase ASP flood) was similarly performed, however, 0.5% ammonia was added to the surfactant slug. The effluent samples were similarly processed to obtain surfactant adsorption. Note that in coreflood CF-11, AN-125 was used as the polymer in the surfactant slug, while FP 3630S was used as the polymer in the polymer drives. In SP

corefloods (CF-10 and CF-12), FP 3630S was used in both surfactant slug and polymer drives. Coreflood CF-12 was a repetition of coreflood CF-10 to confirm the adsorption number. No alkali was added to the surfactant slug of coreflood CF-12. A summary table of surfactant adsorptions in these corefloods is given in Table 4.33(b). The surfactant adsorption in the case of SP floods (CF-10 and CF-12) was found to be about 0.20 mg/g rock. In the case of single-phase ASP coreflood (CF-11), the surfactant adsorption was found to be about 0.24 mg/g rock. These adsorption values were very close to their respective surfactant retention values obtained from oil recovery corefloods CF-8 and CF-9; the surfactant adsorption values in the single-phase corefloods was also very similar with and without ammonia, although a high pH propagation was observed in the case of ASP flood suggesting that perhaps high pH is not the sole factor responsible for reduction in surfactant adsorption on carbonate surfaces in the presence of gypsum. The rock type and ionic composition of the brine perhaps have a large influence in governing surfactant adsorption values. About 10,000 ppm sodium sulfate was added in ASP and SP corefloods and sulfate ions might have reduced adsorption of surfactant since sulfate ions are known to lower the zeta potential of carbonate surfaces. Note that different polymers were used in the ASP and the SP slugs (AN-125 and FP3630, respectively) which may have also affected the surfactant retention values.

Table 4.30: Surfactant adsorption in single-phase surfactant floods in a carbonate core containing gypsum

Coreflood	Alkali amount	Surfactant adsorption (mg/g rock)
CF-10	No alkali	0.19
CF-11	0.5% NH_3	0.24
CF-12	No alkali	0.20

Experiment 4.19: Oil recovery ASP coreflood CF-13 in a sandstone core containing gypsum

An oil recovery coreflood was performed in a sandstone core containing gypsum using crude oil-1 and the surfactant formulation 4.14(a). This core was previously used to perform oil recovery corefloods using sodium metaborate; the same core was used to compare the retention values with sodium metaborate and ammonia. Note that the surfactant formulation used with sodium metaborate was not effective with ammonia because the formulation did not show low IFT in the presence of calcium ions (from gypsum). Therefore, another similar formulation (formulation 4.14(a)) was developed for ammonia.

The core was cleaned using the cleaning procedure to remove oil, polymer and surfactant from the previous coreflood. The core properties and experimental conditions are shown in Tables 4.31 and 4.32. The presence of gypsum in the core was confirmed by measuring the effluent calcium and sulfate ions obtained by injecting sodium chloride brine at 1 ft/d. The core was saturated with formation brine and then oil was flooded at constant pressure to establish initial oil saturation. The core was then waterflooded which

resulted in reducing oil saturation from 57% to 30%. 0.4 pore volume of surfactant slug was then injected at 1 ft/d followed by 2 pore volumes of polymer drive. The details of the surfactant and polymer slugs are given in Table 4.33(a). Note that sodium sulfate was added to the surfactant slug and polymer drive. The effluent ions were collected and analyzed for oil recovery, surfactant concentration, pH, salinity, polymer viscosity and pressure drop. The tertiary and cumulative oil recovery from the coreflood was about 72% and 88%, respectively. The residual oil saturation was reduced from 30%, after waterflood, to 8%. A good oil bank of 50% and pH increase to 10.2 was observed. The surfactant retention in the core was about 0.25 mg/g rock. This retention number was similar to the retention numbers obtained using sodium metaborate in these cores.

Table 4.31: Properties of the core used in the ASP coreflood CF-13

Core	Length (inches)	Diameter (inches)	Porosity (%)	Permeability (md)	Temperature (°C)	Gypsum
Sandstone	11.19	1.48	19.2	80	55	Yes

Table 4.32: Composition of the brines used in coreflood CF-13

Ions	Formation/Waterflood brine (ppm)	ASP slug (ppm)	Polymer drive 1 (ppm)
Ca^{2+}	1,500	0	0
Mg^{2+}	644	0	0
Na^{+}	56,100	24863	4419
Cl^{-}	86,488	33376	1820
SO_4^{2-}	3,875	6760	6760
NH_3	-	0.9 wt%	0
TDS	**147,509**	**65,000**	**13,000**

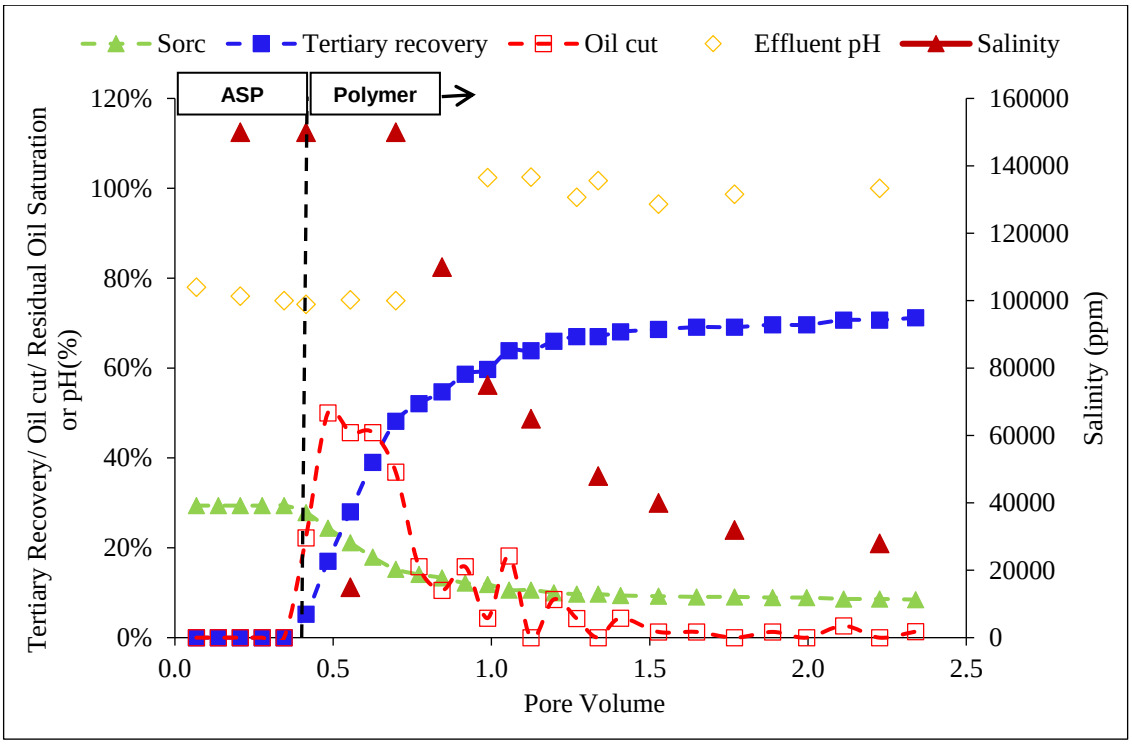

Figure 4.57: Oil recovery, oil cut, residual oil saturation, effluent salinity and pH obtained during the ASP coreflood CF-13

Table 4.33 (a): Summary of corefloods CF5-CF7 and coreflood CF13

Experiment (Core)		CF-5	CF-6	CF-7	CF-13
Core		Berea Sandstone	Berea Sandstone	Berea Sandstone	Sandstone with gypsum
ASP Slug	Surfactants	0.65% C_{28}-25PO-45EO-carboxylate, 0.45% C_{15-18} IOS, 0.25% C_{19-28} IOS	0.65% C_{28}-25PO-45EO-carboxylate, 0.45% C_{15-18} IOS, 0.25% C_{19-28} IOS	0.65% C_{28}-25PO-45EO-carboxylate, 0.45% C_{15-18} IOS, 0.25% C_{19-28} IOS	0.5% C_{12-13}-13PO-SO_4 0.5% C_{15-18} IOS
	Co-solvent	1% TEGBE	1% TEGBE	1% TEGBE	0.5% IBA-3EO
	Alkali	1% NH_3	0.9% NH_3	0.9% NH_3	1% NH_3
	TDS (ppm)	65,000	70,000	80,000	55,000 ppm
	Polymer	3500 ppm FP 3630S	3500 ppm FP 3630S	3500 ppm FP 3630S	6000 ppm AN-125
	Slug size	0.25 PV	0.25 PV	0.4 PV	0.4 PV
Polymer Drive 1	Alkali	0.5% NH_3	0.45% NH_3	0.45% NH_3	-
	TDS (ppm)	45,000	52,500 ppm	60,000	13,000
	Polymer	3500 ppm FP 3630S	3500 ppm FP 3630S	3500 ppm FP 3630S	6000 ppm AN-125
	Slug size	0.5 PV	1.75 PV	1.5 PV	2 PV
Polymer Drive 2	Alkali	-	-	-	-
	TDS (ppm)	25,000	-	-	-
	Polymer	3000 ppm FP 3630S	-	-	-
	Slug size	1.4 PV	-	-	-
Oil Saturation After Chemical Flood (Sorc)		13%	9.7%	7.1%	8.4%
Total Oil Recovery		81%	85.1%	88%	87.5%
Surfactant Retention (mg/g rock)		Injected surfactant retained	Injected surfactant retained	Injected surfactant retained	0.25

Table 4.33(b): Summary of corefloods CF8-CF12

Experiment (Core)		CF-8	CF-9	CF-10	CF-11	CF-12
Core		Carbonate core with gypsum	Carbonate core with gypsum	Carbonate core with gypsum	Carbonate core with gypsum	Carbonate core with gypsum
ASP Slug	Surfactants	Same as CF5-CF7	Same as CF5-CF7	Same as CF5-CF7	Same as CF5-CF7	Same as CF5-CF7
	Co-solvent	1% TEGBE	1% TEGBE	1% TEGBE	1% TEGBE	1% TEGBE
	Alkali	0.5% NH_3	-	-	0.5% NH_3	-
	TDS	80,000	80,000	80,000	80,000	80,000
	Polymer	5500 ppm AN-125	2500 ppm FP 3630S	2500 ppm FP 3630S	5500 ppm AN-125	2500 ppm FP 3630S
	Slug size	0.4 PV	0.4 PV	0.4 PV	0.4 PV	0.4 PV
Polymer Drive 1	Alkali	-	-	-	-	-
	TDS	50,000	50,000	50,000	50,000	50,000
	Polymer	2500 ppm FP 3630S	2500 ppm FP 3630S	2500 ppm FP 3630S	2500 ppm FP 3630S	2500 ppm FP 3630S
	Slug size	0.5 PV	0.5 PV	0.45 PV	0.5 PV	0.45 PV
Polymer Drive 2	Alkali	-	-	-	-	-
	TDS	35,000	35,000	35,000	35,000	35,000
	Polymer	2500 ppm FP 3630S	2500 ppm FP 3630S	2500 ppm FP 3630S	2500 ppm FP 3630S	2500 ppm FP 3630S
	Slug size	1.2 PV	1.2 PV	1.2 PV	1.2 PV	1.2 PV
Oil Saturation After Chemical Flood (Sorc)		5.5%	4%	Single-phase flood	Single-phase flood	Single-phase flood
Total Oil Recovery		91%	94%	-	-	-
Surfactant Retention (mg/g rock)		0.24	0.20	0.19	0.24	0.21

4.3 Use of ammonia in cores without gypsum

The study with ammonia was extended to sandstone and carbonate cores which did not contain gypsum and comparisons were made with a conventional alkali such as sodium carbonate. Zeta potential measurements were performed on sandstone and carbonate cores in the presence of ammonia and sodium carbonate. Single-phase static and dynamic surfactant adsorption experiments were performed, in cores without gypsum, to compare ammonia with sodium carbonate. Surfactant formulations were developed with ammonia and tested in oil recovery corefloods in outcrop cores. These results will be discussed in the following section.

4.3.1 Static experiments

Experiment 4.20 (a): Zeta potential measurements on sandstones

Zeta potential measurements were performed on crushed Bandera brown using the procedure described in chapter 3. It is proposed that an alkali can lower the zeta potential of sandstones by giving hydroxyl ions which can then interact with positive silica sites as per the following reaction.

$$>SOH + OH^- = >SO^- + H_2O$$

A decrease in zeta potential results in lowering the adsorption of anionic surfactants on the rock surface. The purpose of this experiment was to compare the effectiveness of ammonia and sodium carbonate in lowering zeta potential on sandstones.

A 250 g sample consisting of 1 wt% crushed Bandera brown sandstone (140-200 mesh) was prepared in a 4500 ppm ammonium acetate brine and left to equilibrate overnight. The sample was brought in contact with zeta probe and left to equilibrate for 10 minutes. 30 wt% ammonia was added in small quantities to adjust the pH and measurements were performed. Another set of measurements was performed in the presence of sodium carbonate, using the procedure described above. Sodium carbonate and sodium bicarbonate salts were mixed in different proportions, keeping the total salinity of 4500 ppm, to obtain a wide range of pH values. The zeta potential of each sample was measured five times at 25 °C and the mean value is reported. The results for ammonia and sodium carbonate are shown in Figures 4.58 and 4.59, respectively. The zeta potential values were found to be negative even at a neutral pH in both the cases and decreased further with increasing pH.

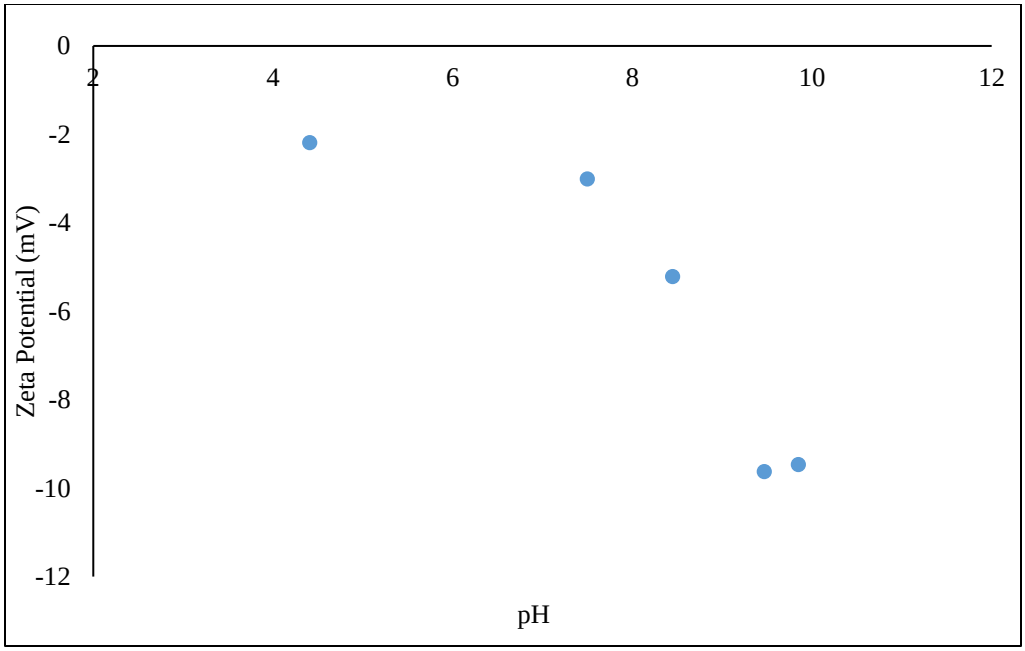

Figure 4.58: Zeta potential measurements obtained on Bandera brown sandstone by increasing pH with ammonia

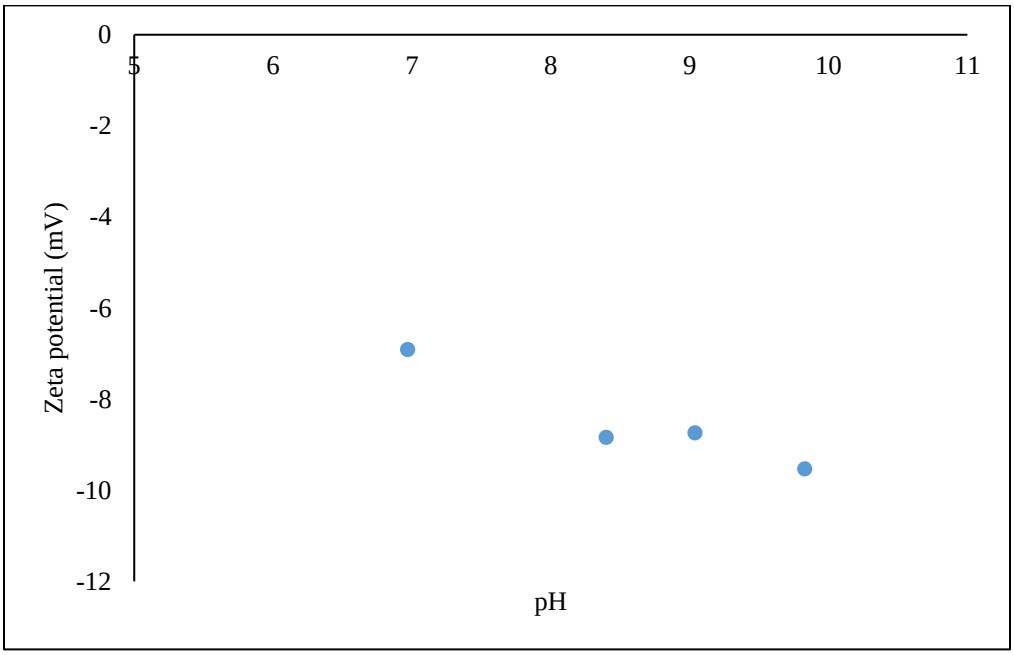

Figure 4.59: Zeta potential measurements obtained on Bandera brown sandstone by increasing pH with sodium carbonate

Experiment 4.21 (b): Zeta potential measurements on carbonates

Zeta potential measurements were similarly performed using crushed Silurian dolomite (140-200 mesh size) using ammonia and sodium carbonate. The results shown in Figures 4.60 and 4.61 showed a reduction in zeta potential of Silurian dolomite in both the cases.

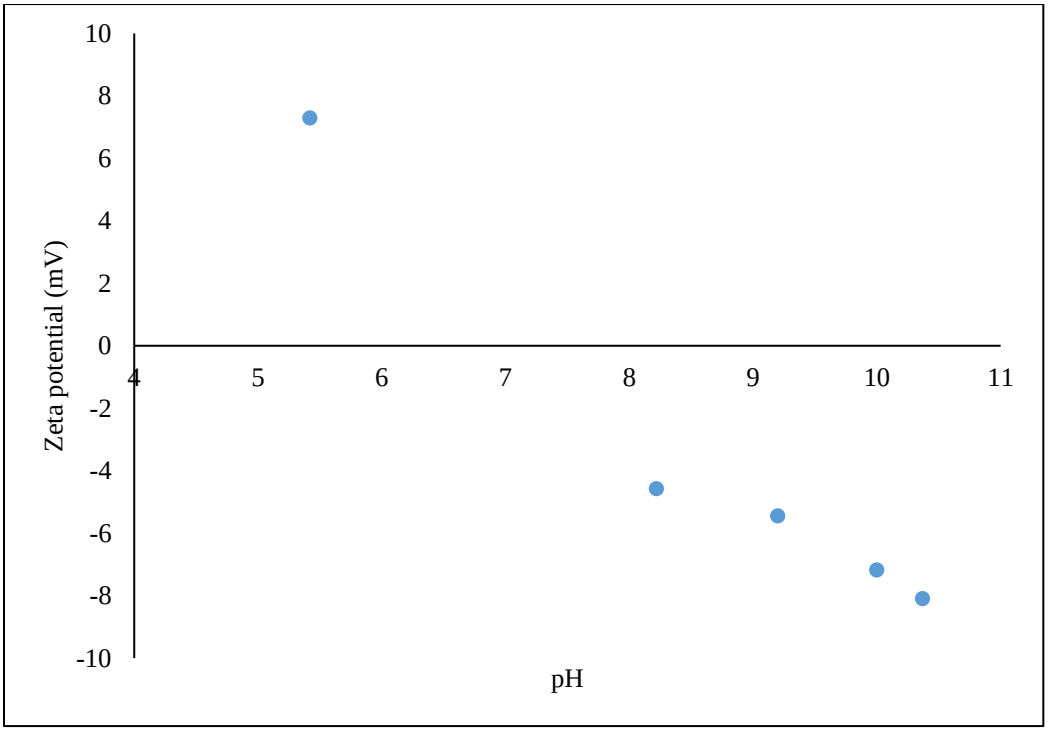

Figure 4.60: Zeta potential measurements obtained crushed Silurian dolomite by increasing pH with ammonia

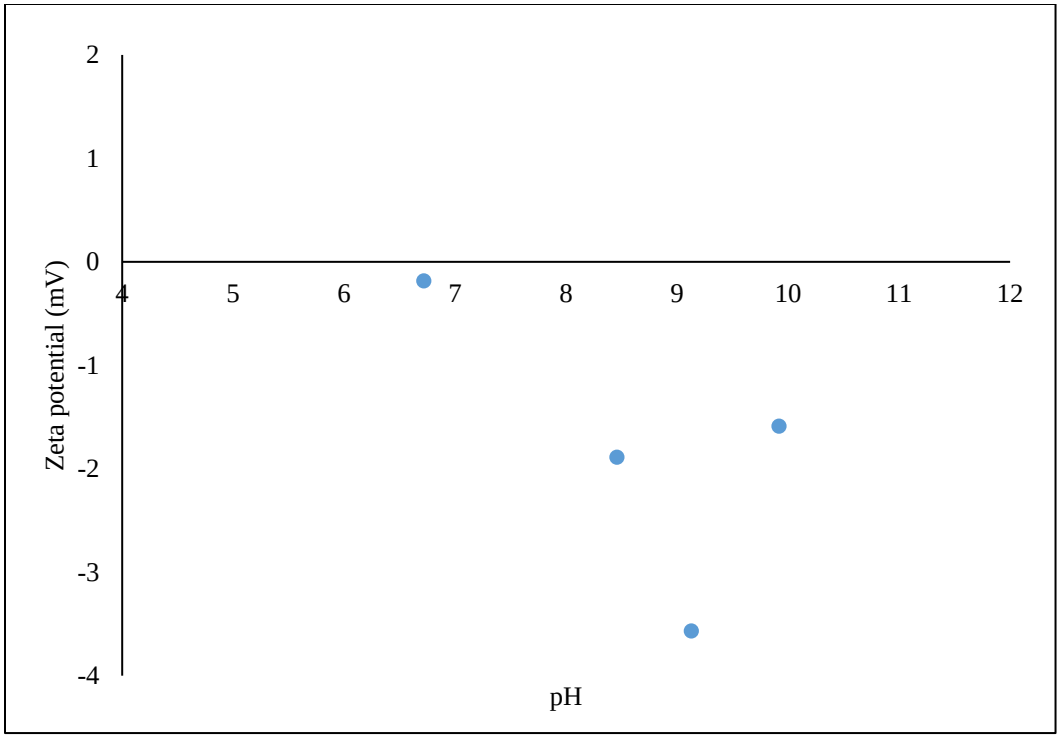

Figure 4.61: Zeta potential measurements obtained crushed Silurian dolomite by increasing pH with sodium carbonate

Experiment 4.21: Single-phase static surfactant adsorption on sandstone

Static surfactant adsorption experiments were performed on crushed Bandera brown sandstone core to compare the advantages of sodium carbonate and ammonia in lowering surfactant adsorption. Note that the surfactant adsorption numbers during static adsorption experiments are usually much higher than dynamic corefloods, due to a higher specific surface area. These results should, therefore, be used to make a qualitative comparison between different cases. Static surfactant adsorption samples were prepared at their respective optimum salinities using the surfactant formulation previously developed for crude oil-1 (see experiment 4.8) and crushed Bandera brown. The mineralogy of the Bandera brown core is shown in Table 4.34. The samples were allowed

to equilibrate, and surfactant adsorption values were determined. The detailed procedure to prepare the samples and obtain adsorption numbers is discussed in chapter 3. A comparison was made between three cases; no alkali was added in experiment 4.21(a), sodium carbonate was added in experiment 4.21(b) and ammonia was added in experiment 4.21(c). In experiment 4.21(a), 0.67 mg/g rock of surfactant adsorption was observed (Table 4.35). The surfactant adsorption was reduced to 0.40 mg/g rock and 0.37 mg/g rock by adding sodium carbonate and ammonia, respectively. These results showed that both ammonia and sodium carbonate were effective in lowering surfactant adsorption on Bandera brown sandstone.

Table 4.34: Mineralogy of the Bandera brown sandstone core

Species	Bandera brown sandstone (%)
Quartz	68.6
Montmorillonite	1.4
Kaolinite	0.7
Illite & Mica	5.2
Chlorite	7.4

Table 4.35: Static surfactant adsorption results for crushed Bandera brown sandstone

Experiment	Alkali	Surfactant adsorption at optimum salinity (mg/g rock)
4.18 (a)	No Alkali (NaCl only)	0.67
4.18 (b)	1.0 wt% Na_2CO_3	0.40
4.18 (c)	0.35 wt% NH_3	0.37

Experiment 4.22: Single-phase static surfactant adsorption in carbonates

Static surfactant adsorption experiments were similarly performed using the same surfactant formulation and crushed Silurian dolomite core. The results are shown in Table 4.36. In Experiment 4.22(a), where no alkali was added, and the surfactant adsorption was found to be 3.24 mg/g-rock. On adding 1 wt% sodium carbonate (Experiment 4.22(b)), the adsorption was lowered to 1.03 mg/g-rock. On adding 0.35 wt% ammonia (Experiment 4.22(c)) the surfactant adsorption was found to be 2.59 mg/g-rock. Note that all the measurements were performed at their respective optimum salinities and the values reported in Table 4.36 are the average values of two samples prepared for each case. From these results, it can be observed that a large reduction in surfactant adsorption on Silurian dolomite was observed on adding sodium carbonate; however, much less reduction in adsorption was observed on adding ammonia.

Table 4.36: Static surfactant adsorption results obtained on crushed Silurian dolomite

Experiment	Alkali	Surfactant adsorption at optimum salinity (mg/g rock)
4.19 (a)	No Alkali (NaCl only)	3.24
4.19 (b)	1.0 wt% Na_2CO_3	1.03
4.19 (c)	0.35 wt% NH_3	2.59

4.3.2 Single-phase transport experiments

Experiment 4.23: Single-phase dynamic surfactant adsorption experiments in sandstone

Single-phase dynamic surfactant adsorption experiments were performed in Bandera brown sandstone cores using the surfactant formulation previously developed for crude oil-1 (see experiment 4.8). The experimental conditions and core properties are given in Table 4.37 and 4.38. The core was saturated with a 10,000 ppm NaCl brine and displaced with 5-6 pore volumes of 100,000 ppm NaCl brines to remove the divalent ions present in them. This step was especially important for Bandera brown sandstone cores since these cores have large amounts of divalent ions attached to the clays. This brine was then displaced by injecting 2-3 pore volumes of the formation brine of 40,000 ppm NaCl. This brine was then displaced with a surfactant solution at the optimum salinity at 1 ft/day, and the effluent samples were collected using a fractional collector. The injected surfactant concentration was fixed to 1 wt%. The coreflood effluents were collected and analyzed for pH, salinity and surfactant concentration. The delay in surfactant concentration compared to the tracer was used to estimate the surfactant adsorption. The detailed procedure is described in chapter 3. In experiment 4.23(a), 0.5% ammonia was added to the surfactant formulation. In experiment 4.23(b), no alkali was added. The results of experiments 4.23(a) and 4.23(b) are shown in Figures 4.62 and 4.63, respectively. From the results, it can be seen that the surfactant was retarded compared to the tracer front due to adsorption on the rock matrix. The surfactant adsorption for experiment 4.23(a), calculated based on the area between the surfactant and tracer fronts, was found to be 0.30 mg/g-rock. For experiment 4.23(b), performed similarly without adding alkali, the surfactant adsorption was found to be 0.52 mg/g rock. Thus, ammonia reduced the adsorption significantly.

Table 4.37: Properties of the Bandera brown sandstone core used in experiment 4.23(a)

Core	Length (inches)	Diameter (inches)	Porosity (%)	Permeability (md)
Sandstone	11.8	1.48	23.3	106

Table 4.38: Properties of the Bandera brown sandstone core used in experiment 4.23(b)

Core	Length (inches)	Diameter (inches)	Porosity (%)	Permeability (md)
Sandstone	11.9	1.48	23	168

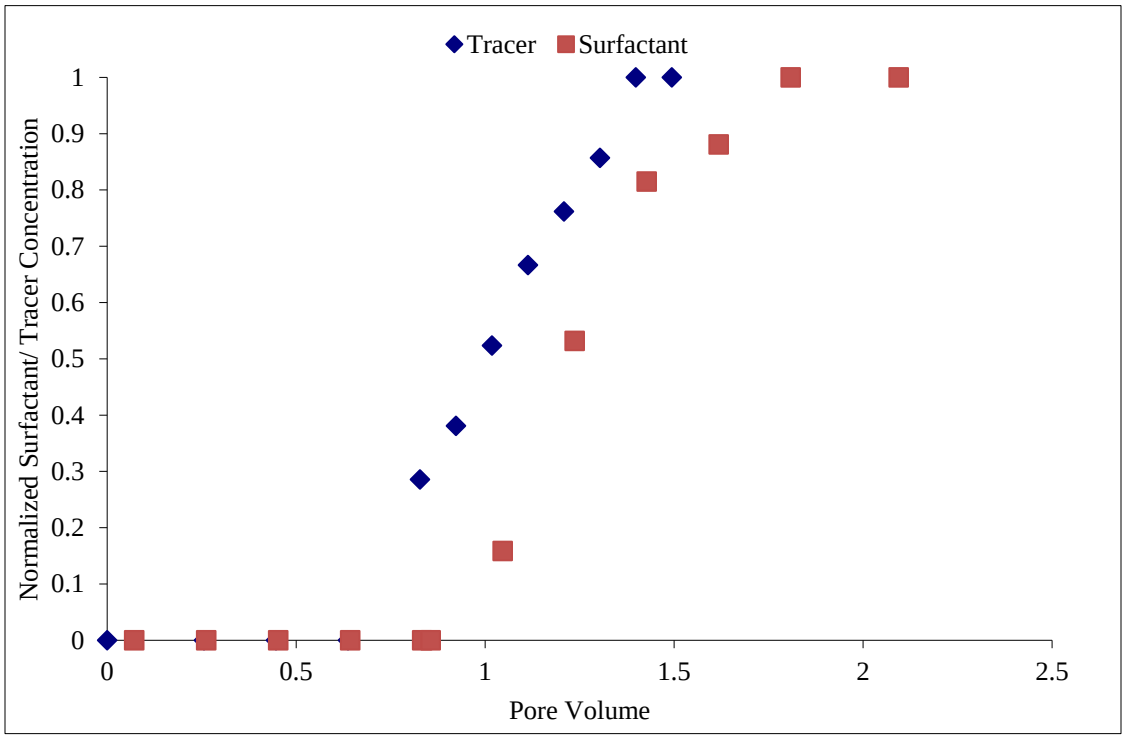

Figure 4.62: Effluent surfactant and tracer profile during the continuous single-phase alkali surfactant flood in a Bandera brown sandstone core

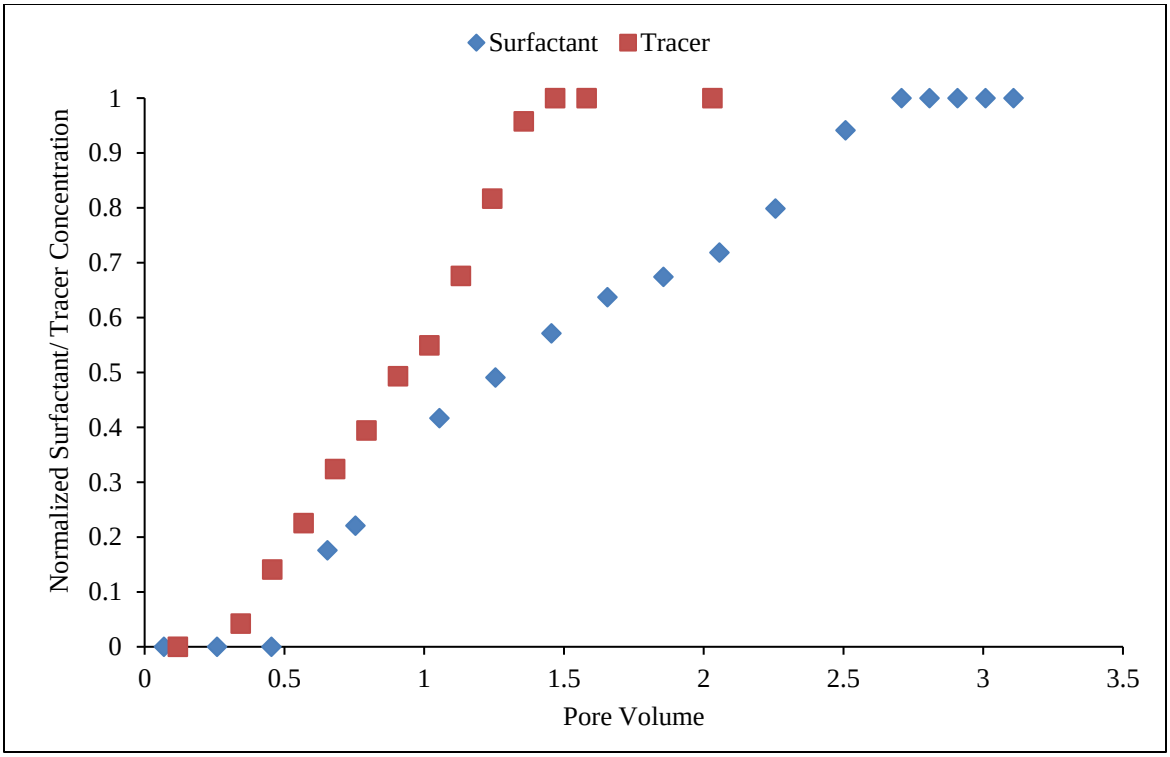

Figure 4.63: Effluent surfactant and tracer profile during the continuous single-phase surfactant flood (no alkali) in a Bandera brown sandstone core

Experiment 4.24: Single-phase dynamic surfactant adsorption experiments in carbonate

Single-phase dynamic surfactant adsorption experiments 4.24(a) and 4.24(b) were performed similarly, with the same surfactant formulation as the previous experiment, by injecting continuous surfactant slug of 1 wt% surfactant in an Estaillades limestone core with and without ammonia, respectively, at 1 ft/day. The core properties and other details are shown in Table 4.39. After experiment 4.24(a), the same core was cleaned, by injecting a large quantity of methanol until no surfactant was observed in the effluent,

and reused for experiment 4.24(b). In experiment 4.24(a), ammonia was added to the surfactant formulation. No alkali was added to the surfactant formulation in experiment 4.24(b). The results of experiments 4.24(a) and 4.24(b) are shown in Figures 4.64 and 4.65, respectively. The surfactant adsorption was calculated based on the delay on the surfactant front compared to the tracer and was found to be 0.19 mg/g rock for experiment 4.24(a). Experiment 4.24(b), performed similarly using the same surfactant formulation without alkali, showed an adsorption of 0.12 mg/g rock. Dynamic adsorption on the Estaillades limestone core was small (without any alkali) and increased slightly in the presence of ammonia. Based on these results, the benefits of adding ammonia to carbonate cores is not obvious.

Table 4.39: Properties of the core used in the single-phase surfactant transport in Estaillades limestone

Core	Length (inches)	Diameter (inches)	Porosity (%)	Permeability (md)
Sandstone	11.8	1.48	28.4	154

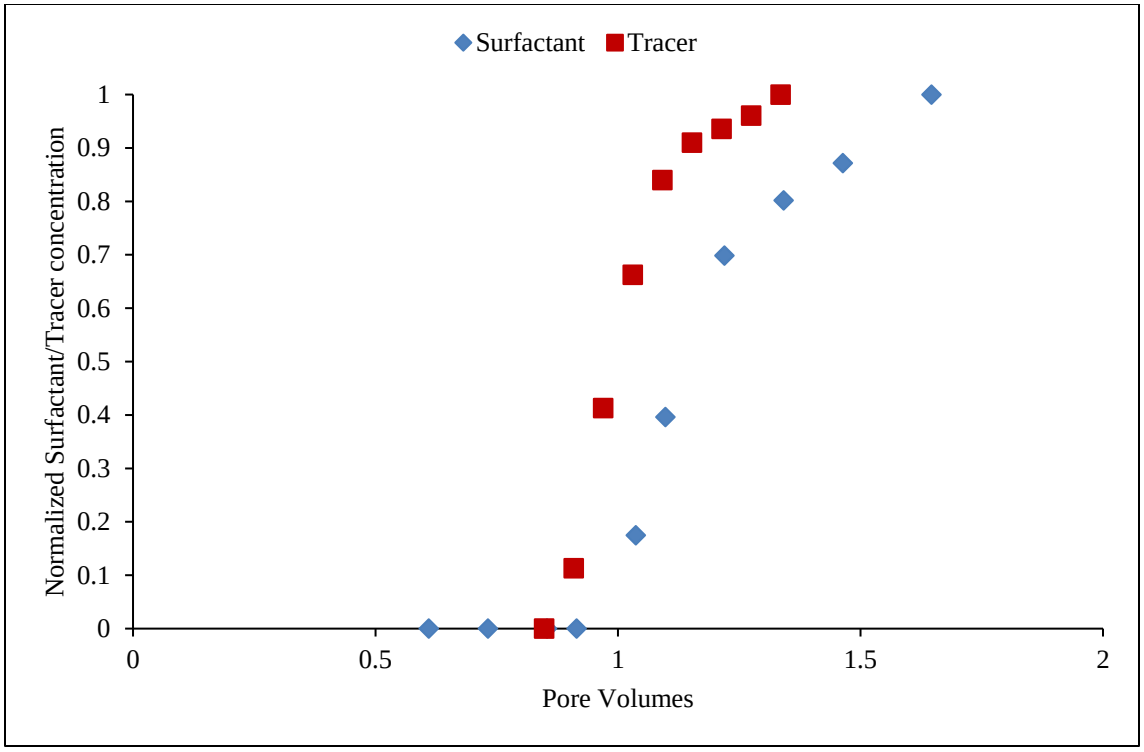

Figure 4.64: Effluent surfactant and tracer profile for single-phase surfactant coreflood, containing 0.5 wt% NH_3, in an Estaillades limestone core

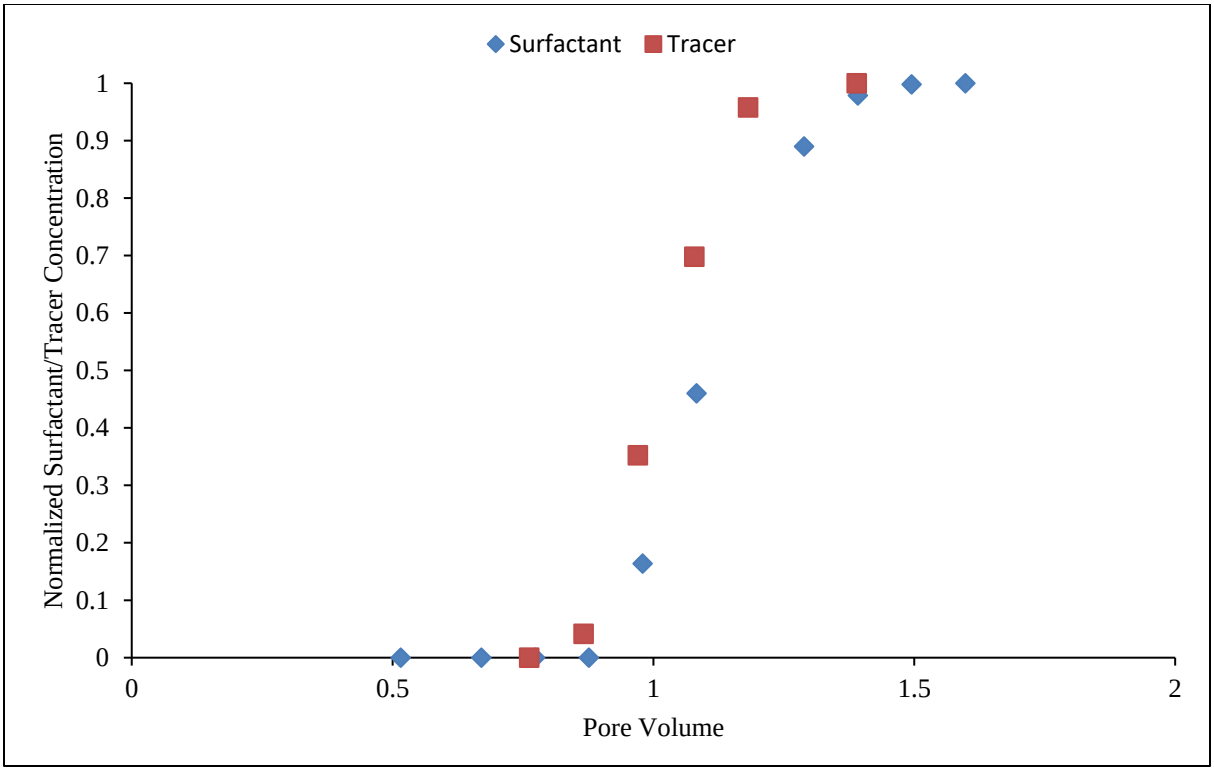

Figure 4.65: Effluent surfactant and tracer profile for the single-phase surfactant flood in an Estaillades limestone core without adding alkali

4.3.3 Surfactant phase behavior experiments

Experiment 4.25: Surfactant phase behavior experiment with crude oil-3

Surfactant phase behavior experiments were performed with crude oil-3 to develop ultralow IFT surfactant formulations with and without ammonia at 45 °C. These formulations were later used in oil recovery corefloods in Berea sandstone cores and surfactant retentions in these floods were compared. The brines used in the experiment consisted of only sodium chloride salt. A surfactant formulations consisting of 0.5 wt% $C_{12\text{-}13}$-13PO-SO_4 and 0.5 wt% $C_{20\text{-}24}$-IOS surfactants showed ultralow IFT with the oil

and was aqueous stable at salinities beyond the optimum salinity. 2 wt% TEGBE co-solvent was added to the formulation to reduce the equilibration time and improve the aqueous stability. NaCl was used to increase the salinity. Another similar experiment was performed where 0.5 wt% ammonia was added to the phase behavior samples, in addition to the other species. The solubilization ratio plots as a function of salinity are shown in Figure 4.66 for the ammonia case. From this plot, it can be seen that the solubilization ratio at the optimum salinity (17,500 ppm NaCl) was about 17, corresponding to the ultra-low IFT value of 0.001 dyne/cm. The surfactant formulation without ammonia also showed an ultra-low IFT at an optimum salinity of 20,000 ppm NaCl. The same surfactant formulation showed ultralow IFT without ammonia; the equilibration time was however much longer without ammonia. Note that little difference was observed on adding 0.5 wt% ammonia to the surfactant phase behavior.

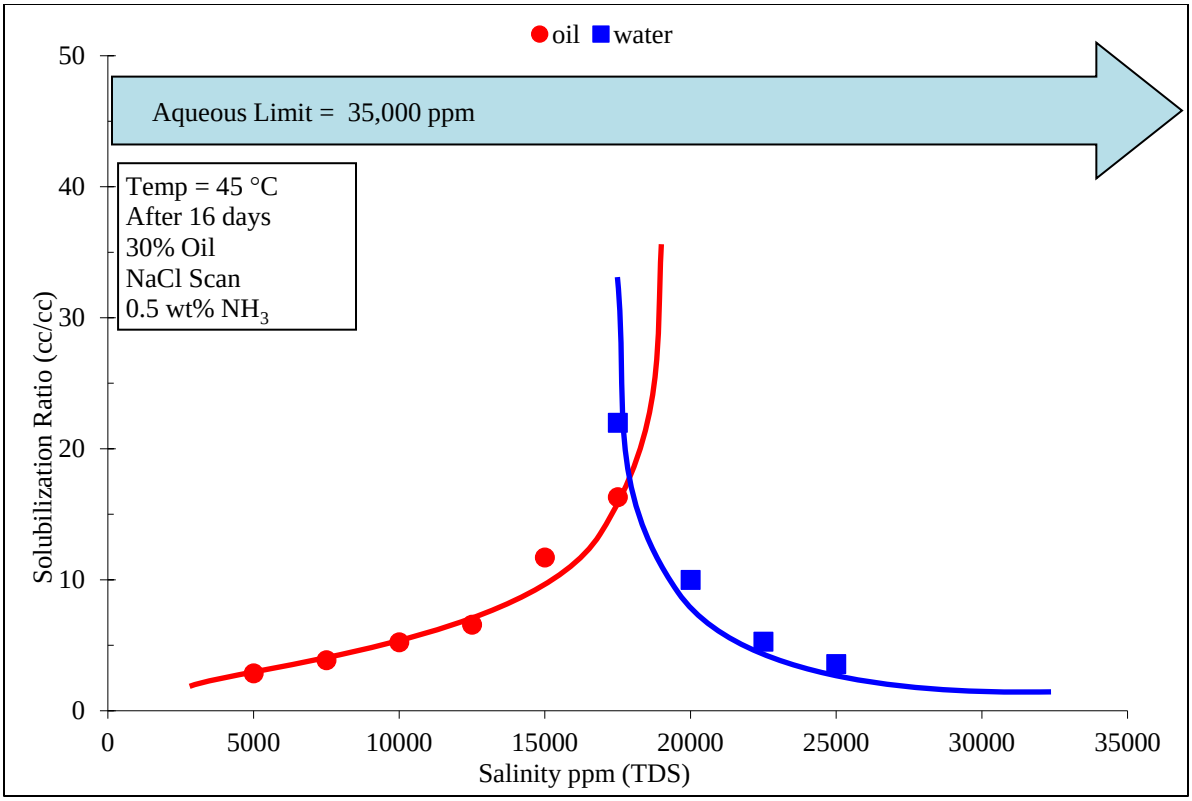

Figure 4.66: Oil and water solubilization ratios as a function of salinity for the surfactant formulation with crude oil-3

4.3.4 Oil recovery corefloods in sandstones using ammonia

Experiment 4.26 (a): Oil recovery ASP coreflood CF-14 in Berea sandstone

Oil recovery experiments were performed in low permeability Berea sandstone cores using the surfactant formulation developed by the surfactant phase behavior experiments to compare surfactant retention with and without adding ammonia. The cores were prepared by the procedure described previously. The properties of the core and the brines are given in Table 4.40 and 4.41. The divalent ions from the cores, especially on the clays, were removed by injecting many pore volumes of 100,000 ppm NaCl brine.

This brine was then replaced with the formation brine followed by oil to establish initial oil saturation. Waterflood was then performed using 27,500 ppm NaCl brine which resulted in reducing oil saturation from 55% to 34%. Chemical flood CF-14 was then performed in which 0.4 PV of ASP slug having 0.5 wt% ammonia, 1 wt% surfactant and 3500 ppm Floppam 3330S was injected at optimum salinity. This was followed by 0.2 PV of polymer drive-1 consisting of 3500 ppm Floppam 3330S and 1.4 PV of polymer drive-2 consisting of 3000 ppm of Floppam 3330S. The effluent samples from the coreflood were collected in graduated tubes at regular intervals using a fractional collector and then analyzed for oil recovery, pH, salinity, viscosity, and surfactant concentration. Further details of the coreflood are given in Table 4.44.

The chemical flood resulted in reducing oil saturation from about 34% to 0.86%, recovering 97.5% of the oil left after waterflood. It can be seen from this Figure 4.67 that more than 90% of the residual oil left after waterflood was recovered within 0.8 PV. A good oil bank with an oil cut of about 50-60% was observed, and the residual saturation after 1 PV was about 1.4%. The pH after 1.2 PV was about 9.9 showing that even 0.5 wt% ammonia is sufficient to propagate a high pH through a low permeability Berea sandstone. A low surfactant retention of 0.057 mg/g-rock was observed.

Table 4.40: Properties of the core used in coreflood CF-14

Core	Length (inches)	Diameter (inches)	Porosity (%)	Permeability (md)	Temperature (°C)
Berea Sandstone	11.9	1.49	19.6	59	45

Table 4.41: Composition of the brines used for waterflood and chemical flood

Salt	Formation/Waterflood brine (ppm)	ASP slug (ppm)	Polymer drive 1 (ppm)	Polymer drive 2 (ppm)
NaCl	27,500	17,500	12,500	7,500
NH_3	-	0.5 wt%	0	0
TDS	**27,500**	**17,500**	**12,500**	**7,500**

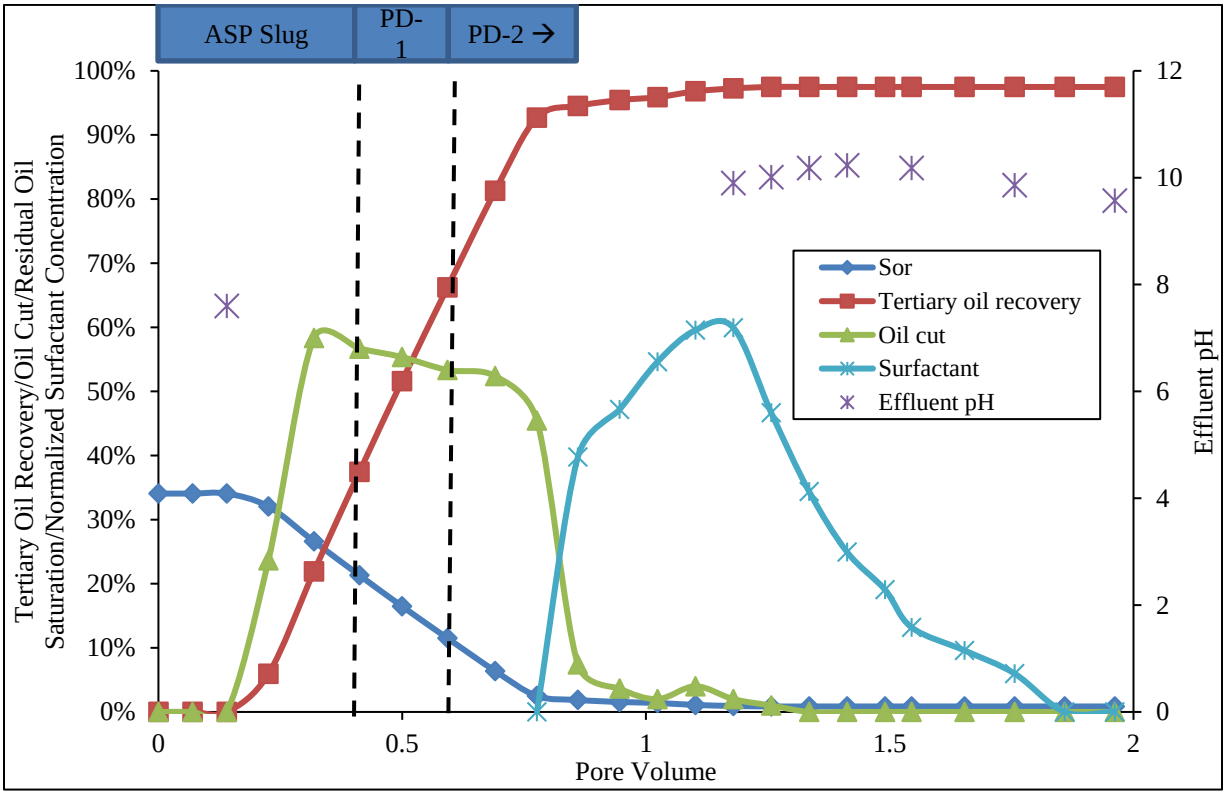

Figure 4.67: Oil recovery profile for the alkali surfactant flood, performed with 0.5 wt% NH_3 as alkali, in a Berea sandstone. Effluent surfactant concentration is normalized with the injected surfactant concentration

Experiment 4.26 (b): Oil recovery SP coreflood CF-15 in Berea sandstone

Coreflood CF-15 was performed similar to coreflood CF-14, except no ammonia was added to the surfactant formulation. The properties of the core and composition of the brines are given in Table 4.42 and 4.43. The coreflood was performed in a similar Berea sandstone core which was characterized and then flooded with many pore volumes of 100,000 ppm NaCl brine to remove divalent ions at reservoir temperature. This brine was then displaced with the formation brine. Oil was then injected at a constant pressure to establish initial oil saturation. Waterflood was performed by using 27,500 ppm NaCl brine which resulted in lowering the oil saturation from 56% to 31 %. A chemical flood consisting of 0.4 PV SP slug followed by two polymer drives of lower salinities was performed. Additional details of the coreflood are given in Table 4.44. The effluent samples were analyzed for oil recovery, pH, viscosity, salinity and surfactant concentration. The results of coreflood CF-15 (Figure 4.68) were found to be very similar to that of the coreflood CF-14. High oil recovery, high oil cut, and low residual oil saturation after the chemical flood were observed. About 90% of the residual oil after waterflood was recovered by 0.9 pore volume of the chemical flood. A good oil bank having an oil cut of about 50-60% was observed. The tertiary oil recovery after 2 pore volumes was about 94%, reducing oil saturation to 1.8%. The images of the cores after the corefloods CF-14 and CF-15 (Figure 4.69) show that almost no oil is visible inside the core, further corroborating the high oil recovery values. The surfactant retention during the ASP and SP floods were found to be 0.057 mg/g rock and 0.069 mg/g rock, respectively.

Table 4.42: Properties of the core used in coreflood CF-15

Core	Length (inches)	Diameter (inches)	Porosity (%)	Permeability (md)	Temperature (°C)
Berea Sandstone	11.9	1.49	19.4	91	45

Table 4.43: Composition of the brines used for waterflood and chemical flood

Salt	Formation/Waterflood brine (ppm)	SP slug (ppm)	Polymer drive 1 (ppm)	Polymer drive 2 (ppm)
NaCl	27,500	20,000	12,500	7,500
NH_3	-	0	0	0
TDS	**27,500**	**20,000**	**12,500**	**7,500**

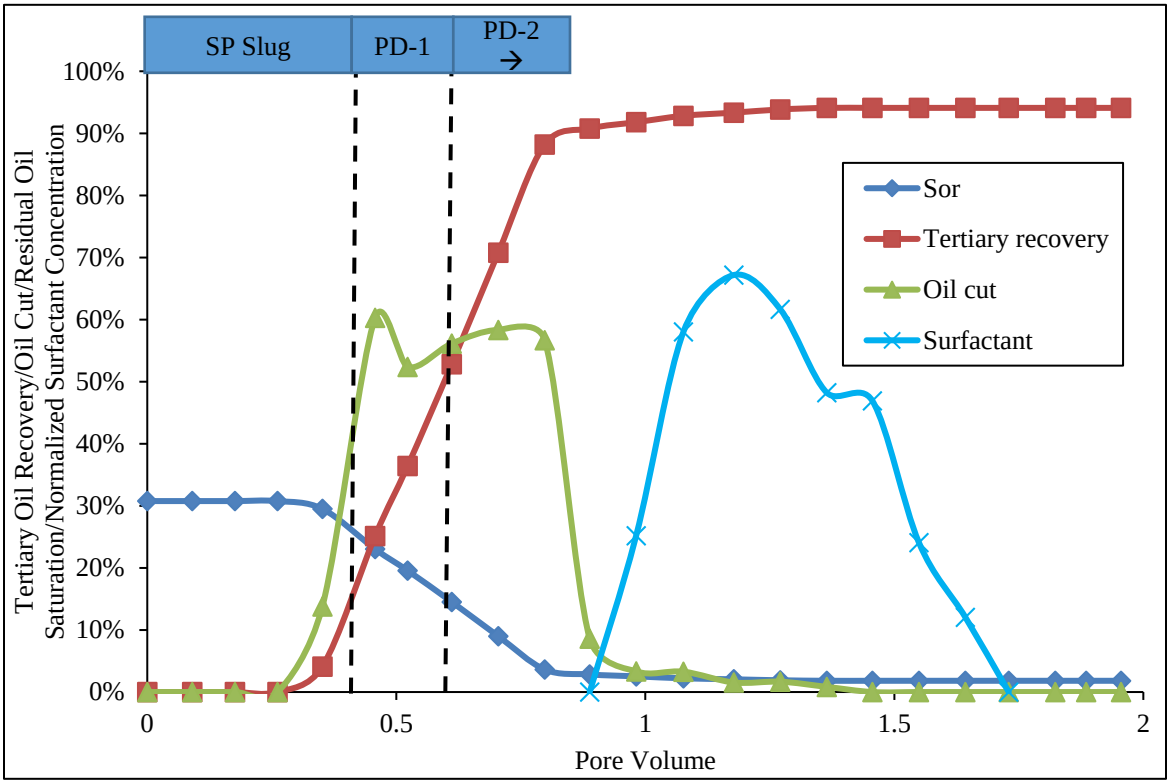

Figure 4.68: Oil recovery profile for the surfactant flood performed in a Berea sandstone. The effluent surfactant concentration is normalized by the injected surfactant concentration

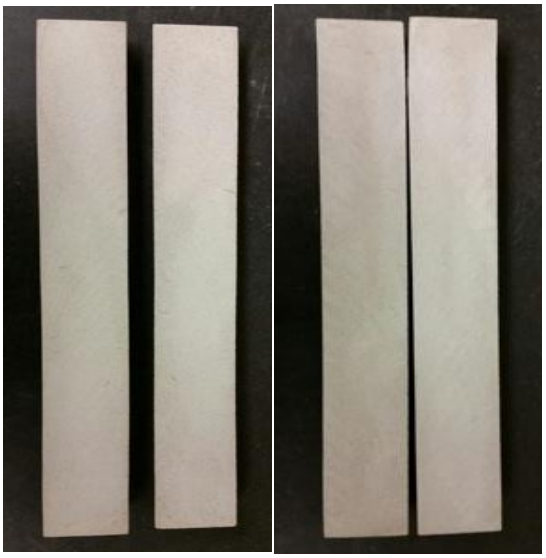

Figure 4.69: Images of the cores after corefloods CF-14 (left) and CF-15 (right). The images further corroborate that almost all the oil was recovered during the corefloods

Table 4.44: A summary of corefloods CF-14 and CF-15

Experiment		CF-14	CF-15	Units
Surfactant Slug	TDA-13PO-SO_4	0.5	0.5	wt%
	C_{20-24} IOS	0.5	0.5	
	TEGBE	2.0	2.0	
	NaCl	1.75	2.0	
	NH_3	0.50	0	
	FP 3330S	0.35	0.35	
	Size	0.40 PV	0.40 PV	
	pH	11.01	8.1	
Polymer Drive 1	NaCl	1.25	1.25	wt%
	FP 3330S	0.35	0.35	
	Size	0.20 PV	0.20 PV	
Polymer Drive 2	NaCl	0.75	0.75	wt%
	FP 3330S	0.30	0.30	
	Size	1.6 PV	1.6 PV	
Oil Saturation After Chemical Flood (Sorc)		0.86	1.81	%
Tertiary oil Recovery		97.49	94.10	%
Surfactant Retention		0.057	0.069	mg of surfactant/g of rock

A summary of the results obtained using ammonia is given below:

1. Ammonia was investigated as an alternative alkali. Due to its low molecular mass, less mass of ammonia is required in chemical floods, compared to other alkalis. This serves as an advantage for transportation and storage of alkali in the field.

2. A pH of about 11 was obtained by adding a small amount of ammonia to aqueous solutions. Only a fraction of the added ammonia participated in increasing the pH because of a low dissociation constant of ammonia. Most of the added ammonia existed as NH_3(aq), while some dissociated to NH_4^+ and OH^- ions. The presence of NH_3(aq) and NH_4^+ species allows ammonia to make a buffer system, with a pKa of 9.25. As a result, high pH propagation was observed in sandstone and carbonate cores using ammonia.

3. Single-phase static and transport experiments in cores containing gypsum using ammonia as the alkali showed high equilibrium pH and no calcium precipitation. In addition, no calcium precipitation was observed in presence of ammonia. Magnesium precipitation was, however, observed. The effluents obtained on injecting ammonia at 1 ft/d were found to be in equilibrium with gypsum.

4. Surfactant formulations were developed by fixing the ammonia concentration and increasing the salinity with sodium chloride. A classical Winsor type phase behavior was observed. A lowering of optimum salinity was observed on addition of calcium ions to surfactant formulations developed with ammonia. In some cases, an increase in IFT

and transformation to Winsor type II phase behavior was observed on adding a small amount of calcium ions.

5. Polymer stability experiments were performed to identify polymers for ASP floods in cores containing gypsum using ammonia as the alkali. AN-125 polymer showed better stability compared to HPAM polymers in the presence of up to 2000 ppm calcium ions and pH of 11.

6. Good oil recoveries were observed during ASP and SP corefloods in carbonate cores containing gypsum. The surfactant retention values during both SP and ASP corefloods were very similar, thus not clearly showing the benefit of adding an alkali to the surfactant formulation.

7. Static surfactant adsorption experiments were performed using crushed Bandera brown sandstone and Silurian dolomite cores. Lowering of surfactant adsorption on sandstone core on adding ammonia was observed. The extent of reduction with ammonia was similar to that with sodium carbonate. No obvious reduction in surfactant adsorption on Silurian dolomite was observed on adding ammonia. However, lowering of surfactant adsorption was observed with sodium carbonate.

8. Zeta potential measurements were performed on sandstone and carbonate cores at different pH values. The pH values were adjusted with sodium carbonate and ammonia, respectively. A decrease in zeta potential of sandstone and carbonate cores was observed, both using ammonia and sodium carbonate.

9. Oil recovery ASP (using ammonia as alkali) and SP corefloods showed good oil recovery and low surfactant retention in sandstone cores. Lower surfactant retention was observed on adding ammonia to the surfactant formulation.

4.4 ACP floods using alternative alkalis

It is well known that one of the key reasons to add an alkali to surfactant formulations is that the alkali generates in-situ surfactant on reacting with acidic crude oils. These in-situ surfactants, also known as soaps, is not only beneficial from the viewpoint of economics but is also considered to be very good surfactants in terms of lowering IFT and improving surfactant phase behavior. However, soaps themselves are not suitable for chemical floods, mainly because they result in forming viscous emulsions and the ultralow IFT region often occur at a very low salinity. Synthetic hydrophilic surfactants are therefore added in surfactant floods which result in moving the ultralow IFT region to a higher salinity. Such a design is practical and can be applied in the field. Cosolvents are often added to improve surfactant phase behavior by lowering the microemulsion viscosity and eliminating viscous phases. A recent study by Fortenberry et al. (2013) has found that the requirement of synthetic surfactants can be all-together removed in case of sufficiently acidic crude oils. Since the soap is sufficiently large in these oils, only cosolvent (such IBA, Phenol, TEGBE) is added which results in lowering the viscosity of emulsions. Further, newer ethoxylated cosolvents such as IBA-$(EO)_n$, Phenol-$(EO)_n$ can be used to increase the salinity of the low IFT region and reduce the positive slope of the activity map diagram. These cosolvents have also shown to reduce

the emulsion viscosity and improve the surfactant phase behavior. So far only sodium carbonate has been used in ACP floods. Ammonia has shown to reduce surfactant adsorption on sandstone surfaces similar to a conventional alkali, such as sodium carbonate, and offers many benefits due to its low molecular mass such as ease of transportation and storage at offshore locations. Many recent studies have shown successful alkali surfactant polymer corefloods using ammonia as the alkali. The objective of this study is to understand the interaction of ammonia with acidic crude oils since these interactions affect the surfactant phase behavior in the porous media. Another objective of this study is to develop low interfacial tension (IFT) alkali cosolvent polymer (ACP) formulations for acidic crude oils since such formulations could be economical compared to ASP floods under certain conditions. In this study, alkali scans were performed with various alkalis (NaOH, Na_2CO_3, $NaBO_2$, NH_3) and an acidic crude oil. Similar scans were performed by also adding different cosolvents to study the effect of cosolvents and also to develop optimum low IFT formulations with ammonia. The effect of divalent cations on low IFT region was studied for the cases where NH_3 was used as alkali. Another set of experiments were performed to develop low IFT cosolvent-polymer formulations, without adding additional alkali using amine cosolvents. The crude oils properties are given in Table 4.45. Preliminary alkali scans were performed with these oils, without cosolvent, using ammonia to compare with sodium carbonate. In these scans, sodium chloride concentration was varied, keeping ammonia concentration fixed to about 0.5-1 wt%. Alkali scans with different alkalis were performed next, keeping the cosolvent type and amount fixed, to compare the phase behavior with these alkalis. The

effect of divalent ions on the phase behavior was studied. The effect of cosolvent type and the amount was studied for different alkalis and the formulations were optimized to obtain phase behaviors which are considered to be favorable for an oil recovery coreflood. Oil recovery corefloods were then performed in sandstone cores. The list of experiments performed to develop ACP floods with acidic crude oils is shown in Table 4.45.

Table 4.45: Properties of the acidic crude oils used in ACP floods

Oil	Viscosity	Acid number (mg KOH/g oil)
Oil-5	113 cP at 59 °C	5.0
Oil-6	14 cP at 59 °C	2.0
Oil-7	350 cP at 30 °C	3.5

Table 4.46: List of experiments performed with alkalis and acidic crude oils

4.27	Alkali scans using ammonia as alkali with crude oil-5 and oil-6
4.28	Alkali scans with the acidic oil-7 (a) NaOH (b) $NaBO_2$ (c) NH_3 (d) Na_2CO_3
4.29	Ammonia and acidic crude oil-7 in the presence of calcium ions (a) No calcium (b) 100 ppm calcium (c) 250 ppm calcium
4.30	Activity maps with oil-7 for different alkalis using IBA-3EO cosolvent (a) NaOH (b) $NaBO_2$ (c) NH_3 (d) Na_2CO_3
4.31	Activity map obtained on adding ammonia to the formulation developed using oil-7 and Na_2CO_3
4.32	Optimization of ACP formulations (a) crude oil-7 (b) crude oil-6
4.33	Oil recovery experiments in sandstone cores using crude oil-6 and ACP formulations developed in experiment 4.32

4.4.1 Alkali scans

Alkali scans involved mixing oil and aqueous solutions in desired proportions, typically ranging from 10 % to 50% oil (v/v), in glass tubes. The aqueous solutions consisted on alkali, salts and cosolvents, depending on the experiment. The concentration of cosolvent was kept fixed and the salinity of the solution was increased by adding an alkali. In the case of ammonia, the concentrations of ammonia and cosolvent were fixed and salinity was increased by adding NaCl. The glass tubes were then sealed using a gas torch, after replacing the air inside the tube with argon. These samples were mixed for four hours at 59 °C and then kept at the required temperatures. The samples were mixed from time to time. The low IFT regions were recorded at regular intervals to observe any changes due to equilibration.

Experiment 4.27: Alkali scans using ammonia as alkali

Alkali scans were performed with ammonia and acidic crude oils to test if ammonia gave a pH high enough to generate soap. In the first experiment, the concentration of ammonia was varied from 0-2.5 wt%, starting from DI water and oil was added such that oil fraction was 30%. Soap formation was observed, however, the typical Winsor type phase behavior was not observed because ammonia did not dissociate completely and did not add much to salinity as was discussed in experiment 4.14. The alkali concentration was, therefore, fixed to 0.5-1 wt% in subsequent experiments and sodium chloride concentration was systematically increased.

Alkali scans were performed with crude oils 5 and 6, keeping the oil amount to 30%. The aqueous solutions consisted of a fixed amount of ammonia; sodium chloride concentration was increased systematically. The samples were kept at 59 °C for equilibration and mixed from time to time. This preliminary experiment was performed to verify that ammonia can also give low IFT formulation with acidic crude oils, similar to sodium carbonate. The pictures of the phase behavior tubes for oil-5 and 6 are shown in Figures 4.70 and 4.71, respectively. The images clearly show the generation of soap on using ammonia with acidic crude oils and a Winsor type phase behavior going from type II- to type II+ on increasing sodium chloride concentration.

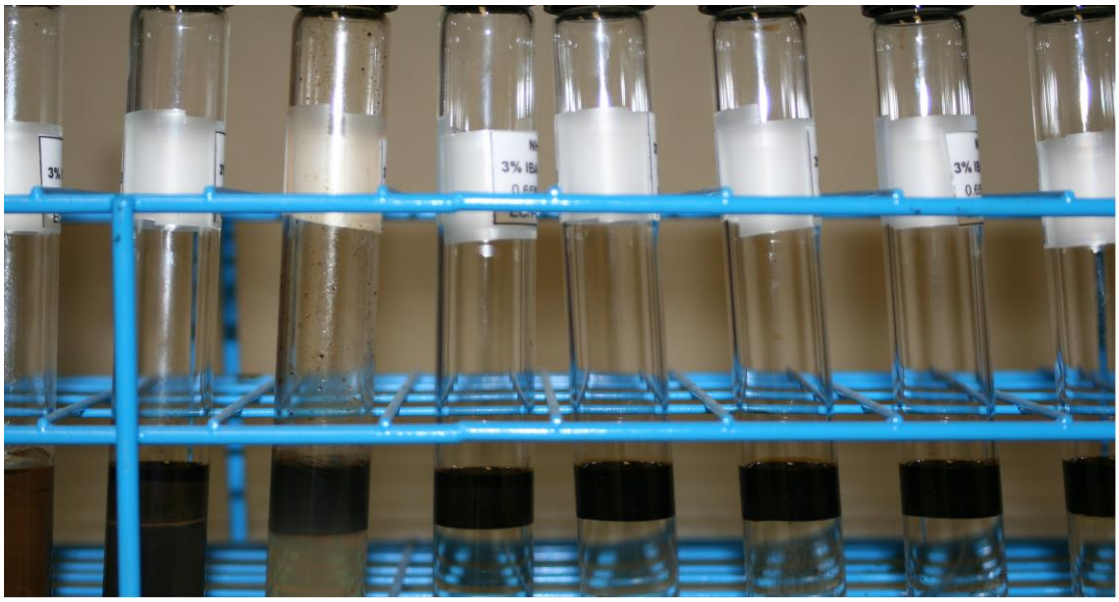

Figure 4.70: Alkali scan samples obtained on mixing 30% fraction of crude oil-5 and aqueous solution consisting of fixed ammonia and increasing NaCl concentration

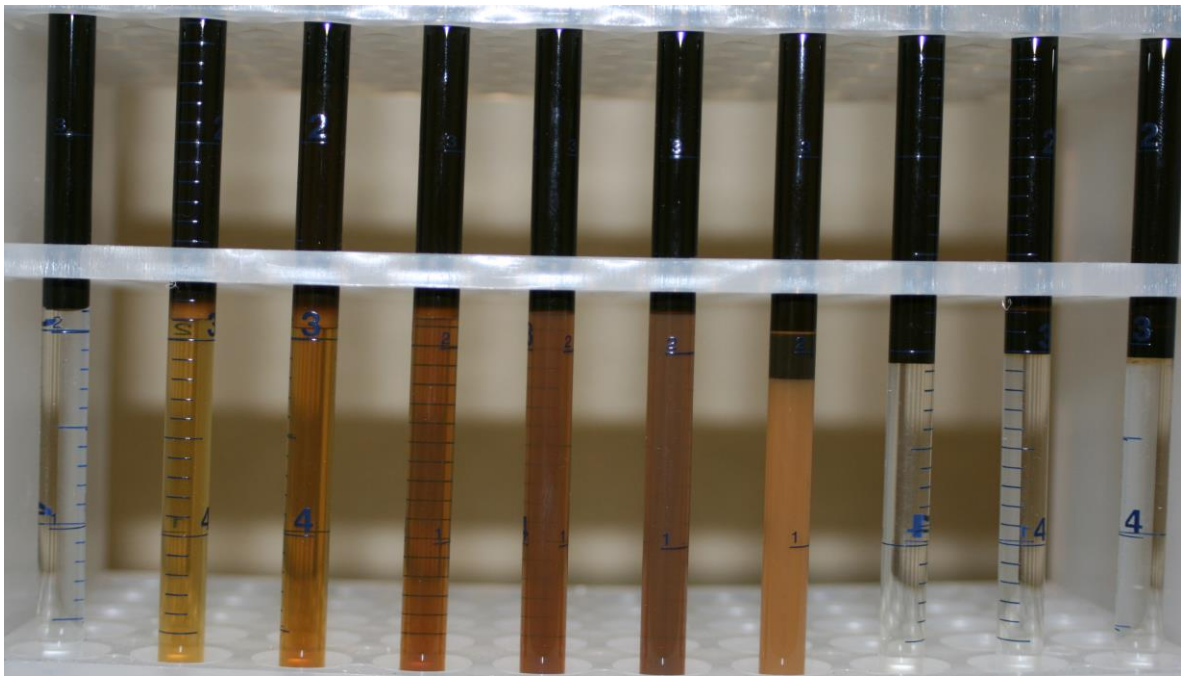

Figure 4.71: Alkali scan samples obtained on mixing 30% fraction of crude oil-6 and aqueous solution consisting of fixed ammonia and increasing NaCl concentration

Experiment 4.28: Alkali scans with different alkalis (a) $NaBO_2$ (b) NH_3

Alkali scans were performed with crude oil-7 to compare low IFT regions with different alkalis in the absence of cosolvent. The concentration of an alkali was systematically increased, keeping the oil volume fraction to 30%. The samples were prepared in glass tubes and sealed as described previously. The samples were then equilibrated at 30 °C, mixed from time to time and low IFT region was identified, visually.

The results of the experiment are given in Table 4.47. With sodium metaborate, low IFT was observed at around 0.12-0.15 meq/Kg, corresponding to about 8,000-10,000

ppm $NaBO_2$. In the case of ammonia, the concentration of ammonia was fixed to 0.4 wt% and sodium chloride was used to increase the salinity. The low IFT, in this case, was observed at around 0.051 meq/Kg, corresponding to 3000 ppm NaCl. From these results, it can be seen that sodium metaborate showed low IFT region at a higher salinity compared to that of ammonia. A possible reason for this difference could be the difference in the type of soap that is generated with these alkalis. It appears that ammonia, being a Lewis base, can interact with the acids directly. However, further research is needed to confirm this hypothesis.

Table 4.47: Low IFT region of different alkalis with crude oil-7

Alkali	Low IFT region
NaBO2	8,000-10,000 ppm
NH3	3,000 ppm NaCl

Experiment 4.29: Effect of divalent ions on ACP formulations

While calcium precipitates with sodium carbonate, sodium metaborate and sodium hydroxide, it stays soluble in the presence of ammonia. Calcium ions, being divalent cations, have shown to significantly affect the surfactant phase behavior, as was discussed in experiment 4.14, and thus can interact with soap and affect ACP formulations developed using ammonia. Magnesium ions, on the other hand, precipitate even with ammonia and are not likely to affect the formulations. The effect of calcium ions on low IFT alkali formulations developed using ammonia (and crude oil-5) as the alkali was studied. This experiment was critical because the concentration of calcium

ions in the porous media could increase due to geochemical interactions such as mineral dissolution, ion exchange, and so on, and affect IFT and low IFT region.

Separate alkali scans were performed with a given amount of calcium ions (between 0 to 250 ppm), fixed ammonia concentration and crude oil-5. The concentration of ammonia was kept fixed to 0.4 wt% and the salinity scans were performed using NaCl. The change in IFT and low IFT region was recorded. The low IFT region was around 3000 ppm NaCl when no calcium was present. The low IFT region shifted up to around 10,000 ppm NaCl when 100 ppm calcium was added and low IFT was not observed when 250 ppm calcium was added. A possible reason for the change in low IFT region on adding calcium ions is the complexation of soap with calcium ions. When calcium concentration was increased from 0 ppm to 100 ppm calcium, some of the soap complexed with calcium ions, became more hydrophobic and possibly went into the oil phase. However, even after losing some soap to the oil phase, there was enough soap left to give a low IFT. On increasing the calcium ions to 250 ppm, all the soap was complexed with calcium and went into oil phase. Thus, no low IFT region was encountered. These results show that even a small amount of free calcium ions can alter the low IFT region and hence the oil recovery process, significantly. This is especially important when ammonia is used as an alkali since ammonia does not precipitate calcium ions up to a very high concentration. A possible way to make the ACP floods with ammonia more robust is to add a small amount of sodium carbonate, along with ammonia, so that the divalent ions can be precipitated.

4.4.2 ACP formulations with different alkalis

Experiment 4.30: Alkali scans using different alkalis using IBA-3EO as cosolvent

Alkali scans were performed with different alkalis using crude oil-7. The oil to water ratio was systematically changed to obtain activity diagrams for different alkalis. Activity diagrams are used in identifying the effect of oil to water ratio on low IFT regions. 1% IBA-3EO was used as the cosolvent in these experiments. The objective of these experiments was to understand the dependence of low IFT region on alkali type. The activity maps obtained for different alkalis are shown in Figures 4.72-4.79.

Figure 4.72 and 4.73 show activity maps obtained using NaOH. This scan was performed by increasing the amount of NaOH in DI water. The low IFT region was observed up to 400 meq/Kg, corresponding to 16,000 ppm NaOH. A similar experiment was performed with $NaBO_2$, Figures 4.74 and 4.75, showed low IFT up to about 600 meq/Kg, corresponding to about 40,000 ppm $NaBO_2$. The low IFT region with Na_2CO_3 was up to about 700 meq/Kg and 950 meq/kg for 30% oil and 50% oil, respectively (Figures 4.76). These values correspond to about 37,000 ppm and 50,000 ppm Na_2CO_3, respectively (Figure 4.77). The results of experiments performed with ammonia (Figure 4.78 and 4.79), where ammonia concentration was fixed to about 0.5 wt% and the concentration of NaCl was varied, showed low IFT region up to 188 meq/Kg, corresponding to about 11,000 ppm NaCl.

These results show that the low IFT regions for $NaBO_2$ and Na_2CO_3 were at higher salinities compared to NaOH and NH_3 when the cosolvent the same cosolvent was

used in these cases. A possible reason for this difference is that the type of soaps formed with NaOH and NH_3 were more hydrophobic compared to that with $NaBO_2$ and Na_2CO_3. Due to their more hydrophobic nature, the low IFT regions were observed at lower salinities with NaOH and NH_3.

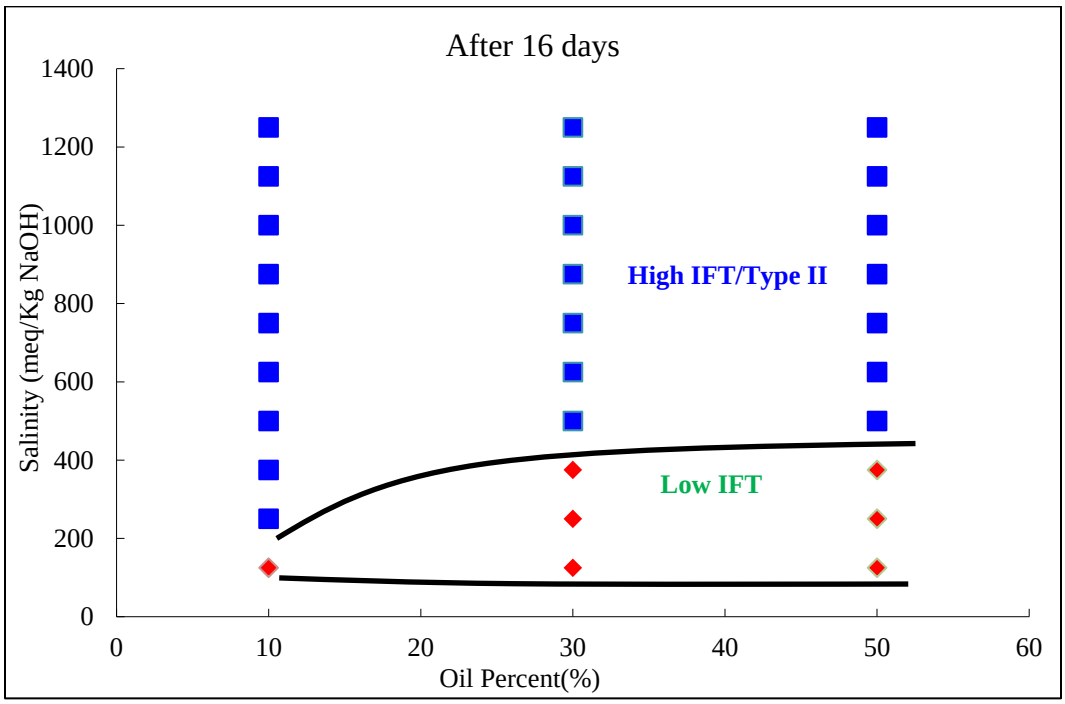

Figure 4.72: Activity map obtained using NaOH as alkali and IBA-3EO as cosolvent

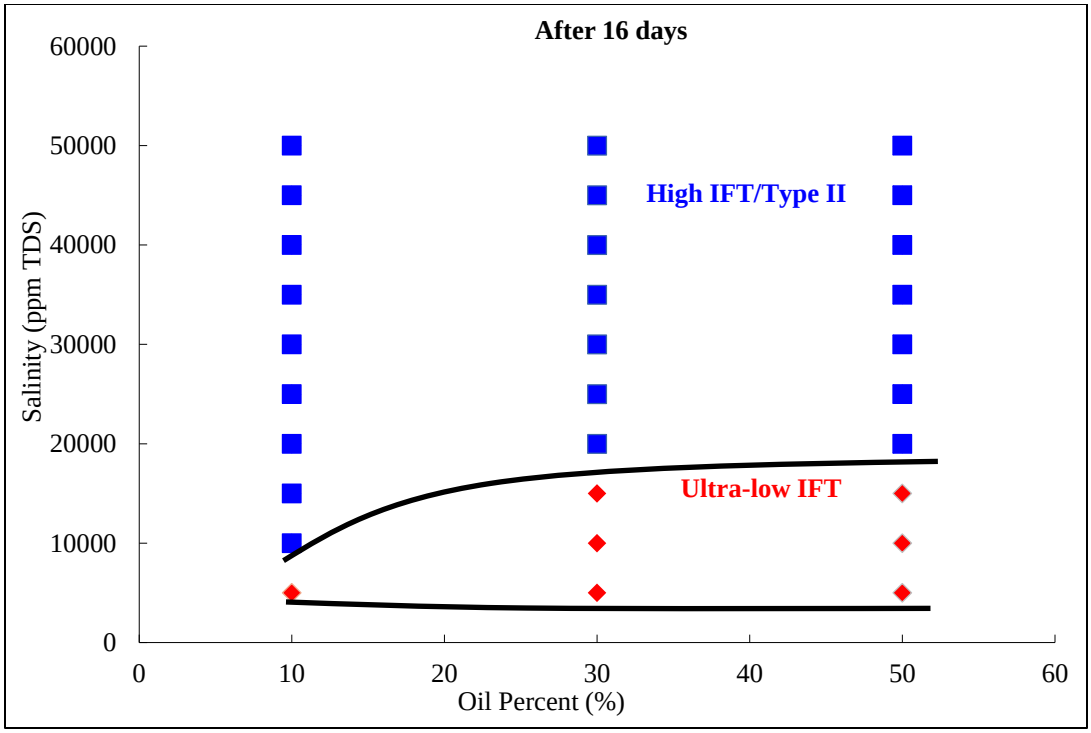

Figure 4.73: Activity map obtained using NaOH as alkali and IBA-3EO as cosolvent

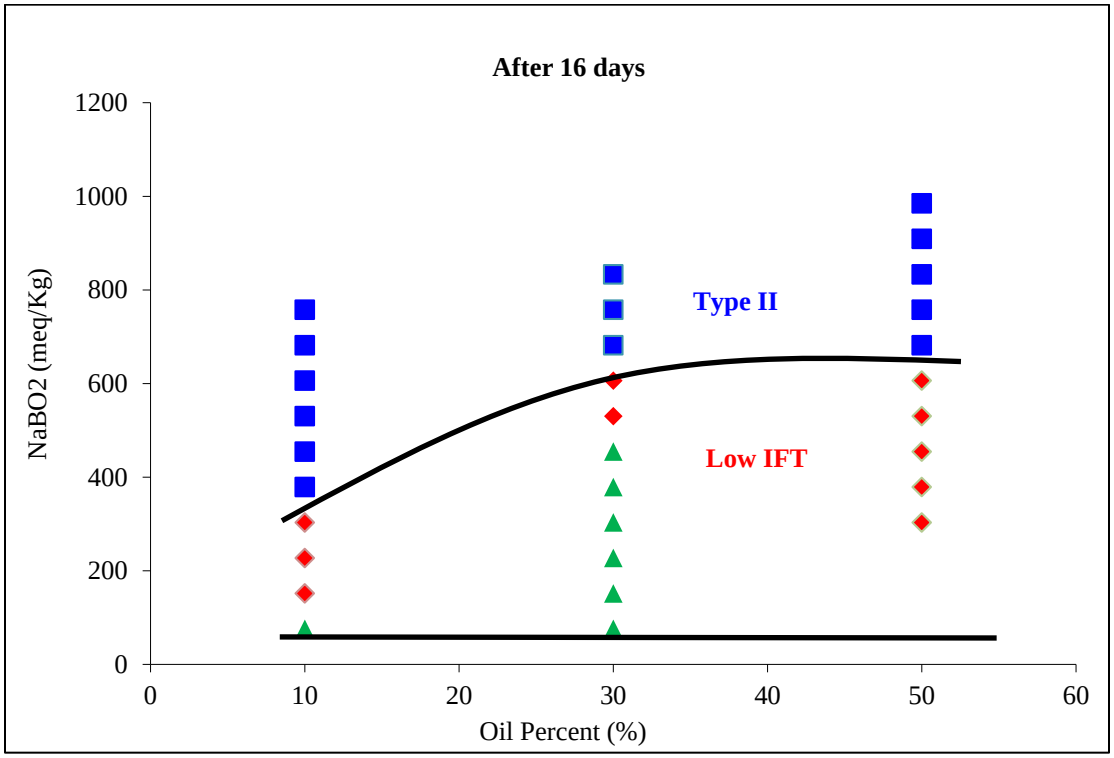

Figure 4.74: Activity map obtained using $NaBO_2$ as alkali and IBA-3EO as cosolvent

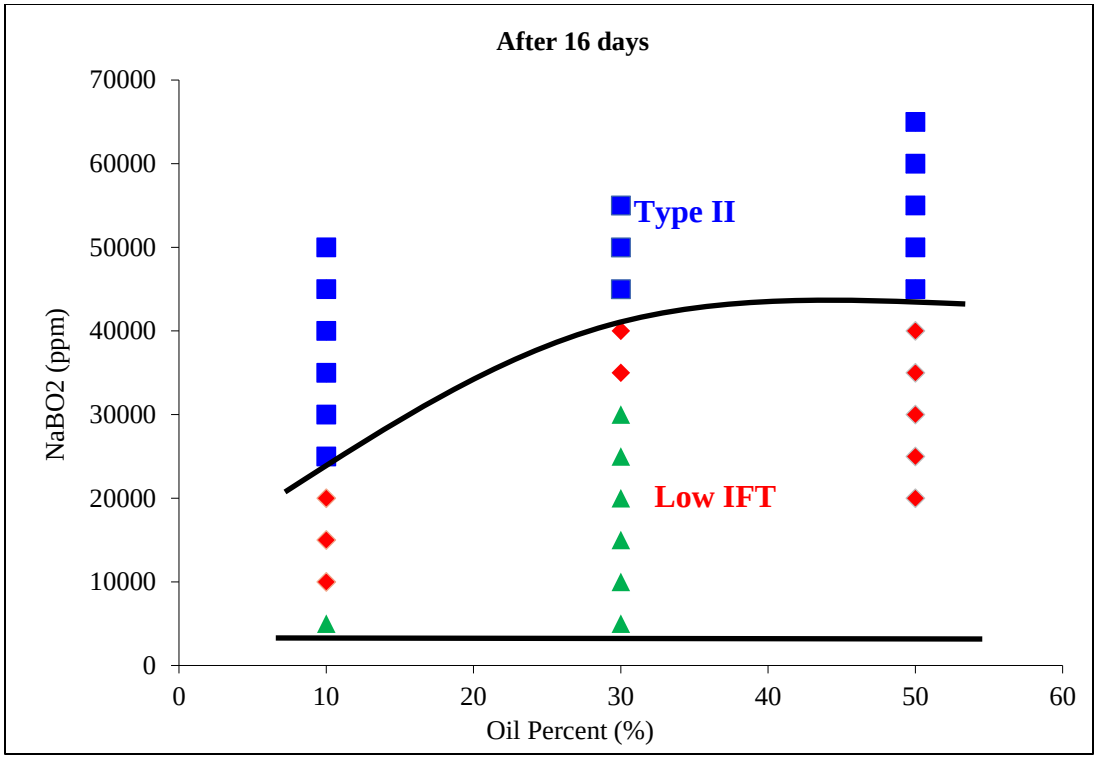

Figure 4.75: Activity map obtained using $NaBO_2$ as alkali and IBA-3EO as cosolvent

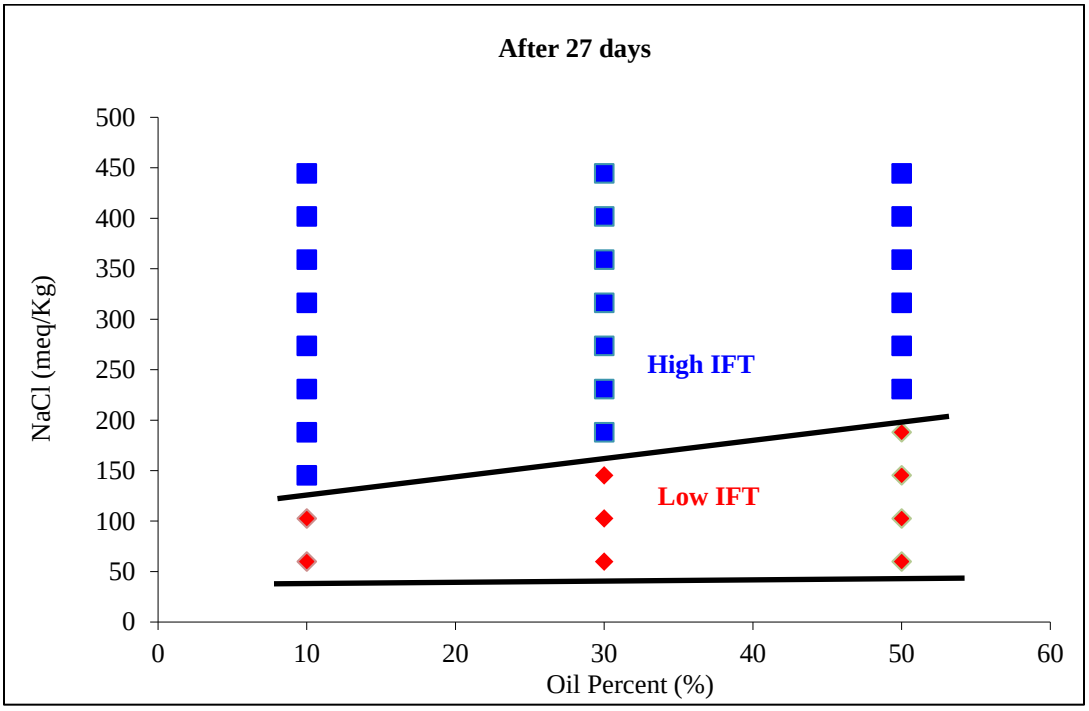

Figure 4.76: Activity map obtained using ammonia as alkali and IBA-3EO as cosolvent. Ammonia concentration was fixed to 0.5 wt% and NaCl was used to increase the salinity

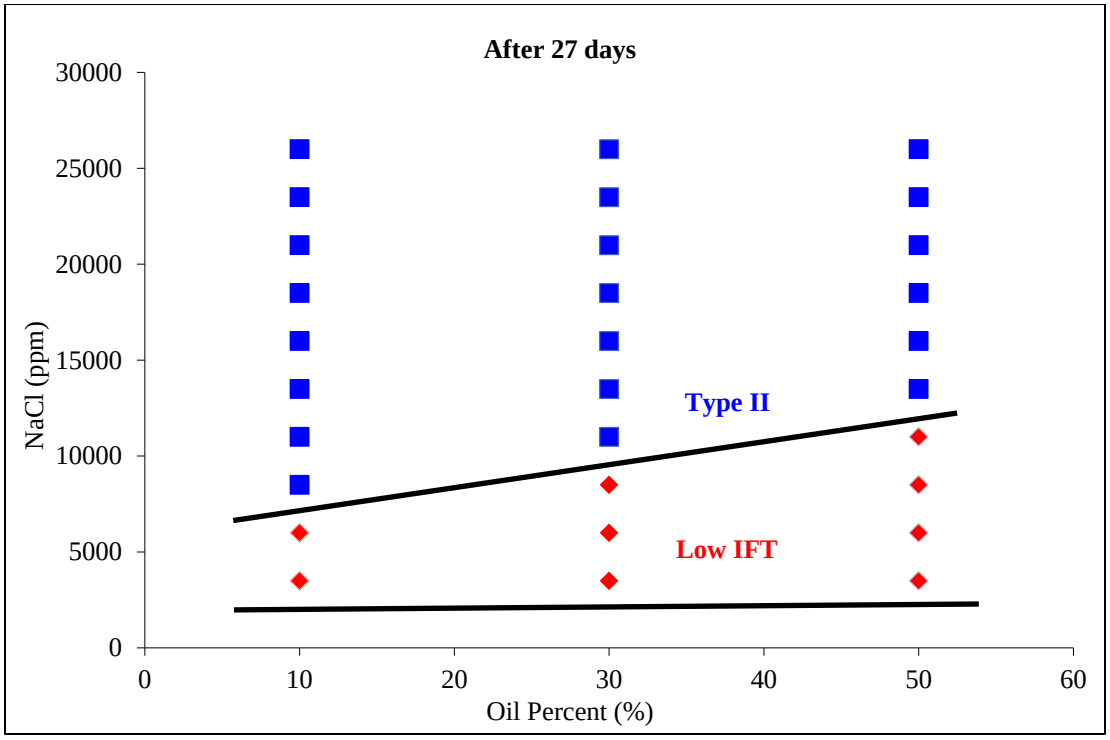

Figure 4.77: Activity map obtained using ammonia as alkali and IBA-3EO as cosolvent. Ammonia concentration was fixed to 0.5 wt% and NaCl was used to increase the salinity

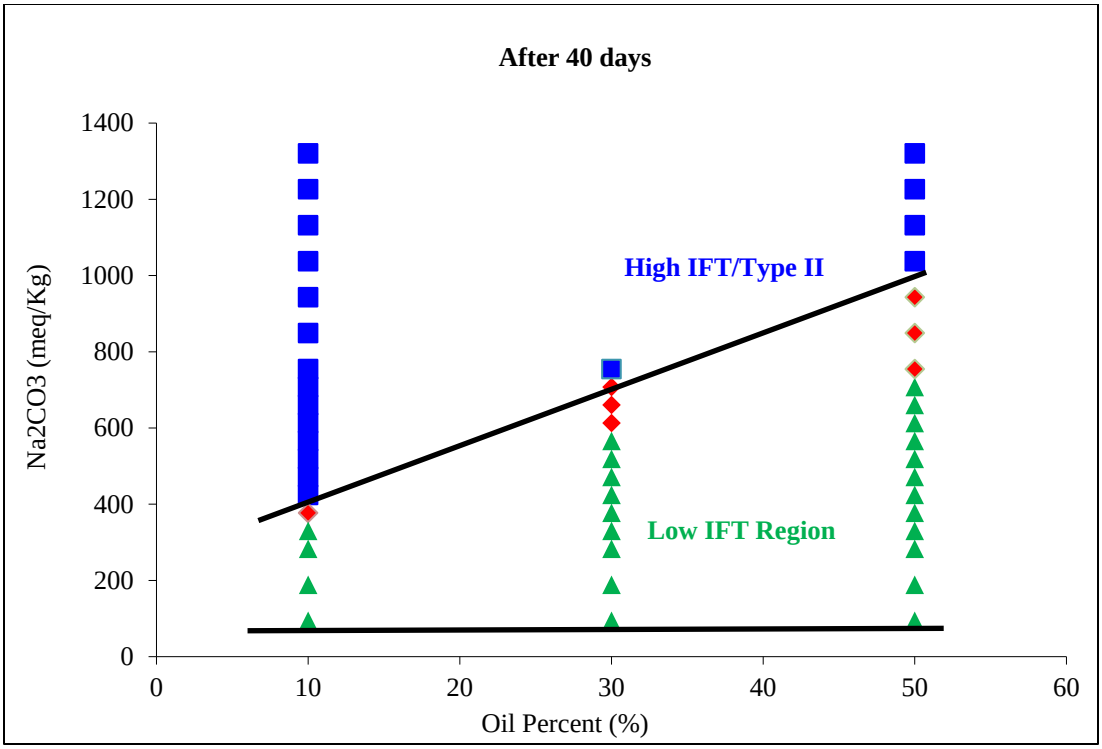

Figure 4.78: Activity map obtained using Na_2CO_3 as alkali and IBA-3EO as cosolvent

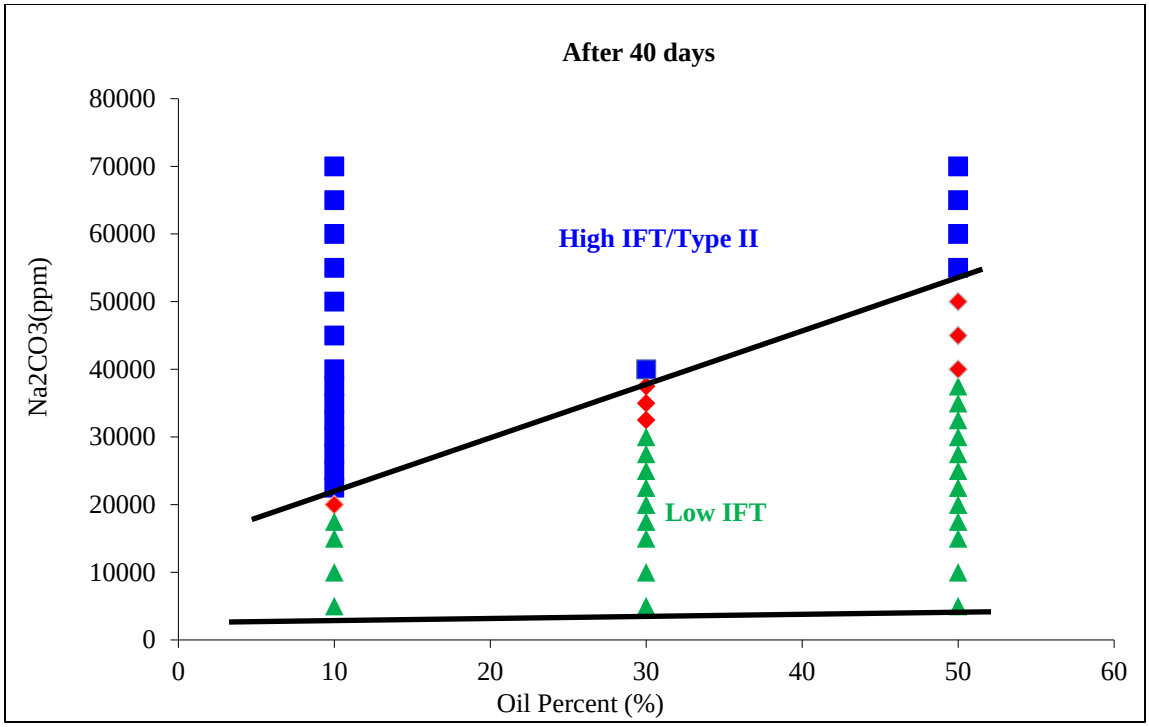

Figure 4.79: Activity map obtained using Na_2CO_3 as alkali and IBA-3EO as cosolvent

Experiment 4.31: Effect of adding ammonia on formulation 4.26 (d)

An experiment was performed to study the effect of adding NH_3 to the low IFT formulations that were obtained with Na_2CO_3. The purpose of this experiment was to test the hypothesis that if NH_3 is able to generate hydrophobic soaps, which was more difficult to make, then a shift in low IFT region should be observed when it is added to the formulations prepared using enough Na_2CO_3. The results of this experiment are shown in Figures 4.80 and 4.81. Figure 4.80 shows the original formulation prepared using Na_2CO_3. The low IFT region, in this case, was up to 40,000 ppm Na_2CO_3 and 50,000 ppm Na_2CO_3 for 30% and 50 % oil, respectively. On adding 0.5 wt% NH_3 (Figure 4.81), the low IFT is observed up to 26,000 ppm Na_2CO_3 and 36,000 ppm Na_2CO_3,

respectively. Clearly, a shift in the low IFT region to lower salinities was observed on adding NH_3 to the ACP formulation developed with Na_2CO_3, indicating that possibly more hydrophobic soap was generated when NH_3 was added.

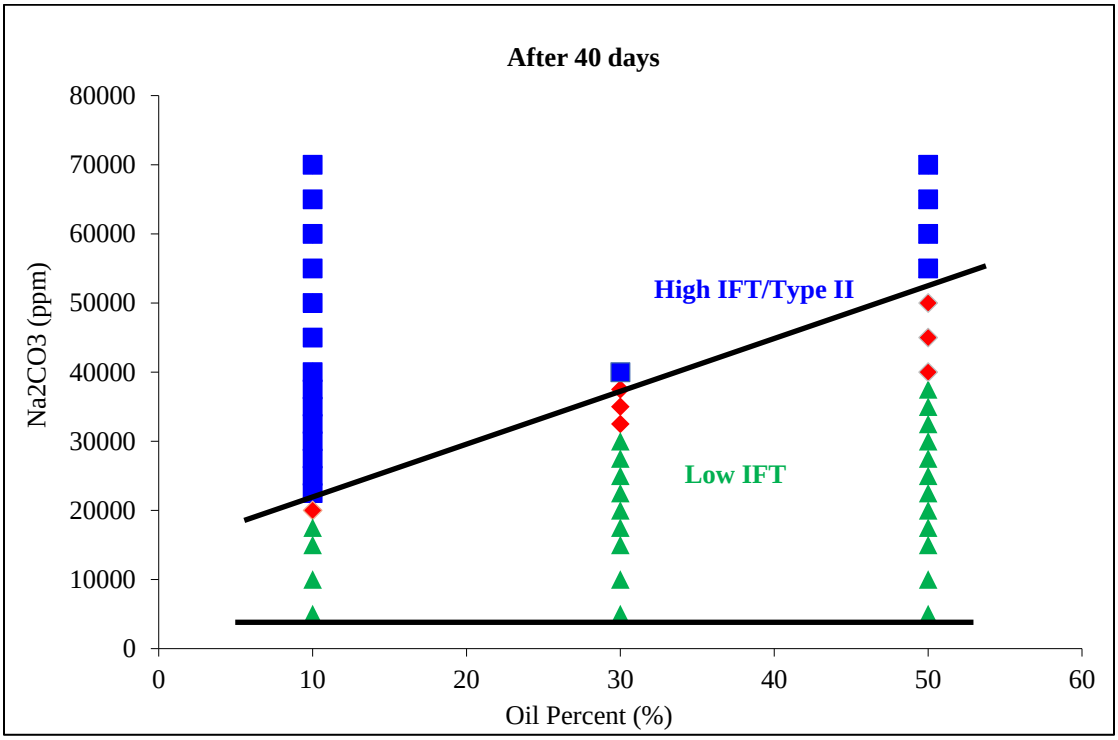

Figure 4.80: Activity map of an ACP formulation developed with Na2CO3 (experiment4.26)

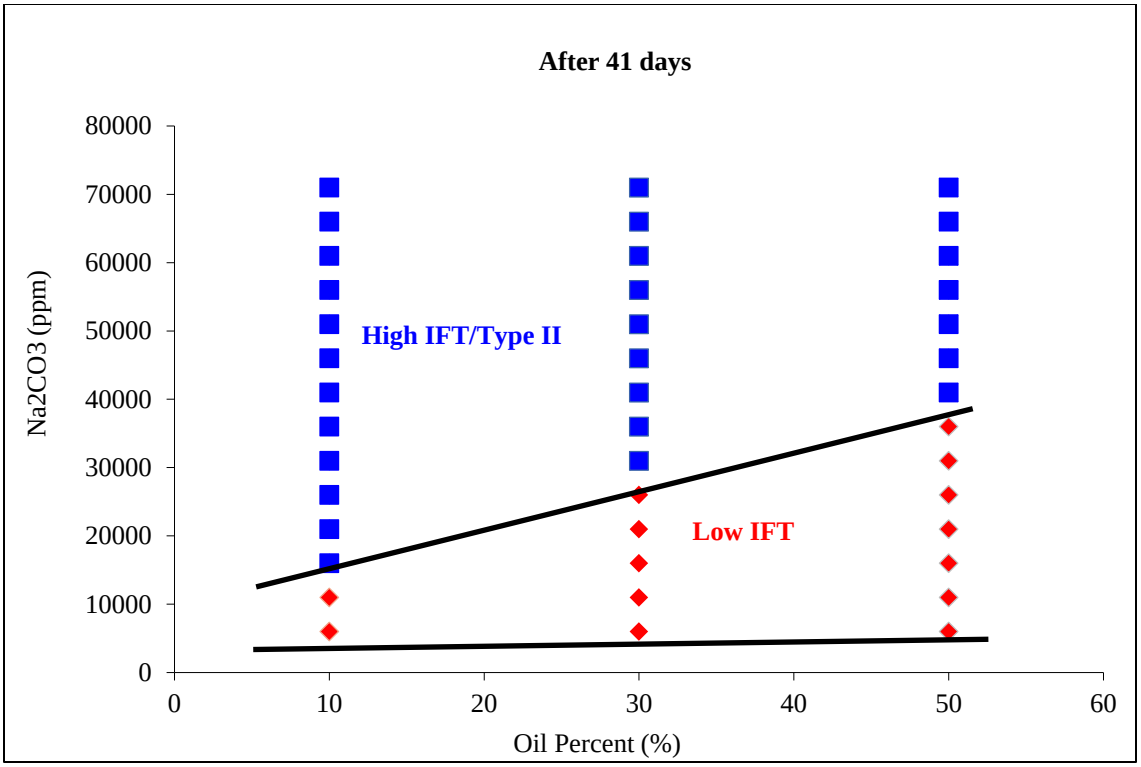

Figure 4.81: Activity map obtained on adding 0.5% NH_3 to the formulation developed using Na_2CO_3 as alkali and IBA-3EO as cosolvent in experiment 4.26

Experiment 4.32(a): Formulation optimization for crude oil-7

The ACP formulations developed using NH_3 and IBA-3EO showed the low IFT region at lower salinities compared to Na_2CO_3 and $NaBO_2$. However, it is possible to adjust the low IFT region as per the requirements by choosing a suitable cosolvent. A cosolvent adds hydrophilicity to the formulation which results in shifting the low IFT region to a higher salinity. In this situation, therefore, a cosolvent more hydrophilic than IBA-3EO was used. The ACP formulations developed using Phenol-10EO (Figure 4.83)

showed low IFT region at higher salinities compared to IBA-3EO (Figure 4.82). Increasing the number of EOs from 10 to 20 did not show significant additional benefit.

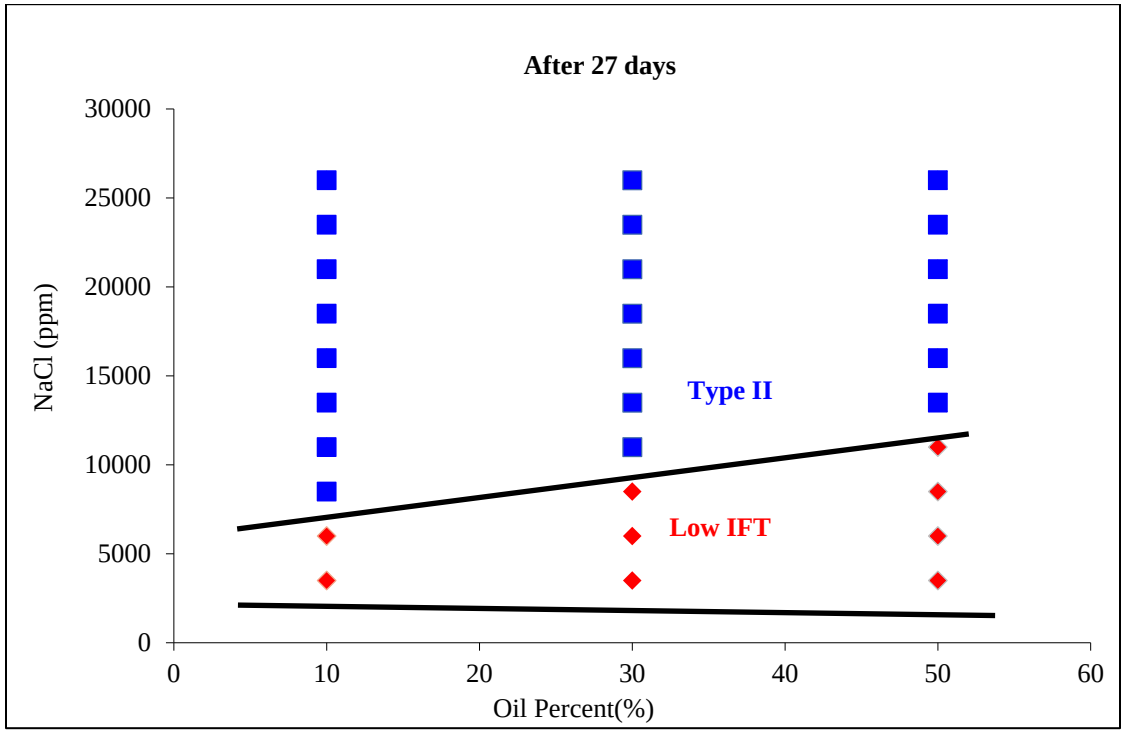

Figure 4.82: Low IFT ACP formulation developed using IBA-3EO as cosolvent and ammonia as alkali

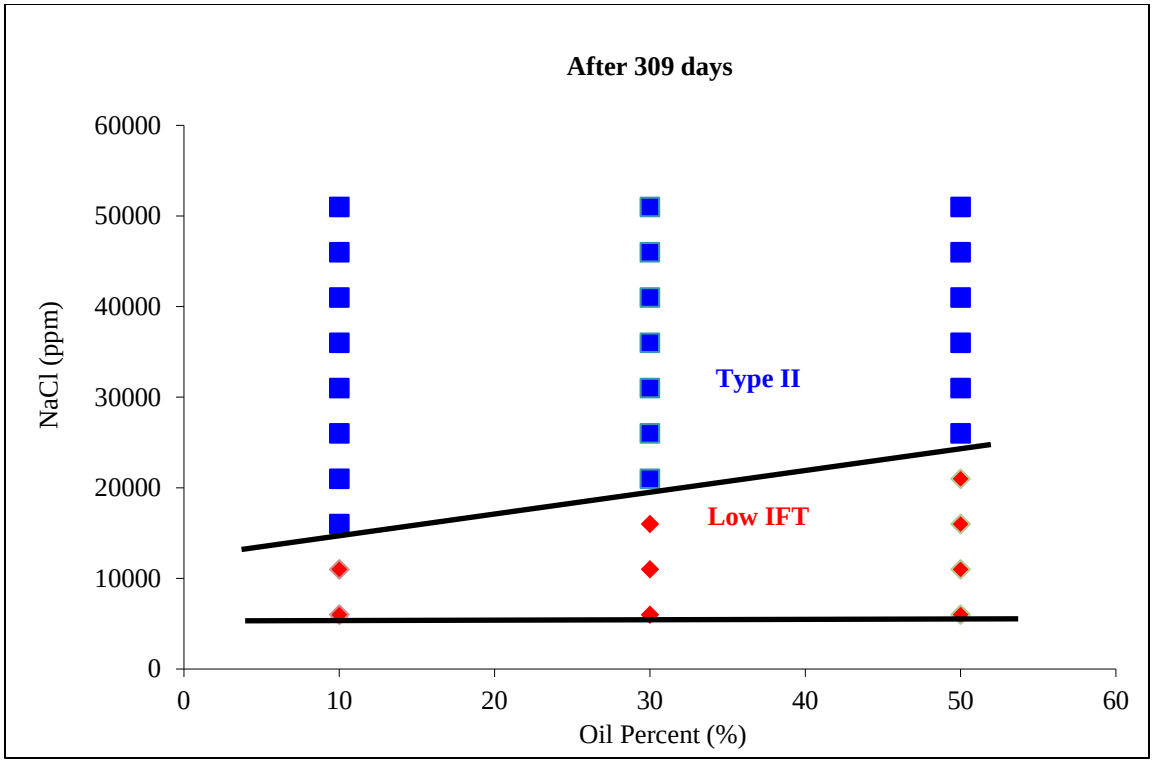

Figure 4.83: Low IFT ACP formulation developed using Phenol-10EO as cosolvent and ammonia as alkali

Experiment 4.32 (b): Formulation optimization for crude oil-6

ACP formulations were developed with crude oil-6, similarly. Note that although this crude oil was relatively less acidic compared to crude oils 5 and 7, it also had a lower viscosity. A moderately high acid number and a relatively lower viscosity made crude oil-6 an interesting candidate for ACP floods. The polymer requirement for this oil seem feasible for a stable flood in the field and the addition of a small amount of alkali may increase the oil recovery dramatically. The objective of this study was, therefore, to compare ACP floods using crude oil 6 with the ASP floods previously performed with

the same oil by Panthi et al. (2016). Alkali scans were performed using sodium carbonate keeping the cosolvent concentration fixed to 0.5 wt%. The phase behavior tubes were prepared as discussed in chapter 3 after which they allowed to equilibrate at 59 °C and mixed from time to time. The scans were performed for 10% oil, 30% oil and 50% oil and activity maps were prepared. In these experiments, sodium carbonate scans were performed using DI water, instead of the base brine of 20,000 ppm NaCl. These are preliminary results and optimization work later performed for this particular reservoir is not presented here.

The list of cosolvents tested in developing ACP formulations is listed in Table 4.48. The first experiment was performed with 0.5 wt% IBA-3EO which showed the low IFT region with 10% and 30% oil at high alkali concentrations of about 3.5 % and up to 8.5% sodium carbonate, respectively. The low IFT region with 50% oil was likely to be higher than 8.5. In second experiment, 0.5 wt% IBA-3EO cosolvent was replaced with 0.5 wt% IBA-2EO cosolvent. The low IFT region was still at a high sodium carbonate concentration and Winsor type-I phase behavior was observed up to 5 wt% sodium carbonate. In the third experiment, 0.5 wt% IBA-2PO was used as the cosolvent, which resulted in giving low IFT region around 3-3.5 wt% sodium carbonate. The formulation was aqueous stable at room conditions but was not aqueous stable at 59 °C, the reservoir temperature. In the next experiment, 0.5 wt% IBA-2PO-2EO was used as the cosolvent which resulted in showing low IFT at a high sodium carbonate concentration of around 6 wt% for 30% oil scan. In the fifth experiment, 0.5 wt% IBA was used without any EO groups which resulted in showing low IFT region from 1.5 wt% to 6.5 wt% sodium

carbonate as the oil volume fraction was increased from 10% to 50%. The formulation using IBA was however aqueous stable at 59 °C. However, because of a steep slope with IBA, a combination of IBA and IBA-2PO in equal proportion (0.25 wt% each) was used. The formulation was aqueous stable also at 59 °C, unlike IBA-2PO alone but resulted in making viscous emulsions.

The activity maps for the formulations developed using IBA-2PO and IBA are shown in Figures 4.84 and 4.85, respectively. With IBA-2PO, the low IFT region was observed between 1.5% to about 4% sodium carbonate as the oil volume fraction was increased from 10% to 50%. With IBA, the low IFT region was observed between 1.5% to about 6.5% sodium carbonate. From the figures, it can be seen positive slopes were seen in the activity maps for both the cosolvents. However, the slope was steeper with IBA. Oil recovery ACP corefloods were performed with these formulations in sandstone cores.

Table 4.48: List of cosolvents tested with crude oil-6 to obtain favorable ACP formulation

Cosolvents	Observations
0.5% IBA-3EO	Low IFT region with 10% oil~3.5% Na2CO3; 30% oil~6.5-8.5% Na2CO3
0.5% IBA-2EO	All Type I
0.5% IBA-2PO	Low IFT around 3% Na2CO3; Not aqueous stable at 59 °C
0.5% IBA-2EO-2PO	Low IFT region with 30% oil~5.5-6%
0.5% IBA	Positive slope between 1.5%-6% Na2CO3; Aqueous stable at 59 °C
0.25% IBA-2PO + 0.25%IBA	Viscous emulsions; Aqueous stable at 59 °C

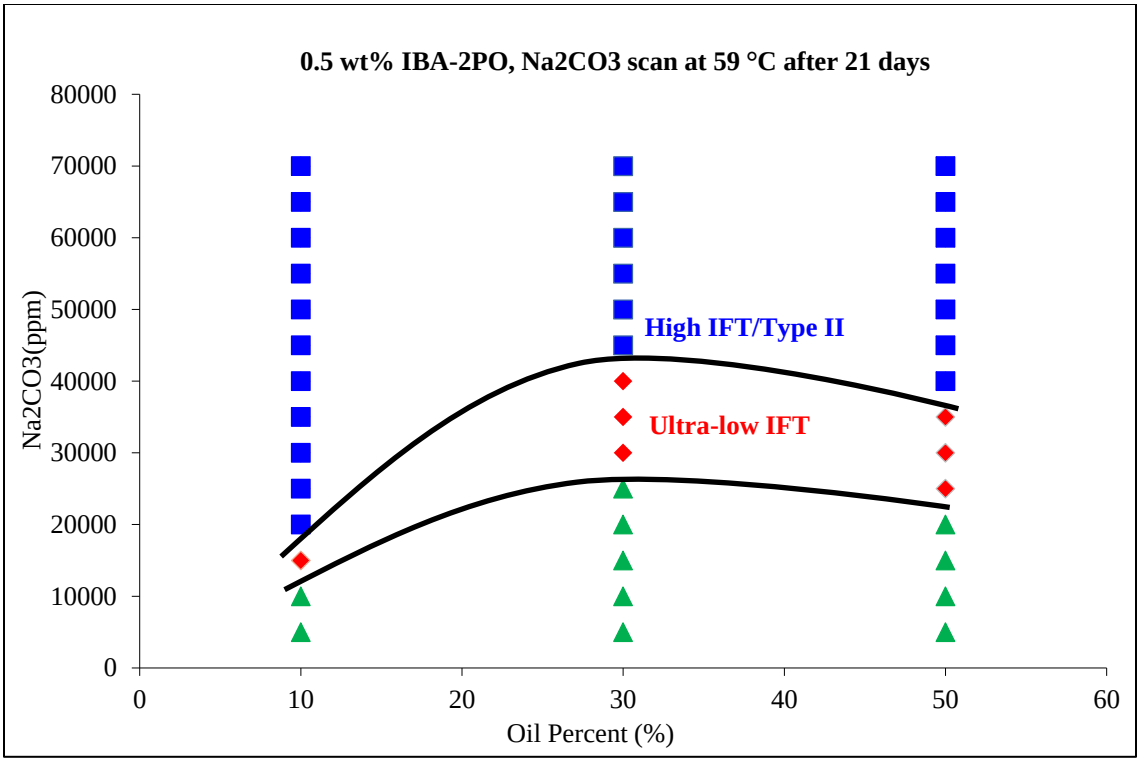

Figure 4.84: Activity map obtained with crude oil-6, 0.5% IBA-2PO cosolvent and Na2CO3 scan

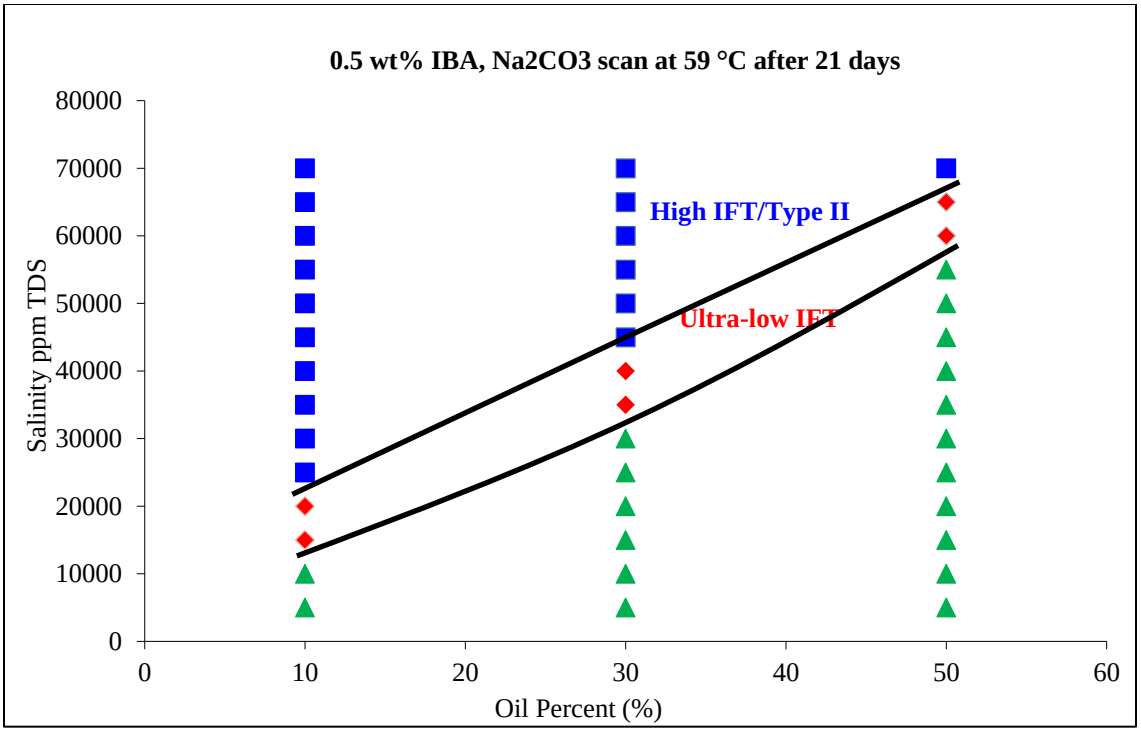

Figure 4.85: Activity map obtained with crude oil-6, 0.5% IBA cosolvent and Na2CO3 scan

4.4.3 Oil recovery ACP corefloods

Experiment 4.33: ACP oil recovery coreflood CF-16

The ACP formulation developed with crude oil-6 using IBA-2PO as the cosolvent (see Table 4.48) was used in an oil recovery coreflood in a Berea sandstone core. The properties of the core are given in Table 4.51. The core was characterized to obtain the porosity and permeability. The core was saturated with a formation brine and initial oil saturation was established by following the procedure described chapter 3. The ionic compositions of the formation brine, waterflood brine and chemical slugs are given in Table 4.52. Waterflood was performed at 1 ft/d and effluent samples were collected using

an automatic fractional collector. The amount of oil recovered was measured to obtain the residual oil saturation after waterflood.

A 0.3 pore volume ACP slug injection was performed next, followed by two polymer drives of 0.2 pore volume and 1.5 pore volume, each, of decreasing salinities. The ACP slug consisted of 0.5% IBA-2PO, 0.35% FP 3330S and 3.5% Na_2CO_3. The formulation was injected from outside the oven since the formulation was not aqueous stable at 59 °C. The slug heated up while it was being injected in the injection line. The ACP slug was followed by the first polymer drive consisting of 0.5% IBA-2PO, 0.35% FP 3330S and 2.5% Na_2CO_3. Another polymer drive of even lower salinity, 1.0% Na_2CO_3, was injected. In addition to sodium carbonate, 0.5% IBA-2PO and 0.3% FP 3330S was present in the second polymer drive. Note that in these preliminary corefloods, cosolvent was added to the ACP slug as well as the polymer drives. The recovery results from the coreflood are shown in Figure 4.87. During the ACP flood, the oil recovery increased from about 30% OOIP (after waterflood) to about 86% OOIP. The residual oil saturation decreased from about 43% (after waterflood) to about 8%. A good oil bank of about 50% oil-cut was observed during the coreflood. Note that no synthetic surfactant was added in this chemical flood and additional oil recovery during the chemical flood was due to lowering of IFT by the soap generated on reacting with (injected) sodium carbonate.

Table 4.51: Properties of the core used in the ACP coreflood CF-16

Core	Length (inches)	Diameter (inches)	Porosity (%)	Permeability (md)	Temperature (°C)
Berea Sandstone	1.5	11.8	21	58	59

Table 4.52: Composition of the formation brine, the waterflood brine and the chemical slugs

Salt	Formation/Waterflood brine (ppm)	ACP slug (ppm)	Polymer drive 1 (ppm)	Polymer drive 2 (ppm)
NaCl	45,000	-	-	-
Na_2CO_3	-	**35,000**	**25,000**	**10,000**
TDS	**45,000**	**35,000**	**25,000**	**10,000**

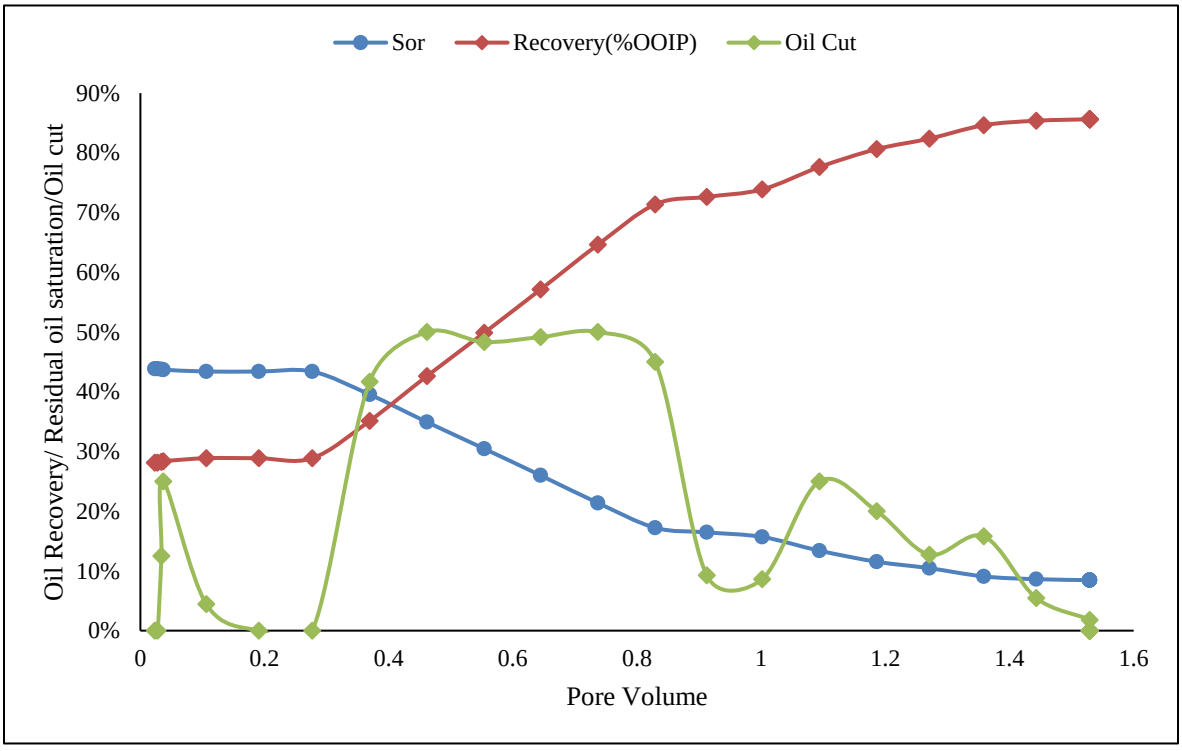

Figure 4.87: Oil recovery data from the ACP coreflood CF-16

A summary of the results obtained using ammonia for developing ACP floods is given below:

1. Alkali scans were performed with active oils using sodium carbonate, ammonia, sodium metaborate and sodium hydroxide. The low IFT regions were found to be at different salinities with these alkalis. Similar results were obtained when the experiment was repeated with a given amount of cosolvent (keeping cosolvent type fixed). The low IFT regions were observed at lower salinity when ammonia and sodium hydroxide were used. This difference was attributed to the type of soap formed with various alkalis; it appears more hydrophobic soap was generated using ammonia and sodium hydroxide compared to that with sodium carbonate or sodium metaborate.

2. The addition of calcium ions to ACP formulations developed using ammonia showed a transition to Winsor type II. Since calcium ions do not precipitate in the presence of ammonia, they are free to attach to the soap that is generated by adding alkali to acidic crude oils. The resulting calcium-soap, being very hydrophobic, transforms the phase behavior towards Winsor type II.

3. ACP formulations were developed for acidic crude oils. The type of cosolvent was changed to optimize the formulations. It was found that more hydrophilic cosolvents, with higher EO groups, were better in giving a favorable activity diagram. ACP oil recovery coreflood performed in a sandstone core showed good oil recovery.

CHAPTER 5. SIMULATIONS OF ASP COREFLOODS

In the previous chapter, experimental results showed the significance of geochemical interactions in designing a robust chemical flood. These interactions can greatly alter the composition of the brine in the porous media, resulting in changing surfactant phase behavior, affecting polymer and surfactant stability, increasing surfactant retention, reducing rock permeability and so on. In this chapter, results of modeling and simulation study conducted to further investigate the role of geochemical interactions on surfactant floods are presented. Single-phase and multiphase flow studies were performed to understand geochemical interaction between injected alkalis/brines, reservoir fluids, and minerals. Sensitivity study was performed to study these interactions at different salinities and temperatures. Precipitation/dissolution and ion exchange reactions were identified to be the key reactions that could affect surfactant floods. Methods were developed to make a chemical flood more robust. PHREEQC, the USGS geochemistry tool, was used for conducting single-phase studies. Multiphase flow studies were performed in UTCHEM, the University of Texas chemical flooding simulator. UTCHEM-EQBATCH and UTCHEM-IPHREEQC were used for incorporating geochemistry in multiphase flow simulations. The list of simulations is given in Table 5.1

Table 5.1: List of single-phase and multiphase simulations

Simulation	Description
5.1	UTCHEM-EQBATCH simulations of ASP corefloods performed using sodium metaborate as alkali (a) Tertiary ASP coreflood CF-3 (b) Secondary ASP coreflood CF-4
5.2	Single-phase geochemical interactions of various alkalis in presence of gypsum during static experiments (a) Sodium carbonate (b) Sodium metaborate
5.3	Single-phase geochemical interactions of various alkalis with gypsum during transport experiments
5.4	Simulation of ASP coreflood CF-8 performed in a carbonate core containing gypsum using ammonia as alkali in UTCHEM-IPHREEQC
5.5	Simulation of ASP coreflood CF-14 (using ammonia as alkali) and the effect of ion exchange reactions on these corefloods

5.1 UTCHEM simulation of ASP corefloods CF-3 and CF-4

In ASP coreflood CF-3, tertiary ASP coreflood was performed in a Silurian dolomite core with the surfactant formulation discussed in experiment 4.8. Sodium metaborate was used as the alkali in the surfactant formulation. The core was waterflooded with a soft brine, which lowered the oil saturation to 43%. A preflush solution was injected after the waterflood to increase the salinity ahead of the surfactant slug. The properties of the core and ionic compositions of the aqueous solutions are shown in Tables 5.2(a) and 5.2(b), respectively.

Table 5.2(a): Properties of the core used in ASP corefloods CF-3 and CF-4

Core	Length (inches)	Diameter (inches)	Porosity (%)	Permeability (md)	Temperature (°C)	Gypsum
Silurian dolomite	11.95	1.47	18.8	80.1	38	No

Table 5.2(b): Composition of the various brines used in the ASP corefloods CF-3 and CF-4

Salt	Formation/Waterflood brine (ppm)	Preflush	ASP slug (ppm)	Polymer drive 1 (ppm)	Polymer drive 2 (ppm)
NaCl	30,700	30,700	30,700	30,700	30,700
Na_2SO_4	4,800	4,800	4,800	4,800	4,800
$NaBO_2$	-	10,000	10,000	10,000	-
TDS	**35,500**	**45,500**	**45,500**	**45,500**	**35,500**

Changes in ionic compositions of the injected solutions due to their interactions with Silurian dolomite was studied in PHREEQC. Dissolution of dolomite in an aqueous solution can be described as shown below. The reaction could result in increasing calcium and magnesium ions in the injected brine and affecting the chemical flood.

$$CaMg(CO_3)_2 = Ca^{2+} + Mg^{2+} + 2CO_3 \quad (5.1)$$

PHREEQC is a geochemistry tool, developed by USGS, that can perform single-phase static and transport calculations of brine-rock and brine-brine interactions and brine stability calculations. These calculations can be performed assuming local equilibrium or with reaction kinetics. Reactions such as dissolution/precipitation, ion exchange and surface complexation can be modeled easily with PHREEQC. In addition, aqueous speciation calculations can be performed to investigate the stability of a brine. These calculations are useful to investigate brine stability at reservoir conditions or estimate changes in brine composition due to depressurization at production wells. The reaction constants for performing calculations are obtained from the geochemistry databases that

have been designed for PHREEQC. Each database serves its purpose and works best under a certain condition. Additional reactions can be added by the user as needed. The program takes into account the effect of salinity and temperature on equilibrium constants.

Table 5.3: Final pH, calcium and magnesium concentration in CF-3 and CF-4 coreflood brines on coming in equilibrium with dolomite

Brine	Calcium concentration (ppm)	Magnesium concentration (ppm)	Initial/Final pH
Formation/Waterflood/Polymer drive 2	10.7	6.4	7/9.6
Preflush/ASP/Polymer drive 1 (with 10,000 ppm NaBO2)	14.6	2.8	10.8/10.7

The calcium and magnesium concentrations due to dissolution of dolomite in the formation/waterflood brine, preflush and chemical flood brines are shown in Table 5.3. Note that calcium or magnesium ions were not initially present in these brines. PHREEQC estimated dolomite dissolution to add about 10.7 ppm calcium ions and 6.4 ppm magnesium ions in the formation brine, waterflood brine and polymer drive 2. The surfactant slug is not likely to be affected on mixing with these equilibrated brines. Note that PHREEQC predicted the final pH of these brines to be about 9.7, higher than the initial pH value of 7. This increase in pH is the result of carbonate ions released due to dissolution of dolomite (equation 5.1). The dissolution of dolomite results in introducing carbonate ions to the aqueous solution, which results in increasing the pH. The increase

in pH may not be observed in the laboratory corefloods, unless they are conducted at a sufficiently slow injection rates due to slow dissolution reaction kinetics of dolomite. Also, note that in spite of the high pH of the brines equilibrated with dolomite, the aqueous solution has almost negligible alkalinity. Similar calculation performed for the preflush solution and the ASP slug showed calcium and magnesium ions in the equilibrated solutions to be around 14.6 ppm and 2.8 ppm, respectively. Such low concentrations of divalent ions are not likely to affect the surfactant phase behavior. The final pH value was almost the same as the initial pH, indicating that sodium metaborate can propagate through a dolomite core without interacting noticeably.

The surfactant phase behavior is modeled in UTCHEM using the Hand representation of the ternary diagram. The UTCHEM input parameters for modeling surfactant phase behavior were obtained by matching the experimental surfactant phase behavior data. For active oils, surfactant phase behavior experiments must be performed at different water-oil ratio (WOR) when an alkali is included in the formulation. An alkali reacts with acidic components in an active crude oil and generates in-situ soap. Due to different amount of soap in samples prepared at different WOR, the soap to surfactant ratio in these samples differ. This results in changing the optimum salinity and solubilization at the optimum salinity as discussed by Salager et al. (1979) and Mohammadi et al. (2009). During an ASP flood, WOR ratio differ at various stages of the flood. A prior knowledge of expected change in optimum salinity with a change in WOR is helpful in designing a robust salinity gradient. The equations to calculate a change in

optimum salinity and a change in solubilization ratio at the optimum salinity with changing WOR are given below.

$$ln(S_M^*) = X_{soap}.ln(S_{soap}^*) + X_{surfactant}.ln(S_{surfactant}^*) \quad (5.2)$$

$$\sigma_M^* = X_{soap}.\sigma_{soap}^* + X_{surfactant}.\sigma_{surfactant}^* \quad (5.3)$$

where S_M^*, S_{soap}^*, $S_{surfactant}^*$ are the optimum salinities of the mixture, soap and surfactant, respectively. $\sigma_M^*, \sigma_{soap}^*$, $\sigma_{surfactant}^*$ are the solubilization ratios at their respective optimum salinities. X_{soap} and $X_{surfactant}$ are mole fractions of soap and surfactant, respectively. A comparison of the modeled and the measured solubilization ratio for water-oil-ratio (WOR) of 1 is shown in Figure 5.1. The parameters that showed a reasonable comparison with the experimental data is given in Table 5.4.

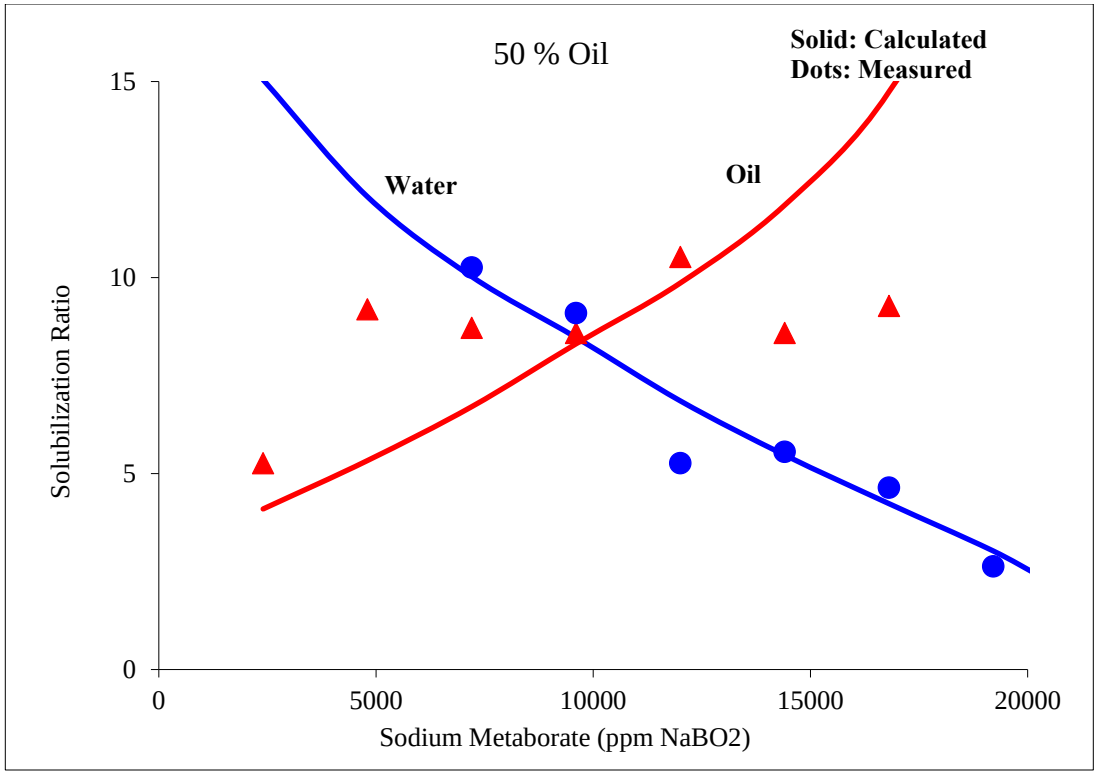

Figure 5.1: Comparison of solubilization plots obtained experimentally and calculated from Hand's rule

The amount of soap generated in the presence of an alkali is calculated based on the total acid number of the oil and the partitioning coefficient of soap in the aqueous phase. The partitioning of soap in the aqueous phase is shown in the equation below. The partitioned soap reacts with an alkali to generate soap.

$$HA_o \leftrightarrow HA_w$$

$$K_d = \frac{[HA_w]}{[HA_o]}$$

$$HA_w + OH^- \leftrightarrow A_w^- + H_2O$$

$$K_a = \frac{[A_w^-]}{[HA_w][OH^-]}$$

The net equilibrium constant for the conversion of naphthenic acids to soap can be written as

$$K_s = K_d K_a$$

The concentration of soap in the aqueous phase can now be obtained from the equation given below.

$$C_s = \frac{K_s(TAN)S_2\rho_2}{S_1(MW_{KOH})} \tag{5.4}$$

Surfactant adsorption in UTCHEM is modeled using a Langmuir-type isotherm as shown in equation 5.5. The dependence of total surfactant adsorption on permeability and salinity is modeled by using equation 5.6. The adsorption is assumed to be irreversible with respect to surfactant concentration and reversible with respect to salinity. Further details are available in the UTCHEM technical manual.

$$\hat{c}_k = min\left(\tilde{c}_k, \frac{a_k(\tilde{c}_k - \hat{c}_k)}{1 + b_k(\tilde{c}_k - \hat{c}_k)}\right) \qquad \text{k=3} \tag{5.5}$$

$$a_3 = (a_{31} + a_{32}C_{SE})\left(\frac{K_{ref}}{K}\right)^{0.5} \tag{5.6}$$

where C_{SE} is the effective salinity, a & b are the constants for the Langmuir model, K_{ref} is the reference permeability at which adsorption parameters are specified.

Table 5.4: Surfactant and polymer parameters used in UTCHEM simulations

Polymer parameters	**Surfactant parameters**
Ap1= 700 Ap2= 900 Ap3= 1700 Sp= -0.39 γ_c= 3 $\dot{\gamma}_{1/2}$= 0.8 P_α= 1.8	CSEL7=0.6; CSEU7=1.3 Hblc71=0.08; Hblc71=0.06; Hblc72=0.08

The UTCHEM parameters for modeling polymer viscosity are based on the Flory-Huggins equation given below.

$$\mu_p^0 = \mu_w\left(1 + \left(A_{p1}C_{4l} + A_{p2}C_{4l}^2 + A_{p3}C_{4l}^3\right)C_{SEP}^{Sp}\right) \tag{5.7}$$

where A_{p1}, A_{p2} and A_{p3} are the input parameters used for calculating polymer viscosity as a function of polymer concentration at zero shear rate. Polymer concentration in phase l is shown as C_{4l} in the equation above.C_{SEP} is the effective salinity of the solution obtained from the equation shown below

$$C_{SEP} = \frac{C_{51}+(\beta_p-1)C_{61}}{C_{11}} \tag{5.8}$$

where C_{51}, C_{61} and C_{11} are the total anion concentration in water, the total divalent cation concentration in water and the total water concentration in the aqueous phase, respectively. β_p is the input parameter to account for change in polymer viscosity due to divalent cations. S_p is the parameter to account for the change in polymer viscosity with

an increase in effective salinity; obtained from the slope of viscosity vs effective salinity on a log-log plot.

Polymer viscosity (μ_p) at a given shear rate is calculated in UTCHEM as per the Meter's equation shown below

$$\mu_p = \mu_w + \frac{\mu_p^0 - \mu_w}{1+\left(\frac{\dot{\gamma}}{\dot{\gamma}_{1/2}}\right)^{P_\alpha - 1}} \tag{5.9}$$

where $\dot{\gamma}$ is the effective shear rate in the core and $\dot{\gamma}_{1/2}$ is the shear rate at which viscosity is the average of μ_w andμ_p^0. P_α takes into account the reduction in polymer viscosity with a change in shear rate. The effective shear rate in the core is calculated from the equation given below

$$\dot{\gamma} = \left[\frac{3n+1}{4n}\right]^{\frac{n}{n-1}} \left[\frac{u_w}{\sqrt{k k_{rw} S_w \varphi}}\right] \tag{5.10}$$

Additional details such as modeling of polymer resistance factors, polymer adsorption and inaccessible pore volumes is available in the UTCHEM technical manual.

In coreflood CF-3 and CF-4, FP 3630S was used for mobility control. The parameters to model the rheology of FP3630S in UTCHEM simulations were obtained by comparing with lab measurements. Figure 5.2 shows the comparison of measured and calculated polymer viscosity at zero shear rate as a function of polymer concentration. Figure 5.3 shows the comparison of measured and calculated viscosity of the polymer drive (used in corefloods CF-3 and CF-4) as a function of shear rate. Figure 5.5 shows the comparison of measured and calculated polymer viscosity as a function of effective

salinity. Sp is obtained from the slope of this line. The parameters obtained for modeling polymer rheology in UTCHEM are given in Table 5.4.

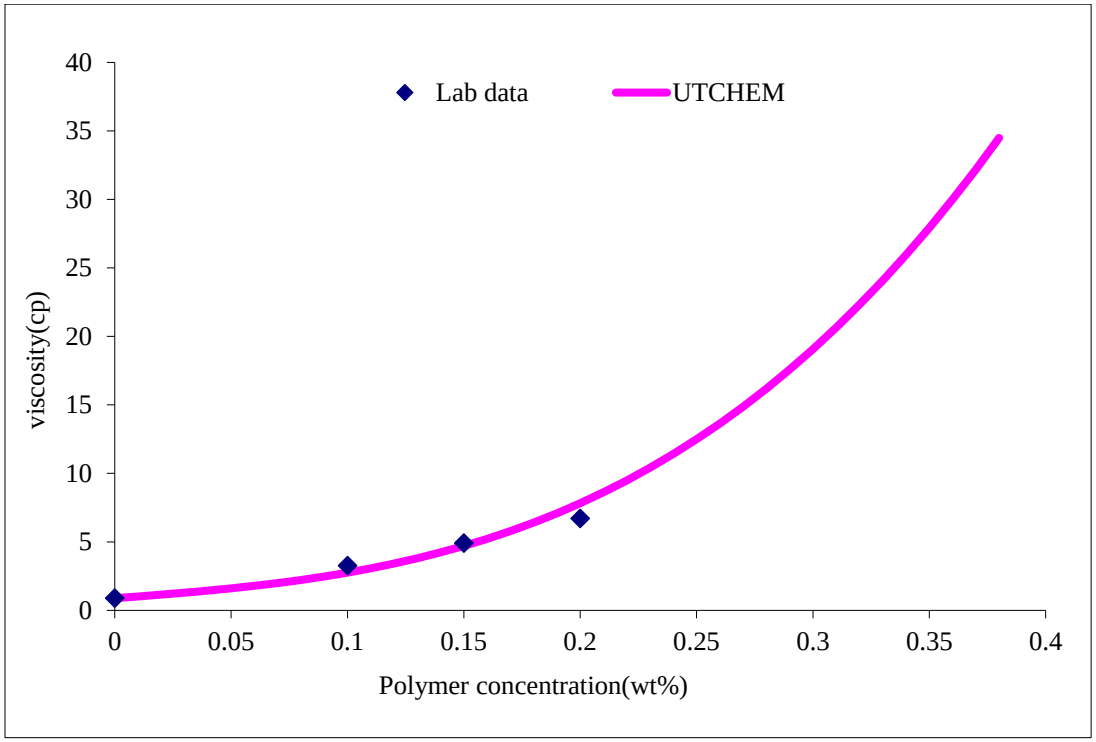

Figure 5.2: Comparison of measured and calculated polymer viscosity at zero shear rate as a function of polymer concentration

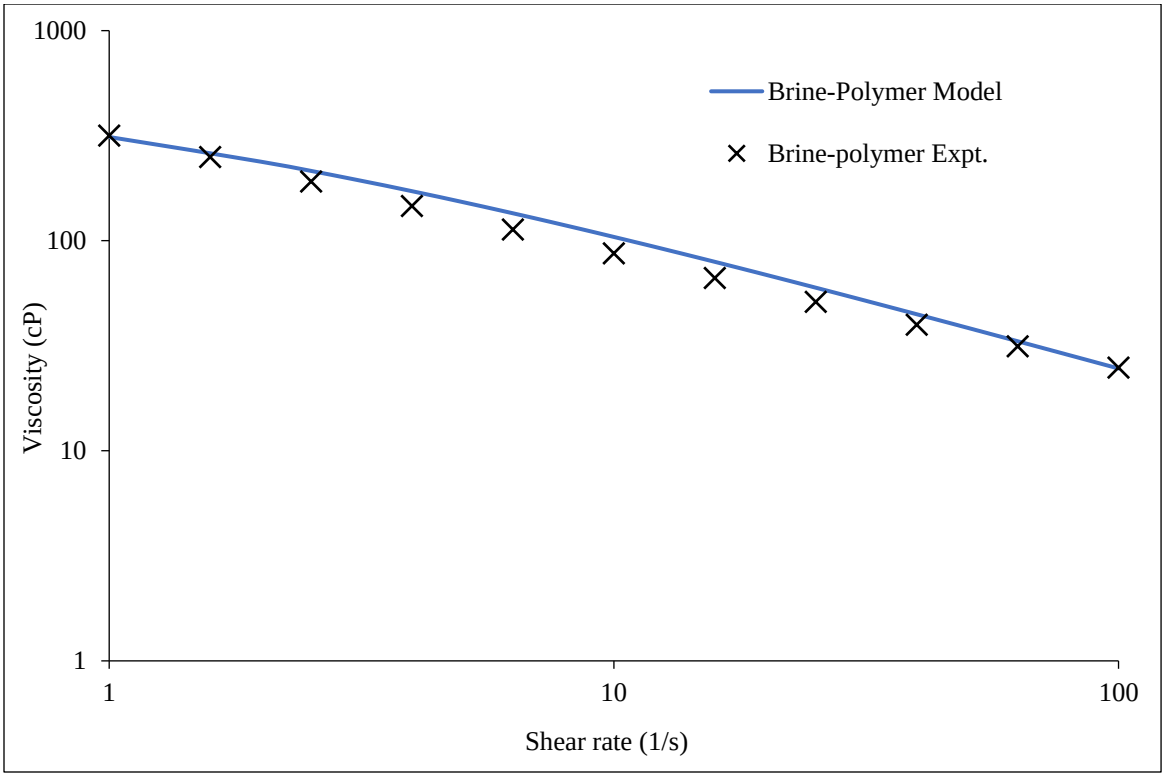

Figure 5.3: Comparison of measured and calculated polymer viscosity as a function of shear rate

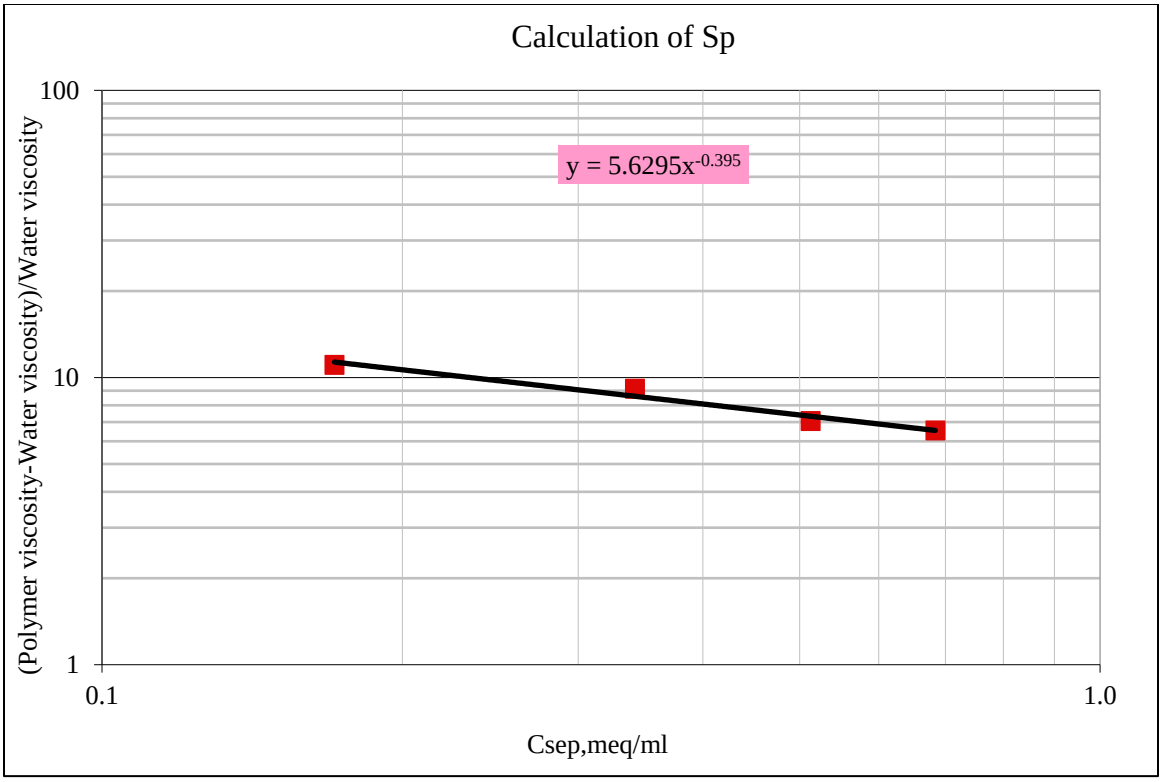

Figure 5.4: Normalized polymer viscosity as a function of effective salinity

Since alkali generates in-situ surfactants and lowers surfactant adsorption during ASP floods, its consumption in the reservoir should be minimum. Alkali consumption in corefloods CF-3 and CF-4 is modeled in UTCHEM by including relevant geochemical interactions of sodium metaborate. The aqueous and solid species included in these simulations are given in Table 5.5. For simplicity, aqueous species that are less likely to participate in geochemical reactions under the experimental conditions were not considered in these calculations. The calculations were performed assuming local equilibrium. The equilibrium thermodynamic data for various reactions was obtained from the literature. EQBATCH was used for performing the equilibrium calculations.

Other input parameters of the UTCHEM simulations are listed in Table 5.6. Further details of the chemical slugs are given in Table 4.17.

Table 5.5: Aqueous and solid species included in geochemical calculations

Elements or pseudo-elements	Calcium, Magnesium, Sodium, Hydrogen(reactive), Sulfate, Tetrahydroxy Borate, Oleic Acid
Independent species	Ca^{2+}, Mg^{2+}, Na^{+}, H^{+}, SO_4^{2-}, CO_3^{2-},$B(OH)_4$-, HAo, H_2O
Dependent species	OH-, H_2CO_3, HCO_3-, $B(OH)_3$, HAw, A^{-}
Surfactant associated cations	Na^{+}, Ca^{2+}
Solid species	$CaMg(CO_3)_2$

Table 5.6: UTCHEM input parameters used for modeling corefloods CF-3 and CF-4

Number of grids	1x1x50
Components	Water, Oil, Surfactant, Polymer, Chloride, Calcium, Magnesium, Carbon (as carbonate), Sodium, Hydrogen (reactive), Sulfate, $B(OH)_4$-, HAo
Porosity	0.18
Permeability	80 mD
Water viscosity	0.85 cP
Oil viscosity	105 cP
Residual oil saturation	0.43
Residual water saturation	0.30
Water endpoint relative permeability	0.05
Oil endpoint relative permeability	1.0
Injection Schedule	0.3 PV ASP Slug 0.5 PV Polymer drive 1 0.5 PV Polymer drive 2

Table 5.7: List of important aqueous and solid reactions

Reaction	Equilibrium constant
$H_2O = H^+ + OH^-$	log_k -14
$HAw = H^+ + A_w^-$	log_k -4.01
$B(OH)_3 + H_2O = B(OH)_4^- + H^+$	log_k -9.239
$CaMg(CO_3)_2\ (s) = Ca^{2+} + Mg^{2+} + 2CO_3^{2-}$	log_k -17.083
$Ca(OH)_2\ (s) = Ca^{2+} + 2OH^-$	log_k -5.190
$Mg(OH)_2\ (s) = Mg^{2+} + 2OH^-$	log_k -10.88

A comparison of experimental and simulated oil recovery data for ASP floods CF-3 and CF-4 are shown in Figures 5.5 and 5.6, respectively. In tertiary ASP coreflood CF-3, the oil cut was zero before the breakthrough of the oil bank at around 0.25 pore volumes. The oil cut increased to about 50% before decreasing to zero again at about 0.8 pore volumes in the simulation. In secondary ASP coreflood CF-4, only oil is produced at the start of the experiment, then the oil cut drops to about 60% before decreasing to zero in about 1 PV injection. In both the cases, the simulation results agree reasonably well with the experimental data; the oil production continues for a longer time in the experiments. Experimental data for surfactant phase behavior, polymer viscosity, and surfactant adsorption were critical in obtaining match with the experimental results.

Figure 5.7 shows the simulated in-situ oil saturation profiles at 0.2 pore volumes for both the ASP corefloods. Three changes in oil saturations were observed in each case. At about $x_d = 0.075$, oil saturation jumps from 0 to 0.15; between $x_d = 0.2$ to 0.4, oil saturation increases slowly from 0.15 to about 0.6 and at $x_d = 0.72$, it jumps from 0.6 to

its initial value. The initial oil saturations in corefloods CF-3 and CF-4 were 70% and 43%, respectively. These saturation profiles are similar to the fractional flow theory of ASP floods discussed by Pope (1980).

As salinity increases, the microemulsion phase behavior transitions from Winsor type I to Winsor type III to Winsor type II. For a successful ASP flood, it is important to attain an ultralow IFT in the reservoir; Winsor type III microemulsion gives ultralow IFT. It is necessary to have a correct salinity gradient design in an ASP flood to be able to encounter the type III region. The simulated salinity profile shows that type III salinity was achieved in corefloods CF-3 and CF-4.

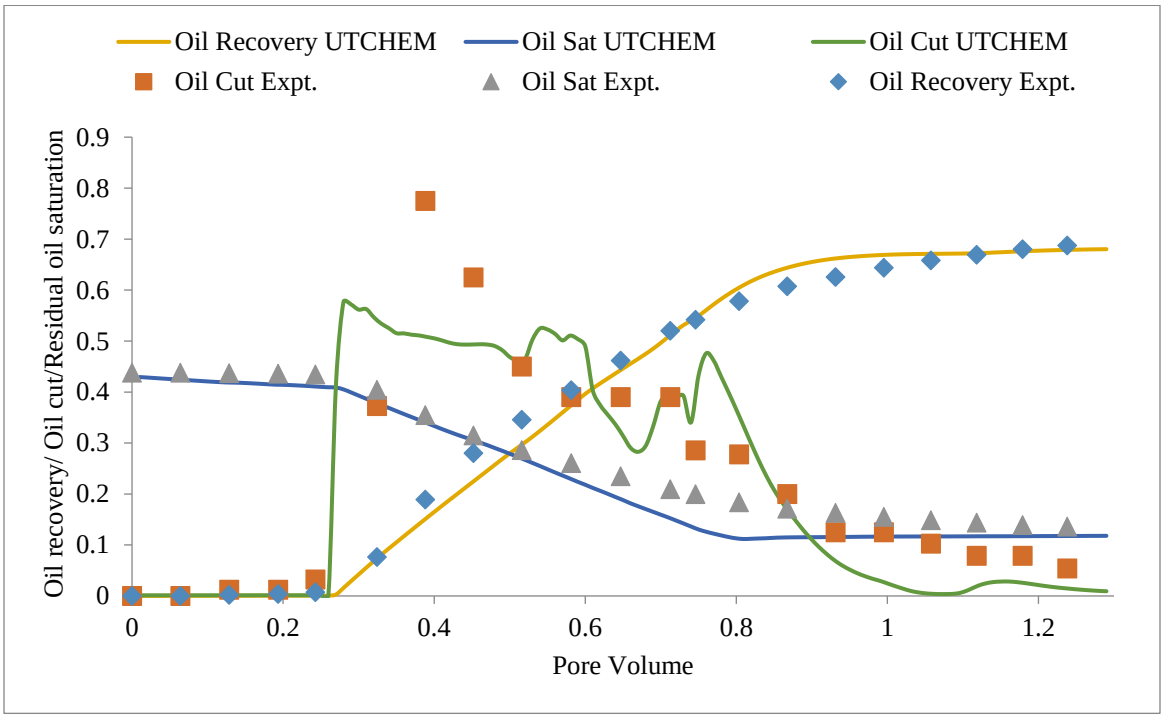

Figure 5.5: Comparison of oil recovery data obtained from coreflood CF-3 and UTCHEM simulations

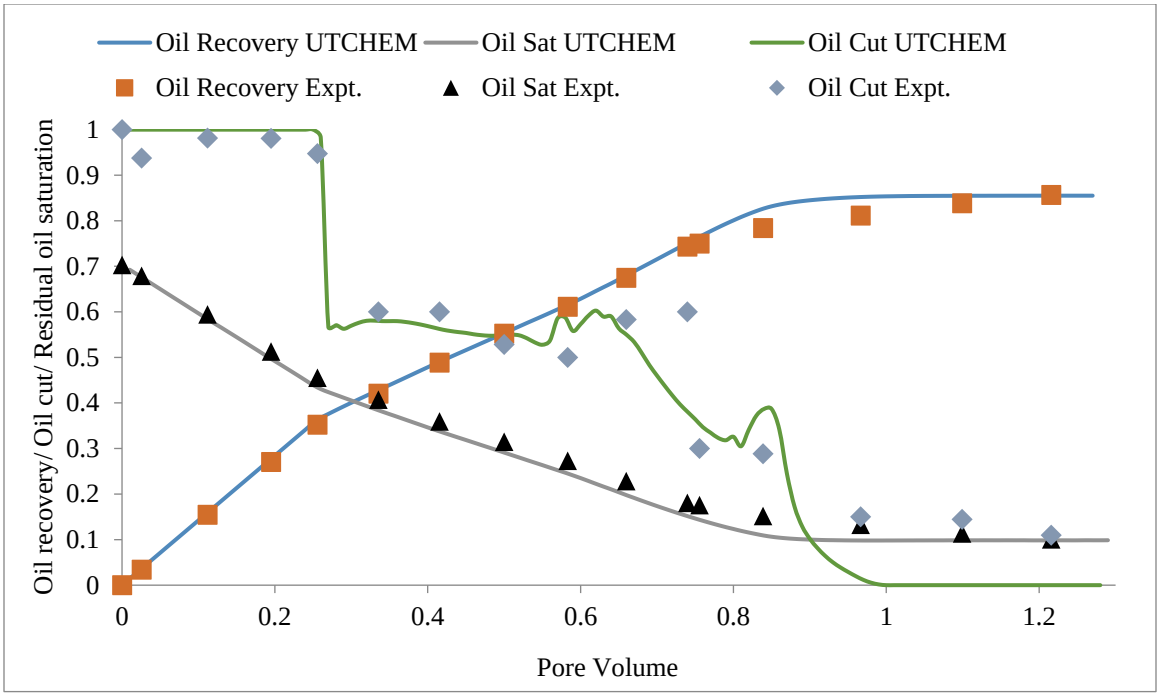

Figure 5.6: Comparison of oil recovery data obtained from coreflood CF-4 and UTCHEM simulations

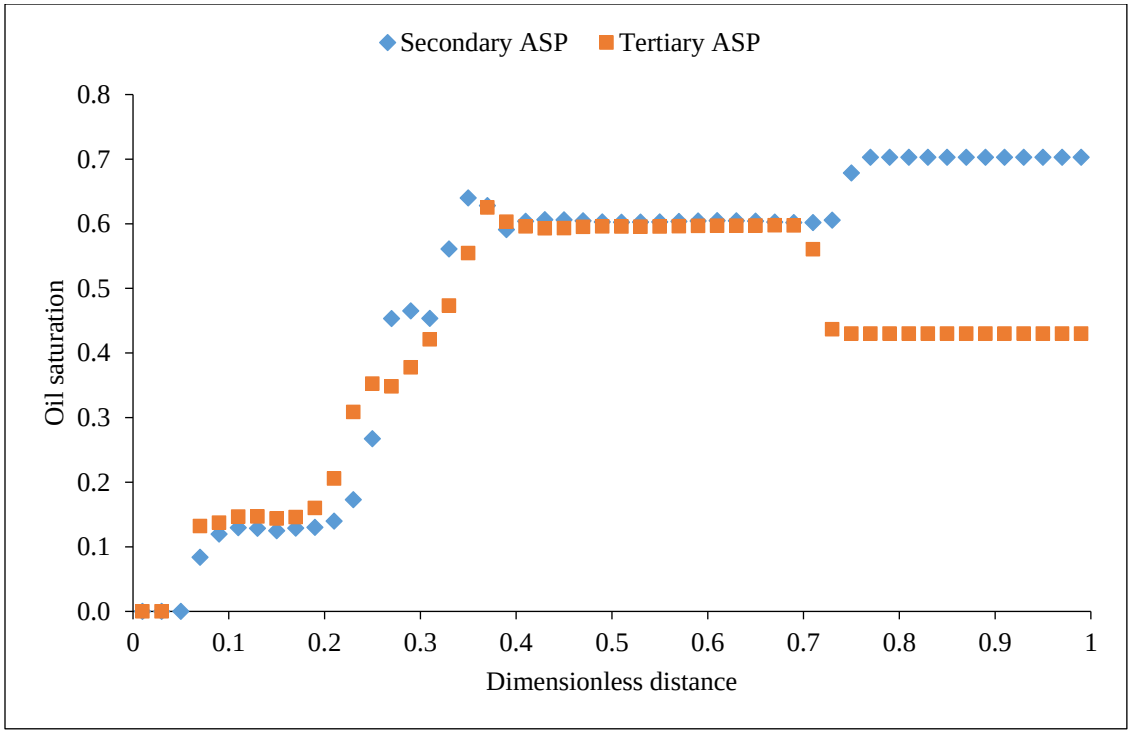

Figure 5.7: UTCHEM simulations of in-situ oil saturation profiles for corefloods CF-3 and CF-4 at 0.2 pore volumes

5.2 Single-phase static interactions of alkalis with gypsum

Geochemical interaction of sodium carbonate, sodium metaborate and ammonia with gypsum was studied by performing single-phase static and transport calculations in PHREEQC. The effluent pH and effluent ions results obtained from PHREEQC was compared with the respective experimental results.

The results obtained from static experiments, shown in Table 4.2 and 4.11(a), were compared with PHREEQC calculations. In these experiments, various alkalis (sodium carbonate, sodium metaborate and ammonia) were allowed to equilibrate with excess amount of gypsum, after which pH and ionic composition of the supernatant

solutions were reported. Note that no divalent cations were present initially in the alkali solutions. The presence of divalent cations ions in the final solutions was due to gypsum dissolution. A comparison of results obtained from experiments and PHREEQC is shown in Table 5.8.

Table 5.8: Comparison of PHREEQC simulations with alkali-rock static experiments data

Case	Alkali	Calcium (ppm)	Sulfate (ppm)	pH	Boron (ppm)
5.2 (a)	No alkali (exp.)	1,082	2,560	6.9	-
	PHREEQC	1,313	3,151	7.0	-
5.2 (b)	0.58 M Na_2CO_3 (exp.)	441	53,302	8.3	-
	PHREEQC	237	56,246	9.0	-
5.2 (c)	0.58 M $NaBO_2$ (exp.)	1,489	26,551	10.9	2490
	PHREEQC	1,455	20,323	10.6	2347
5.2 (d)	0.19 M $NaBO_2$ (exp.)	1,600	7,974	10.3	1594
	PHREEQC	1,906	7,107	10.4	1468
5.2 (e)	0.58 M NH_3 (exp.)	1,312	2,584	11.1	-
	PHREEQC	1,323	3,175	10.7	-

Note that the base brine consisted of 1.25% NaCl and the experiments (and calculations) were performed at 53 °C in the experimental and PHREEQC calculations shown in Table 5.8. Also note that, technically, gypsum ($CaSO_4.2H_2O$) exist in anhydrite ($CaSO_4$) form at temperatures greater than about 45 °C but for the sake of simplicity, we use both the terms interchangeably unless we refer to a specific instance. In case 5.2(a), a

solution consisting of 1.25% NaCl was brought in equilibrium with gypsum. The pH, calcium and sulfate concentration of the supernatant after a few days of equilibration was found to be 6.9, 1082 ppm and 2560 ppm, respectively. The results obtained from PHREEQC calculations are shown in the row below. The pH, calcium and sulfate concentration from calculations were found to be 7.0, 1313 ppm and 3151 ppm. Note that a reasonable agreement was observed between experimental results and the calculations. Note that no parameter was tuned in obtaining these results. The results were obtained by considering the thermodynamic equilibrium constants reported in the literature. From these results, it can be seen that PHREEQC calculations slightly over-estimate gypsum dissolution in this case. Nevertheless, the results compare reasonably.

In case 5.2(b), 0.58 M Na_2CO_3 was added to 1.25% NaCl brine and was allowed to equilibrate with excess amount of gypsum at 53 °C. The pH, calcium and sulfate concentrations of the supernatant solution after equilibrating samples for a few days were found to be 8.3, 441 and 53,302 ppm, respectively. These results show that sodium carbonate cannot be used in the presence of gypsum due to excessive dissolution of gypsum and a concomitant precipitation of calcium carbonate leading to loss of alkali and pH. The calculation results, shown in the row below, were found to be 9.0, 237 ppm and 56,246 ppm, respectively. Note that these results were obtained without tuning any parameters in PHREEQC, similar to the previous case. Note that PHREEQC over-estimated the pH, however, gave a good comparison of calcium and sulfate ions.

In case 5.2(c), 0.58 M of $NaBO_2$ was added to 1.25% NaCl brine and allowed to equilibrate in presence of excess amount of gypsum at 53 °C. The pH, calcium, sulfate,boron concentration in the supernatant solution after a few days were 10.9, 1489 ppm, 26,551 ppm and 2490 ppm, respectively. The results of PHREEQC calculations for the same case were found to be 10.6, 1455 ppm, 20,323 ppm and 2347 ppm, respectively. A reasonable comparison was obtained between experimental results and PHREEQC calculations. Note that the existing databases of PHREEQC were not complete to model these results. The calculations performed with existing databases did not show any calcium precipitation in the presence of sodium metaborate, however, experimental results discussed in sections 4.1 and 4.2 clearly showed calcium precipitation in presence of sodium metaborate. This difference was due to an incomplete PHREEQC database. A solid species named calcium borate was included to model the precipitation reaction as shown below.

$$Ca(B(OH)_4)_2 = Ca^{2+} + 2B(OH)_4^- \tag{5.11}$$

$$\log k = -5.1$$

A reasonable agreement was observed between experimental results and PHREEQC calculations. To further confirm the validity of this reaction, another calculation was performed in PHREEQC to compare with the experimental results obtained when 0.19 M sodium metaborate was added to 1.25% NaCl brine and equilibrated with gypsum at 53 °C (case 5.2d). The pH, calcium, sulfate and boron concentrations in the supernatant solution were found to be 10.3, 1600 ppm, 7974 ppm

and 1594 ppm, respectively. PHREEQC calculations showed a pH of 10.4 and calcium, sulfate and boron concentrations of 1900 ppm, 7107 ppm and 1468 ppm, respectively for case 5.2(d). A reasonable agreement was observed between experimental results and PHREEQC on equilibrating sodium metaborate in presence of gypsum. The reaction included to account for calcium and boron precipitation in cases 5.2(c) and 5.2(d) was found to be reasonable to model these experiments.

In case 5.2(e), 0.58 M ammonia was added to 1.25% NaCl brine and equilibrated with excess amount of gypsum at 53 °C. The final pH, calcium and sulfate concentrations from the experiment were found to be 11.1. No calcium precipitation was observed in the experiments. PHREEQC calculations also did not show any precipitation on bring ammonia in contact with gypsum. The equilibrium pH, calcium and sulfate concentrations were found to be 10.7, 1323 ppm and 3175 ppm, respectively. A reasonable agreement between experimental results and PHREEQC calculations was observed. Note that reported thermodynamic equilibrium constants were used, without tuning them to match the results.

5.3 Single-phase alkali-gypsum interactions during transport experiments

Single-phase alkali transport experiments discussed in sections 4.3 and 4.4 showed excessive gypsum dissolution and subsequent calcium carbonate precipitation on injecting sodium carbonate in a core containing gypsum. Sodium metaborate, on the other hand, was able to propagate a high pH. Reaction of sodium metaborate with gypsum was

found to be dependent on injection rate. These experiments were modeled in PHREEQC to further investigate interactions of these alkalis with gypsum.

(a) Sodium carbonate injection

Calculations of sodium carbonate injection in a carbonate core containing anhydrite was performed with PHREEQC. The compositions of the initial brine and injected alkali solution, and core properties are shown in Table 5.9 and 5.10. The core is assumed to contain 5% anhydrite by weight, distributed evenly throughout the core. Local equilibrium assumption is made for these calculations. The results of the calculations are shown in Figures 5.8 and 5.9.

Table 5.9: Composition of formation brine and injected solutions

Salts (ppm)/Brines	Formation brine	Sodium carbonate solution
NaCl	30,000	30,000
Na2CO3	-	30,000
TDS (ppm)	30,000	60,000
pH	7.8	10.9

Table 5.10: Properties of the core used in experiment 4.3

Core	Length (inches)	Diameter (inches)	Porosity (%)	Permeability (md)	Temperature (°C)	Gypsum
Carbonate	3.0	1.5	24	101	50	Yes

From Figure 5.8, it can be seen that the effluent pH does not reach the injected pH of 10.9, even after injecting 3 pore volumes of the alkali solution. In addition, the effluent sulfate and calcium concentrations are about 32,000 ppm and 300 ppm, indicating large gypsum dissolution and subsequent calcium carbonate precipitation as per the reactions shown below. These reactions result in alkali loss, pH propagation delay and permeability damage.

$$CaSO_4 = Ca^{2+} + SO_4^{2-} \tag{5.12}$$

$$Ca^{2+} + Na_2CO_3 = CaCO_3 + 2Na^+ \tag{5.13}$$

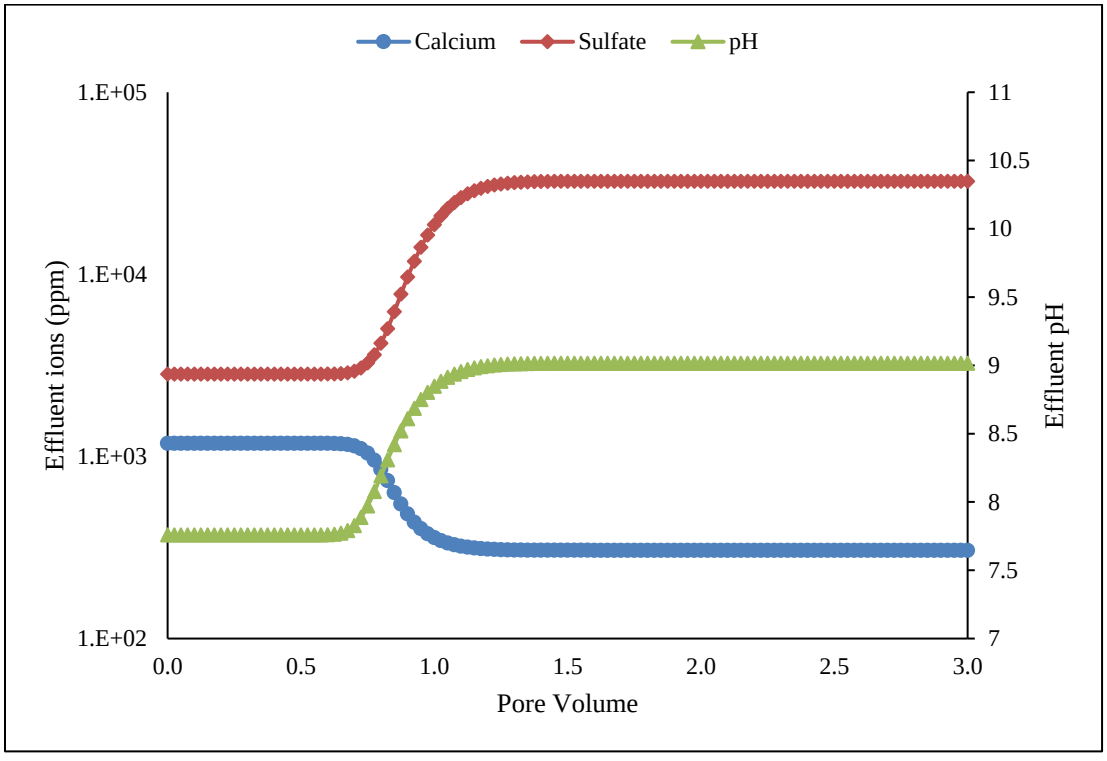

Figure 5.8: PHREEQC simulation results of effluent pH, calcium and sulfate concentrations on injecting sodium carbonate in a core containing gypsum

The concentrations of solid species and pH, after injecting 3 pore volumes of sodium carbonate solution, is plotted against the dimensionless distance in Figure 5.9. The figure shows dissolution of anhydrite and precipitation of calcium carbonate till xd=0.175. Note that before xd=0.175, the in-situ pH is same as the injected pH of about 11. However, after xd=0.175, the pH drops to about 9 due to reaction of sodium carbonate with anhydrite. The figure also shows that dissolution/precipitation front moves much slower compared to the tracer front.

The effluent pH values from Figure 5.8 were compared with the pH values obtained on injecting sodium carbonate in a core without gypsum. The results (Figure 5.10) clearly show good pH propagation when gypsum was not present in the core.

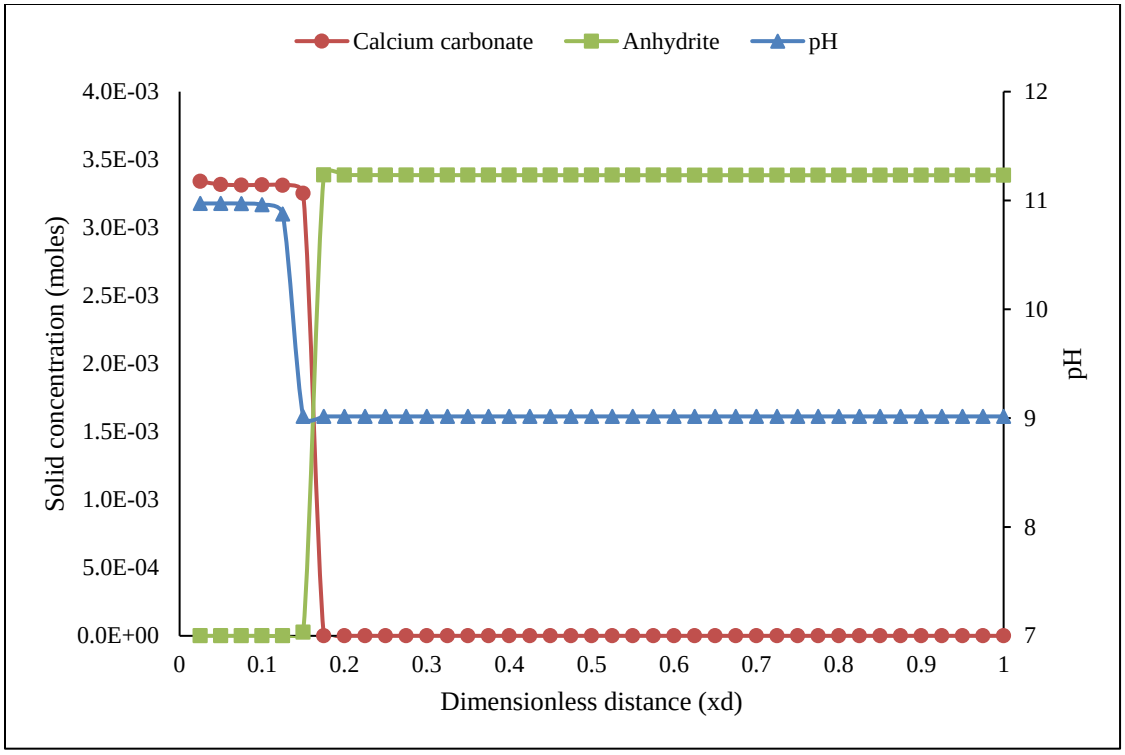

Figure 5.9: PHREEQC simulation results of in-situ pH and concentrations of solid species on injecting sodium carbonate in a core containing anhydrite

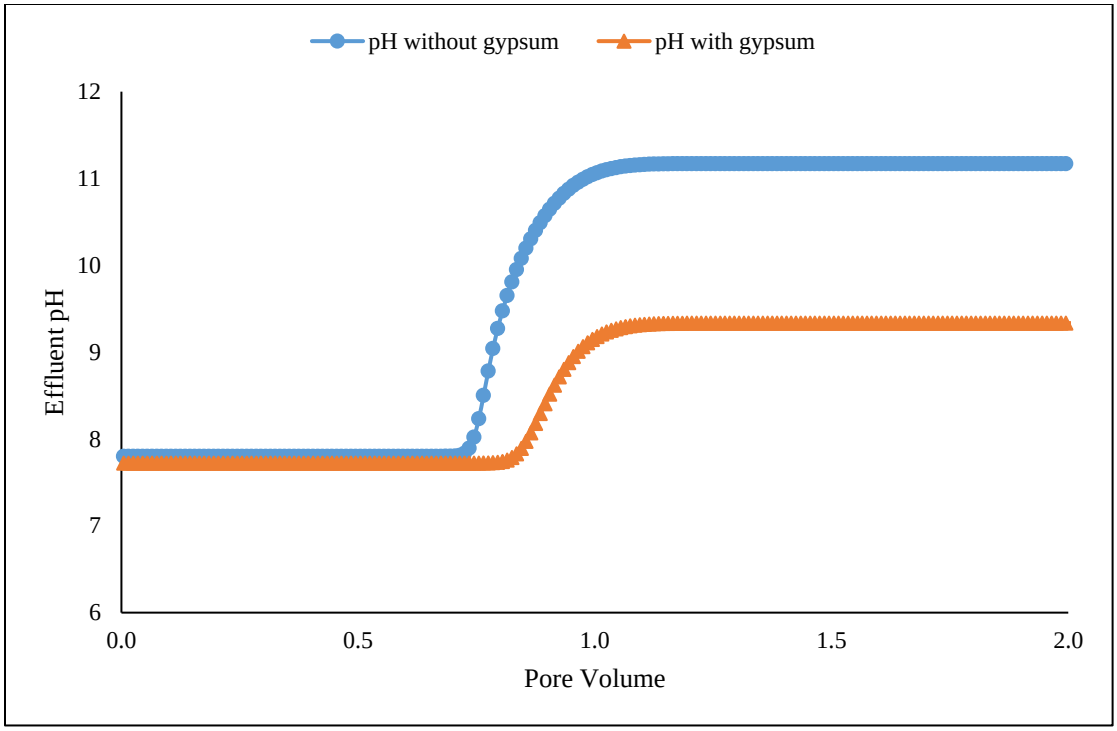

Figure 5.10: Effluent pH results from PHREEQC on injecting sodium carbonate in cores with and without gypsum

Note that the effluent pH of about 9 was observed in the results shown in Figures 5.8 and 5.9. However, the effluent pH during the experiment was steady increasing and approaching the injected pH (section 4.3). In addition, effluent sulfate concentration in the experiment was about 25,000 ppm, instead of 32,000 ppm shown in Figure 5.8. From these results, it appears that the local equilibrium assumption made for performing PHREEQC calculations does not hold true for modeling the lab experiment with sodium carbonate (section 4.3). The injection rate in the lab may not be slow enough to allow these reactions to come to equilibrium. The calculations were repeated again in PHREEQC by considering reaction kinetics. A simple model (Aagaard et al., 1982) is

assumed to include dissolution kinetics of anhydrite. Calcium carbonate precipitation is assumed to take place instantaneously.

$$R_k = k_k \left(\frac{A_0}{V}\right)\left(\frac{m_k}{m_{0k}}\right)\left[1 - \left(\frac{IAP}{K_{sp}}\right)^{\sigma}\right] \tag{5.14}$$

where, k_k= reaction rate; $\left(\frac{A_0}{V}\right)$= specific surface area; m_k= moles of solid species k at any time, m_{0k}= moles of solid species k at time t=0, IAP= ion activity product for solid species k, K_{sp}= solubility product of solid species k, σ= average stoichiometric number

A results of PHREEQC calculations and the experimental results (Figure 5.11) show good agreement between experimental results and PHREEQC calculations on including reaction kinetics in the calculations. The in-situ concentrations obtained from the calculations (Figure 5.12) show that, unlike Figure 5.9, the dissolution and precipitation fronts are more smeared out; reactions are observed throughout the core, not just at the inlet.

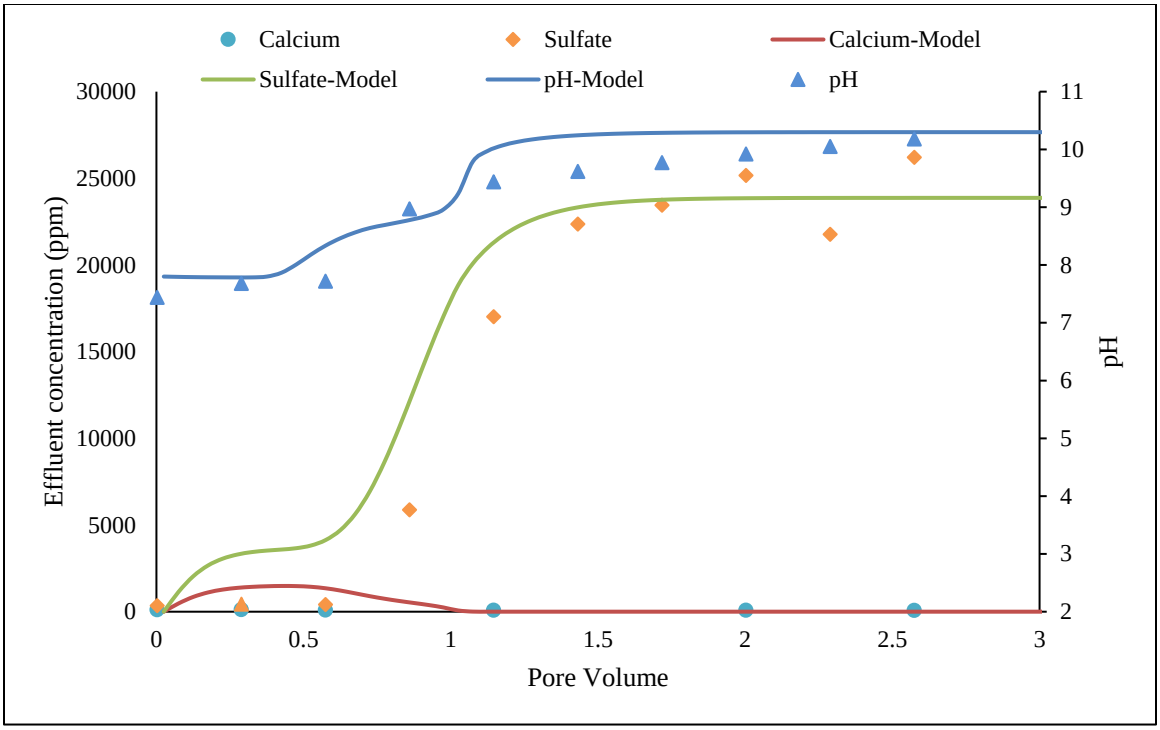

Figure 5.11: Comparison of experimental results of sodium carbonate injection in a core containing gypsum with PHREEQC calculations. Anhydrite dissolution kinetics was included

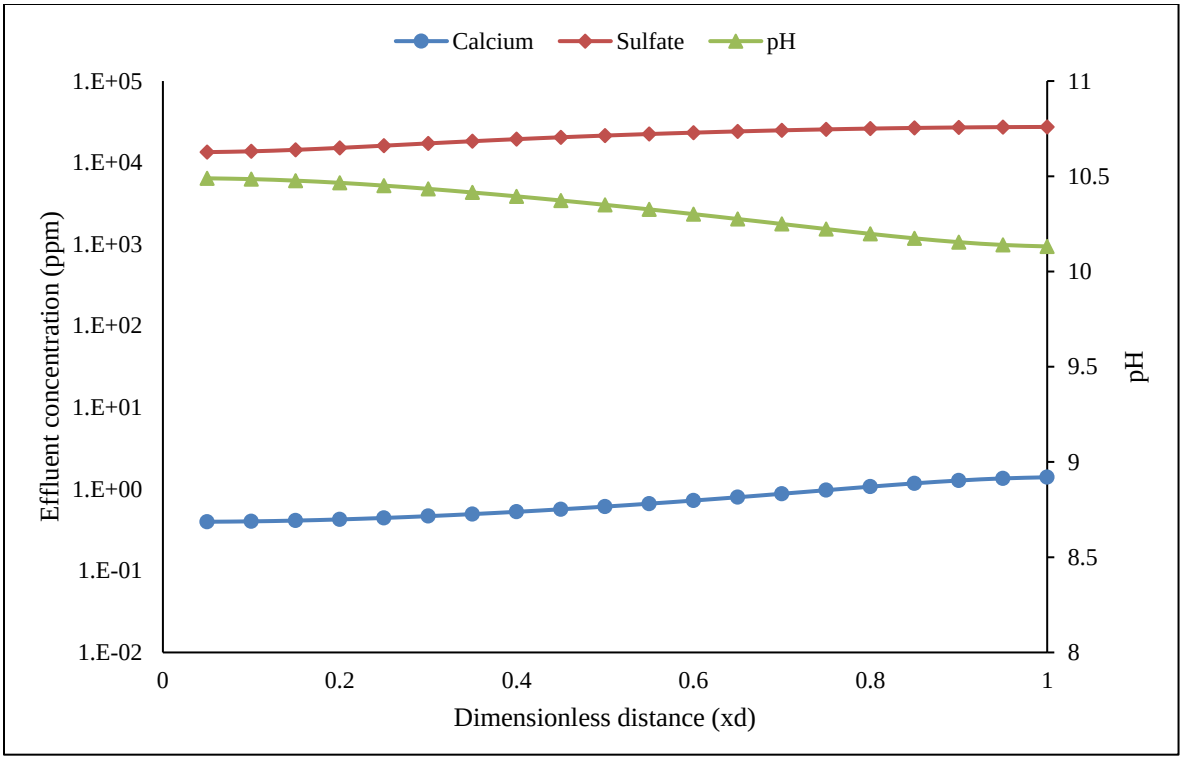

Figure 5.12: In-situ concentrations obtained from PHREEQC calculations on injecting sodium carbonate in a core containing gypsum. Anhydrite dissolution kinetics was included

(b) Sodium metaborate injection

PHREEQC calculations of sodium metaborate injection in a core containing anhydrite is discussed next. These calculations were performed to compare with experimental results discussed in section 4.4. The compositions of initial brine, injected alkali solution, and core properties are shown in Table 5.11 and 5.12, respectively.

Table 5.11: Composition of formation brine and injected solutions

Salts (ppm)/Brines	Formation brine	Sodium metaborate solution
NaCl	10,000	10,000
NaBO2	-	30,000
TDS (ppm)	10,000	40,000
pH	7	10.8

Table 5.12: Properties of the core used in experiment 4.4

Core	Length (inches)	Diameter (inches)	Porosity (%)	Permeability (md)	Temperature (°C)	Gypsum
Carbonate	7.93	1.485	19.3	68	55	Yes

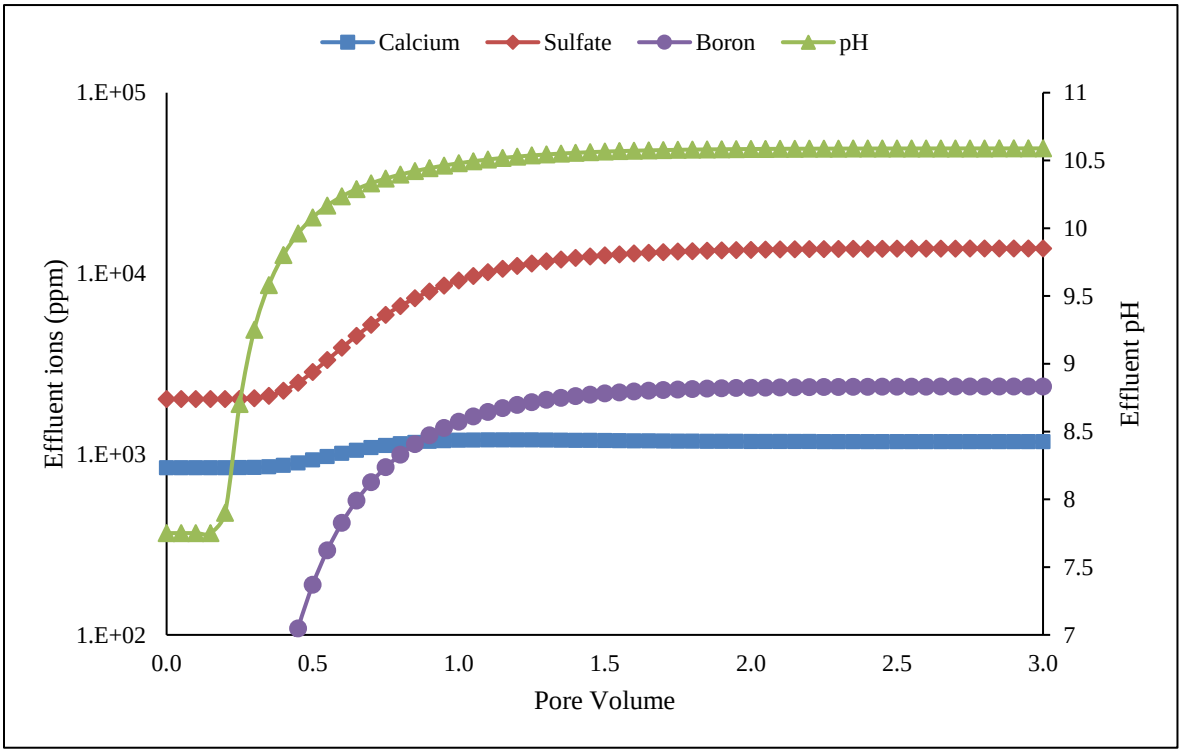

Figure 5.13: PHREEQC calculations of sodium metaborate injection in a core containing gypsum assuming local equilibrium

The results shown in Figure 5.13 are the PHREEQC results of sodium metaborate injection in a core containing gypsum assuming local equilibrium. The effluent pH of about 10.5 was observed at 1 pore volume. The effluent pH obtained a steady state value of 10.6 at about 1.5 pore volumes. The effluent boron concentration became steady at about 2350 ppm, lower than the injected boron concentration of about 4900 ppm indicating boron loss. Note that sodium metaborate concentration is reported as total boron concentration in these results. The steady state effluent sulfate concentration was about 13,100 ppm, higher than the steady state calcium concentration of about 1180 ppm. In molar terms, the steady state concentrations of sulfate and calcium are 0.136 mM and 0.029 mM, respectively. The higher steady state sulfate concentration, compared to the calcium, clearly indicate precipitation of calcium ions on injecting sodium metaborate. The in-situ pH, calcium borate and anhydrite concentrations, shown in Figure 5.14, show dissolution/precipitation reaction at the inlet of the core. Note that similar dissolution/precipitation profile was observed when similar calculations were performed with sodium carbonate. However, unlike sodium carbonate, a high pH was observed on injecting sodium metaborate in a core containing gypsum.

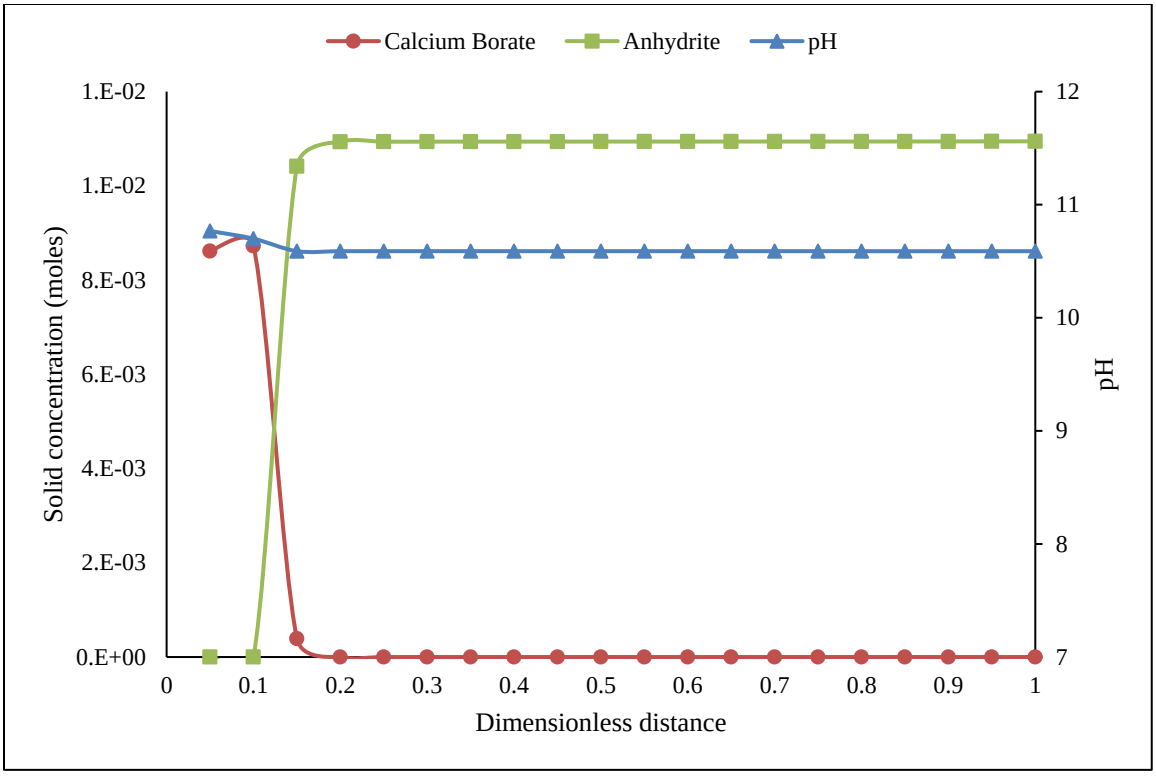

Figure 5.14: PHREEQC results of in-situ pH, anhydrite and calcium borate concentrations assuming local equilibrium

The PHREEQC results shown previously were obtained assuming local equilibrium. The experimental results, however, differ significantly. The experimental results, shown in Figure 5.15, were previously discussed in section 4.4. During this experiment, first 2 pore volumes were injected at 0.1 ft/d, corresponding to the residence time of 6.5 days. Then the flow rate was changed to 0.17 ft/d, corresponding to the residence time of 4 days, from 2-4 pore volume. Last 2 pore volumes were injected at 0.32 ft/d, corresponding to the residence time of 1 day. Change in steady state value of sulfate concentration was observed on varying flow rate, indicating that the reactions did not reach an equilibrium. The flow rate was further reduced to 0.044 ft/d, corresponding

to the residence time of 15 days and an increase in effluent sulfate concentration was observed.

This experiment was modeled in PHREEQC by including anhydrite dissolution kinetics as discussed in equation 5.14. Calcium borate precipitation kinetics was lumped with anhydrite dissolution kinetics by assuming anhydrite dissolution to depend on sodium metaborate concentration. Calcium borate precipitation was assumed to take place instantaneously. The results of the PHREEQC calculations with the above mentioned assumptions are shown in Figure 5.15.

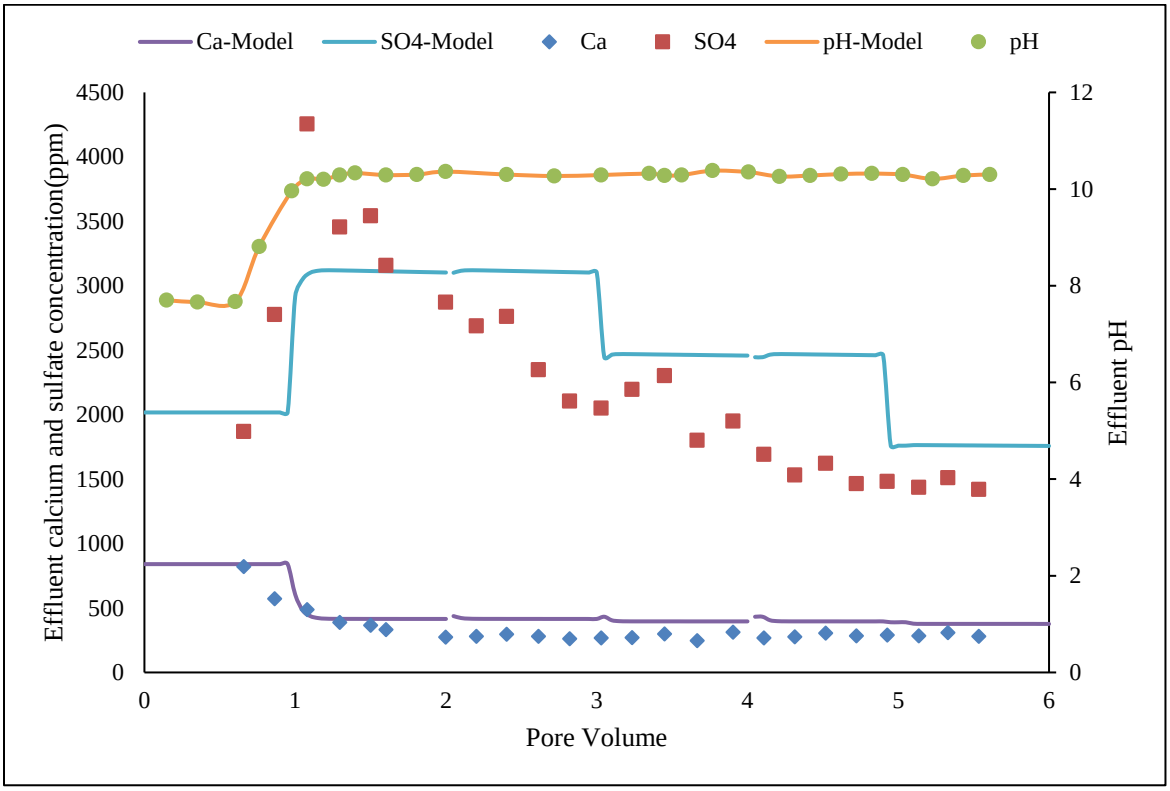

Figure 5.15: Comparison of experimental results and PHREEQC calculations on injecting sodium metaborate in a carbonate core containing anhydrite

A good agreement can be seen between the experimental results and PHREEQC calculations. Note that the effluent pH obtained from PHREEQC compares very well with the experimental result. No significant change in pH was observed on changing the flow rate; both in the experiment and the calculations. The effluent calcium concentration obtained from the experiment and PHREEQC calculations agree well. A steady state calcium concentration of about 300 ppm was observed. A change in sulfate concentration with change in injection rate was observed in PHREEQC and the calculation results agree fairly well with experimental results. Note that no dispersion was included in PHREEQC calculations for simplicity. The steady state sulfate concentration obtained from PHREEQC were compared with the values obtained experimentally. The results (Figure 5.16) show reasonable agreement between experimental results and PHREEQC calculations.

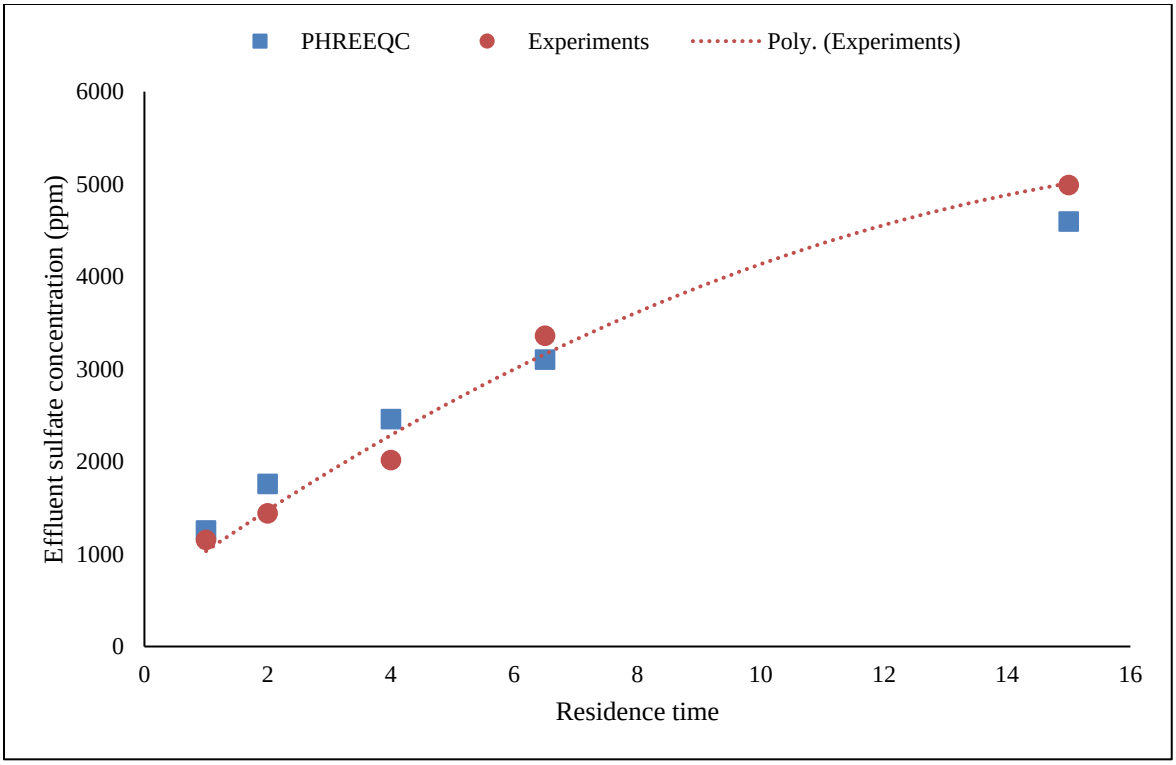

Figure 5.16: Comparison of steady state sulfate concentrations obtained from experiments and PHREEQC on injecting sodium metaborate in a carbonate core containing gypsum

(c) Ammonia injection

Before performing an ASP coreflood using ammonia in a carbonate core containing gypsum, preliminary calculations were performed with PHREEQC to estimate expected calcium concentrations during the coreflood at experimental conditions. The calculations were critical for designing a robust salinity gradient as surfactant phase behavior is found to depend on calcium ions (section 4.14). Pitzer.dat was used for performing these calculations. An alkali solution containing ammonia was injected, similarly, in a carbonate core containing gypsum and effluent pH and ions were measured

(see section 4.13). The injection rate was performed at 0.5 ft/d. The compositions of the initial brine, injected alkali solution, and core properties are given in Tables 5.13 and 5.14, respectively. An effluent pH of 10 was observed at about 1 pore volume and no calcium precipitation took place in the core. The experiment was modeled in PHREEQC, assuming local equilibrium, and the results were compared with the experimental results (Figure 5.17). As shown in Figure 5.17, a good comparison was observed between the effluent pH and ions obtained experimentally and from PHREEQC calculations. Note that local equilibrium assumption was able to model the experimental results; indicating that reactions reached to equilibrium at the injection rate of 0.25 ft/d. From Figure 5.17, it can also be seen that gypsum dissolution is dependent on the salinity of the aqueous solution. At high salinity, more gypsum dissolution is observed leading to higher calcium ion concentrations. Such dissolution pattern is favorable for designing a surfactant flood in gypsum containing cores as an additional salinity gradient is provided by calcium ions. In negative salinity gradient design, high salinity is maintained ahead of the surfactant slug. This means that, if gypsum is present, higher amount of calcium would exist ahead of the surfactant slug which would further drive the process into Winsor type-II phase behavior. As the salinity decreases in the polymer drive, lower calcium concentration would contribute in obtaining Winsor type-I phase behavior.

Table 5.13: Properties of the core used in single-phase ammonia coreflood

Core	Length (inches)	Diameter (inches)	Porosity (%)	Permeability (md)	Temperature (°C)	Gypsum
Carbonate	12	1.48	19.5	453	22	Yes

Table 5.14: Compositions of the initial brine and injected alkali solution

Salts (ppm)/Brines	Formation brine (ppm)	Ammonia solution (ppm)
NaCl	80,000	10,000
NH_3	-	0.3 wt%
TDS (ppm)	80,000	10,000
pH	7.5	11.1

Simulations were performed in PHREEQC to investigate if gypsum dissolution can be reduced by adding sodium sulfate (Figure 5.18**)**. Figure 5.18 shows concentration of calcium ions in the aqueous solution due to dissolution of gypsum at two different salinities and two different temperatures with increasing Na_2SO_4 concentration. From the figure, a sharp decrease in calcium uptake can be seen on adding up to 10,000 ppm Na_2SO_4 at both salinities and temperatures. About 50% reduction in calcium concentration was observed on adding about 10,000 ppm Na_2SO_4 to the injection slugs. Not a significant reduction in gypsum dissolution was observed on adding Na_2SO_4 beyond 10,000 ppm. Note that less gypsum dissolution was observed at higher temperatures.

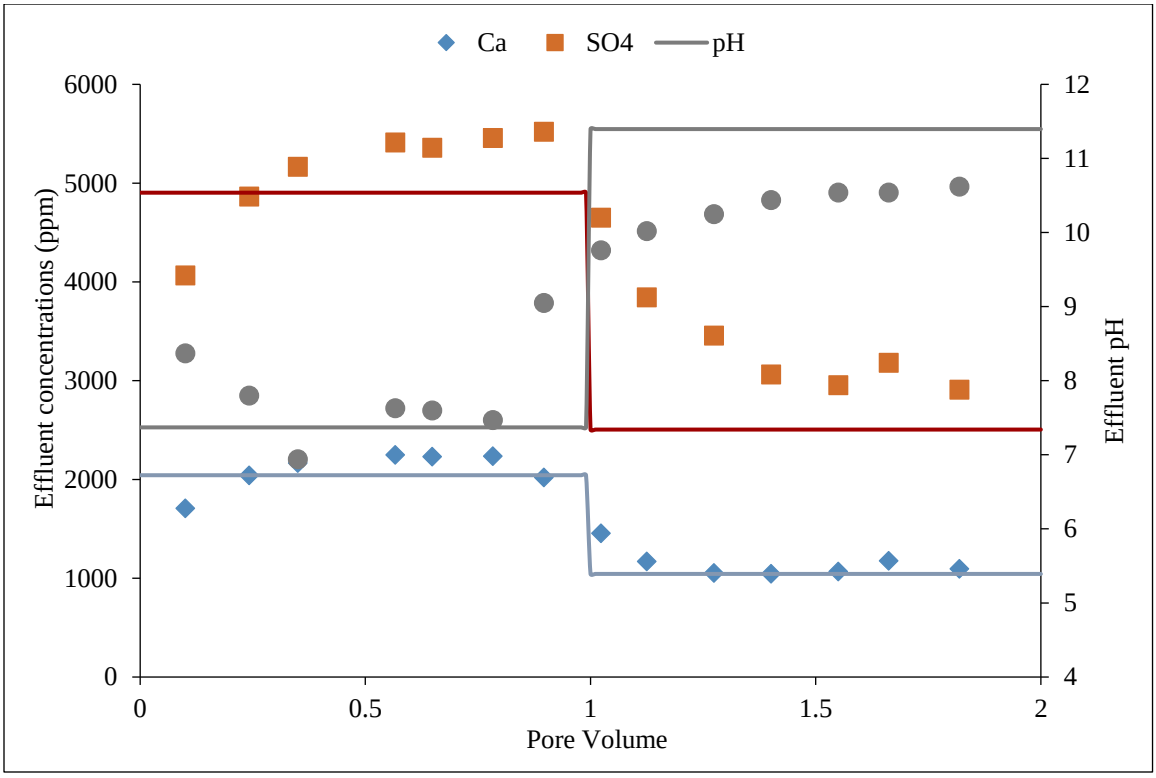

Figure 5.17: Comparison of effluent pH and ions obtained experimentally and PHREEQC on injecting ammonia in a carbonate core containing gypsum

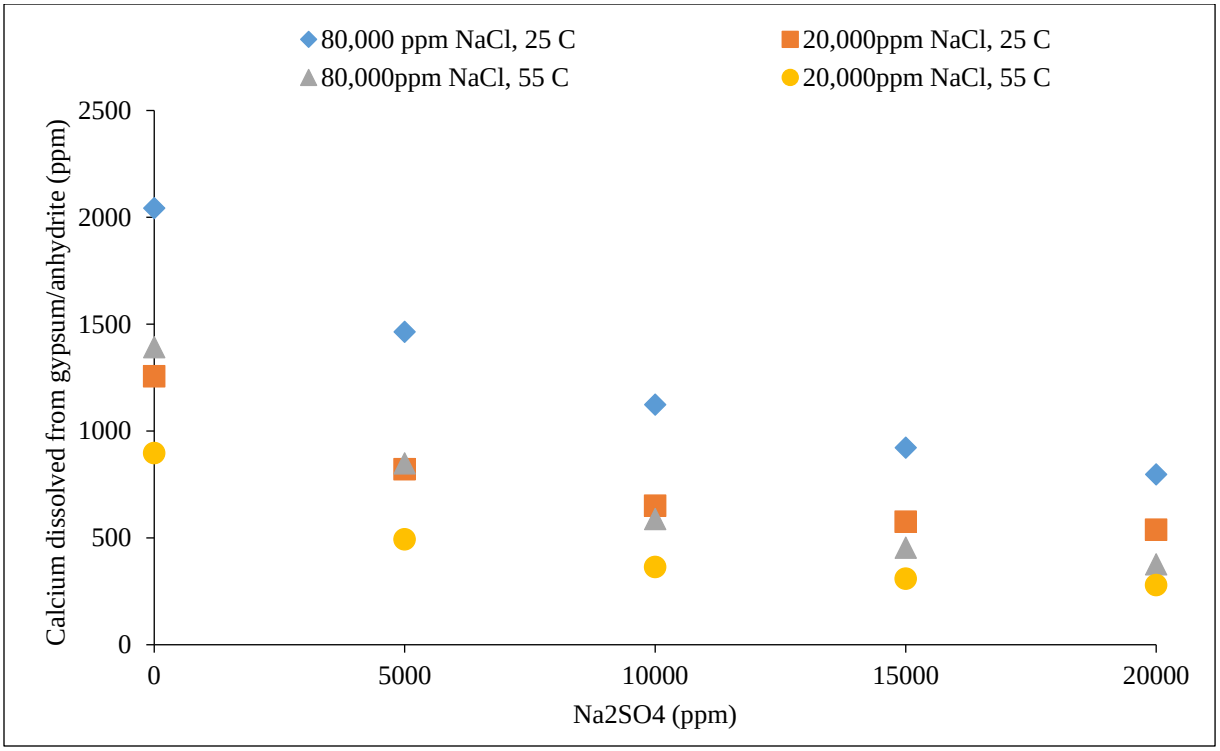

Figure 5.18: Effect of sodium sulfate addition on lowering anhydrite/gypsum dissolution

5.4 UTCHEM simulation of ASP coreflood CF-8

The ASP coreflood CF-8 performed using ammonia as the alkali in a carbonate core containing anhydrite was modeled in UTCHEM-IPHREEQC. UTCHEM was recently coupled with IPHREEQC by Kazemi et al. (2014), which allows complex geochemical reactions to be included in multiphase flow UTCHEM simulations. The coupled simulator has many attractive features such as being able to directly use databases developed for PHREEQC, include diverse set of geochemical reactions and include the effect of temperature and salinity on equilibrium constants. In addition, multiphase simulations can be performed by including desired reaction kinetics.

The properties of the core and the ionic compositions of various brines used in the coreflood are shown in Table 5.15 and 5.16, respectively. Further details of the ASP slug and polymer drives are given in Table 4.33(b). The parameters for modeling surfactant phase behavior and polymer rheology were obtained by following the procedure described previously. A comparison of calculated surfactant phase behavior with the experimental data is shown in Figure 5.19. Note that two different types of polymers were used in the surfactant slug and polymer drives; AN-125 in the surfactant slug and FP 3630S in the polymer drives. Since UTCHEM cannot handle different types of polymers in the surfactant slug and polymer drives, FP 3630S was assumed in the surfactant slug as well to model the coreflood. The concentration of FP 3630S was obtained by comparing with the measured viscosity of the surfactant slug. Other polymer parameters were obtained by following the procedure described previously (see Figures 5.20-5.22). A list of parameters used for modeling surfactant phase behavior and polymer rheology are given in Table 5.17. Since calcium concentration during ASP corefloods using ammonia as the alkali can be up to 2000 ppm, the effect of these ions on surfactant phase behavior must be considered. In these UTCHEM simulation, the effect of calcium ions on surfactant phase behavior was considered by including a parameter β_s. A 10,000 ppm NaCl shift in optimum salinity was observed on adding 1000 ppm calcium ions (see section 4.14).

A comparison of UTCHEM simulation results with the experimental data is shown in Figures 5.23 and 5.24, respectively. The thermodynamic reactions constants were obtained from Pitzer.dat database. The oil recovery data agreed well with the

UTCHEM simulations. Calcium and sulfate ions were measured in the effluent ions. These ions were produced due to gypsum dissolution as the ASP slug and polymer drives were prepared in soft brines. The simulation results showed good agreement with the effluent ions obtained experimentally.

Table 5.15: Properties of the core used for ASP coreflood CF-8

Core	Length (inches)	Diameter (inches)	Porosity (%)	Permeability (md)	Temperature (°C)	Gypsum
Carbonate	12	1.48	19.5	453	22	Yes

Table 5.16: Ionic compositions of the formation brine, injection brine and polymer drives

Salt	Formation/Waterflood brine (ppm)	ASP slug (ppm)	Polymer drive 1 (ppm)	Polymer drive 2 (ppm)
NaCl	90,000	70,000	40,000	25,000
Na_2SO_4	-	10,000	10,000	10,000
NH_3	-	0.9 wt%	0.45 wt%	-
TDS	**90,000**	**80,000**	**50,000**	**35,000**

Table 5.17: UTCHEM surfactant and polymer parameters

Polymer parameters	Surfactant parameters
Ap1= 350 Ap2= 500 Ap3= 1000 Sp= -0.83 γ_c= 4 $\dot{\gamma}_{1/2}$= 12 P_α= 1.8	CSEL7=1.1; CSEU7=1.53 Hblc71=0.05; Hblc71=0.04; Hblc72=0.05

Table 5.18: List of key geochemical reactions included in the calculations

Aqueous reactions	
$NH_4^+ = NH_3(aq) + H^+$	log_k -9.252
$Ca^{+2} + SO_4^{-2} = CaSO4(aq)$	log_k 2.3
$Ca^{+2} + CO_3^{-2} = CaCO3(aq)$	log_k 3.224
$Mg^{+2} + SO_4^{-2} = MgSO_4(aq)$	log_k 2.37
$Mg^{+2} + CO_3^{-2} = MgCO_3(aq)$	log_k 2.98
$H_2O = H^+ + OH^-$	log_k -14.0
Solid reactions	
$CaSO_4(s) = Ca^{2+} + SO_4^{2-}$	log_k -4.36
$CaMg(CO_3)_2 = Ca^{2+} + Mg^{2+} + 2\ CO_3^{2-}$	log_k -17.09
$Ca(OH)_2(s) = Ca^{2+} + 2\ OH^-$	log_k -5.5

Table 5.19: UTCHEM input parameters used for modeling CF-8

Number of grids	1x1x40
Components	Water, Oil, Surfactant, Polymer, Anion, Calcium, alc1 alc2 (Geochemical species were included separately with IPHREEQC)
Porosity	0.195
Permeability	453 mD
Water viscosity (@ 38 ºC)	0.47 cP
Oil viscosity (@ 38 ºC)	8.3 cP
Residual oil saturation	0.29
Residual water saturation	0.30
Water endpoint relative permeability	0.05

Table 5.19 (continued)

Oil endpoint relative permeability	0.9
Injection Schedule	0.4 PV ASP Slug 0.5 PV Polymer 1 1.4 PV Polymer 2

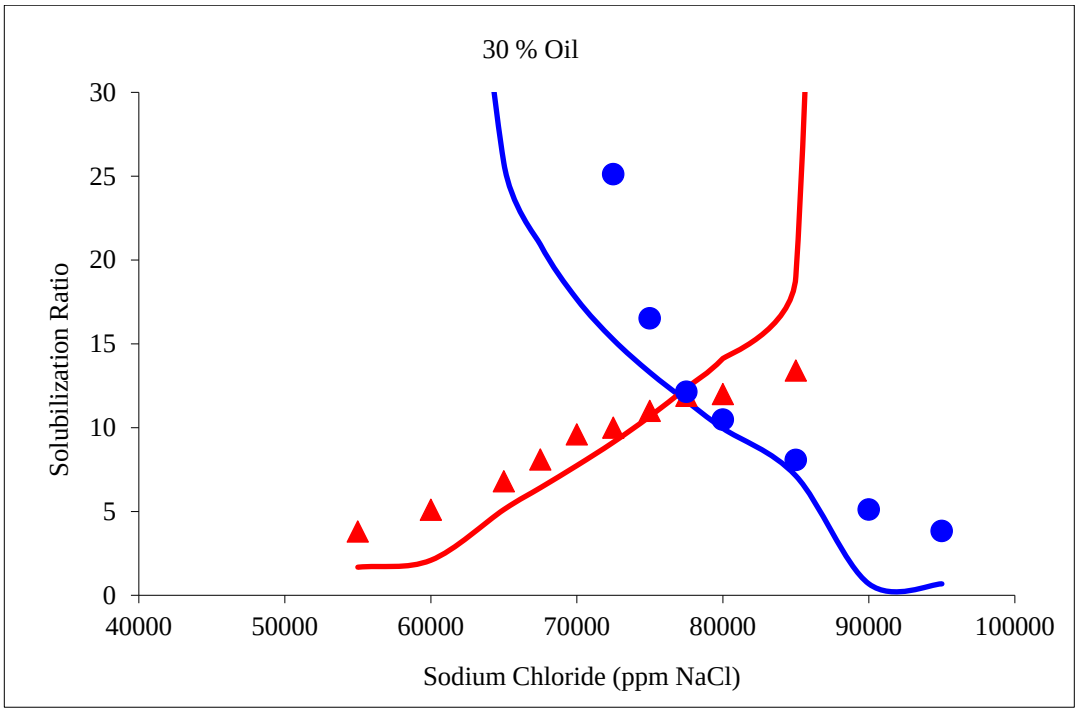

Figure 5.19: Comparison of calculated surfactant phase behavior with experimental data

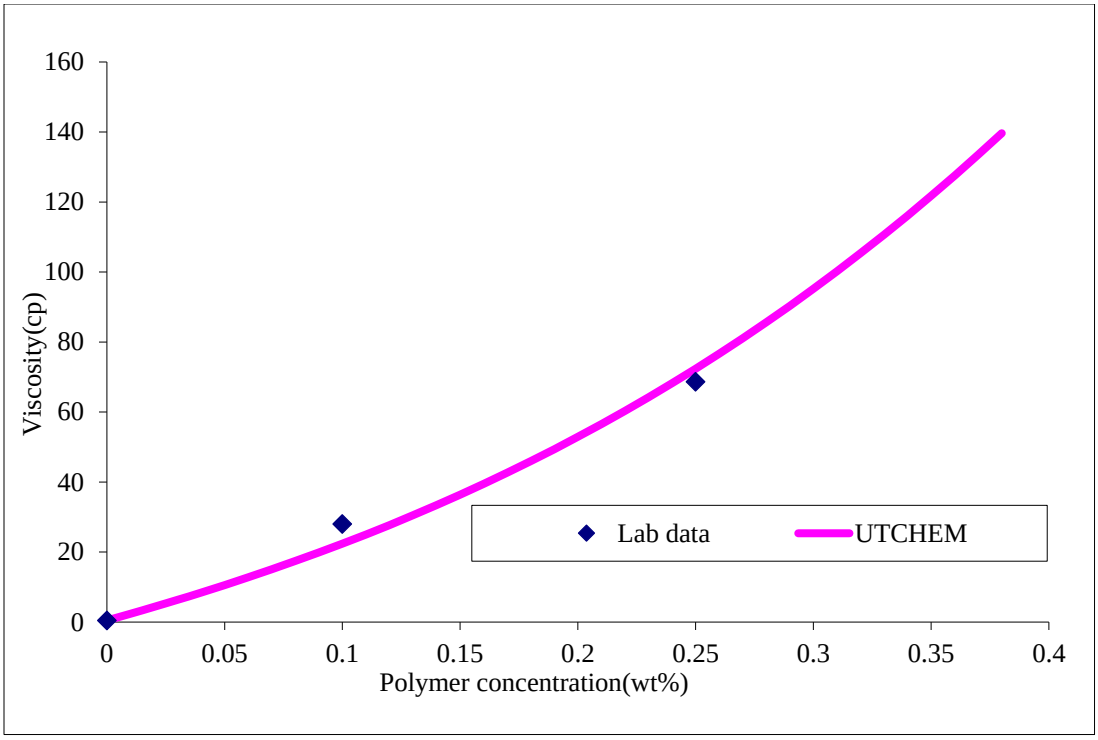

Figure 5.20: Comparison of measured polymer and calculated viscosity as a function of polymer concentration

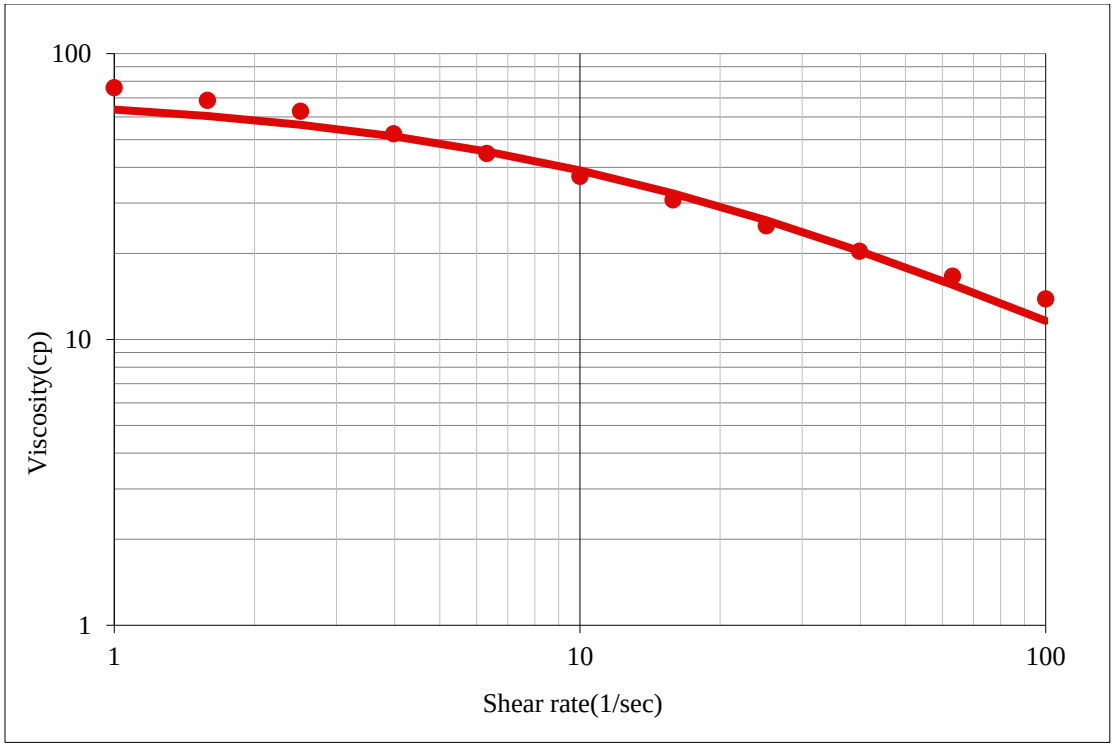

Figure 5.21: Comparison of measured and calculated viscosity as a function of shear rate

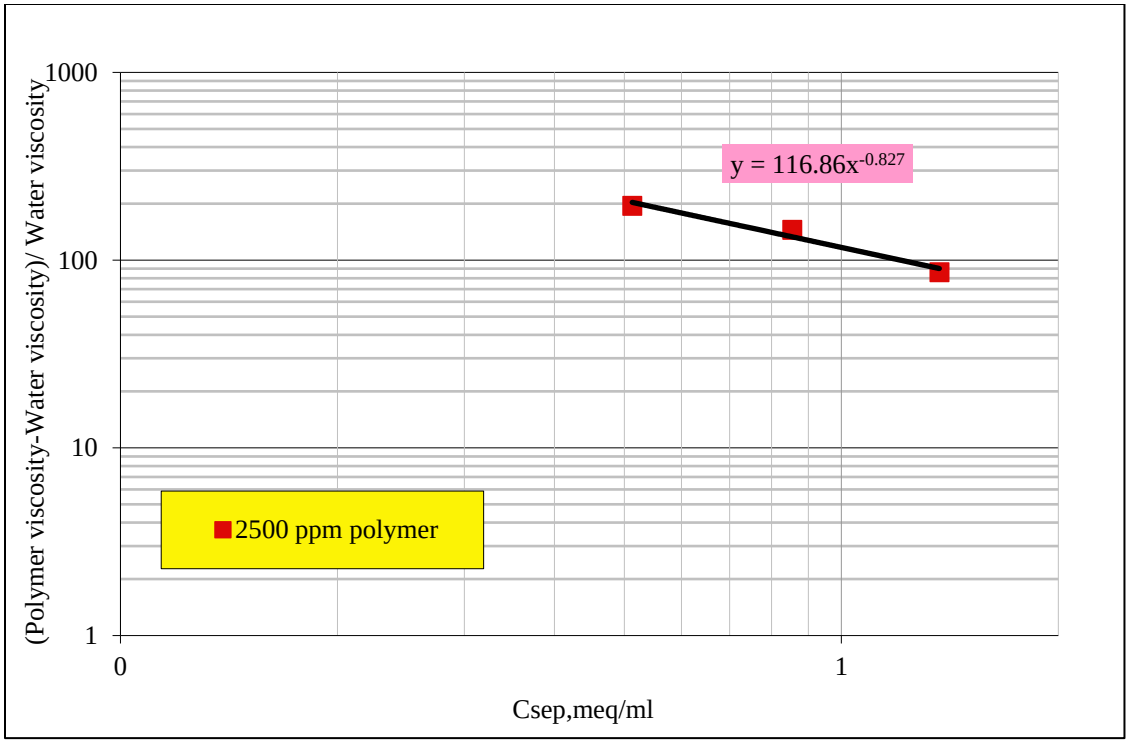

Figure 5.22: Comparison of measured and calculated viscosity as a function of effective salinity

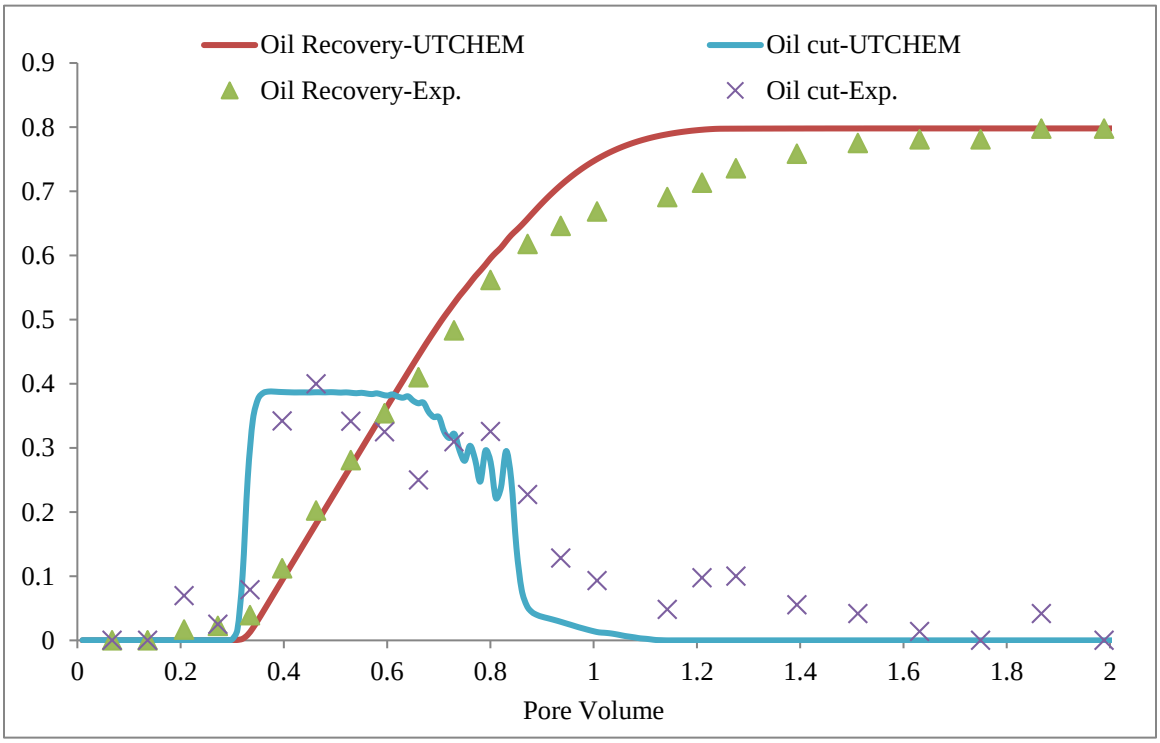

Figure 5.23: Comparison of oil recovery results obtained experimentally and UTCHEM simulations

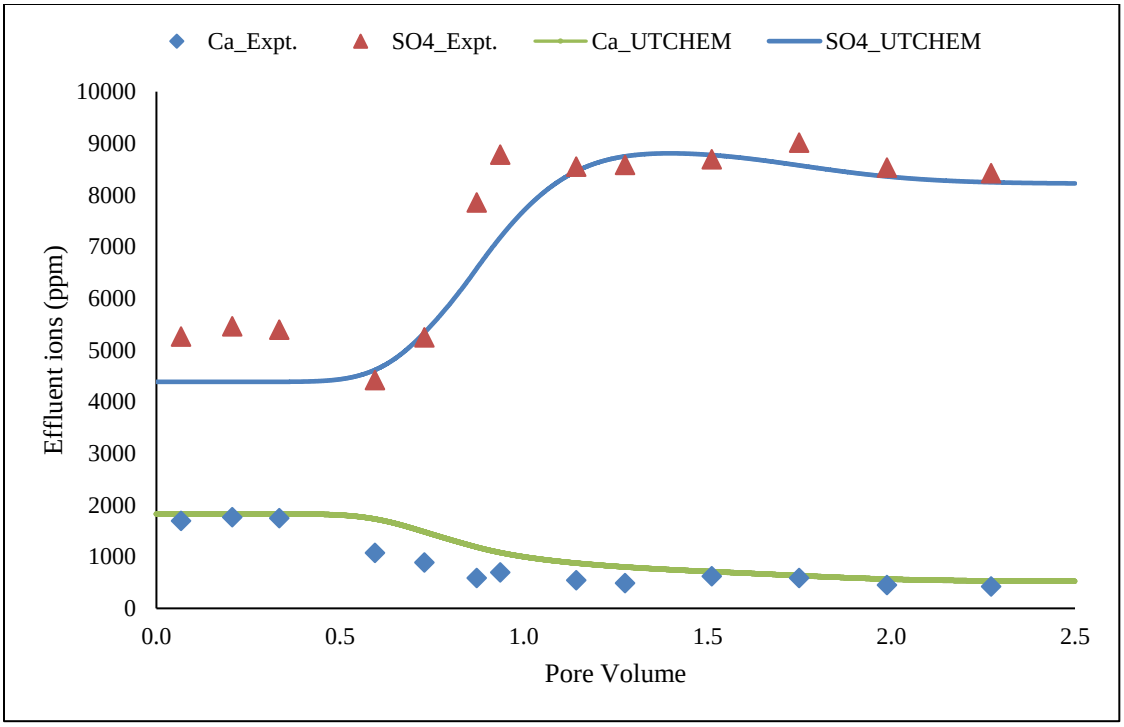

Figure 5.24: Comparison of ASP coreflood effluent ions with UTCHEM simulations

5.5 (a) UTCHEM simulation of ASP coreflood CF-14

ASP coreflood CF-14, discussed in section 4.26, was simulated in UTCHEM-IPHREEQC. This coreflood was performed in a Berea sandstone core using ammonia as the alkali. The properties of the core and the composition of the formation/waterflood brines and the chemical slugs are given in Tables 5.20 and 5.21, respectively. Further details of the coreflood, including the type and amounts of surfactants and polymer used in the chemical slugs are given in Table 4.44.

Parameters used for modeling surfactant phase behavior and polymer rheology in UTCHEM were obtained as per the procedure described previously. A list of the

parameters is shown in Table 5.22. A comparison of experimental data and calculated surfactant phase behavior curves is shown in Figure 5.25. Good agreement was observed between the measured and calculated polymer rheology data from the parameters given in Table 5.22 (not shown here). The oil recovery data obtained from UTCHEM simulations showed good agreement with the experimental results (Figure 5.26). Note that in this experiment, the core was cleaned initially by injecting many pore volumes of 100,000 ppm NaCl brine. The cleaning was performed mainly to remove the divalent ions attached to the clays. In this UTCHEM simulation, therefore, ion exchange reactions between cations in the aqueous phase with the cations attached to the clays were not considered. A detailed discussion on this topic is presented next.

Table 5.20: Properties of the core used in coreflood CF-14

Core	Length (inches)	Diameter (inches)	Porosity (%)	Permeability (md)	Temperature (°C)
Berea Sandstone	11.9	1.49	19.6	59	45

Table 5.21: Ionic compositions of the formation/waterflood brines and chemical slugs

Salt	Formation/Waterflood brine (ppm)	ASP slug (ppm)	Polymer drive 1 (ppm)	Polymer drive 2 (ppm)
NaCl	27,500	17,500	12,500	7,500
NH_3	-	0.5 wt%	0	0
TDS	27,500	17,500	12,500	7,500

Table 5.22: Parameters to model surfactant phase behavior and polymer rheology in UTCHEM

Polymer parameters	**Surfactant parameters**
Ap1= 60 Ap2= 300 Ap3= 1500 Sp= -0.428 $\dot{\gamma}_{1/2}$= 4.2 P_{α}= 1.7	CSEL7=0.26; CSEU7=0.34 Hblc71=0.03; Hblc71=0.028; Hblc72=0.03

Table 5.23: UTCHEM input parameters used for modeling CF-14

Number of grids	1x3x100
Components present	Water, Oil, Surfactant, Polymer, Anion, Calcium. Other geochemical species were included with IPHREEQC similar to the previous case.
Porosity	0.2
Permeability	60 mD
Water viscosity (@ 38 ºC)	0.45 cP
Oil viscosity (@ 38 ºC)	3 cP
Residual oil saturation	0.34
Residual water saturation	0.34
Water endpoint relative permeability	0.1
Oil endpoint relative permeability	0.7
Injection Schedule	0.4 PV ASP Slug 0.2 PV Polymer 1 1.6 PV Polymer 2

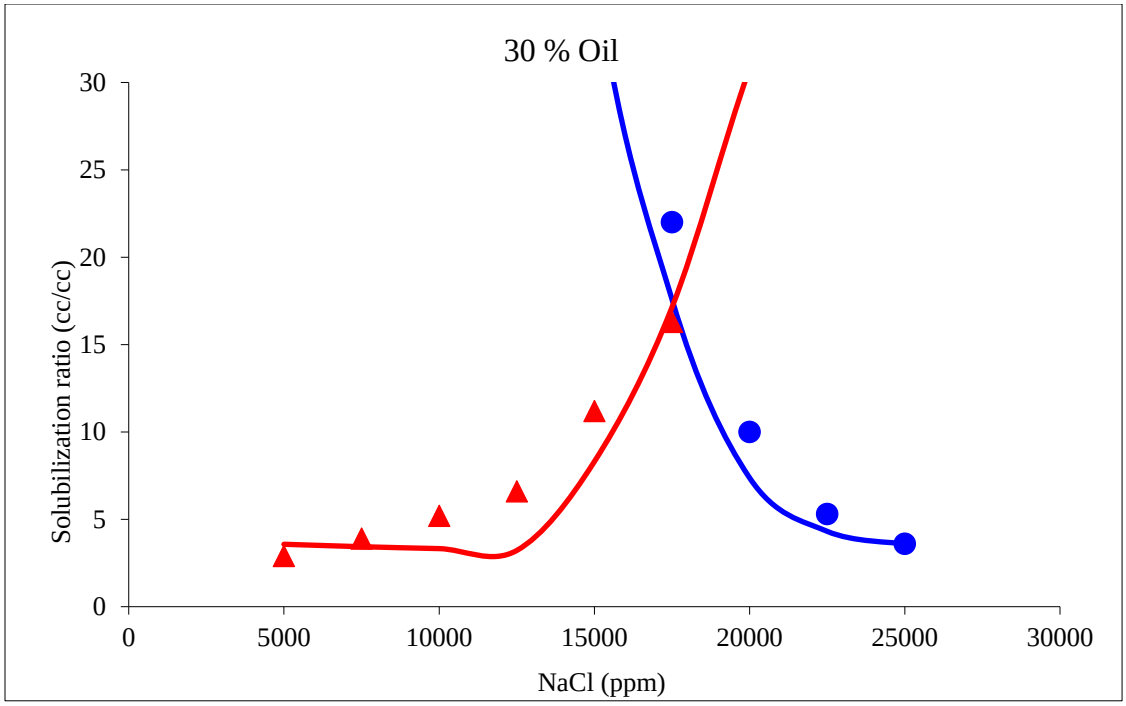

Figure 5.25: Comparison of calculated surfactant phase behavior with the experimental data

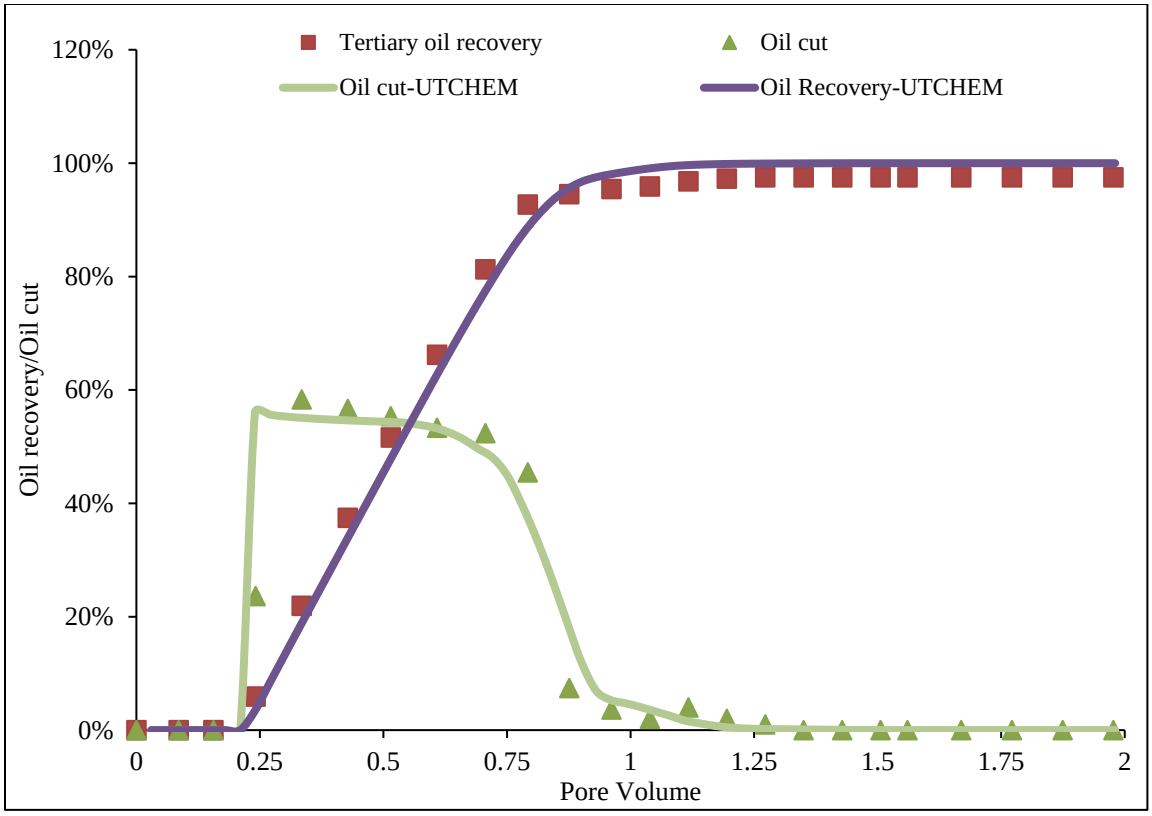

Figure 5.26: Comparison of experimental oil recovery data with UTCHEM simulations

5.5(b) Sensitivity of ASP floods to cation exchange reactions

Cation exchange reactions in sandstone reservoirs can significantly alter the composition of the chemical slugs, thus affecting the surfactant phase behavior, polymer viscosity and alkali transport. This section discusses cation exchange reactions for scenarios commonly encountered in surfactant floods. In addition, the effect of cation exchange reaction on ASP floods using ammonia as the alkali is specifically discussed. For simplicity, the analysis was kept limited to single-phase flow. The calculations were performed in PHREEQC, and effluent ions and in-situ solid concentrations were monitored.

Case 1: Base case

The base case consisted of an injection brine displacing the formation brine from a sandstone core. The injection brine had lower salinity and hardness compared to the formation brine. The compositions of the brines are shown in Table 5.24. No alkali was added to the injection brine; this case is thus similar to a surfactant polymer (SP) flood. The cation exchange capacity (CEC) of the sandstone core was assumed to be 0.125 meq/mL. Similar CEC values are reported in the literature for reservoir and outcrop sandstone cores (Southwick et al., 2014). The effluent ions profile obtained from PHREEQC calculations are shown in Figure 5.27. From the results, it can be seen that chloride concentration in the effluent changes from its initial value (in the formation brine) to a final value (in the injection brine) without undergoing any reaction. The behavior of chloride ions is similar to an unreactive tracer. Sodium, calcium and magnesium ions, on the other hand, show a delay in reaching to their injected concentrations because of the cation exchange reactions. The cations almost reach to their respective injected concentrations at about 1.6 pore volumes, about 0.45 pore volumes after the chloride ions. Calcium and magnesium concentrations remain 10-20 ppm higher than the injected concentrations even after 2 pore volumes.

The results show that if a surfactant slug, prepared in the injected brine, is introduced in a core initially saturated with formation brine, the calcium and magnesium concentrations in the slug could be much higher than the initial concentrations. These divalent ions can significantly alter the surfactant phase behavior (see section 4.14), drive

the phase behavior into (high IFT) Winsor type II and, in worst cases, result in surfactant precipitation.

Table 5.24: Brine compositions for case 1

Ions	Formation brine (ppm)	Injection brine (ppm)
Na^+	41,411	23,590
Ca^{2+}	11,686	36,410
Mg^{2+}	2700	200
Cl^-	103,000	300
SO_4^{2-}	200	0
TDS	**148,740**	**61,624**

Table 5.25: Brine compositions used case 2

Ions	Formation brine (ppm)	Injection brine (ppm)
Na^+	41411	23590
Ca^{2+}	11686	36410
Mg^{2+}	2700	0
Cl^-	103000	0
SO_4^{2-}	200	0
TDS	**148,740**	**60,000**

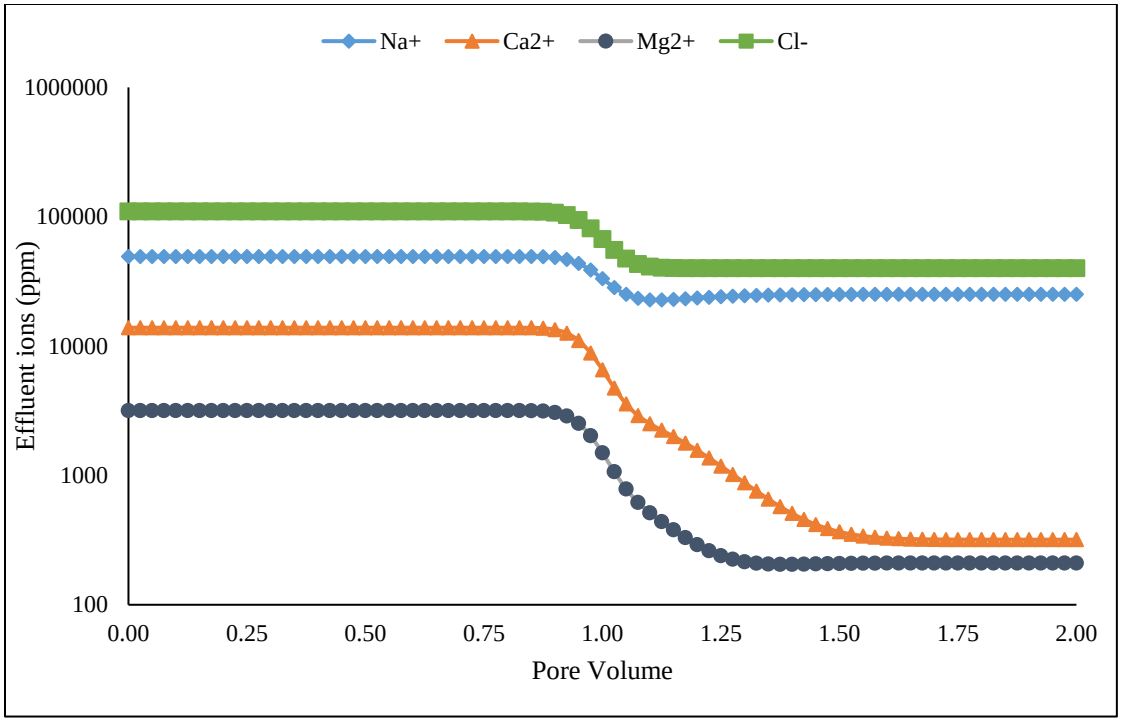

Figure 5.27: Effluent ions from PHREEQC calculations of case 1 (base case)

Case 2: Surfactant slug in soft brine

In this case, change in ionic composition of a surfactant slug prepared in soft brine and injected in a sandstone core initially saturated with hard brine is discussed. PHREEQC calculations were performed using the same system which was used in case 1, except divalent cations were removed from the injection brine. The compositions of injection brine and formation brine are shown in Table 5.25. The effluent ions from the calculations are shown in Figure 5.28. Similar to the previous case, cations show delay in reaching to the injected concentrations. The chloride ions reach the injected concentration at about 1.15 pore volumes. Calcium and Magnesium concentrations even after 1.5 pore

volumes are about 200 ppm and 1.4 ppm, respectively. A surfactant formulation prepared in a soft brine can alter significantly on contacting divalent cations, especially if the surfactant formulation is not tolerant to divalent cations. For example, surfactant formulations prepared using alkyl benzene sulfonates (ABS) are not tolerant to divalent cations and are likely to show high IFT on contacting them. Surfactant formulations that have some tolerance for divalent cations can show transition into Winsor type II. The amount of shift in effective salinity is dependent on the surfactant formulation.

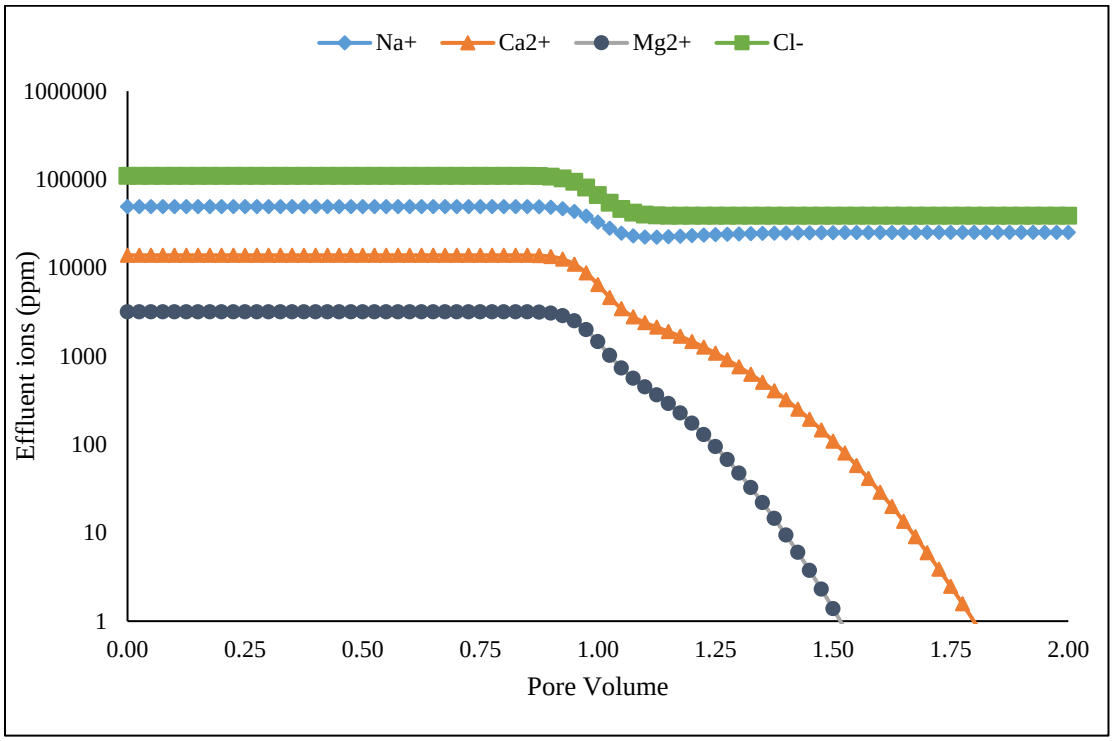

Figure 5.28: Effluent ions from PHREEQC calculations for case 2

Case 3: Ammonia as alkali for ASP floods

In this case, the effect of ion exchange reactions on the ASP floods, using ammonia as the alkali, was investigated using PHREEQC. The ionic compositions of the formation brine, the ASP slug and the polymer drive are given in Table 5.26. Note that the ASP slug contained 0.5 wt% ammonia while no alkali was present in the polymer drive brine. The pH values of the ASP slug and the polymer drive were about 11.4 and 7, respectively. The properties of the core were the same as the previous cases. The results of the calculations are shown in Figures 5.29(a) and 5.29(b). The effluent data (Figure 5.29(a)) showed precipitation of magnesium ions on coming in contact with the ASP slug brine. Calcium ions, however, did not precipitate. Free calcium ions could, therefore, affect the surfactant phase behavior in cases where only ammonia is used as the alkali in ASP slugs. The pH values showed a delay in reaching the injected value due to the precipitation of magnesium ions as magnesium hydroxide. These magnesium ions were present in the mixing zone and on the clays. The precipitation profile of magnesium hydroxide (Brucite) is shown in Figure 5.29(b).

The effect of injecting a polymer drive, without ammonia, after the ASP slug (containing ammonia) was investigated next. The ionic composition of the polymer drive brine is shown in Table 5.26. The effluent ions on injecting the polymer drive is shown in Figure 5.30. The results show no change in calcium ions, suggesting that calcium ions were removed by the ASP slug brine. Note that calcium ions were removed not by precipitation but were ion-exchanged by the ASP slug brine and eluted. The magnesium

ions showed an increase on injecting the polymer drive brine because of re-dissolution of magnesium hydroxide. Note that the magnesium concentration reached a maximum value of 50 ppm and then stabilized at about 7 ppm. These ions could affect the surfactant phase behavior significantly, unless the formulation is tolerant to at least some divalent ions. Also note that the pH of the polymer drive was 7. However, the effluent pH, shown in Figure 5.30, remained at around 10.4 even after injecting 2 pore volumes of the polymer drive. The increase in pH is the result of magnesium hydroxide re-dissolution.

These calculations show that ammonia by itself would not precipitate calcium ions. In addition, the precipitated magnesium ions could re-dissolve unless ammonia is also added to the polymer drives. The results obtained on adding sodium carbonate along with ammonia to the surfactant slug is discussed next.

Table 5.26: Brine compositions used case 3

Ions	**Formation brine (ppm)**	**ASP slug brine (ppm)**	**Polymer drive brine (ppm)**
Na^+	41,411	23,590	23,590
Ca^{2+}	11,686	36,410	36,410
Mg^{2+}	2700	0	0
Cl^-	103,000	0	0
SO_4^{2-}	200	0	0
NH_3	**0**	**0.5 wt%**	**0**
TDS	**148,740**	**60,000**	**60,000**

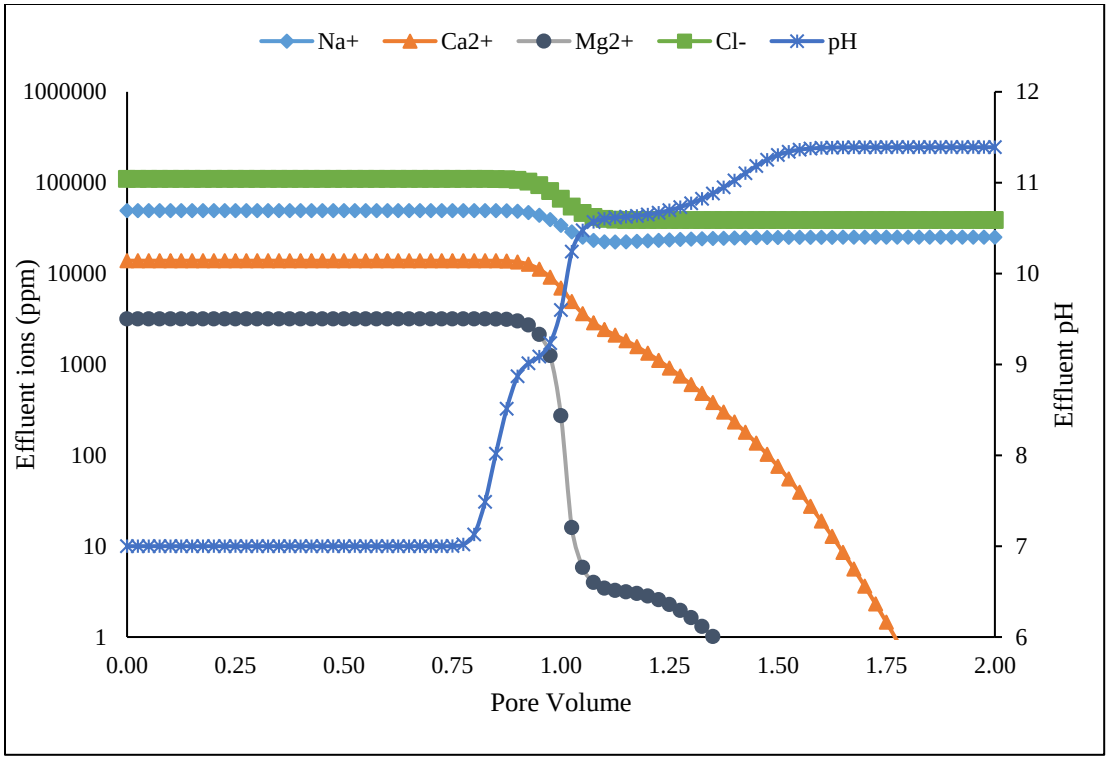

Figure 5.29 (a): Effluent ions from PHREEQC calculations of case 3

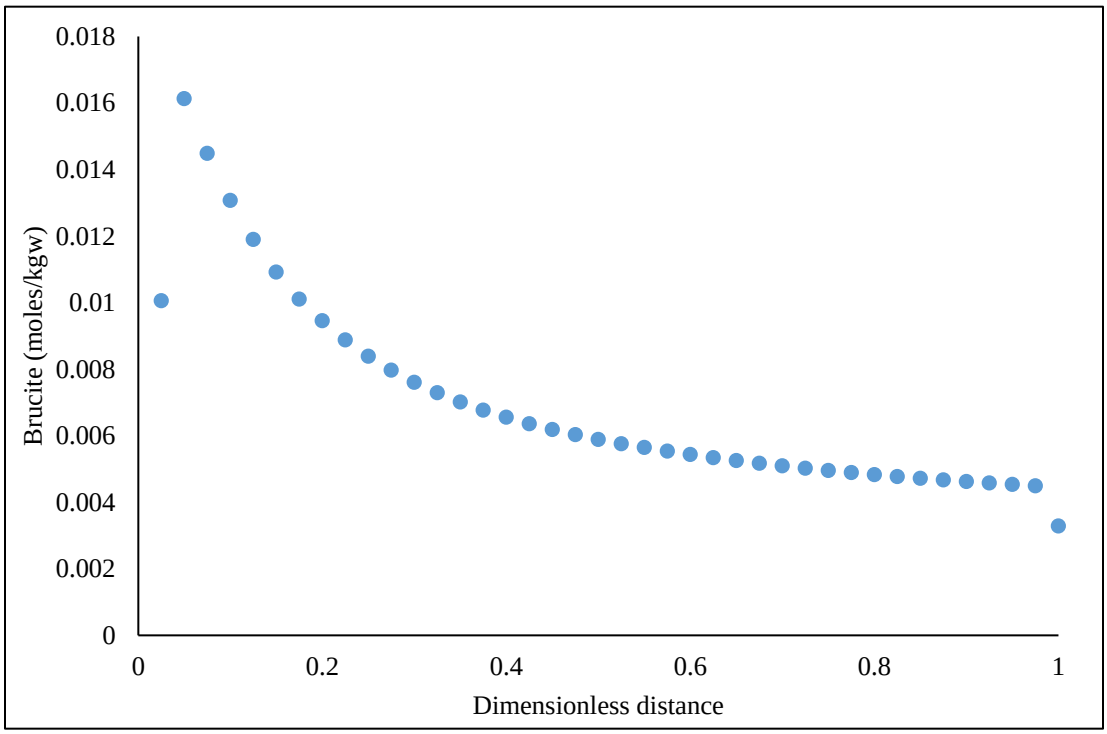

Figure 5.29 (b): Precipitation profile of magnesium hydroxide in the core on injecting injection brine containing ammonia

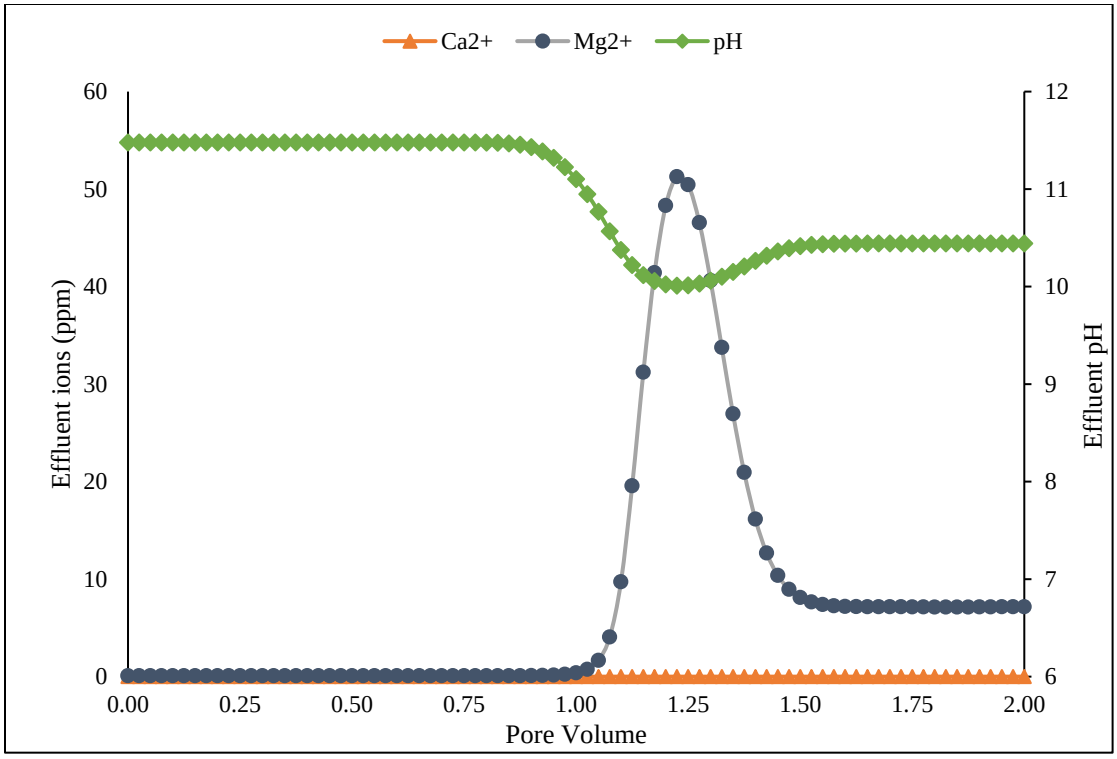

Figure 5.30: Results of PHREEQC calculations showing effluent ions on injecting the polymer drive brine after the ASP slug brine in case 3

Case 4: Ammonia-Na_2CO_3 as alkali for ASP floods

In this case, sodium carbonate was also added, along with ammonia, to the surfactant formulation. Other parameters were kept the same as the previous runs. The compositions of the brines are shown in Table 5.26. The results of the PHREEQC calculations are shown in Figure 5.31(a) and 5.31(b). Figure 5.31(a) shows the effluent ions from the sandstone core on injecting ASP slug brine prepared by adding both ammonia and sodium carbonate as alkalis. The core was initially saturated with the formation brine. Note that both magnesium and calcium ions precipitate to very low

values on coming in contact with the ASP slug. The solids that precipitated on injecting the ASP slug brine is shown in Figure 5.31(b). Note that mainly calcite and brucite precipitated on injecting the ASP slug brine. A small amount of magnesite precipitation was also observed.

The ASP slug brine was displaced with the polymer drive brine, containing no alkali. The results of the PHREEQC calculations for this case is shown in Figures 5.32(a) and 5.32(b). The results show re-dissolution of calcium and magnesium ions on injecting the polymer drive brine. The maximum concentrations of calcium and magnesium ions in this case were found to be about 60 ppm and 80 ppm, respectively. The resulting total divalent ions concentration of about 140 ppm could significantly affect the surfactant phase behavior, unless the formulation is tolerant to divalent cations. The concentration of solid species along the core after injecting 2 pore volumes of the polymer drive is shown in Figure 5.32(b). The solid lines on the figure show the concentration of solid species before injecting the polymer drive brine. The dots on the figure represent solid concentration along the core after 2 pore volumes injection of the polymer drive brine. On injecting the polymer drive brine, re-dissolution of brucite, magnesite and some calcite was observed. Note that the calculations were performed assuming the local equilibrium. As a result, the change in solid concentrations is observed only at the beginning of the core.

The PHREEQC calculations of case 4 show that both calcium and magnesium ions precipitated on injecting the ASP slug brine, containing both ammonia and sodium

carbonate, in a core initially saturated with a formation brine containing large amounts of these divalent cations. Therefore, addition of at least a small amount of sodium carbonate is recommended when ammonia is used as the main alkali in the surfactant slug. The addition of a small amount of sodium carbonate to the polymer drive is also recommended to avoid the re-dissolution of the precipitated solids.

Table 5.27: Brine compositions used case 4

Ions	**Formation brine (ppm)**	**ASP slug brine (ppm)**	**Polymer drive brine (ppm)**
Na^+	41,411	23,590	23,590
Ca^{2+}	11,686	36,410	36,410
Mg^{2+}	2700	0	0
Cl^-	103,000	0	0
SO_4^{2-}	200	0	0
NH_3	**0**	**0.5 wt%**	**0**
Na_2CO_3	**0**	**10,000**	**0**
TDS	**148,740**	**70,000**	**60,000**

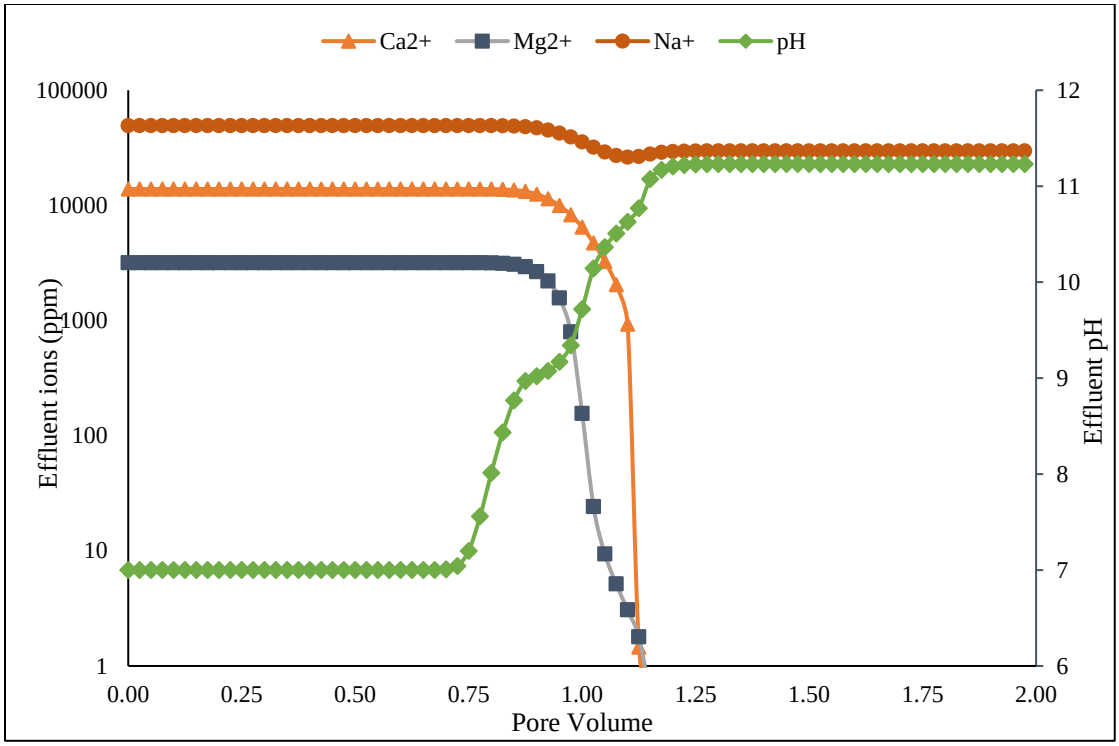

Figure 5.31(a): Effluent ions from PHREEQC calculations when the ASP slug was injected in case 4

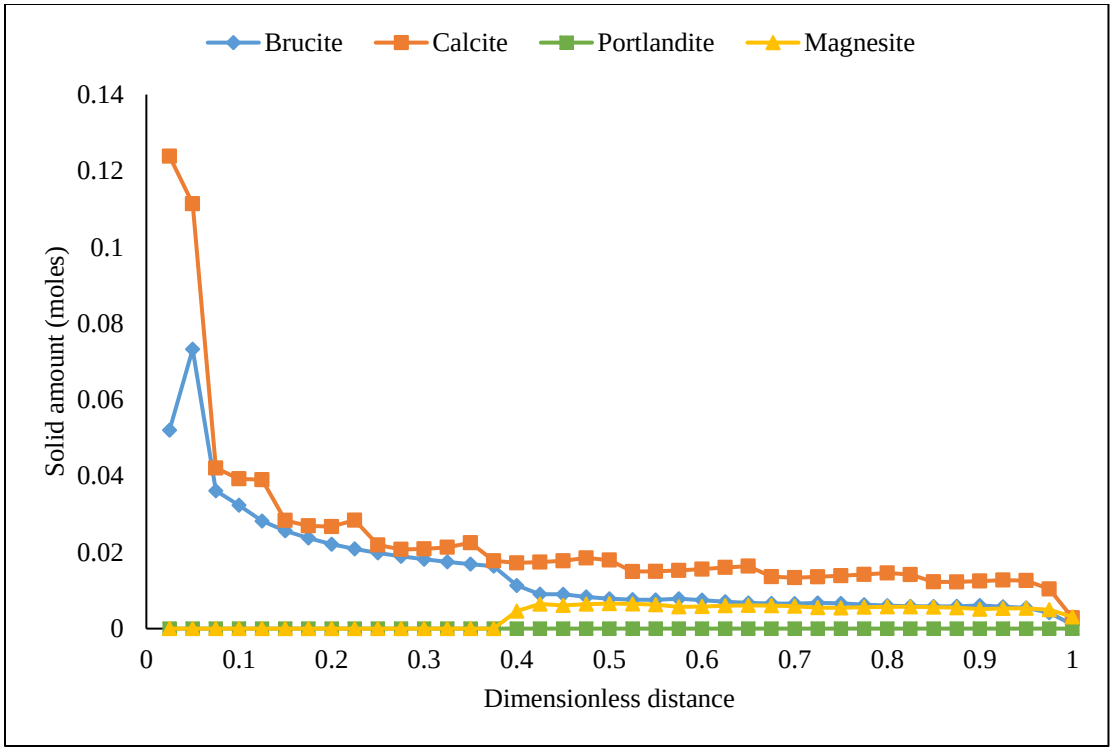

Figure 5.31(b): Precipitation profile on injecting the ASP slug in case 4

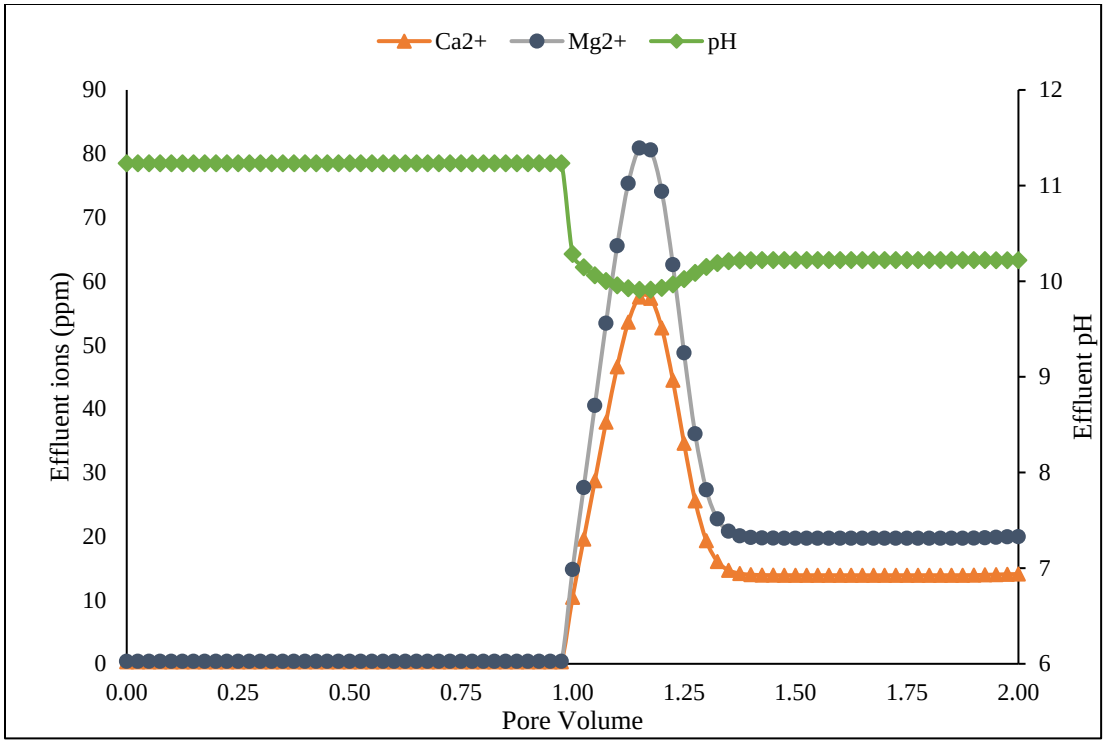

Figure 5.32 (a): Effluent ions on injecting the polymer drive in case 4

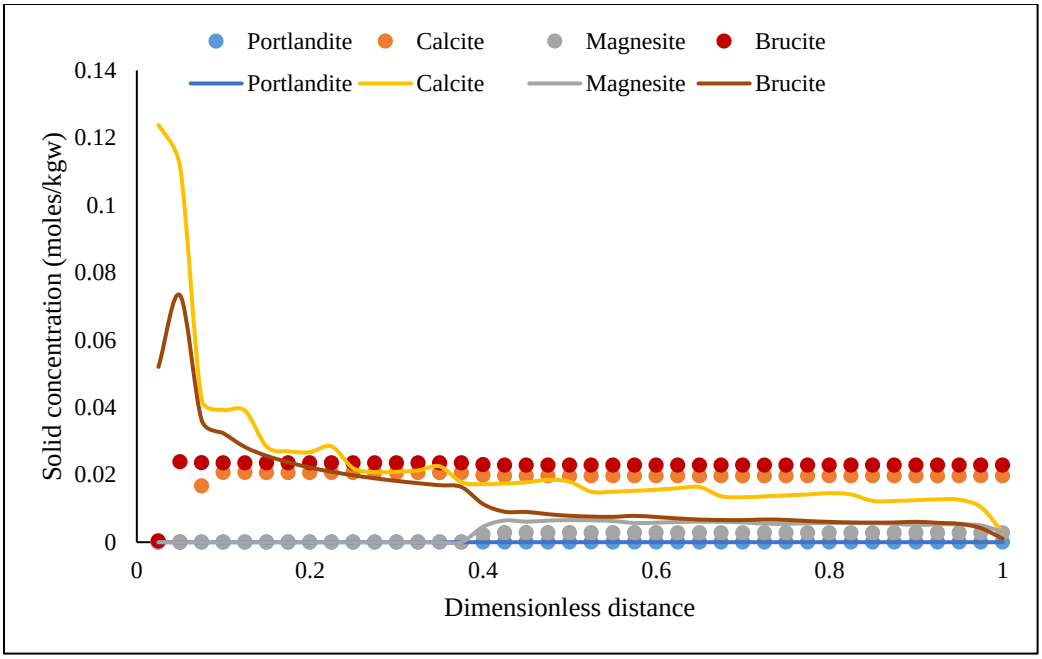

Figure 5.32 (b): Change in concentrations of solids (precipitated in the core when the ASP slug was injected in case 4) on injecting 2 pore volumes of the polymer drive brine

A summary of simulation results is given below:

1. Sodium metaborate ASP corefloods in Silurian dolomite cores were simulated in UTCHEM. EQBATCH was used for including the geochemical reactions. A good agreement was observed between experimental and modeling results. In addition, PHREEQC calculations were performed to study the interaction of sodium metaborate with Silurian dolomite. PHREEQC calculations showed very little dissolution of Silurian dolomite in the presence of sodium metaborate.

2. Single-phase static and transport alkali-rock experiments performed using sodium metaborate and sodium carbonate in the presence of gypsum were modeled in PHREEQC. A good agreement was observed between the results of static experiments

and PHREEQC calculations. The concentration of effluent ions obtained during sodium carbonate experiment with a core containing gypsum corresponded to their equilibrium concentrations. Similar results with sodium metaborate, however, were far from the equilibrium. A simple reaction kinetics was included to model sodium metaborate flow experiments. A good agreement was seen between experimental and PHREEQC results.

3. ASP coreflood performed in a carbonate core containing gypsum, using ammonia as the alkali, was simulated in UTCHEM-IPHREEQC. UTCHEM-IPHREEQC was used mainly because of the dependence of gypsum dissolution on brine salinity; higher calcium concentration was observed in high salinity brine. UTCHEM-IPHREEQC takes into account the effect of ionic strength on activity coefficients. The effect of calcium ions on surfactant phase behavior was considered in the simulations. A good agreement was observed between the oil recovery data and effluent ions was observed from experiments and simulations.

4. Sensitivity study in PHREEQC showed that surfactant phase behavior can alter significantly from ion exchange of divalent cations. Ammonia was found to precipitate magnesium ions but not calcium ions. Sodium carbonate, on the other hand, precipitated both calcium and magnesium ions. Injection of polymer drive, without any alkali, could re-dissolve the precipitates from the ASP slug. These factors must be considered when designing a surfactant flood.

CHAPTER 6. LOW SALINITY WETTABILITY ALTERATION IN CARBONATES

A substantial amount of oil is known to exist in carbonate reservoirs. Most of these reservoirs are mixed-wet or oil-wet due to which the recovery from these reservoirs is low during primary and secondary floods. The presence of fractures further lowers the oil recovery due to bypassing of injected fluids through fractures. Furthermore, a substantial portion of these reservoirs are at high temperature and high salinity which makes them difficult targets for applying enhanced oil recovery (EOR) techniques. Oil recovery from these reservoirs can be improved by wettability alteration. Wettability alteration involves changing the wetting state of an oil-wet rock towards a water-wet state, thus improving the oil recovery. Injections of brines with carefully designed ionic compositions in oil-wet carbonate rocks at high temperatures have shown to alter their wettability towards a water-wet state and improve oil recovery. Various mechanisms have been postulated for this wettability alteration such as calcite dissolution and interaction of potential determining ions, such as Ca^{2+}, Mg^{2+} and SO_4^{2-}, with the carbonate surface. Although these mechanisms are not completely understood, recent studies agree that geochemical interactions between injected brines and carbonate rocks are responsible for altering the wettability. In this chapter, results of experimental and modeling work performed to gain further insights into the geochemical interactions between carbonate rocks and modified brines is discussed. Single-phase static and transport experiments were performed to understand the interactions of injected brines

with carbonate rocks. Based on the experimental results, a mechanistic model was developed in UTCHEM-IPHREEQC to model the wettability alteration process in carbonates. The list of experiments and simulations discussed in this chapter are given in Table 6.1.

6.1 Single-phase experiments

Single-phase static and transport experiments were performed to understand the interactions of various ions present in the low salinity brines with carbonate rocks. The brines ionic composition of the brines used in this study are shown in Table 6.2. The properties of the limestone core used in single-phase static and transport experiments are shown in Table 6.3. The core predominantly consisted of calcite with trace amounts of dolomite and other minerals.

6.1.1 Static experiments

Single-phase static experiments were performed to study the interactions of crushed limestone cores with modified brines at 120 °C. These experiments were performed to also calibrate the model (discussed later) since the existing geochemical databases have limitations at high temperature and high salinity. In these experiments, a given amount of crushed limestone was mixed with modified brines in glass ampules. The glass ampules were sealed with a propane torch and the samples were allowed to equilibrate at 120 °C for 4-5 days. Brine samples, without crushed limestone, were prepared, similarly, and equilibrated at 120 °C. These samples were prepared to study

effect of heating on brine compositions. After equilibrating for 4-5 days, supernatant solutions were collected from the ampules, filtered and analyzed for Na^+, Ca^{2+}, Mg^{2+}, Cl^-, SO_4^{2-} ions using ion chromatography. The composition of a brine equilibrated at 120 °C, without limestone, was compared with its original composition (at room conditions) to understand the effect of heating. Brines equilibrated with crushed limestone were compared with brines equilibrated without limestone to understand the interaction of brines with crushed limestone at 120 °C.

The experimental results, given in Table 6.4, show original compositions of various brines at 25 °C and their respective compositions on equilibrating, with and without crushed limestone, at 120 °C. Formation brine (FB), seawater (SW), diluted seawaters and 4xSO_4 SW (4S-SW) brine were investigated. From the results, it can be seen that sodium and chloride concentrations did not change on heating the brines, with or without limestone, indicating that these ions were under-saturated in the solutions and also did not show any interaction with limestone at 120 °C. The concentration of sulfate ions did not change on heating the brines to 120 °C, with or without limestone, except for 4S-SW brine. For the 4S-SW brine, concentration of sulfate and calcium ions decreased on heating to 120 °C, without limestone, and a white precipitate was observed in the glass ampule. The precipitate indicated that the brine was supersaturated with respect to anhydrite at 120 °C. The final calcium and sulfate concentrations at 120 °C in 4S-SW brine was 221 ppm and 12,119 ppm, respectively; lower than their concentrations in the original brine. A decrease in calcium and sulfate ions confirmed that anhydrite precipitation from 4S-SW brine at 120 °C.

Large changes in concentrations of calcium and magnesium ions were observed on equilibrating SW, SW/2, SW/50 and 4S-SW brines with crushed limestone at 120 °C. It can be seen from Table 6.4 that the concentration of calcium ions increased and that of magnesium ions decreased in these brines. This change in calcium and magnesium concentrations was the result of two possible reactions; calcite dissolution and surface dolomitization. For a better comparison, molar concentrations of calcium and magnesium ions in these brines are shown in molar terms in Figure 6.1. The figure shows that the increase in calcium ions in these brines was almost equivalent to the corresponding decrease in magnesium ions, indicating that dolomitization was more dominant than calcite dissolution in bringing these changes. Note that even in the case of SW/50, which was the most diluted brine, dolomitization was more dominant in increasing the concentration of calcium ions than calcite dissolution.

6.1.2 Single-phase brine corefloods

Single-phase brine corefloods were performed at 0.5 ft/d to study geochemical interactions of various brines with limestone cores at 120 °C. The purpose of these experiments was to identify additional interactions that were possibly not captured by the static experiments. Another reason to perform these experiments was to understand if the geochemical reactions during low salinity floods reach to equilibrium at the flow rates typically used in laboratory experiments. The procedure to setup a coreflood is described in chapter 3. A limestone core of known dimensions was placed in a core holder, characterized and saturated with formation brine. The coreholder was placed in a

convection oven set at 120 °C. Brines, preheated to 120 °C, were injected through the core at 0.5 ft/d and effluent samples were collected using an automated fractional collector. The effluent samples were filtered and analyzed for cations and anions using ion chromatography. The injection sequences used in these experiments are given in Table 6.1. These injection schemes were used as they have shown to improve oil recovery in various studies (Chandrasekhar et al., 2013; Yousef et al., 2010). In experiment B1, the formation brine was first displaced with seawater, which was then displaced with SW/50. In experiment B2, the core was first saturated with 0.1 NaCl brine which was then displaced by seawater followed by SW/50. Experiment B2 was performed to remove the effect of any anhydrite that might have precipitated due to the mixing of seawater and formation brine in experiment B1. In experiment B3, the formation brine was first displaced with seawater, which was then displaced with 4S-SW. Throughout these experiments, a 100 psi backpressure was used to avoid boiling at 120 °C.

Experiment B-1.1 (SW displacing FB):

In this experiment, seawater was injected through a limestone core which was previously saturated with formation brine. The actual concentrations and normalized concentrations of effluent ions are plotted in Figures 6.2 and 6.3, respectively. From Figure 6.2, it can be seen that the calcium concentration at 2.5 PV (~920 ppm) was more than the injected concentration (~511 ppm) and magnesium concentration (1,360 ppm) was less than the injected concentration (1,600 ppm). Similar to static experiments,

dolomitization was observed in the dynamic experiments. Note that the increase in calcium concentration was mainly due to dolomitization. The effluent sulfate concentration at 2.5 PV was equal to the injected concentration indicating that no noticeable anhydrite precipitation occurred in the core on injecting SW. Figure 6.3 shows a delay in effluent sulfate concentration compared to other ions suggesting that sulfate ions were getting adsorbed on the rock surface. This result was not observed during the static experiments, possibly due to a small solid to water ratio, and signifies the importance of performing dynamic experiments.

Experiment B-1.2 (SW/50 displacing SW):

After experiment B-1.1, the seawater inside the core was displaced with SW/50 brine and the effluent ions were measured. The actual concentrations and normalized concentrations of effluent ions are plotted in Figures 6.4 and 6.5, respectively. From Figure 6.4, it can be observed that, unlike sodium and chloride ions, the effluent concentrations of calcium, magnesium and sulfate ions did not reach to steady state values even after injecting 2.5 PV of SW/50 brine. It appears that SW/50 brine was not injected long enough to allow these reactions to reach to steady state values. The effluent concentrations of calcium, magnesium and sulfate ions at 2.5 PV (~78 ppm, 52 ppm and 239 ppm, respectively) were much higher than the injected values of about 10 ppm, 32 ppm and 71 ppm, respectively. The sodium and chloride concentrations, however, reached the injected values at about 1.5 PV. The delay in potential determining ions to reach to the injected concentrations, in this case, was possibly the result of slow

geochemical interactions. After 1.5 pore volumes, the concentration of sodium and chloride ions decrease to their respective concentrations in SW/50. However, the concentrations of potential determining ions remain higher, thus making them interact more effectively with the surface. These interactions might be responsible for wettability alteration on injecting diluted seawater in limestone cores without anhydrite. The concentration of calcium ions at 2.5 PV is close to the equilibrium value obtained from experiment A4, however, the concentration of magnesium ions at 2.5 PV is much larger than the corresponding value obtained from the static experiment (3.8 ppm). It appears that the sulfate adsorption and dolomitization reactions that occurred when seawater was injected in experiment B-1.1 affected the results during SW/50 injection. Figure 6.5 shows that sulfate ion was delayed compared to other ions, similar to the previous case when seawater was injected. However, since the sulfate concentration did not reach to a steady state value, it is not clear if the delay was due to adsorption of sulfate ions or due to slow desorption of sulfate ions previous adsorbed during seawater injection (experiment B-1.1).

Experiment B-2.1 (SW displacing 0.1 NaCl brine):

This experiment was performed similar to the previous experiments, except the core was initially saturated with 0.1% NaCl, instead of the formation brine. The reason to perform this test was to make sure that the sulfate delay was due to the adsorption of sulfate on limestone rather than precipitation of anhydrite on the mixing of seawater with formation brine (experiment B-1.1). The results obtained in this case were similar to

experiment B-1.1. Normalized concentrations of chloride and sulfate ions are shown here (Figure 6.6). A delay in sulfate ions was observed compared to chloride ions, similar to experiment B-1.1, suggesting that the delay in sulfate is due to adsorption of sulfate ions on limestone surface.

Experiment B-2.2 (SW/50 displacing SW):

Seawater inside the core, from the previous experiment, was displaced with SW/50 brine. The concentration of effluent ions and their normalized concentrations are shown in Figures 6.7 and 6.8, respectively. From Figure 6.7, it can be seen that the concentrations of calcium, magnesium and sulfate ions did not reach steady state values, similar to experiment B-1.2. The concentrations of calcium, magnesium and sulfate ions at 3 pore volumes were about 58 ppm, 45 ppm and 155 ppm, respectively, much higher than their injected values. Figure 6.8 shows that sulfate ion was delayed compared to other ions suggesting that sulfate adsorption was taking place in this case also, similar to experiment B-1.2. However, since the sulfate concentration did not reach a steady state, it is not clear if the delay was due to adsorption of sulfate ions or due to slow desorption of sulfate ions previous adsorbed during experiment B-2.1.

Experiment B-3.1 (SW displacing formation brine):

Another set of experiments was performed to study the effect of injecting 4S-SW brine after seawater. First, the formation brine was displaced with seawater and results similar to experiments B-1.1 and B-2.1 were obtained (Figures 6.9 and 6.10). The concentrations of effluent calcium and magnesium ions at 2.5 PV were higher and lower,

respectively, than the corresponding injected values. A large delay in sulfate ions was observed compared to other ions similar to experiments B-1.1 and B-2.1.

Experiment B-3.2 (4S-SW displacing SW):

The seawater in the core was then displaced with 4S-SW brine. The results of this experiment are shown in Figures 6.11 and 6.12. Figure 6.11 shows that sodium and chloride ions did not interact with the surface and travelled, similar to a non-reactive conservative tracer, as was expected. The sulfate ions showed a slight delay compared to chloride concentration (Figure 6.12), but less delayed compared to the results presented previously. The calcium ion concentration decreased from the initial value to a final value (~350 ppm) around 2 PV. This final value was higher than the injected concentration of 221 ppm. The magnesium ions remained more or less constant at about 1,400 ppm, lower than the injected values of 1,600 ppm. From Figure 6.11, a slight decrease in magnesium concentration can be observed around 1 pore volume possibly due to dolomitization.

6.2 Mechanistic model for low salinity wettability alteration

A mechanistic model was developed for the wettability alteration process in UTCHEM-IPHREEQC, a coupled multiphase multicomponent three-dimensional reservoir simulator of the University of Texas at Austin. The simulator combines the capabilities of PHREEQC, the USGS geochemistry tool, with UTCHEM. This includes being able to include the dependence of reaction constants on salinity and temperature, use geochemical databases originally developed for PHREEQC and incorporate

additional reactions. The simulator was developed and calibrated against UTCHEM and PHREEQC (Kazemi et al., 2014).

The wettability alteration model assumed calcite surface to consist of positively charged calcium and negatively charged carbonate sites which could interact with calcium, magnesium and sulfate ions. Surface complexation reactions were assumed to occur between the lattice-bound ions of the exposed surface with water and dissolved species. These interactions and their respective equilibrium constants governed the distribution of surface species.

At equilibrium, a reaction on the carbonate surface (> CO_3H) with a divalent cation (Me^{2+}) can be expressed as shown below.

$$> CO_3H + Me^{2+} \Leftrightarrow > CO_3Me^{+} + H^{+} \tag{6.1}$$

$$K_{int}^{s} = \frac{\{>CO_3Me^{+}\}\{H^{+}\}_s}{\{>CO_3H\}\{Me^{2+}\}_s} \tag{6.2}$$

where K_{int}^{s} and $\{S\}_s$ are the intrinsic equilibrium constant of the reaction and the activity of species S on or near the surface, respectively. Since the surface species are not directly accessible, this reaction is often expressed in terms of an apparent equilibrium constant and the activity of a species in the aqueous solution as shown below.

$$K^{s} = \frac{\{>CO_3Me^{+}\}_s\{H^{+}\}_{aq}}{\{>CO_3H\}_s\{Me^{2+}\}_{aq}} \tag{6.3}$$

$$K^{s} = K_{int}^{s} exp\left(\frac{-zF\psi}{RT}\right) \tag{6.4}$$

where $\{S\}_{aq}$ is the activity of the species S in the aqueous phase, z is the charge of the surface complex formed, F is the Faraday constant and ψ is the surface potential.

To model limestone surface reactions, the surface was assumed to consist of two primary species, that is, hydrated calcium ($>CaH_2O^+$) and carbonate species ($>CO_3^-$). The surface is assumed to consist of equal number of these primary surface species. About 2-3 surface sites per nm^2 were assumed. Interactions of primary surface species with ions dissolved in the aqueous phase were included assuming local equilibrium. Key surface reactions included in the model are given in Table 6.5. These reactions were modeled in UTCHEM-IPHREEQC, using its surface complexation module. In addition to surface reactions, aqueous phase reactions and solid phase reactions (dissolution/precipitation reactions) were also included. The equilibrium constants for aqueous and solid reactions were obtained from PHREEQC.dat (Pakrhurst et al., 1999) and those of surface reactions were reported by Van Cappellen et al. (1993) and Brady et al. (2012).

The wettability of the rock surface was assumed to depend on the amount of naphthenic acid, here represented by "HA", attached on the surface. Naphthenic acids could attach on positively charged calcium sites or calcium/magnesium complexed (or adsorbed) carbonate sites (Equations 11, 21 and 22 in Table 6.5). The wettability alteration in the model was based on the mechanisms postulated by Zhang et al. (2007) as shown in Figure 6.13. It was assumed that sulfate ions facilitate the removal of naphthenic acids in the presence of calcium and magnesium ions, thus altering the wettability.

The model was used to simulate single-phase static and transport experiments (reported in this study), zeta potential results reported by Zhang and Austad (2006) and Mahani et al. (2015), and oil recovery experiments reported by Yousef et al. (2010) and Austad et al. (2015). The list of experiments and simulations performed in this study is given in Table 1. Note that most reaction constants for the equations reported in Table 4 were taken from the literature[20,24,25].

In this section, simulation results obtained with the proposed mechanistic model will be discussed. The results of the single-phase static experiments were used to calibrate the model, since most databases are not very accurate at the experimental conditions of high temperature and salinity used in this study. Once the model was calibrated, it was used to model single-phase transport experiments, zeta potential measurements and oil recovery experiments.

6.2.1 Modeling of single-phase static experiments

The results obtained from the model for single-phase static experiments are given in Table 6.6. These results were obtained by running the model in IPHREEQC, rather than UTCHEM-IPHREEQC, for simplicity. The concentrations of potential determining ions are presented. From Table 6.6, it can be seen that no change in formation brine composition was observed in the experiments or simulations. An increase in calcium concentration and a decrease in magnesium concentration was observed in case of seawater. The model results agree well with the experimental results. Similarly, reasonable agreement between experimental and modeling results was observed for other

cases, that is, SW/2, SW/50 and 4S-SW. Calcite dissolution and dolomitization reactions were mainly responsible in bringing the observed changes in brine compositions in these cases. The contribution of calcite dissolution was, however, smaller compared to dolomitization.

6.2.2 Modeling of single-phase transport experiments

The single-phase transport experiments, shown previously, were simulated with the proposed model in UTCOMP-IPHREEQC. The calibrated model, obtained after modeling single-phase static experiments, was used to model these experiments. The concentrations and normalized concentrations (normalized between injected and produced ions at the end of experiment) of individual effluent ions are plotted as a function of the pore volume injected.

Case D-1 (Seawater displacing formation brine):

The model was used to simulate the experimental results obtained from experiment B-1.1. A limestone core initial saturated with formation brine was displaced with seawater at 120 °C. The comparison of concentrations and normalized concentrations of individual ions obtained from the model and the experiment B-1.1 are shown in Figures 6.2 and 6.3, respectively. From these results, it can be seen that, besides calcite dissolution and dolomitization, sulfate adsorption was also an important reaction in this case. A good agreement was observed between the experimental and modeling results.

Case D-2 (SW/50 displacing SW):

The results obtained from experiment B-1.2 were modeled next. In this case, the seawater from experiment B-1.1 was displaced with SW/50 and effluent ions were measured. A comparison of the results obtained from the model and the experiments are shown in Figures 6.4 and 6.5, respectively. From these results, some key observations can be made. The effluent ions, except sodium and chloride, did not reach to a steady state even after injecting 2.5 pore volumes. The concentration of calcium, magnesium and sulfate ions decreased slowly in the effluent ions suggesting that the reactions occurring in this step were reversing the changes made to surface in the previous step when seawater was injected. Although the effluent ions did not reach a steady state, normalizing effluent ions between the injected concentrations and concentrations obtained at 2.5 PV show that sulfate ions were lagging behind other ions, possibly due to a slow desorption of ions adsorbed during seawater injection. Figures 6.4 and 6.5 show that good agreement between experimental and modeling results.

Case D-3 (4S-SW displacing Seawater):

In this case, the experimental results obtained from experiment B-3.2 was modeled. A comparison of modeling results with experimental data is shown in Figures 6.11 and 6.12, respectively. It can be observed from the results that, unlike the previous case, the effluent ions reach to steady state values after 2.5 pore volumes. A good agreement was observed between the effluent ions obtained from the experiment and model.

6.2.3 Modeling of zeta potential of calcite in low salinity brines

Surface potential results obtained from the model were compared with the zeta potential data reported in the literature. The intent of this work was not to compare the actual values, but to understand if the model was able to explain the changes observed on the surface on bringing it in contact with different brines. A comparison of surface potential obtained from the model and the zeta potential measurements reported by Zhang and Austad (2006) and Mahani et al. (2015) are shown in Figures 6.14 and 6.15, respectively. Zhang and Austad (2006) observed an increase and a decrease in zeta potential of calcite surface on addition of magnesium and sulfate ions, respectively. From Figure 6.14, it can be seen that the surface potential results obtained from the model (solid lines) agreed well with the zeta potential measurements. Mahani et al. (2015) observed lower zeta potential was observed in seawater and SW/25 compared to formation brine (Figure 6.15). The model results showed similar trend. It can be observed from Figures 6.14 and 6.15 that the surface reactions included in the model are able to make reasonable predictions of calcite surface potential in presence of different brines.

6.2.4 Modeling of oil recovery experiments

The model was used to simulate oil recovery experiments reported by Yousef et al. (2010) and Austad et al. (2015). The list of experiments modeled is given in Table 6.1. The brine injection sequences for each experiment is also shown in Table 6.1. The core properties, oil viscosity, temperature, and brine compositions are given in Tables 6.7-6.9.

In experiment F-1.1, an oil wet carbonate core was flooded with seawater followed by its dilutions. Incremental oil recovery was observed on injected SW/2 and SW/10, however, not much oil was recovered on injecting SW/20 and SW/100. The model predicted reduction in the amount of acid adsorbed on the surface on injecting seawater and its dilutions as shown in Figure 6.16 (a). A good comparison was obtained between simulations and experimental results shown in Figure 6.16 (b). Experiment F-1.2 was similarly performed in a different set of cores from the same reservoir and observed incremental oil recovery on injecting dilutions of seawater, similar to experiment F-1.1. Similar to the previous case, a reduction in surface acid concentration was observed on injecting seawater and its dilutions and a good agreement was obtained between experimental and modeling results (Figure 6.17).

Austad et al. (2015) reported oil recovery experiments in limestone cores containing anhydrite. They observed incremental oil recovery even by injecting dilutions of formation brine and postulated the role of sulfate ions, dissolved from anhydrite, in altering the wettability in these cases. The oil recovery experiments, shown in Table 6.1, were simulated and oil recovery data and effluent ions were compared. In experiment F-2.1, the core was first flooded with FW0S followed by SW and SW0Na. Incremental oil recovery was obtained on injecting SW and then SW0Na. It was shown in this experiment by the authors that removing sodium ions helped in further improving oil recovery because potential determining ions could interact easily with the surface. The model showed reduction in surface concentration of naphthenic acids on injecting SW and SW0Na and showed good agreement with the experimental results as shown in

Figures 6.18 (a) and 6.18 (b), respectively. In experiment F-2.2, incremental oil recovery was observed even on injecting dilution of formation brine containing no sulfate ions (FW0S/100) because sulfate ions were dissolved from anhydrite. The model results were in agreement with the experimental observations and showed reduction in surface concentration of naphthenic acids due to the interaction of sulfate ions obtained from anhydrite as shown in Figure 6.19 (a). A good agreement between experimental and modeling oil recovery results was obtained as shown in Figure 6.19 (b). In experiment F-2.3, an oil wet core was first flooded with FW0S followed by SW and SW/10 which showed incremental oil recovery. The model predicted reduction in surface acid concentration on injecting SW and SW/10 as shown in Figure 6.20 (a). A good agreement was observed between the experimental and modeling oil recovery results (Figure 6.20 (b)). Similarly, in experiments F-2.4 and 2.5, the cores were first flooded with FW0S brine followed by SW/10 and SW/30, respectively and incremental oil recovery was observed. The model showed decrease in surface acid concentration on injecting SW/10 and SW/30 following FW0S and good agreement was observed between experimental and modeling oil recovery results (Figure 6.21). The effluent ions obtained from experiments F-2.4 showed reasonable agreement with the modeling results (Figure 6.22). Critical parameters used for modeling these oil recovery corefloods are given in Tables 6.9-6.16.

A summary of the experiments and simulations on wettability alteration is given below:

1. Single-phase static experiments showed dolomitization reaction to occur in various low salinity brines. In addition, the experiments showed that the higher calcium concentration in the equilibrated samples was mainly due to dolomitization. The contribution of calcite dissolution was much smaller.

2. Single-phase injection of seawater in limestone cores, initially saturated with formation brine, showed a delay in sulfate ions relative to other ions. This delay was attributed to the adsorption of sulfate ions on limestone surface at high temperature. In addition, dolomitization and calcite dissolution reactions were observed similar to the static experiments. The injection rate of 1 ft/d was slow enough to bring the system.

3. Injection of fifty-times-diluted seawater in cores initially flooded with seawater showed a delay in potential determining ions to reach a steady state. Sodium and chloride ions reached to their respective injected concentration in 1.5 pore volumes. However, the concentration of calcium, sulfate and magnesium ions remained much higher than their injected concentrations and kept decreasing slowly. No steady state was achieved even after injecting more than 3 pore volumes.

4. Seawater with four-times-sulfate (4S-SW) showed precipitation of anhydrite on heating up to 120 °C. Injection of 4S-SW brine in a limestone core, initially flooded with seawater, showed a delay in sulfate ions, similar to that of seawater. However, the extent of delay was much less than that of seawater. In addition, dolomitization and calcite dissolution reactions was observed.

5. A mechanistic model was developed in UTCHEM-IPHREEQC for low salinity wettability alteration in carbonates by taking into account the relevant geochemistry; aqueous reactions, solid reactions and surface reactions. Calcite surface was assumed to consist of positive calcium and negative carbonate sites. The interaction of potential determining ions with these sites was considered assuming the local equilibrium.

6. The equilibrium constants of reactions were the values reported in the literature and PHREEQC.dat, the geochemical database. A good agreement was observed between the results of the static experiments and the model.

7. Local equilibrium assumption was found to be valid for modeling the single-phase transport experiments. A good agreement was observed between the simulations and single-phase transport experiments. The number of sites per unit area was used as the matching parameter; the number of sites were varied between 2-4 sites/nm^2.

8. The zeta potential data of calcite reported in the literature was modeled and a good agreement was observed with the simulation results. A lower zeta potential was observed in the presence of low salinity brines. The model was able to account for the surface changes in the presence of low salinity brines.

9. The oil recovery corefloods reported in the literature were modeled. The wettability of the surface was assumed to depend on the surface concentration of acids. A good agreement was observed between the experimental data and the simulation results.

Table 6.1: List of experiments and simulations

Experiments	
A	Static interactions of crushed limestone with (1) Formation brine (2) Seawater (3) Twice-diluted seawater (SW/2) (4) Fifty-times-diluted seawater (SW/50) (5) Four-times-sulfate seawater (4S-SW) at 120 °C
B	Single-phase corefloods in a limestone core at 120 °C (1.1) Seawater displacing formation brine (1.2) SW/50 displacing seawater (2.1) Seawater displacing 0.1% NaCl brine (2.2) SW/50 displacing seawater (3.1) Seawater displacing formation brine (3.2) 4S-SW displacing seawater
Simulations	
C	Comparison of modeling results with results of static experiments A1-A5
D	Comparison of modeling results with results of single-phase brine experiments (1) Comparison with experiment B-1.1 (2) Comparison with experiment B-1.2 (3) Comparison with experiment B-3.2
E	Modeling of zeta potential data reported by Zhang and Austad (2006) and Mahani et al. (2015)
F	Modeling of oil recovery experiments reported in the literature (1) Diluted SW corefloods reported by Yousef et al. (2010) (1.1) First coreflood using SW and its dilutions (1.2) Second coreflood using SW and its dilutions (2) Oil recovery experiments in anhydrite containing cores reported by Austad et al. (2015) (2.1) Coreflood using FW0S, SW, SW0Na (2.2) Coreflood using FW0S followed by FW0S/100 (2.3) Coreflood using FW0S, SW, SW/10 (2.4) Coreflood using FW0S followed by SW/10 (2.5) Coreflood using FW0S followed by SW/30

Table 6.2: Composition of brines used in static and single-phase corefloods

Ions/Concentration (ppm)	Formation Brine (FB)	Seawater (SW)	SW/50	4xSO_4 SW (4S-SW)
Na^+	41,411	12,891	239	9,700
Ca^{2+}	11,686	510	10.2	510
Mg^{2+}	2,763	1,600	29	1,600
SO_4^{2-}	215	3,485	67	13,940
Cl^-	103,002	26,578	501	13,428
TDS	**149,160**	**41,127**	**822**	**41,237**

Table 6.3: Properties of the outcrop limestone core

Core	Diameter (in) x Length (in)	Porosity (%)	Permeability (mD)	XRD Data
Limestone	1.5 x 12	28	20	97.7% Calcite, 0.1 % Dolomite, 1.2% Fluorapatite, 0.3% Quartz, 0.6% Chlorite

Table 6.4: Change in brine composition due to equilibration with crushed limestone at 120 °C

Formation brine					
Ions (ppm)	**Na^+**	**Ca^{2+}**	**Mg^{2+}**	**SO_4^{2-}**	**Cl^-**
Brine composition at 25 °C	41,411	11,686	2,763	215	103,002
Brine equilibrated at 120 °C	40,287	11,235	2,815	214	107,309
Brine equilibrated with crushed limestone at 120 °C	40,207	11,334	2,804	200	106,450
Seawater					
Brine composition at 25 °C	12,891	510	1,600	3,485	26,578
Brine equilibrated at 120 °C	12,378	511	1,600	3,589	26,657

Table 6.4 (continued)

Brine equilibrated with crushed limestone at 120 °C	12,951	894	1,362	3,482	26,972
SW/2					
Brine composition at 25 °C	6,445	255	800	1,742	13,289
Brine equilibrated at 120 °C	6,189	255	800	1,794	13,328
Brine equilibrated with crushed limestone at 120 °C	6,296	470	632	1,668	13,033
SW/50					
Brine composition at 25 °C	257	10	32	531	70
Brine equilibrated at 120 °C	247	10	32	533	72
Brine equilibrated with crushed limestone at 120 °C	294	61	4	546	69
4S-SW					
Brine composition at 25 °C	9,700	510	1,600	13,940	13,428
Brine equilibrated at 120 °C	9,720	221	1,467	12,119	13,428
Brine equilibrated with crushed limestone at 120 °C	9,768	279	1,322	11,843	13,580

Table 6.5: List of important reactions considered in the model. The complete set of reactions are given in PHREEQC database. Only log_k values are given; these values are dependent on temperature and salinity

Aqueous reactions		
1	$HA = H^+ + A^-$	log k= 3.98
2	$Ca^{2+} + A^- = CaA^+$	log k= -2.2
3	$Mg^{2+} + A^- = MgA^+$	log k= -3.3
4	$Ca^{2+} + SO_4^{2-} = CaSO_4$ (aq)	log k= 2.25
5	$Mg^{2+} + SO_4^{2-} = MgSO_4$ (aq)	log k= 2.37
6	$HCO_3^- = H^+ + CO_3^{2-}$	log k= -10.39
7	$CO_3^{2-} + 2H^+ = CO_2 + H_2O$	log k= 16.68
Dissolution/Precipitation reactions		
8	$CaCO_3(s) = Ca^{2+} + CO_3^{2-}$	log k= -8.48
9	$CaMg(CO_3)_2(s) = Ca^{2+} + Mg^{2+} + 2CO_3^{2-}$	log k= -17.09
10	$CaSO_4(s) = Ca^{2+} + SO_4^{2-}$	log k= -4.58
Surface complexation reactions		
11	$>CaH_2O^+ + A^- = >CaH_2OA$	log k= 0.4
12	$>CaH_2O^+ = >CaOH + H^+$	log k= -12.8
13	$>CaH_2O^+ + HCO_3^- = >CaCO_3^- + H^+ + H_2O$	log k= -5.65
14	$>CaH_2O^+ + HCO_3^- = >CaHCO_3 + H_2O$	log k= 1.68
15	$>CaH_2O^+ + SO_4^{2-} = >CaSO_4^- + H_2O$	log k= 3.3
16	$>CO_3^- + H^+ = >CO_3H$	log k= 5.48
17	$>CO_3^- + Ca^{2+} = >CO_3Ca^+$	log k= 1.74
18	$>CO_3^- + Mg^{2+} = >CO_3Mg^+$	log k= 1.74

Table 6.5 (continued)

19	$>CO_3Ca^+ + SO_4^{2-} = >CO_3CaSO_4^-$	log k= 3.3
20	$>CO_3Mg^+ + SO_4^{2-} = >CO_3MgSO_4^-$	log k= 3.3
21	$>CO_3Mg^+ + A^- = >CO_3MgA$	log k = 0.4
22	$>CO_3Ca^+ + A^- = >CO_3CaA$	log k = 0.4

Table 6.6: Comparison of static experimental results with modeling results on equilibration brines with crushed calcite at 120 °C

FB			
Ions	**Ca^{2+}**	**Mg^{2+}**	**SO_4^{2-}**
Experimental results	11334	2804	200
Model results	11400	2825	207
SW			
Experimental results	894	1,362	3482
Model results	891	1360	3584
SW/2			
Experimental results	470	632	1668
Model results	451	672	1720
4S-SW			
Experimental results	279	1,322	11,843
Model results	273	1423	12100
SW/50			
Experimental results	61	3.8	69
Model results	54	3.5	57

Table 6.7: Core properties and injection sequence during oil recovery corefloods

Experiment	Core dimensions (Diameter x Length) (cm)	Initial oil saturation	Porosity/ Permeability (mD)	Oil viscosity(cP)/ Reservoir temperature (°C)	Core type
F-1.1	3.8 x 16.24	0.89	0.25/39.6	0.716/100	Carbonate
F-1.2	3.81 x 23.65	0.85	0.246/68.3	0.716/100	Carbonate
F-2.1	3.8 x 8.4	0.9	0.25/51	2.03/100	Limestone core with Anhydrite
F-2.2	3.8 x 4.7	0.9	0.28/51	2.03/100	Limestone core with Anhydrite
F-2.3	3.8 x 4.7	0.9	0.28/51	2.03/100	Limestone core with Anhydrite
F-2.4	3.8 x 4.7	0.9	0.28/51	2.03/100	Limestone core with Anhydrite
F-2.5	3.8 x 4.7	0.9	0.28/51	2.03/100	Limestone core with Anhydrite

Table 6.8: Composition of brines (in ppm) used by Yousef et al. (2010)

Ions/Brine	Formation Brine	Seawater
Na^+	59,491	18,300
Ca^{2+}	19,040	650
Mg^{2+}	2,439	2,110
Cl^-	132,060	32,200
SO_4^{2-}	350	4,290
HCO_3^-	354	120
TDS	213,734	57,670

Table 6.9: Composition of brines (in mM) used by Austad et al. (2015)

Ions/Brine	FW0S	SW	SW0Na	FW0S/10	SW/10
Na^+	2577.1	797.5	92	257.7	79.8
Ca^{2+}	475	16	16	47.5	1.6
Mg^{2+}	100	86	86	10	8.6
Cl^-	3721.1	909.5	204	372.1	91
SO_4^{2-}	0	45	45	0	4.5
HCO_3^-	6	2.0	2	0.6	0.2
TDS (mg/L)	213,000	57,760	16,530	21,300	5,776

Table 6.10: Modeling parameters for simulation F 1.1

Parameter	Initial	Final
Kro	0.4	0.8
Krw	0.5	0.2
Sorw	0.17	0.1
Sw	0.1044	0.3
no	3	2
nw	4	1
Surf. acid concentration (mM)	0.95	0.83

Table 6.11: Modeling parameters for simulation F 1.2

Parameter	Initial	Final
Kro	0.4	0.8
Krw	0.5	0.2
Sorw	0.13	0.06
Sw	0.144	0.3
no	2.5	1.5
nw	4	1.5
Surf. acid concentration(mM)	0.945	0.83

Table 6.12: Modeling parameters for simulation F 2.1

Parameter	Initial	Final
Kro	0.4	0.8
Krw	0.5	0.2
Sorw	0.66	0.6
Sw	0.1	0.1
no	3	2
nw	2	1
Surf. acid concentration (mM)	3.8	2.71

Table 6.13: Modeling parameters for simulation F 2.2

Parameter	Initial	Final
Kro	0.4	0.8
Krw	0.5	0.2
Sorw	0.62	0.42
Sw	0.1	0.1
no	3	2
nw	2	1
Surf. acid concentration(mM)	4.0	2.75

Table 6.14: Modeling parameters for simulation F 2.3

Parameter	Initial	Final
Kro	0.4	0.8
Krw	0.5	0.2
Sorw	0.67	0.6
Sw	0.1	0.1
no	3	2
nw	2	1
Surf. acid concentration(mM)	4.0	2.3

Table 6.15: Modeling parameters for simulation F 2.4

Parameter	Initial	Final
Kro	0.2	0.8
Krw	0.8	0.2
Sorw	0.63	0.60
Sw	0.1	0.1
no	3	2
nw	2	1
Surf. acid concentration(mM)	3.9	0.5

Table 6.16: Modeling parameters for simulation F 2.5

Parameter	Initial	Final
Kro	0.4	0.8
Krw	0.5	0.2
Sorw	0.73	0.55
Sw	0.1	0.1
no	3	2
nw	4	1
Surf. acid concentration(mM)	10	0.5

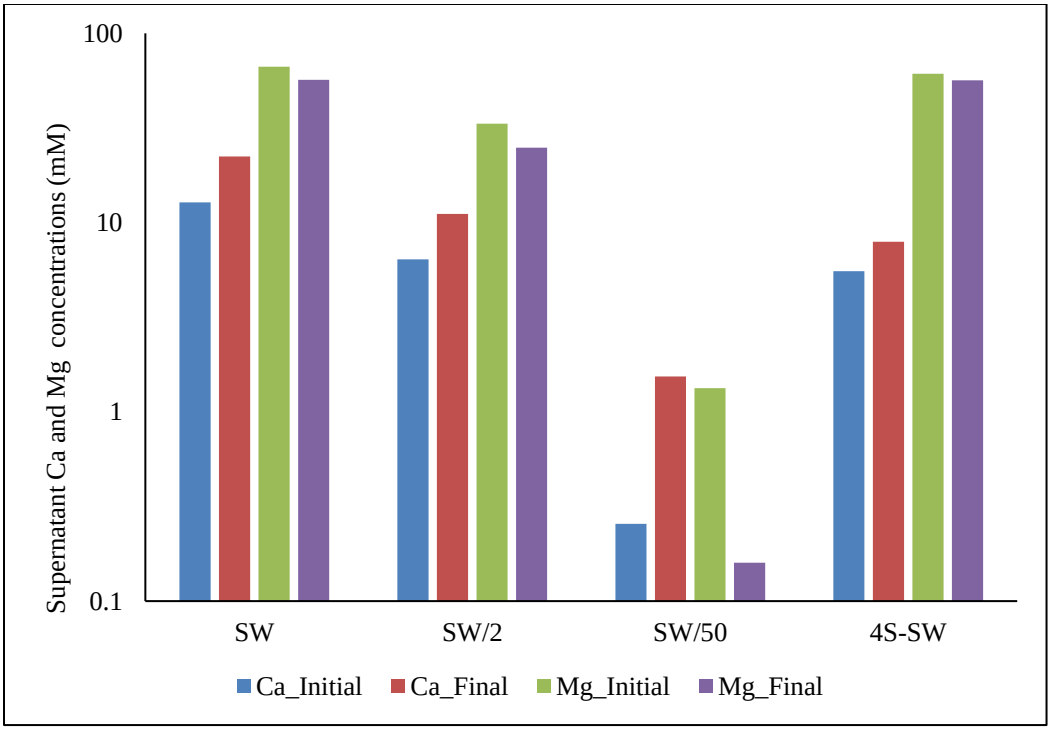

Figure 6.1: Concentration of calcium and magnesium ions after equilibrating at 120 °C with ('Final') and without ('Initial') crushed limestone core.

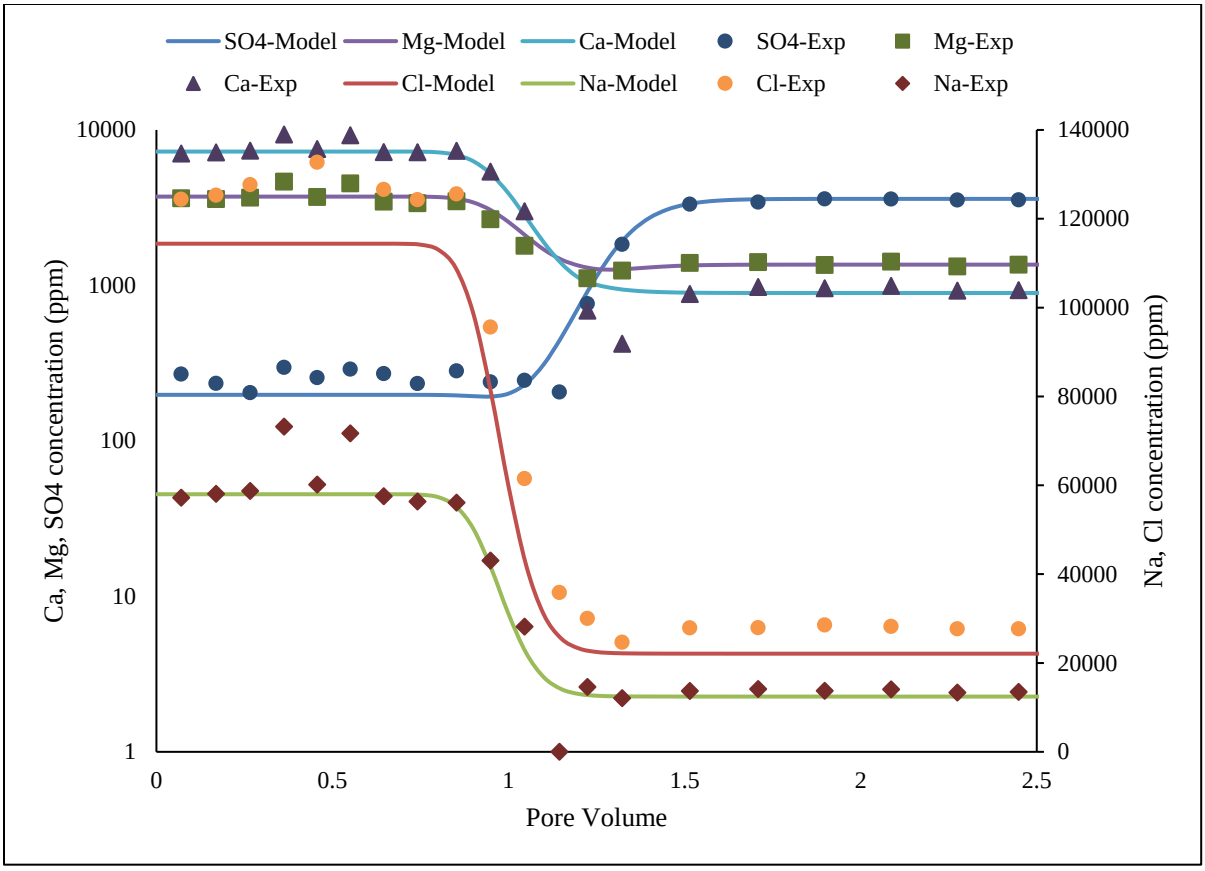

Figure 6.2: Concentration of effluent ions as a function of pore volume when the formation brine was displaced with seawater at 0.5 ft/d through a limestone core at 120 °C

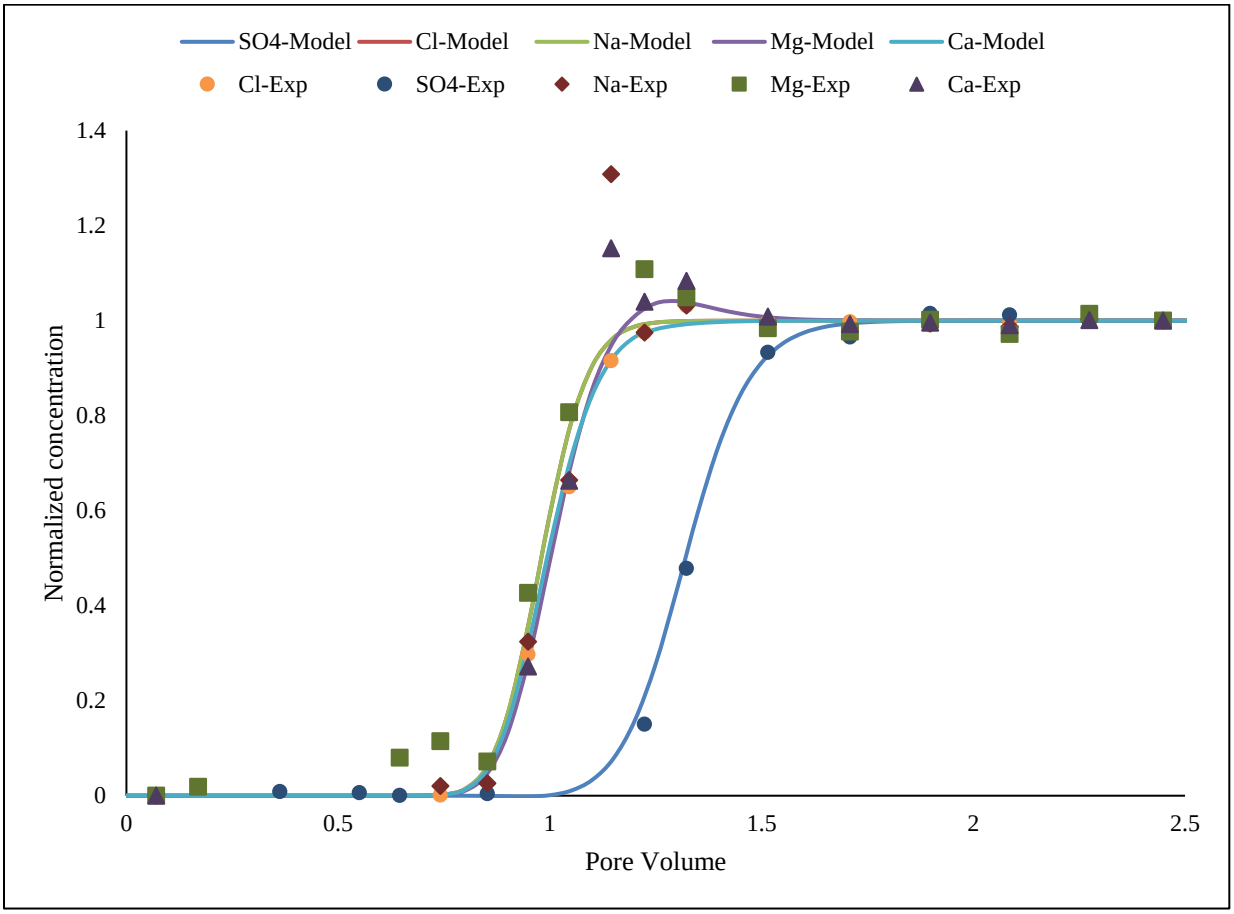

Figure 6.3: Normalized concentration of effluent ions as a function of pore volume when the formation brine was displaced with seawater through a limestone core at 120 °C. The concentrations were normalized between the initial and the injected concentrations

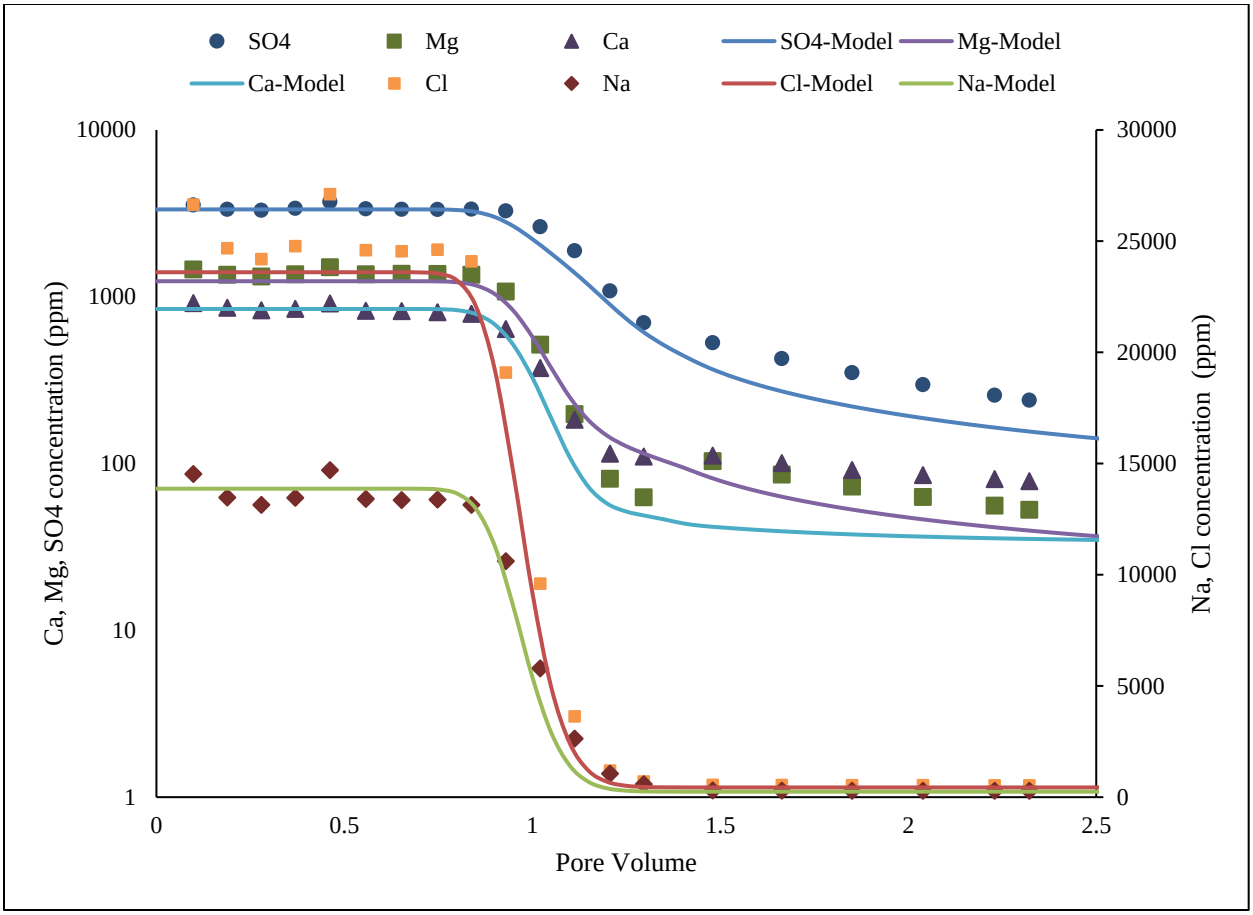

Figure 6.4: Concentration of effluent ions as a function of pore volume when the seawater was displaced with SW/50 at 0.5 ft/d through a limestone core at 120 °C

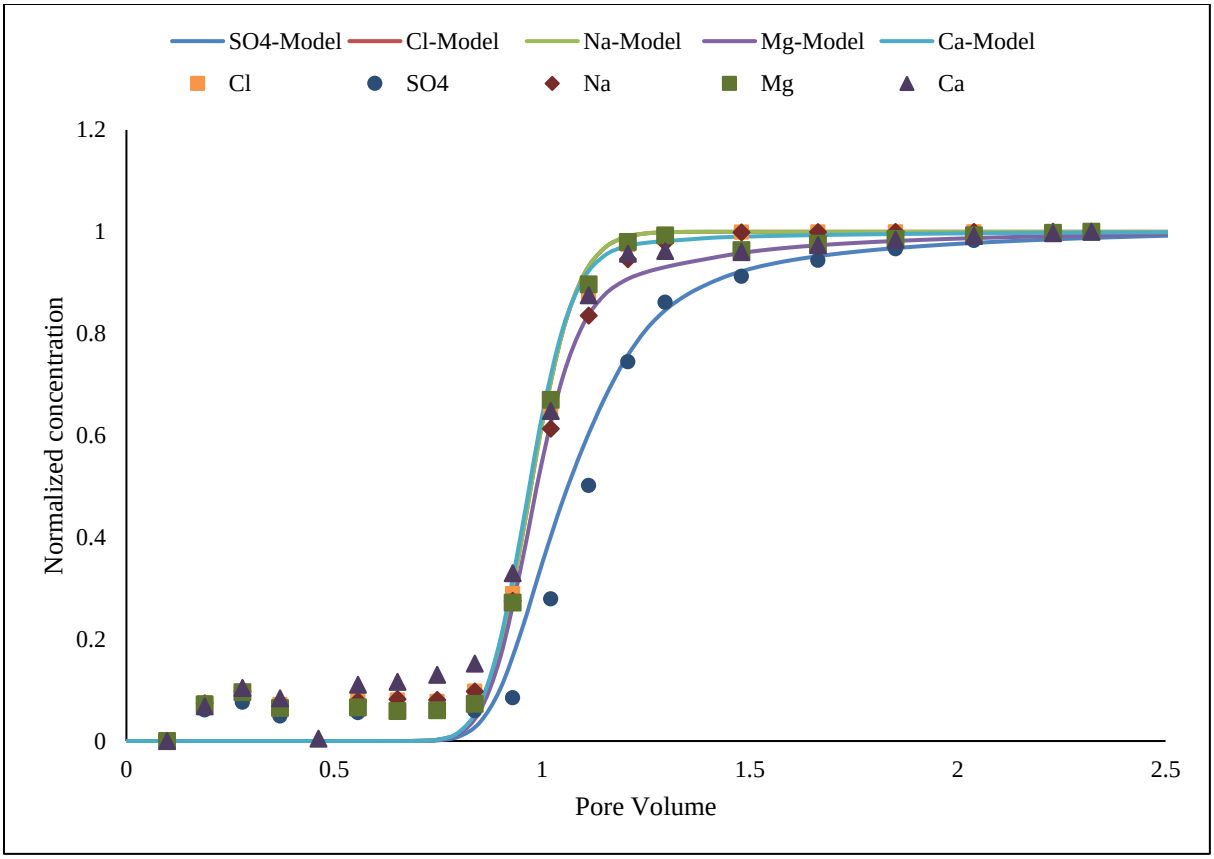

Figure 6.5: Normalized concentration of effluent ions as a function of pore volume when the seawater was displaced with SW/50 through a limestone core at 120 °C. The concentrations were normalized between the initial and the injected concentrations

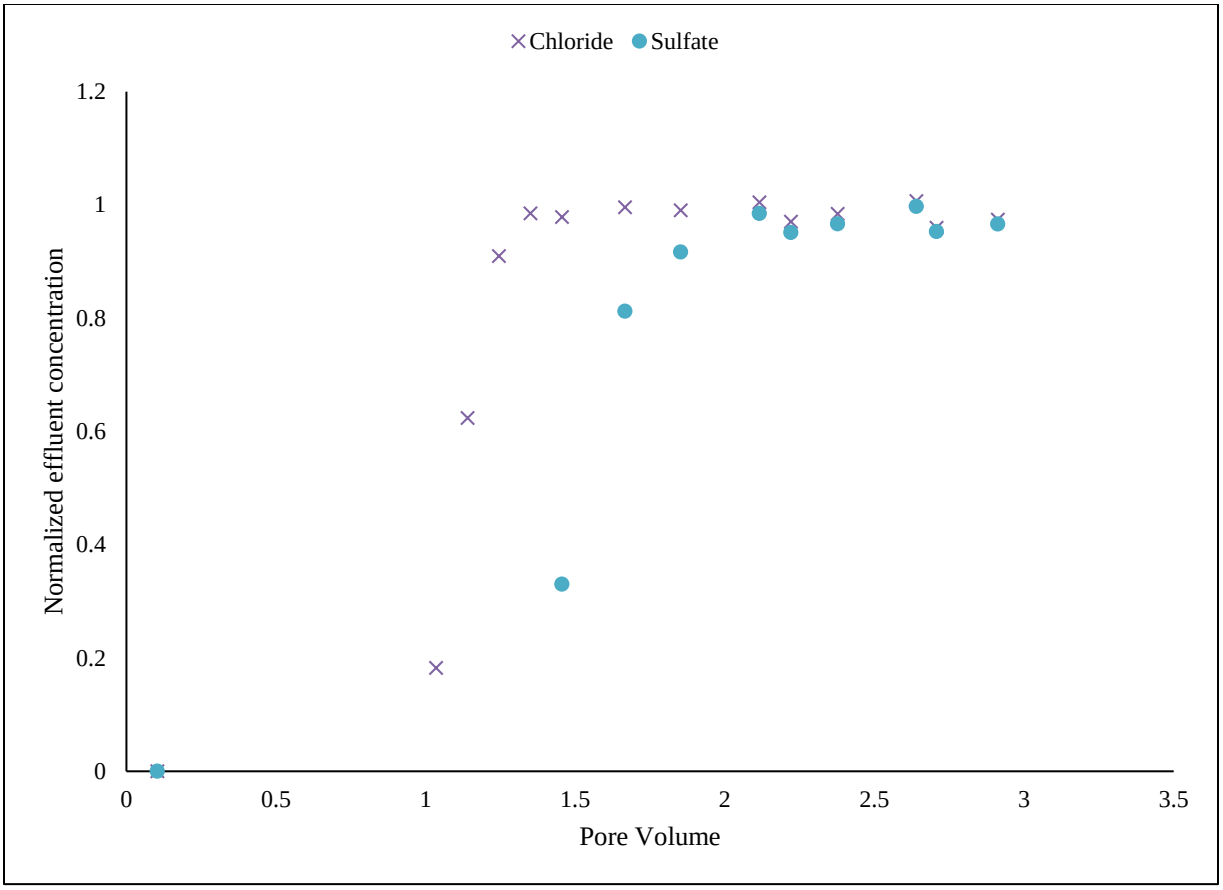

Figure 6.6: Normalized concentration of chloride and sulfate ions as a function of pore volume when the 0.1%NaCl brine was displaced with seawater through a limestone core at 120 °C. The concentrations were normalized between the initial and the injected concentrations

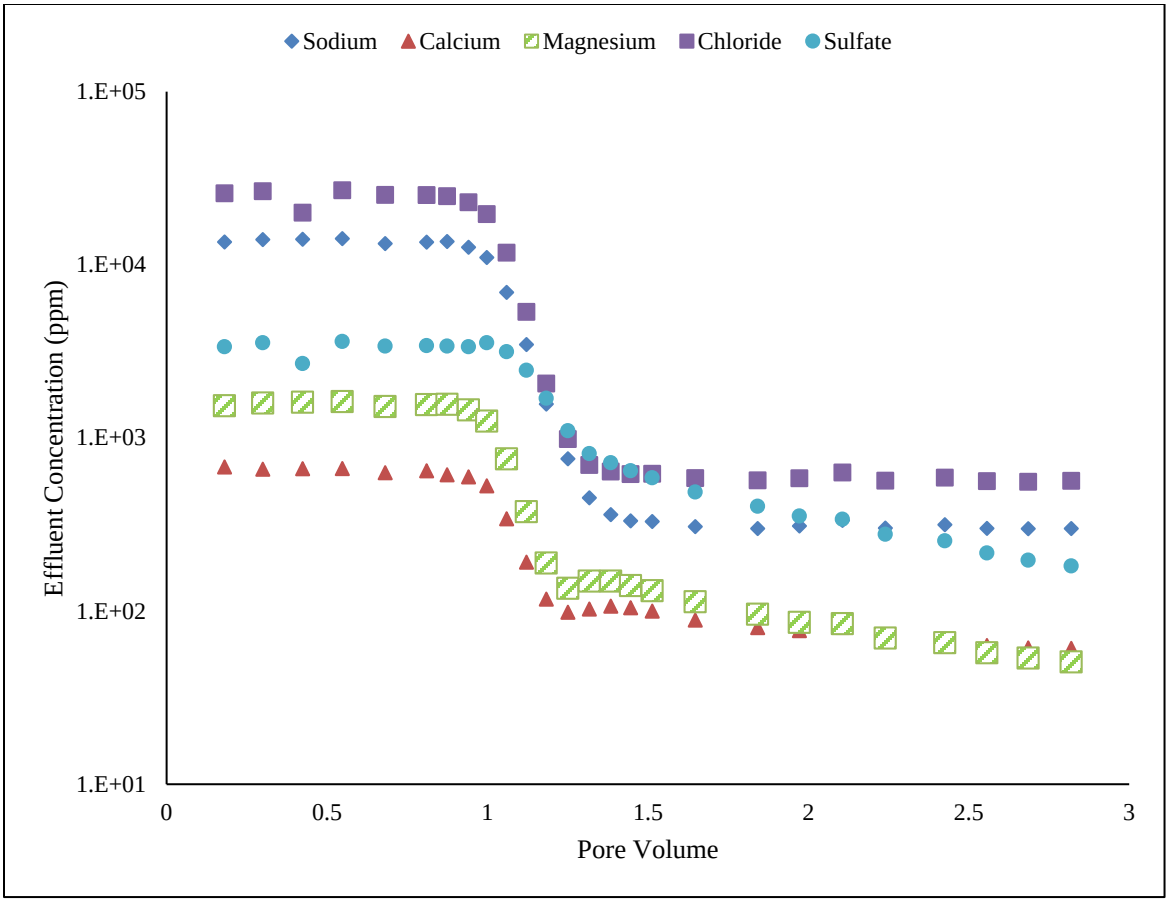

Figure 6.7: Concentration of effluent ions as a function of pore volume when the seawater was displaced with SW/50 brine at 0.5 ft/d through a limestone core at 120 °C

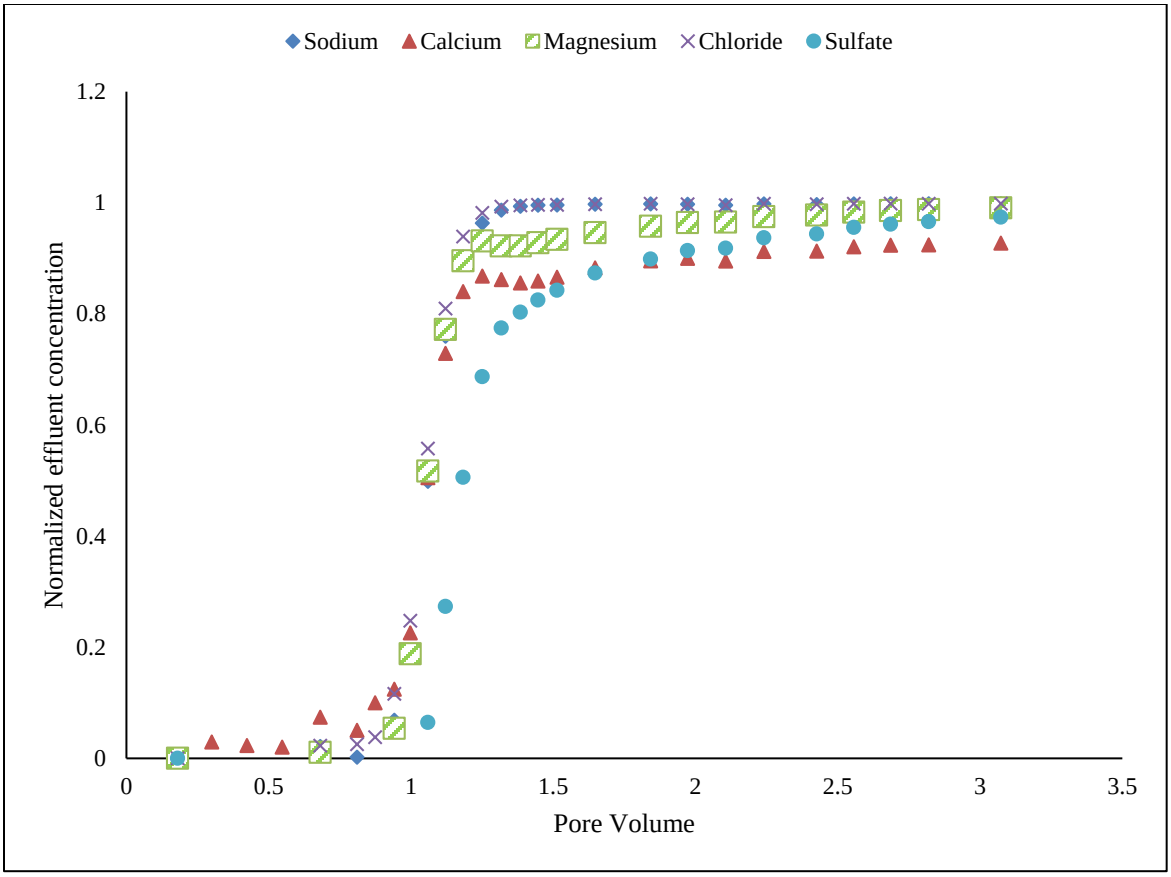

Figure 6.8: Normalized concentration of effluent ions as a function of pore volume when the seawater was displaced with SW/50 brine through a limestone core at 120 °C. The concentrations were normalized between the initial and the injected concentrations

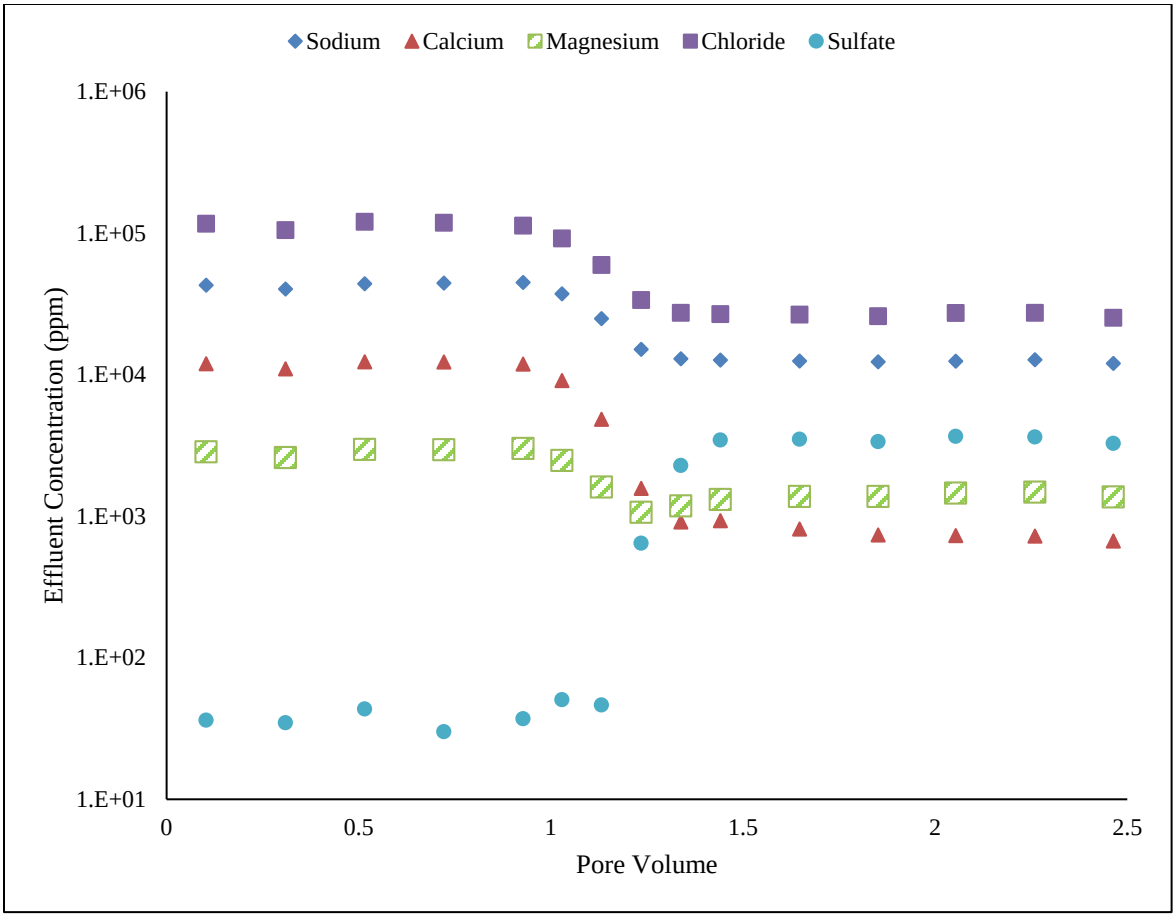

Figure 6.9: Concentration of effluent ions as a function of pore volume when the formation brine was displaced with seawater at 0.5 ft/d through a limestone core at 120 °C

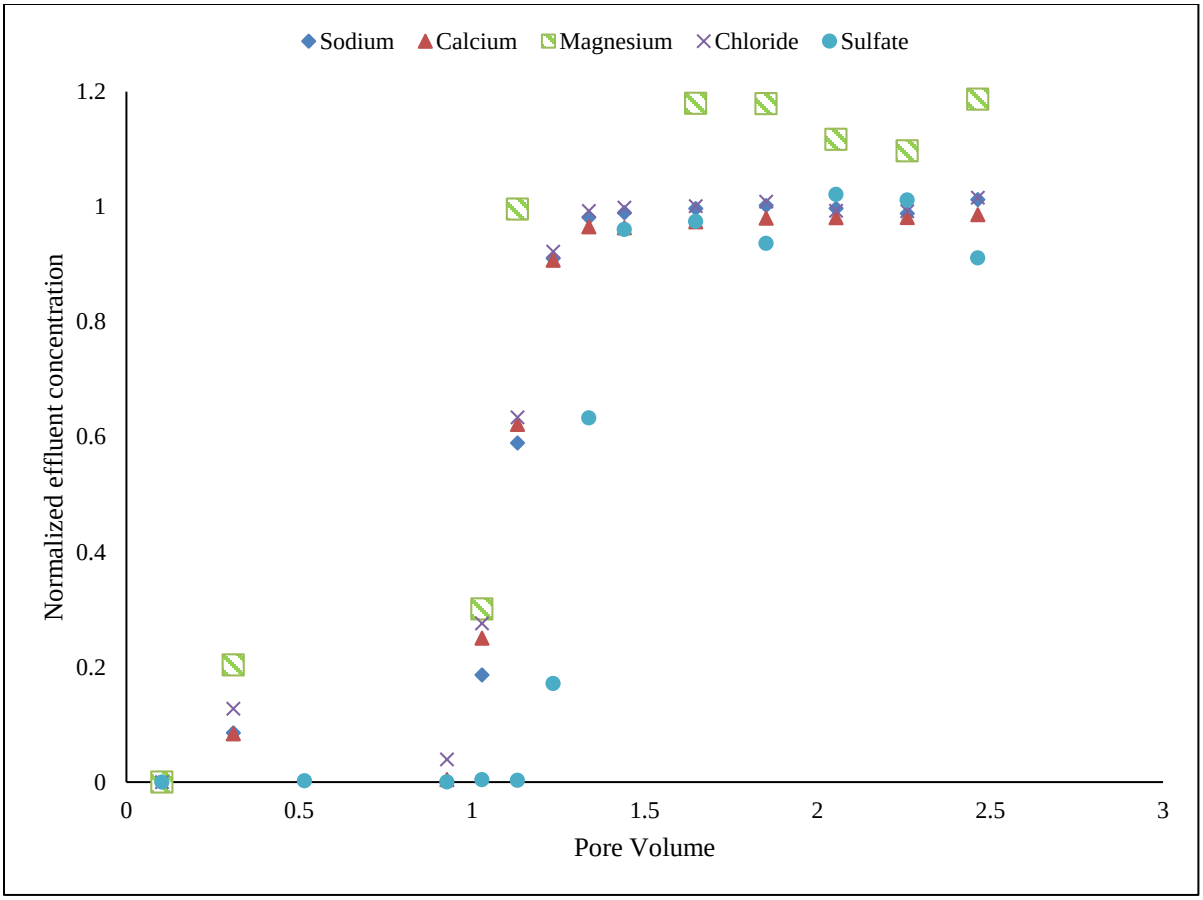

Figure 6.10: Normalized concentration of effluent ions as a function of pore volume when the formation brine was displaced with seawater through a limestone core at 120 °C. The concentrations were normalized between the initial and the injected concentrations

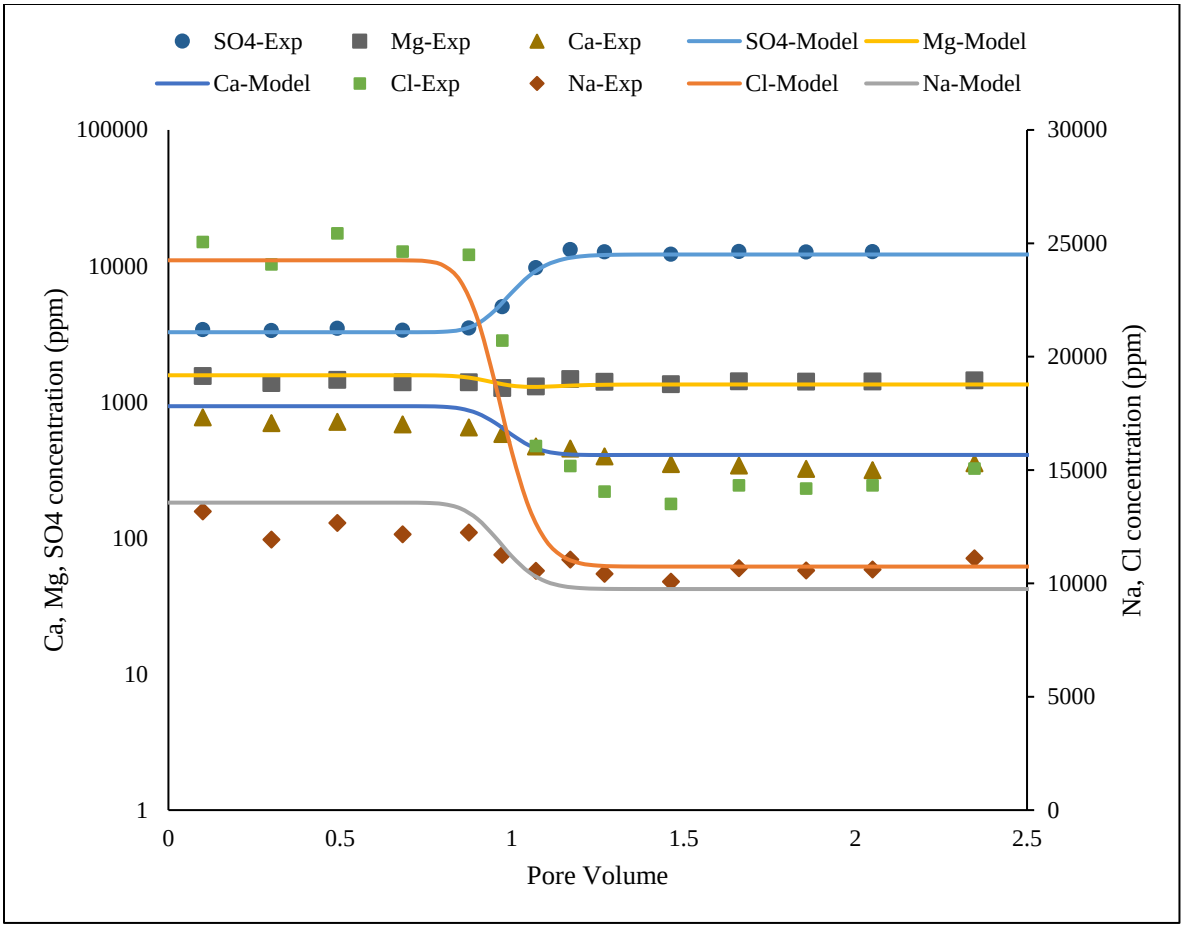

Figure 6.11: Concentration of effluent ions as a function of pore volume when the seawater was displaced with 4S-SW brine at 0.5 ft/d through a limestone core at 120 °C

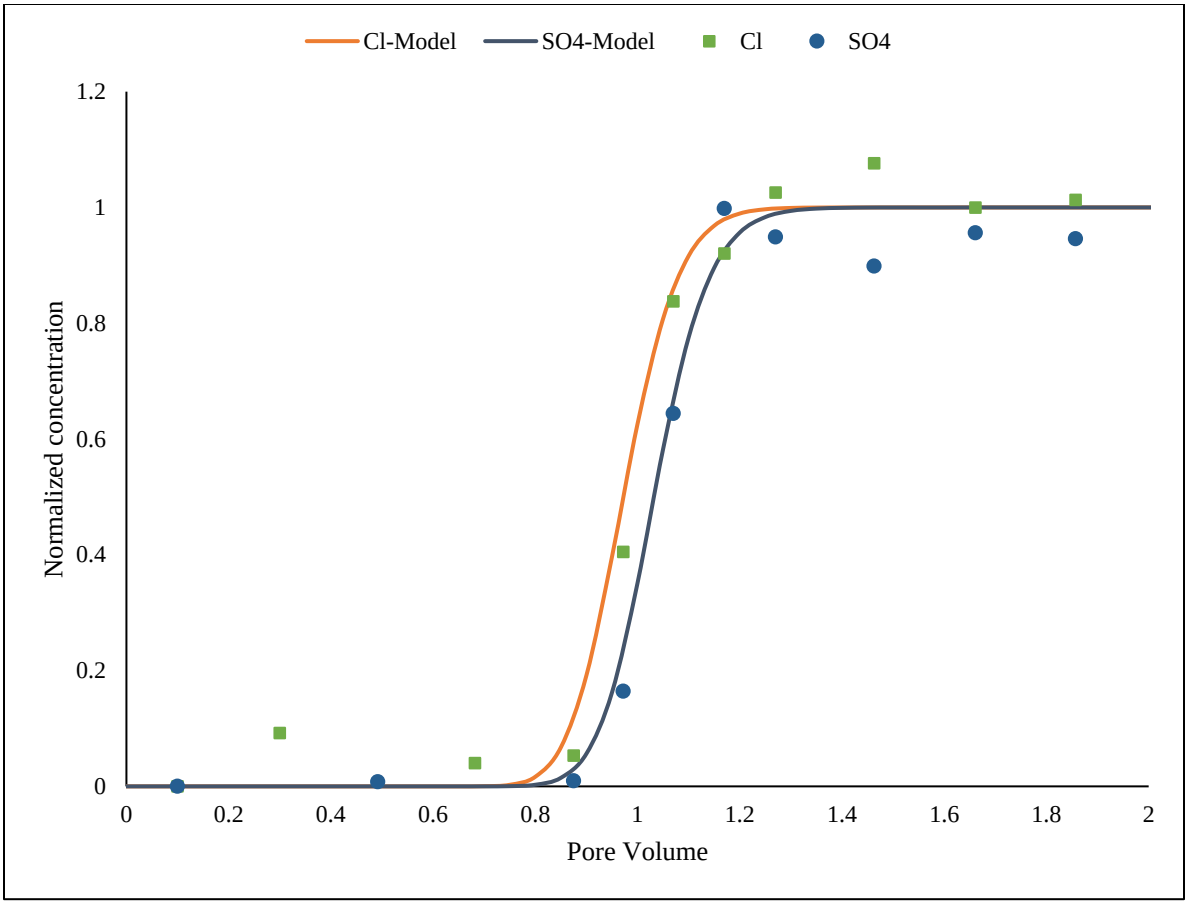

Figure 6.12: Normalized concentration of chloride and sulfate ions as a function of pore volume when the seawater was displaced with 4S-SW brine through a limestone core at 120 °C. The concentrations were normalized between the initial and the injected concentrations

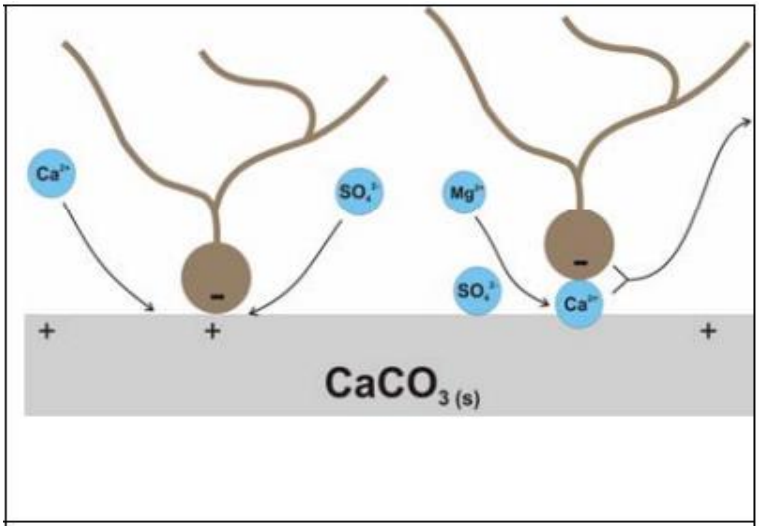

Figure 6.13: Wettability alteration mechanism as postulated by Zhang et al. (2007)

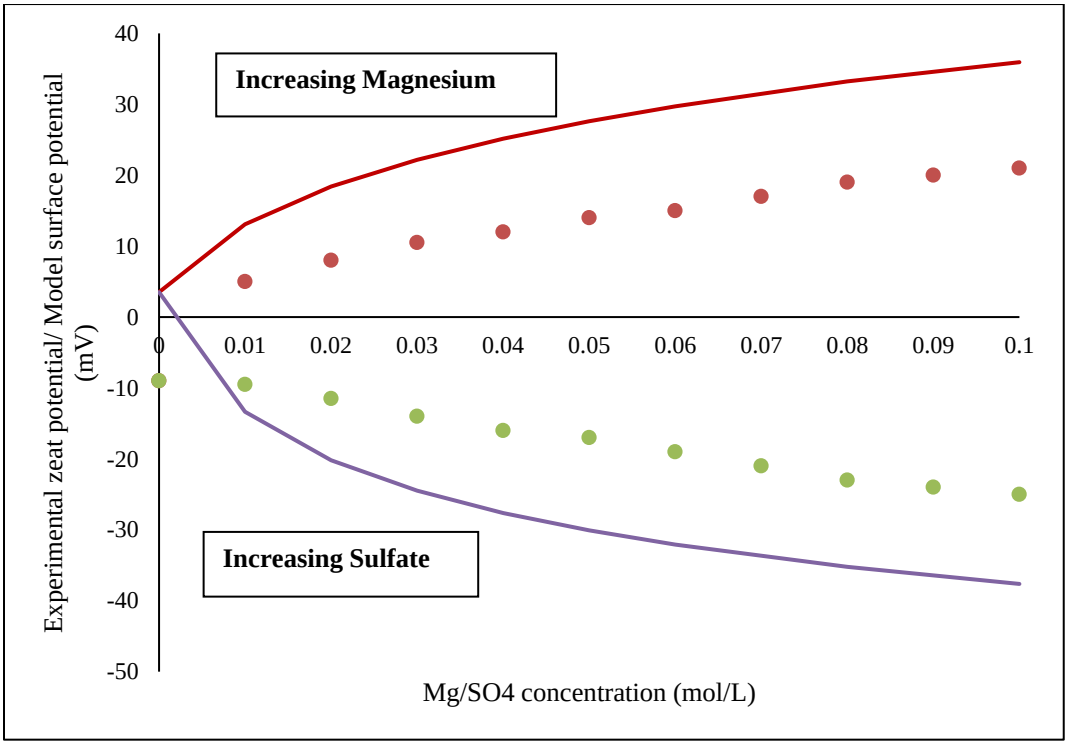

Figure 6.14: Comparison of zeta potential values of calcite in 0.573 NaCl with increasing magnesium and sulfate ions (reported by Zhang and Austad, 2006) with the surface potential values obtained from the model

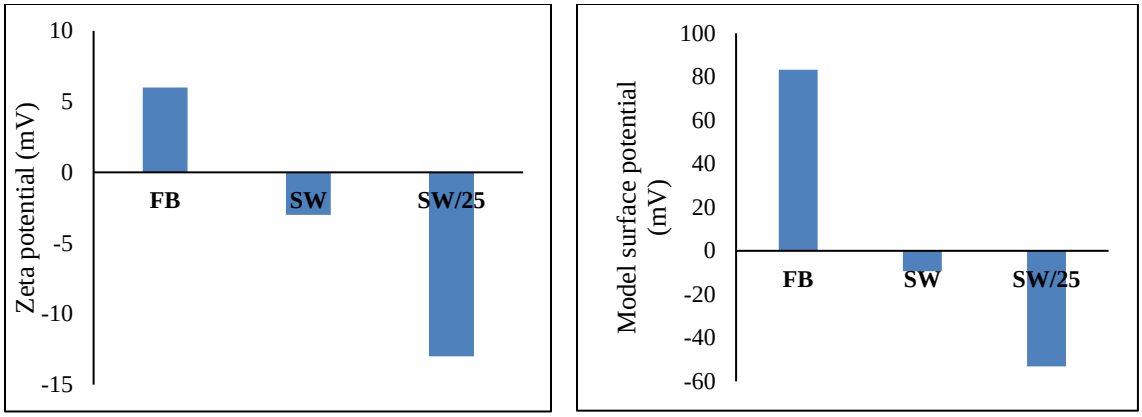

Figure 6.15: Comparison of zeta potential values obtained by Mahani et al., 2015 (left) and the surface potential obtained from model (right)

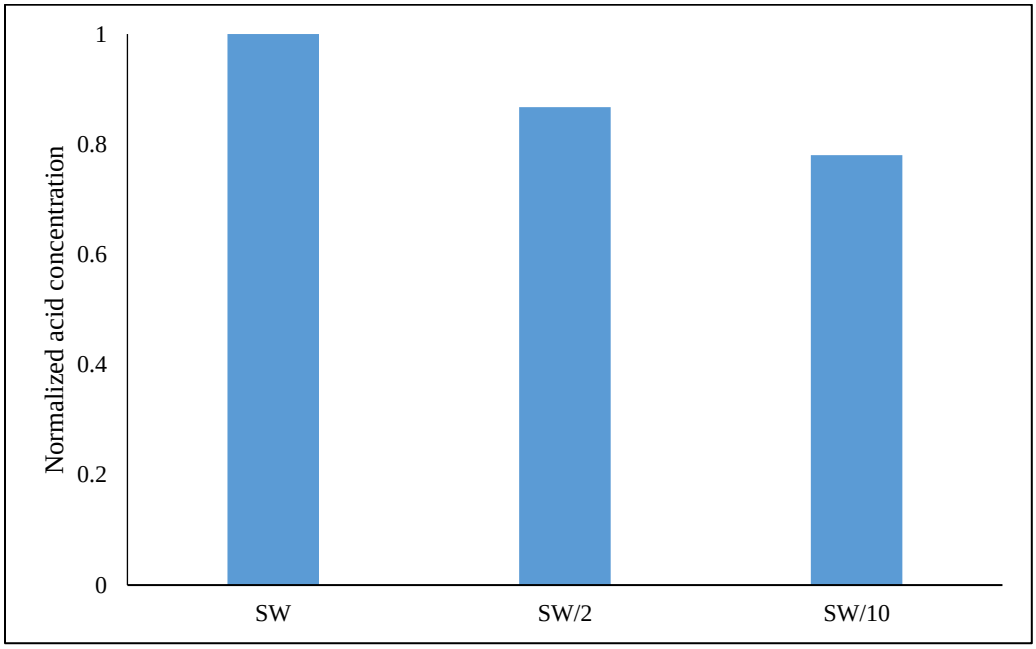

Figure 6.16 (a): Normalized acid concentration on the surface as a function of brine composition

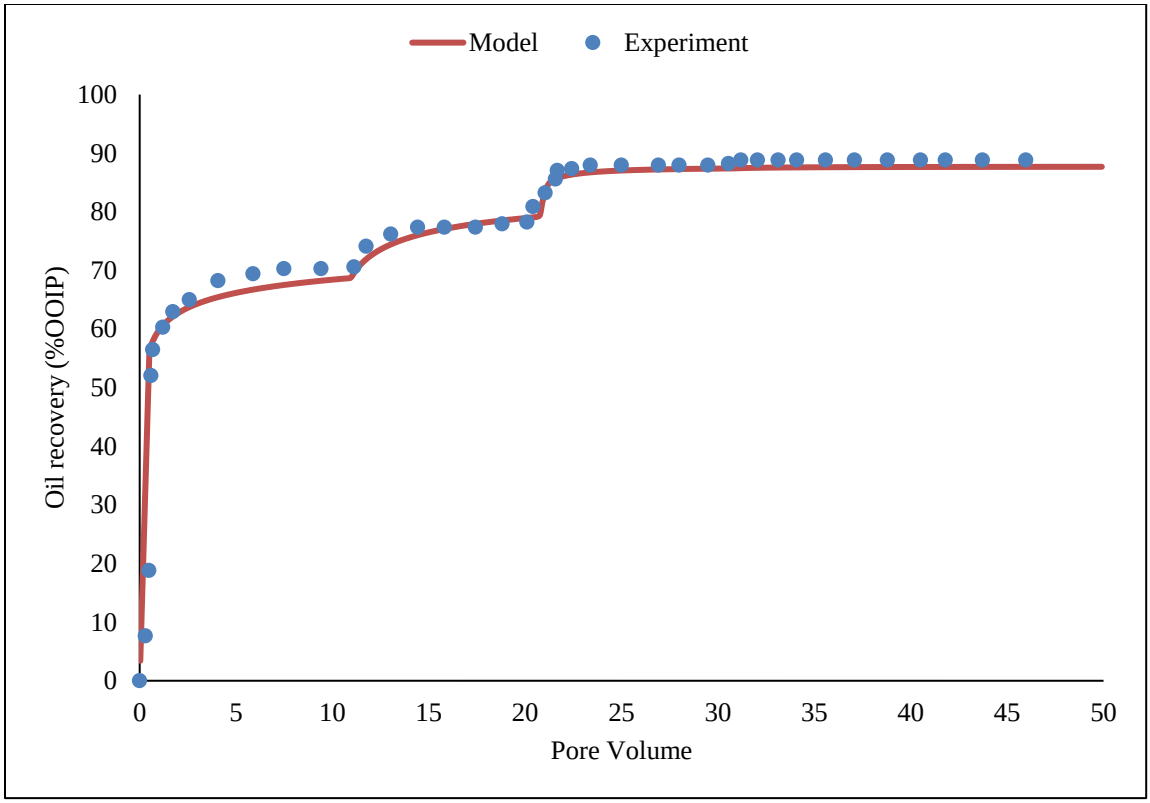

Figure 6.16 (b): Comparison of oil recovery results obtained from simulations with experimental results reported by Yousef et al. (2010)

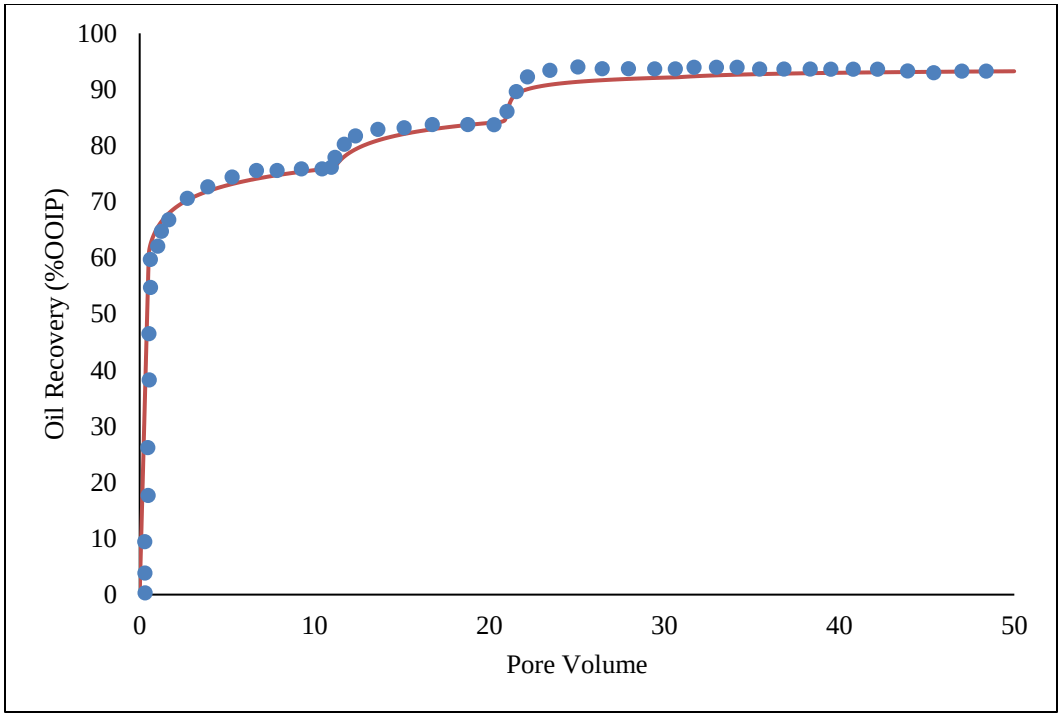

Figure 6.17: Comparison of oil recovery results obtained from simulations with experimental results reported by Yousef et al. (2010)

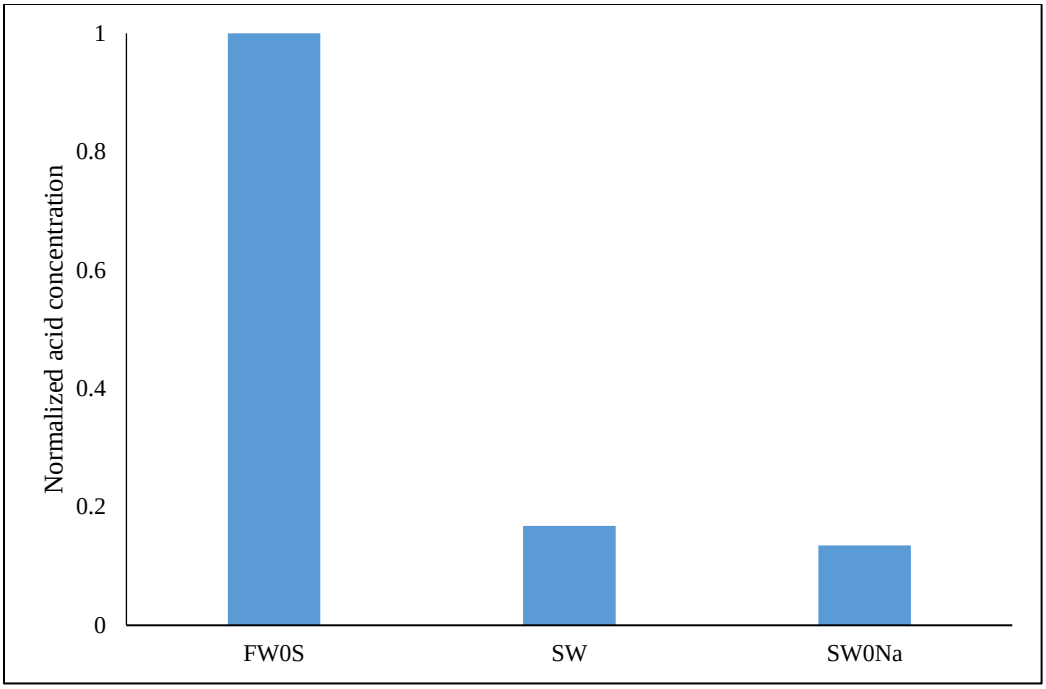

Figure 6.18 (a): Normalized surface acid concentration as a function of brine

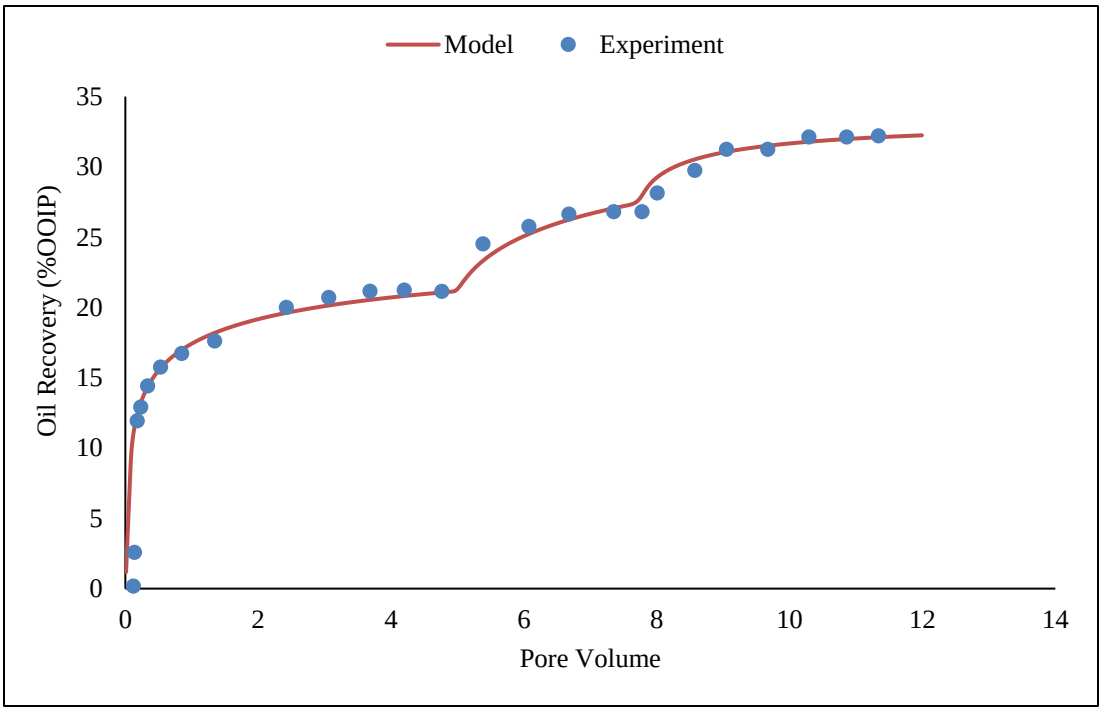

Figure 6.18 (b): Comparison of experimental and modeling oil recovery results for coreflood F-2.1 reported by Austad et al. (2015)

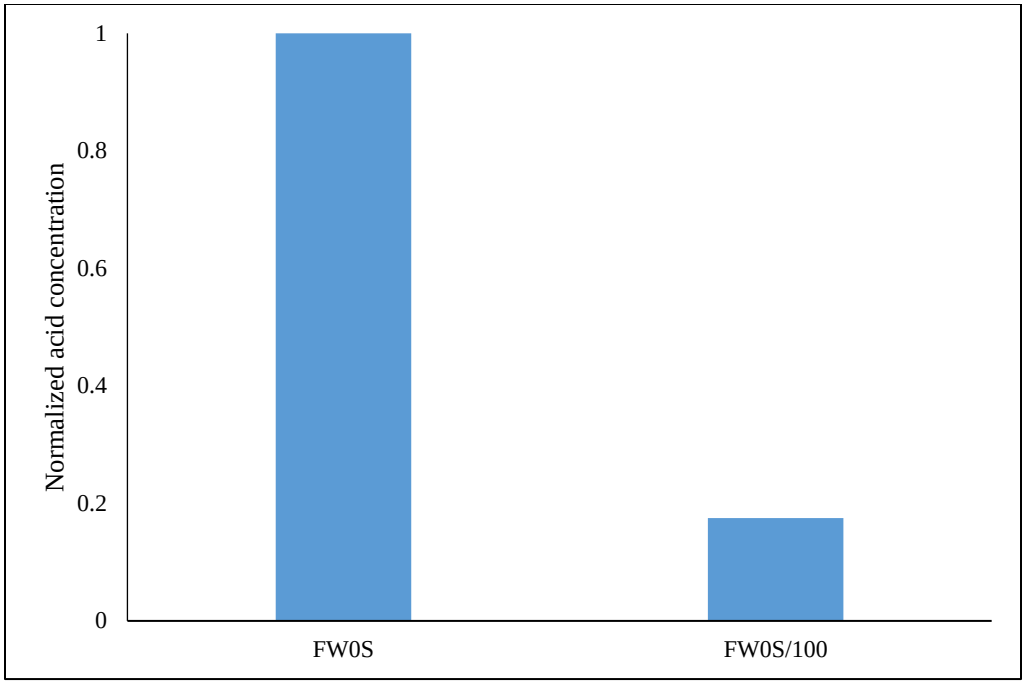

Figure 6.19 (a): Normalized surface acid concentration as a function of brine

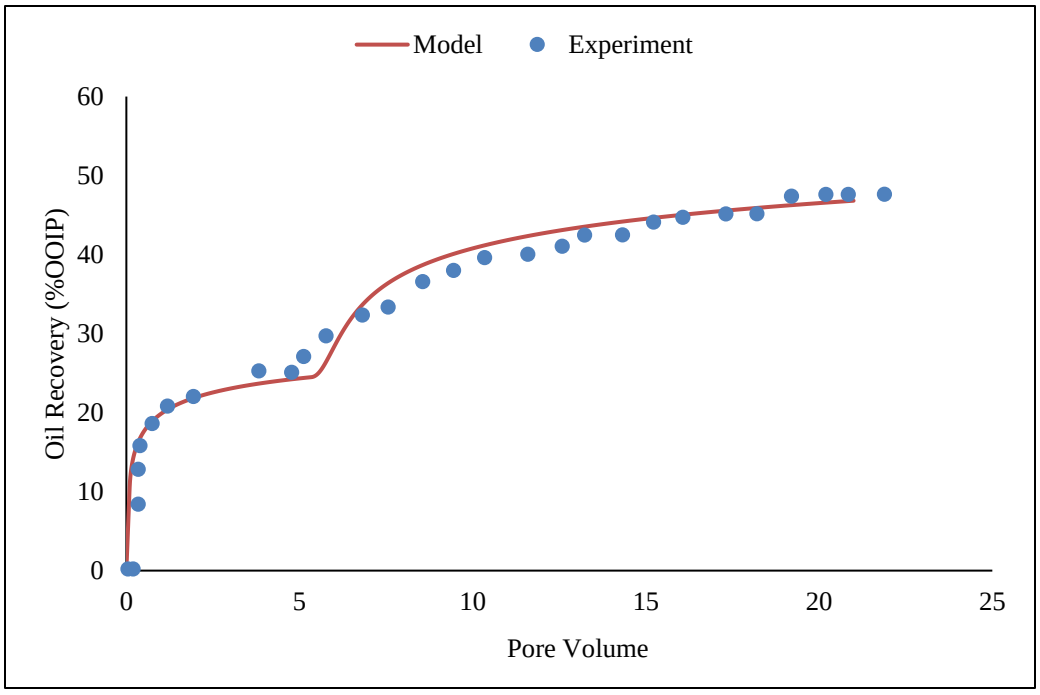

Figure 6.19 (b): Comparison of experimental and modeling oil recovery results for coreflood F-2.2 reported by Austad et al. (2015)

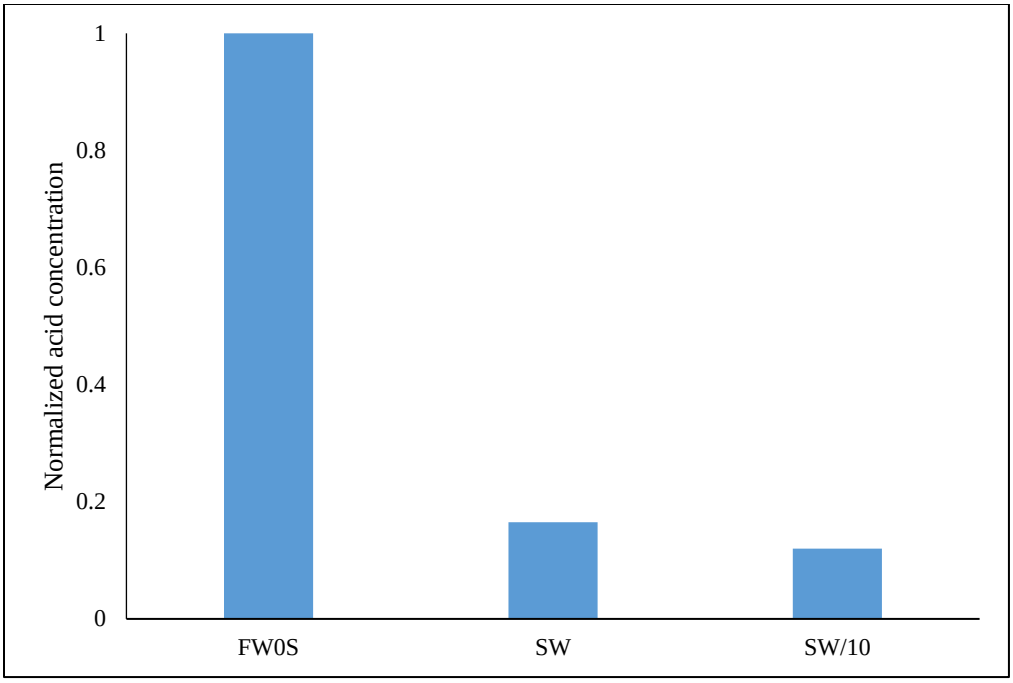

Figure 6.20 (a): Normalized surface acid concentration as a function of brine

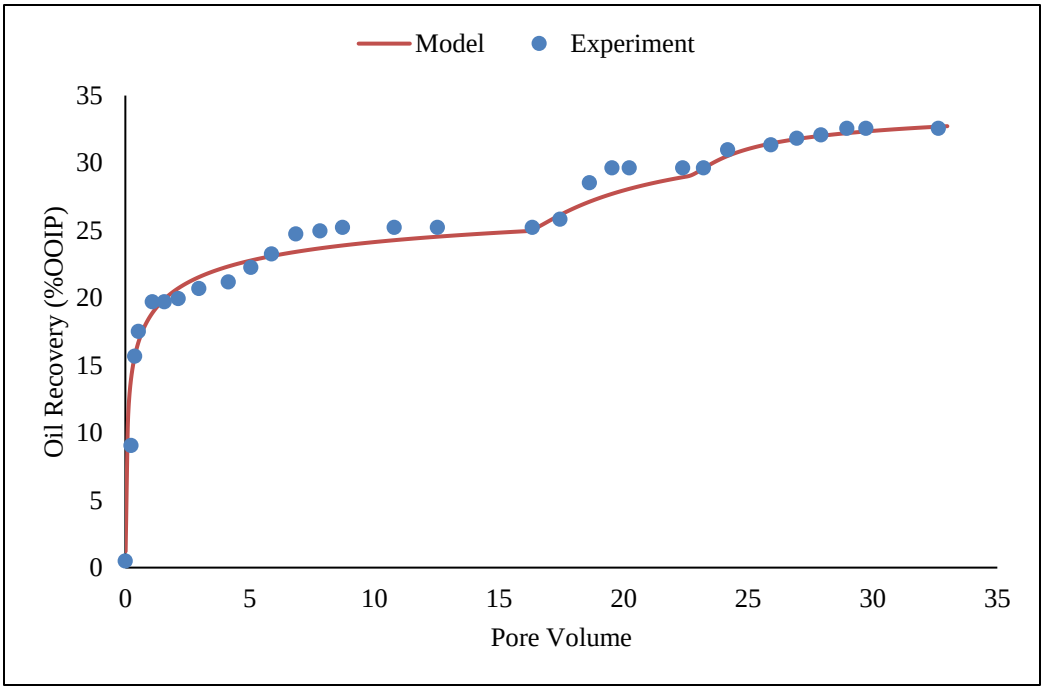

Figure 6.20 (b): Comparison of experimental and modeling oil recovery results for coreflood F-2.3 reported by Austad et al. (2015)

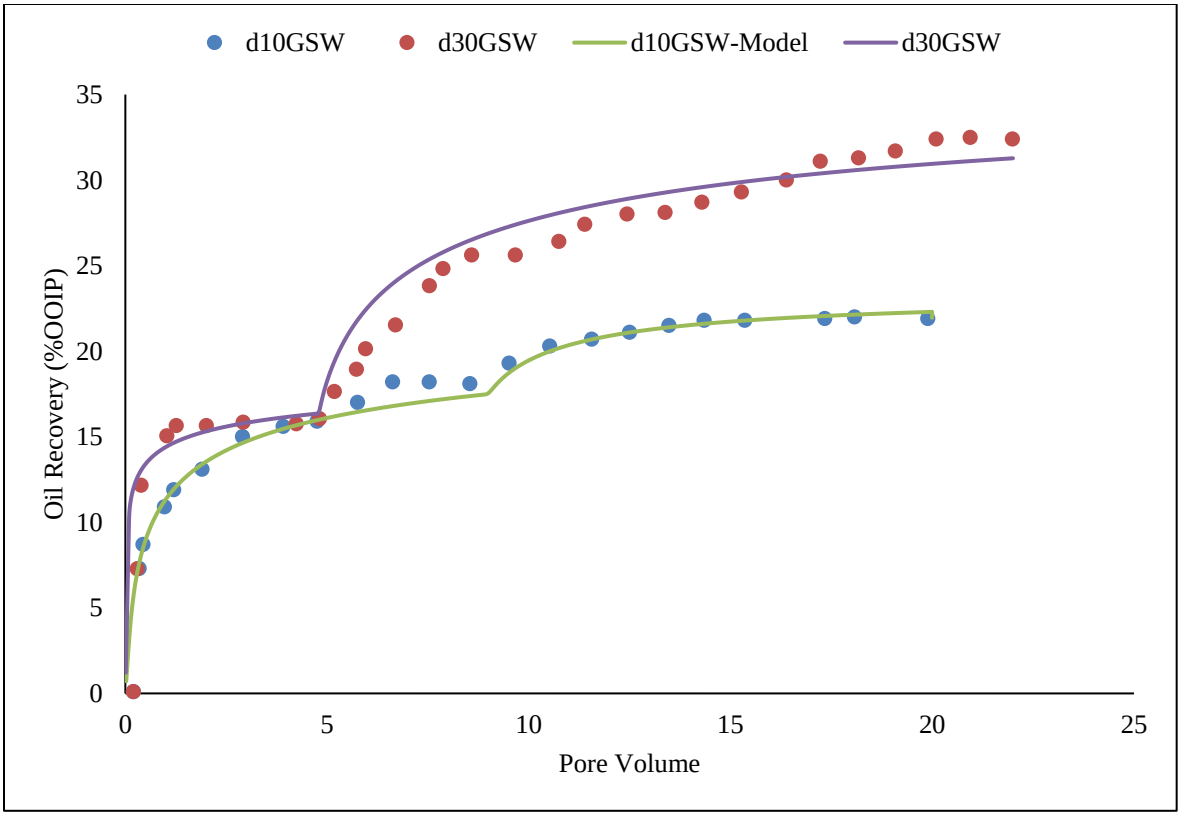

Figure 6.21: Comparison of experimental and modeling oil recovery results for coreflood F-2.4 and F-2.5 reported by Austad et al. (2015)

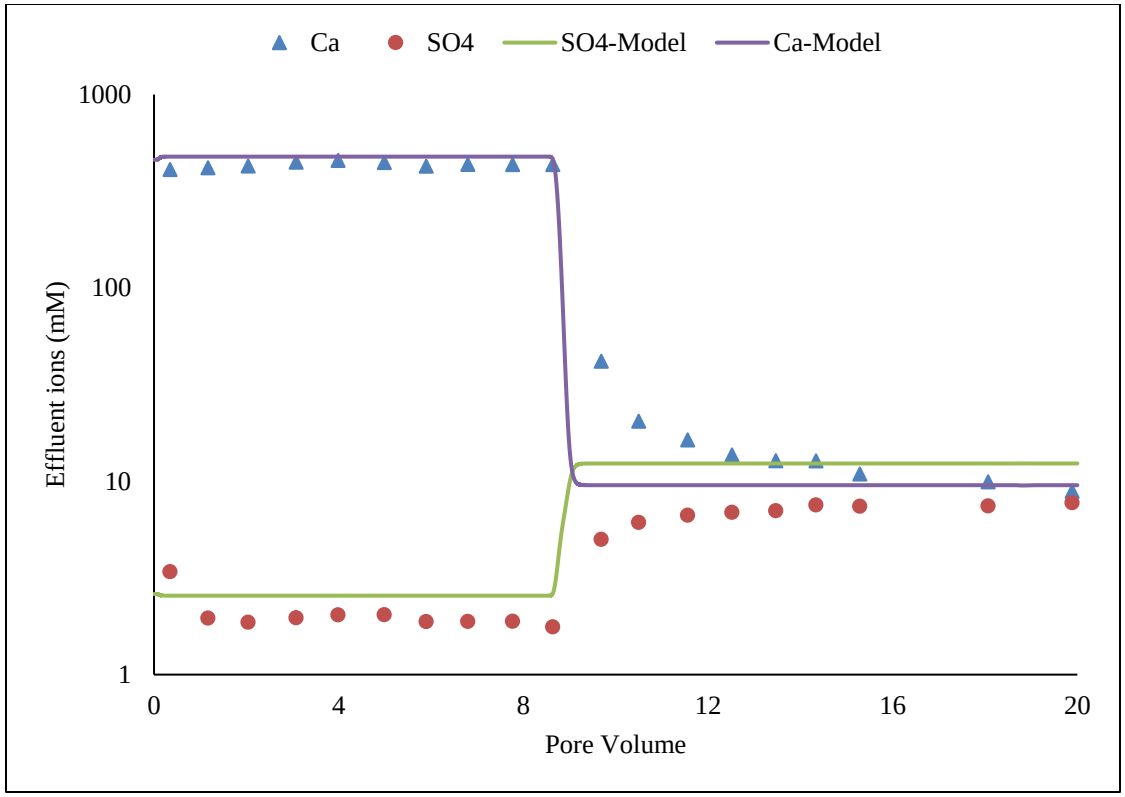

Figure 6.22: Effluent calcium and sulfate ions obtained from experiment F-2.4 and comparison with simulation results

CHAPTER 7: CONCLUSIONS AND RECOMMENDATIONS

The objective of this work was to understand the role of geochemical interactions during chemical EOR processes. Experimental as well as modeling and simulation work was conducted to achieve this objective. The study was performed mainly for two such chemical EOR techniques; these are ASP/ACP floods and low salinity wettability alteration in carbonates. Main conclusions from the study are summarized in this chapter. Towards the end, recommendations are made to further investigate the topic in future.

7.1 Conclusions

In this study, sodium metaborate and ammonia were investigated as alternative alkalis of sodium carbonate for performing ASP floods, particularly for reservoirs containing gypsum. Single-phase experiments were performed to understand the interactions of these alkalis with sandstone and carbonate cores containing gypsum. Surfactant phase behavior experiments were performed, and the effect of alkali-rock interactions on the surfactant phase behavior was investigated. Polymer stability experiments were performed to identify polymers suitable for ASP floods in reservoirs containing gypsum. Finally, oil recovery experiments were performed to test surfactant formulations in sandstone and carbonate cores. Sodium metaborate experiments showed high pH propagation in the presence of gypsum. The reaction of sodium metaborate with gypsum was found to be dependent on the injection velocity. Some calcium precipitation was observed in single-phase sodium metaborate experiments, however, the precipitation

was far less compared to that with sodium carbonate. Sodium carbonate showed excessive dissolution of gypsum and subsequence precipitation of calcium carbonate. In addition, sodium carbonate was not able to maintain a high pH in the presence of gypsum. ASP corefloods performed using sodium metaborate as the alkali in sandstone cores containing gypsum showed a high pH propagation, good oil recovery and low surfactant retention. Very little change in permeability was observed during single-phase and oil recovery corefloods. Single-phase surfactant adsorption and oil recovery ASP corefloods were performed with sodium metaborate using dolomite cores (without gypsum). A reduction in surfactant adsorption on dolomite was observed on adding sodium metaborate. A similar reduction was observed on adding sodium carbonate to the surfactant formulation. ASP corefloods using sodium metaborate as the alkali showed a high pH propagation, good oil recovery and low surfactant retention in dolomite cores. Calculations were performed in PHREEQC to investigate the interactions of sodium metaborate and sodium carbonate with gypsum. These calculations were also performed to understand if equilibrium was reached during the corresponding lab experiments.

PHREEQC calculations showed minimal interaction of sodium metaborate with dolomite, however, calcium precipitation was observed in the presence of gypsum. The effluent sulfate concentration obtained on injecting sodium metaborate in a core containing gypsum, even at 0.044 ft/d, was much lower than the equilibrium results obtained from PHREEQC. This showed that reactions of sodium metaborate with gypsum did not reach to equilibrium in the single-phase corefloods. A reaction kinetics model was included in PHREEQC calculations to model the coreflood results. Similar

calculations performed for sodium carbonate showed a good agreement with the experimental results, even without adding the reaction kinetics.

Since some calcium precipitation was observed due to the interaction of sodium metaborate with gypsum, ammonia was investigated as an alternative alkali under such conditions. In addition, ammonia offered other advantages due to its lower molecular mass in terms of storage and transportation during a field operation. Single-phase experiments performed using ammonia in the presence of gypsum showed ammonia to maintain a high pH without showing any calcium precipitation. Due to no calcium precipitation, calcium ions remained soluble in the presence of ammonia. As a result, the effect of these ions on surfactant phase behavior and polymer stability was investigated. The surfactant phase behavior experiments showed that the effect of free calcium ions on the phase behavior can be minimized by selecting suitable surfactants. A shift in the optimum salinity towards a lower salinity was observed in the presence of calcium ions. The aqueous stability was similarly affected. Polymer stability experiments in the presence of 1000 ppm calcium ions and ammonia showed precipitation of hydrolyzed polyacrylamide polymers at 60 °C. AN-125 and SAV 550 polymers remained stable under similar conditions. PHREEQC calculations were performed to estimate gypsum dissolution in the presence of ammonia. Effect of adding sodium sulfate to lower gypsum dissolution was investigated in PHREEQC. These calculations were helpful in designing the ASP and SP corefloods. ASP (using ammonia as the alkali) and SP corefloods were performed in carbonate cores containing gypsum which showed good oil recovery and low surfactant retention. Single-phase ASP and SP corefloods were similarly performed

to compare the surfactant retention values with and without adding ammonia. The surfactant retention values with and without adding ammonia were very similar in these corefloods, although a high pH of about 10.5 was observed in the ASP corefloods. The benefits of adding ammonia were not obvious.

Ammonia was also investigated as an alternative of sodium carbonate for sandstone and carbonate reservoirs not containing gypsum. Lowering of the zeta potential measurements of sandstone and carbonate rocks was observed on increasing the pH using ammonia. Single-phase and oil recovery experiments showed reduction in surfactant adsorption on sandstone cores on adding ammonia. However, very little reduction in surfactant adsorption was observed on carbonate rocks was observed on adding ammonia.

Ammonia was also investigated for developing ACP formulations in the case of acidic crude oils. The effects of alkali type, cosolvent type and calcium ions were investigated to compare ammonia with sodium metaborate, sodium carbonate and sodium hydroxide. Ammonia showed low IFT region at a lower salinity, similar to sodium hydroxide. The low IFT regions were at higher salinities for sodium metaborate and sodium carbonate. The addition of calcium ions to ACP formulations developed using ammonia shifted them to Winsor type II region due to the complexation of naphthenic acids with calcium ions. Low IFT ACP formulations were developed with acidic crude oils. An ACP coreflood performed in a low permeability sandstone core an incremental oil recovery of about 85% ROIP.

Single-phase experiments were performed to investigate geochemical interactions during low salinity wettability alteration in carbonates at high temperatures. The change in ionic composition due to these interactions was carefully monitored. The experiments showed calcite dissolution, surface dolomitization and sulfate adsorption as a result of these interactions. The reactions reached to equilibrium at 1 ft/d when the formation brine was displaced with seawater (SW). However, the reactions did not reach equilibrium when the SW was subsequently displaced with SW/50. A mechanistic model for the wettability alteration process was developed in UTCHEM-IPHREEQC. Single-phase lab experiments, as well as zeta potential and oil recovery corefloods reported in literature were modeled. The calculations were performed assuming local equilibrium using the thermodynamic data available in the literature. A good agreement between the simulation and experimental results was observed.

7.2 Recommendations

1. Surfactant adsorption on sandstone and carbonate surfaces are usually considered to depend greatly on the pH. However, besides the pH, the surfactant adsorption can be affected by other ions present in the aqueous solutions. Divalent cations can result in affecting the surfactant adsorption, especially at high pH. Very little work has been performed to understand the effect of other ions on surfactant adsorption in sandstones and carbonates. In addition, most surfactant adsorption studied reported in the literature are performed with clean minerals. However, the presence of trace amounts of other minerals could significantly affect these numbers. Iron minerals, especially, tend

to have a large surface area which could result in greatly affecting the surfactant adsorption. These effects must be understood to reliably upscale the lab results.

2. The interaction of acidic crude oils with alkalis are often represented by a simple acid-base reaction. However, in reality, the naphthenic acids present in the crude oil are of various kinds and the kind of soap that is generated can also depend on the type of alkali. Very little work has been performed to understand these interactions.

3. Interaction of alkalis in the reservoir can be very different from that in the core because of much longer residence times in the field. Therefore, long-term interactions of alkalis with reservoir fluids and minerals must be carefully understood to reliably upscale these reactions.

4. One of the concerns during surfactant floods is that the surfactants must not chromatically separate inside the porous media. Several lab experiments have found no chromatographic separation of surfactants in single-phase and oil recovery corefloods. However, most lab experiments are performed with foot long cores. Surfactant transport studies performed in longer cores must be used to further investigate the topic.

5. Formation damage during ASP floods remains a topic of interest. During an ASP flood, precipitation is often observed on mixing of the surfactant slug with the reservoir brines (often containing divalent cations). Although, no appreciable formation damage is observed in the lab, the cores used in lab experiments are often smaller and they may not be representative of the field situation. In addition, formation damage may occur at the production wells due to depressurization (and cooling) of the produced

fluids. This could result in precipitation of dissolved species. These effects should be studied to avoid formation damage in the field.

6. Lab experiments are often performed in oxidized state and the results of these experiments may not be applicable to field conditions. For example, low salinity wettability alteration experiments are often conducted in an oxidized environment. The degree of wetness of a surface can depend greatly on the redox state of the core. In addition, geochemical reactions can also be affected based on the redox state.

7. Low salinity waterfloods must be investigated further to develop a better understanding of the topic. For example, low salinity effects have been observed in some carbonate cores but not in others. In addition, some rocks show great response to low salinity brines while other show only a very little improvement in oil recovery. A better understanding of the process is required to be able to identify situations where low salinity wettability alteration may be useful.

8. Although low salinity waterfloods have shown improvement in oil recovery in various lab studies and pilot studies, their fate at the field scale remains unclear. Most lab studies are performed in foot long cores, which typically have much less residence times than the field. Long-term interaction and propagation of low salinity brines must be studied to make reliable field predictions. In addition, the effect of trace minerals must be studied.

9. Although, the model developed for low salinity waterfloods showed good agreement with the lab results, further improvement is needed in the model to make it

more reliable. This is especially true in the case of oil recovery simulations. In the current model, the amount of acid attached on the surface is used to alter the wettability. However, no direct measurements of this acid concentration exist, and thus, it becomes purely a fitting parameter. A more realistic parameter must be included to model the oil recovery floods.

NOMUNCLATURE

ASP	Alkaline-surfactant-polymer
$CaCO_3$	Calcium carbonate
$CaSO_4$	Calcium sulfate (Anhydrite)
$CaSO_4$	Calcium sulfate dehydrate (Gypsum)
HPAM	Hydrolyzed polyacryamide
HPLC	High performance liquid chromatography
ICP	Inductively coupled plasma
IC	Ion chromatograph
IFT	Interfacial Tension
KHP	Potassium hydrogen phthalate
md	Millidarcy
NH_3	Ammonia
NH_4OH	Ammonium hydroxide
NaCl	Sodium chloride
Na_2CO_3	Sodium carbonate
$NaBO_2{\cdot}4H_2O$	Sodium metaborate tetrahydrate
OOIP	Original oil in place
ppm	Parts per million
PV	Pore volume
TDS	Total dissolved solids
TEGBE	Triethylene glycol monobutyl ether
wt%	Percentage by weight
µS	Micro siemens

APPENDIX A

UTCHEM Input Files

Simulation 5.1 (a)

```
CC*****************************************************************
CC
CC   BRIEF DESCRIPTION OF DATA SET : UTCHEM (VERSION 2011_9)      *
CC
CC*****************************************************************
CC                                                                                *
CC  ALKALI SURFACTANT POLYMER   FLOODING                          *
CC                                        *
CC  LENGTH (FT) :                          PROCESS : A/S/P FLOODING       *
CC  THICKNESS (FT) :              INJ. PRESSURE (PSI) :          *
CC  WIDTH (FT) : .                COORDINATES : CARTESIAN        *
CC  POROSITY :                                *
CC  GRID BLOCKS : 50X1X1                                  *
CC  DATE :   Dec 2012                                     *
CC                                        *
CC*****************************************************************
CC
CC*****************************************************************
CC                                        *
CC   RESERVOIR DESCRIPTION                              *
CC                                        *
CC*****************************************************************
CC
CC
*----RUNNO
Chev-1
CC
CC
*----HEADER
 coreflood  Borate-ASP
 Experiment  38 C
*************************************************************
CC
CC SIMULATION FLAGS
*---- IMODE IMES IDISPC ICWM ICAP IREACT IBIO ICOORD ITREAC ITC IGAS IENG
      1  4   3     0   0    3     0   1    0     0   0  0
CC
CC NUMBER OF GRID BLOCKS AND FLAG SPECIFIES CONSTANT OR VARIABLE GRID SIZE
*----NX   NY  NZ  IDXYZ  IUNIT
    50   1  1  0      0
CC
CC  CONSTANT GRID BLOCK SIZE IN X, Y, AND Z
*----DX        DY         DZ
    0.01993   0.1225   0.1225
CC
CC TOTAL NO. OF COMPONENTS, NO. OF TRACERS, NO. OF GEL COMPONENTS
*----N   no NTw nta ngc ng noth
    15  0  0   0   7   0   0
CC
CC
*---- SPNAME(I),I=1,N
WATER
OIL
SURFACTANT
POLYMER
Chloride
```

```
CALCIUM
alc1
alc2
Magnesium
SODIUM
hydrogen
Sulfate
Carbonate
Bor
HAo
CC
CC FLAG INDICATING IF THE COMPONENT IS INCLUDED IN CALCULATIONS OR NOT
*----ICF(KC) FOR KC=1,N
   1 1 1 1 1 1  0 0 1 1 1 1 1 1 1
CC
CC*************************************************************************
CC                                        *
CC   OUTPUT OPTIONS                                *
CC                                        *
CC*************************************************************************
CC
CC
CC  FLAG FOR PV OR DAYS FOR OUTPUT AND STOP THE RUN
*----ICUMTM  ISTOP   IOUTGMS  IS3G
     1       1   0      0
CC
CC FLAG INDICATING IF THE PROFILE OF KCTH COMPONENT SHOULD BE WRITTEN
*----IPRFLG(KC),KC=1,N
   1 1 1 1 1 1 0 0 1 1 1 1 1 1 1
CC
CC FLAG FOR PRES,SAT.,TOTAL CONC.,TRACER CONC.,CAP.,GEL, ALKALINE PROFILES
*----IPPRES IPSAT IPCTOT IPBIO IPCAP IPGEL IPALK ITEMP    IPOBS
    1     1     1     0     0    0   1     0       0
CC
CC FLAG FOR WRITING SEVERAL PROPERTIES
*----ICKL IVIS IPER ICNM  ICSE IFOAM IHYST  INONEQ
    1    1   1   1   1   0    0      0
CC
CC FLAG FOR WRITING SEVERAL PROPERTIES TO PROF
*----IADS  IVEL IRKF IPHSE
    1    0   1   1
CC
CC*************************************************************************
CC                                        *
CC   RESERVOIR PROPERTIES                              *
CC                                        *
CC*************************************************************************
CC
CC
CC MAX. SIMULATION TIME ( PV)
*---- TMAX
   1.3
CC
CC ROCK COMPRESSIBILITY (1/PSI), STAND. PRESSURE(PSIA)
*----COMPR   PSTAND
    0.      14.7
CC
CC FLAGS INDICATING CONSTANT OR VARIABLE POROSITY, X,Y,AND Z PERMEABILITY
*----IPOR1 IPERMX IPERMY IPERMZ  IMOD   ITRANZ  INTG
     0     0    0     0     0      0     0
CC
CC CONSTANT POROSITY
*----PORC1
   .18853
CC
```

```
CC CONSTANT X-PERMEABILITY (MILIDARCY) FOR LAYER K = 1,NZ
*----PERMX
    240.0
CC
CC
*---- CONSTANT Y DIRECTION PERMEABILITY
    240.0
CC
CC
*---- CONSTANT Z DIRECTION PERMEABILITY
    240.0
CC
CC FLAG FOR CONSTANT OR VARIABLE DEPTH, PRESSURE, WATER SATURATION
*----IDEPTH  IPRESS  ISWI  ICWI
     0       0      0    -1
CC
CC CONSTANT DEPTH (FT)
*----D111
    0.
CC
CC INITIAL PRESSURE (PSIA)
*----PINIT   DEPTH
     14.7    0.0
CC
CC CONSTANT INITIAL WATER SATURATION (residual oil)(Sw=0.5623)
*----SWI
   0.57
CC
CC CONSTANT CHLORIDE AND CALCIUM CONCENTRATIONS (MEQ/ML)
*----C50       C60
   0.5924     0.0
CC
CC**********************************************************************
CC                                          *
CC    PHYSICAL PROPERTY DATA                *
CC                                          *
CC**********************************************************************
CC
CC 3.4.1 OIL CONC. AT PLAIT POINT FOR TYPE II(+)AND TYPE II(-), CMC
CC                 CMC
*---- c2plc  c2prc   epsme   ihand
       0      1     0.0001     0
CC
CC 3.4.2 flag indicating type of phase behavior parameters
*---- ifghbn=0 for input height of binodal curve; =1 for input sol. ratio
       0
CC 3.4.3 SLOPE AND INTERCEPT OF BINODAL CURVE AT ZERO, OPT., AND 2XOPT SALINITY
CC FOR ALCOHOL 1
*---- hbns70   hbnc70   hbns71   hbnc71   hbns72   hbnc72
       0    0.09       0     0.07     0     0.09
CC 3.4.5 SLOPE AND INTERCEPT OF BINODAL CURVE AT ZERO, OPT., AND 2XOPT SALINITY
CC FOR ALCOHOL 2
*---- hbns80  hbnc80  hbns81  hbnc81  hbns82  hbnc82
       0       0.08       0       0.06       0       0.08
CC
CC 3.4.6 LOWER AND UPPER EFFECTIVE SALINITY FOR ALCOHOL 1 AND ALCOHOL 2
*---- csel7   cseu7   csel8   cseu8
      0.6      1.3     0.62       1.0
CC 3.4.7 THE CSE SLOPE PARAMETER FOR CALCIUM AND ALCOHOL 1 AND ALCOHOL 2
CC    Ca     Alcohol#1  Alcohol#2
*---- beta6    beta7    beta8
       0        0        0
CC
CC 3.4.8 FLAG FOR ALCOHOL PART. MODEL AND PARTITION COEFFICIENTS
*---- ialc   opsk7o   opsk7s   opsk8o   opsk8s
```

```
      0     0       0       0       0
CC  these are used only for alcohol partitioning in a two alcohol system:
CC 3.4.9 NO. OF ITERATIONS, AND TOLERANCE
*---- nalmax     epsalc
      30       0.0001
CC 3.4.10 ALCOHOL 1 PARTITIONING PARAMETERS IF IALC=1
CC   aq-oleic   aq-oleic  surf-oleic
*---- akwc7     akws7     akm7      ak7      pt7
     4.671    1.79      48      35.31    0.222
CC
CC 3.4.11 ALCOHOL 2 PARTITIONING PARAMETERS IF IALC=1
*---- akwc8     akws8    akm8    ak8     pt8
      0        0       0     0      0
CC
CC 3.4.22 ift model flag
*----  ift=0 for Healy&Reed; =1 for Chun Huh correl.
      1
CC 3.4.24 INTERFACIAL TENSION PARAMETERS
CC    typ=.1-.35   typ=5-20
*---- chuh         ahuh
    0.3          9
CC 3.4.25 LOG10 OF OIL/WATER INTERFACIAL TENSION
CC     units of log 10 dynes/cm = mN/m
*---- xiftw
     1.3
CC 3.4.26 ORGANIC MASS TRANSFER FLAG
CC    imass=0 for no oil sol. in water.  icorr=0 for constant MTC
*---- imass   icor
      0       0
cc
cc
* iwalt iwalf
0 0
CC 3.4.31 CAPILLARY DESATURATION PARAMETERS FOR PHASE 1, 2, AND 3 (prev t22=59000)
CC              AQ     OLEIC     ME
*---- itrap      t11      t22      t33
      2        1865    6000    394
CC
CC  3.4.32 FLAG FOR RELATIVE PERMEABILITY AND CAPILLARY PRESSURE MODEL
*---- iperm=0 for constant; =1 varies by layer; =2 varies by gridblock
      0     0
CC
CC 3.4.35 FLAG FOR CONSTANT OR VARIABLE REL. PERM. PARAMETERS
*---- isrw    iprw    iew
      0     0       0
CC
CC CONSTANT RES. SATURATION OF PHASES 1,2,AND 3 AT LOW CAPILLARY NO.0.18,0.4377
*----S1RWC  S2RWC  S3RWC
    0.3     .42    0.3
CC
CC CONSTANT ENDPOINT REL. PERM. OF PHASES 1,2,AND 3 AT LOW CAPILLARY NO.
*----P1RW  P2RW  P3RW
    .05   1.0   .05
CC
CC CONSTANT REL. PERM. EXPONENT OF PHASES 1,2,AND 3 AT LOW CAPILLARY NO.
*----E1W     E2W  E3W
   4.0     1.5   4.0
CC
CC  RES. SATURATION OF PHASES 1,2,AND 3 AT HIGH CAPILLARY NO.
*----S1RC  S2RC  S3RC
   0.12    0.12    0.12
CC
CC ENDPOINT REL. PERM. OF PHASES 1,2,AND 3 AT HIGH CAPILLARY NO.
*----P1RC    P2RC  P3RC
   1.0     1.0   1.0
```

```
CC
CC REL. PERM. EXPONENT OF PHASES 1,2,AND 3 AT HIGH CAPILLARY NO.
*----E13CW  E23C  E31C
   1.4    1.4  1.4
CC 3.4.61 WATER AND OIL VISCOSITY , RESERVOIR TEMPERATURE
CC  water    oil      =0 for isothermal modeling
*---- VIS1    VIS2  TSTAND
     0.8    105     100
CC
CC 3.4.80 COMPOSITIONAL PHASE VISCOSITY PARAMETERS for microemulsion
*----  ALPHAV1  ALPHAV2  ALPHAV3  ALPHAV4  ALPHAV5
        0.0     0.0    0     0     0
CC
CC 3.4.81 PARAMETERS TO CALCULATE POLYMER VISCOSITY AT ZERO SHEAR RATE
*---- AP1     AP2     AP3
    700     900     1700
CC
CC 3.4.82 PARAMETER TO COMPUTE CSEP,MIN. CSEP, AND SLOPE OF LOG VIS. VS. LOG CSEP
*---- BETAP   CSE1    SSLOPE
     1     0.01    -0.38
CC
CC 3.4.83 PARAMETER FOR SHEAR RATE DEPENDENCE OF POLYMER VISCOSITY(prev rweff=0.25)
*---- GAMMAC  GAMHF  POWN  IPMOD  ishear  rweff  gamhf2
     3.0    0.8   1.8   0     0      0.003    0
CC
CC 3.4.84  FLAG FOR POLYMER PARTITIONING, PERM. REDUCTION PARAMETERS
*---- IPOLYM   EPHI3   EPHI4   BRK    CRK    rkcut
      1      1.0     1     100     0.005  10
CC 3.4.85 SPECIFIC WEIGHT FOR COMPONENTS 1,2,3,7,8 ,Coeffient of oil and GRAVITY FLAG
CC  if IDEN=1 ignore gravity effect; =2 then include gravity effect
*---- DEN1    DEN2     DEN23    DEN3     DEN7   DEN8   IDEN
    0.43    0.44  0.45    0.42    0.41   0.42      1
CC  ISTB=0:BOTTOMHOLE CONDITION , 1: STOCK TANK
CC 3.4.93 FLAG FOR CHOICE OF UNITS when printing
*----- ISTB
      0
CC
CC 3.4.95 COMPRESSIBILITY FOR VOL. OCCUPYING COMPONENTS 1,2,3,7,AND 8
*----  COMPC(1)   COMPC(2)    COMPC(3)  COMPC(7)  COMPC(8)
       0.      0.       0.       0        0
CC  IOW=0 water wet, =1 oil wet, =2 mixed wet
CC 3.4.99 CONSTANT OR VARIABLE PC PARAM., WATER-WET OR OIL-WET PC CURVE FLAG
*---- ICPC   IEPC   IOW
     0      0     0
CC
CC 3.4.100 CAPILLARY PRESSURE PARAMETER, CPC0
*---- CPC0
     0
CC
CC 3.4.103 CAPILLARY PRESSURE PARAMETER, EPC0
*---- EPC0
     0.0
CC
CC 3.4.117 MOLECULAR DIFFUSION COEF. KCTH COMPONENT IN PHASE 1
*---- D(KC,1),KC=1,N
      0       0       0       0       0       0       0       0       0       0       0.001       0   0.001   0   0
CC
CC 3.4.118 MOLECULAR DIFFUSION COEF. KCTH COMPONENT IN PHASE 2
*---- D(KC,2),KC=1,N
      0       0       0       0       0       0       0       0       0       0       0.001       0   0.001   0   0
CC
CC 3.4.119 MOLECULAR DIFFUSION COEF. KCTH COMPONENT IN PHASE 3
*---- D(KC,3),KC=1,N
      0       0       0       0       0       0       0       0       0       0       0.001       0   0.001   0   0
CC
```

CC 3.4.121 LONGITUDINAL AND TRANSVERSE DISPERSIVITY OF PHASE 1
*---- ALPHAL(1) ALPHAT(1)
  0.01 0.001
CC
CC 3.4.122 LONGITUDINAL AND TRANSVERSE DISPERSIVITY OF PHASE 2
*---- ALPHAL(2) ALPHAT(2)
  0.01 0.001
CC
CC 3.4.124 LONGITUDINAL AND TRANSVERSE DISPERSIVITY OF PHASE 3
*---- ALPHAL(3) ALPHAT(3)
  0.01 0.001
CC
CC 3.4.125 flag to specify organic adsorption calculation
*---- iadso=0 if organic adsorption is not considered
  0
CC
CC 3.4.130 SURFACTANT AND POLYMER ADSORPTION PARAMETERS (0.5 0.9)
*---- AD31 AD32 B3D AD41 AD42 B4D IADK IADS1 FADS REFK
  0.8 0.2 1000 0.0 0.0 100 0 0 0 100
2 1 800
7 13 13 0.1
0.62 1.0
0
9 15 5 0 2 1
9 0 6 11
4 3 1 2 6
0 0 0
8
Ca 2.00
Mg 2.00
Na 1.00
H 1.00
SO4 -2.00
CO3 -2.00
B(OH)4- -1.00
HAo -1.00
Chlorine -1.00
Ca
Mg
Na
H
SO4
CO3
B(OH)4-
HAo
H2O
OH-
A-
H2CO3
HCO3-
B(OH)3
HAw (* FLDSPS *)
CaMg(CO3)2
Ca(OH)2
Mg(OH)2
Boric acid
Borax (* SLDSPS *)
Surf Sodium
Surf Calcium (*Surf exc *)
1. 0. 0. 0. 0. 0. 0. 0. 0. 0. 0. 0. 0. 0. 0.
0. 1. 0. 0. 0. 0. 0. 0. 0. 0. 0. 0. 0. 0. 0.
0. 0. 1. 0. 0. 0. 0. 0. 0. 0. 0. 0. 0. 0. 0.
0. 0. 0. 1. 0. 0. 0. 1. 2. 1. 0. 2. 1. 1. 1.
0. 0. 0. 0. 1. 0. 0. 0. 0. 0. 0. 0. 0. 0. 0.
0. 0. 0. 0. 0. 1. 0. 0. 0. 0. 0. 1. 1. 0. 0.

0. 0. 0. 0. 0. 0. 1. 0. 0. 0. 0. 0. 0. 1. 0.
0. 0. 0. 0. 0. 0. 0. 1. 0. 0. 1. 0. 0. 0. 1.
1. 1. 0. 0. 0.
1. 0. 1. 0. 0.
0. 0. 0. 0. 2.
0. 2. 2. 1. 2.
0. 0. 0. 0. 0.
2. 0. 0. 0. 0.
0. 0. 0. 1. 4.
0. 0. 0. 0. 0.
0. 1.
0. 0.
1. 0.
0. 0.
0. 0.
0. 0.
0. 0.
0. 0.
1.0 0.0 0.0 0.0 0.0 0.0 0.0 0.0 0.0 0.0 0.0
0.0 1.0 0.0 0.0 0.0 0.0 0.0 0.0 0.0 0.0 0.0
0.0 0.0 1.0 0.0 0.0 0.0 0.0 0.0 0.0 0.0 0.0
0.0 0.0 0.0 1.0 0.0 0.0 0.0 0.0 0.0 0.0 0.0
0.0 0.0 0.0 0.0 1.0 0.0 0.0 0.0 0.0 0.0 0.0
0.0 0.0 0.0 0.0 0.0 1.0 0.0 0.0 0.0 0.0 0.0
0.0 0.0 0.0 0.0 0.0 0.0 1.0 0.0 0.0 0.0 0.0
0.0 0.0 0.0 0.0 0.0 0.0 0.0 1.0 0.0 0.0 0.0
0.0 0.0 0.0 0.0 0.0 0.0 0.0 0.0 1.0 0.0 0.0
0.0 0.0 0.0 -1.0 0.0 0.0 0.0 0.0 0.0 0.0 0.0
0.0 0.0 0.0 -1.0 0.0 0.0 0.0 1.0 0.0 0.0 0.0
0.0 0.0 0.0 2.0 0.0 1.0 0.0 0.0 0.0 0.0 0.0
0.0 0.0 0.0 1.0 0.0 1.0 0.0 0.0 0.0 0.0 0.0
0.0 0.0 0.0 1.0 0.0 0.0 1.0 0.0 0.0 0.0 0.0
0.0 0.0 0.0 0.0 0.0 0.0 0.0 1.0 0.0 0.0 0.0
0.0 0.0 0.0 0.0 0.0 0.0 0.0 0.0 0.0 1.0 0.0
0.0 0.0 0.0 0.0 0.0 0.0 0.0 0.0 0.0 0.0 1.0
1.0 1.0 0.0 0.0 0.0 2.0 0.0 0.0 0.0
1.0 0.0 0.0 -2.0 0.0 0.0 0.0 0.0 0.0
0.0 1.0 0.0 -2.0 0.0 0.0 0.0 0.0 0.0
0.0 0.0 0.0 1.0 0.0 0.0 1.0 0.0 0.0
0.0 0.0 2.0 2.0 0.0 0.0 4.0 0.0 0.0
2.0 2.0 1.0 1.0 -2.0 -2.0 -1.0 0.0 0.0 -1.0 -1.0 0.0
-1.0 0.0 0.0
0.1000000000000E+01 0.1000000000000E+01 0.1000000000000E+01
0.1000000000000E+01 0.1000000000000E+01 0.1000000000000E+01
0.1000000000000E+01 0.1000000000000E+01 0.1000000000000E+01
0.2580000000000E-13 0.7270126443377E-12 0.3430000000000E+17
0.1710000000000E+11 0.1680000000000E+10 0.7270126443377E-04
0.3250000000000E-18 0.4397440000000E+22 0.4250000000000E+16
0.3529390000000E-09 0.2499770000000E-25
1.0 2.0
0.4000000000000E+00
-1.0 0.0 2.0 0.0 0.0 0.0 0.0 0.0 0.0 -2.0 1.0
0.6699319020164E-06 0.1022322963357E-21
0.5248000000000E+00 0.5966164510056E-03
0.5966164510056E-03
0.5924000000000E+00
0.1111000000000E+03
0.6760000000000E-01
0.2553232902017E-02
0.3090459402411E-11
0.3105494085134E-05
0.3350096043152E-01
0.2983082255028E-03 0.2983082255028E-03 0.5923993300681E+00
0.3635536949034E-07 0.3380000000000E-01 0.1911069369907E-05
0.4978427388078E-13 0.2539689450591E-01 0.5553661929034E+02

```
0.1124580994525E+02 0.0000000000000E+00 0.0000000000000E+00
0.0000000000000E+00 0.0000000000000E+00
0.9999975156109E+00 0.9738987648126E+00
0.1000000000000E-07 0.8000000000000E+03
CC
CC*********************************************************************
CC                                          *
CC   WELL DATA                                    *
CC                                          *
CC*********************************************************************
CC
CC
CC FLAG FOR PRESSURE CONST. BOUNDARIES
*---- IBOUND  IZONE
     0    0
CC
CC TOTAL NUMBER OF WELLS, WELL RADIUS FLAG, FLAG FOR TIME OR COURANT NO.
*----NWELL   IRO   ITIME  NWREL
    2     2     1     2
CC
CC WELL ID,LOCATIONS,AND FLAG FOR SPECIFYING WELL TYPE, WELL RADIUS, SKIN
*----IDW   IW    JW    IFLAG    RW     SWELL  IDIR   IFIRST  ILAST  IPRF
    1   1     1     1   .003      0.    3     1     1    0
CC
CC WELL NAME
*---- WELNAM
INJECTOR
CC
CC ICHEK MAX. AND MIN. ALLOWABLE BOTTOMHOLE PRESSURE AND RATE
*----ICHEK   PWFMIN   PWFMAX  QTMIN   QTMAX
    0    0.0    5000.  0.0    50000.
CC
CC WELL ID, LOCATION, AND FLAG FOR SPECIFYING WELL TYPE, WELL RADIUS, SKIN
*----IDW  IW   JW   IFLAG    RW     SWELL  IDIR  IFIRST   ILAST    IPRF
   2   50    1    2      .003    0.     3    1      1      0
CC
CC WELL NAME
*---- WELNAM
PRODUCER
CC
CC MAX. AND MIN. ALLOWABLE BOTTOMHOLE PRESSURE AND RATE
*----ICHEK  PWFMIN   PWFMAX  QTMIN   QTMAX
    0    0.0    5000.  0.0    50000.
CC
CC ID,INJ. RATE AND INJ. COMP. FOR RATE CONS. WELLS FOR EACH PHASE (L=1,3)
*----ID  QI(M,L)  C(M,KC,L)    P    Cl         Ca  alc1  alc2  mg   na   H  SO4  Co3  Bor  Hao
     1   0.002543   0.968   0.  0.032    0.45   0.524786   0.0001  0.0  0.0 0.0001  0.743907  111.10  0.067605  0.003872  0.151515
0.0001
     1      0.   0.   0.  0.    0.    0.    0.   0.   0.    0.   0.    0.   0.   0.    0.   0
     1      0.   0.   0.  0.    0.    0.    0.   0.   0.    0.   0.    0.   0.   0.    0.   0
CC
CC ID,
*----ID   PWF
   2    14.7
CC
CC CUM. INJ. TIME , AND INTERVALS (PV OR DAY) FOR WRITING TO OUTPUT FILES
*----TINJ    CUMPR1   CUMHI1    WRHPV   WRPRF     RSTC
   0.3      0.01     0.01      0.01    0.01      0.3
CC
CC FOR IMES=2 ,THE INI. TIME STEP,CONC. TOLERANCE,MAX.,MIN. COURANT NO.
*----DT      DCLIM     CNMAX   CNMIN
   0.000001   15*0.001     0.1     0.001
CC******     INJECT Polymer 1**********************
CC FLAG FOR INDICATING BOUNDARY CHANGE
*---- IBMOD
```

```
      0
CC
CC  IRO, ITIME, NEW FLAGS FOR ALL THE WELLS
*----  IRO    ITIME     IFLAG
      2      1        1  2
CC
CC  NUMBER OF WELLS CHANGES IN LOCATION OR SKIN OR PWF
*----  NWEL1
       0
CC
CC  NUMBER OF WELLS WITH RATE CHANGES, ID
*---- NWEL2     ID
      1        1
CC
CC ID,INJ. RATE AND INJ. COMP. FOR RATE CONS. WELLS FOR EACH PHASE (L=1,3)
*----ID  QI(M,L)  C(M,KC,L)                      P    Cl   Ca  alc1  alc2  mg   na   H  SO4  Co3  Bor  Hao
     1   0.002543    1.0   0.  0.0    0.45   0.524786   0.0001  0.0  0.0 0.00001  0.743907  111.11  0.067605  0.004  0.151515  0.
     1      0.    0.    0.   0.     0.     0.     0.    0.    0.     0.    0.     0.    0.    0.    0.  0
     1      0.    0.    0.   0.     0.     0.     0.    0.    0.     0.    0.     0.    0.    0.    0.  0
CC
CC  CUM. INJ. TIME , AND INTERVALS (PV) FOR WRITING TO OUTPUT FILES
*---- TINJ          CUMPR1         CUMHI1     WRHPV      WRPRF     RSTC
    0.8       0.01      0.01       0.01    0.01        2.0
CC
CC  FOR IMES=4 ,THE INI. TIME STEP,CONC. TOLERANCE,MAX.,MIN. TIME STEPS
*----  DT           DCLIM       CNMAX      CNMIN
      0.0000001       15*0.001      0.1         0.001
CC******     INJECT Polymer 2 **********************
CC FLAG FOR INDICATING BOUNDARY CHANGE
*---- IBMOD
      0
CC
CC  IRO, ITIME, NEW FLAGS FOR ALL THE WELLS
*----  IRO    ITIME     IFLAG
      2      1        1  2
CC
CC  NUMBER OF WELLS CHANGES IN LOCATION OR SKIN OR PWF
*----  NWEL1
       0
CC
CC  NUMBER OF WELLS WITH RATE CHANGES, ID
*---- NWEL2     ID
      1        1
CC
CC ID,INJ. RATE AND INJ. COMP. FOR RATE CONS. WELLS FOR EACH PHASE (L=1,3)
*----ID  QI(M,L)  C(M,KC,L)                      P    Cl   Ca  alc1  alc2  mg   na   H  SO4  Co3  Bor  Hao
     1   0.002543  1.0   0.  0.0    0.45   0.5248   0.0001  0.0  0.0 0.0001  0.5925  111.10  0.06760  0.0014  0.0001  0.0001
     1      0.    0.    0.   0.     0.     0.     0.    0.    0.     0.    0.     0.    0.    0.    0.  0
     1      0.    0.    0.   0.     0.     0.     0.    0.    0.     0.    0.     0.    0.    0.    0.  0
CC
CC  CUM. INJ. TIME , AND INTERVALS (PV) FOR WRITING TO OUTPUT FILES
*---- TINJ          CUMPR1         CUMHI1     WRHPV      WRPRF     RSTC
    1.3       0.01      0.01       0.01    0.01        2.0
CC
CC  FOR IMES=4 ,THE INI. TIME STEP,CONC. TOLERANCE,MAX.,MIN. TIME STEPS
*----  DT           DCLIM       CNMAX      CNMIN
      0.0000001       15*0.001      0.1         0.001
```

Simulation 5.4

UTCHEM Input file

```
CC*************************************************************************
CC *
CC BRIEF DESCRIPTION OF DATA SET : UTCHEM (VERSION 9.9) *
CC *
CC*************************************************************************
CC *
CC History match of ASP core flood *
CC *
CC LENGTH (FT) : PROCESS : A/S/P FLOODING *
CC THICKNESS (FT) : INJ. PRESSURE (PSI) : *
CC WIDTH (FT) : COORDINATES : CARTESIAN *
CC POROSITY : *
CC GRID BLOCKS : 1X1X25 *
CC DATE : *
CC *
CC*************************************************************************
CC
CC*************************************************************************
CC *
CC RESERVOIR DESCRIPTION *
CC *
CC*************************************************************************
CC
CC
*----RUNNO
#C1
CC
CC
*----HEADER
ASP coreflood
Experiment
************************************************************
CC
CC SIMULATION FLAGS
*---- IMODE IMES IDISPC ICWM ICAP IREACT IBIO ICOORD ITREAC ITC IGAS IENG  IPhreeqc
     1    4    0     0   0   3     0    1     0    0  0   0     1
CC
CC NUMBER OF GRID BLOCKS AND FLAG SPECIFIES CONSTANT OR VARIABLE GRID SIZE
*----NX NY NZ IDXYZ IUNIT
1 1 25 0 0
CC
CC CONSTANT GRID BLOCK SIZE IN X, Y, AND Z (Himanshu: in ft)
*----DX DY DZ
0.123 0.123 0.0388
CC
CC TOTAL NO. OF COMPONENTS, NO. OF TRACERS, NO. OF GEL COMPONENTS
*----N no NTw nta ng noth
8 0 0 0 0 0
CC
CC
*---- SPNAME(I),I=1,N
WATER
OIL
SURFACTANT
POLYMER
ANION
CALCIUM
alc1
alc2
CC
```

```
CC FLAG INDICATING IF THE COMPONENT IS INCLUDED IN CALCULATIONS OR NOT
*----ICF(KC) FOR KC=1,N
1 1 1 1 1 1 0 0
CC
CC**********************************************************************
CC *
CC OUTPUT OPTIONS *
CC *
CC**********************************************************************
CC
CC
CC FLAG FOR PV OR DAYS FOR OUTPUT AND STOP THE RUN
*----ICUMTM ISTOP IOUTGMS
1 1 0
CC
CC FLAG INDICATING IF THE PROFILE OF KCTH COMPONENT SHOULD BE WRITTEN
*----IPRFLG(KC),KC=1,N
   1 1 1 1 1 1 0 0
CC
CC FLAG FOR PRES,SAT.,TOTAL CONC.,TRACER CONC.,CAP.,GEL, ALKALINE PROFILES
*----IPPRES IPSAT IPCTOT IPBIO IPCAP IPGEL IPALK ITEMP IPOBS
1 1 1 0 0 0 1 0 0
CC
CC FLAG FOR WRITING SEVERAL PROPERTIES
*----ICKL IVIS IPER ICNM ICSE IFOAM IHYST INONEQ
1 1 1 1 1 0 0 0
CC
CC FLAG FOR WRITING SEVERAL PROPERTIES TO PROF
*----IADS IVEL IRKF IPHSE
1 0 1 1
CC
CC**********************************************************************
CC *
CC RESERVOIR PROPERTIES *
CC *
CC**********************************************************************
CC
CC
CC MAX. SIMULATION TIME ( PV)
*---- TMAX
2.5
CC
CC ROCK COMPRESSIBILITY (1/PSI), STAND. PRESSURE(PSIA)
*----COMPR PSTAND
0. 14.7
CC
CC FLAGS INDICATING CONSTANT OR VARIABLE POROSITY, X,Y,AND Z PERMEABILITY
*----IPOR1 IPERMX IPERMY IPERMZ IMOD ITRANZ INTG   ITRZ
     0 0 3 3 0 0 0   0
CC
CC CONSTANT POROSITY
*----PORC1
.20
CC
CC CONSTANT X-PERMEABILITY (MILIDARCY) FOR LAYER K = 1,NZ
*----PERMX
480
CC
CC Y DIRECTION PERMEABILITY IS DEPENDENT ON X DIRECTION PERMEABILITY
*---- CONSTANT PERMEABILITY MULTIPLIER FOR Y DIRECTION PERMEABILITY
1
CC
CC Z DIRECTION PERMEABILITY IS DEPENDENT ON X DIRECTION PERMEABILITY
*---- CONSTANT PERMEABILITY MULTIPLIER FOR Z DIRECTION PERMEABILITY
1
```

```
CC
CC FLAG FOR CONSTANT OR VARIABLE DEPTH, PRESSURE, WATER SATURATION
*----IDEPTH IPRESS ISWI ICWI
0 0 0 -1
CC
CC CONSTANT DEPTH (FT)
*----D111
0.
CC
CC INITIAL PRESSURE (PSIA)
*----PINIT DEPTH
14.7 0.0
CC
CC CONSTANT INITIAL WATER SATURATION (residual water)
*----SWI
0.71
CC
CC CONSTANT CHLORIDE AND CALCIUM CONCENTRATIONS (MEQ/ML)
*----C50 C60
0.1 0.0
CC
CC**********************************************************************
CC *
CC PHYSICAL PROPERTY DATA *
CC *
CC**********************************************************************
CC
CC 3.4.1 OIL CONC. AT PLAIT POINT FOR TYPE II(+)AND TYPE II(-), CMC
CC CMC
*---- c2plc c2prc epsme ihand
0 1 0.001 0
CC
CC 3.4.2 flag indicating type of phase behavior parameters
*---- ifghbn=0 for input height of binodal curve; =1 for input sol. ratio
0
CC 3.4.3 SLOPE AND INTERCEPT OF BINODAL CURVE AT ZERO, OPT., AND 2XOPT SALINITY
CC FOR ALCOHOL 1
*---- hbns70 hbnc70 hbns71 hbnc71 hbns72 hbnc72
0 0.06 0 0.04 0 0.06
CC 3.4.5 SLOPE AND INTERCEPT OF BINODAL CURVE AT ZERO, OPT., AND 2XOPT SALINITY
CC FOR ALCOHOL 2
*---- hbns80 hbnc80 hbns81 hbnc81 hbns82 hbnc82
0 0.0 0 0.0 0 0.0
CC
CC 3.4.6 LOWER AND UPPER EFFECTIVE SALINITY FOR ALCOHOL 1 AND ALCOHOL 2
*---- csel7 cseu7 csel8 cseu8
1.111  1.5384 0 0
CC 3.4.7 THE CSE SLOPE PARAMETER FOR CALCIUM AND ALCOHOL 1 AND ALCOHOL 2
CC Ca Alcohol#1 Alcohol#2
*---- beta6 beta7 beta8
3.42 0 0
CC
CC 3.4.8 FLAG FOR ALCOHOL PART. MODEL AND PARTITION COEFFICIENTS
*---- ialc opsk7o opsk7s opsk8o opsk8s
0 0 0 0 0
CC these are used only for alcohol partitioning in a two alcohol system:
CC 3.4.9 NO. OF ITERATIONS, AND TOLERANCE
*---- nalmax epsalc
20 0.0001
CC 3.4.10 ALCOHOL 1 PARTITIONING PARAMETERS IF IALC=1
CC aq-oleic aq-oleic surf-oleic
*---- akwc7 akws7 akm7 ak7 pt7
4.671 1.79 48 35.31 0.222
CC
CC 3.4.11 ALCOHOL 2 PARTITIONING PARAMETERS IF IALC=1
```

*---- akwc8 akws8 akm8 ak8 pt8
0 0 0 0 0
CC
CC 3.4.22 ift model flag
*---- ift=0 for Healy&Reed; =1 for Chun Huh correl.
1
CC 3.4.24 INTERFACIAL TENSION PARAMETERS
CC typ=.1-.35 typ=5-20
*---- chuh ahuh
0.3 12
CC 3.4.25 LOG10 OF OIL/WATER INTERFACIAL TENSION
CC units of log 10 dynes/cm = mN/m
*---- xiftw
1.3
C 3.4.26 ORGANIC MASS TRANSFER FLAG
CC imass=0 for no oil sol. in water. icorr=0 for constant MTC
*---- imass icor
0 0
CC
CC
*---- IWALT IWALF
0 0
CC 3.4.31 CAPILLARY DESATURATION PARAMETERS FOR PHASE 1, 2, AND 3
CC AQ OLEIC ME
*---- itrap t11 t22 t33
2 1865 59074 364.2
CC
CC 3.4.32 FLAG FOR RELATIVE PERMEABILITY AND CAPILLARY PRESSURE MODEL
*---- iperm=0 IRTYPE
0 0
CC
CC 3.4.35 FLAG FOR CONSTANT OR VARIABLE REL. PERM. PARAMETERS
*---- isrw iprw iew
0 0 0
CC
CC CONSTANT RES. SATURATION OF PHASES 1,2,AND 3 AT LOW CAPILLARY NO.
*----S1RWC S2RWC S3RWC
0.30 0.29 0.30
CC
CC CONSTANT ENDPOINT REL. PERM. OF PHASES 1,2,AND 3 AT LOW CAPILLARY NO.
*----P1RW P2RW P3RW
.05 0.9 .05
CC
CC CONSTANT REL. PERM. EXPONENT OF PHASES 1,2,AND 3 AT LOW CAPILLARY NO.
*----E1W E2W E3W
4.0 1.5 4.0
CC
CC RES. SATURATION OF PHASES 1,2,AND 3 AT HIGH CAPILLARY NO.
*----S1RC S2RC S3RC
0.095 0.095 0.095
CC
CC ENDPOINT REL. PERM. OF PHASES 1,2,AND 3 AT HIGH CAPILLARY NO.
*----P1RC P2RC P3RC
1.0 1.0 1.0
CC
CC REL. PERM. EXPONENT OF PHASES 1,2,AND 3 AT HIGH CAPILLARY NO.
*----E13CW E23C E31C
1.0 1.0 1.0
CC 3.4.61 WATER AND OIL VISCOSITY , RESERVOIR TEMPERATURE
CC water oil =0 for isothermal modeling
*---- VIS1 VIS2 TSTAND
0.47 8.3 0
CC
CC 3.4.80 COMPOSITIONAL PHASE VISCOSITY PARAMETERS for microemulsion
*---- ALPHAV1 ALPHAV2 ALPHAV3 ALPHAV4 ALPHAV5

```
1.0 1.0 0.0 0.5 0.5
CC
CC 3.4.81 PARAMETERS TO CALCULATE POLYMER VISCOSITY AT ZERO SHEAR RATE
*---- AP1 AP2 AP3
350 500 1000
CC
CC 3.4.82 PARAMETER TO COMPUTE CSEP,MIN. CSEP, AND SLOPE OF LOG VIS. VS. LOG CSEP
*---- BETAP CSE1 SSLOPE
20 0.01 -0.827
CC
CC 3.4.83 PARAMETER FOR SHEAR RATE DEPENDENCE OF POLYMER VISCOSITY
*---- GAMMAC GAMHF POWN IPMOD
4.0 13.0 1.9 0   0     0     0     0
CC
CC 3.4.84 FLAG FOR POLYMER PARTITIONING, PERM. REDUCTION PARAMETERS
*---- IPOLYM EPHI3 EPHI4 BRK CRK RKCUT
      1     1.0 0.95  100  0.05 10    0
CC 3.4.85 SPECIFIC WEIGHT FOR COMPONENTS 1,2,3,7,8 ,Coeffient of oil and GRAVITY FLAG
CC if IDEN=1 ignore gravity effect; =2 then include gravity effect
*---- DEN1 DEN2 DEN23 DEN3 DEN7 DEN8 IDEN
     0.44 0.4065 0.4065 0.42 0.346 0 2
CC ISTB=0:BOTTOMHOLE CONDITION , 1: STOCK TANK
CC 3.4.93 FLAG FOR CHOICE OF UNITS when printing
*----- ISTB
       1
CC 3.4.94 FORMATION VOLUME FACTOR - may set all these to 1.0 and just factor in post-proc
CC water oil me
*----- FVF(I), I=1 TO MXP (IGAS=0 MXP=3,IGAS=1 MXP=4)
1.0 1.0 1.0
CC
CC 3.4.95 COMPRESSIBILITY FOR VOL. OCCUPYING COMPONENTS 1,2,3,7,AND 8
*---- COMPC(1) COMPC(2) COMPC(3) COMPC(7) COMPC(8)
0.0 0.0 0 0 0
CC IOW=0 water wet, =1 oil wet, =2 mixed wet
CC 3.4.99 CONSTANT OR VARIABLE PC PARAM., WATER-WET OR OIL-WET PC CURVE FLAG
*---- ICPC IEPC IOW
0 0 0
CC
CC 3.4.100 CAPILLARY PRESSURE PARAMETER, CPC0
*---- CPC0
0
CC
CC 3.4.103 CAPILLARY PRESSURE PARAMETER, EPC0
*---- EPC0
0.0
CC
CC 3.4.117 MOLECULAR DIFFUSION COEF. KCTH COMPONENT IN PHASE 1
*---- D(KC,1),KC=1,N
0 0 0 0 0 0 0 0
CC
CC 3.4.118 MOLECULAR DIFFUSION COEF. KCTH COMPONENT IN PHASE 2
*---- D(KC,2),KC=1,N
0 0 0 0 0 0 0 0
CC
CC 3.4.119 MOLECULAR DIFFUSION COEF. KCTH COMPONENT IN PHASE 3
*---- D(KC,3),KC=1,N
0 0 0 0 0 0 0 0
CC
CC 3.4.121 LONGITUDINAL AND TRANSVERSE DISPERSIVITY OF PHASE 1
*---- ALPHAL(1) ALPHAT(1)
0.02 0.
CC
CC 3.4.122 LONGITUDINAL AND TRANSVERSE DISPERSIVITY OF PHASE 2
*---- ALPHAL(2) ALPHAT(2)
0.02 0.
```

```
CC
CC 3.4.124 LONGITUDINAL AND TRANSVERSE DISPERSIVITY OF PHASE 3
*---- ALPHAL(3) ALPHAT(3)
0.02 0.
CC
CC 3.4.125 flag to specify organic adsorption calculation
*---- iadso=0 if organic adsorption is not considered
0
CC
CC 3.4.130 SURFACTANT AND POLYMER ADSORPTION PARAMETERS
*---- AD31 AD32 B3D AD41 AD42 B4D IADK IADS1 FADS REFK
     3  0.1  1000 2.0 0.1 100 0 0 0 50
CC
CC**********************************************************************
CC *
CC WELL DATA *
CC *
CC**********************************************************************
CC
CC
CC FLAG FOR PRESSURE CONST. BOUNDARIES
*---- IBOUND IZONE
0 0
CC
CC TOTAL NUMBER OF WELLS, WELL RADIUS FLAG, FLAG FOR TIME OR COURANT NO.
*----NWELL IRO ITIME NWREL
2 2 1 2
CC
CC WELL ID,LOCATIONS,AND FLAG FOR SPECIFYING WELL TYPE, WELL RADIUS, SKIN
*----IDW IW JW IFLAG RW SWELL IDIR IFIRST ILAST IPRF
1 1 1 1 .003 0. 3 25 25 0
CC
CC WELL NAME
*---- WELNAM
INJECTOR
CC
CC ICHEK MAX. AND MIN. ALLOWABLE BOTTOMHOLE PRESSURE AND RATE
*----ICHEK PWFMIN PWFMAX QTMIN QTMAX
0 0.0 5000. 0.0 50000.
CC
CC WELL ID, LOCATION, AND FLAG FOR SPECIFYING WELL TYPE, WELL RADIUS, SKIN
*----IDW IW JW IFLAG RW SWELL IDIR IFIRST ILAST IPRF
2 1 1 2 .003 0. 3 1 1 0
CC
CC WELL NAME
*---- WELNAM
PRODUCER
CC
CC MAX. AND MIN. ALLOWABLE BOTTOMHOLE PRESSURE AND RATE
*----ICHEK PWFMIN PWFMAX QTMIN QTMAX
0 0.0 5000. 0.0 50000.
CC
CC ID,INJ. RATE AND INJ. COMP. FOR RATE CONS. WELLS FOR EACH PHASE (L=1,3)
*----ID QI(M,L) C(M,KC,L)
1 0.00213 0.9865 0. 0.0135 0.225 0.0 0.0 0. 0.
1 0. 0. 0. 0. 0. 0. 0. 0.  0.
1 0. 0. 0. 0. 0. 0. 0. 0.  0.
CC
CC
*---- INJ_SOLUTION
      101
CC
CC ID,
*----ID PWF
2 14.7
```

```
CC
CC CUM. INJ. TIME , AND INTERVALS (PV OR DAY) FOR WRITING TO OUTPUT FILES
*----TINJ CUMPR1 CUMHI1 WRHPV WRPRF RSTC
0.4 0.01 0.01 0.01 0.01 2.5
CC
CC FOR IMES=2 ,THE INI. TIME STEP,CONC. TOLERANCE,MAX.,MIN. COURANT NO.
*----DT DCLIM CNMAX CNMIN
0.000001 16*0.01 0.1 0.005
CC****** Polymer drive 1 **********************
CC FLAG FOR INDICATING BOUNDARY CHANGE
*---- IBMOD
0
CC
CC IRO, ITIME, NEW FLAGS FOR ALL THE WELLS
*---- IRO ITIME IFLAG
2 1 1 2
CC
CC NUMBER OF WELLS CHANGES IN LOCATION OR SKIN OR PWF
*---- NWEL1
0
CC
CC NUMBER OF WELLS WITH RATE CHANGES, ID
*---- NWEL2 ID
1 1
CC
CC ID,INJ. RATE AND INJ. COMP. FOR RATE CONS. WELLS FOR EACH PHASE (L=1,3)
*---- ID QI(M,L) water oil surf polymer Chlor divalent
1 0.00213 1.0 0. 0.0 0.25 0.0 0.0 0. 0.
1 0. 0. 0. 0. 0. 0. 0. 0.
1 0. 0. 0. 0. 0. 0. 0. 0.
CC
CC
*---- INJ_SOLUTION
      102
CC
CC CUM. INJ. TIME , AND INTERVALS (PV) FOR WRITING TO OUTPUT FILES
*---- TINJ CUMPR1 CUMHI1 WRHPV WRPRF RSTC
0.9 0.01 0.01 0.01 0.01 2.5
CC
CC FOR IMES=4 ,THE INI. TIME STEP,CONC. TOLERANCE,MAX.,MIN. TIME STEPS
*---- DT DCLIM CNMAX CNMIN
0.000001 16*0.01 0.1 0.005
CC****** Polymer drive 2 **********************
CC FLAG FOR INDICATING BOUNDARY CHANGE
*---- IBMOD
0
CC
CC IRO, ITIME, NEW FLAGS FOR ALL THE WELLS
*---- IRO ITIME IFLAG
2 1 1 2
CC
CC NUMBER OF WELLS CHANGES IN LOCATION OR SKIN OR PWF
*---- NWEL1
0
CC
CC NUMBER OF WELLS WITH RATE CHANGES, ID
*---- NWEL2 ID
1 1
CC
CC ID,INJ. RATE AND INJ. COMP. FOR RATE CONS. WELLS FOR EACH PHASE (L=1,3)
*---- ID QI(M,L) water oil surf polymer Chlor divalent
1 0.00213 1.0 0. 0.0 0.25 0.0 0.0 0. 0.
1 0. 0. 0. 0. 0. 0. 0. 0.
1 0. 0. 0. 0. 0. 0. 0. 0.
CC
```

```
CC
*---- INJ_SOLUTION
      103
CC
CC CUM. INJ. TIME , AND INTERVALS (PV) FOR WRITING TO OUTPUT FILES
*---- TINJ CUMPR1 CUMHI1 WRHPV WRPRF RSTC
2.5 0.01 0.01 0.01 0.01 2.5
CC
CC FOR IMES=4 ,THE INI. TIME STEP,CONC. TOLERANCE,MAX.,MIN. TIME STEPS
*---- DT DCLIM CNMAX CNMIN
0.000001 16*0.001 0.1 0.005
```

GCINPUT

```
CC
CC*********************************************************
CC                                      *
CC          GEOCHEMISTRY SECTION                *
CC                                      *
CC*********************************************************
CC
CC
*---- IRSPS   IPHAD  EQW(Equivalent weight of surfactant)
      2       1   400
CC
CC
*--- PHC PHT PHT1 HPHAD(The constant by which the surfactant adsorption is reduced)
     7   13  13   0.1
CC
CC
*---- CSELP(meq/ml) CSEUP(meq/ml)
         0.1         0.2
CC
CC
*-----IMIX
     0
CC
CC
*------HBN0 HBN1 HBN2

CC
CC
*----   AW_MW      EQWPS       Log(Kp) (HAo=HAw)     Log(Kd) (HAw= H+ + Aw-)
      59.05       500.0        -3.966082235              -8.0
CC
CC*********************************************************
CC                                      *
CC          GEOCHEMISTRY OUTPUT  SECTION          *
CC                                      *
CC*********************************************************
CC
CC
```

```
*---- PRINT_NUMBER_ELEMENT   ELEMENT_HISTORY   ELEMENT_MAP    FREQUENCY_HIS(TIME STEP)
FREQUENCY_MAP(TIME STEP)
          0              1              1                1                1
CC
CC
*---- NSLDP  SOLID_HISTORY   SOLID_MAP    FREQUENCY_HIS (TIME STEP)    FREQUENCY_MAP(TIME STEP)
      0     1              1              1         1
CC
CC
*----  NAQSP   AQS_HISTORY   AQS_MAP    FREQUENCY_HIS(TIME STEP)    FREQUENCY_MAP(TIME STEP)
       0       1           1              1                    1
CC
CC
*---- NSORBP  SORBED_HISTORY   ELEMENT_MAP    FREQUENCY_HIS (TIME STEP)   FREQUENCY_MAP (TIME STEP)
       0        1              1              1                    1
CC
CC
*---- NPRINTG    PRINTG_HISTORY   PRINTG_MAP    FREQUENCY_HIS (TIME STEP)  FREQUENCY_MAP(TIME STEP)
       3           1            1              1                   10
cc
cc
*-----
1
cc
cc
*------
1
1
1
cc
cc
*-----
TOT("Ca")
TOT("S")
-la("H+")
```

IPHREEQC INPUT

```
## ****************************************************************************
##                    GRIDBLOCK INITIALIZATION
## ****************************************************************************

SOLUTION 1-25
 -units  ppm
 -water 1## in Kg
## it is converted to PV/gridblock automatically
-pH    7.5
temp 59
Na  35384
Cl  54615 charge
END

use solution 1-25
equilibrium_phases 1-25
       Anhydrite 0 0.217    #changing from 0.217
save solution 1-25
END

## ---------------------------------------------------------------------
```

```
##                    INJECTION SOLUTIONS
## -----------------------------------------------------------------

SOLUTION 101
  -water  1  ## kg
  -units   ppm
#pH 11.1
temp 59
Na  30760.8
Cl  42478.6 charge
S(6) 6760.6
end

use solution 101
equilibrium_phases 101
NH3(g) -1 0.294 #orig 0.294
save solution 101
end

SOLUTION 102
  -water   1  ## kg
  -units   ppm
temp 59
Na  18965.9
Cl  24273.5 charge
S(6) 6760.56
END

SOLUTION 103
  -water   1  ## kg
  -units   ppm
temp 59
Na  11102.68
Cl  12136.75 charge
S(6) 6760.56
END
```

PHREEQC Input File for Low Salinity Wettability Alteration

```
## INITILIZATION
Solution_Master_Species
A  A-  0  A  350

Solution_Species
A- = A-
        log_k 0.0

H+ + A- = HA
        log_k 3.98  #orig 3.98

#HA + Ca+2 = CaA+ + H+
#       log_k -2.20

#HA + Mg+2 = MgA+ + H+
#       log_k -3.30
end

Surface_master_species
#Ca_s  Ca_sOH
#Co_s  Co_sH

Ca_s  Ca_sH2O+
Co_s    Co_s-


Surface_Species
Ca_sH2O+ = Ca_sH2O+
                log_k 0.0

Ca_sH2O+ = Ca_sOH + H+
    log_k  -12.8 #different K value

Ca_sH2O+ + HCO3- = Ca_sCO3- + H+ + H2O
        log_k = -5.65

Ca_sH2O+ + HCO3- = Ca_sHCO3 + H2O
                log_k  1.68  #original k value

Ca_sH2O+ + SO4-2 = Ca_sSO4- + H2O
         log_k 2.8

Ca_sH2O+ + A- = Ca_sH2OA
         log_k 2.5 #orig 5.4

Co_s- = Co_s-
        log_k 0.0

Co_s- + H+ = Co_sH
        log_k 5.48  #different K value

Co_s- + Ca+2 = Co_sCa+
        log_k 1.74

Co_s- + Mg+2 = Co_sMg+
        log_k 1.74

Co_sCa+ + A- = Co_sCaA
        log_k 2.5

Co_sMg+ + A- = Co_sMgA
        log_k 2.5
```

```
Co_sCa+ + SO4-2 = Co_sCaSO4-
        log_k 5.0

Co_sMg+ + SO4-2 = Co_sMgSO4-
        log_k 5.0
end


#Formation Brine
SOLUTION 1-20
-temp   120   ## degree C
-water 0.005 #100 grams solution
-pH         7.5
-units mg/L
Na          57231
Ca          7056
Mg          3636
Cl          124389 charge
S(6)        268
A 1000
save solution 1-20


equilibrium_phases 1-20
Calcite 0 10
Dolomite -0.07 0
#Anhydrite 0.34 0

SURFACE 1-20
                    -sites_units density sites/nm^2
                    #Surface    number_sites_in_moles  specific_SurfaceArea(m2/g)  Mass_solid_in_gram
    Ca_s     3    0.5  30 #4 grams caco3
          Co_s     3    0.5  30
        #-diffuse_layer
        #-only_counter_ions
-no edl
save solution 1-20
end



#Seawater
SOLUTION 0
-temp   120   ## degree C
-water 0.005 #5 grams solution
-units mg/L
-pH 7.5
Na          12378.16
Ca          511.64
Mg          1600
Cl          26657.23 charge
S(6)        3589.06
A 1000
save solution 0
end

#PRINT

TRANSPORT
-Cells 20
-shifts 60
-lengths 0.012
-flow_direction forward
-boundary_conditions flux flux
```

```
-dispersivities 0.001

Selected_output
 -file FB-SW.sel
 -selected_output true
 -solution true
 -totals Ca Na Mg Cl S
 -molalities Ca_sH2OA Co_sCaA Co_sMgA
# -equilibrium_phases Calcite Dolomite Anhydrite
 #-water true
 -ph true
 -distance true
 -time true
END
```

REFERENCES

Abdallah, W., Buckley, J.s., Carnegie, A., Edwards, J., Herold, B., Fordham, E., Graue, A., Habashy, T., Seleznev, N., Signer, C., Hussain, H., Montaron, B., and Ziauddin, M. (2007). Fundamentals of Wettability. Schlumberger Oilfield Review **19** (2): 44-61

Adibhatla, B., & Mohanty, K. K. (2008, February 1). Oil Recovery From Fractured Carbonates by Surfactant-Aided Gravity Drainage: Laboratory Experiments and Mechanistic Simulations. Society of Petroleum Engineers. doi:10.2118/99773-PA

Adkins, S., Liyanage, P.L., Arachchilage, G.W.P., Mudiyanselage, T., Weerasooriya, U., Pope, G.A. (2010). A new process of manufacturing and stabilizing high performance EOR surfactants at low cost for high temperature, high salinity oil reservoirs. Paper SPE 129923 presented at the SPE Improved Oil Recovery Symposium, 24-28 April, Tulsa, Oklahoma, USA

Adkins, S., Pinnawala Arachchilage, G. W. P., Solairaj, S., Lu, J., Weerasooriya, U., & Pope, G. A. (2012, January 1). Development of Thermally and Chemically Stable Large-Hydrophobe Alkoxy Carboxylate Surfactants. Society of Petroleum Engineers. doi:10.2118/154256-MS

Aitkulov, A., & Mohanty, K. K. (2016, April 11). Timing of ASP Injection for Viscous Oil Recovery. Society of Petroleum Engineers. doi:10.2118/179606-MS

Alvarado, V., Manrique, M. (2010). Enhanced oil recovery: An update review. Energies 3(9) 1529-1575

Anderson, W. G. (1986, October 1). Wettability Literature Survey- Part 1: Rock/Oil/Brine Interactions and the Effects of Core Handling on Wettability. Society of Petroleum Engineers. doi:10.2118/13932-PA

Atkinson, H. (1927). Recovery of petroleum from oil-bearing sands. US patent 1651311A

Austad, T. (2009). Is wettability alteration of carbonates by seawater caused by rock dissolution? Paper presented at the International symposium of society of core analyst, The Netherlands

Austad, T., Strand, S., Madland, M. V., Puntervold, T., and Korsnes, R. I. (2008). Seawater in chalk: An EOR and compaction fluid. SPE Reservoir Evaluation & Engineering, 11(04), 648-654. doi: http://dx.doi.org/10.2118/118431-PA

Barnes, J. R., Dirkzwager, H., Smit, J., Smit, J., On, A., Navarrete, R. C., Buijse, M. A. (2010, January 1). Application of Internal Olefin Sulfonates and Other Surfactants to EOR. Part 1: Structure - Performance Relationships for Selection at Different Reservoir Conditions. Society of Petroleum Engineers. doi:10.2118/129766-MS

Berger, P.D., Lee, C.H. (2006). Improved ASP process using organic alkali. 2006. Paper SPE 99581-MS presented at the SPE/DOE symposium on Improved Oil Recovery, 22-26 April, Tulsa, Oklahoma, USA.

Bhuyan, D., Pope, G. A., & Lake, L. W. (1991, January 1). Simulation of High-pH Coreflood Experiments Using a Compositional Chemical Flood Simulator. Society of Petroleum Engineers. doi:10.2118/21029-MS

Bourrel, M., Schechter, R.S. (2010). Microemulsions and related systems. ISBN: 9782710809562

Brady, P. V., Krumhansl, J. L., & Mariner, P. E. (2012, January 1). Surface Complexation Modeling for Improved Oil Recovery. Society of Petroleum Engineers. doi:10.2118/153744-MS

Bragg, J. R., Gale, W. W., & Canning, J. W. (1983, January 1). Loudon Surfactant Flood Pilot-Overview and Update. Society of Petroleum Engineers. doi:10.2118/11505-MS

Buckley, J. S., Liu, Y., Xie, X., & Morrow, N. R. (1997, June 1). Asphaltenes and Crude Oil Wetting - The Effect of Oil Composition. Society of Petroleum Engineers. doi:10.2118/35366-PA

Bunge, A. L., & Radke, C. J. (1982, December 1). Migration of Alkaline Pulses in Reservoir Sands. Society of Petroleum Engineers. doi:10.2118/10288-PA

Bunge, A.L., Radke, C.J.1985. The origin of reversible hydroxide uptake on reservoir rock. Paper SPE 11798

Burk, J. H. (1987, February 1). Comparison of Sodium Carbonate, Sodium Hydroxide, and Sodium Orthosilicate for EOR. Society of Petroleum Engineers. doi:10.2118/12039-PA

Campbell, T. C. (1977, January 1). A Comparison of Sodium Orthosilicate And Sodium Hydroxide For Alkaline Waterflooding. Society of Petroleum Engineers. doi:10.2118/6514-MS

Cappellen, P.V., Charlet, L., Stumm, W., Wersin, P. (1993). A surface complexation model of the carbonate mineral-aqueous solution interface. Geochimica et Cosmochimica Acta 57(15): 3505-3518

Chatzis, I., & Morrow, N. R. (1984, October 1). Correlation of Capillary Number Relationships for Sandstone. Society of Petroleum Engineers. doi:10.2118/10114-PA

Chuoke, R.L., van Meurs, P., and van der Poel, C. (1959). The Instability of Slow, Immiscible, Viscous Liquid-Liquid Displacements in Permeable Media, Aime 216

Cooke, C.E., Williams, R.E., Kolodzie, P.A. (1974). Oil recovery by alkaline waterflooding. Paper SPE 4739

Cui, L., Ma, K., Abdala, A. A., Lu, L. J., Tanakov, I., Biswal, S. L., & Hirasaki, G. J. (2014, April 12). Adsorption of a Switchable Cationic Surfactant on Natural Carbonate Minerals. Society of Petroleum Engineers. doi:10.2118/169040-MS

De Zabala, E.F., Vislocky, J.M., Rubin, E., Radke, C.J. (1982). A chemical theory for linear alkaline flooding. Paper SPE 8997-PA

Delamaide, E., Zaitoun, A., Renard, G., & Tabary, R. (2013, July 2). Pelican Lake Field: First Successful Application of Polymer Flooding in a Heavy Oil Reservoir. Society of Petroleum Engineers. doi:10.2118/165234-MS

Delshad, M., Bhuyan, D., Pope, G. A., & Lake, L. W. (1986, January 1). Effect of Capillary Number on the Residual Saturation of a Three-Phase Micellar Solution. Society of Petroleum Engineers. doi:10.2118/14911-MS

Delshad, M., Pope, G.A., and Sepehrnoori, K. (1996). A Compositional Simulator for Modeling Surfactant Enhanced Aquifer Remediation. Journal of Contaminant Hydrology, 23, 303-327

Demin, W., Zhenhua, Z., Jiecheng, C., Jingchun, Y., Shutang, G., & Li, L. (1997, November 1). Pilot Test of Alkaline Surfactant Polymer Flooding in Daqing Oil Field. Society of Petroleum Engineers. doi:10.2118/36748-PA

Doe, P.H., Wade, W.H., Schechter, R.S. (1976). Alkyl benzene sulfonate for producing low interfacial tensions between hydrocarbons and water. Journal of colloid and interface science 59 (3) 525-531

Doorwar, S., & Mohanty, K. K. (2015, February 23). Fingering Function for Unstable Immiscible Flows. Society of Petroleum Engineers. doi:10.2118/173290-MS

Doorwar, S., & Mohanty, K. K. (2016, July 1). Viscous-Fingering Function for Unstable Immiscible Flows. Society of Petroleum Engineers. doi:10.2118/173290-PA

Emery, L. W., Mungan, N., & Nicholson, R. W. (1970, December 1). Caustic Slug Injection in the Singleton Field. Society of Petroleum Engineers. doi:10.2118/2425-PA

Falls, A.H., Thigpen, D.R., Nelson, R.C., Ciaston, J.W., Lawson, J.B., Good, P.A., Ueber, R.C., Shahin, G.T. (1994). Field Test of Cosurfactant-Enhanced Alkaline Flooding. *SPE Res Eng*, **9**(3): 217-223. SPE 24117-PA. doi: 10.2118/24117-PA

Farajzadeh, R., Krastev, R., Zitha, P.L.J. (2008). Foam films stabilized with alpha olefin sulfonate (AOS). Colloids and surfaces A: Physicochemical and engineering aspects 324 (1-3) 35-40

Fathi, S. J., Austad, T., and Strand, S. (2012). Water-Based Enhanced Oil recovery (EOR) by “Smart Water” in Carbonate Reservoirs. SPE EOR Conference at Oil and Gas West Asia. Muscat, Oman. 16-18 April. doi:10.2118/154570-MS

Fortenberry, R., Kim, D. H., Nizamidin, N., Adkins, S., Arachchilage, G. W. P. P., Koh, H. S., Pope, G. A. (2015, April 1). Use of Cosolvents to Improve Alkaline/Polymer Flooding. Society of Petroleum Engineers. doi:10.2118/166478-PA

French, M. S., Keys, G. W., Stegemeier, G. L., Ueber, R. C., Abrams, A., & Hill, H. J. (1973, February 1). Field Test of an Aqueous Surfactant System for Oil Recovery, Benton Field, Illinois. Society of Petroleum Engineers. doi:10.2118/3799-PA

Gao, C.H. (2011). Scientific research and field applications for polymer flooding in heavy oil recovery. J Petrol Explor Prod Technol (1) 65-70. doi 10.1007/s13202-011-0014-6

Ghosh, P., & Mohanty, K. K. (2016, April 11). Foams with Wettability Alteration for Oil-Wet Carbonate Rocks. Society of Petroleum Engineers. doi:10.2118/179598-MS

Gilliland, H. E., & Conley, F. R. (1976, January 1). A Pilot Test of Surfactant Flooding in the Big Muddy Field. Society of Petroleum Engineers. doi:10.2118/5891-MS

Glover, C. J., Puerto, M. C., Maerker, J. M., & Sandvik, E. L. (1979, June 1). Surfactant Phase Behavior and Retention in Porous Media. Society of Petroleum Engineers. doi:10.2118/7053-PA

Graue, D. J., & Johnson, C. E. (1974, December 1). Field Trial of Caustic Flooding Process. Society of Petroleum Engineers. doi:10.2118/4740-PA

Green, D. W. and Willhite, G. P. (1988). Enhanced oil recovery, SPE Textbook Series, Volume 6, Society of Petroleum Engineers, Richardson, TX, USA

Hahn, R. (2015). Novel cationic surfactants for CO2-foam flooding in carbonate reservoirs. MS Thesis, The University of Texas at Austin

He, L., Gang, C., & Guochen, S. (2007, January 1). Technical Breakthrough in PCP's Scaling Issue of ASP Flooding in Daqing Oilfield. Society of Petroleum Engineers. doi:10.2118/109165-MS

Healy, R. N., Reed, R. L., & Stenmark, D. G. (1976, June 1). Multiphase Microemulsion Systems. Society of Petroleum Engineers. doi:10.2118/5565-PA

Hill, H. J., Helfferich, F. G., Lake, L. W., Reisberg, J., & Pope, G. A. (1977, October 1). Cation Exchange and Chemical Flooding. Society of Petroleum Engineers. doi:10.2118/6642-PA

Hirasaki, G. (1982, April 1). Ion Exchange with Clays in the Presence of Surfactant. Society of Petroleum Engineers. doi:10.2118/9279-PA

Hirasaki, G. J. (1981, April 1). Application of the Theory of Multicomponent, Multiphase Displacement to Three-Component, Two-Phase Surfactant Flooding. Society of Petroleum Engineers. doi:10.2118/8373-PA

Hirasaki, G. J. (1982, December 1). Interpretation of the Change in Optimal Salinity with Overall Surfactant Concentration. Society of Petroleum Engineers. doi:10.2118/10063-PA

Hirasaki, G. J., Miller, C. A., & Puerto, M. (2008, January 1). Recent Advances in Surfactant EOR. Society of Petroleum Engineers. doi:10.2118/115386-MS

Hirasaki, G. J., van Domselaar, H. R., & Nelson, R. C. (1983, June 1). Evaluation of the Salinity Gradient Concept in Surfactant Flooding. Society of Petroleum Engineers. doi:10.2118/8825-PA

Huang, L., Yang, P., Qin, T. (1986). A study of caustic consumption by clays. SPE/DOE 14945

Huh, C., and Pope, G. A. (2008). Residual Oil Saturation from Polymer Floods: Laboratory Measurements and Theoretical Interpretation, Society of Petroleum Engineers. doi:10.2118/113417-MS

Humphry, K. J., van der Lee, M., Southwick, J. G., Ineke, E. M., & van Batenburg, D. W. (2013, July 2). Microemulsion Flow in Porous Media: Implications for Alkaline-Surfactant-Polymer Flooding. Society of Petroleum Engineers. doi:10.2118/165233-MS

International energy agency (IEA). (2015). Storing CO2 through enhanced oil recovery-Combining EOR with CO2 storage (EOR+) for profit, Insights series

Jang, S. H., Liyanage, P. J., Tagavifar, M., Chang, L., Upamali, K. A. N., Lansakara-P, D., Pope, G. A. (2016, April 11). A Systematic Method for Reducing Surfactant Retention to Extremely Low Levels. Society of Petroleum Engineers. doi:10.2118/179685-MS

Jennings, H.Y. (1975). A study of caustic solution-crude oil interfacial tensions. Paper SPE 5049

Jennings, H.Y., Johnson, C.E., McAuliffe, C.D.1974. A caustic waterflooding process for heavy oils. Paper SPE 4741

Johnson, C. E. Jr. (1976). Status of Caustic and Emulsion Methods, J. Pet. Tech. 28 (1): 85-92. SPE 5561-PA

Kamath, J., Meyer, R. F., & Nakagawa, F. M. (2001, January 1). Understanding Waterflood Residual Oil Saturation of Four Carbonate Rock Types. Society of Petroleum Engineers. doi:10.2118/71505-MS

Kazemi Nia Korrani, A., Sepehrnoori, K., & Delshad, M. (2014, April 12). A Mechanistic Integrated Geochemical and Chemical Flooding Tool for Alkaline/Surfactant/Polymer Floods. Society of Petroleum Engineers. doi:10.2118/169094-MS

Kazempour, M., Sundstrom, E., Alvarado, V. (2011). Geochemical modeling and experimental evaluation of high pH floods: Impact of water-rock interactions in sandstone. Paper SPE 143479 presented at the SPE EUROPAC/EAGE Annual Conference and Exhibition, 23-26 May, Vienna, Austria, USA.

Koh, H., Lee, V. B., & Pope, G. A. (2016, April 11). Experimental Investigation of the Effect of Polymers on Residual Oil Saturation. Society of Petroleum Engineers. doi:10.2118/179683-MS

Koning, E., Mentzer, E., Heemskerk, J. (1988). Evaluation of a pilot polymer flood in the Marmul field Oman. SPE 18092 presented at annual technical conference and exhibition, Houston, Texas, 2–5 October 1988

Koval, E. J. (1963, June 1). A Method for Predicting the Performance of Unstable Miscible Displacement in Heterogeneous Media. Society of Petroleum Engineers. doi:10.2118/450-PA

Krumrine, P. H., Falcone, J. S., & Campbell, T. C. (1982, August 1). Surfactant Flooding 1: The Effect of Alkaline Additives on IFT, Surfactant Adsorption, and Recovery Efficiency. Society of Petroleum Engineers. doi:10.2118/8998-PA

Kulawardana, E. U., Koh, H., Kim, D. H., Liyanage, P. J., Upamali, K., Huh, C., Pope, G. A. (2012, January 1). Rheology and Transport of Improved EOR Polymers under Harsh Reservoir Conditions. Society of Petroleum Engineers. doi:10.2118/154294-MS

Lager, A., Webb, K. J., Collins, I. R., and Richmond, D. M. (2008). LoSal Enhanced Oil Recovery: Evidence of Enhanced Oil Recovery at the Reservoir Scale. SPE: Society of Petroleum Engineers. doi:10.2118/113976-MS

Lake, L. W., & Helfferich, F. (1978, December 1). Cation Exchange in Chemical Flooding: Part 2--The Effect of Dispersion, Cation Exchange, and Polymer/Surfactant Adsorption on Chemical Flood Environment. Society of Petroleum Engineers. doi:10.2118/6769-PA

Lake, L.W (2010). Enhanced oil recovery. ISBN: 978-1-55563-305-9

Leach, R. O., Wagner, O. R., Wood, H. W., and Harpke, C. F. (1962). A Laboratory and Field Study of Wettability Adjustment in Waterflooding, J. *Per. Tech.* (Feb. 1962) 206-212; ***Trans.*** AIME, 225

Lenormand, R., Touboul, E., & Zarcone, C. (1988). Numerical models and experiments on immiscible displacements in porous media. Journal of Fluid Mechanics, 189, 165-187

Leonhardt, B., Ernst, B., Reimann, S., Steigerwald, A., & Holding, W. (2014). Field Testing the Polysaccharide Schizophyllan : Results of the First Year. The SPE Improved Oil Recovery Symposium-Oklahoma, (April), 1–16. doi:10.2118/169032-MS

Levitt, D. and Pope, G.A. (2008). Selection and screening of polymers for enhanced oil recovery. Paper SPE 113845 presented at the SPE Improved Oil Recovery Symposium, 19-23 April, Tulsa, Oklahoma, USA

Levitt, D. and Pope, G.A. (2011). Chemical degradation of polyacrylamide polymers under alkaline conditions. Paper SPE 129879-PA

Levitt, D., Dufour, S., Pope, G.A., Morel, D.C., Gauer, P.R. (2011). Design of an ASP flood in a High-Temperature, High-Salinity, Low-Permeability Carbonate. Paper IPTC 14915 presented at the International Petroleum Technology Conference, 15-17 November, Bangkok, Thailand

Levitt, D., Jackson, A., Heinson, C., Britton, L. N., Malik, T., Dwarakanath, V., & Pope, G. A. (2006, January 1). Identification and Evaluation of High-Performance EOR Surfactants. Society of Petroleum Engineers. doi:10.2118/100089-MS

Levitt, D.B. (2009). The optimal use of enhanced oil recovery polymers under hostile conditions. Ph.D. dissertation, The University of Texas at Austin

Liu, M., Wang, Y., Liao, X., Zhao, C., Yang, Q., Yan, R. (2010). Study and application of profile modification in offshore fields. SPE 133812 presented at SPE Asia Pacific oil and gas conference and exhibition, Brisbane, Australia, 18–20 October 2010

Liu, S., Miller, C. A., Li, R. F., & Hirasaki, G. (2010, June 1). Alkaline/Surfactant/Polymer Processes: Wide Range of Conditions for Good Recovery. Society of Petroleum Engineers. doi:10.2118/113936-PA

Lopez-Salinas, J.L., Hirasaki, G.J., Miller, C.A. (2011). Determination of anhydrite in reservoirs for EOR. Paper SPE 141420 presented at the SPE International Symposium on Oilfield Chemistry, 11-13 April, Woodlands, Texas, USA

Lu, J., & Pope, G. A. (2015, April 27). Optimization of Gravity-Stable Surfactant Flooding. Society of Petroleum Engineers. doi:10.2118/174033-MS

Lu, J., Britton, C., Solairaj, S., Liyanage, P. J., Kim, D. H., Adkins, S., Pope, G. A. (2014, December 1). Novel Large-Hydrophobe Alkoxy Carboxylate Surfactants for Enhanced Oil Recovery. Society of Petroleum Engineers. doi:10.2118/154261-PA

Luo, H., Al-Shalabi, E. W., Delshad, M., Panthi, K., & Sepehrnoori, K. (2016, February 1). A Robust Geochemical Simulator to Model Improved-Oil-Recovery Methods. Society of Petroleum Engineers. doi:10.2118/173211-PA

Mahani, H., Keya, A.L., Berg, S., Bartels, W.B., Nasralla, R., Rossen, W.R. (2015). Insights into the mechanisms of wettability alteration by low salinity flooding (LSF) in carbonates. Energy Fuels 29(3): 1352-1367

Manichand, R., Mogollon, J., Bergwijn, S., Graanoogst, F., Ramdajal, R. (2010). Preliminary assessment of Tambaredjo heavy oilfield polymer flooding pilot test. SPE 138728 presented at SPE Latin American and Caribbean petroleum engineering conference, Lima, Peru, 1–3 December 2010

Manrique, E. J., Muci, V. E., & Gurfinkel, M. E. (2006, January 1). EOR Field Experiences in Carbonate Reservoirs in the United States. Society of Petroleum Engineers. doi:10.2118/100063-MS

Martin, F.D., Oxley, J.C. (1985). Effect of various alkaline chemicals on phase behavior of surfactant/brine/oil mixtures. Paper SPE 13575 presented at the International Symposium on Oilfield and Geothermal Chemistry, 9-11 April, Arizona, USA

Mayer, E.H., Berg, R.L., Carmichael, J.D., Weinbrandt, R.M. (1983). Alkaline injection for enhanced oil recovery-A status report. Paper SPE 8848-PA

McAuley, R. G. (1977, January 1). Sodium Hydroxide Enhanced Waterflood In The Wainwright Field. Petroleum Society of Canada. doi:10.2118/77-14

McGuire, P. L., Chatham, J. R., Paskvan, F. K., Sommer, D. M., and Carini, F. H. (2005). Low Salinity Oil Recovery: An Exciting New EOR Opportunity for Alaska's North Slope. SPE Western Regional Meeting. Irvine, California. 30 March-1 April. doi:10.2118/93903-MS

Mohammadi, H., Delshad, M., & Pope, G. A. (2009, August 1). Mechanistic Modeling of Alkaline/Surfactant/Polymer Floods. Society of Petroleum Engineers. doi:10.2118/110212-PA

Mohanty, K. K., Davis, H. T., & Scriven, L. E. (1987, February 1). Physics of Oil Entrapment in Water-Wet Rock. Society of Petroleum Engineers. doi:10.2118/9406-PA

Mohnot, S.M., Bae, J.H. (1989). A study of mineral/alkali reactions-Part 2. Paper SPE 13576-PA

Mohnot, S.M., Bae, J.H., Foley, W.L. (1987). A study of mineral/alkali reactions. Paper SPE 13032-PA

Muller, G. (1981a). Thermal Stability of High-molecular-weight Polyacrylamide Aqueous Solutions. Polymer Bulletin 5: 31-37

Muller, G. (1981b). Thermal Stability of Polyacrylamide Solutions: Effect of Residual Impurities in the Molecular-weight-degradation Process upon Heating. Polymer Bulletin 5: 39-45

Nadeeka Upamali, K., Liyanage, P. J., Cai, J., Lu, J., Jang, S. H., Weerasooriya, U. P., & Pope, G. A. (2016, April 11). New Surfactants and Co-Solvents Increase Oil Recovery and Reduce Cost. Society of Petroleum Engineers. doi:10.2118/179702-MS

Nelson, R. C. (1982, April 1). The Salinity-Requirement Diagram - A Useful Tool in Chemical Flooding Research and Development. Society of Petroleum Engineers. doi:10.2118/8824-PA

Nelson, R. C., & Pope, G. A. (1978, October 1). Phase Relationships in Chemical Flooding. Society of Petroleum Engineers. doi:10.2118/6773-PA

Nelson, R.C., Lawson, J.B., Thigpen, D.R., Stegemeier, G.L. (1984). Cosurfactant-enhanced alkaline flooding. Paper SPE 12672 MS presented at the SPE Enhanced Oil Recovery symposium, 15-18 April, Tulsa, Oklahoma, USA

Novosad, Z., Novosad, J. (1984). Determination of Alkalinity Losses Resulting from Hydrogen Ion Exchange in Alkaline Flooding. Paper SPE 10605-PA

Nutting, P. G. (1925). Chemical Problems in the Water-driving of Petroleum Reservoirs, *Ind.Eng. Chem.*, **17**, 1035–1036, 1925

Pakrhurst, D.L., Appelo, C.A.J. (1999). User's guide to PHREEQC (Version 2): A computer program for speciation, batch-reaction, one-dimensional transport, and inverse geochemical calculations. US Geological Survey

Pandey, A., Koduru, N., Stanley, M., Pope, G. A., & Weerasooriya, U. P. (2016, April 11). Results of ASP Pilot in Mangala Field: A Success Story. Society of Petroleum Engineers. doi:10.2118/179700-MS

Peters, E. J., & Flock, D. L. (1981, April 1). The Onset of Instability During Two-Phase Immiscible Displacement in Porous Media. Society of Petroleum Engineers. doi:10.2118/8371-PA

Peters, E.J. 2012. Advanced Petrophysics, ISBN-978-1-936909-44-5

Pope, G. A. (1980, June 1). The Application of Fractional Flow Theory to Enhanced Oil Recovery. Society of Petroleum Engineers. doi:10.2118/7660-PA

Pope, G. A., & Nelson, R. C. (1978, October 1). A Chemical Flooding Compositional Simulator. Society of Petroleum Engineers. doi:10.2118/6725-PA

Pope, G. A., Lake, L. W., & Helfferich, F. G. (1978, December 1). Cation Exchange in Chemical Flooding: Part 1--Basic Theory Without Dispersion. Society of Petroleum Engineers. doi:10.2118/6771-PA

Prasad, D., Pandey, A., Suresh Kumar, M., & Koduru, N. (2014, April 12). Pilot to Full-field Polymer Application in One of the Largest Onshore Field in India. Society of Petroleum Engineers. doi:10.2118/169146-MS

Puntervold, T., Strand, S., Ellouz, R., Austad, T. (2015). Modified seawater as a smart EOR fluid in chalk. Journal of Petroleum Science and Engineering (133) 440-443

Pursley, S.A., Healy, R.N., Sandvik, E.I. (1973). A field test of surfactant flooding, Loudon, Illinois. Paper SPE 3805

Qi, Q., Gu, H., Li, D., & Dong, L. (2000, January 1). The Pilot Test of ASP Combination Flooding in Karamay Oil Field. Society of Petroleum Engineers. doi:10.2118/64726-MS

Qiao, C., Li, L., Johns, R. T., & Xu, J. (2014). A Mechanistic Model for Wettability Alteration by Chemically Tuned Water Flooding in Carbonate Reservoirs. Society of Petroleum Engineers. doi:10.2118/170966-MS

Raicar, J., and Procter, R. M. (1984). Economic considerations and potential of heavy oil supply from Lloydminster – Alberta, Canada, in Meyer, R.F., Wynn, J.C., and Olson, J.C., eds., The Second UNITAR International Conference on Heavy Crude and Tar Sands, Caracas, February 7-17, 1982: New York, McGraw-Hill, p. 212-219

Ramsden, D.K. and McKay, K. (1986). The Degradation of Polyacrylamide in Aqueous Solutions Induced by Chemically Generated Hydroxyl Radicals: Part I – Fenton's Reagent. Polymer Degradation and Stability 14: 217-229

Ramsden, D.K. and McKay, K. (1986). The Degradation of Polyacrylamide in Aqueous Solutions Induced by Chemically Generated Hydroxyl Radicals: Part II -Autoxidation of Fe2+. Polymer Degradation and Stability 15: 15-31

Rivenq, R. C., Donche, A., & Nolk, C. (1992). Improved Scleroglucan for Polymer Flooding Under Harsh Reservoir Conditions. SPE Reservoir Engineering, 7(01), 15–20. doi:10.2118/19635-PA

Sahni, V.M. 2009. Experimental evaluation of co-solvents in development of high performance alkali/surfactant/polymer formulations for enhanced oil recovery. MS Thesis. The University of Texas at Austin

Salager, J. L., Bourrel, M., Schechter, R. S., & Wade, W. H. (1979, October 1). Mixing Rules for Optimum Phase-Behavior Formulations of Surfactant/Oil/Water Systems. Society of Petroleum Engineers. doi:10.2118/7584-PA

Salathiel, R. A. (1973, October 1). Oil Recovery by Surface Film Drainage in Mixed-Wettability Rocks. Society of Petroleum Engineers. doi:10.2118/4104-PA

Sandiford, B. B. (1964, August 1). Laboratory and Field Studies of Water Floods Using Polymer Solutions to Increase Oil Recoveries. Society of Petroleum Engineers. doi:10.2118/844-PA

Sanz, C.A. and Pope, G.A., "Alcohol-Free Chemical Flooding: From Surfactant Screening to Coreflood Design," Proceedings of the SPE International Symposium on Oilfield Chemistry, San Antonio, TX, February 14-17, 1995

Seethepalli, A., Adibhatla, B., & Mohanty, K. K. (2004, December 1). Physicochemical Interactions During Surfactant Flooding of Fractured Carbonate Reservoirs. Society of Petroleum Engineers. doi:10.2118/89423-PA

Seright, R. S., & Henrici, B. J. (1990). Xanthan Stability at Elevated Temperatures. SPE Reservoir Engineering, 5(1). doi:10.2118/14946-PA

Seright, R., & Skjevrak, I. (2015, June 1). Effect of Dissolved Iron and Oxygen on Stability of Hydrolyzed Polyacrylamide Polymers. Society of Petroleum Engineers. doi:10.2118/169030-PA

Sharma, G., & Mohanty, K. (2013, April 22). Wettability Alteration in High-Temperature and High-Salinity Carbonate Reservoirs. Society of Petroleum Engineers. doi:10.2118/147306-PA

Sheng, J.J. (2016). Critical review of alkaline-polymer flooding. J Petrol Explor Prod Technol. doi:10.1007/s13202-016-0239-5

Shupe, R.D. (1981). Chemical Stability of Polyacrylamide Polymers. JPT 1513-1529

Singh, R., & Mohanty, K. K. (2015). Synergy between nanoparticles and surfactants in stabilizing foams for oil recovery. Energy & Fuels, 29(2), 467-479

Singh, R., & Mohanty, K. K. (2016). Foams with Wettability-Altering Capabilities for Oil-Wet Carbonates: A Synergistic Approach. SPE Journal,21(04), 1,126-1,139. doi:10.2118/175027-PA

Somasundaran, P., & Hanna, H. S. (1979, August 1). Adsorption of Sulfonates on Reservoir Rocks. Society of Petroleum Engineers. doi:10.2118/7059-PA

Somasundaran, P., Ananthapadmanabhan, K. P., & Viswanathan, K. V. (1983, January 1). Adsorption of Sulfonate on Kaolinite and Alumina in the Presence of Gypsum. Society of Petroleum Engineers. doi:10.2118/11780-MS

Somasundaran, P., Zhang L. (2006). Adsorption of surfactants on minerals for wettability control in improved oil recovery processes. Journal of Petroleum Science and Engineering (52) 198-212

Sorbie, K.S. (1991). Polymer improved oil recovery. ISBN: 0-8493-7137-6

Southwick, J.G. (1985). Solubility of silica in alkaline solutions: Implications for alkaline flooding. Paper SPE 12771-PA

Standnes, D.C. and Austad, T. (2000). Wettability alteration in chalk 2. Mechanism for wettability alteration from oil-wet to water-wet using surfactants. Journal of Petroleum Science and Engineering, 28, 123-143

Standnes, D.C. and Austad, T. (2003). Wettability alteration in carbonates: Interaction between cationic-surfactant and carboxylates as a key factor in wettability alteration from oil-wet to water-wet conditions Colloids and Surfaces A: Physicochemical Engineering Aspects, 216, 243-259

Stegemeier, G.L. (1977). Mechanism of Entrapment and Mobilization of Oil in Porous Media. New York City: Academic Press

Strand, S., Standnes, D. C., and Austad, T. (2006). New wettability test for chalk based on chromatographic separation of SCN− and SO42−. 2006. Journal of Petroleum Science and Engineering, 52(1), 187-197. doi: 10.1016/j.petrol.2006.03.021

Subkow, P. (1942). Process for the Removal of Bitumen from Bituminous Deposits. U.S Patent No. 2,288,857

Tagavifar, M., Herath, S., Weerasooriya, U. P., Sepehrnoori, K., & Pope, G. (2016, April 11). Measurement of Microemulsion Viscosity and Its Implications for Chemical EOR. Society of Petroleum Engineers. doi:10.2118/179672-MS

Talley, L. D. (1988, February 1). Hydrolytic Stability of Alkylethoxy Sulfates. Society of Petroleum Engineers. doi:10.2118/14912-PA

Thomas, S. 2008.Enhanced oil recovery-an overview, Oil & Gas Science and Technology – Rev.IFP, Vol.63

Topguder, N. (2010). A review on utilization of crosslinked polymer gels for improving heavy oil recovery in Turkey. SPE 131267 presented at SPE/EUROPEC/EAGE annual conference, Barcelona, Spain, 14–17 June 2010

Tweheyo, M. T., Zhang, P., and Austad, T. (2006). The Effects of Temperature and Potential Determining Ions Present in Seawater on Oil Recovery from Fractured Carbonates. SPE/DOE Symposium on Improved Oil Recovery. Tulsa, Oklahoma, USA. 22-26 April. doi:10.2118/99438-MS

Venkataraman, A. (2014). Gibbs free energy minimization for flow in porous media. PhD Dissertation, The University of Texas at Austin

Vargo, J., Turner, J., Bob, V., Pitts, M. J., Wyatt, K., Surkalo, H., & Patterson, D. (2000, December 1). Alkaline-Surfactant-Polymer Flooding of the Cambridge Minnelusa Field. Society of Petroleum Engineers. doi:10.2118/68285-PA

Vermolen, E. C. M., Van Haasterecht, M. J. T., Masalmeh, S. K., Faber, M. J., Boersma, D. M., & Gruenenfelder, M. A. (2011, January 1). Pushing the envelope for polymer

flooding towards high-temperature and high-salinity reservoirs with polyacrylamide based ter-polymers. Society of Petroleum Engineers. doi:10.2118/141497-MS

Viebke, C. (2005). Order-disorder conformational transition of xanthan gum. Polysaccharides: Structural Diversity and Functional Versatility, 2. In S. Dumitriu (Ed.), Polysaccharides: Structural Diversity and Functional Versatility , Second Edition (2nd ed., pp. 459–474). CRC Press

Vledder, P., Gonzalez, I. E., Carrera Fonseca, J. C., Wells, T., and Ligthelm, D. J. (2010). Low Salinity Water Flooding: Proof of Wettability Alteration On a Field Wide Scale. SPE: Society of Petroleum Engineers. doi:10.2118/129564-MS

Wagner, O.R and Leach, R.O. (1959). Improving Oil Displacement by Wettability Adjustment. Trans. AIME 216, 65-72

Walker, D., Britton, C., Kim, D. H., Dufour, S., Weerasooriya, U., & Pope, G. A. (2012, January 1). The Impact of Microemulsion Viscosity on Oil Recovery. Society of Petroleum Engineers. doi:10.2118/154275-MS

Wang, D., Seright, R. S., Shao, Z., & Wang, J. (2008, December 1). Key Aspects of Project Design for Polymer Flooding at the Daqing Oilfield. Society of Petroleum Engineers. doi:10.2118/109682-PA

Wang, F. H. L. (1993, May 1). Effects of Reservoir Anaerobic, Reducing Conditions on Surfactant Retention in Chemical Flooding. Society of Petroleum Engineers. doi:10.2118/22648-PA

Wassmuth, F., Arnold, W., Green, K., Cameron, N. (2009) Polymer flood application to improve heavy oil recovery at East Bodo. J Can Pet Technol 48(2):55–61

Webb, K. J., Black, C. J. J., and Al-Ajeel, H. 2004. Low Salinity Oil Recovery - Log-Inject-Log. SPE: Society of Petroleum Engineers. doi:10.2118/89379-MS

Worawutthichanyakul, T. (2016). Unstable immiscible displacement study in oil-wet rocks. MS Thesis, The University of Texas at Austin

Yang, H. T., Britton, C., Liyanage, P. J., Solairaj, S., Kim, D. H., Nguyen, Q. P., Pope, G. A. (2010, January 1). Low-Cost, High-Performance Chemicals for Enhanced Oil Recovery. Society of Petroleum Engineers. doi:10.2118/129978-MS

Yousef, A. A., Al-Saleh, S., & Al-Jawfi, M. S. (2012, January 1). Improved/Enhanced Oil Recovery from Carbonate Reservoirs by Tuning Injection Water Salinity and Ionic Content. Society of Petroleum Engineers. doi:10.2118/154076-MS

Zaitoun, A., Potie, B. Limiting conditions for the use of hydrolyzed polyacrylamides in brines containing divalent ions. (1983). Paper SPE 11785-MS presented at the SPE Oilfield and Geothermal Chemistry Symposium, June 1-3, Denver, Colorado, USA

Zhang, R., Somasundaran, P. (2006). Advances in adsorption of surfactants and their mixtures at solid/solution interfaces. Advances in colloid and interface science (123-126) 213-229

Zhao, P., Jackson, A., Britton, C., Kim, D. H., Britton, L. N., Levitt, D., & Pope, G. A. (2008, January 1). Development of High-Performance Surfactants for Difficult Oils. Society of Petroleum Engineers. doi:10.2118/113432-MS

Zhijian, Q., Yigen, Z., Xiansong, Z., & Jialin, D. (1998, January 1). A Successful ASP flooding Pilot in Gudong Oil Field. Society of Petroleum Engineers. doi:10.2118/39613-MS